RECEIVED
LAWRENCE
BERKELEY LABORATORY
OCT 9 1984

LBL-16870
UC-34 c.2

LIBRARY AND
DOCUMENTS SECTION

NUCLEAR SCIENCE DIVISION

ANNUAL REPORT 1982-1983

August 1984

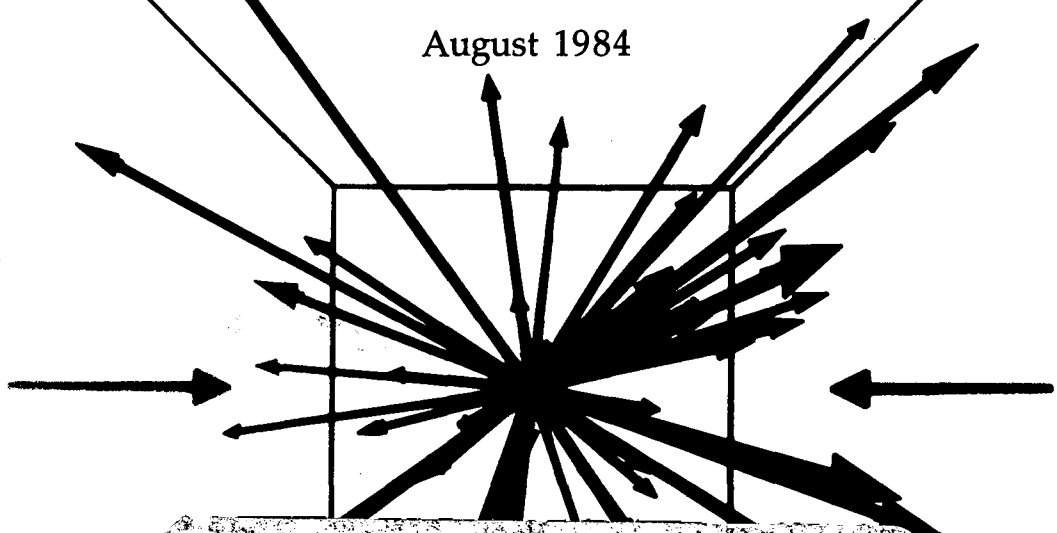

TWO-WEEK LOAN COPY
This is a Library Circulating Copy
which may be borrowed for two weeks.

LAWRENCE BERKELEY LABORATORY
UNIVERSITY OF CALIFORNIA

LBL-16870 c.2

Prepared for the U.S. Department of Energy under Contract DE-AC03-76SF00098

DISCLAIMER

This document was prepared as an account of work sponsored by the United States Government. While this document is believed to contain correct information, neither the United States Government nor any agency thereof, nor the Regents of the University of California, nor any of their employees, makes any warranty, express or implied, or assumes any legal responsibility for the accuracy, completeness, or usefulness of any information, apparatus, product, or process disclosed, or represents that its use would not infringe privately owned rights. Reference herein to any specific commercial product, process, or service by its trade name, trademark, manufacturer, or otherwise, does not necessarily constitute or imply its endorsement, recommendation, or favoring by the United States Government or any agency thereof, or the Regents of the University of California. The views and opinions of authors expressed herein do not necessarily state or reflect those of the United States Government or any agency thereof or the Regents of the University of California.

LBL-16870

Nuclear Science Division

Annual Report for the Period
October 1, 1982 – September 30, 1983

Division Head
Joseph Cerny

Assistant Division Head
Janis Dairiki

Editor
Jeannette Mahoney

Editorial Committee
David Clark, Jørgen Randrup, James Symons, Gordon Wozniak

Lawrence Berkeley Laboratory
University of California
Berkeley, California, 94720, USA

This work was supported by the Director, Office of Energy Research, Office of High Energy and Nuclear Physics, Division of Nuclear Physics and by the Office of Basic Energy Sciences, Division of Nuclear Sciences, of the U.S. Department of Energy under Contract No. DE-AC03-76SF00098

Cover: Some of the collisions observed by the Plastic Ball, which when analyzed showed the collective flow of nuclear matter.

Introduction

This report summarizes the scientific research carried out within the Nuclear Science Division between October 1, 1982 and September 30, 1983. Heavy-ion investigations continue to dominate the experimental and theoretical research efforts. Complementary programs in light-ion nuclear science, in nuclear data evaluation, and in the development of advanced instrumentation are also carried out. Experimental research utilizes the Bevalac-SuperHILAC complex and the 88-Inch Cyclotron, to support a broad program involving scientists from institutions throughout the world.

Exploring the nature of matter at extreme densities and temperatures is one of the most exciting challenges facing nuclear physics. Interest in this realm is demonstrated by the Nuclear Science Advisory Committee's 1983 recommendation to build a 30A GeV x 30A GeV heavy-ion collider. The Bevalac scientific program has been able to delve into new regions of the nuclear equation of state by making high-temperature (100 MeV or 10^{12}K) compressed matter. Studies with the Streamer Chamber for Ar - KCl and Ar - Pb collisions gave indirect evidence for collective flow of nuclear matter. The very high statistics from the GSI/LBL Plastic Ball/Wall detector (in Nb - Nb collisions at 400 MeV/nucleon) have identified two collective flow effects – bounce-off and side-splash – which had been predicted by nuclear hydrodynamical calculations.

The past year has been especially notable for the excellent new and high-quality beams from the upgraded Bevalac. Significant measurements have been made of the atomic properties of the new ion beams, particularly uranium, and the acceleration for the first time anywhere of a beam of completely stripped uranium nuclei (U^{92+}) opens up a variety of experimental possibilities.

Reaction mechanism studies dominate the heavy-ion research at the 88-Inch Cyclotron and the SuperHILAC. Investigations of transfer reactions at the cyclotron were enhanced by a new 4π scintillation detector, the Plastic Box, and will be further enhanced by completion in 1984 of the Electron Cyclotron Resonance (ECR) high charge state heavy-ion source. Complex fragment emission in compound nucleus and deep-inelastic reactions is being studied to explore the transition between evaporation and fission. Nuclear structure studies at both accelerators, aimed mainly at understanding nuclei with large angular momenta, have begun to use the new and unique High Resolution Ball detector system which will eventually consist of 21 Compton-shielded Ge detector modules. Research continues on the newly discovered decay mode of beta-delayed two-proton radioactivity, with emphasis on exploring the mechanism for two-proton emission and searching for new isotopes which decay by the same mode.

Division members published 158 reports and journal articles including 5 Ph.D. theses. Affiliated with the Nuclear Science Division during this period were 5 faculty senior scientists, 21 staff senior scientists, 29 staff scientists, 18 postdoctoral fellows, 28 graduate students, and 35 technical, adminstrative, and clerical support staff. Our research programs continue to be enriched by our many visiting scientists and by productive relationships with the UC campus and other LBL divisions.

The Division is actively engaged in looking to meet very high energy heavy-ion physics needs beyond the 1980s. To extend the study of relativistic heavy ion physics to higher energies, LBL has joined with GSI to propose experiments at CERN. These have been approved for early 1986, for ^{16}O beams at energies up to 40 GeV/nucleon. Taken in combination with the ongoing program at the Bevalac, with the very heaviest ions available, this program of light ion experiments at much higher energies will provide a glimpse of what may be anticipated at accelerators such as the Relativistic Nuclear Collider or the Mini-Collider, which are still on the drawing boards.

Joseph Cerny

PART I: PROGRAMS

Exotic Nuclei	1
Isotopes Project	2
New Element and Isotope Synthesis	4
Heavy Element Radiochemistry	6
Relativistic Heavy Ion Physics	7
Nuclear Structure	8
Polarization Phenomena in Nuclear Physics	10
Heavy Ion Reactions	12
Deep Inelastic Heavy Ion Reactions and Compound Nucleus Studies	14
Nucleus-Nucleus Collisions	16
HISS-A Group	18
Light Particle Emission in High Energy Nuclear Collisions	20
High Energy Nuclear Collisions	22
Heavy Ion Studies/Pion Studies	24
High Energy Nucleus-Nucleus Collisions	26
Relativistic Heavy Ion Collisions	30
High Energy Heavy Ion Collisions	31
Detector Research and Development	32
Nuclear Theory	33
High Energy Nuclear Beams at Berkeley	36

PART II: ACCELERATORS

88-Inch Cyclotron Operations 41
D.J. Clark, D. Elo, L. Glasgow, Y. Jongen, R. Lam, C.M. Lyneis, R.G. Stokstad

88-Inch Cyclotron Research Program 46
R.G. Stokstad

Bevalac Research Program 49
Howel G. Pugh

SuperHILAC Research Program 55
R.M. Diamond

PART III: EXPERIMENTS

Nuclear Structure

Discovery of Beta-Delayed Two-Proton Radioactivity: ^{22}Al* 59
M.D. Cable, J. Honkanen, R.F. Parry, S.H. Zhou, Z.Y. Zhou, and Joseph Cerny

Beta-Delayed Two-Proton Decay of ^{26}P* 61
J. Honkanen, M.D. Cable, R.F. Parry, S.H. Zhou, Z.Y. Zhou, and Joseph Cerny

Wide Angle Measurement of Beta-Delayed Two-Proton Radioactivity of ^{22}Al* 62
M.D. Cable, J. Honkanen, J.E. Reiff, E.C. Schloemer, S.H. Zhou, Z.Y. Zhou, and Joseph Cerny

Beta-Delayed Proton Emission Observed in New Lanthanide Isotopes 65
J.M. Nitschke, W.-D. Zeitz, P.A. Wilmarth, P.K. Lemmertz, J. A. Honkanen

Interpretation of Beta-Delayed Proton Spectra 69
P.K. Lemmertz, J.M. Nitschke, J. Honkanen, P.A. Wilmarth

Recent Attempts to Produce Superheavy Elements in the ^{48}Ca + ^{248}Cm Reaction 71
A. Ghiorso, K.E. Gregorich, D. Lee, M. Leino, K.J. Moody, G.T. Seaborg, R.B. Welch, P. Wilmarth, S. Yashita, Y.K. Agarwal, P. Armbruster, W. Brüchle, M. Brügger, J.P. Dufour, H. Gäggeler, S. Hoffman, F.P. Hessberger, P. Lemmertz, G. Münzenberg, K. Poppensieker, W. Reisdorf, M. Schädel, K.-H. Schmidt, J.H.R. Schneider, W.F.W. Schneider, K. Sümmerer, D. Vermeulen, G. Wirth, C. Frink, N. Greulich, G. Herrmann, U. Hickmann, N. Hildebrand, J.V. Kratz, N. Trautmann, M.M. Fowler, D.C. Hoffman, H.R. von Gunten, H. Dornhöfer

Actinide Production from Reactions of ^{129,132}Xe with ^{248}Cm 72
R.B. Welch, K.J. Moody, D. Lee, K.E. Gregorich, W. Kot and G.T. Seaborg

Large Einsteinium Accelerator Program (LEAP) for the Increased Production of Ultra Heavy Elements 73
G.T. Seaborg and A. Ghiorso

The Decay of ^{251}Bk 75
Y.-F. Liu, K.J. Moody, D. Lee, Y. Morita, G.T. Seaborg and H.R. von Gunten

The Half-Life and Absolute Gamma Ray Intensities of ^{157}Er 77
K.E. Gregorich, K.J. Moody, P. Juergens, D. Lee, and G.T. Seaborg

Compound Nuclei at High Angular Momentum

High-Spin γ-Ray Spectroscopy: Past Successes, Future Hopes 79
R.M. Diamond

Shell Effects at High Angular Momentum 81
M.A. Deleplanque, A.O. Macchiavelli, R.M. Diamond, F.S. Stephens, E.L. Dines, and J.E. Draper

Nuclear Moments of Inertia at High Spins 84
M.A. Deleplanque

Transient Magnetic Fields for Large Z Atoms Recoiling Through Gadolinium 86
O. Häusser, H.R. Andrews, D. Horn, M.A. Lone, P. Taras, P. Skensved, R.M. Diamond, M.A. Deleplanque, E.L. Dines, A. Macchiavelli, F.S. Stephens

Evidence for Reduced Neutron Pairing Correlations in ^{165}Yb 88
C. Schuck, N. Bendjaballah, R.M. Diamond, Y. Ellis-Akovali, K.H. Lindenberger, J.O. Newton, F.S. Stephens, J.D. Garrett, and B. Herskind

E2 Properties of the Ground-State Band in ^{248}Cm 91
T. Czosnyka, D. Cline, L. Hasselgren, C.Y. Wu, R.M. Diamond, H. Kluge, C. Roulet, E.K. Hulet, R.W. Lougheed, C. Baktash

Future Directions for High-Spin Studies 93
F.S. Stephens

Polarization Studies

Separation of Projectile and Ejectile Spin-Orbit Distortions in an $\ell = 0$ (d,^{3}He) Reaction 96
J.D. Brown, J.M. Barnwell, S. Roman, H.E. Conzett, D. Eversheim, R.M. Larimer, J. Birchall, C. Lapointe, J.S.C. McKee, N.M. Clarke, R.J. Griffiths, J.S. Hanspal, R.A. McCulloch

Spin-Polarization Observables at the $J=\frac{3}{2}^+$ Resonance in the Reactions ^{3}H(d,n)^{4}He and ^{3}He(d,p)^{4}He 98
H.E. Conzett

Insensitivity in Some Tests of Time-Reversal Invariance 100
H.E. Conzett

Scattering of Polarized Protons from ^{24}Mg, ^{27}Al, ^{32}S and
Anomalies in the Giant-Resonance Regions of ^{25}Al, ^{28}Si, and ^{33}Cl 101
R. Roy, C.R. Lamontagne, R.J. Slobodrian, J. Arvieux, J. Birchall, and H.E. Conzett

Time-Reversal Asymmetry: Polarization and Analyzing Power in Nuclear Reactions 101
C. Rioux, R. Roy, R.J. Slobodrian, and H.E. Conzett

Elastic and Inelastic Scattering of Polarized Protons from ^{6}Li 102
D. Rowley, C.H. Poppe, F.S. Dietrich, H.E. Conzett, D. Eversheim, and C. Rioux

Damped Collisions and Transfer Reactions

Compound Nucleus Decay Via the Emission of Large Fragments 104
L.G. Sobotka, M.L. Padgett, G.J. Wozniak, G. Guarino, A.J. Pacheco, L.G. Moretto, Y. Chan, R.G. Stokstad, I. Tserruya, and S. Wald

Complex Nuclei Emission In Compound Nucleus and Deep-Inelastic Reactions 106
G.J. Wozniak

Excitation Function for ^{3}He + ^{nat}Ag 107
M.L. Padgett, L.G. Sobotka, G.J. Wozniak, G. Guarino, A.J. Pacheco, L.G. Moretto, Y. Chan, R.G. Stokstad, I. Tserruya, and S. Wald

Bridging the Gap between Evaporation and Fission 108
L.G. Sobotka, R.J. McDonald, C. Signarbieux, G.J. Wozniak, M.L.Padgett, H.H. Gu, Z.Q. Yao, Z.H. Liu, L.G. Moretto

Incomplete and Complete Fusion at Intermediate Energies 109
W. Loveland, K. Aleklett, Wing Kot, D.J. Morrissey, T.T. Sugihara, and G.T. Seaborg

Angular Momentum Transfer and Alignment for ^{208}Pb- and ^{197}Au-Induced Reactions 113
G.J. Wozniak, A.J. Pacheco, G. Guarino, J.H. Gu, R.J. McDonald, L.G. Sobotka, and L.G. Moretto

Coincidence Measurements of Fusion-Like Residues in the ^{16}O + ^{40}Ca Reaction at $E^{Lab}_{^{16}O}$ = 313 MeV 115
A. Budzanowski, Y. Chan, R.G. Stokstad, I. Tserruya, S. Wald, and M. Blann

Velocity Distributions of Fusion-like Products for Medium Mass Heavy-Ion Systems 117
Y. Chan, C. Albiston, M. Bantel, P. Countryman, D. DiGregorio, H. Homeyer, R. Stokstad, S. Wald, S.H. Zhou, Z.Y. Zhou, A. Budzanowski, K. Grotowski, and R. Planeta

Excitation Functions for Fragments Produced in the ^{20}Ne + ^{197}Au Reaction 122
H. Homeyer, C. Albiston, M. Bantel, K. Van Bibber, Y.D. Chan, P. Countryman, R.G. Stokstad, S. Wald

Production of Neutron Rich Bi Isotopes by Transfer Reactions 123
K. Eskola, P. Eskola, M.M. Fowler, H. Ohm, E.N. Treher, J.B. Wilhelmy, D. Lee, and G.T. Seaborg

Excitation Functions for Production of Heavy Actinides from Reactions of ^{40}Ca and ^{48}Ca with ^{248}Cm 124
D. Lee, K. Moody, K. Gregorich, R. Welch, G.T. Seaborg, H. von Gunten, D.C. Hoffman, M. Fowler, W.R. Daniels, G.S.I. Mainz Collaboration

Alpha Particle Emission from the Reaction 484 MeV ^{56}Fe + ^{nat}Ag 125
L.G. Sobotka, G.J. Wozniak, G. Guarino, R.J. McDonald, J.H. Gu, Z.Q. Yao, and L.G. Moretto

Identification of Complete Charge Transfer Reactions for ^{20}Ne + ^{197}Au with the Plastic Box 127
S. Wald, C.R. Albiston, M. Bantel, Y.D. Chan, B.G. Harvey, M.J. Murphy, I. Tserruya, R.G. Stokstad, P.J. Countryman, K. Van Bibber, H. Homeyer

Transfer Reactions with Very Heavy Ions 130
A.O Macchiavelli, M.A. Deleplanque, R.M. Diamond, F.S. Stephens, E.L. Dines, J.E. Draper

Below-Target Transfers in the ^{136}Xe + ^{249}Cf Reaction 132
K.E. Gregorich, K.J. Moody, R.B. Welch, W. Kot, D. Lee and G.T. Seaborg

Mass Distributions in the Reaction of 240 MeV ^{12}C with ^{197}Au 134
H. Kudo, K.J. Moody, and G.T. Seaborg

Transfer Reaction Cross Sections from the Interactions of ^{20}Ne and ^{22}Ne with ^{232}Th 136
S. Tanaka, K.J. Moody and G.T. Seaborg

Relativistic Nuclear Collisions

Heavy Target Fragmentation and the Energy Dependence of Nucleus-Nucleus Total Reaction Cross Sections 139
W. Loveland, C.P. Oertel, D.J. Morrissey, P.L. McGaughey, G.T. Seaborg, and K. Aleklett

The ^{139}La + ^{139}La Reaction at 245 MeV/nucleon 141
Li Wenxin, W. Loveland, K. Aleklett, and G.T. Seaborg

Au Target Fragmentation in Intermediate Energy Heavy Ion Reactions 142
W. Loveland, K. Aleklett, P.L. McGaughey, K.J. Moody, R.M. McFarland, R.H. Kraus, Jr., and G.T. Seaborg

Target Fragment Angular Distributions for the Interaction of 86 MeV/nucleon ^{12}C with ^{197}Au 145
R.H. Kraus, Jr., W. Loveland, K. Aleklett, P.L. McGaughey, T.T. Sugihara, G.T. Seaborg, T. Lund, Y. Morita, E. Hagebø, and I.R. Haldorsen

First Results from a Repeat Experiment on the Mean Free Path of Projectile Fragments from 1.88 GeV/nucleon ^{56}Fe – Emulsion Interactions 147
Y.J. Karant, H.H. Heckman, and E.M. Friedlander

Evidence Against "Anomalon" Production in High-Energy Heavy Ion Collisions 149
J.D. Stevenson, J.A. Musser and S.W. Barwick

Observation of Anomalons in CR-39 Track Detectors 151
M.L. Tincknell and P.B. Price

Search for Short-Lived Anomalons in Projectile Fragmentation 153
H.A. Gustafsson, H.H. Gutbrod, B. Kolb, B. Ludewigt, A. M. Poskanzer, T. Renner, H. Riedesel, H.G. Ritter, A.I. Warwick, and H.H. Wieman

Radiochemical Search for Anomalons 154
G.Dersch, K. Aleklett, R. Beckman, R. Brandt, E.M. Friedlander, W. Loveland, T. Lund, P.L. McGaughey, N.T. Porile, G.T. Seaborg, and R.M. Weiner

Search for Relativistic Projectile Fragments with Charges of 4/3, 5/3, 7/3, and 8/3 155
M.A. Bloomer, E.M. Friedlander, H.H. Heckman, and Y.J. Karant

Search for Fractional Charges Produced in Heavy-Ion Collisions at 1.8 GeV/nucleon 156
*M.A. Lindgren, D.C. Joyce, P.C. Abrams, R.W. Bland, R.T. Johnson, T.D.Knoop, M.H. Savage, M.H. Scholz, B.A. Young, C.L. Hodges, A.A. Hahn, G.L. Shaw, K.S. Lackner,**H.G. Pugh, R. Slansky*

Two-Particle Correlations Observed with the Plastic Ball Detector 160
H. Wieman, H.H. Gutbrod, H.A. Gustafsson, B. Kolb, H. Löhner, B. Ludewigt, A.M. Poskanzer, T. Renner, H. Riedesel, H.G. Ritter, A. Warwick, and F. Weik

Angular Correlations Between Target and Projectile Fragments Emitted from ^{238}U + Ag(Br) Collisions at 0.85 GeV/nucleon 163
H.H. Heckman, E.M. Friedlander and Y.J. Karant

Spectator-Velocity Pions from Heavy Ions 165
J. Ridout, D. Murphy, H.M.A. Radi, and J.O. Rasmussen

Interaction of 4.22 GeV and 7.54 GeV ^{20}Ne with Cu 169
K.H. Hicks, T.E. Ward, H. Bowman, J.G. Ingersoll, J.O. Rasmussen, J.P. Sullivan, M. Koike, and J. Peter

Charged Particle Multiplicity Distributions in the Reaction ^{139}La + ^{139}La at 1 GeV/nucleon 172
G. Odyniec, D. Bangert, R. Brockmann, A. Dacal, J.W. Harris, M. Maier, M. Ortiz, H.G. Pugh, W. Rauch, R.E. Renfordt, A. Sandoval, R. Stock, H. Stroebele, D. Schall, and K.L. Wolf

Uranium Fragmentation at 900 MeV/nucleon 175
D.E. Greiner, T.J.M. Symons, H. Crawford, P.J. Lindstrom, H. Gould, J. Kidd, and W. Schimmerling

Charge Distributions of 962 and 430 MeV/nucleon U in Matter 179
H.J. Crawford, H. Gould, D.E. Greiner, P.J. Lindstrom, and T.J.M. Symons

Particle-Gamma Coincidence Measurements in ^{12}C + ^{12}C and ^{12}C + Pb Collisions at 2.1 GeV/nucleon Incident Energy, First Results – γ-Ray Spectrum 180
G. Roche, J. Carroll, C.C. Chang, T. Hallman, P.N. Kirk, R. Koontz, G. Krebs, L. Madansky, T. Mulera, H. Pugh, L. Schroeder, J. Vicente

Inclusive Measurements of Pions and Light Fragments in 800 MeV/nucleon $^{139}_{57}$La + $^{139}_{57}$La Collisions 183
X. Bai, H. Hamagaki, O. Hashimoto, K. Kimura, T. Kobayashi, Y. Miake, S. Nagamiya, G. Shapiro, Y. Shida and I. Tanihata

Measurement of High P_T Light Fragments at 90° C.M. in 800 MeV/nucleon ^{12}C + ^{12}C Collisions 184
X.X. Bai, H. Hamagaki, O. Hashimoto, S. Kadota, K. Kimura, Y. Miake, S. Nagamiya, K. Omata, Y. Shida, I. Tanihata, and N. Yoshikawa

The Production of Negative Pions at $\Theta_{c.m.}$ = 90° from the 246 MeV/nucleon ^{139}La + ^{139}La Reaction 186
G.F. Krebs, J.-F. Gilot, P.N. Kirk, L.S. Schroeder, J. Miller, H.G. Pugh, G. Roche, J. Vicente, W. Benenson, K. Beard, H. van der Pflicht, B. Sherill, and J.W. Harris

Subthreshold K^- Production in Nucleus-Nucleus Collisions 188
A. Shor, J. Carroll, E. Barasch, S. Abachi, V. Perez-Mendez, T. Mulera, P. Fischer, G. Igo, S. Trentalange, K. Ganezer, F. Kazeminzhad

Charge, Mass and Energy Measured in the Plastic Ball 189
H.-A. Gustafsson, H.H. Gutbrod, B. Kolb, H. Löhner, B. Ludewigt, A.M. Poskanzer, T. Renner, H. Riedesel, H.G. Ritter, A. Warwick, F. Weik, H. Wieman

Thermalization in High Energy Nuclear Collisions 190
H.-A. Gustafsson, H.H. Gutbrod, B. Kolb, H. Löhner, B. Ludewigt, A.M. Poskanzer, T. Renner, H. Riedesel, H.G. Ritter, A. Warwick and H. Wieman

Pion Spectra from the Interaction of Intermediate and Heavy Nuclear Systems 191
R. Brockmann, D. Bangert, A. Dacal, J.W. Harris, M. Maier, G. Odyniec, M. Ortiz, H.G. Pugh, W. Rauch, A. Sandoval, R.E. Renfordt, R. Stock, H. Stroebele, and D. Schall

Momentum Flow in the 800 MeV/nucleon Ar + Pb Reaction 192
R.E. Renfordt, D. Bangert, R. Brockmann, J.W. Harris, M. Maier, G. Odyniec, H.G. Pugh, A. Sandoval, R. Stock, H. Stroebele, D. Schall, L.S. Schroeder, K. Tittel, and K.L. Wolf

Part IV: THEORY

Static Nuclear Properties

An Update on Droplet Model Charge Distributions 197
W.D. Myers and K.-H. Schmidt

Combining the Droplet Model and the Yukawa-plus-Exponential Macroscopic Model 198
P. Möller and W.D. Myers

Note on Nuclear Disintegration Widths 198
W.J. Świątecki

The Surface Energy of Multi-Component Systems 199
W.D. Myers, W.J. Świątecki and C.S. Wang

On the Coulomb Sum Rule in the Relativistic Nuclear Many-Body Problem 200
T. Matsui

Low Energy Nuclear Dynamics

Dynamical Evolution of Angular Momentum in Damped Nuclear Reactions:
I. Accumulation of Angular Momentum by Nucleon Transfer 202
T. Døssing and J. Randrup

Dynamical Evolution of Angular Momentum in Damped Nuclear Reactions:
II. Observation of Angular Momentum through Sequential Decay 205
T. Døssing and J. Randrup

Dissipative Resistance Against Changes in the Mass Asymmetry Degree of Freedom in Macroscopic Nuclear Dynamics: The Completed Wall-and-Window Formula 207
J. Randrup and W.J. Świątecki

Dynamics of Nucleus-Nucleus Collisions 208
J. Blocki and W.J. Świątecki

A Simple Model for Fermi Jets 210
K. Möhring, W.J. Świątecki and M. Zielińska-Pfabé

An Overlap Model for Fragment Yields in Heavy Ion Reactions 212
B.G. Harvey and H. Homeyer

Monte Carlo Studies of Alpha-Accompanied Fission 214
H.M.A. Radi, J.O. Rasmussen, R. Donangelo, L.F. Canto, and L.F. Oliveira

Feedback and Self-Regulation in Energy and Mass Exchange Between Heavy Ions 217
L.G. Moretto

A Feedback Process Controlling Energy Partition and Mass Exchange Between Heavy Ions 220
L.G. Moretto, E.G. Lanza

New Statistical and Non-Statistical Effects in Deep Inelastic Heavy Ion Collisions 223
L.G. Moretto

The Phenomenology of Deep-Inelastic Processes 224
L.G. Moretto

Statistical Properties of Deep Inelastic Reactions 224
L.G. Moretto

High Energy Collisions

Effect of Fluctuations on Global Analysis of Fluid Dynamical Calculations for High-Energy Nuclear Collisions 225
L.P. Csernai, G. Fai, and J. Randrup

Global Event Analysis as a Tool to Study the Nuclear Matter Equation of State 227
H. Stöcker, G. Buchwald, G. Graebner, J. Haruhn, W. Greiner, K. Frankel, M. Gyulassy

Jacobian-Free Global Event Analysis 227
P. Danielewicz and M. Gyulassy

Non-Binary Effects in High-Energy Nuclear Collisions 229
K.C Chung, R. Donangelo, S.B. Duarts, T. Kodama, R.A.M.S. Nazareth, J.Randrup

Quantum Theory of Nonequilibrium Processes 229
P. Danielewicz

Quark-Gluon Plasma Evolution in Scaling Hydrodynamics 230
M. Gyulassy and T. Matsui

Deflagrations and Detonations in Quark-Gluon Plasmas 231
M. Gyulassy, K. Kajantie, H. Kurki-Suonio, L. McLerran

Creation of a $q\bar{q}$ Pair in a Chromoelectric Flux Tube 233
N.K. Glendenning, and T. Matsui

Achieving Maximum Baryon Densities 236
M. Gyulassy

Evaporation of Mesons from Quark-Gluon Plasma by Fission of Chromoelectric Flux Tubes 236
B. Banerjee, N.K. Glendenning, and T. Matsui

Charge-Exchange Products of Bevalac Projectiles 241
John Rasmussen

Heavy Ion Pion Production: Spectral Irregularities 243
John O. Rasmussen

Monte Carlo Studies of Pion Distributions from Heavy Ion Collisions 247
Hafez M.A. Radi, J.O. Rasmussen, K.A. Frankel, J.P. Sullivan, and H.C. Song

PART V: INSTRUMENTATION AND TECHNIQUES

General

A Method for Precise Charge Measurements for Relativistic Light Nuclei, $Z \geqslant 3$, in Nuclear Track Emulsion 251
M.A. Bloomer, H.H. Heckman, and Y.J. Karant

Development of a New Type of On-Line Mass Analyzer – RIMA 252
A. Ghiorso, K. Halback, and S. Yashita

A Monopole Search 253
F. Beiser, D. Greiner, and R. Hagstrom

Mapping the HISS Dipole 254
C. McParland, F. Bieser

Status Report on the ECR Ion Source for the 88-Inch Cyclotron 256
D.J. Clark, Y. Jongen, C.M. Lyneis

High Charge State Ion Sources 258
D.J. Clark

Global Analysis of Relativistic Nuclear Collisions Detected by the Plastic Ball 260
H.A. Gustafsson, H.H. Gutbrod, B. Kolb, H. Löhner, B. Ludewigt, A.M. Poskanzer, T. Renner, H. Riedesel, H.G. Ritter, A. Warwick, F. Weik, and H. Wieman

Minimal-Spanning-Tree Analysis of Plastic Ball Events 262
H. Löhner, A. Baden, H. Gutbrod, A.M. Poskanzer, T. Renner, H. Riedesel, H.G. Ritter, A. Warwick, H. Wieman

Enhanced Adhesion of Thin Films by Heavy Ion Bombardment 264
M. Mendenhall, T. Tombrello, R.G. Stokstad

Detectors

Large Solid Angle Bragg-Curve Spectrometer 266
R.J. McDonald, L.G. Sobotka, Z.Q. Yao, G.J. Wozniak, and G.Guarino

A Large Solid Angle Ion Chamber 267
L.G. Sobotka, J.B. Hunter and G.J. Wozniak

A Threshold Čerenkov Counter for Isotopic Identification of High-Energy Heavy Ions 269
J. Stevenson, J. Musser, and P.B. Price

HISS Drift Chamber Resolution 270
D.F. Greiner and F. Bieser

Multi-Angle Gas and Si Detector Particle Telescope 271
R.J. McDonald, L.G. Sobotka, and G.J. Wozniak

Status of the HISS MUSIC Detector 272
H.J. Crawford, I. Flores, F. Bieser, D. Greiner, P. Lindstrom, C. McParland, P. Brady, C. Castenada, W. Christie, J. Romero, C. Tull, H. Sann

Status of the HISS TOF Wall 274
M. Baumgartner, H. Crawford, Ryoichi Wada,

A Position-Sensitive "Phoswich" Detector 275
M. Bantel, R.G. Stokstad, Y.D. Chan, S. Wald, and P.J. Countryman

The Plastic Box: A 4π Detector for Intermediate Energy Heavy Ion Physics 277
K. Van Bibber, P.J. Countryman, M.J. Murphy, Y.D. Chan, R.G. Stokstad, I. Tserruya, S. Wald

Improvements to the Plastic Ball 279
R. Albrecht, H.-A. Gustafsson, H.H. Gutbrod, B. Kolb, H. Löhner, B. Ludewigt, A.M. Poskanzer, T. Renner, H. Riedesel, H.G. Ritter, H. Stelzer, A. Warwick, H. Wieman

A New Detection System for OASIS 280
P.A. Wilmarth, J.M. Nitschke, W.D. Zeitz, P.K. Lemmertz

A Forward Scintillator Hodoscope for the Streamer Chamber Facility 283
R. Brockmann, D. Bangert, A. Dacal, P. Eitner, J.W. Harris, W. Hou, M. Maier, G. Odyniec, M. Ortiz, H.G. Pugh, W. Rauch, A. Sandoval, R.E. Renfordt, R. Stock, H. Stroebele, and D. Schall

Monitoring System for a Scintillator Hodoscope using an UV Laser 284
R.E. Renfordt, D. Bangert, R. Brockmann, P. Eitner, W. Hou, J.W. Harris, M. Maier, G. Odyniec, H.G. Pugh, W. Rauch, A. Sandoval, R. Stock, H. Stroebele, and D. Schall

On Line Streamer Chamber Monitoring System 285
R.E. Renfordt, D. Bangert, R. Brockmann, J.W. Harris, G.Odyniec, H.G. Pugh, W. Rauch, A. Sandoval, M. Maier, R. Stock, H. Stroebele, and D. Schall

Computers

WC – A General Purpose Computer Program for Off-Line Analysis 287
S. Wald

Bevalac Software Project Status 287
C. McParland, M. Bronson, P. Lindstrom

Installation Progress of the NSD-Bevalac VAX 289
C. McParland

LULU Analysis Program 290
H.J. Crawford and P.J. Lindstrom

Status of HISS Maps 292
E. Beleal, M. Bronson, C.McParland, D. Olson

ICAMS A New System for Automated Emulsion Data Acquisition and Analysis 293
A.A. Arthur, W.L. Brown, Jr., E.M. Friedlander, H.H. Heckman, R.W. Jones, Y.J. Karant, and A.D. Turney

MONA, the Plastic Ball Data Acquisition System 294
B. Kolb

GAMUT, a Computer Code for Statistical Analysis of γ-Ray Data 295
R.B. Firestone and E. Browne

PART VI: APPENDICES

Appendix I — Publications
Appendix II — Thesis Abstracts
Appendix III — Seminars
Appendix IV — Author Index

PART I: PROGRAMS

Exotic Nuclei

Group Leader
Joseph Cerny

M. Cable
J. Honkanen
R. Parry
*J.E. Rieff**
E.C. Schloemer

S.H. Zhou,
Institute of
Atomic Energy
Beijing,
Peoples Republic
of China

Z.Y. Zhou
Nanking Univ.
Peoples Republic
of China

**Graduate student*

Studies of nuclei very far from the valley of stability may reveal new radioactivities; provide tests of theoretical models that predict the existence, masses, and shapes of exotic nuclei; and develop spectroscopic data on nuclides with abnormal neutron to proton ratios. Several techniques are in use for studying such nuclei produced in low-yield reactions. Current experiments at the 88-Inch Cyclotron are concentrated primarily, but not exclusively, on exploring the light-mass nuclei that are expected to define the proton drip line.

In the light-mass region, the odd-odd $T_z = -2$ nuclides ^{22}Al and ^{26}P have been discovered using the (^{3}He,p4n) reaction at 110 – 130 MeV on ^{24}Mg and ^{28}Si targets. The experimental technique employed used a minimal length helium jet to transport these short-lived nuclides ($T_{1/2} < 100$ ms) from the target region to a collection point in front of a semiconductor counter telescope. Observation of the beta-delayed (isospin-forbidden) proton decay of these nuclei (~7–8 MeV protons) established their existence. In addition to being of interest for studies of charge-dependent effects in nuclei, the measurement of these protons confirmed Gol'danskii's hypothesis that these nuclei were prime candidates to exhibit the new decay mode of beta-delayed two-proton radioactivity. Subsequent proton-proton coincidence experiments detected this decay branch.

Two specially constructed detector systems were used to measure these two-proton events at both narrow (~40°) and wide (~120°) relative proton angles. These measurements showed that the dominant decay mechanism for two-proton emission in each isotope appears to be sequential decay; however, a small component of the two-proton decay proceeding by another mechanism (such as ^{2}He emission) remains a possibility, particularly for ^{22}Al. Efforts are being made to detect these other possible decay mechanisms.

In addition to the light mass beta-delayed two-proton emitters already observed, heavier nuclei are expected also to exhibit this decay mode. Initial efforts have been made to find beta-delayed two-proton emitters in the mass 40–60 region. These nuclei, however, are not only expected to have smaller two-proton decay branches, but must be produced using lower intensity heavy ion beams. No new emitters have been detected in preliminary searches.

A new beta-delayed single proton emitter, ^{58}Zn, was also characterized this year. Its beta decay properties are being studied and compared to existing (p,n) data on ^{58}Ni.

Isotopes Project

Group Leader
J.M. Dairiki

E. Browne
R.B. Firestone
C.M. Lederer
V.S. Shirley

The Isotopes Project compiles and evaluates nuclear structure and decay data and disseminates these data to the scientific community. From 1940–1978 the Project had as its main objective the production of the *Table of Isotopes.* Since publication of the seventh (and last) edition in 1978, the group now coordinates its nuclear data evaluation efforts with those of other data centers via national and international nuclear data networks. The group is currently responsible for the evaluation of mass chains A = 167–194. All evaluated data are entered into the international Evaluated Nuclear Structure Data File (ENSDF) and are published in *Nuclear Data Sheets.* In addition to the evaluation effort, the Isotopes Project is responsible for production of the *Radioactivity Handbook.*

During the past year the evaluations of nuclear structure data for all nuclides with masses A = 169, 187 and 190 were published in *Nuclear Data Sheets.* Evaluations of A = 192, A = 174, and A = 181 have been submitted for review; an updated evaluation of A = 171 is nearing completion.

Approximately half of the group's efforts were directed toward production of the *Radioactivity Handbook.* The purpose of the *Handbook* is to provide a compilation of recommended decay data that is detailed enough for use in sophisticated applications, but that is organized clearly so as to be usable in simple routine applications. Recommended decay data will be taken from the current version of ENSDF, with no further updating. Additional calculations and evaluation will be done to provide recommended data for atomic radiations and conversion electrons.

ENSDF data are restructured into a data base which is accessed via DATATRIEVE, a DEC data base management system. Several major computer codes have been developed to facilitate the *Handbook* production. These production mechanisms are now largely in place; future efforts will concentrate on the processing of mass-chain data and the tabular output formats. Plans call for submitting the completed manuscript to the publisher by the end of 1984.

Many of the codes and procedures developed for production of the *Radioactivity Handbook* can also be used as tools to increase the efficiency of the evaluation process. For example, the code SPINOZA is a valuable physics checking program; it is especially useful in deriving spin/parity assignments for complicated level schemes. The code GAMUT presents the evaluation network with a uniform, statistical process for deriving gamma-ray energies and intensities.

The group has presented a proposal for production of a complementary volume – the *Nuclear Structure Handbook* – to the NAS/NRC Panel on Basic Nuclear Data Compilations which advises DOE. This handbook is intended to address the needs of the basic nuclear physics community for a compilation of nuclear structure data. Recommended data will be taken from the ENSDF file and the production mechanisms already developed for the *Radioactivity Handbook* can be used directly for the *Nuclear Structure Handbook.* Plans for this publication will be finalized in 1985.

One of the goals of the U.S. Nuclear Data Network is to make ENSDF data available to remote users by on-line retrieval. A procedure has been implemented at LBL to allow access to the LBL Nuclear Structure Numerical Database which currently contains ENSDF data for mass chains A = 200–263. During 1984 ENSDF data for all other mass chains will be implemented into the database; these data can be accessed by telephone lines or via DECNET and

MILNET.

In response to a request from the NAS Panel at its 1982 meeting, the Isotopes Project has designed a form to solicit author input for the preparation of nuclear-structure keyword abstracts. The check-list/matrix form style resulted from consideration of the prime criteria: author cooperation, completeness and uniformity of keywords, and efficiency of keyword preparation. A complete summary report was submitted to the Panel.

The seventh edition of the *Table of Isotopes* continues to be the most up-to-date general reference source available for nuclear structure and decay data. Sales through April 1983 total 7844 copies (3708 clothbound and 4136 paperback). The *Table of Nuclear Moments,* a compilation of nuclear magnetic and quadrupole moments published by the Isotopes Project, has been the only such table maintained on a continuing basis. The most recent version was published as an appendix to the *Table of Isotopes.* User response has led to plans for expanding the amount of data and its presentation in the next edition. Nearly all 7000 copies of the *Nuclear Wallet Cards,* produced in 1979 by the Isotopes Project on behalf of the US. Nuclear Data Network, have been distributed to the user community.

Promoting the science of data evaluation and providing assistance to the user community are both important aspects of the Project's role. Project members organized the very successful First Annual Conference on Nuclear Structure Data Evaluation, held at Asilomar October 27–30, 1981. In addition to answering specific data requests, the Isotopes Project encourages general use of its extensive library, which contains comprehensive data files and major nuclear physics journals.

New Element and Isotope Synthesis

Group Leaders
A. Ghiorso
J.M. Nitschke

*L. Frank**
*K.E. Gregorich**
D.M. Lee
P. Lemmertz
K.J. Moody
M.J. Nurmia
L.P. Somerville
G.T. Seaborg
*P.A. Wilmarth**
*S. Yashita**

W.-D. Zeitz,
Hahn-Meitner
Institut, Berlin
West Germany

D. Hoffman,
M. Fowler,
Los Alamos
National
Laboratory

E.K. Hulet,
R. Lougheed,
Lawrence
Livermore
National
Laboratory

**Graduate students*

The research program of the Heavy Elements Research group is directed toward the synthesis of new nuclides and the determination of the radioactive properties of known nuclides. Graduate students play an important role in this work and thereby are trained in the experimental techniques of nuclear physics. Experiments are conducted both at the 88-Inch Cyclotron and at the SuperHILAC, and often there are extensive collaborations with scientists at other laboratories of the USA and foreign countries. Some of the delayed proton experiments were carried out in collaboration with J. Cerny's RAMA group.

Our research in the transuranium element region has now matured to the point where it is imperative to make exact identification of the interesting spontaneous fission activities that have been uncovered in recent years using conventional, non-specific methods. To do so we are confronted with a major challenge because their production cross sections are very small and their half-lives are in the seconds to milliseconds region. We have been developing a fast and efficient on-line mass separator for this purpose called RIMA (Recoil Ion Mass Analyzer) which should be ready for testing early in 1984.

The key to expanding our knowledge of the heaviest region of the periodic system is the use of 276-d ^{254}Es as a target; so we have been active in helping to launch a proposal to make a large jump in the production of this reactor-produced nuclide. This proposal, under the sponsorship of the U.S. Transplutonium Program Committee, is called LEAP (Large Einsteinium Accelerator Program) and envisions an order of magnitude increase in the production of this nuclide to 40 micrograms. This target material will be used for accelerator-based research on elements with Z greater than 100 to learn about their chemistry and their neutron-rich isotopes, and to enhance the possibilities of making superheavy elements. LEAP will bring together far-flung qualified nuclear chemistry groups for joint researches in these fields. To this end, SASSY, our gas-filled magnetic spectrometer and RIMA will be modified to make it possible to bombard the highly radioactive material with absolute safety and high efficiency.

Another major research tool of the heavy element group is OASIS (an acronym for On-line Apparatus for SuperHILAC Isotope Separation). Recoils from heavy-ion-induced nuclear reactions are stopped in a tantalum catcher, which is kept at a temperature just below its melting point inside an ion source. The recoils diffuse out of the catcher, are ionized and then accelerated to an energy of 50 keV. An analyzing magnet selects the desired isotopes and focuses them onto various detectors. The isotopically-pure beam can also be guided to a shielded room 4 meters above OASIS where low-background proton-, $\beta^{\pm}$-, γ- and x-ray experiments can be carried out. A fast tape system transports the selected isotope within 65 ms to a detection system that consists of a high purity Ge detector for $\beta^{\pm}$- and x-ray spectroscopy, and an n-type Ge detector for γ- and x-ray measurements. In addition a $\Delta E/E$ telescope is placed in front of one of the Ge detectors to identify charged particles. All detectors provide coincidence information.

Presently most of the physics with OASIS is focused on the region between the magic numbers of $Z > 50$ and $N \leqslant 82$. This region is of particular interest because of the recent discovery of proton radioactivity. In the search for other examples of this exotic decay mode many new beta-delayed proton emitters were found. With the new tape system now fully operational it was possible to identify these new isotopes uniquely according to A and Z. The A identification is inherent in the isotope separation process while Z-identification is achieved by measuring $K_{\alpha,\beta}$-x-rays in coincidence with beta-delayed protons. Information

about the spin of the proton precursor is obtained by measuring gamma radiation from the daughter nucleus in coincidence with protons. In the same experiment the level scheme of the proton emitting nucleus can be studied through positron/gamma- and x-ray/gamma- coincidences. One of the Ge-detectors also measures positron endpoint energies which are directly related to electron capture Q-values. The most important information is, however, obtained from the proton spectrum itself. It is the result of a two step process – β^+ decay followed by proton emission – and reflects β^+-transition rates to excited states via the intermediate nucleus and the competition between proton- and gamma-decay of these states. By comparing calculations of this process with the experimental proton spectrum a beta-strength function can be obtained which itself can be compared to calculations using for instance the gross theory of beta decay or the random phase approximation method. Beta delayed proton emission is a powerful tool to investigate nuclei far from stability because the large energy window available from the decay of the precursor allows the population of regions of high level density and excitation energies in the intermediate nucleus. This gives rise to a statistical model to interpret the decay of such a nucleus and the fluctuations associated with it.

It is expected that for a group of nuclei located in the region $65 < Z < 71$, $73 < N < 79$ α-emission may become a possible decay mode besides positron- and proton decay. This group of nuclei is located on or near the proton drip line and therefore very difficult to synthesize with reasonable cross sections. Combining the most neutron deficient targets with neutron deficient projectiles from the SuperHILAC OASIS will be used to look for weak α-lines of about 4.3 MeV among a vast "background" of beta particles and protons.

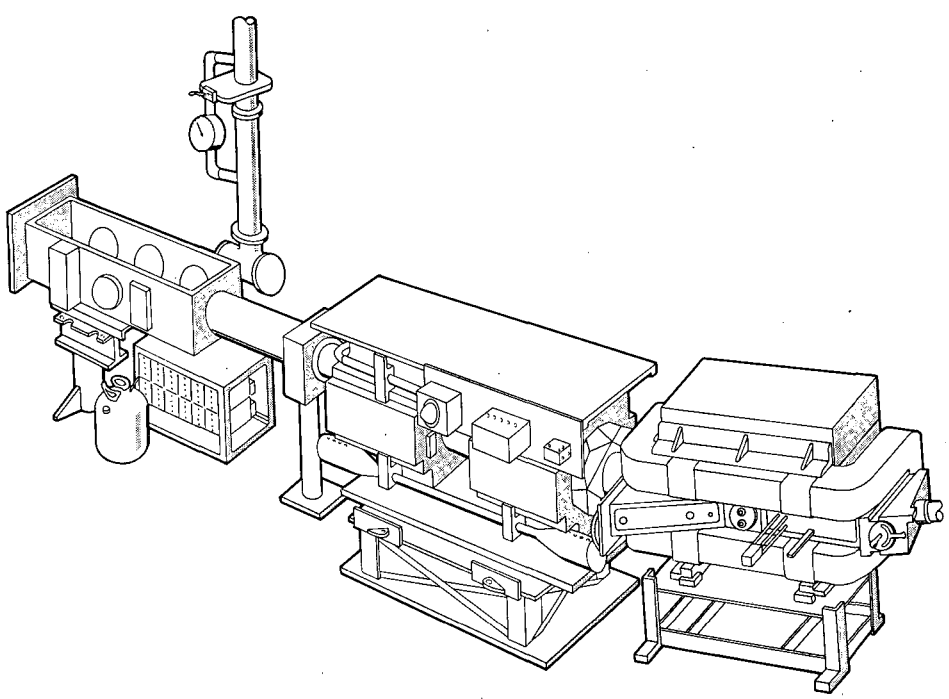

Fig. 1. Artist's view of the gas-filled magnetic spectrometer SASSY at the SuperHILAC. XBL 8312-6900

Heavy Element Radiochemistry

Group Leader
G.T. Seaborg

E. Bicknese†
*K. Gregorich**
P. Juergens†
*W. Kot**
D. Lee
*R. Welch**
*P. Wilmarth**
*S. Yashita**

K. Aleklett,
Studsvik Science
Research Laboratory
Sweden

D. Hoffman,
Los Alamos National
Laboratory

H. Kudo,
Niigata University,
Niigata, Japan

W. Li,
Institute of Modern
Physics, Lanzhou,
People's Republic
of China

Y.-F. Liu,
Peking University
People's Republic
of China

W. Loveland,
Oregon State
University

S. Tanaka,
University of Tokyo
Japan

H. von Gunten,
University of Bern
Switzerland

**Graduate students*
†*Undergraduate students*

This group uses all three of the LBL accelerators to identify and characterize new elements and isotopes, to study nuclear mechanisms, and to train students in modern radiochemical techniques. Currently, research is focused on (1) the synthesis and identification of new isotopes and elements in the actinide and transactinide region, along with attempts to synthesize superheavy elements, (2) the study of low-energy heavy ion reaction mechanisms such as massive transfer, complete fusion and deep inelastic scattering, potentially useful in the synthesis of new elements and isotopes and (3) the characterization of the mechanisms operating in intermediate energy (10–100 MeV/nucleon) and relativistic ($\geqslant$250 MeV/nucleon) heavy ion (RHI) reactions through studies of the target fragment yields, energies, angular distributions, etc.

With light ($A < 25$) heavy ion reaction studies at the 88-Inch Cyclotron, the primary emphasis has been on the use of "transfer" reactions to produce heavy actinides and the study of the mechanism of these reactions. These studies have indicated surprisingly large probabilities for the synthesis of the nuclear species ranging in mass from the target mass to that of the compound nucleus. The group is systematically exploring these reactions by studying the variation of product yields, energies, angular distributions, etc., with projectile and target mass and energy.

Members of the group have also used the 88-Inch Cyclotron and SC synchrotron at CERN to study intermediate energy heavy ion reaction mechanisms. In particular, they are concerned with studies of the target fragment yields, energies, and angular distributions in light ion-heavy target reactions.

Research at the SuperHILAC has been directed toward the use of deep inelastic transfer and "cold fusion" processes to produce new isotopes or elements and to obtain an understanding of the mechanisms involved. Efforts are being concentrated on the reactions of ^{48}Ca and the heaviest projectiles (Kr, Xe) with very heavy targets (^{248}Cm, ^{249}Cf, ^{254}Es). Future work will involve the use of heavier projectiles such as ^{238}U.

Research on target fragmentation at the Bevalac has involved single particle inclusive survey measurements of the energy dependence of target fragmentation.

Recent work has focused on very heavy ion-heavy nucleus collisions. An international collaborative radiochemical search for anomalons is being pursued.

An international collaborative program (LEAP, Large Einsteinium Accelerator Program) is being planned to utilize some 40 micrograms of 276-day ^{254}Es (to be produced in the HFIR/TRU facility at ORNL) for the production and study of the nuclear properties of known, and especially new, nuclides at the upper reaches of the periodic table and the study of the largely or completely unknown chemical properties of the transactinide elements.

Relativistic Heavy Ion Physics

Group Leader
H.H. Heckman

M. Bloomer
S. Chatterji
C. Connolly
E. Friedlander
R. Guzman
Y. Karant
H. Yee
C. Zeitlin

M. Ghoniem,
Cairo University
Cairo, Egypt

B. Judek,
National Research
Council, Ottawa

The Relativistic Heavy Ion Group's experimental program employs nuclear emulsion visual track detectors to carry out studies on the interaction of relativistic nuclei in matter. At the Bevalac, experiments on the interaction properties of relativistic projectile fragments of ~2 GeV/nucleon ^{56}Fe nuclei are in progress. The availability of uranium beams up to ~1 GeV/nucleon at the Bevalac has extended the scope of our program, with studies beginning on the topological characteristics of high-multiplicity ^{238}U-nucleus events and the target-projectile fragment correlation therefrom, and the kinematics of the fission reactions of ^{238}U at relativistic energies. Complementary to the above experiments are our technical advances related to the measurement of nuclear charge for particle tracks in emulsion. For light nuclei, $1 < Z < 6$, at relativistic energies, charge information is extracted from the linear structure of the ionization track, whereas for high Z nuclei, i.e., ^{238}U and fission fragments, such information is extracted from the area profiles of stopping tracks. The development of an Interactive Computer Assisted Measuring System (ICAMS) as part of our data acquisition and measurement program continues to be a major activity of the group.

An experiment on the interactions of 12 GeV/nucleon ^{4}He nuclei in matter became possible with the irradiation of nuclear emulsions by the first such ^{4}He beam extracted from the CERN-PS. The initial physics application of the emulsions will be to intercompare the multiplicity distributions of shower particles (relativistic $Z = 1$ particles, including mesons and projectile fragments) and non-relativistic (target-related) fragments with those produced in ^{4}He- and proton-nucleus interactions at energies of 2 GeV/nucleon and $6 < E < 69$ GeV, respectively.

Concurrent with the above experiment, the group collaborated with the University of Marburg in a radioanalytical experiment to investigate possible variations in the production of radioactive isotopes that take place in identical pairs of Cu targets bombarded by 12 GeV/nucleon ^{4}He and the secondary projectile fragments therefrom, where the distance of separation between the two Cu targets are varied from 0 to 20 cm. The analysis of the interaction topologies of 12 GeV/nucleon ^{4}He interactions in emulsion as described above are pertinent to the interpretation of the radioanalytical results. Both of these analyses are in progress. Similar exploratory studies have been carried out at the Bevalac using 1.9 GeV/nucleon ^{40}Ar beams for irradiating Cu targets. An experiment of this type using an improved target design, will be performed as Exp. # 660H.

The group is also involved in an electronic experiment, Bevalac Exp. 681H, that will use segmented solid state Si(Li) detectors to study the mean-free-paths of projectile fragments produced in the interaction of 2 GeV/nucleon ^{6}Li beam nuclei with Si (and other) target nuclei. The key feature of this experiment is that, in addition to measuring the $\Sigma_i Z_i^2$ of the projectile fragments, it has the capability of locating the origins of the interactions by simultaneously detecting the low-energy, target related fragments that are emitted in the interaction.

An integral part of the Group's program this FY was our participation in, and contributions to the organization of, the Second Anomalon Workshop held as part of the Sixth High Energy Heavy Ion Study held at LBL, 28 June – 1 July, 1983. This workshop brought together a major fraction of Bevalac researchers who specialize in visual techniques and offered the opportunity for in-depth discussions on the short-mean-free path phenomenon.

Nuclear Structure

Group Leaders
R.M. Diamond
F.S. Stephens

M-A. Deleplanque

J.E. Draper,
*E.L. Dines,**
U.C. Davis

*A.O. Macchiavelli,**
Buenos Aires,
Argentina

**graduate students*

Essentially the whole range of spins possible for many nuclei in the periodic table is available with the use of the 88-Inch cyclotron and SuperHILAC accelerators. Nuclei carry angular momentum principally in two ways: by aligning individual high j nucleons, and by a collective rotation of the nucleus as a whole. Deformed nuclei use both modes and it is the interplay between the single-particle and collective modes that leads to the great diversity of nuclear properties at high spin.

Information about these states and their properties is obtained only by detailed γ-ray spectroscopy of their de-exciting transitions. But for the higher spins the population is usually spread over so many states that only average values of continuum properties can be determined. So one of the goals of present-day research is to push discrete spectroscopic studies to higher spin states, reducing the continuum region. To do this requires that the number of cascade pathways observed be reduced to a small enough number so that individual transitions can show. One way is to use a combination of sum-energy and multiplicity selection, that is, to define a smaller entry region. This is what the NaI crystal balls can do. Another technique is to set gates on the highest-lying discrete transitions observed and look at what is in coincidence (ahead) of them. Either method requires a drastic decrease in the number of cascades selected, so very good statistics are needed and this means many detectors as close as possible to the target.

Our idea is to use both techniques simultaneously. We plan to place 21 Ge detectors at only 5-6 inches from the target. This makes possible higher order coincidence studies than ever done before, triple and even quadruple coincidence events. Each of these detectors will have a Compton-suppression shield of bismuth germanate (BGO) scintillator, and the arrangement will permit the most searching look upwards for higher-spin discrete transitions so far attempted. In addition, we propose a small central ball of 44 BGO sectors which form almost as good sum-energy selectors as the much larger NaI crystal balls, though poorer in multiplicity selection (44 sectors vs. 72 or 162).

The planning for this multi-detector array has taken an increasing amount of time and effort of the group during the past 2-3 years, and now the testing of the first units is taking place. At the time of writing this report (November, 1983), five BGO-shielded Ge detectors have been used in a first experiment and worked very successfully. The array will grow to its final size at the rate of one additional unit per month, and will be the focus of the group's experimental efforts during the coming year.

Although work on the array has been of major concern the past year, a number of experiments have been carried out. A study of the continuum γ-spectra of the even-even erbium nuclei (160, 158, 156, 154) has given the systematics of the band crossings (particle alignments) in these nuclei at high spin. As one goes to the lighter nuclei, the valence-shell alignments come closer together and a minimum in the spectra develops around 1 MeV for ^{156,154}Er. This suggests that the valence-shell alignments are used up and that significantly higher rotational frequencies are needed to bring down the $i_{13/2}$ and $h_{9/2}$ protons from the shell above to provide further aligned angular momentum.

As mentioned earlier, more detailed information about nuclear states and properties can be obtained from discrete γ-ray studies. Such a study of the high-spin levels in ^{165}Yb produced by ^{20}Ne and ^{40}Ar at the LBL 88-Inch Cyclotron showed that at rotational frequencies above 0.4 MeV the bands observed had

nearly constant values of $\mathscr{I}^{(1)}$ and that $\mathscr{I}^{(2)}_{\text{band}}$ was approximately as large and surprisingly constant. Certainly the neutron pairing is very much reduced at these rotational frequencies, but this behavior is not what is expected from most calculations with the loss of neutron pairing. It would appear that something might be missing in the calculations performed so far, perhaps the possibility of changing deformation and shell effects occurring simultaneously with the pairing decrease under rotation.

Another study performed during the past year concerned determining the transient magnets field in cooled ferromagnetic Gd acting on high-velocity (up to 7% c) nuclear recoils produced by inverse reactions (Xe on Mg targets) at the SuperHILAC, and then using these calibrated fields to determine g-factors through the backbend region of a rare earth nucleus. This was a collaborative project with a Chalk River group. Additional work has been done on 1- and 2-neutron transfer reactions on rare earth targets with Xe projectiles, and on giant resonances observed in competition with neutron emission from compound nuclei at rotatively high excitation energy and spin. The latter is a collaborative effort with a Copenhagen group.

Polarization Phenomena in Nuclear Physics

Group Leader
H.E. Conzett

D. Eversheim
C. Rioux
R.M. Larimer

W.J. Knox,
U.C. Davis

P. von Rossen,
U. von Rossen,
University of Bonn, West Germany

This group's research uses the polarized beams from the 88-Inch Cyclotron and is concerned with spin-polarization effects in nuclear scattering and reactions. It particularly addresses such fundamental questions as parity violation by the weak interaction component in pp scattering, time-reversal invariance in reactions, and charge symmetry of the nucleon-nucleon interaction. A most important feature of polarization effects is that they often display uniquely the operation of a basic symmetry property of the nuclear interaction, and we continue to pursue fundamentally important experiments of this nature.

1.) A collaborative experiment is being pursued at TRIUMF to investigate the isospin-mixing, charge-symmetry breaking (CSB) component in the n-p interaction. The experiment will measure the difference ΔA between the neutron and proton analyzing powers A_n and A_p in n-p elastic scattering at 500 MeV. Designed as a null-measurement requiring no accurately known polarization standards, the experiment will determine the difference in angle at which A_n and A_p cross through zero. It will provide unambiguous tests for the existence of CSB effects to the level of $\Delta A = 0.001$, corresponding to a laboratory angle difference at zero crossing of $\simeq 0.05°$. The major equipment development is a polarized-proton target at TRIUMF. Components of the wire-chamber detection system have been fabricated at LBL. The experimental runs and data acquisitions are scheduled to start during the latter part of this year.

2.) In collaboration with a group from Laval University, we have made tests of the principle of time-reversal invariance in nuclear reactions. This principle results in the polarization-analyzing power equality, i.e., the polarization in a reaction A(a,b)B is equal to the analyzing power in the inverse reaction with polarized projectile B(b,a)A. Previous tests of time-reversal invariance in nuclear reactions have been limited to tests in elastic proton scattering, and we have shown that those results were inadequate, due to lack of accuracy in some experiments and lack of sensitivity to time-reversal violations in others. In addition to pursuing the experimental tests, we are preparing a report that describes both the inadequacies of most of the previous experiments and the conditions which must be satisfied in order that a valid test of time-reversal invariance be made.

Spin-polarization measurements also provide information concerning nuclear structure and reaction mechanisms that is not otherwise available. Thus, studies are made of analyzing powers and polarization transfer in inelastic nucleon scattering and nucleon-transfer reactions in order to deduce the specific spin-dependent nature of the nuclear interactions. For example, the inelastic nucleon scattering results provide detailed information about the spin-dependent components of the effective nucleon-nucleon force in nuclei, which is a subject of considerable current interest. Measurements also are made of polarization-transfer in elastic proton-nucleon scattering, since these results will provide a unique means of establishing the existence of a spin-spin component of this nuclear interaction. Specifically:

a) In collaboration with research groups from the Universities of Birmingham and Manitoba, we are continuing studies of polarization analyzing powers in both (p,d) and (d,^{3}He) reactions and their inverses, (d,p) and (^{3}He,d). From these data, the specific spin-orbit interactions for the separate p,d, and ^{3}He particles are determined.

b) In collaboration with a group from Lawrence Livermore National Laboratory, we have begun studies of polarization effects in elastic and inelastic proton scattering from light nuclei. Microscopic model calculations, employing effective nucleon-nucleon interactions, are being made for comparison with these results. From these studies, detailed information about the various components (central, spin-orbit, tensor) of the effective nucleon-nucleon force can be obtained.

In future work this group plans to continue to focus on experiments with polarized particles which examine the operation of the basic symmetries – time-reversal invariance, parity conservation, and charge symmetry – in nuclear scattering and reactions. Also, the study of selected polarization observables to answer specific questions concerning nuclear structure and reactions will be pursued.

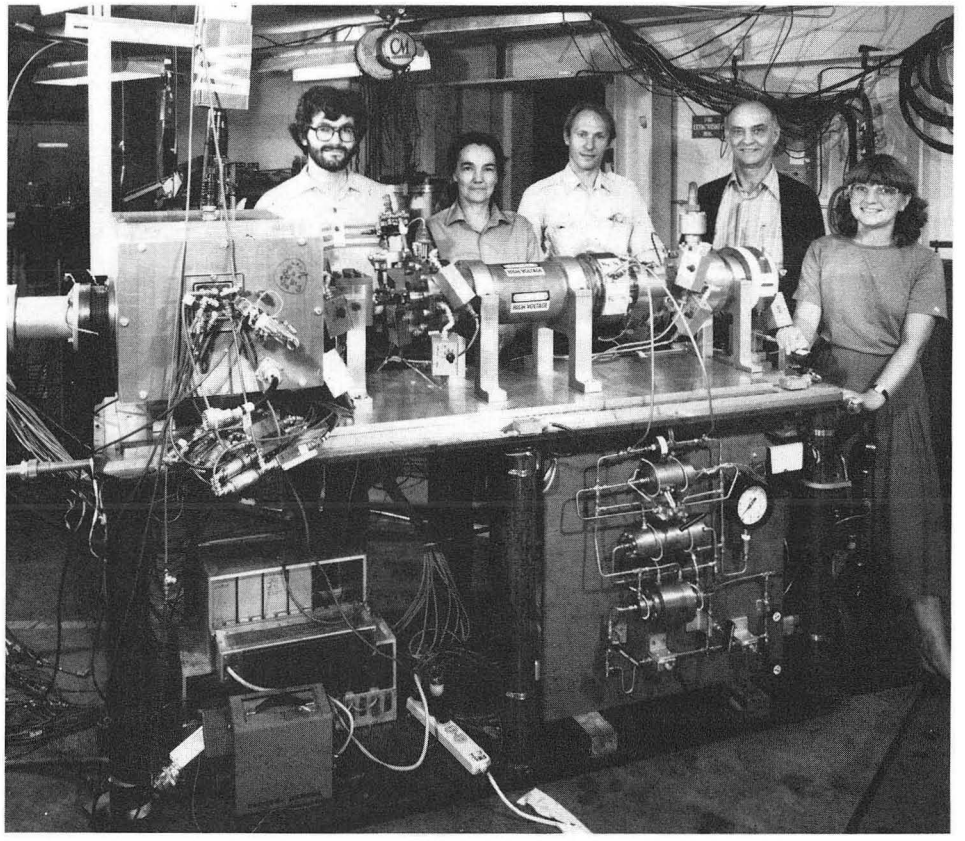

Fig. 1. Group members with experimental equipment for measurements of parity non-conservation in pp scattering near 50 MeV. From left to right, C. Rioux, R.M. Larimer, P. von Rossen, H.E. Conzett, U. von Rossen. CBB 8311-9864

Heavy Ion Reactions

Group Leaders
B.G. Harvey
R.G. Stokstad

*C. Albiston**
*M. Bantel**
Y.D. Chan
S. Wald

H. Homeyer,
Hahn-Meitner
Institut, Berlin

K. Van Bibber,
*P.J. Countryman,**
Stanford University

**Graduate students*

In the energy range from a few MeV/nucleon to 20–30 MeV/nucleon there are rapid changes in the nature of nuclear reactions induced by heavy ions. The complete fusion of projectile and target becomes less probable while the cross sections for emission of small fragments such as α-particles and Li isotopes with velocities close to that of the beam increase. At the upper end of the range, these cross sections are strikingly similar to those measured in the fragmentation of relativistic heavy ions. The group's goal is to gain a detailed understanding of heavy ion reactions in this transition energy range and, if possible, to arrive at a description of them that will tie together the phenomena that are observed from the lowest to the highest beam energies.

The Plastic Box, a major new 4π detector for the study of heavy ion reactions, became fully operational during the period under review. It consists of six $8'' \times 8''$ double plastic paddles arranged as a cube around the target. The use of double walls permits the rejection of signals from neutrons and γ-rays. A slot in a front wall allows one or more E-ΔE telescopes to identify forward-going projectile-like fragments while the plastic walls record the presence (or absence) of additional charged particles. An additional plastic wall behind the telescope detects particles that passed through the slot without hitting a telescope. The plastic walls are able to distinguish between hydrogen and helium isotopes.

Several combinations of projectile and target have been studied: ^{20}Ne + ^{197}Au, ^{16}O + ^{60}Ni, ^{16}O + ^{208}Pb and ^{16}O + ^{12}C. The results for ^{20}Ne + ^{197}Au at 11 and 17 MeV/nucleon have been fully analyzed and complementary inclusive measurements for the same system have been made at six energies between 5.4 and 11 MeV/nucleon. The Plastic Box experiments show that the transfer of at least 14 projectile nucleons can occur in events with no associated charged particles. The most likely number of associated particles is just one. This, combined with the observation that the energy spectra of fragments in coincidence with one charged particle are shifted down in energy by comparison with fragments without an associated particle, is entirely consistent with the production of excited fragments that subsequently decay by α or proton emission.

Particle identification by the walls of the Plastic Box is limited mainly by the large solid angle subtended by each wall and the concomitant large range of angles of incidence. If X-Y position measurements could be obtained within each wall, the particle identification would be vastly improved. To achieve this goal, studies have been made of a prototype wall consisting of a sandwich of two different scintillators (Phoswich) viewed by a photomultiplier on each of its four edges. A position resolution of about 1 cm has been demonstrated. At least the forward walls of the Plastic Box will now be replaced with Phoswich walls.

The process of incomplete projectile fusion must lead to target-like recoils whose velocities are lower than those coming from complete fusion. The emission of fast forward-going nucleons arising from Fermi jets or pre-equilibrium phenomena could also contribute to the reduction of recoil velocity that has been observed in many systems for projectile energies more than just a few MeV/nucleon above the Coulomb barrier. The time-of-flight spectrometer at the 88-Inch Cyclotron has been used to measure the recoil velocities of fusion-like residues. Our previous studies with an oxygen beam and a variety of heavier targets were extended to include different projectiles, e.g., ^{14}N, ^{19}F and ^{20}Ne. The same gross systematic behavior – that the recoil velocity reduction depends mainly on the relative velocity of the colliding nuclei – was found to hold as well for these different projectiles.

All models predict that the velocity reduction must vanish when projectile and target are identical, but they make differing predictions about just how this limit is approached. Therefore, measurements of more symmetric systems, ^{20}Ne and ^{22}Ne projectiles with targets of ^{24}Mg and ^{26}Mg, were begun and are in progress.

The Wilczynski sum rule model of complete and incomplete fusion has been extensively used for the interpretation of experimental fragment cross sections and the recoil velocity reduction. Its predictions are not in agreement with fragment cross sections measured with the Plastic Box and with the Berlin neutron ball detector, nor with recoil velocity results.

A new model (the overlap model) has been developed. Its prime assumption – borrowed from the Fireball model for relativistic heavy ion collisions – is that the formation of an ejectile takes place only when the nucleons removed from the projectile overlap in space with the target nucleus. Thus the formation of a small ejectile requires a larger overlap than that for an ejectile close in mass to the projectile. Good agreement is obtained with experimental yields of fragments from ^{4}He to $^{18,19}F$ in the system $^{20}Ne + ^{197}Au$ from near the Coulomb barrier to 20 MeV/nucleon. The model is also in excellent agreement with the recoil velocity of fissioning nuclei produced in $^{20}Ne + ^{197}Au$ at 290 MeV, and with the angular momentum measurements in coincidence with different fragments in the reaction $^{20}Ne + ^{181}Ta$ at 200 MeV. The success of the overlap model represents an important step toward a unified description of fragment yields and other phenomena from the lowest to the highest energies.

During the period under review the group benefited from the contributions of several visiting scientists. H. Homeyer (HMI, Berlin) spent seven months with us. M. Bantel, having received a diploma from the University of Munich, spent a year with us, supported partly by a German fellowship. He is now studying at the University of Heidelberg. Again during this year we enjoyed short visits from colleagues in Cracow – A. Budzanowski in the Fall of 1982 and K. Grotowski and R. Planeta in the Spring of 1983.

Deep Inelastic Heavy Ion Reactions and Compound Nucleus Studies

Group Leader
L.G. Moretto

G. Guarino
J.B. Hunter
M.A. McMahan
*M. Padgett**
L. G. Sobotka
G.J. Wozniak

J. Gu,
Z. Yao,
Shanghai,
Peoples Republic
of China

Z.H. Liu,
Institute of Atomic
Energy, Beijing,
Peoples Republic
of China

C. Signarbieux,
CEN, Saclay

**Graduate student*

Our theoretical and experimental work is directed along two different lines. On the one hand we study deep-inelastic reactions with special attention to the role of angular momentum; on the other we have started working on the compound nucleus emissions of complex particles.

The elucidation of the role of rotational degrees of freedom in the intermediate dinuclear complex has been guided by a statistical model that predicts the distributions and correlations of the spin components in the two fragments. On the experimental side, we have explored the angular momentum transfer and alignment as a function of Q-value and mass asymmetry with a variety of techniques. We have been successful in establishing the rise and fall of angular momentum alignment as a function of Q-value by means of continuum γ-ray angular distributions. We have established the rigid rotation limit by measuring the α-particle angular distributions from one of the two fragments as a function of mass asymmetry. We have successfully tested the asymmetric angular momentum misalignment predicted by the model at large mass asymmetries by measuring in-plane sequential fission angular distributions.

Some recent theoretical work carried out in our group has indicated that the angular momentum transfer should be strongly affected by the magicity of the target and/or projectile. In a search for such effects, we have measured the magnitude and alignment of the spin transferred to the fragments in the deep-inelastic reactions of 7.4 MeV/nucleon ^{208}Pb on ^{208}Pb, ^{197}Au and ^{165}Ho using continuum γ-ray multiplicity and anisotropy techniques. In contrast to the rise and fall of the γ-ray anisotropy with increasing Q-value observed for the Ho + Ho system, the γ-ray anisotropy is smaller and essentially independent of Q-value for these Pb-induced reactions.

The in- and out-of-plane angular distributions for fission fragments in coincidence with projectile-like products from the reaction of 238 MeV ^{32}S with ^{197}Au and ^{238}U have been measured. An in-plane anisotropy of the fission fragments is observed similar to that seen in the Ne + Au and Ne + U systems. In contrast to the Ne data, which were consistent with statistical model calculations, the S sequential fission data show larger in-plane anisotropies than the model calculations and the opposite trend with mass asymmetry. At present this disagreement is not understood.

Two striking, apparently unrelated, open problems in our understanding of deep-inelastic processes are the lack of drift in mass asymmetry on one hand and the unexpected thermal partition of the energy between fragments even at small Q-values on the other. The former effect can be observed in the reluctance of the Kr-like fragment in reactions such as Kr + Er or Kr + Au to drift toward symmetry, as suggested by the potential energy surface, except at the largest energy losses. The latter effect is the surprising interfragment thermal equilibration, which is observed even at small Q-values and short interaction times. While these two features seem to be unrelated at first glance, we have shown that they can be explained in terms of a dynamical driving force toward larger mass asymmetries because of the attempt of the smaller fragment to contain its temperature gradient (with respect to the heavy fragment) at the expense of its particle number. We have shown that such a feedback could be operative in actual nuclei when the barrier height between the two nuclei as seen by the nucleons being exchanged is close to the Fermi surface.

The production of three or more major fragments is expected to be a dominant mechanism in the region of 10 to 50 MeV/nucleon and higher. In the wake of the success of the statistical theory for angular momentum in binary (deep-inelastic) processes, a statistical theory for the distribution of angular momentum between the fragments has been developed for the case of multifragmentation (three or more fragments). From the generalized partition function, the average energy and angular momentum of each fragment have been derived as well as the corresponding variances.

We have undertaken a major effort to characterize experimentally the compound nucleus emission of large particles. At the 88-Inch Cyclotron we have measured the kinetic energy distributions, angular distributions, charge distributions and excitation functions of the particles emitted in the reaction Ag + ^{3}He with atomic numbers as high as 10. Simultaneously at the SuperHILAC we have studied a variety of compound nucleus reactions with the inverse kinematics technique, such as Be and C targets + Ge, Nb and La projectiles. With this technique we have been successful in measuring the complete charge distribution from protons to symmetric splitting. The charge distributions of the fragments have shown the transition from a minimum at symmetry below the Businaro-Gallone point to a maximum at symmetry above the Businaro-Gallone point.

An extensive study of the alpha particles emitted in coincidence with deep-inelastic fragments for the reaction 484 MeV Fe + Ag has been made. The plots of the invariant cross section in the v_x, v_y plane for various exit channel atomic numbers show that the two fragments are the major sources of the alpha particles. However, when one nears symmetric splitting a central component, possibly arising from evaporation preceding fission, is observed.

We have constructed a large solid angle, segmented anode, position-sensitive ion chamber of the double gridded design. The detector is designed to function both inside a large scattering chamber and outside a small scattering chamber.

Nucleus-Nucleus Collisions

Group Leader
P.B. Price

*S. Barwick**
*T. Coan**
*J. Drach**
*T. Liss**
*J. Musser**
M. Salamon
M. Solarz
J. Stevenson
G. Tarlé
*M. Tincknell**

L. Garwin,
University of
Cambridge, England

Shi-lun Guo,
Institute of
Atomic Energy,
Beijing, People's
Republic of China

**Graduate students*

All this group's offices and equipment are located in Birge Hall on the UCB campus, which makes it easy to attract new students but restricts to some extent interaction with Nuclear Science Division staff. Current research falls into the following five principal areas:

1. Relativistic heavy ion research (DOE support)
   a. Production of heavy ion fragments, including exotic neutron-rich nuclides near the dripline
   b. Detailed properties of secondary nuclei with anomalously short interaction lengths ("anomalons")
   c. Production of high-energy gamma rays
   d. Search for Lee-Wick matter
   e. High-order effects in electrodynamics of slowing heavy ions
   f. Response of various detectors to heavy ions
   g. Hadron calorimetry for nucleus-nucleus collisions
   h. Search for quark-nucleon complexes;
2. Search for highly ionizing particles in e^+e^- annihilation (PEP-2 experiment, supported by NSF) and in $\bar{p}p$ annihilation (NSF support);
3. Cosmic-ray astrophysics (NASA and NSF support)
   a. Final engineering design and tests of prototype instruments for a 50 m^2 detector for a two-year space exposure beginning 1986
   b. Construction of an experiment to detect anti-iron nuclei in cosmic rays at a level 3×10^{-7} of iron;
4. New detectors (NASA support)

   CR-39 with charge resolution $\sigma_z \simeq 0.05e$; other plastics with $\sigma_z < 0.2e$ in the vicinity of uranium;
5. Search for grand-unification magnetic monopoles (NSF and Calspace support)
   a. Sea-level search with huge, thick plastic scintillator slab
   b. Search with mica detector at sensitivity $\lesssim 10^{-19}$ cm^{-2} sr^{-1} s^{-1}.

Doctors Stevenson and Tarlé play a major role in conceiving new experiments and in training students. There is much overlap among the various projects. Detectors devised to solve one problem frequently make possible the solution of all or part of another problem. A result obtained with plastic detectors may stimulate the construction of an electronic system to do a second-generation experiment. Expertise gained in resolving isotopes in a balloon-borne cosmic-ray experiment may be used at PEP or the next-generation neutron-rich nuclide experiment. In all these projects, both post-graduate and undergraduate students play an active part.

Among the experiments in progress or planned for the next two years at the Bevalac are a high-energy gamma-ray experiment with 100 times higher collecting power; detection of many new nuclides delineating the neutron dripline; hadron calorimetry with large solid angle; search for Lee-Wick matter in U-U collisions; measurement of higher order electrodynamics in dE/dx and Čerenkov radiation by ions up to U; detailed studies of anomalons, including measurement of

lifetimes, with detectors capable of resolving nonintegral charge; and determination of the response of plastic track detectors to relativistic ions up to U (the latter being of crucial importance for the proof that cosmic rays come from freshly synthesized supernova debris).

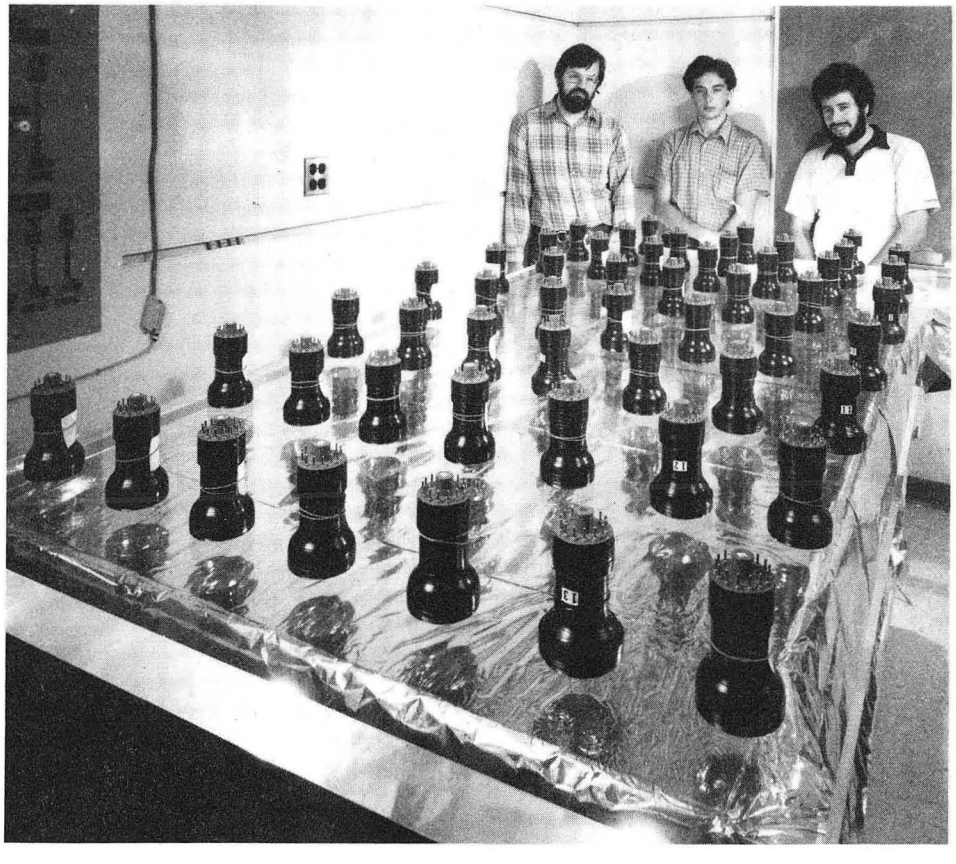

Shown here is the largest slab of plastic scintillator ever cast. It was recently used to search for super-massive magnetic monopoles moving with velocities between $5 \times 10^{-4}c$ and $5 \times 10^{-3}c$. Such monopoles have been predicted to exist by recently-developed Grand Unification Theories of particle physics.

CBB 820-9777

HISS-A Group

Group Leader
D. Greiner

E. Beleal
F. Bieser
M. Bronson
P. Lindstrom
J. Wolf

H. Crawford,
I. Flores,
*L. Greiner,**
C. McParland,
U.C. Space Science Laboratory

M. Baumgartner,
Accelerator and Fusion Research Division, LBL

J. Porter,
Environmental and Technical Services Division, LBL

**undergraduate student*

The first months of FY83 were devoted to setting up for the multi-particle measurements of experiments 513H and 517H.

Experiment 513H is a semi-exclusive measurement of the particle spectra produced by a carbon projectile over the region of rigidities 1–10 GV and angles up to 10 degrees out of the horizontal plane. The object is to determine the excitation spectra of the reaction which allows a test of the various reaction mechanisms. The second goal is to examine the invariant masses of the various particle combinations to determine if there are any short lived states produced.

Experiment 517H is designed to look at the specific reaction $^{16}0 \rightarrow {}^{15}N + {}^{1}H$. The purpose is to determine the amount of the time the reaction proceeds via the giant dipole resonance on heavy targets. Sufficient accuracy will allow the determination of the shape of the dipole excitation spectrum.

Both of these experiments completed data taking in June of 1983.

Measurements of the equilibrium charge state of the uranium beam formed a digression during the first months of FY83. The HISS group was asked to perform the measurements in order to support the TEVALAC proposal. We found that U^{92+} could be best produced by a copper target at 430 MeV/nucleon while a tantalum target is better for a 962 MeV/nucleon beam. A side benefit was the chance to measure the reaction cross sections for uranium on a variety of elemental targets. The results are reported elsewhere in this volume.

Most of the time between June and September was spent mapping the fields used in the experiments which have completed data taking at HISS. There were major tasks in the mechanical, electronic and software areas necessary in order to complete and use the automatic mapping apparatus. The end result was that the five maps necessary for the first three completed experiments were completed.

In August 1983 data analysis became the prime focus of our efforts. At the time of this writing much of the preliminary work has been done. All calibrations for the TOF walls are complete. The preliminary calibration of the drift chambers is allowing trajectory calculation to proceed. The prime limitation now is sufficient computer time to process all the data tapes.

Another digression, dictated by the physics interests of the group, occurred when several months were dedicated to a measurement of the interaction mean free paths of the secondary fragments from argon and iron beams. This work was done in collaboration with the Symons Group using a Čerenkov technique. The goal was to see if the reports of a short mean free path component seen in emulsions could be verified at much a higher statistical level using electronic techniques. The experiment worked quite well, the result being that no short mean free path component was seen down to the 1% level.

A small experiment designed to detect magnetic monopoles using silicon detectors was begun in collaboration with Ray Hagstrom of ANL. The niche this experiment fills is the velocity range where scintillator signals are too low to be seen. Fortunately, those velocities (10^{-3} to 10^{-5} c) are just the region where GUTS monopoles moving under the local gravitational forces should appear. The apparatus will run for several years here in Berkeley and the data will be analyzed at Argonne.

The BEVALAC software effort, led by Chuck McParland, is also a part of HISS group. This year, in spite of the low level of support, much was accomplished. The order for the second VAX at the BEVALAC was placed and the site

is almost prepared. The most outstanding result was the breakthrough that allowed data rates to increase a factor of 4-5 for the typical large experiment. This was accomplished by developing a memory module which resides in CAMAC and stores the data during a beam spill, breaking the bottleneck of data transfer to the data taking computer during the pulse. Chuck McParland and Peter Lindstrom deserve a word of thanks from all the experimenters for this result.

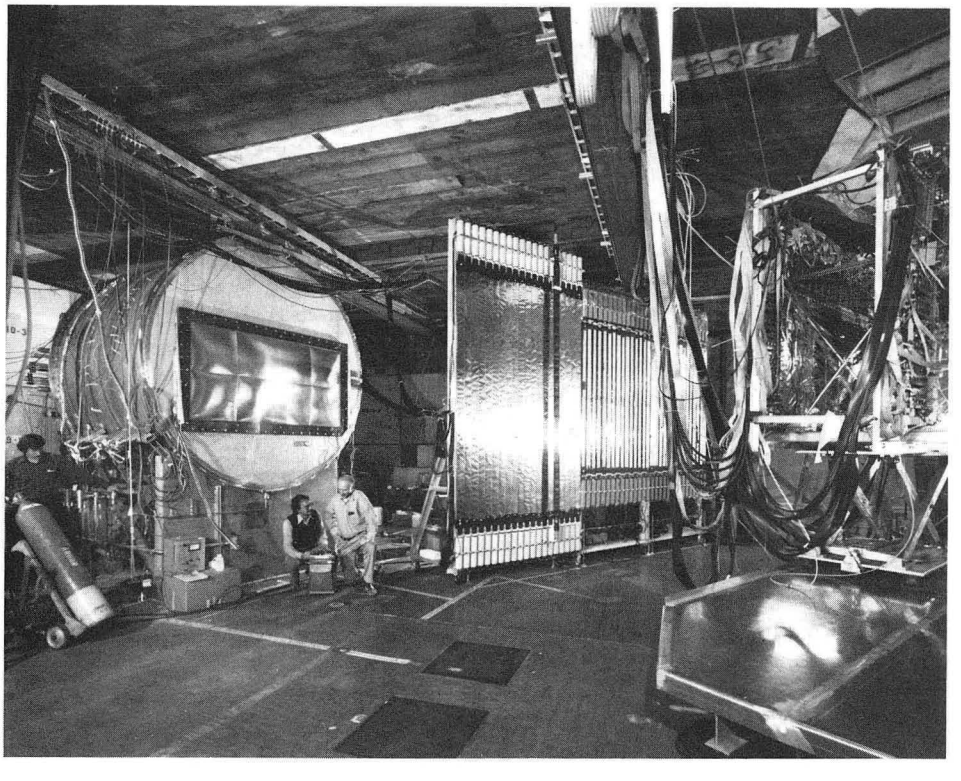

HISS cave with TOF walls and MUSIC detector. CBB 828-7538

Light Particle Emission in High Energy Nuclear Collisions

Group Leaders
O. Chamberlain
H. Steiner
O. Hashimoto

H. Hamagaki,
T. Kobayashi,
K. Nakayama,
Y. Shida,
I. Tanihata,
N. Yoshikawa,
INS, Univ. of Tokyo, Japan

S. Nagamiya,
Y. Miake,
University of Tokyo, Japan

K. Kimura,
Kyushu University, Japan

X. Bai,
Institute of Atomic Energy, Beijing, China

O. Yamakawa,
Nagoya University, Japan

Our group's research program emphasizes the study of the reaction mechanisms involved in high-energy nuclear collisions. This experimental program includes both inclusive and particle correlation studies. Most of the measurements involve the detection and identification of light particles, e.g., $\pi^{\pm}$, K^{+}, p, d, α, etc., over a wide kinematic range. The group utilizes two spectrometers for these studies. One is a compact magnetic spectrometer which was built and has been used for various experiments by the group. The other is the Heavy Ion Spectrometer System (HISS) which utilizes a large superconducting magnet (2 m diameter and 1 m gap). The HISS detection system consists of time-of-flight scintillators covering an area of 2 m $\times$ 2 m and 2.5 m $\times$ 4 m and two 1 $\times$ 2 m 6-plane drift chambers. In the past year most of the effort was directed toward two experiments using HISS (E512H and E593H). These experiments, together with E472H and E618H, were carried out under the INS (University of Tokyo)-LBL collaboration program.

The data of E472H have been intensively analyzed. In this experiment, two-particle correlations, e.g., p-p, p-d, . . ., were measured in the reactions of protons and Ne on various targets at 400 MeV/nucleon and 800 MeV/nucleon. The incident proton data suggest that the production of backward protons is predominantly due to scattering from a two-nucleon cluster in the target. Quasi-elastic pd scatterings were also studied and interpreted in terms of two-nucleon momentum distributions. Analysis of nucleus-nucleus data seems to suggest the presence of hydrodynamical flow in heavy ion reactions.

In experiment 618H, inclusive spectra of light particles and pions were measured in 800 MeV/nucleon La + La collisions. This experiment was an extension of previous measurements with lighter projectiles such as C, Ne and Ar. E618H was one of the first counter experiments with ultra-heavy projectiles accelerated by the up-graded Bevalac. Light particles, i.e, p, d, t, ^{3}He, ^{4}He, and negative pions were detected. The general characteristics of the observed spectra were found to be very similar to those produced in collisions involving lighter-mass systems, but for La + La the system looks more equilibrated. However, for La + La the 90° center of mass (CM) slope parameter for pions seems somewhat steeper than that for Ar + KCl. This is contrary to a general trend observed previously with lighter nuclei and further studies are needed.

In experiment 512H, we have collected both inclusive and correlation data for particles emitted at 90° CM with very high transverse momentum in 800 MeV/nucleon ^{12}C + ^{12}C reaction. The high magnetic field of HISS coupled with its large volume effectively swept out the low momentum particles which otherwise would have constituted an unmanageable background. Five 3-plane wire chambers, a 0.9 m $\times$ 1.6 m time of flight wall as well as several other scintillators were installed in HISS to provide a two arm spectrometer for detection of particles emitted at 90° CM. The spectra for p, d and t have been measured for P_T up to 1.8 GeV/c(proton), 2.5 GeV/c(deuteron) and 2.8 GeV/c(triton). The inclusive proton cross sections decrease monotonically with increasing P_T by 8 orders of magnitude. A significant inward deviation from an exponential slope was observed at a high P_T region. It is very likely that this effect can be attributed at least in part to phase space constraints, but further comparison with theory is needed. In addition it was found that the deuteron (and triton) spectra at 90° CM are remarkably well reproduced by the squares (and cubes) of the observed proton spectrum.

The first part of E593H was carried out at the end of FY83, also at HISS. The aim of this experiment is to study time evolution of high-energy heavy-ion collisions by utilizing the Coulomb interaction. The experiment was designed to measure correlations of both positive and negative pions emitted at 0° with respect to projectile fragments. We expect that the effect of the Coulomb field on low energy pion spectra will be greatly enhanced with ultra heavy beams. A two-arm spectrometer system to detect both positive and negative pions was constructed and added to the HISS facility. The first run was successful and further data taking is under way using Ar and La beams at 800 MeV/nucleon.

A part of the group in front of the HISS magnet CBB 8312-10964

High Energy Nuclear Collisions

LBL
Group Leader
A.M. Poskanzer

M. Doss
H.-A. Gustafsson
T. Renner
H. Riedesel

GSI
Group Leaders
H.H. Gutbrod
H.-G. Ritter

B. Kolb
H. Löhner
B. Ludewigt
A. Warwick
H. Wieman

This group is a continuing collaboration between GSI (Gesellschaft für Schwerionenforschung, Darmstadt, West Germany) and LBL. The work of the group centers on the use of the Plastic Ball to study central collisions of relativistic nuclei with the aim of learning about nuclear matter at high temperature and density.

The Plastic Ball covers 96% of 4π with 815 modules, each consisting of a CaF_2 ΔE detector and a plastic scintillator E detector. The two scintillators are observed by the same photomultiplier tube and the signals are separated electronically by taking advantage of their different decay characteristics. In addition, positive pions are identified by their $\pi^+ \rightarrow \mu^+ \rightarrow e^+$ decay. The small forward angle region is covered by the Plastic Wall placed 6m downstream. The Wall consists of 177 plastic scintillators and identifies particles by their time of flight and energy loss. Data have been taken for ^{40}Ca on a Ca target at two energies and for ^{93}Nb on a Nb target at six energies.

The large number of detectors in the Plastic Ball and Wall very effectively measures the multiplicity of charged particles in each event, and thus gives an indication of the impact parameter of the collision. It has been found that the event momentum shapes become more isotropic in the center of mass as the multiplicity increases. At the highest multiplicities the Ca + Ca events are still somewhat prolate along the beam axis, but the larger Nb + Nb events appear spherical, indicating stopping and possible thermalization. Apparent temperatures have been extracted for these events. Further global analysis indicates collective flow effects for the Nb system which are not present in the lighter Ca system or in cascade calculations.

The deuteron-yield/proton-yield has been found to be a strong function of multiplicity. This is significant because it is hoped that the ratio of composite particles relative to nucleons will be an indicator of the entropy produced in the nuclear collision.

Because the Ball has 815 detectors it very efficiently measures two-particle correlations. From the proton-proton correlation, the size of the emitting source has been obtained as a function of multiplicity. Correlations between the composite particles indicate interesting nuclear structure effects caused by unbound states. A search for clusters of particles in momentum space by a minimum-spanning tree analysis has fairly successfully been able to separate out those particles originating from the target and projectile spectators from other particles which are mainly the participants.

In addition a separate experiment was performed to search for short-lived anomalons. The yield in the Plastic Wall was compared for a solid and a dilute target. It was concluded that if anomalons exist their disappearance in the first few centimeters of emulsion is not due to decay.

The Plastic Ball Group standing in front of the Bevalac high bay experimental area. Left center is the Plastic Ball house. Left to right first row: Hans-Georg Ritter, Mohan Doss, Howard Wieman, Burkhard Kolb. Second row: Tim Renner, Tony Warwick, Karl-Heinz Kampert. Third row: Herbert Löhner, Hans-Ake Gustafsson, Bernhard Ludewigt, Hans Gutbrod, Art Poskanzer.

CBB 8311-10362

Heavy Ion Studies/Pion Studies

Group Leaders
K.M. Crowe
J.O. Rasmussen

J.A. Bistirlich
*R.R. Bossingham**
H.R. Bowman
*A.D. Chacon**
D. Fitzgerald†
S. Folkman†
K.A. Frankel
T.J. Humanic
*J.M. Kurck**
*C.A. Meyer**
*D.L. Murphy**

R. Anholt,
W. Meyerhof,
Stanford University
Stanford, California

O. Hashimoto,
Institute for Nuclear Studies, University of Tokyo, Tanashi, Tokyo, Japan

J.P. Sullivan,
Texas A&M University, College Station, Texas

J.S. Xu,
Z.Z. Xu,
Fudan Univ., Shanghai

W.A. Zajc,
University of Pennsylvania, Philadelphia, PA

**Graduate students*
†Undergraduate students

The Berkeley research activities of our group center mainly on the study of charged pions or correlated pairs of particles produced in high-energy heavy-ion collisions at the Bevalac. The technical approach involves a large (~4 meter flight path) dipole-dipole magnetic spectrometer (JANUS) and combinations of fast scintillators and wire chambers interfaced with a CAMAC-PDP 11/45 data acquisition system.

One major part of the work is the determination of the cross sections (with an exploration of the angular dependence) for pion production in heavy-ion reactions. The existence of both positively and negatively charged pions facilitates determinations of simple Coulomb effects and therefore the charge density evolution in heavy-ion collisions by observation of the π^-/π^+ ratio as a function of pion energy, bombarding energy, and target-projectile charges. In fact, we found that pions produced with low energy in the projectile frame have large π^-/π^+ ratios due to the Coulomb fields of the projectile fragments. Systematic observations of the sharp anomaly were made to compare with various models for production. The effects due to esoteric mechanisms, i.e., condensates, etc., are expected to modify the conventional modes, and these phenomena are being explored.

We are also studying the production cross section for low-energy π^- and π^+ at 90° in the center of mass, where an enhancement in the π^+ production has been observed. We want to ascertain that this 90° peak does disappear at low energy and to attempt to measure the threshold for its appearance. In addition, we are studying production of charged pions below the single nucleon-nucleon threshold to probe the importance of Fermi momentum in the nucleus. By measuring the center-of-mass angular distribution, we want to distinguish between thermal and single particle production modes. We have undertaken thick target studies in order to evaluate the practicality of heavy-ion production of useful π^- beams.

Another major part of our research effort involves pion interferometry studies. In the past ten years theorists have predicted that exotic phenomena such as pion condensation and quark-gluon plasmas occur in relativistic heavy-ion collisions. One way to obtain information about these phenomena is to measure the radius, lifetime and coherence of the pion-emitting source produced in the collision. The Hanbury-Brown,Twiss effect, which has been used extensively in astronomy to measure the radii of stars, provides a direct method to measure these pion source parameters. In practice, we measure the momenta ($\vec{p}_1$ and $\vec{p}_2$) of coincident like-charged pions in our spectrometer and, using the two pion yields thus obtained, form the correlation function C ($\vec{p}_1,\vec{p}_2$). This experimental correlation function is then fitted to a model, which assumes a Gaussian space-time distribution for the sources, and the source parameters are extracted. Thus far we have used this technique to measure source parameters for the systems 1.8 GeV/nucleon ^{40}Ar on KCl and 1.7 GeV/nucleon ^{56}Fe on Fe.

In a collaborative effort with the Tokyo group (INS), we are studying pion production through coherent isobar formation in relativistic heavy-ion collisions. A theory exists which predicts significant pion production through the mechanism of simultaneous production of a coherent Δ resonance in the target with the excitation of an isobar resonance in the projectile for peripheral collisions. We are presently studying pion production from the system 2.1 GeV/nucleon ^{12}C on C within the context of this theory.

Future work that our group intends to pursue will utilize the experimental techniques and apparatus that we have built. The availability of Bevalac beams of the heavier elements (Au, Pb, or U) and our upgraded experimental apparatus (addition of a kicker magnet) will call for new pion spectroscopic measurements to search for evidence of highly compressed nuclear matter effects. The π^-/π^+ ratios will again be exploited for heavier beams to measure the dynamic charge evolution in relativistic heavy-ion collisions, and the pion interferometry method will be applied to these heavier elements.

Now that heavy elements can be accelerated at the Bevalac, there are new opportunities in atomic physics. Our earliest Bevalac work involved measuring K x-ray production cross sections. With Stanford collaborators we have measured extensively the x-ray spectra from 190 MeV/nucleon Xe ions and 375 MeV/nucleon U ions. We observed not only target and projectile x-rays but also the radiative electron capture peak.

Various members of the group are involved in collaborative work centered at other laboratories: muon fusion experiments at SIN; muon and pion experiments at TRIUMF; theoretical nuclear studies by the Classical Limit S-Matrix Method with collaborators at the Universities of Tennessee, Brazil, and Kuwait; and hybrid plastic and emulsion studies of relativistic heavy ions with collaborators in Nagoya and Cairo.

High Energy Nucleus-Nucleus Collisions

Group Leaders
LBL
H.G. Pugh
L.S. Schroeder

GSI
A. Sandoval
R. Stock

This group has two complementary research components in relativistic heavy ion physics at the Bevalac. One uses electronic detection techniques and operates the TASS two-arm spectrometer system in collaboration with the P. Kirk group from Louisiana State University. This is suitable for a wide range of charged particle inclusive measurements and for precise two-particle coincidence experiments where a large solid angle is not required. The other operates the STREAMER CHAMBER as a Gesellschaft für Schwerionenforschung (GSI)-LBL collaboration to study 4π charged particle exclusive data with this low-data-rate visual-data-storage device. The groups of K. Wolf at Texas A&M University and A. Dacal at the University of Mexico have also made major commitments to the Streamer Chamber research program.

TASS

LBL
G. Claesson
H.S. Matis
J. Miller
G. Roche

GSI
J.W. Harris

P.N. Kirk,
G. Krebs,
J.-F. Gilot,
Louisiana State University

J. Vicente,
University of Clermont-Ferrand

The Two-Arm Spectrometer System (TASS) consists of two fully rotatable magnets with accompanying wire chambers and scintillation hodoscopes for particle identification. It was first operated in July 1980 and the first phase of instrumentation and experiments was completed in mid-1983. The present activities on TASS are:

599H This experiment looks at the possible differences of π^- and π^+ inclusive yields primarily in the central region of rapidity but extending also into the projectile fragmentation domain. The chosen system is ^{40}Ca + ^{40}Ca at 1.05 GeV/nucleon, which apart from Coulomb effects, should yield a π^-/π^+ ratio of unity. A ratio different from unity has previously been reported for the ^{40}Ar + KCl system at the same energy. For the experiment, a multiplicity detector system was added to TASS at zero degrees to provide a "streamer-chamber-type" tagging of central and peripheral interactions. For ion identification at low momenta it was found essential to add helium bags around the target and to add a Čerenkov detector to veto electrons and positrons. Data acquisition has been completed, and final analysis is in progress. Early results from this study are reported elsewhere in this report.

630H This experiment was to search for anomalous nuclear fragments in the target fragmentation region. The "anomalon" phenomenon has so far been seen only in the projectile fragmentation region but should also occur in the target fragmentation region if target and projectile are interchanged. The difficulty in the target fragmentation region is that the only signature so far observed – shortened mean free path – is more or less unusable because of the rapid variations of mean free path with energy in this regime. In experiment 630H, various targets were bombarded with 2.1 GeV/nucleon carbon ions and a search was made for unusual structure in the energy spectra of protons, deuterons, and photons. A thin-walled scatter chamber previously used by the Poskanzer-Gutbrod group was equipped with several ΔE-E charged-particle telescopes provided by the University of Maryland. Two large photon detectors, a large NaI crystal, and a Pb-glass array were provided and operated by the Johns Hopkins and UCLA groups (486H). The photon spectra up to 400 MeV have been studied to look for sharp peaks that might occur from the decay of an excited anomalon at rest in the target frame; none was observed. The charged-particle spectra are smooth and roughly consistent with those previously measured. A final study of the particle-photon correlation data

has been made to see if some peak might occur in the effective mass reconstruction that was not visible in the inclusive data. No unusual structure has been observed in the γp or γd mass distributions (see Roche *et al.*, this report). Upper limits are being obtained for the production of anomalons, subject to the constraint that they would have to decay in the relatively simple fashion that we could have observed.

628H This experiment (in association with Michigan State University) involved a search for pionic condensation effects in the 90° c.m. inclusive spectrum from La + La collisions at 246 MeV/nucleon. The pion spectrum is observed to fall exponentially, with no hint of a "bump" due to production of the condensate phase in the collisions (see G. Krebs *et al.*, this report). In addition, proton spectrum at 90° c.m. where measured to study the "nuclear temperatures" achieved relatively low Bevalac energies with heavy nuclei analysis is continuing. Pion and proton measurements at more forward angles will be carried out in late 1984.

631H A hydrogen target has been completed and should be installed on TASS in late 1984 or early 1985 to study Δ production in p-p and p-A collisions by detecting the decay proton and pion in coincidence.

670H Following a series of workshops a collaboration has been formed, involving LBL, Johns Hopkins University, Louisiana State University, Northwestern University, UCLA, and the University of Clermont-Ferrand to make a major study of lepton and dilepton production in heavy ion collisions. These particles are believed to be the most reliable probes of the hot conditions produced in the high density phase of the reaction. The problem in their study is the low yield. TASS is suitable, with the addition of Čerenkov detectors, for measurement of single leptons, and 300 hours of beam time for such a study have been approved. Installation of equipment was completed in late 1983 and the first data taken. These runs will continue throughout 1984. For the more definitive dilepton measurement a very large acceptance device is required. Tentatively, use is planned for the Lampshade Magnet, which is a large acceptance toroidal magnetic field device constructed by CERN. Permission has been received from CERN to borrow this. A detailed plan is being developed for total instrumentation of this new facility called the Dilepton Spectrometer (DLS). The first experiments using it are planned for 1986.

ISR Experiment R 418

Two of us (LSS and HGP) are involved with T.J.M. Symons and C.R. Gruhn, in a large collaboration studying α-α collisions at the CERN ISR. This experiment, one of the last to be carried out on the ISR before its final shutdown, was completed in August 1983, and the data are being analyzed.

LBL
J.B. Brannigan
P. Eitner
W. Hou
I.W. Muskovich
G. Odyniec
H.G. Pugh
P. Renteln
L.M. Tinay

GSI
R. Brockmann
J.W. Harris
M. Maier
S. Reinsch
A. Sandoval
R. Stock
H. Stroebele

D. Bangert,
W. Rauch,
University of
Marburg,
West Germany

A. Dacal,
M. Ortiz,
Instituto
de Fisica,
UNAM,
Mexico D.F.,
Mexico

R.E. Renfordt,
D. Schall,
University of
Heidelberg,
W. Germany

K.L. Wolf,
Texas A&M
University

Streamer Chamber

The Streamer Chamber allows the study of charged particle as well as K^0 and Λ production over most of the 4π solid angle in high energy heavy ion collisions. Detailed 4π exclusive data is necessary to study the behavior of nuclear matter under conditions of extreme temperature and density. Up to now projectiles from protons to ^{40}Ca have been used extensively in Streamer Chamber experiments. With completion of the Bevalac upgrade much heavier beams (up to U) are now available and in the near future the Streamer Chamber research will concentrate on these heavier beams.

Our group has upgraded the LBL Streamer Chamber to be able to use metallic targets and has reduced the loading effect of the Chamber voltage due to high energy delta rays from heavy projectiles. Instrumentation has been implemented to monitor the chamber performance with, among other things, an UV laser that produces tracks with a well defined ionization. This has enabled us to optimize the Streamer Chamber parameters to obtain the most stable running conditions. All this is necessary to obtain high quality data for the heavy projectiles.

Furthermore, a forward angle 400 element scintillator hodoscope detector was designed and constructed to complement the Streamer Chamber particle identification capabilities in the region of momenta above 1 GeV/c. The signal processing of this detector is done with a Large Scale Digitizer system with 512 ADC's and 384 TDC's which was used previously in a SLAC experiment and modified to meet our needs. A calibration and monitoring system for the hodoscope using a light fiber coupled N_2 laser was constructed.

Besides the work on instrumentation in preparation for experiments with heavy beams, the analysis of previous experiments has continued.

401H In this experiment the excitation function of Ar-induced reactions on KCl from energies between 0.4 and 1.8 GeV/nucleon and the central collisions of Ar on Pb at 800 MeV/nucleon was measured. From the energy dependence of the negative pion production and use of a cascade model, an equation of state of nuclear matter at high density was extracted. A new theoretical approach to interpret the data independently of the intranuclear cascade model is in progress. This experiment has also been analyzed in terms of the total charged-particle final state. This involves the measuring, reconstruction and identification of all charged particles emitted in the interaction as measured in the Streamer Chamber. Work here has concentrated on the 1.8 GeV/nucleon Ar + KCl and 800 MeV/nucleon Ar + KCl and Ar + Pb reactions. Results from a larger statistical sample for the Ar + Pb system, analyzed in terms of the momentum flow tensor, show that for intermediate impact parameters there is a measurable sideward deflection of the emitted particles, while the more central collisions approach a thermal, isotropic distribution.

564H This experiment is a high statistics run of the ^{40}Ca + Ca reaction at 2.1 GeV/nucleon. The main thrust of this experiment is the study of Λ and K^0 production in central collisions of heavy ions at the top Bevalac energy. The production cross sections, transverse momenta and polarization are of great interest. The neutral strange particles are detected by their charged-particle decay (vee). The film of this experiment has been scanned for vees, which have been measured and reconstructed, and the analysis is in progress.

629H This, our active proposal, focuses on the study of interactions of ^{139}La + ^{139}La over the Bevalac energy range. An integral part of this proposal is the detection and identification of the forward emitted particles using a newly developed 400-element scintillator hodoscope. This detector was designed and constructed during this report period and will see its first beam in the spring of 1984. Two test runs with 1 GeV/nucleon ^{139}La have been taken to further develop the Streamer Chamber capabilities for heavy beams.

SPS experiment.

Within the LBL/GSI collaboration our group, together with the Plastic Ball group, has an accepted proposal to measure the interactions of ^{16}O with nuclear targets at energies between 10 and 40 GeV/nucleon at the CERN SPS. The necessary injector developments are well in progress; GSI has placed the order for the ion source, and LBL is in the process of commissioning an RFQ for the Bevatron Local Injector similar to the one to be built for the CERN experiment. Furthermore, CERN has started the necessary upgrade of their diagnostics instrumentation. The vertex magnet that will be used for the Streamer Chamber is in place and operational in the West Hall. The Streamer Chamber from the Max Planck Institut in Munich to be used in the experiment is being upgraded and a forward angle calorimeter has been offered to us.

Members of the Streamer Chamber group with a life-size picture of an event as seen in the chamber. BBC 830-9674

Relativistic Heavy Ion Collisions

Group Leader
V. Perez-Mendez

P. Fisher
T. Mulera

University of California at Los Angeles
Group Leader
G. Igo

*S. Abachi**
*S. Carlson**
J. Carroll
A. Shor
S. Trentalange

*E. Barasch,**
University of California at Davis

**Graduate students*

In addition to the staff listed here, which comprises a long standing collaboration led by V. Perez-Mendez and G. Igo, other collaborations have been formed. A current collaboration, formed to study the production of single leptons and lepton pairs in relativistic heavy ion collisions (RHIC), consists of the above listed people plus members of other LBL groups and groups led by L. Madansky at the Johns Hopkins University, D. Miller at Northwestern University and P. Kirk at Louisiana State University.

The group carries on a diverse program of research in relativistic heavy ion physics using projectiles supplied by the Bevalac. The unifying theme of this research program is the search for evidence for the possible formation of a new or "anomalous" states of nuclear matter in RHIC.

Anomalous production of particles below threshold (for nucleon-nucleon collisions at equal energy/nucleon) provides evidence for collective effects that may lead to the production of new states of matter. In the past we have reported the observation of a surprisingly high rate of K^- production in 2.1 GeV/nucleon $^{28}Si + {}^{28}Si$ collisions. During the past year we have extended this investigation by measuring the momentum distribution of these subthreshold K^-. This momentum spectrum is approximately exponential in shape with a slope corresponding to a temperature of $\sim$80 MeV. This result indicates that it is unlikely that subthreshold K^- production is due to a ϕ-bremsstrahlung mechanism or is the result of $K\bar{K}$-condensation. Further studies are planned which should shed more light on the nature of the production mechanism. In preparation for some of these studies, a new beam line/spectrometer has been designed and approved for construction. The remainder of the program will be carried out using our existing instrumentation in Beam 40.

Changes in the effective mass spectra of lepton pairs produced in RHIC, as a function of bombarding energy, may provide the clearest signature of the postulated phase transition to the quark-gluon plasma. We are collaborators in an effort to construct a new major facility at the Bevalac, the dilepton spectrometer, which will be used to study the production of e^+e^- pairs in RHIC. As a prelude to this effort, an experiment will be started during the coming year to measure the yield of single direct electrons at the Bevalac.

Development of instrumentation remains a major part of our effort. As well as developing instrumentation for the experiments described above, a good deal of long range development of radiation detectors was carried out.

High Energy Heavy Ion Collisions

Group Leader
T.J.M. Symons

J.-P. Dufour
J. Girard
D. Olson

This group is engaged in a wide variety of experiments using beams accelerated by the Bevalac. In recent years, interests have ranged from nuclear structure physics to reaction mechanism studies at very high energies.

We are currently involved in two major development projects. The first is our segmented Čerenkov detector which we have built to measure the interaction mean free paths of secondary fragments produced in relativistic heavy ion collisions. The development of this device was spurred by the observation first in the cosmic rays and later in experiments at the Bevalac that a fraction of projectile fragments produced in relativistic heavy ion collisions have interaction mean free paths that are very much shorter than normal. "Anomalons," the particles responsible for this effect, are the subject of great current interest. Our detector was first used in August 1983 to investigate the charge-changing cross sections of secondary fragments from ^{40}Ar and ^{56}Fe beams. The detector worked well during this first experiment although we observed no anomalons. We are making several improvements to increase the sensitivity of the detector. These include the development of radiators only 2mm thick that will allow us to measure the interaction rate of the secondary fragments closer to the interaction point than before.

Our second major project is the development of a Čerenkov detector to be used at the HISS facility. This is a novel device, the design of which has been very much influenced by the experience with Čerenkov detectors that we have gained during our anomalon experiment. The detector will be a hodoscope of total internal reflection counters capable of measuring both the charge and the velocity of projectile fragments at least up to mass 100. The most significant aspect of the device is that we have been able to design a detector that is well matched to the energy range of the Bevalac without using exotic materials such as silica aerogels. First tests of the detector will be made this year with full operation commencing next year. It will be used first for experiments investigating the limits of particle stability but should also be useful for other general HISS experiments.

We are also continuing, in collaboration with HISS Group A and B. Berman of LLNL, the study of electromagnetic dissociation of light nuclei using the HISS spectrometer. The first run for this experiment will take place this year. Finally, we are continuing our collaboration with Professor G. Westfall's group at Michigan State University.

Next year we plan to complete and put into use our Čerenkov detector hodoscope at HISS. We believe that this device will greatly improve the flexibility and usefulness of the HISS facility. Second, we are becoming involved as collaborators in an experiment to study strange baryon production (e.g. Λ, $\bar{\Lambda}$) in relativistic heavy ion collisions at the CERN SPS. If approved, this experiment will run in 1986 using the ^{16}O beam that will be available then, at which time it will be necessary to assemble the apparatus at CERN. This experiment is a collaborative effort of several groups led by LBL.

Detector Research and Development

C.R. Gruhn

The function of this group is to explore new concepts in detectors and to develop systems that optimize the accuracy of measurement in the specific uses for which they are designed. Experiments this year have been conducted entirely at CERN.

High-Density Time-Projection Chambers

Two high-density time-projection chambers (HDPC's) for tagging spectator neutrons in colliding alpha beam experiments at the CERN ISR were constructed, installed, and successfully operated during the August run at the Split Field Magnet (SFM) facility of the CERN ISR. Although the main effort has been associated with the HDPC spectator neutron tagging, some initial thoughts have been given to an experiment (concerned with strange baryon production and the associated instrumentation) to be proposed and conducted at the CERN SPS in 1986.

Strange Baryon Antibaryon ($B\bar{B}$) Production at the CERN SPS

An experiment is being designed and proposed which will take advantage of new opportunities for study of high energy nucleus-nucleus collisions made available with the construction by LBL and GSI of an injector for the CERN SPS. Beam energies up to 225 GeV/nucleon will become available.

The tentative design of the experiment is as follows: A split superconducting-solenoid magnet would be placed at 0° in front of the target to serve as a low momenta filter, thus allowing the larger portion of the pions (associated with large multiplicities) to be swept free from the forward cone (0°). The more massive $B(\bar{B})$, having higher momenta, are transmitted through the filter and appear in the forward cone relatively free of the high multiplicity pion background. At one side of the beam in this forward cone we would place a high resolution micro TPC which would provide particle identification for the detection of $p\bar{p}$, $\Lambda\bar{\Lambda}$, $\Sigma^+\bar{\Sigma}^-$, $\Sigma^-\bar{\Sigma}^+$, $\Xi^-\bar{\Xi}^+$, and $\Omega^-\bar{\Omega}^+$. We would thus measure particle production having strangeness, $|S| = 0, 1, 2, 3$. The filter magnet has the added advantage of compressing the length of the apparatus, thus accommodating the short decay lengths of the particles of interest.

A cost savings on the data acquisition system and electronics is being realized by sharing in the prototype efforts for the ALEPH LEP central detector (TPC). We would use their computer and TPC electronics on loan.

The design of this experiment is expected to be completed and a proposal submitted to the CERN SPSC this year. Assuming the proposal is approved, a prototype micro TPC would then be constructed and tested at CERN.

Nuclear Theory

Group Leaders
N.K. Glendenning
M. Gyulassy
W.D.Myers
J. Randrup
W.J. Świątecki

J. Boguta
P. Danielewicz
T. Døssing
T. Matsui
M. Redlich

C.S. Wang,
Beijing, China

K. Möhring,
Berlin
West Germany

P. Möller,
Lund
Sweden

M. Weiss,
Lawrence Livermore
National Laboratory

I. Hadronic and Quark Matter at High Energy Density

The work of the theory group continues to include a broad range of nuclear-, particle-, and astrophysical aspects, addressed by a variety of approaches and techniques. We have found it possible to sustain the momentum in the direction of ultra relativistic nuclear physics and the quark-gluon plasma and to strengthen our effort in the astrophysical domain, while actually broadening our support to ongoing experiments at all of LBL's accelerators.

A major undertaking is the study of matter at very high energy densities. The regime of supernuclear densities is of great interest, impinging as it does on the fields of ultra-relativistic nuclear collisions and astrophysics. At densities below the deconfinement threshold, matter can be discussed in terms of hadrons and their interactions. Fortunately, not all pieces of the most general interaction Lagrangian are relevant, since certain baryon source currents, which possess symmetries that are different from the normal ground state, must vanish. The coupling constants of the nonvanishing terms can be determined empirically from known bulk properties of nuclear matter. Other terms are associated with phase transitions, of which the pion-condensed state has been most thoroughly studied. The development of a pion condensate or hyperon population or both, precludes the possibility of other exotic condensates. The neutral rho-meson which contributes to the isospin symmetry energy, plays an important role in determining the particle composition of neutron stars. The critical neutron star mass is found to be 1.8 solar masses and in such a star 15–20% of the baryons are hyperons. Considerable effort has been directed toward the study of the very high energy density domain that is expected to be formed in ultrarelativistic nuclear collisions. Particular interest has focused on the transition from nuclear to quark matter and the experimental signatures that are expected to be associated with this transition. Estimates have been made of the maximum energy and baryon densities that can be achieved for collisions involving massive nuclei with energies up to 1 TeV/nucleon. A well-developed quark-gluon plasma is predicted for such collisions. The formation of such a plasma is estimated to begin at much lower energies, even before the maximum baryon density is achieved at about 10 GeV/nucleon. A quark-gluon plasma (once formed) may disassemble by hydrodynamic expansion or by evaporation or both. The chromoelectric flux tube model provides a phenomenological description of the confinement of color, and it is shown how it provides a mechanism for the formation and radiation of mesons from the plasma surface. This evaporation process together with the external bag pressure due to the non-perturbative vacuum outside the plasma, impose boundary conditions on the hydro-expansion. For cylindrical geometry with Bjorken longitudinal expansion the resulting disassembly has the following characteristics. The plasma shrinks in the radial direction accompanied by the radiation of mesons from this space-like surface. The interior of the plasma meanwhile retains an almost spatially uniform temperature, which falls due to the longitudinal expansion. A global phase transition resulting from the homogeneity of the plasma defines a time-like surface on which energy-momentum conservation and the second law of thermodynamics require a transition from a supercooled plasma to a superheated hadron gas. This subsequently undergoes a rapid expansion to freezeout. The hadronic and di-lepton spectra characterizing this unusual disassembly are being calculated.

II. Relativistic Nuclear Collisions

A wide range of phenomena are under investigation in connection with nuclear collisions at relativistic energies. These include the nature of the explosive disassembly process, the mechanisms underlying observed particle production rates, and the continuing search for signatures of collective behavior. Encouraging agreement has been obtained between measured fragment yields and a simple two-stage statistical model. This model idealizes the process as a fast explosion into excited residues followed by a slower evaporation stage. This work has been extended to provide a complete description of multi-fragment events at medium energies. In the initial stage of the event the complete microcanonical many-fragment distribution is generated by a method of statistical simulation. These events are then subjected to the same sort of analysis employed in the actual experiments. The model is currently being used by various experimental groups in their attempts at understanding observational biases and assessing the significance of measurements that seem to imply collective effects. A quantum description of the nuclear collision process is being developed using Green's function perturbation techniques for studying the time evolution. Numerical calculations of collisions in an interpenetrating nuclear matter model have been performed, and the quantum dynamics results have been compared with classical dynamics from the Boltzmann equation, emphasizing the role of the uncertainty principle. Using the perturbation expansion developed in this work the space-time structure of particle production in the high-energy collisions has been studied. This is of importance for the energy-density formation in the nuclear collisions at beam energies of $\sim$10 GeV/nucleon and the possible occurrence of the quark-plasma phase transition. Intranuclear cascade calculations have been performed that provide quantitative, parameter-free predictions of charged particle inclusive (and deuteron) yields that are in good agreement with experiment at bombarding energies greater than 50 MeV/nucleon. Discrepancies found below 50 MeV/nucleon seem to indicate the importance of the mean field effects that are neglected in these calculations. In this connection, a rigorous derivation of the coalescence model has been obtained using the density matrix formalism. Finite multiplicity distortions in the flow analysis of heavy-ion collisions are also being investigated. The research revealed a phase-space Jacobian in the distributions of the flow variables, whose removal allows for a more model-independent analysis of the experimental results. Pion yields and energy spectra have been estimated for production associated with collision-induced collective spin-isospin instabilities. The consequences of this mechanism for pion pair-correlation measurements have been determined. One of our major interests continues to be the search for experimental signatures for the observation of pion-field instabilities. Thus far, there is no evidence experimentally for coherence phenomena.

III. Low Energy Nuclear Dynamics

Studies continue of the "Chaotic Regime" nuclear dynamics (a new type of dynamics resulting from the assumption of chaotic motions of the nucleons in the nuclear mean field). In particular, new theoretical results have been obtained on the "sticking time" of two nuclei in deep-inelastic and fast-fission reactions. Typical times range from about 2×10^{-21} s to 2×10^{-20} s, the latter figure representing a U + U collision, for which recent experimental evidence suggests $1\text{-}1.5 \times 10^{-20}$ s.

IV. Damped Nuclear Reactions

The dynamics of damped nuclear reactions is being studied with a particular view towards the role played by the multiple transfer of nucleons. Current efforts have been devoted to studying the accumulation of angular momentum in the two reacting nuclides and the subsequent disposition of spin through sequential decays. A set of first order differential equations is derived for the evolution of the averages, variances, and covariances of the spin distributions in the two nuclides during the collisions. The stationary solution to the dynamical equations can be interpreted in terms of the six angular momentum bearing modes of the disphere in thermal equilibrium with the remaining intrinsic degrees of freedom. The relaxation times of these modes have been estimated in a model where the angular momenta are generated by nucleon transfers. Relative to the collision time, some of the relaxation times are very short and some are quite long. This implies very specific properties of the distribution of spins in the two nuclei when they separate after the collision. The sequential decay of nuclei resulting from damped reactions is considered with an emphasis of multiplicity distributions and angular correlations. The effect of prior particle evaporation is included. The existence of covariances between the spins of the two reaction products implies that the detection of a decay product from one nucleus may break the reflection symmetry of the angular correlation of decays from the other nucleus; this important effect is presently being probed in a fission-fission experiment. Overall good agreement with a broad range of data is found, but for small energy losses the calculated spin increases too rapidly, which may signify the simultaneous action of an additional dissipative mechanism not carrying angular momentum.

V. Static Nuclear Properties

The Droplet Model predictions of nuclear charge distributions have been updated in order to check the agreement with a large number of new measurements. So far the overall agreement is excellent, and the differences are associated with well-understood static or dynamic deformation effects. The study will continue in order to gain a better understanding of the dynamic effects and to determine whether there is any evidence for shell effects in the volume of the charge distribution.

VI. Nuclear Astrophysics

The study of semi-infinite nuclear surfaces is continuing in order to determine the nature of the phase transition that takes place when an increasing neutron excess goes over suddenly to neutron matter. The Thomas-Fermi method is employed with a simple saturating force. The results of these calculations are important for formulating a description of nuclei as they evolve during the collapse of a supernova or for describing nuclei in the surface of neutron stars.

High Energy Nuclear Beams at Berkeley Present and Future Possibilities*

L.S. Schroeder

The Bevalac

In 1974 the era of relativistic heavy-ion physics with moderately heavy ($A \leq 56$) projectiles began at LBL when the SuperHILAC was coupled via a transfer-line to the Bevatron. The SuperHILAC serves as the heavy-ion injector (at 8.5 MeV/nucleon) for the Bevatron. After injection into the Bevatron, the beams are accelerated and extracted for physics research, as well as for a major bio-medical program. In this early period of operation the Bevalac provided beams up to Fe at energies of approximately 2.1 GeV/nucleon. In addition, protons at 4.9 GeV were available from the Bevatron's local 20 MeV linac. The primary goal of the research program was, and continues to be, the study of nuclear matter under *extreme conditions* of high temperature and baryon density. At the same time an active program addressing more conventional aspects of nuclear physics such as momentum distributions of fragmentation products and production of new neutron-rich isotopes was started.

It was clear from the beginning that one wanted to extend the range of available projectiles for research all the way up the periodic table to uranium. This "uranium capability" was realized in 1982 after the addition of a third injector at the SuperHILAC (to provide the heaviest beams) and the improvement of the Bevatron's vacuum from the range of 10^{-7} torr to about 10^{-10} torr. The improved vacuum is necessary to allow partially stripped ions to survive acceleration in the Bevatron without suffering catastrophic losses through interactions with residual gas atoms. With this improvement the Bevalac became the first machine to provide beams of uranium ions at relativistic energies of about 1 GeV/nucleon.

Recent Plans for Going Beyond the Bevalac

As early as 1979, LBL was developing a concept for a machine capable of achieving nucleus-nucleus collisions in a colliding beam mode. It was called VENUS, which stood for Variable Energy Nuclear Synchrotron.[1,2] The physics behind this was the possibility of producing *quark matter* (the term quark-gluon plasma was not generally in vogue at this time) in high energy heavy-ion collisions. The central feature of this concept involved two superconducting accelerating rings capable of operation at energies up to 20 GeV/nucleon in either a fixed target or colliding beam mode. This type of dual operation clearly called for high-field ($\sim$4.5 T), rapid-cycling ($\sim$1 T/sec) superconducting magnets.

In 1982, due to the relatively tight fiscal climate in the United States, we decided to step back and investigate the possibilities of less expensive options. The basic idea was to look for a facility which would be a natural extension of the Bevalac to higher energies allowing us to provide a rich program of conventional nuclear physics, and at the same time have the capability to strike out and explore the domain of the quark-gluon plasma in the region of maximum baryon density. These studies resulted in the Tevalac concept,[3] a facility which would be capable of delivering uranium beams at 10 GeV/nucleon for physic research. Again, high-field ($\sim$6 T), rapid-cycling ($\sim$1 T/sec) superconducting magnets were an essential feature.

In 1983, two significant events occurred – both associated with actions of the Nuclear Science Advisory Committee (NSAC) – which help shape our plans at LBL. The first was the NSAC recommendation for the construction of a 4 GeV cw electron machine. One of the by-products of this recommendation is that it helps establish a new scale in nuclear science, allowing the community to think about more ambitious projects. The second event was the decision by NSAC, at the Wells College meeting called to update the Long Range Plan for Nuclear Science in the United States, to recommend as the next major construction project (*after* the 4 GeV electron machine) a heavy ion collider to produce and study the quark-gluon plasma. In a real sense this bring us full circle, back to a device like VENUS.

Future Plans – Relativistic Nuclear Collider (RNC)

Fig. 1 shows our present concept for a relativistic nuclear collider (RNC) at LBL. It consists of the following elements:

- Improved SuperHILAC as the heavy-ion injector.

- An intermediate energy conventional synchrotron to serve as a booster for the final stage of the RNC. The energy for this stage is dictated by the need to strip off all the electrons on the heavy-ion being accelerated. Recent Bevalac results[4] show that approximately 1 GeV/nucleon would be adequate for the energy of this booster. As shown, the booster could also have a physics program of its own.

- The final stage contains two superconducting rings, operating for either fixed target (single ring only) or colliding beam (both rings) physics. As in earlier LBL concepts, high-field, rapid cycling magnets would be used.

Physics Regimes of the RNC

The central theme of the physics to be studied at the RNC is shown in Fig. 2. There are two regions of interest, both leading to quark-gluon plasma formation:

- At laboratory energies in the 10–20 GeV/nucleon range theoretical estimates[3] indicate that maximum baryon density will be achieved. In such a domain one would create a baryon-rich plasma. This regime would be accessed by single ring operation of the RNC, a natural extension to the present Bevalac program.

- At the much higher energies available to a collider, the two nuclei interpenetrate and disassemble, but do not stop in the overall center of mass. Instead, a hot plasma rich in mesons and low in baryons is left behind, with net baryon number residing in the out-going target and projectile fragmentation regions. It has been suggested[5] that about 30 GeV/nucleon per beam is required to produce sufficient separation in rapidity for these conditions to be met.

General Requirements for RNC

The final machine parameters required for formation of the quark-gluon plasma at an RNC will be clarified at future workshops over the period of the next one to two years. Clearly, careful consideration will have to be given to the overall operating costs including the necessary instrumentation to address the challenge of this physics. In the meantime, there are, however, a number of conclusions that can be drawn at this point concerning general requirements for an RNC. These include:

- Research versatility – such a facility must solve a wide range of problems in nuclear, particle, and atomic physics, astrophysics and cosmology.

- Full nuclear spectrum – must deliver all elements (p to U) for physics research.

- Collider operation
  - — $E_{c.m.} \leqslant 30$ GeV/nucleon for each beam.
  - — $\mathscr{L}_{min} \sim 10^{25} cm^{-2} sec^{-1}$ – based on using ~1% of the U-U interactions ($\sigma^{geom}_{U-U} \sim 10$ barns) this yields 1 central U-U collision/sec.
  - — $\mathscr{L}_{max} \sim 10^{28}-10^{29} cm^{-2} sec^{-1}$ yields 10^3-10^4 central collisions/sec. (There will always be some experimenters who are looking at either very rare processes or using small acceptance requiring large luminosity.)
  - — 2–3 well-instrumented interaction regions will be needed.

- Fixed-target capability – must provide continuity of energy from existing fixed-target machines to collider energies.

A facility to meet the above requirements at LBL, would, of course, require superconducting magnets with high-field and rapid pulsing capabilities. One of the chief goals of the LBL program will be to further develop and refine such a magnet.

Footnote and References

*Condensation of an invited talk given at the Quark Matter '83 Conference, Brookhaven National Laboratory, September 1983.

1. The VENUS Project, LBL PUB-5029 (June 1979).
2. H. Pugh, Proceedings of the Bielefeld Workshop on Quark Matter Formation and Heavy Ion Collisions, eds. M. Jacob and M. Satz (World Scientific)., p 329 (1982)
3. The Tevalac, LBL PUB-5081 (1982).
4. H. Gould (LBL), private communication.
5. G. Baym, summary talk, Quark Matter '83 Conference, Brookhaven National Laboratory, September 1983.

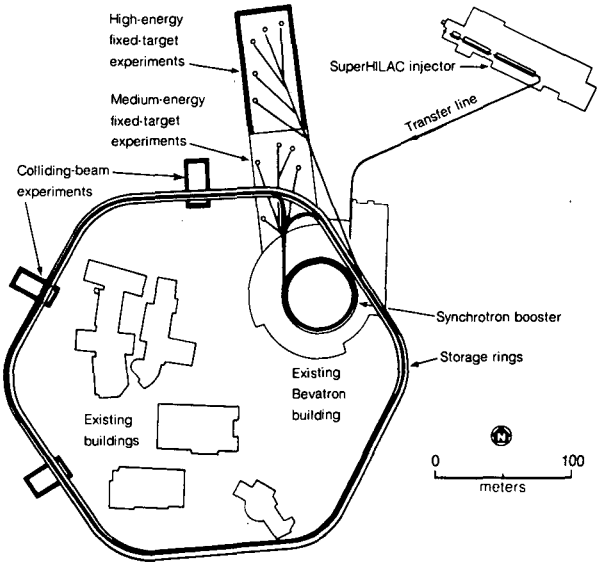

Fig. 1. Conceptual layout for a relativistic nuclear collider (RNC) at LBL. Various components of such an accelerator are indicated. XBL 8310-605

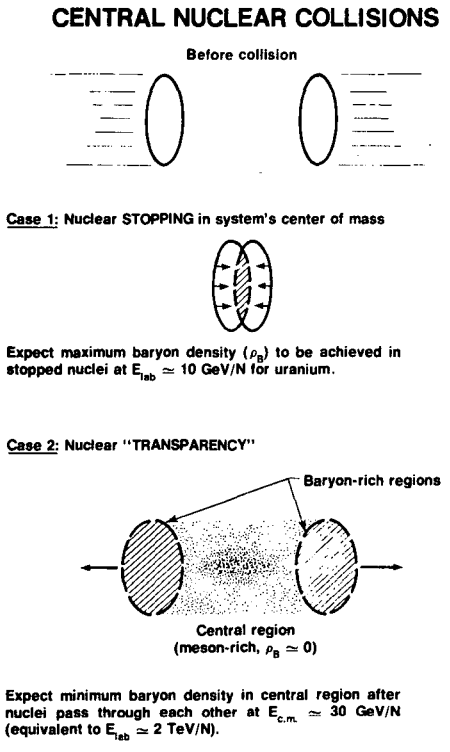

Fig. 2. Characterization of the physics to be probed in fixed target (case 1) and in colliding beam (case 2) operation of the RNC. XBL 8310-12112

PART II: ACCELERATORS

88-Inch Cyclotron Operations

D.J. Clark, D. Elo, L. Glasgow, Y. Jongen, R. Lam, C.M. Lyneis, R.G. Stokstad*

Operations

The 88-Inch Cyclotron, operated by the Nuclear Science Division, provides a large fraction of the beam time that is used by Division scientists. Variable energy high resolution beams from hydrogen through argon are produced and used for studies of nuclear structure and nuclear reaction mechanisms. The cyclotron is also the Laboratory's major source of medical isotopes and its only source of polarized proton and deuteron beams. Ions as heavy as ^{40}Ar can be accelerated to the Coulomb barrier of 5 MeV/nucleon, while lighter heavy ions can reach 20-30 MeV/nucleon. The cyclotron thus operates in the important transition region between low and high energies: 10–30 MeV/nucleon.

As a national accelerator laboratory the 88-Inch Cyclotron is used extensively by outside groups from many institutions in the U.S. and abroad. Table I shows the number of users from LBL and elsewhere. Scheduling of experiments for the cyclotron is done in an open meeting on a weekly basis with a lead time of eight days. Outside users who must make travel arrangements in advance are accommodated with advance scheduling. A users' organization has been formed and a Program Advisory Committee instituted. The members of the Users' Executive Committee are Karl Van Bibber (Stanford University), Chairman; Frank S. Dietrich (Lawrence Livermore National Laboratory); and Marie-Agnes Deleplanque (LBL). The Program Advisory Committee consists of C. Konrad Gelbke (Michigan State University), Chairman, Charles Goodman (Indiana University) and Jørgen Randrup (LBL).

The 88-Inch Cyclotron plays a significant educational role. In 1983 twelve graduate students from the University of California at Berkeley employed this facility in their research toward the Ph.D. degree. Five students received their doctorates from UCB in 1983 for research done at the cyclotron. Eleven graduate students from other universities participated in research at the cyclotron.

The cyclotron now operates 14 1/2 eight hour shifts per week with one additional shift for maintenance at the beginning of the week and one half shift for shutdown for the weekend. It was operated for 20 shifts per week until October 1981 when increased power rates and budget limitations made the reduction in running time necessary. The distribution of cyclotron time is shown in Table II. The list of beams available is given in Table III. The particle distribution of ion beams during the past years is shown in Fig. 1.

Improvement Programs

The new internal PIG source developed last year is now in routine operation. Additional anodes will be fabricated so that they are available at the source changes. A hydrofluoric acid cleaning procedure has been put into regular service for source anodes. This procedure replaces a mechanical cleaning operation that was very hard on anodes. The new procedure preserves anode geometry and significantly reduces the manpower required for servicing and fabricating anodes.

The polarized ion source vacuum system has been improved and simplified. Two 10″ mercury diffusion pumps with LN traps have been replaced with two oil diffusion pumps which are untrapped. A new pump design and special oil permit this desirable change. Additionally, a liquid nitrogen trap on another oil diffusion pump has been replaced with a new one with more vacuum reliability. The Electron Cyclotron Resonance (ECR) high charge state heavy ion source was well into the construction stage in FY83. This project is described in more detail in a separate article in this annual report.

Work is in progress on modification of the drive system for the rf matching capacitor. This project will increase coupling efficiency between the power amplifier tube and the system. This will in turn reduce the power required from the power amplifier tube, increase the tube life and provide experience for a possible conversion to a less expensive tube.

Electronic improvements include the replacement of two tube type 100 kV deflector power supplies with solid state supplies, for the middle and exit deflectors. A new trim-coil control panel was nearly completed and will replace the old one in the near future. Eight regulators for the quadrupole power supplies have been built and are ready to replace the old chopper-type regulators. New intercom chassis have been built and will replace old ones gradually. A digital controller has been built for the RAMA magnet.

In the experimental area the installation of a mechanical vacuum pump venting system to replace a temporary system has been started and is nearing completion. The new installation will ease the problems of removing the exhaust and simplify installing new equipment. The 36″ scattering chamber and its associated control circuits have been moved to cave 4c. The emergency power system now handles more critical cyclotron components and building equipment. This will ease recovery from power outages, which occur more frequently since the building is now on an interruptible power line to obtain lower power rates.

*On leave from Cyclotron Laboratory, Louvain-la-Neuve, Belgium.

Table I. Number of users of the Cyclotron during FY83

LBL Staff, University of California, Berkeley Campus			21
Graduate Students			
	U.C. Berkeley	12	
	Other Universities	11	
			23
Post-doctoral scientists			
	LBL	7	
	Other laboratories	0	
			7
Outside users and visitors			
	Industry	41	
	Universities, National Labs.	62	
			103
	TOTAL		154

Table II.

Cyclotron operating and maintenance time distribution for the 12 month period 10/1/82 to 9/30/83 covered by this Annual Report

		Hours	%
Operating Time	Machine Studies	427	7.0
	Tuning	478	7.9
	Optics	267	4.4
	On target	3131	51.6
	Waiting for experimenter	246	4.1
	Subtotal	4549	75.0
Maintenance Time			
	Weekly maintenance	360	5.9
	Shutdown maintenance	452	7.5
	Ion source preparation	374	6.2
	Unscheduled maintenance	259	4.3
	Other	68	1.1
	Subtotal	1513	25.0
	Total	6062	100.0
	Holiday/Shutdown	2698	
	Total Time	8760	

Table III. 88-Inch Cyclotron Beam List 1983

Ion	Energy[a] (MeV)	Ext. Beam Intensity (eμA[b])
p	0.2 – 55	100 – 20
p (polarized)	6 – 50	.7 – .4
d	0.5 – 65	100 – 20
	65 – 70	~0.5
d (polarized)	10 – 65	.7 – .4
$^{3}He^{1+}$ c)	2 – 47	>20
$^{3}He^{2+}$ c)	4 – 140	100 – 10
$^{4}He^{2+}$	3 – 130	100 – 10
	130 – 140	~0.5
$^{6}Li^{1+}$ c)	2 – 23	5
$^{6}Li^{2+}$ c)	23 – 93	1
$^{6}Li^{3+}$ c)	93 – 195	0.1
$^{7}Li^{2+}$	20 – 80	1
$^{7}Li^{3+}$	80 – 180	0.1
$^{9}Be^{2+}$	15 – 62	5
$^{9}Be^{3+}$	62 – 140	2
$^{9}Be^{4+}$	140 – 249	.05
$^{10}B^{2+}$ c)	14 – 56	10
$^{10}B^{3+}$ c)	56 – 126	50
$^{10}B^{4+}$ c)	126 – 224	0.3
$^{10}B^{5+}$ c)	224 – 320	0.001
$^{11}B^{2+}$	12 – 51	10
$^{11}B^{3+}$	51 – 115	50
$^{11}B^{4+}$	115 – 204	0.3
$^{12}C^{2+}$	12 – 47	>20
$^{12}C^{3+}$	47 – 105	30
$^{12}C^{4+}$	105 – 212	5 – .5
$^{12}C^{5+}$	187 – 306	.05 – .001
$^{12}C^{6+}$	292 – 384	10^{5} p/s
$^{13}C^{3+}$ c)	43 – 97	>20
$^{14}N^{2+}$	10 – 40	20
$^{14}N^{3+}$	40 – 90	15
$^{14}N^{4+}$	90 – 160	15
$^{14}N^{5+}$	160 – 250	2
$^{14}N^{6+}$	250 – 360	10^{6} p/s
$^{14}N^{7+}$	360 – 448	100 p/s
$^{15}N^{4+}$ c)	84 – 150	15
$^{16}O^{1+}$	9	1
$^{16}O^{2+}$	9 – 35	>5
$^{16}O^{3+}$	35 – 79	20
$^{16}O^{4+}$	79 – 155	30 – .2
$^{16}O^{5+}$	140 – 219	5
$^{16}O^{6+}$	219 – 315	0.3
$^{16}O^{7+}$	315 – 429	10^{7} p/s
$^{16}O^{8+}$	429 – 512	0.2 p/s
$^{18}O^{3+}$ c)	31 – 70	20
$^{18}O^{4+}$ c)	70 – 124	>10
$^{18}O^{5+}$ c)	124 – 194	5
$^{19}F^{3+}$	30 – 66	5
$^{19}F^{4+}$	66 – 118	10
$^{19}F^{5+}$	118 – 184	2
$^{20}Ne^{3+}$	28 – 63	>10
$^{20}Ne^{4+}$	63 – 112	10
$^{20}Ne^{5+}$	112 – 175	5
$^{20}Ne^{6+}$	175 – 252	1
$^{20}Ne^{7+}$	252 – 343	0.01
$^{20}Ne^{8+}$	343 – 448	~50 epA
$^{22}Ne^{5+}$ c)	102 – 159	~5
$^{22}Ne^{6+}$ c)	159 – 229	1
$^{24}Mg^{4+}$	50 – 93	2
$^{24}Mg^{5+}$	93 – 146	0.2
$^{25}Mg^{4+}$ c)	50 – 90	2
$^{26}Mg^{4+}$ c)	48 – 86	2
$^{26}Mg^{5+}$	86 – 145	.08
$^{28}Si^{5+}$	80 – 125	1
$^{28}Si^{6+}$	125 – 180	0.2
$^{28}Si^{7+}$	180 – 245	0.05
$^{32}S^{6+}$	100 – 158	2
$^{32}S^{7+}$	158 – 238	0.2 – .03
$^{35}Cl^{7+}$	144 – 196	0.5
$^{35}Cl^{8+}$	196 – 256	0.05
$^{37}Cl^{6+}$	95 – 136	0.3
$^{37}Cl^{7+}$	136 – 185	0.08
$^{40}Ar^{2+}$	3.5- 14	0.4
$^{40}Ar^{6+}$	87 – 126	4
$^{40}Ar^{7+}$	126 – 172	2
$^{40}Ar^{8+}$	172 – 224	0.5
$^{40}Ar^{9+}$	224 – 280	10^{5} p/s
$^{40}Ar^{10+}$	280 – 350	10^{3} p/s
$^{40}Ca^{6+}$	87 – 126	1
$^{40}Ca^{7+}$	126 – 172	0.2
$^{56}Fe^{10+}$	180 – 250	1 p/s
$^{63}Cu^{9+}$	142 – 180	5 enA
$^{63}Cu^{10+}$	180 – 222	0.1 enA
$^{63}Cu^{11+}$	222 – 269	$5x10^{3}$ p/s
$^{84}Kr^{2+}$	1.6- 6.6 d)	.001
$^{84}Kr^{8+}$	82 – 107	.250
$^{84}Kr^{9+}$	107 – 135	.120
$^{84}Kr^{10+}$	135 – 167	.030
$^{84}Kr^{11+}$	167 – 202	.003
$^{197}Au^{13+}$	102 – 120	2 p/s
$^{197}Au^{14+}$	120 – 140	0.1 p/s

a) Heavy ion energy range shows nominal maximum energy for a particular charge state down to energy which can be reached by the next lowest charge state. The maximum energy for several heavy-ion beams has been increased to $E = 160\ Q^2/A$ MeV. Beams can also be run at energies below 1 MeV/nucleon.
b) Electrical microamperes except as noted, $\Delta E/E \sim 0.3\%$. Intensity on target will be less, depending on mode of beam transport.
c) Isotopically-enriched source feed.
d) 15th harmonic.

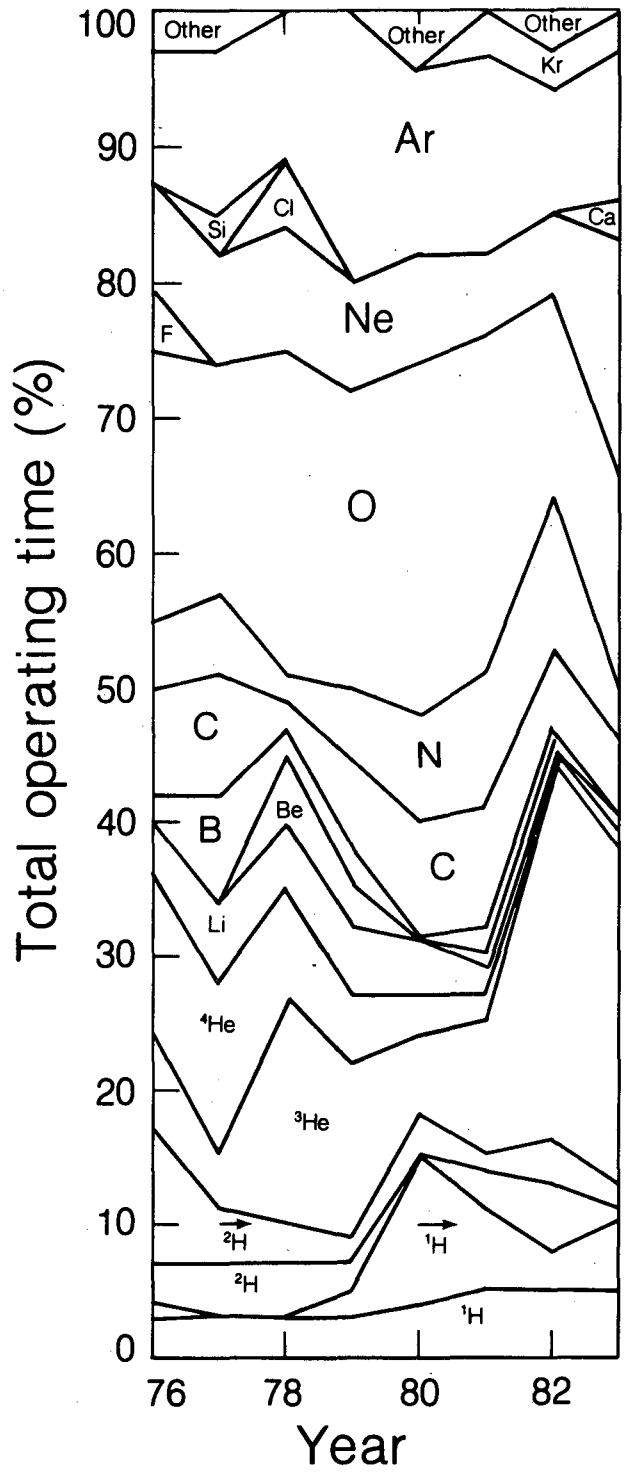

Fig. 1. Distribution of particle type during last 8 years.

XBL 8312-6915A

88-Inch Cyclotron Research Program

R.G. Stokstad

The research programs at the 88-Inch Cyclotron comprise a broad and diversified enterprise that reflects in part the versatility of the accelerator. Basic research in nuclear physics is done with heavy ion and light ion beams. These probes are used to study nuclear structure and nuclear reaction mechanisms. Interspersed in this effort is a series of applications of nuclear techniques to other disciplines. The following overview categorizes the research in terms of heavy ion reaction mechanisms, nuclear structure, exotic nuclei, heavy element research, light ion research and applications.

Heavy Ion Reaction Mechanisms

The study of nuclear reaction mechanisms continues to form one of the main thrusts of the overall research program. Previous developments of beams of beryllium through neon at energies up to ~20 MeV/nucleon have made possible a wide range of investigations into the nature of peripheral reactions, incomplete fusion, fission and evaporation.

The behavior of heavy ion reactions changes rapidly as the bombarding energy is increased significantly above 8 MeV/nucleon. Between this energy and about 100 MeV/nucleon a transition occurs from the characteristics of low energy phenomena (transfer reactions, complete fusion) to those of relativistic heavy ion reactions (fragmentation, participant-spectator mechanisms). The mechanisms of heavy ion reactions in this regime are being studied in order to identify and understand the competing processes and their dependence on the bombarding energy. Two main thrusts of this work are in the areas of transfer and fragmentation reactions and of incomplete fusion. Transfer reactions are being studied by a new device, the "plastic box", a 4π array of scintillators arranged in the form of a cube which provides the means to distinguish between transfer and fragmentation. The plastic box is being used in a number of experiments where the separation of two-body and three-body reactions is crucial. Studies of ^{20}Ne + Au show large probabilities for the transfer of up to 7 charge units (~14 amu). A new position sensitive plastic scintillator has been developed for the plastic box. Incomplete fusion is being investigated with the time-of-flight facility. Systematic measurements for a wide range of targets and projectiles reveal an onset of incomplete linear momentum transfer at about 5 MeV/nucleon above the Coulomb barrier. An important step toward describing the transition from low energies to high energies is the development of the overlap model for transfer reactions. This semiclassical model reproduces very well the excitation function for fragments produced in the ^{20}Ne + Au reaction up to 20 MeV/nucleon.

The transition between evaporation and fission is also being explored. As the evaporated particle increases in mass beyond helium, the distinction between the two mechanisms blurs and the question of how to describe the production of complex intermediate-mass fragments arises. This is being approached experimentally by observing the yields of helium through neon produced in the reaction of ^{3}He and Ag and characteristic changes which occur in the shapes of the energy spectra as the mass of the fragment increases (from a Maxwellian shape to a Gaussian shape). These experimental characteristics are being studied as a function of bombarding energy.

Analysis of data from a series of radiochemical survey measurements of Au target fragmentation at intermediate energies was completed recently by a University of Oregon-LBL collaboration. The most interesting unexpected new finding from this work was the general success of the nuclear firestreak model in describing the

fragment yield distributions and the measurement of excitation functions for fragments with A < 60 which were consistent with the Bertsch-Siemens prediction of a lower threshold for production of these fragments in nucleus-nucleus as compared to p-nucleus collisions.

Radiochemical studies of incomplete fusion in reactions of light heavy ions with neutron-rich rare earth nuclei showed the general inapplicability of the Wilczynski sum rule model for reactions induced by projectiles of energy 20–86 MeV/nucleon.

Nuclear Structure

The nuclear structure studies are aimed mainly at understanding nuclei with large angular momentum. The viewpoint is now generally accepted that angular momentum represents a dimension, not unlike proton or neutron numbers, along which nuclear properties can be studied. Up to now, shell effects and changes in the shape and in the pairing correlations have been studied as a function of angular momentum. Experiments at the 88-Inch Cyclotron have been directed toward measuring shell effects with increasing angular momentum. It was found that the valence shells and the next higher major proton shell produce separate bumps in the unresolved γ-ray spectra at frequencies (spins) around 0.35 MeV ($25\hbar$) and 0.6 MeV ($45\hbar$), respectively, in ^{154}Er and ^{156}Er. This is not the case for heavier (well deformed) rare-earth nuclei, but does seen to occur in several lighter-mass regions.

A major effort in the high-spin studies was expended to get the first parts of the High Resolution Ball detector system into operation. Two experiments, one with four and the other with five Compton-suppressed Ge detector systems (out of 21 planned systems) were performed. The nuclei ^{156}Er and ^{144}Gd were studied. Extremely clean (peak/total ~0.45) and high-resolution (FWHM ~3 keV) γ-γ coincidence spectra were obtained and are currently being analyzed. This system already takes data several times faster than any other in the world, and will improve roughly as the square of the number of detectors, which are arriving at the rate of one per month. It is clear that most future nuclear structure studies at the cyclotron will be done with this detector system.

Some studies of giant resonance γ-ray decays following compound nucleus formation were also made. Most previous studies were done on the giant dipole resonance at ~15 MeV in rare earth nuclei. Current studies were aimed at the giant quadrupole decay in the 20–30 MeV range. Although radiation was observed in this energy range, it is not yet clear whether it is the tail of the giant dipole decay or represents evidence for giant quadrupole decay.

Exotic Nuclei

Research in the area of exotic nuclei consists primarily of decay studies of light to medium mass very neutron-deficient isotopes. Techniques used for these studies involve charged-particle and β-γ spectroscopy of nuclides produced in ^{3}He or heavy ion bombardments of neutron-deficient targets. These nuclides are transported from the target area via a helium jet system which can be used either to prepare a source directly or to feed the on-line mass separator, RAMA.

Work this year has focused on studies of the newly discovered decay mode of beta-delayed two-proton radioactivity. Experiments have been performed at two different relative proton angles and have shown the decay mechanism probably to be largely (if not completely) sequential emission for each of the two known beta-delayed two-proton activities, ^{22}Al and ^{26}P. Some initial and, as yet, unsuccessful searches have also been made for other beta-delayed two-proton emitters in the mass 40–60 region. In addition to the two-proton work, the new isotope ^{58}Zn was also produced and its beta-delayed proton decay studied.

Heavy Element Research

Heavy element research at the 88-Inch Cyclotron is conducted mainly by a group from Lawrence Livermore National Laboratory. Measurements they have made for ^{259}Md and ^{260}[104] indicate a major and abrupt transition in the fission behavior of neutron-rich transfermium nuclei. Fission-fragment measurements for ^{258}No, though made on a very small number of events, tend to support the same conclusion. These studies employ a spinning-wheel analysis for millisecond isotopes (SWAMI) that enables coincident fission fragment energies to be measured for isotopes with half lives as short as 1 millisecond.

Light Ion Research

Light ion research using the polarized proton and deuteron beams is generally concerned with spin-polarization phenomena in nuclear reactions and scattering. A most important feature of polarization effects is that they often display uniquely the operation of, hence the possible violation of, a basic symmetry property of the nuclear interaction. Thus, several fundamental experiments have been designed to make significant tests of parity conservation, charge symmetry, and time-reversal invariance in this interaction.

Spin-polarization measurements also provide information concerning nuclear structure and reaction mechanisms that is not otherwise available. Thus, studies are made of analyzing powers and polarization transfer in inelastic nucleon scattering and nucleon-transfer reactions in order to deduce the specific spin-dependent nature of the nuclear interactions. For example, the inelastic nucleon scattering results provide detailed information about the spin-dependent components of the effective nucleon-nucleon force in nuclei, which is a subject of considerable current interest. Measurements also are made of polarization-transfer in elastic proton-nucleus scattering, since these results will provide a unique means of establishing the existence of a spin-spin component of this nuclear interaction. This research with polarized beams involves collaborations with several groups from different universities and laboratories.

Applications

Grouped as applied research are the activities of (i) the Division of Biology and Medicine, which include radioisotope production and cellular studies of radiobiological effects with low energy heavy ions; (ii) the investigation of cosmic-ray induced errors in digital semiconductor devices; (iii) a study of the enhanced adhesion of thin films through heavy ion bombardment.

Bevalac Research Program

Howel G. Pugh

The Bevalac has the unique capability world-wide to produce beams of all ions in the relativistic energy regime. The new ideas of nuclear physics which emerge from relativistic field theories devised to describe nucleus-nucleus collisions at these energies are often radically different from our preconceptions of nuclear behavior. New configurations of nuclear particles are found to be possibly stable and in the extreme limit it is found that the colliding nuclei may be converted into a new state of nuclear matter called the quark-gluon plasma. Such ideas cannot be investigated with conventional probes such as electrons or protons since they involve raising large volumes of nuclear matter to conditions of high density and pressure such as can only be produced when very large projectiles, i.e., nuclei themselves, are used. The Bevalac program consists of a systematic study of the behavior of nuclei under these conditions, with hot pursuit of any unusual phenomena that seem to be encountered.

The Facility and Its Users

The Bevalac provides beams of ions up to uranium at energies from 20 MeV/nucleon to 2.1 GeV/nucleon (1.0 GeV/nucleon for uranium). Table I shows energies and intensities of some of the beams used in FY83.

Table I

Partial Bevalac Beam Inventory, 1983

Ion	Charge States	E_{max} (MeV/nucleon)	Intensity (Particles/Pulse)
Neon	10+	2100	$1 \cdot 10^{10}$
Iron	24+	1700	$1 \cdot 10^{8}$
Lanthanum	29+	590	$8 \cdot 10^{7}$
"	48+	1260	$1 \cdot 10^{6}$
Gold	35+	450	$1 \cdot 10^{7}$
"	61+	1080	$2 \cdot 10^{6}$
Uranium	38+	380	$1 \cdot 10^{6}$
"	68+	960	$2 \cdot 10^{5}$

To use these beams a large number of user groups converge on LBL from all parts of the United States. Major groups from GSI, Darmstadt, West Germany, and INS, Tokyo, Japan, lead the contingent of international users, while there are many other smaller groups from abroad engaged, for example, in emulsion experiments. A recent count showed that over 200 individuals are engaged in nuclear science research at the Bevalac, representing 18 U.S. universities, 5 U.S. National Laboratories, and 19 foreign institutions. Approximately 40 graduate students are using the Bevalac for some part of their thesis research.

Experiments are selected by the Bevalac Nuclear Science Program Advisory Committee which meets twice

a year. The present members are: P. Siemens, Texas A&M University, Chairman; R. Klapisch, CERN, Geneva, Switzerland; T. Ludlam, Brookhaven National Laboratory; D.K. Scott, Michigan State University; H. Stocker, Michigan State University; E. Vogt, TRIUMF and University of British Columbia, Canada; T. Yamazaki, University of Tokyo, Japan. Within the very limited beam time available, collaborations typically receive 100 hours of beam time per year. Under these circumstances there is a strong emphasis on complex, flexible, and efficient detectors and data acquisition methods, or else on experiments of a decisive quality.

The Bevalac Physical Sciences Users' Association meets annually and its Executive Committee holds regular telephone conference calls to discuss current problems. The present membership of the Executive Committee is: P.N. Kirk, Louisiana State University, Chairman; H.J. Crawford, University of California Space Sciences Laboratory, Berkeley; G.J. Igo, University of California, Los Angeles; G. Westfall, Michigan State University; two others to be elected (election in progress); and ex officio members representing the Laboratory management: J. Alonso, Accelerator and Fusion Research Division; H.S. Matis, Nuclear Science Division; and H.G. Pugh, Nuclear Science Division. The 1984 Users' Association meeting is planned for May 16–17, when workshops on several developing research areas will also be held. In 1983 the 6th High Energy Heavy Ion Study and 2nd Workshop on Anomalons, held from June 28 to July 1, attracted over 200 participants including 60 foreign visitors.

The New Very Heavy Ion Beams

The past year has been specially notable for the excellent performance of the upgraded Bevalac. Many new beams have been developed and excellent quality, good intensity beams of all ions are now a routine matter. For the heavier beams, accelerated in a partially ionized state, it has been possible to produce extremely clean external beams by the use of thin defining slits which change the charge state of unwanted ions so that they are not accepted by the subsequent magnetic analysis. The slits, because of their thinness, do not produce fragmentation of the wanted ions.

A variety of measurements have been made of the atomic properties of the new ions, uranium in particular. Studies have been made of the charge state distribution of ions after passing through foils of various thicknesses. It is found, for example, that 962 MeV/nucleon uranium ions reach an equilibrium charge distribution after about 20 mg/cm^2 of copper, at about 90% U^{92+} and 10% of U^{91+}. This first production of bare uranium nuclei in the laboratory opens up a variety of experimental possibilities. Two experiments approved for Bevalac running are a measurement of the Lamb shift in hydrogen-like uranium (U^{91+}) and an attempt to produce polarized U^{91+} ions by a channeling technique. Studies of the range-energy relationship for uranium ions, published during 1982, have aroused interest from the inertial fusion community, and a program to study energy loss mechanisms for uranium ions up to a few mm range has been initiated.

Equilibration, Compression, and Collective Flow

Of central interest in the Bevalac research program is the question of what reaction mechanisms come into play when fast nuclei collide. Substantial progress has been made in the past year in several areas and using various techniques.

The most striking results have been produced by the Plastic Ball/Wall. In studies of Ca-Ca and Nb-Nb collisions the average transverse momenta and average longitudinal momenta of secondary particles from individual events have been studied. From these it can be deduced that in central Nb-Nb collisions (impact parameter b = 0) the secondary particles are emitted nearly isotropically in the c.m. system. In other words, to a good approximation the two nuclei stop each other prior to disintegration. This conclusion is very significant for attempts to deposit the maximum possible energy density into the nuclear volume, since it implies that all or

most of the energy available at the Bevalac can be used. Earlier studies with the Streamer Chamber for Ar-KCl and Ar-Pb collisions reached the same conclusion. The very high statistics available from the Plastic Ball/Wall have enabled more detailed studies to be carried out, and using the method of energy-flow analysis it has been possible in Nb-Nb collisions at 400 MeV/nucleon to identify two effects which had been predicted by nuclear hydrodynamical calculations. In the projectile fragmentation region, a deflection of the average motion of projectile fragments which depends on impact parameter was found, confirming the predicted "bounce-off" effect. At smaller impact parameters, for nearly central collisions, a large deflection of the average direction of motion of secondary particles confirmed the predicted "side-splash." These studies need to be continued, and we look with excitement to the results of a very successful Au-Au run in which secondary multiplicities of up to 200 were observed. Hydrodynamical effects may become dominant in collisions between such large nuclei.

Studies of the high compressions produced in relativistic heavy ion collisions have so far been carried out only by studying pion production, which is suppressed in comparison with expectations from intranuclear cascade calculations. Attribution of the deficiency of pions to loss of energy into compressional modes of excitation led to derivation of a nuclear equation of state up to densities of 3.5 times normal, which showed no phase changes but a continuation of nuclear incompressibility at the same level as had been deduced from breathing mode excitation energies. During the past year this method has been extended up to a density of 3.8 times normal with a preliminary data point from La + La at 1.0 GeV/nucleon, where pion production is suppressed by as much as a factor of three. Extensive discussion of the assumptions made in this analysis has led to a useful clarification of the difference between chemical freezeout and thermal freezeout. From a detailed analysis of the microscopic development of heavy ion collisions, it can be shown that it is indeed reasonable that at the maximum density stage both thermal and chemical equilibria are established between nucleons, pions and delta particles. However, as the temperature of the system drops off, the inelastic nucleon-nucleon cross section falls and chemical equilibrium cannot be maintained. Nonetheless, thermal equilibrium is maintained during the expansion because it depends only on total cross sections, which remain large. Thus is resolved the apparent paradox that the number of pions produced is frozen at the time of maximum density, while the observed temperature of the pions seems to correspond to a much later stage of the collision.

The Plastic Ball/Wall has produced another result of a striking nature relevant to this discussion. Measurements of deuteron production as a function of multiplicity had earlier been parameterized in such a way as to suggest that deuterons are formed at a very late stage, at nuclear densities of about one quarter normal nuclear density. Recent results of a Hanbury-Brown, Twiss analysis of two-proton correlations measured with the Plastic Ball show a striking relationship between the radius of the emitting source and the multiplicity of emitted particles. Once again this is consistent with the idea that the protons remain in equilibrium until the density has dropped to one quarter nuclear density. These new observations seem to be permitting a rapid follow-up of the picture described by Nagamiya of the nucleus-nucleus interaction as consisting of a series of quasi equilibria, each of which could be tested by adoption of a suitable measurement technique.

Finally, the observation of collective flow (as well as the necessity to fit data) has led to a revival of the "blast-wave" model of the expansion of the nucleus-nucleus system after collision. This permits the proton spectra to be boosted by outward flow, giving apparent temperatures higher than those of the pions, even though the protons and pions are in thermal equilibrium with each other. These considerations were necessitated by new measurements of inclusive spectra for La + La at 800 MeV/nucleon.

Anomalous Projectile Fragments

Two major steps forward were taken in the past year in the study of the controversial "anomalons," projectile fragments that interact much more strongly than can be predicted for normal nuclear processes.

From June 28 to July 1 the Second Workshop on Anomalons was held in conjunction with the 6th High Energy Heavy Ion Study. A roughly tenfold increase in the world data concerning anomalons led to a consensus that the effect is real, but that probably a smaller proportion of projectile fragments (1–3%) is involved than had previously been accepted. Furthermore, much of the new data showed anomalous mean free paths of less than 1 cm, compared with the 2.5 cm indicated by the early emulsion data. The workshop ended in anticipation of results from planned experiments with electronic techniques.

The results from two experiments using stacked Čerenkov detectors became available in November, 1983. With over a million secondary interactions observed, these experiments simulate with much better statistics the previous experiments with plastic track detectors. No anomalous effect was observed, though the data were limited to the study of interactions beyond about 1 cm from the primary production point. This presents a challenge to the anomalon enthusiasts since the statistics are so good that, assuming exponential absorption of the anomalons, a mean free path substantially shorter than 1 cm could have been observed. However, since the characteristic feature of the anomalon phenomenon is the failure of exponential absorption, the assumption of exponential absorption of the anomalous component may be dangerous. Another caveat is that there is only about 20% overlap between the Čerenkov (and plastic track detector) experiments and the emulsion experiments. This arises from a restriction to interactions of highly charged secondaries. Furthermore, the absence of heavy nuclei, silver and bromine, in the medium may influence the result. Fortunately, there seem to be ways to test these differences by modifications of the Čerenkov experiments, and these are being pursued.

Beams of Unstable Nuclei

The Bevalac has for several years provided beams of ^{11}C and ^{18}F for biomedical purposes, and has also been recognized as a potent source of nuclei far from stability which are produced in projectile fragmentation, sixteen new isotopes having been discovered in a single run with ^{48}Ca beams a few years ago. The past year has seen two accepted proposals for experiments using secondary beams. Table II shows estimates of the beam intensities, in particles per pulse, for some selected isotopes.

Table II

Isotope	Expected Intensity (Particles/Pulse) [6]
^{8}He	500
^{8}Li	10^{7}
^{9}Li	$5 \cdot 10^{6}$
^{11}Li	250
^{55}Ni	10^{4}

In the field of nuclear structure studies, an initial experiment will be carried out to study the interaction cross sections of ^{4}He, ^{6}He, and ^{8}He on various nuclei. Hartree-Fock calculations predict that the proton distributions of all three nuclei are about the same, while there will be a neutron-rich skin on the ^{6}He and ^{8}He. These studies will eventually make use of the HISS facility where small beam intensities can be used very effectively, and some nuclear structure studies have already been carried out involving the electrodisintegration of ^{16}O into ^{15}N and a proton.

Another, even more ambitious, experiment will measure the magnetic moments of unstable nuclei to permit the comparison of mirror nuclei in the $f_{7/2}$ shell. In this experiment the isotope-separated beam will be slowed down, spin-polarized by the tilted-foil technique, and then implanted in a stopping foil. The polarization will be preserved by means of a superimposed magnetic field, and the asymmetric β-decay distribution of the polarized nuclei will be measured. Finally, the magnetic moment will be determined by studying the resonant destruction of the polarization by an RF field (nuclear magnetic resonance).

Because of these and other experiments anticipated with secondary beams, the original plan to build an "isotope loop" solely for HISS has been changed, and an isotope production facility has been designed for the exit of the machine. This will permit delivery of secondary beams to any of the beam lines in the Bevalac experimental area.

Fractional Charge Search

The availability of new, intense beams at the Bevalac, coupled with a suggestion that fractionally charged particles might be liberated in high energy collisions between large nuclei, led to an interesting venture. A collaboration of essentially all the "quark search" groups was formed to analyze materials bombarded at the Bevalac.

The target for a 1.9 GeV/nucleon ^{56}Fe beam consisted of several materials including copper for subsequent analysis by electrostatic Van de Graaff techniques, tiny iron balls for magnetic levitation experiments, mercury for mercury droplet experiments, and lead, to enhance the probability of production. The target was surrounded by approximately two tons of carbon tetrachloride to slow down and capture light fractionally charged particles that might escape from the target.

After a one-day bombardment, the target materials have been distributed. One analysis is so far completed: the mercury droplet experiment. This included material from the target as well as samples produced from the carbon tetrachloride by an electrostatic concentration technique. An upper limit of one fractionally charged particle per $2 \cdot 10^6$ interactions has been obtained. This limit can be improved substantially when all the target has been analyzed and perhaps by a more intense beam exposure at the Bevalac.

The logistical success of the procedure has led to the idea that the method can be extended to other accelerators as new beams become available. A repeat of the experiment is, for example, under consideration for the Tevatron at Fermilab.

Status of Major Detectors

As discussed above, the Plastic Ball/Wall has had great success and is opening the doors to the next phase of relativistic heavy ion studies. This capability has recently been expanded by inclusion of gas detectors in the vacuum chamber to permit detection of the heavier fragments.

Users of the HISS facility are in a data analysis phase after a variety of successful runs. In order to study further some problems encountered as a result of the large number of fast delta rays produced by highly charged fragments, implementation of the Phase II detector system is being delayed by about a year for the construction and testing of new prototype drift chambers. The first published results from HISS were presented at the 6th High Energy Heavy Ion Study and consisted of measurements of proton production at extremely high transverse momenta. It was found that the proton spectra deviate substantially from the Boltzmann form at these momenta, roughly 2.5 GeV/c.

The Streamer Chamber facility has been upgraded to accommodate heavier beams, to incorporate better optimization and stabilization procedures, and to add a 384-element dE/dx and time-of-flight detector array in the forward direction. This will add substantially to the particle identification capabilities of the streamer chamber, as well as assist in resolving close tracks near zero degree.

A second VAX 11/780 computer has been purchased to complete the network of three at the Bevalac (one belongs to GSI, Darmstadt). It and the GSI computer have been installed in a new house. The new machine will primarily serve Beam 30 and the Low Energy Beam Line. A front-end VAX 11/750 has been purchased for Beam 30 and another one for the dilepton production experiment. It is hoped eventually to replace all the front-end computers at the Bevalac with VAX 11/750's.

Future Plans

Major detector construction will in the near future consist of the Dilepton Spectrometer which will provide definitive tests of the high temperatures reached in heavy ion collisions, as well as other significant measures of the reaction mechanism such as the rate of virtual $\pi^+ \pi^-$ annihilation as indicated by the yield of rho mesons.

The first detailed considerations of the next 4π detector, to replace the Plastic Ball/Wall, are now beginning. Preliminary ideas are for a superconducting solenoidal magnetic spectrometer to be placed upstream from HISS. These ideas will be developed further in conjunction with the Users' Association.

Proposal pressure has led to a concept for a new beam line which will serve a dual purpose. It will provide an improved low energy beam line capable of high intensity uranium beams up to 100 MeV/nucleon and moderate intensity beams at 200 MeV/nucleon. It will also permit a variety of experiments studying K^+, K^-, and $\bar{p}$ production with much higher efficiency than was possible in previous experiments using Beam 40.

Finally, to extend the study of relativistic heavy ion physics to higher energies, LBL has joined with GSI to propose experiments at CERN. These have been approved for early 1986, for ^{16}O beams at energies up to 40 GeV/nucleon. As part of the agreement between CERN, GSI, and LBL, a new injector will be constructed for the CERN accelerator complex. GSI will provide an electron cyclotron resonance (ECR) ion source, LBL will provide a radio-frequency quadrupole (RFQ) acceleration stage similar to the one installed recently at the Bevalac, and CERN will upgrade the LINAC and beam monitoring capabilities at the PS and SPS. Taken in combination with the ongoing program at the Bevalac, with the very heaviest ions available, this program of light ion experiments at much higher energies will provide a glimpse of what may be anticipated at accelerators such as VENUS, the Tevalac, or the Relativistic Nuclear Collider, which are still on the drawing boards.

SuperHILAC Research Program

R.M. Diamond

The SuperHILAC remains the only accelerator in the U.S. capable of producing very heavy ions up to Pb and U at energies above the Coulomb barrier. In the past year the machine has worked well, particularly the new ABEL injector, and has furnished 2220 hours on target to experimenters, which is 79% of the scheduled time. Beams used ranged from ^{20}Ne to ^{238}U. Electrical power costs are not such a critical item as they were 1–2 years ago, and we can hope for stable 8 months' per year operation in the coming period. The first two RF amplifiers of a new design have been put into use, and when all the new amplifiers are in place, they will provide a more efficient operation, conserving power and permitting a larger duty cycle. Currently the duty cycle is 15–25%, depending upon the beam, and an increase is very desirable for the more complex coincidence experiments now being performed and planned. The time-shared mode of operation with two injectors continues as the normal option; 32 pulses/second go to the principal SuperHILAC user, 2 pulses/second of a different beam are injected into the Bevatron, and 2 pulses/second of either beam (at a different energy) go to a parasite user at the SuperHILAC.

A Program Advisory Committee meets twice a year to go over written proposals in order to select the best experiments to be performed during the next six-months' period. During the past year the committee has consisted of Prof. D. Fossan, State University of New York at Stony Brook, Chairman; Prof. K. Gelbke, Michigan State University; Dr. J. Randrup, Nuclear Science Division; Dr. J. Hardy, Chalk River Nuclear Laboratory; and Dr. S. Datz, Oak Ridge National Laboratory. Slightly less than half the time went to LBL groups, and just over half to outside users. The SuperHILAC is a National Facility open to all qualified research groups in the U.S. and Canada and collaborating groups in Europe and Asia. There is a Users' Association, and a SuperHILAC Users' Executive Committee that holds a monthly telephone conference to discuss the current state of the machine and to consider improvements in the operation and procedures and in the equipment and facilities, and to foresee and prevent any problems in the system as far as possible. The committee has been Prof. D. Cline, University of Rochester, Chairman, Prof. A. Mignerey, University of Maryland, and Dr. M. Blann, Lawrence Livermore National Laboratory, elected by the members; and Drs. J.M. Nitschke and R.M. Diamond of the Nuclear Science Division, appointed by the LBL Director. Dr. D.J. McDonald has served as secretary for both committees, and has done a fine job as User Liaison Officer.

The experimental program at the SuperHILAC can be divided into four main categories: heavy-ion reaction mechanisms (~50%), atomic physics (21%), nuclear structure (17%), and exotic nuclei (12%).

Heavy Ion Reaction Mechanisms

The reaction mechanism work remains the backbone of the research program, and is carried out by five outside consortia and one LBL group. One area of investigation involves studies of the energy and angular distributions of protons and alphas emitted from heavy ion fragments and what they tell about the emitting source, that is, whether it is the combined di-nuclear system before separation (possibly its neck) or the deep-inelastic or fusion fragments after breakup. Another study involves the yield of larger fragments, He through O, emitted from deep-inelastic fragments, to give the same sort of information plus the Q-value and Z-dependence of the complex particle emission, and, from a comparison of in-plane and out-of-plane correlations, to determine the deep-inelastic fragment angular momentum and alignment. Still another experiment proposes to answer the question of how the excitation energy is divided between asymmetric deep-inelastic fragments (^{56}Fe + ^{236}U $\rightarrow$) as a function of the inelasticity by measuring the mass asymmetry of the sequential fission of

the heavy fragment. A very different type of experiment hopes to establish an empirical relationship between the reaction time (T) and the total kinetic energy loss ($-Q$) in a deep-inelastic reaction. This is to be done by determining the K-shell ionization probability of the fragments as a function of $-Q$ and comparing this relationship $P_K(-Q)$ with that obtained from atomic collision theory $P_K(T)$. The resulting correlation between T and $-Q$ can then be compared with nuclear model calculations.

Atomic Physics

Atomic physics experiments have gradually grown to take over the next largest block of time. This is because the use of heavy ion beams to furnish highly charged heavy ions has been a major contributor to the renaissance of atomic spectroscopy. The best way yet found to furnish highly charged ions with low kinetic energy is to ionize the appropriate gas with a beam of highly charged heavy ions of adequate intensity. Gold (+53) and uranium (+58) beams of 4–5 MeV/nucleon appear to be optimum for this purpose, and intensities of 1 eμ amp are now available. The resulting spectra from the excited target ions will include a wide distribution of charge states all at the same low ($\sim$1 eV) velocity and at the same spatial location. This makes possible very accurate energy calibrations with the known lower-charge-state species present. Fine-structure splittings in H-like (Lamb shift) and He-like ions have been studied up to Ar, and these measurements provide stringent tests of Q.E.D. in a strong Coulomb field and of relativistic wavefunctions. Lamb-shift measurements can also be carried out by the technique of beam-foil spectroscopy. Such a measurement on H-like Fe has indicated a possible discrepancy in the value of the spin-orbit splitting, perhaps due to the use of solid C foils. So experiments are planned to study this situation by comparing gas and solid strippers for a number of heavy H-like ions. Another experiment is studying the velocity dependence of electron capture by low-energy Ne^{9+} ions from rare gas targets; the Ne ions are again produced by irradiating Ne gas with a Au beam. They are drawn out of the target cell and passed through a velocity spectrometer. The velocity-selected ions are then passed through the target gas where electron capture occurs. The capture cross section is determined by the attenuation of the beam as a function of the target-gas pressure. This method yields results for ion velocities $\sim$50 times smaller than in previous experiments, and is of importance to fusion research and has astrophysical implications. Finally, there is a beam-foil spectroscopic program to determine the energies and lifetimes of the $\Delta n=0$ and $\Delta n=1$ transitions in Ne-like Ho and Xe. These will test the accuracy of relativistic calculations of these wave functions, in which the relativistic contributions are very large. The results are of interest to studies of high-temperature and high density plasmas and to the possibilities of producing x-ray lasers.

Nuclear Structure

Nuclear structure studies primarily make use of the high-Z projectiles available at the SuperHILAC (Xe and Pb) to multiple Coulomb-excite target nuclei, or by use of inverse reactions, to obtain large recoil velocities. The latter use is to measure lifetimes for both discrete and continuum γ rays by Doppler-shift techniques or to measure g-factors of short-lived states. In favorable cases magnetic moments can be determined by perturbed angular distribution experiments employing the enormous transient fields that act on rapidly moving nuclei in ferromagnetic materials (iron and cooled gadolinium). With the new least-square-fit Coulomb excitation computer code developed by Prof. Cline (University of Rochester) and his colleagues, model-independent moments, both transition and static, can be determined if enough experimental data are available from a variety of projectiles from Pb down to O and for a wide range of scattering angles. These moments provide severe tests of current theoretical models.

Exotic Nuclei

The study of exotic nuclei focuses on isotopes of elements beyond uranium and on nuclei far from stability approaching the neutron and proton drip lines. Two major attempts to produce nuclei of a superheavy element by means of (several) week-long ^{48}Ca irradiations of a ^{248}Cm target were carried out by a collaboration of LBL and Gesellschaft für Schwerionenforschung (GSI) and Marburg scientists in late 1982 at the SuperHILAC and early 1983 at the UNILAC. No events ascribable to superheavy element decay were found, with upper limits of the order of 50 picobarns for lifetimes of milliseconds to years. Either new techniques or heavier targets or both will be necessary to achieve significantly better results in this search. The on-line separator OASIS and its new spectroscopy laboratory is in full operation and has produced nearly a dozen new β-delayed proton emitters. Lifetimes, mass and element numbers, and proton spectra have been obtained, and more detailed studies of the coincident γ-ray spectra are in progress.

Except for atomic physics, all the above programs are treated in more detail in this report. Some are expanding, some are scaling down, but the overall picture is a dynamic one with plans for continuing and new experiments in the coming year.

PART III: EXPERIMENTS

Nuclear Structure

Discovery of Beta-Delayed Two-Proton Radioactivity: ^{22}Al*

M.D. Cable, J. Honkanen,† R.F. Parry, S.H. Zhou,‡ Z.Y. Zhou,§ and Joseph Cerny

Two-proton radioactivity has long been proposed (see the review by Gol'danskii[1]) as a potential mode of radioactive decay for some nuclei far from the valley of beta stability. More recently, Gol'danskii has also discussed beta-delayed two-proton radioactivity[2] and has suggested some potential candidates for this decay mode, among them light mass nuclides in the odd-odd, $T_z = -2$ series. The recent discovery[3] of the first known member of this series, ^{22}Al, and the subsequent observation of an additional member, ^{26}P, made these two nuclei prime candidates for a search for this new mode of decay. We would like to report here the discovery of beta-delayed two-proton emission from ^{22}Al. ^{22}Al is an ideal case for investigation since earlier work on its decay[3] by beta-delayed single-proton emission accurately located the T=2 analog state in its ^{22}Mg daughter (fed by the superallowed branch in ^{22}Al beta-decay), concomitantly showing that this state is unbound to two-proton emission by 6.118 MeV.

^{22}Al($t_{1/2}$ ~ 70 ms) was produced via the ^{24}Mg(^{3}He,p4n)^{22}Al reaction with 110 MeV ^{3}He^{+2} beams of 3–7 μA intensities from the 88-Inch Cyclotron. A helium jet system was used to transport the activity to a counting chamber with a high geometry, three element particle telescope (with detectors denoted "ΔE1", "ΔE2", and "E") capable of identifying and observing two protons simultaneously. The "ΔE1" (24 μm) and "ΔE2" (155 μm) detectors were fabricated such that the surface contact on one side was divided down the center, effectively producing two detectors on the same silicon wafer.

The two-dimensional, proton-proton coincidence spectrum obtained following a 690 mC bombardment is shown in Fig. 1(a); the summed proton energy spectrum appears in Fig. 1(b). Laboratory energies of the two-proton total energy peaks shown in Fig. 1(b) are 4.139 ± 0.020 MeV and 5.636 ± 0.020 MeV. Exact corresponding center-of-mass energies depend on the mechanism of two-proton emission; however, these peaks can be shown to correspond to transitions from the ^{22}Mg T = 2 analog state (fed by the superallowed beta decay of ^{22}Al) to the ground state and first excited state of ^{20}Ne (see Fig. 2).

Two possible decay mechanisms are A) single-step ^{2}He emission[1,2] (two protons coupled to a $^1S_0$ configuration) or B) a sequential two-step process proceeding through an intermediate state (or states) in ^{21}Na. Given the currently limited statistics, the proton-proton coincidence spectrum shown in Fig. 1(a) cannot conclusively distinguish the mechanism; the observed variation in yields and energies could result from either a ^{2}He type distribution or sequential decay through several states in ^{21}Na or both. Work is in progress to determine the two-proton decay mechanism(s) of ^{22}Al.

Footnotes and References

*Condensed from LBL-15453, Phys. Rev. Lett. **50**, 404 (1983).

†On leave from: Dept. of Physics, University of Jyväskylä, Finland.

‡On leave from: Institute of Atomic Energy, Beijing, China.

§On leave from: Dept. of Physics, Nanking University, China.

1. V.I. Gol'danskii, Usp. Fiz. Nauk **87**, 255 (1965); Sov. Phys. Uspekhi **8**, 770 (1966).
2. V.I. Gol'danskii, Pisma Zh. Eksp. Teor. Fiz **32**, 572 (1980); JETP Lett. **32**, 554 (1980).
3. M.D. Cable, J. Honkanen, R.F. Parry, H.M. Thierens, J.M. Wouters, Z.Y. Zhou, and J. Cerny, Phys. Rev. **C26**, 1778 (1982).

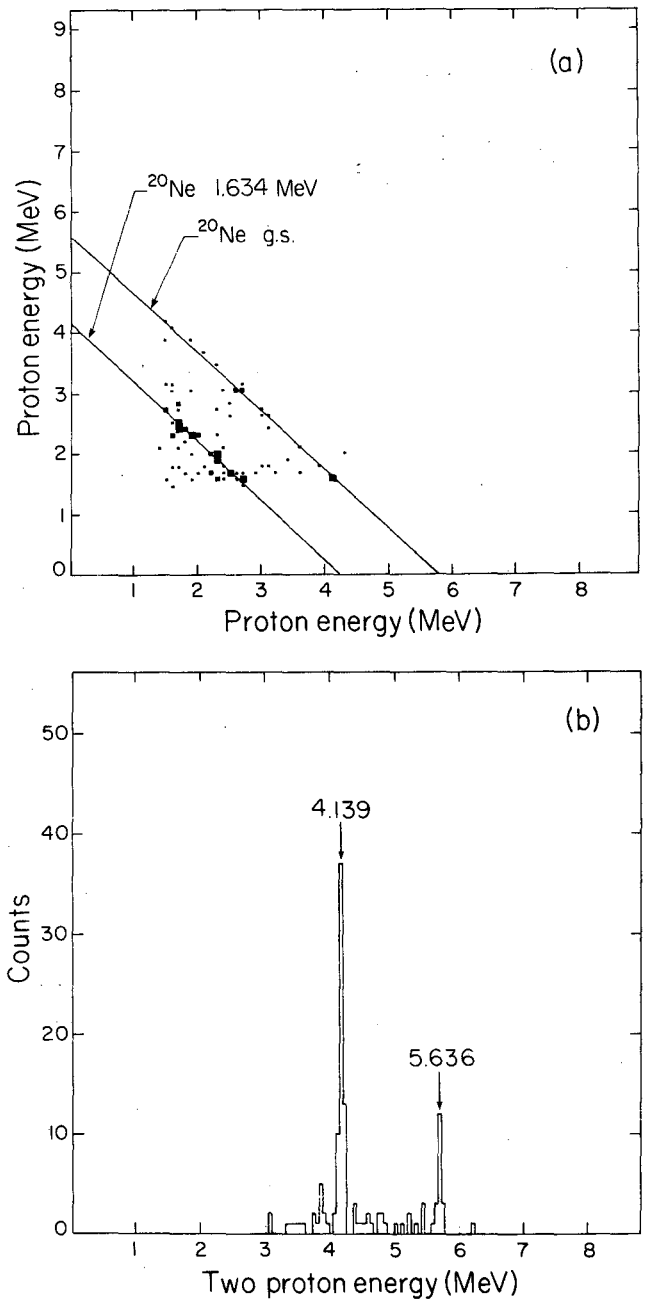

Fig. 1. (a): A proton-proton coincidence spectrum following the beta decay of ^{22}Al (E_p^L vs. E_p^R). Kinematic lines corresponding to decay to the ground state and to the first excited state of ^{20}Ne are shown. Increasing square size corresponds to increasing number of counts.
(b): A summed energy spectrum for the two-proton coincidences in (a): ($E_p^L + E_p^R$). XBL 8211-7365

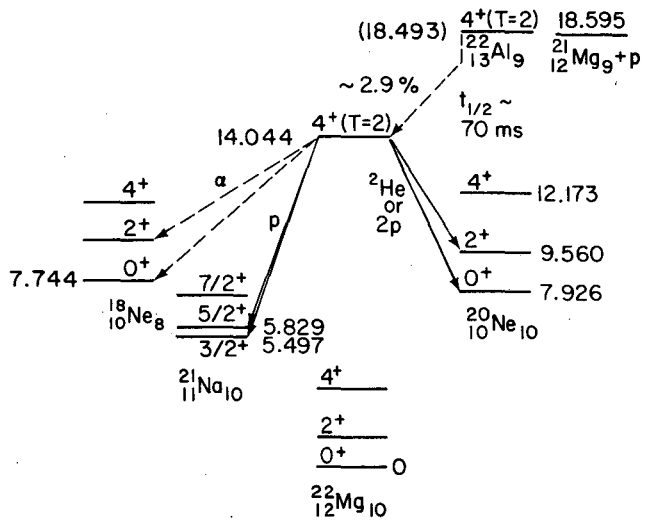

Fig. 2. Proposed partial decay scheme for ^{22}Al.
XBL 829-4626

Beta-Delayed Two-Proton Decay of ^{26}P*

J. Honkanen,[†] M.D. Cable, R.F. Parry, S.H. Zhou,[‡] Z.Y. Zhou,[§] and Joseph Cerný

Beta-delayed emission of two protons has recently been observed for the first time[1] in the decay of ^{22}Al. Observation[2] of beta-delayed single proton emission from another odd-odd $T_z = -2$ nucleus, ^{26}P, showed this nucleus to exist and furthermore indicated that the analog state in ^{26}Si is unbound to two-proton emission by 5291 keV. We would like to report here the observation of beta-delayed two-proton emission from ^{26}P. As opposed to the complex beta-delayed two-proton emission of ^{22}Al, the ^{26}P decay proceeds by a relatively simple mechanism and, as such, is well characterized by the experiments described below.

^{26}P ($t_{1/2} \sim 20$ ms) was produced via the $^{28}Si(^{3}He,p4n)^{26}P$ reaction by bombarding a natural silicon target with 110 MeV ^{3}He beams from the 88-Inch Cyclotron. A helium-jet system was used to transport the recoil atoms through a 70 cm long capillary into a measuring chamber where a specially constructed three element (14 μm $\Delta E1$, 170 μm $\Delta E2$, and 500 μm E) solid state particle telescope was used to observe beta-delayed protons. The ΔE detectors were fabricated such that the surface contact on one side was divided down the center, effectively providing two, two-element ($\Delta E1$ and $\Delta E2$) telescopes capable of detecting low-energy (1.0–4.5 MeV) protons in coincidence. The average angle between these telescopes was 40° with each side subtending 4.5% of 4π sr.

Fig. 1 is a summed energy spectrum of the coincident protons observed in the "left" and "right" low energy telescopes with a 20ns coincidence window. In addition to two-proton groups of ^{22}Al, which were also produced in this bombardment, a new group of 4.914 MeV was observed. This has been assigned to the decay from the ^{26}Si T = 2 analog state (fed by superallowed beta decay of ^{26}P) to the ground state of ^{24}Mg. An arrow at low energy indicates the expected location of the two-proton group corresponding to decay to the ^{24}Mg first excited state.

Possible decay mechanisms for the emission of the two protons can be categorized as sequential or simultaneous emission. Sequential emission is a two-step process in which a proton is emitted to a level in an intermediate nucleus, which is unbound to subsequent emission of a second proton; therefore, the individual proton spectra should show specific proton groups corresponding to these transitions. The individual proton spectra which comprise the 4.914 MeV two-proton group are relatively simple spectra with coincident groups at laboratory energies of 3699 ± 15 keV and 1210 ± 15 keV, indicating a sequential decay through a single intermediate state. Because the emission of the first proton causes a kinematic shift to the laboratory energy of the second proton (since the second proton is emitted from a recoiling nucleus), it is possible to determine the order of the decay by measuring the proton spectra at two different angles. Results of a second experiment performed with two separate telescopes (23 μm $\Delta E1$, 270 μm $\Delta E2$, 1000 μm E) mounted at 120° and each subtending 3.5% of 4π sr show a kinematic shift for the 1.2 MeV individual proton group, which indicates that this group corresponds to the second proton in the sequential process. Thus the intermediate state in ^{25}Al would lie at 3714 ± 21 keV excitation and might correspond to the known $\frac{7}{2}-$ level at 3695.7 ± 0.5 keV. The proposed decay scheme for ^{26}P two-proton emission is shown in Fig. 2.

Further experimentation is of interest to obtain information about the angular correlation of the two protons and to attempt to observe the decay to the ^{24}Mg first excited state. For this decay, ^{2}He emission is allowed and so might contribute. Comparison of the results of the relatively simple ^{26}P decay to the more complex spectra obtained from ^{22}Al decay is also proceeding.

*Condensed from LBL-16606, Phys. Lett. **133B**, 146 (1983).
†On leave from: Dept. of Physics, University of Jyväskylä, Finland.
‡Present address: Institute of Atomic Energy, Beijing, China.
§On leave from: Dept. of Physics, Nanking University, China.

1. M.D. Cable, J. Honkanen, R.F. Parry, S.H. Zhou, Z.Y. Zhou and J. Cerny, Phys. Rev. Lett. **50**, 404 (1983).
2. M.D. Cable, J. Honkanen, R.F. Parry, S.H. Zhou. Z.Y. Zhou and J. Cerny, Phys. Lett. **123B**, 25 (1983).

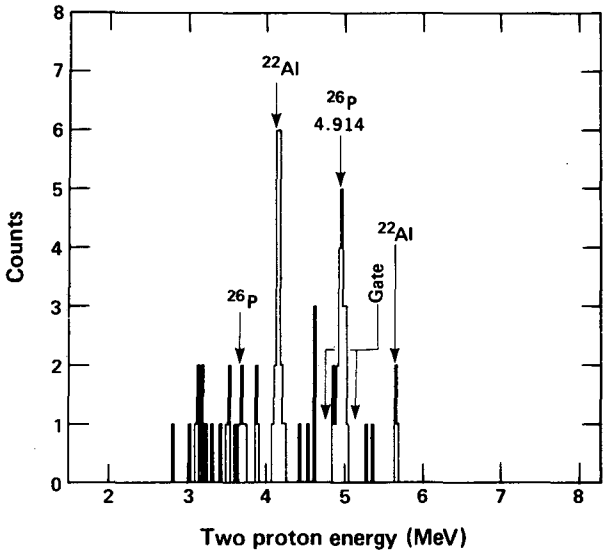

Fig. 1. A summed energy spectrum for two-proton coincidences arising from 110 MeV ^{3}He bombardment of ^{28}Si. The spectrum was measured with telescopes placed at an average separation angle of 40°.
XBL 831-1062

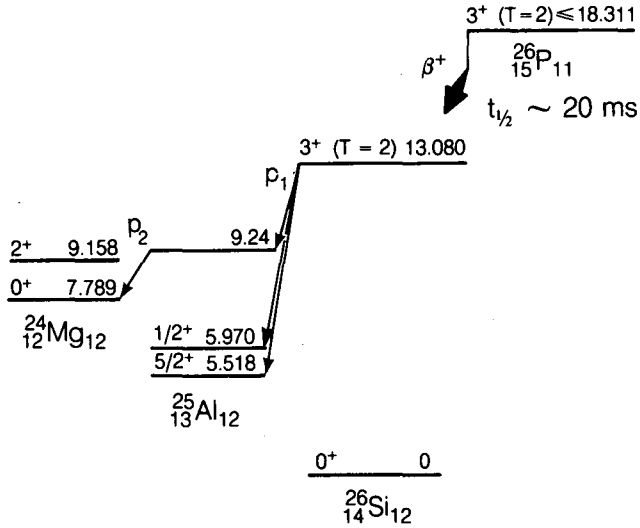

Fig. 2. Proposed decay scheme for the beta-delayed two-proton emission of ^{26}P. XBL 837-1889

Wide Angle Measurement of Beta-Delayed Two-Proton Radioactivity of ^{22}Al

M.D. Cable, J. Honkanen, J.E. Reiff, E.C. Schloemer, S.H. Zhou,† Z.Y. Zhou,‡ and Joseph Cerny*

With the discovery of beta-delayed two-proton radioactivity[1,2] in ^{22}Al and ^{26}P, details of the mechanism of two-proton emission became of immediate interest. The original measurement of each isotope was made with a specially constructed particle telescope described in ref. 1. This telescope was capable of observing proton-proton coincidences at relative angles of 0–70° (with varying efficiencies), and with a mean angle of ~40°. A second measurement at the widest practical angle was desirable in order to obtain more information on the angular correlation of the two protons. As discussed below, this measurement provides some information on the mechanism of two-proton emission.

The wide angle apparatus shown in Fig. 1 was constructed such that two separate telescopes (4.5% of 4π sr each) observe the collection site on the edge of a slowly rotating Al wheel (see ref 1. for more details of the helium jet techniques used). These telescopes observe angles from 70–170° with a mean angle of ~120°. Beta-delayed two-proton decay proceeding via ^{2}He emission is not expected to be observed in this arrangement, since in that case the two protons are expected to be emitted at small relative angles (see ref. 1). Sequential emission, however, should not only be observed but should show an easily measureable kinematic shift (relative to the first measurement) in the energy of the second proton since this proton is emitted from a recoiling nucleus and so has a laboratory energy dependent upon the relative proton angle.

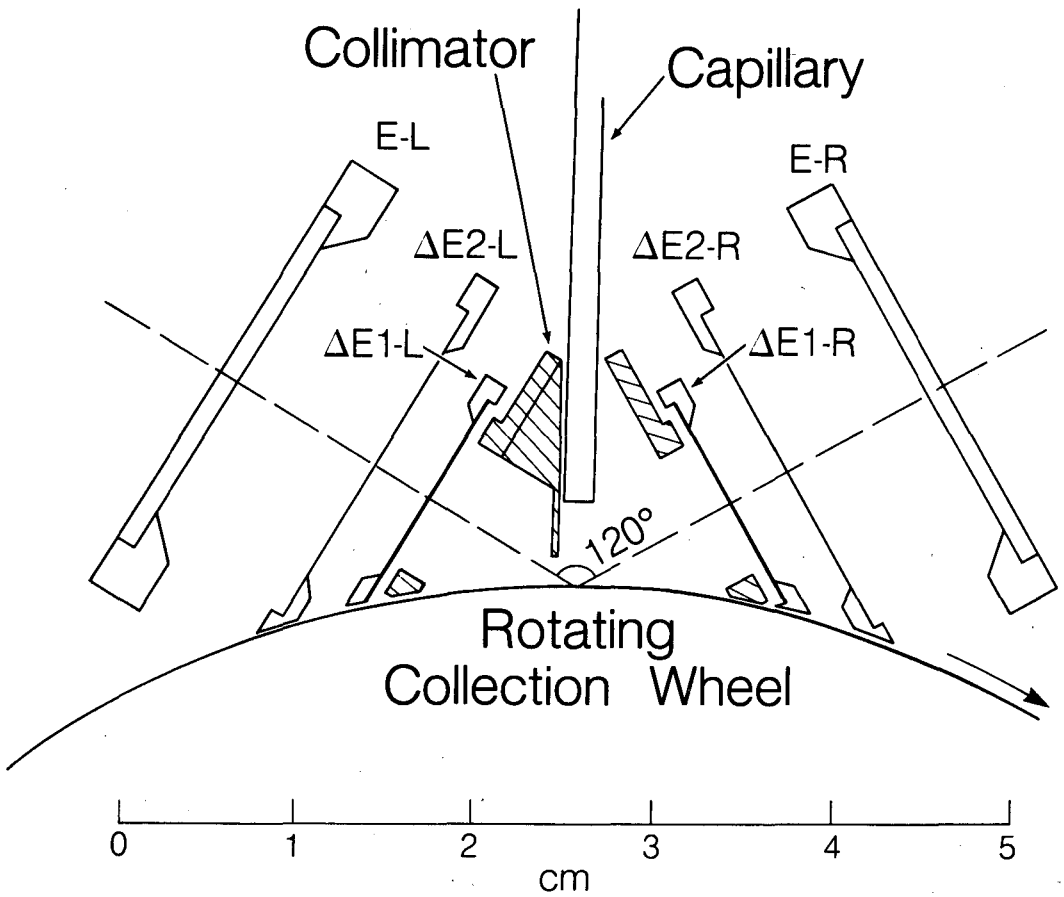

Fig. 1. Apparatus for wide angle two-proton measurements. Activity is transported via a helium jet through the capillary to the collection wheel. XBL 8311-6823

Fig. 2 presents a two-proton summed energy spectrum from experiments at both wide and narrow angles for ^{22}Al. It can be determined that the wide angle spectrum shows the kinematic shift expected for sequential decay; although this shows that sequential decay is indeed a major decay mode, the results do not eliminate the possibility that ^{2}He emission may also be present in the narrow angle data. Detailed studies of the wide and narrow angle individual proton spectra are currently being carried out in an effort to characterize totally this decay. A wide angle measurement has also been made for ^{26}P (see ref. 2) where ^{2}He emission is spin-parity forbidden, and results agree with the expected sequential mechanism.

Footnotes and References

*Present address: Department of Physics, University of Jyväskylä, Finland.

†Present address: Institute of Atomic Energy, Beijing, China.

‡On leave from: Department of Physics, Nanking University, China.

1. M.D. Cable, J. Honkanen, R.F. Parry, S.H. Zhou, Z.Y. Zhou, and J. Cerny, Phys. Rev. Lett. **50**, 404 (1983).
2. J. Honkanen, M.D. Cable, R.F. Parry, S.H. Zhou, Z.Y. Zhou, and J. Cerny, LBL-16606, Phys. Lett. **133B**, 146 (1983).

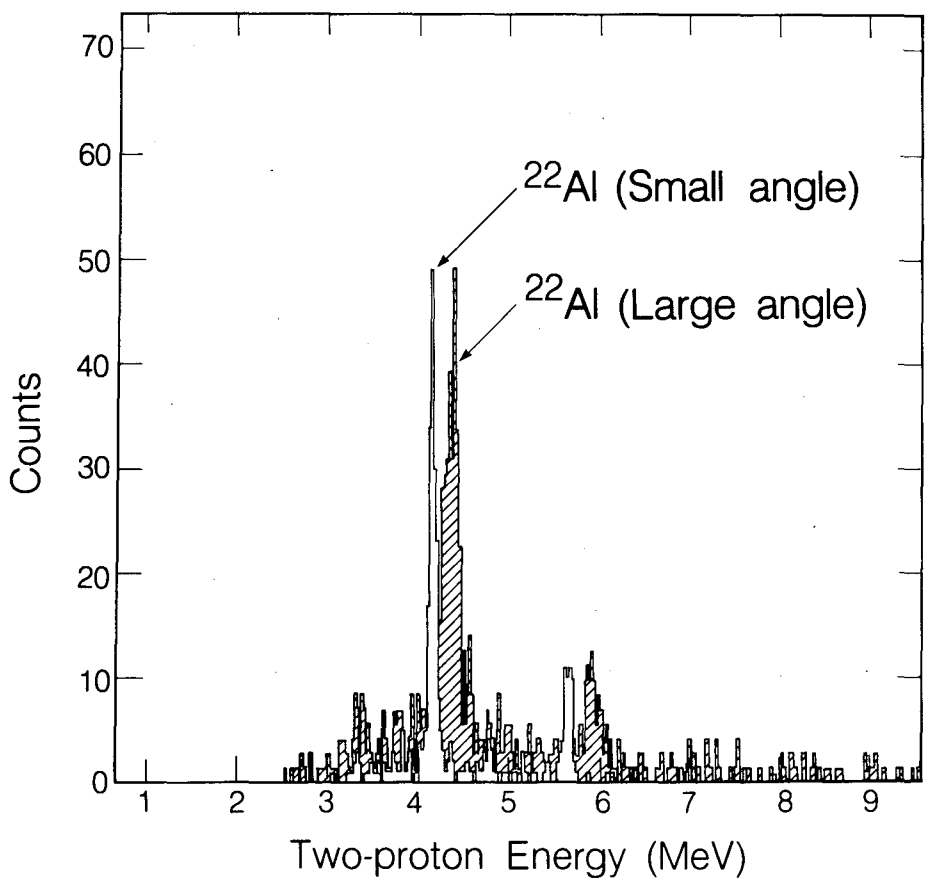

Fig. 2. Two-proton summed spectra for ^{22}Al. Data obtained at both narrow and wide angles are shown. Peak height in the wide angle spectrum is normalized to the narrow angle measurement. XBL 8312-2569

Beta-Delayed Proton Emission Observed in New Lanthanide Isotopes

J.M. Nitschke, W.-D. Zeitz, P.A. Wilmarth, P.K. Lemmertz, J.A. Honkanen†*

We previously reported the discovery of several new beta-delayed proton emitters in the lanthanide region. The masses of these new isotopes were uniquely determined by the on-line isotope separator OASIS[1] and the Z-values were inferred from half-lives, mass-energy systematics and cross sections. A major addition to OASIS, which is described in detail in a separate contribution to this report, now allows us to obtain unique Z-identifications of new isotopes by observing characteristic x-rays in coincidence with beta-delayed protons. The experimental procedure is as follows: the isotope under study is passed through a slit in the focal plane of the isotope separator and transported via ionoptical devices to a low background spectroscopy laboratory. Here the isotope is deposited on a fast-cycling tape and moved within 65 ms to an array of detectors which register protons, α- and β-particles, x-rays and γ-rays. For neutron deficient isotopes two classes of events are of interest: (1) protons (or alphas) in coincidence with positrons, γ's, and x-rays, and (2) positrons and x-rays in coincidence with γ's.

This report covers only events of the first category. The second class of events yields information about members of the isobaric chain which are closer to the valley of beta stability and decay by positron emission, electron capture and γ-decay.

The following new results about beta-delayed proton emitters at different masses have been obtained.

A=143: This mass chain was investigated because $^{143}Ho_{67}$ has been predicted to be a ground state proton emitter.[2] We previous reported the observation of a beta-delayed proton activity with 4.1 s half-life which we assigned to $^{143}Dy_{66}$.[3] This assignment was based on the good agreement with the predicted half-life of 3.1 s from the gross theory of beta decay and a predicted ($Q_{EC} - S_p$) value of 7.56 MeV. (Q_{EC} = Q value for electron capture, S_p = proton separation energy). We have repeated this experiment with our new tape system and observed a low background x-ray spectrum of K_α - and K_β - x-rays from Tb_{65} in coincidence with protons. These protons should be properly called "electron capture delayed protons," because it is the capture of a K-electron which subsequently gives rise to the observed x-ray that is emitted when the K-vacancy is filled from the L- or M-shell of the Tb_{65} atom. This method yields an unambiguous Z-identification of the proton precursor, in this case $^{143}Dy_{66}$. We have also observed γ-rays of 511, 556 and 692 keV in coincidence with protons. These energy values do not, however, correspond to the expected known transitions between members of the rotational band in the daughter nucleus $^{142}Gd_{64}$. The events at 556 keV could be generated as the sum of the 511 annihilation radiation and the K_α x-rays of Tb_{65}. The origin of the 692 keV peak is as yet unknown. Table I summarizes this and two earlier experiments at mass 143. The weighted average for the half-life of the $^{143}Dy_{66}$ delayed proton precursor is $4.1 \pm .3$ s. We have also observed a host of γ-lines in coincidence with positrons. Their half-lives as well as the half-life of the high energy positrons is on the order of 10 s, indicating that they are probably associated with the new isotope $^{143}Tb_{65}$. The predicted half-life for $^{143}Tb_{65}$ is 10 s, and it is not expected to have a significant proton branch because of its low ($Q_{EC} - S_p$) value of 3.50 MeV. The proton-γ and positron-γ coincidence data are still being evaluated.

A=141: The reactions leading to isobars in this mass chain are listed in Table I. Three unknown isotopes, $^{141}Dy_{66}$, $^{141}Tb_{65}$ and $^{141}Gd_{64}$, can be produced with measurable cross sections. $^{141}Dy_{66}$ has the highest calculated ($Q_{EC} - S_p$) value (9.15 MeV), while the other two are 4.98 and 4.96 MeV; the predicted half-lives are 1, 4, and 11 s respectively. Two experiments with tape cycles of 5 and 50 s were carried out. In both cases Tb_{65} and Eu_{63} but no Gd_{64} x-rays in coincidence with protons were observed. The shorter cycle time showed a larger

Tb/Eu x-ray ratio than the 50 s cycle; it also produced a higher average proton energy. Protons in coincidence with Tb_{65} x-rays showed higher energies than protons in coincidence with Eu_{63} x-rays, and the half-life of the Tb_{65} related protons seems to be shorter than the protons coincident with Eu_{63} x-rays. These observations lead us to the conclusion that we are dealing with *two* new beta delayed proton emitters $^{141}Dy_{66}$ and $^{141}Gd_{64}$. No evidence for proton emission from $^{141}Tb_{65}$ was found. From data of the 5 s tape cycle a half-life for *all* observed protons of 1.0 s was calculated. The arguments presented above indicate that this should be due mostly to $^{141}Dy_{66}$ with a small, as yet unknown contribution from $^{141}Gd_{64}$. The half-life of protons in coincidence with Tb_{65} x-rays is approximately 0.7 s with a large error due to poor statistics. Beta-, gamma- and x-ray coincidence data which might address the question of an isometric state in $^{141}Gd_{64}$ have not yet been evaluated.

A=139, 137, and 127: These mass chains were investigated before the completion of the OASIS tape system. Only a dual proton telescope as described in the previous annual report was used to measure half-lives and proton energy spectra. The reaction parameters and the principal results are shown in Table I. The Z-identification of the isotopes is based on a comparison between the observed and predicted values of three parameters: (1) the half-life calculated from the gross theory of β-decay with Q_{EC}-values from the mass table by Liran and Zeldes,[4] (2) the production cross section calculated with the code ALICE, and (3) the predicted ($Q_{EC} - S_p$) value as a function of Z for a known A. The motivation for selecting A=137 and 127 was predictions[2] that $^{137}Tb_{65}$ and $^{127}Pm_{61}$ should be proton ground state emitters.

Table I.

Target-projectile combinations and reaction channels for the production of beta-delayed proton precursors. E_{lab} = bombarding energy, E_p = observed proton energy range, $\overline{E_p}$ = centroid of the proton spectrum, and $T_{½}$ = experimental and calculated half-lives.

Reaction	E_{lab} (MeV)	Precursor	E_p (MeV)	$\overline{E_p}$ (MeV)	$T_{1/2}^{exp}$(s)	$T_{1/2}^{calc}$(s)	x-ray	γ-lines coincident with protons (keV)
$^{92}Mo(^{56}Fe,\alpha n)$	275	^{143}Dy	2.2-6.5	4.2	3.2± .6	3.1	$K_{\alpha,\beta}$(Tb)	511,558,652
$^{92}Mo(^{56}Fe,\alpha n)$	275	^{143}Dy	2.0-5.6	4.1	3.7± .7	3.1	-	-
$^{92}Mo(^{58}Ni,\alpha 2pn)$[a]	292	^{143}Dy	2.1-6.4	4.2	4.3± .3	3.1	-	-
$^{92}Mo(^{54}Fe,\alpha n)$	274	^{141}Dy	2.4-6.1	3.9	1.0± .2	1.0	$K_{\alpha,\beta}$(Tb)	-
$^{92}Mo(^{54}Fe,4pn)$	274	^{141}Gd	-	-	-	11.0	$K_{\alpha,\beta}$(Eu)	-
$^{50}Cr(^{92}Mo,2pn)$	385	^{139}Gd	2.1–5.5	3.8	4.9±1.0	6.5	-	-
$^{50}Cr(^{92}Mo,\alpha n)$	480	^{137}Gd	2.2–6.6	3.8	7±3	2.0	-	-
$^{92}Mo(^{40}Ca,\alpha n)$	213	^{127}Nd	2.0–6.4	3.7	1.9± .4	1.9	-	-
$^{92}Mo(^{36}Ar,\alpha n)$	196	^{123}Ce	2.0–5.8	3.6	3.8± .2[b]	2.7	$K_{\alpha,\beta}$(La)	197,373,513
$^{92}Mo(^{36}Ar,\alpha pn)$	205	^{122}La	2.0–4.6	3.4	8.7±.7	4.0	$K_{\alpha,\beta}$(Ba)	-
$^{58}Ni(^{64}Zn,pn)$	253	^{120}La	2.1–5.6	3.7	2.8± .2	1.2	$K_{\alpha,\beta}$(Ba)	237

[a]Previously reported experiment. [b]Weighted average.

No ground state proton emission characterized by sharp proton lines was found, however. In the case of $^{137}Gd_{64}$ a significant discrepancy exists between the measured and the calculated half-life and it can not be excluded that we are observing an isomeric state associated with the odd-A, N=73 configuration. Cross bombardments with $^{92}Mo_{42}$ + $^{54}Fe_{26}$ in the case of $^{139}Gd_{64}$ and $^{40}Ca_{20}$ + $^{90}Zr_{40}$ in the case of $^{127}Nd_{60}$ were carried out to substantiate the respective Z-assignments.

A=123: In an experiment in which $^{92}Mo_{42}$ was bombarded with $^{36}Ar_{18}$ an intense proton activity was observed. The proton energy spectrum (Fig. 1) is characteristic for beta-delayed proton decay. Due to the high proton production rate a good spectrum of x-rays in coincidence with protons was obtained (Fig. 2). The energies of the two x-ray lines are in excellent agreement with the literature values for La_{57} K_α and K_β radiation, which uniquely identifies the new isotope as $^{123}Ce_{58}$. The half-life obtained

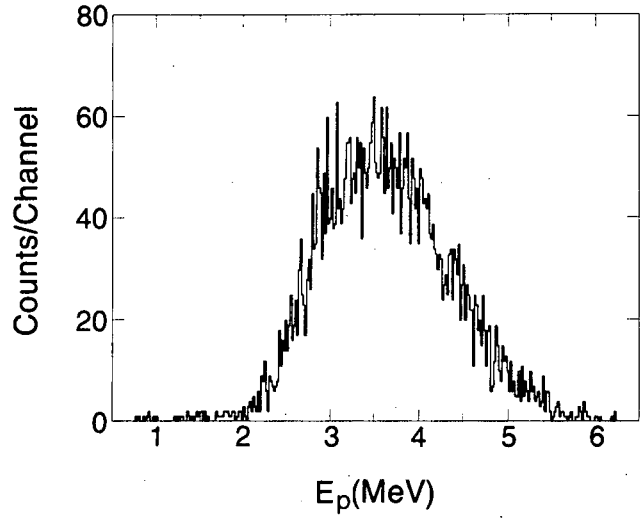

Fig. 1. Beta-delayed proton spectrum observed in the reaction $^{92}Mo(^{36}Ar,\alpha n)^{123}Ce$. XBL 8312-6724

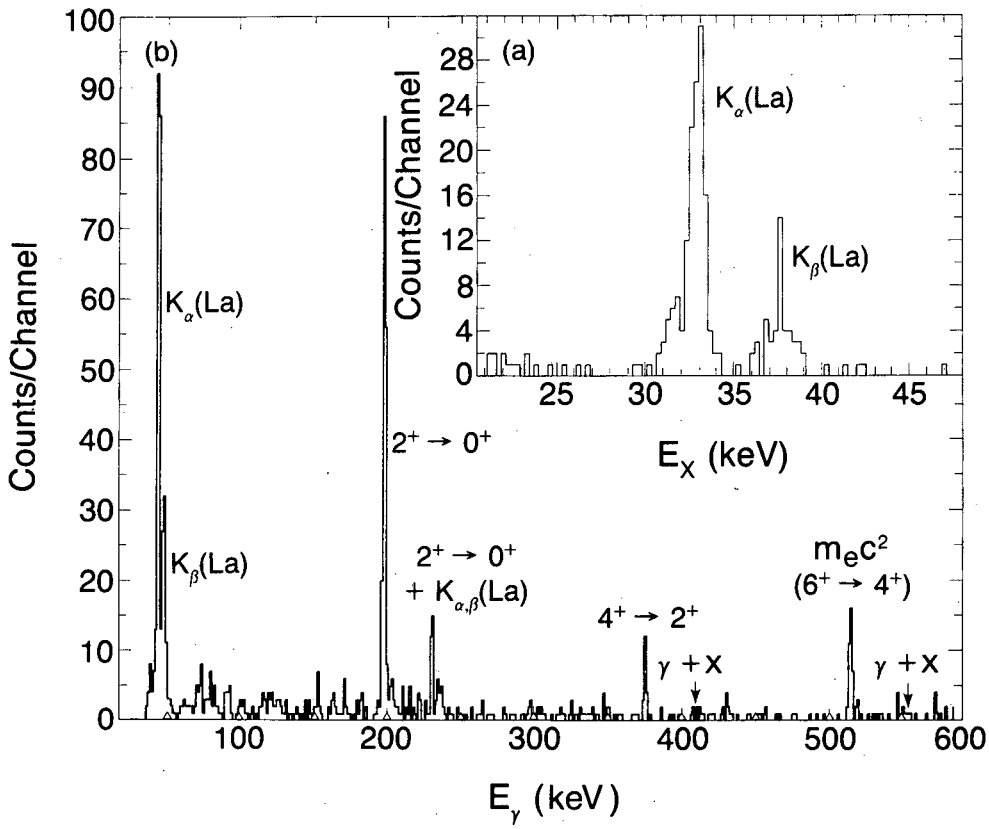

Fig. 2. γ- and x-ray (insert) spectra observed in coincidence with beta-delayed protons from ^{123}Ce.
XBL 8312-6725

from the proton decay data is 3.9 s; the decay of the La_{57} x-rays gives 3.3 s. Additional information about the decay of $^{123}Ce_{58}$ was obtained from a γ-spectrum measured in coincidence with the protons. It clearly shows that the proton decay populates the known rotational 2^+, 4^+, and perhaps 6^+ levels in $^{122}Ba_{56}$ (Fig. 2). Since some of the proton decay is subsequent to electron capture in $^{123}Ce_{58}$, several weak lines in the γ-spectrum are observed at energies which correspond to the sum of transition energies in $^{122}Ba_{56}$ and K_α and K_β x-ray energies in La_{57}. The $6^+ \rightarrow 4^+$ transition was exclusively observed as the x-γ-sum since the energy of the transition itself (513 keV) is too close to the annihilation energy of 511 keV to be resolved by the γ-detector. An evaluation of the branching for different rotational levels and a comparison with detailed calculations[5] will allow us to determine spin and parity of the new $^{123}Ce_{58}$ precursor.

A=122: Two experiments were performed at this mass value: one with the dual proton telescope where a total of about 1800 protons were recorded and one at the tape station where x-rays and gammas were measured in coincidence with protons. The x-ray spectrum in the second experiment shows only Ba_{56} K_α and K_β lines which leads us to the conclusion that the new beta-delayed proton precursor is $^{122}La_{57}$. The calculated low $(Q_{EC} - S_p)$ value of 5.50 MeV is reflected in the observed low upper proton energy of 4.6 MeV.

A=120: The systematics of $(Q_{EC} - S_p)(Z)$ for A=120 predicts that in this mass chain beta-delayed proton emission becomes possible for $Z \geqslant 56$. In an experiment with a ^{64}Zn beam and a ^{58}Ni target we observed beta delayed protons in coincidence with Ba_{56} x-rays and conclude that the new precursor is $^{120}La_{57}$.

The half-life of 2.8 s is in poor agreement with the calculated value of 1.2 s, and it can not be excluded that we are observing an isomer similar to the case of $^{118}Cs_{55}$. Additional evidence for the $^{120}La_{57}$ assignment comes from the γ-spectrum measured in coincidence with protons where we see a weak γ-line at 237 keV which corresponds to the $\frac{11}{2}^+ \rightarrow \frac{9}{2}^+$ (g.s.) transition in $^{119}Cs_{55}$.

The above experiment also served to test the separating power of OASIS which is defined as the intensity that an adjacent mass contributes to the mass under study: In the $^{120}La_{57}$ experiment a very strong delayed proton precursor is produced simultaneously at mass 119 ($^{119}Ba_{56}$). It generates characteristic γ-lines in the mass 119 β-γ coincidence spectrum but none of these lines are visible in the corresponding spectrum at mass 120 at a level of less than 1 part in 10^4.

A=119: At this mass chain only the known beta delayed proton procursor ^{119}Ba was observed with certainty. Its yield from the $^{58}Ni(^{64}Zn, 2pn)$ reaction was so overwhelming that a possible small proton branch from ^{119}La could not be detected.

Footnotes and References

*Present address: Hahn Meitner Institut für Kernforschung, Berlin, West Germany.

†Present address: Department of Physics, University of Jyväskylä, Finland.

1. J.M. Nitschke, Nucl. Inst. and Meth. **206**, 341 (1983).
2. W.F Feix and E.R Hilf, Darmstadt, IKDA 82/12.
3. J.M. Nitschke, M.D. Cable, and W.-D. Zeitz, Z. Phys. A **312**, 265 (1983).
4 S. Liran and N. Zeldes, Atomic Data and Nuclear Data Tables, **17**, 431 (1976).
5. P.K. Lemmertz, J.M. Nitschke, and J. Honkanen, Interpretation of Beta-Delayed Proton Spectra, this report.

Interpretation of Beta-Delayed Proton Spectra

P.K. Lemmertz, J.M. Nitschke, J. Honkanen, P.A. Wilmarth*

Beta-delayed proton emission is a two step process. In the first step, beta-decay of a precursor (Z, A) populates excited states in an intermediate nucleus (Z−1, A), whose energy levels can be unbound to particle emission. Then, in a second step, proton decay to levels in the final nucleus (Z−2, A−1) competes with gamma decay of the intermediate nucleus. Fig. 1 shows such a decay for the new isotope ^{123}Ce as precursor.

A calculation of beta delayed proton spectra has been described by Hornshoi *et al.*[1] The calculated shape of the proton energy spectra and the average intensity, defined as the number of protons per beta decay, are in many cases in good agreement with experimental data.

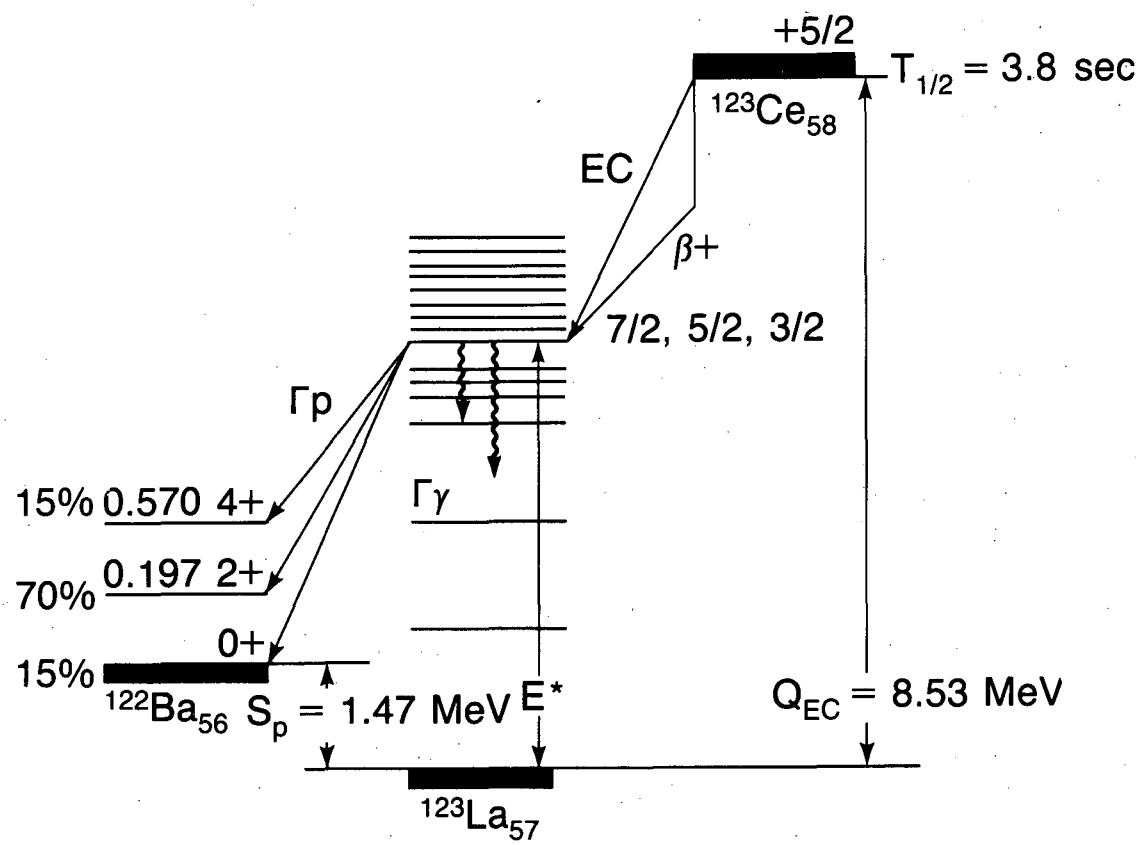

Fig. 1. The beta delayed proton decay of ^{123}Ce. The Q_{EC} and the proton separation energy S_p are taken from the Liran-Zeldes[2] mass table. The Ce ground state spin was determined from the calculated branching values to the excited states in the final nucleus ^{122}Ba. The branching is shown in percent. XBL 8312-6942

The main steps in this calculation† are as follows:

1. The population of levels in the intermediate nucleus is calculated with the statistical rate function for beta particle decay and electron capture. Allowed and first forbidden transitions are assumed to have the same energy dependence. The beta strength function is taken as constant above a certain cut-off value and the population of individual spins is taken into account by a statistical weight function.
2. The partial proton width is obtained from the transmission coefficients through the potential barrier. Shape and height of the potential are described by optical model parameters. Three different sets of parameters can be selected.
3. The level density and the gamma radiation width are calculated according to Gilbert and Camron.

Based on particle-X-ray coincidences, two improvements to this model have, however, been proposed:[3] (i) the level density formula by Gilbert and Camron is replaced by a back-shifted Fermi gas model and (ii) the gamma radiation width is calculated from photoabsorbtion cross sections.

The new prescriptions result in an increased level density and gamma emission width and hence the calculated proton spectra have their maxima shifted to particle energies about 0.5 MeV higher than calculated with Hornshoi's prescription.

For our data on ^{143}Dy and ^{123}Ce the "improved" calculations lead to a poorer agreement with the experimental spectra as long as the beta strength function is held constant. We have therefore introduced a resonance structure in the beta strength function based on the beta strength calculated within the frame of the RPA approximation.[4] Fig. 2a shows the result of a calculation for ^{123}Ce. Unlike the case discussed in ref. 5, it was not possible to fit the asymmetric shape of the proton spectra (Fig. 2b) with a single gaussian. Therefore, each of the major transitions was represented by a gaussian with the area equal to the transition strength and a FWHM of 1.3 MeV. A constant equal to 10% of the highest peak was also added to the beta strength composed of multiple gaussians. Fig. 2b shows the calculated proton spectrum. It can be seen that the smooth part of the spectrum is well reproduced. Calculations are under way to reduce the width of the gaussians in order to account for the fine structure observed in several spectra of other beta delayed proton emitters.

Nilssen model calculations for the ^{123}Ce predict a spin of $\frac{5}{2}+$ with a $\frac{5}{2}-$ state lying close by. Our measured proton branches to the rotational levels in the final nucleus ^{122}Ba are in good agreement with this result.

We are indebted to P. Möller for his calculations of the beta strength function.

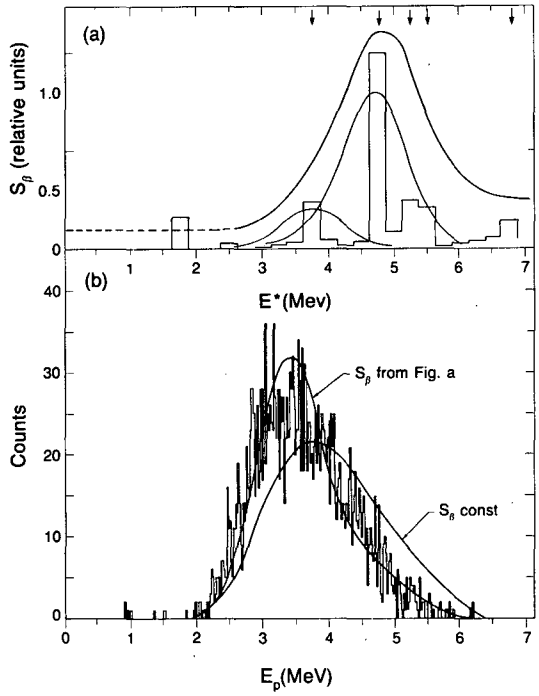

Fig. 2. (a) Calculated beta strength function for ^{123}Ce (histogram) as a function of excitation energy E*. The arrows indicate the five peaks used to represent the beta strength as a multiple gaussian (see text). Examples of the single gaussians are shown only for two peaks, together with the sum used in the calculation;
(b) measured proton spectrum for the decay of ^{123}Ce (histogram) and calculations with constant and resonant beta strength function. The calculations use spins and energies as shown in Fig. 1.

XBL 8312-6943

Footnotes and References

*Present address: Department of Physics, University of Jyväskylä, Finland.
†D. Schardt from GSI kindly provided us with a modified FORTRAN code.

1. P. Hornshoi, K. Wilsky, P.G. Hansen, B. Jonson, O.B. Nielsen, Nucl. Phys. A **187**, 609 (1972).
2. S. Liran and N. Zeldes, Atomic Data and Nuclear Data Tables, **17**, 431 (1976).
3. J. Hardy, Phys. Lett. **109B**, 242 (1982), and CERN 81-09, p. 217.
4. J. Krumlinde, P. Möller, Report LUNFD6 (NFFK-7029), University of Lund, Sweden 1980.
5. P. Tidemand-Petersen, A. Plochocki, Phys. Lett. **118B**, 278 (1982).

Recent Attempts to Produce Superheavy Elements in the ^{48}Ca + ^{248}Cm Reaction

A. Ghiorso, K.E. Gregorich, D. Lee, M. Leino, K.J. Moody, G.T. Seaborg, R.B. Welch, P. Wilmarth, S. Yashita, Y.K. Agarwal, P. Armbruster,* W. Brüchle,* M. Brügger,* J.P. Dufour,* H. Gäggeler,* S. Hoffman,* F.P. Hessberger,* P. Lemmertz,* G. Münzenberg,* K. Poppensieker,* W. Reisdorf,* M. Schädel,* K.-H. Schmidt,* J.H.R. Schneider,* W.F.W. Schneider,* K. Sümmerer,* D. Vermeulen,* G. Wirth,* C. Frink,† N. Greulich,† G. Herrmann,† U. Hickmann,† N. Hildebrand,† J.V. Kratz,† N. Trautmann,† M.M. Fowler,‡ D.C. Hoffman,‡ H.R. von Gunten,§ H. Dornhöfer***

Recent successes in synthesizing transactinide nuclides in "cold fusion" reactions have revived the interest in synthesizing superheavy elements in the reaction of ^{48}Ca with ^{248}Cm. Previous experiments aimed at synthesizing these elements[1,2] were performed at approximately 25 MeV in excess of the nominal fusion barrier. It was thought at that time that this extra energy was required to push the reacting system toward a spherical shape, allowing fusion to occur. However, this resulted in ^{296}116 compound nuclei (if any) with excitation energies between 30 and 50 MeV, which could only be removed by the evaporation of 4 to 5 neutrons and a corresponding departure from the region of stability near the 184 neutron shell. The experiments of 1976 were unsuccessful, establishing the upper limit for superheavy element formation as a function of half life shown in Fig. 1 by a dashed curve.

Recent calculations on the systematics of the fusion of heavy nuclei[3,4] indicate that the ^{48}Ca + ^{248}Cm system may fuse near or even below the nominal barrier. Therefore, it was decided to try to synthesize superheavy elements in the reaction of ^{248}Cm with ^{48}Ca at these lower energies. A first series of experiments was performed at the LBL SuperHILAC in October of 1982, where off-line chemical searches and a search with the gas-filled separator SASSY were performed. The second series of experiments was performed at the GSI UNILAC in March/April of 1983, where on-line chemical searches and search with the velocity separator SHIP were performed. Any ^{296}116 compound nuclei were produced with 16 to 40 MeV of excitation energy. Since the evaporation residues almost certainly either decay directly by spontaneous fission or produce a spontaneously fissile nuclide in their decay toward stability, this decay mode was treated as the signature of the superheavy nuclei produced in the reaction.

No spontaneous fission events which could be attributed to superheavy nuclides were observed. Upper limits in the form of 95% confidence limits (i.e., if no events were observed, then 3 events were assumed in the calculation) are given in the figure

from 1) SASSY experiments, 2) SHIP experiments, 3) high temperature on-line gas phase chemistry experiments, 4) low temperature on-line gas phase chemistry experiments, 5) quasi on-line solution chemistry experiments, and 6) off-line chemistry experiments. The half life range from several microseconds to several years has been examined to a sensitivity of 100 picobarns.

Footnotes and References

*Gesellschaft für Schwerionenforschung, Darmstadt, Fed. Rep. of Germany.
†Universität Mainz, Fed. Rep. of Germany.
‡Los Alamos National Laboratory, USA.
§Universität Bern, Switzerland.
**Universität Göttingen, Fed. Rep. of Germany.

1. E.K. Hulet et al., Phys. Rev. Lett. **39**, 385 (1977).
2. Yu. Ts. Oganessian et al., Nucl. Phys. **A254**, 213 (1978).
3. W.J. Świątecki, Nucl. Phys. **A376**, 275 (1982).
4. S. Bjørnholm and W.J. Świątecki, Nucl. Phys. **A391**, 471 (1982).

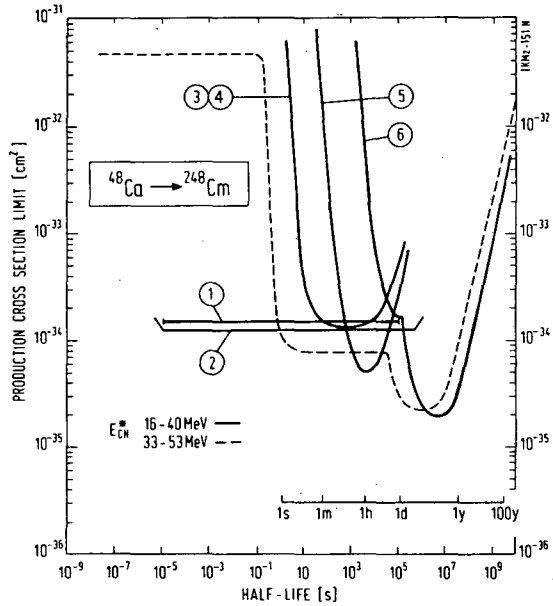

Fig. 1. Upper limits on superheavy element production in the ^{46}Ca+^{248}Cm reaction.
1) SASSY experiments, 2) SHIP experiments, 3) high temperature on-line gas phase chemistry experiments, 4) low temperature on-line gas phase chemistry experiments, 5) quasi on-line solution chemistry experiments, and 6) off-line chemistry experiments.
XBL 841-24

Actinide Production from Reactions of ^{129,132}Xe with ^{248}Cm

R.B. Welch, K.J. Moody, D. Lee, K.E. Gregorich, W. Kot and G.T. Seaborg

We have measured production cross sections for actinide nuclides formed in the reactions of 750 ± 70 MeV ^{129}Xe and 770 ± 70 MeV ^{132}Xe with ^{248}Cm for purposes of studying the effect of different neutron numbers of the projectile in heavy ion induced reactions. Products that are formed through a large net transfer of nucleons between the projectile and target and those involving transfer of unequal number of protons and neutrons should be more sensitive to the N/Z ratio of the composite system, since the N/Z ratio is a rapidly equilibrated mode in deep inelastic reactions. The bombarding energies used correspond to 1.0 to 1.1 times the Coulomb barriers of the systems used. The cross sections for the production of Cf, Es, and Fm nuclides are compared in Fig. 1 with those from a similar ^{136}Xe reaction with ^{248}Cm.[1] Cross sections for some Np, Pu, Am, Cm, and Bk isotopes were also measured in the ^{129}Xe and ^{132}Xe reactions and these results will be reported later. The results from ^{129}Xe bombardments were reported in ref. 2.

A ^{132}Xe beam was obtained by extraction of ^{132}Xe (by the Abel injector of the SuperHILAC) from a natural xenon source (26.9% ^{132}Xe) and accelerated to 1122 MeV by the SuperHILAC into our target

system. After passing through a 1.8 mg/cm^2 havar isolation window, 0.3 mg/cm^2 nitrogen cooling gas and 2.3 mg/cm^2 beryllium target backing, the beam struck a 0.502 mg/cm^2 ^{248}Cm target, present as Cm_2O_3. The energy on target, as measured by a Si(Au) surface barrier detector, was 770 MeV with a FWHM of 70 MeV.

Short bombardments of 1 to 3 hours duration were performed to obtain cross sections for the production of short lived activities, while a single 24 hour bombardment was done for the long lived activities. The average intensity of the beam was 1 electrical microampere of $^{132}Xe^{+29}$ through the target. Reaction products were stopped in a gold or nickel catcher foil and various chemical techniques were used to get Np, Pu, Am, Cm, Bk, Cf, Es, and Fm fractions.[1]

The ^{129,132,136}Xe bombardments were all done at approximately the same energy out of the SuperHILAC and into the same target assembly and are about the same energy on target. As seen in Fig. 1, the production of neutron deficient nuclides is highest for ^{129}Xe and lowest for ^{136}Xe. However, for the most neutron rich nuclides, such as ^{252,253}Cf, ^{254m,255}Es and ^{256}Fm, the cross section for a given nuclide is rather independent of the projectile. One would have expected ^{136}Xe to be better than ^{129}Xe in producing nuclides like ^{253}Cf. We are currently looking for an explanation of this effect.

References

1. K.J. Moody, Ph.D. thesis, 1983, LBL-16249.
2. R.B. Welch, K.J. Moody, D. Lee, K.E. Gregorich, P. Wilmarth, G.T. Seaborg, Nuclear Science Division Annual Report, 1981-1982.

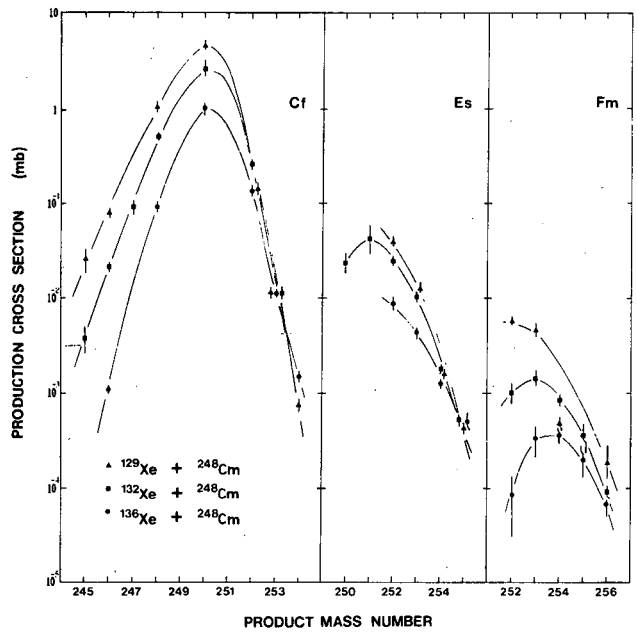

Fig. 1. Comparison of Cf, Es, and Fm product cross sections from 750 MeV ^{129,136}Xe and 770 MeV ^{132}Xe with ^{248}Cm. XBL 8311-718

Large Einsteinium Accelerator Program (LEAP) for the Increased Production of Ultra Heavy Elements

G.T. Seaborg and A. Ghiorso

Recent research with the heaviest elements on mechanisms of nuclear reactions and systematics of yields of heavy nuclides produced by heavy ions now makes it clear that the key to further substantial progress is the use of 276-day ^{254}Es as target material. This nuclide represents a substantial step beyond other available target nuclides in terms of mass number and atomic number and is the heaviest nuclide capable of production in the required multi-microgram quantities within the foreseeable future. Its use as target material makes possible a leap forward in the study of the nuclear properties of known, and especially new, nuclides at the upper reaches of the periodic table and research on the largely or

completely unknown chemical properties of the transactinide elements.

The information to be gained on the radioactive and spontaneous fission properties of these ultra heavy nuclides, near the limits of nuclear stability, should provide unique information for the understanding of nuclear structure in general. More specifically, increased knowledge of reaction mechanisms and nuclear properties in this upward extended region should be helpful in predicting the properties of, and planning reactions for the production of, the superheavy elements. Probably more importantly, the ^{254}Es target (when bombarded with ^{48}Ca) might make it possible to produce a superheavy nuclide containing close to 184 neutrons, a requirement (hitherto not met in any experiments) that could be the key to the observation of superheavy elements.

From the chemical viewpoint, the transition from the actinide to the transactinide elements, which occurs at element 104, represents a sharp discontinuity in chemical properties and is of great interest. Use of ^{254}Es will make it possible to produce sufficient quantitities of elements immediately below (elements 102 and 103) and above (elements 104, 105 and 106) this transition point to allow the study of their chemical properties. For the transactinide elements relativistic effects of electron configuration are expected to become prominent; an actual observation of this will influence the way we think about the chemistry of many of the rest of the lighter, naturally occurring elements. Additionally, knowledge of the chemistry of the transactinide elements will be important in extrapolating to the chemical properties of the superheavy elements, which could be a crucial prerequisite to their discovery.

We are still a long way from the upper boundary of either the periodic table or of the knowledge of nuclear and chemical structure that continued expansion promises. The production and use of ^{254}Es, which we have characterized as the LEAP, is clearly the key to the next strides forward.

Careful analysis and study at Oak Ridge National Laboratory indicates that a dedicated program at the HFIR/TRU facilities can produce the planned amount of 40 micrograms of ^{254}Es, a sufficient quantity for the fabrication of one or two targets for use in an international interlaboratory collaborative effort designed to achieve our goal.

In addition to ^{254}Es it is possible to produce a few hundred nanograms of 40-day ^{255}Es. Although this target would be about a hundred times smaller than the former, the additional neutron could make a tremendous difference in whether superheavy elements can be produced. This comes about because intense competition by fission occurs at each step of the de-excitation process following compound nucleus formation in a heavy ion reaction. The compound nucleus when using ^{48}Ca projectiles has 184 neutrons.

Experiments are being planned to cover three main areas of interest: (1) (fast) chemical experiments of various kinds on transeinsteinium elements, (2) light ion bombardments up to ^{22}Ne to make neutron heavy nuclides, and (3) bombardments with ^{48}Ca to make superheavy elements. It is expected that most of these experiments would take place at the SuperHILAC and the 88-Inch Cyclotron beginning in 1986 or 1987.

This proposal, under the sponsorship of the U.S. Transplutonium Program Committee is being planned with the cooperation of Darleane Hoffman of the Los Alamos National Laboratory, E. Kenneth Hulet of the Lawrence Livermore National Laboratory, and O. Lewin Keller of the Oak Ridge National Laboratory.

The Decay of ^{251}Bk

Y.-F. Liu, K.J. Moody,† D. Lee, Y. Morita,‡ G.T. Seaborg and H.R. von Gunten§*

^{251}Bk was first observed in the 8% alpha decay branch of ^{255}Es.[1,2] Samples prepared by collecting recoiling atoms from isotopically enriched ^{255}Es sources were counted for gamma rays and beta particles. The half life was determined to be 57.0 ± 1.7 minutes. Beta end point energies of ≃1.2 MeV and ≃1 MeV and gamma rays of 152.8 keV and 177.7 keV were measured. The intensity ratio of the two gamma rays was determined to be 0.38, and both arise from the same $\frac{3}{2}+$ state at 177.7 keV in the ^{251}Cf daughter. The decay of ^{251}Bk has also been observed following the beta decay of ^{251}Cm[3], where the beta end point energy was found to be ≈1 MeV.

A relatively high cross section for the direct formation of ^{251}Bk was found in reactions of 97 MeV ^{18}O with ^{248}Cm (≥24 μb).[4] It was possible to produce enough of this nuclide in heavy ion bombardments to remeasure some of the properties of ^{251}Bk decay, and to estimate the absolute intensities of the gamma rays. A target of 560 μg/cm^2 ^{248}Cm was irradiated with as much as 1 particle microampere of ^{18}O ions. Recoiling product atoms were collected with a catcher foil and Bk was chemically isolated.[5] This Bk fraction was counted for both photons and electrons, and the relative intensity data in Table I was determined from the results of seven experiments.

Table I. Relative intensities of the emitted radiations from ^{251}Bk decay

Cf K_{α_2} X-ray	2.02 ± 0.11
Cf K_{α_1} X-ray	3.19 ± 0.14
Cf K_{β_1} X-ray*	1.68 ± 0.09
Cf K_{β_2} X-ray	0.36 ± 0.05
153 keV γ-ray	0.385 ± 0.025
164 keV γ-ray	0.060 ± 0.012
178 keV γ-ray	1
gross β^- activity	≈33

*Including contribution from 129.9 keV γ-ray

The half life of ^{251}Bk was determined from measurements of the gamma ray activity as a function of time; it was found to be 55.6 ± 1.1 minutes (see Fig. 1). The beta endpoint energy of ^{251}Bk, determined by deconvolution of electron spectra taken as a function of time with a plastic scintillator, was found to be 915 ± 10 keV. A very weak (≈5%) component with an end point energy of 1130 ± 35 keV was also observed, corresponding to beta decay directly to the ^{251}Cf ground state. A previously unobserved gamma ray with an energy of 164 keV, arising from beta decays populating the $\frac{5}{2}+$ state of 211.6 keV in the ^{251}Cf daughter, was observed, and its relative intensity was determined holding the half life fixed at 55.6 minutes. The relative intensity of the $K\beta_1$ x-ray is significantly larger than predicted. which allowed us to obtain the intensity of the "missing" 129.9 keV gamma ray in the ^{251}Cf level scheme by subtraction.

From the above information, and assuming that the gamma transitions in ^{251}Cf (all $\Delta J^\pi = 0, \pm 1$, no) were mostly of M1 multipolarity, we were able to estimate an absolute intensity of the 178 keV gamma ray of 5.2 ± 0.6%. The decay scheme of ^{251}Bk is shown in Fig. 2.

Footnotes and References

*Department of Technical Physics, Peking University, Beijing 100871, People's Republic of China.
†Gesellschaft für Schwerionenforschung mbH, Postfach 11 05 41, 6100 Darmstadt 11, West Germany.
‡School of Pharmacy, University of California, San Francisco, Departments S-926, San Francisco, California 94143.
§Universität Bern, Institute für anorganische, analytische und physikalische Chemie, CH-3000 Bern 9, Freistrasse 3, Switzerland.

1. H. Diamond, R. Sjoblom, R. Barnes, J. Lerner, D. Henderson, and P. Fields, J. Inorg. Nucl. Chem. **29**, 601 (1967).
2. R. Hoff, R. Lougheed and P. Johnson, Lawrence Livermore National Laboratory Report UCRL-72090 (1970).
3. R. Lougheed, J. Wild, E. Hulet, R. Hoff and J. Landrum, J. Inorg. Nucl. Chem. **40**, 1865 (1978).
4. D. Lee, K. Moody, M. Nurmia, G. Seaborg, H. von Gunten and D. Hoffman, Phys. Rev. **C27**, 2656 (1983).
5. Y.-F. Liu, C. Luo, K. Moody, D. Lee, G. Seaborg and H. von Gunten, Radioanalytical Chemistry **76**, 119 (1983).

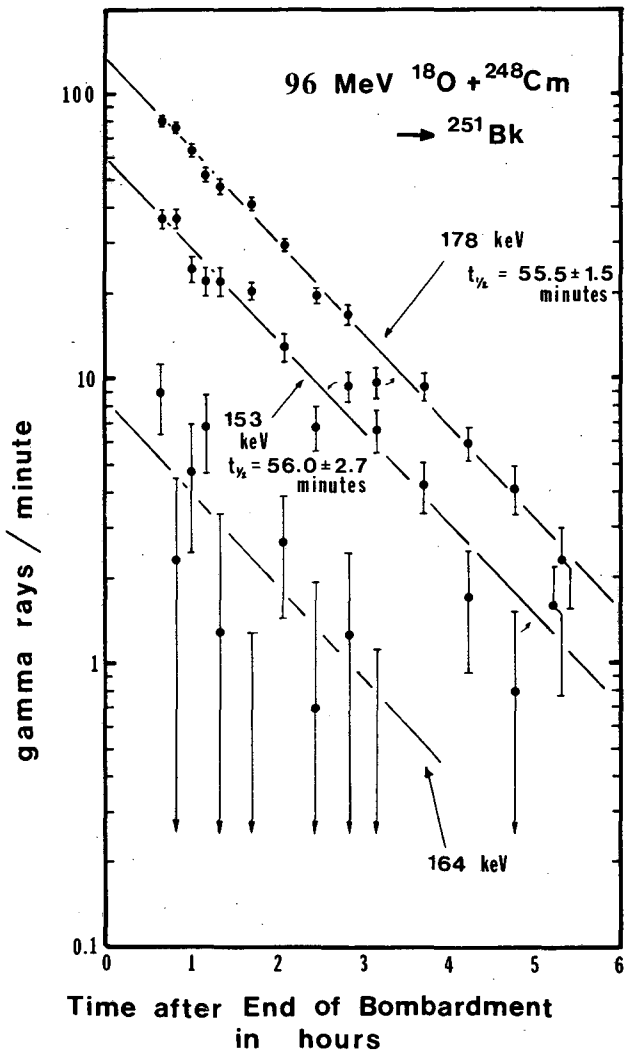

Fig. 1. Decay curves of the 177.7 keV, 152.8 keV, and 163.8 keV gamma rays of ^{215}Bk from one irradiation of ^{248}Cm with 96 MeV ^{18}O. XBL 836-10252

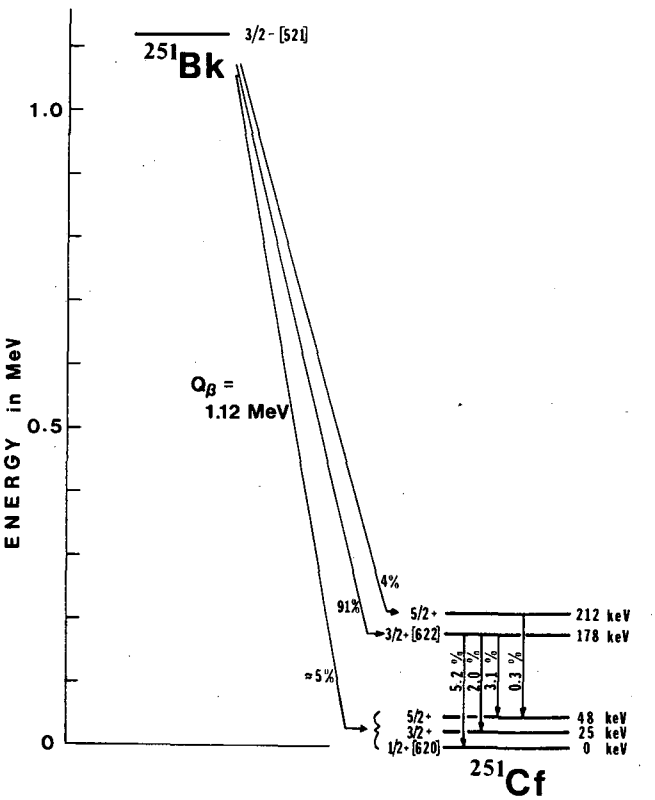

Fig. 2. The decay scheme of ^{251}Bk. Gamma transitions are labeled with absolute photon intensities. XBL 836-10299

The Half-Life and Absolute Gamma Ray Intensities of ^{157}Er

K.E. Gregorich, K.J. Moody, P. Juergens, D. Lee, and G.T. Seaborg

A source of ^{157}Er was produced by the electron capture/positron decay of ^{157}Tm ($t_{1/2}$ = 3.3 m) made in the ^{141}Pr(^{20}Ne,4n)^{157}Tm reaction at the 88-Inch Cyclotron. The target, which was made by a molecular plating procedure,[1] consists of a 0.55 mg/cm^2 layer of Pr as Pr_2O_3 on a 4.6 mg/cm^2 Be backing foil. The bombardment was carried out in the Actinide Recoil Target System[2] and the recoiling reaction products were caught in a 7 mg/cm^2 gold foil. After the bombardment, Er was chemically separated from Ho and other daughter products using an ammonium α-hydroxyisobutyrate cation column procedure similar to that to be described elsewhere.[3]

The gamma rays of the Er and its daughters were measured with a 40 cm^3 Ge(Li) detector coupled with a 4096 channel analyzer. This system had a full width at half maximum resolution for the 1332 keV ^{60}Co peak of 2.0 keV. The energy and efficiency calibration of the detector system were measured with a standard mixed gamma ray calibration source. Spectra were collected over a period of several days.

The decay curves for 15 of the most intense gamma rays of the ^{157}Ho daughter ($t_{1/2}$ = 12.6 m)[4] were given error-weighted least squares fits for growth and decay. From these fits, an approximate half life for the ^{157}Er parent was found. From the ratio of parent to daughter activities in these fits, a time of chemical separation of Er from Ho was determined. Another round of least squares fits was carried out on the same Ho lines with the ^{157}Ho daughter activity fixed at 0 at the time of chemical separation. These fits were used to determine the half life of the ^{157}Er parent to be 18.65 ± 0.04 m. Taking other systematic errors into consideration, we have determined that a more reasonable value for this half-life is 18.65 ± 0.10 m. This value is significantly different from the published value of 24^{+2}_{-4} m.[5]

Many gamma rays were found in the sample which decayed with this half life. The 18.65 m half-life for ^{157}Er is essentially identical to the half-life for ^{156}Er given as 19 ± 1 m.[6] No gamma rays for ^{156}Er are known above 56 keV.[6] This prompted us to measure the excitation functions of these 18.65 m gamma rays to determine if they were due to the decay of ^{156}Er or ^{157}Er. The relative intensities of the 391.6 keV gamma ray[7] remained constant at three different bombarding energies, indicating that all the gamma rays were due to the decay of ^{157}Er.

The absolute intensity of the 326 keV gamma ray of the ^{157}Dy granddaughter of ^{157}Er is known to within 2%.[8] The absolute intensities of the ^{157}Er gamma rays were therefore found by determining the number of mass 157 atoms in the sample at the time of chemical separation by following the decay of the ^{157}Dy granddaughter. The absolute intensity of the 391.6 keV gamma ray has been determined to be $14.2 \pm 1.0\%$ and the relative intensities of the ^{157}Er gamma rays are given in Table I.

References

1. D.C. Aumann, G. Mullen, NIM **115**, 75-81 (1974); G. Mullen, D.G. Aumann, NIM **128**, 425-428 (1975).
2. R.M. McFarland: Ph.D. Thesis, LBL 15027 (1982).
3. K.E. Gregorich, K.J. Moody, G.T. Seaborg, to be published.
4. J.P. Torres *et al.*, Nuc. Phys. A **185**, 574 (1972).
5. Zh. T. Zhelev *et al.*, Sov. J. Nuc. Phys. **2**, 956 (1965).
6. A.A. Aleksandrov *et al.*, Bull. Acad. Sci. USSR Phys. Ser. **39**, 1661 (1975).
7. V. Andrejchev *et al.*, INIS Microfiche 4388.
8. C.M. Lederer *et al.*, **Table of Isotopes** 7th Ed. p. 913 (1977).

TABLE I

The relative intensities of the gamma rays accompanying the decay of ^{157}Er. The absolute intensity of the 391.6 keV line is 14.2 ± 1.0%. The energy uncertainties are 0.2 kev for E < 1000 keV and 0.4 kev for E > 1000 keV.

ENERGY (keV)	REL. INT. (%)	UNCERTAINTY
66.8	–	–
121.0	56.	3.
179.6	8.0	0.4
303.8	9.8	0.5
347.8	11.3	0.6
391.6	100.	4.
431.1	5.8	0.3
503.2	9.8	0.5
527.5	5.4	0.3
549.4	19.9	0.9
574.1	3.4	0.2
584.2	5.9	0.4
611.4	5.0	0.3
641.0	2.0	0.2
652.5	3.2	0.2
673.2	3.3	0.3
722.2	3.8	0.4
747.5	3.5	0.3
786.0	2.6	0.3
792.0	3.6	0.3
807.5	2.4	0.3
1115.3	1.7	0.3
1242.6	3.9	0.3
1422.4	7.2	0.5

Compound Nuclei at High Angular Momentum

High-Spin γ-Ray Spectroscopy: Past Successes, Future Hopes*

R.M. Diamond

The addition of angular momentum to a nucleus presents a whole new dimension, a new coordinate axis, along which to study changes in nuclear behavior and structure. Nuclei can carry angular momentum in two principal ways: by the collective rotation of a deformed nucleus as a whole and by the alignment along the rotation axis of individual high-j nucleons. For spherical (or near-spherical) nuclei, the latter mode is the only one possible. On the right in Fig. 1, the levels of ^{212}Rn illustrate a scheme of particle alignment; it is quite irregular with transitions of a variety of electromagnetic types and with little pattern to the level spacing. On the left, the yrast band of ^{238}U is shown, a predominantly rotational scheme with only strongly enhanced electric quadrupole transitions and a level spacing that approximates that of a rigid rotor, $E = I(I + 1)\hbar^2/2\mathcal{J}$ and $E_\gamma = (4I - 2)\hbar^2/2\mathcal{J}$, where $\mathcal{J}$ is the moment of inertia. Most nuclei, however, combine both types of motion, and it is this interplay between collective and single-particle motion that makes the behavior of nuclei along the angular momentum coordinate so fascinating and so rich in variety.

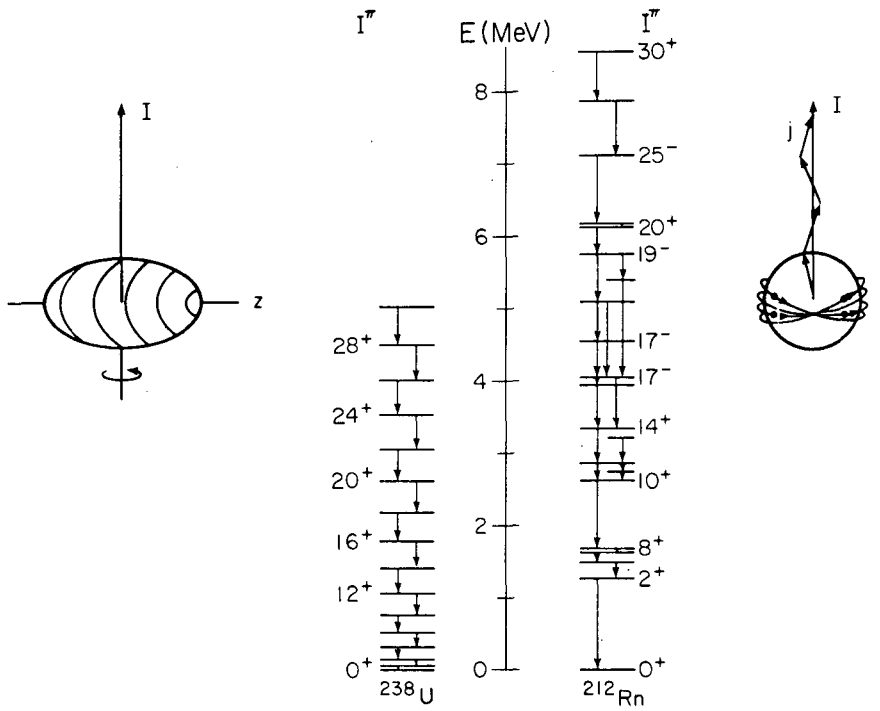

Fig. 1. Level schemes for ^{238}U and ^{212}Rn, illustrating collective rotation and aligned individual particle motion, respectively, as predominant sources of angular momentum. XBL 833-1470

Discrete high-spin γ-ray studies have led to a new "backbending" spectroscopy, which is telling us about the details of particle alignments and monopole and quadrupole pairing. Consider, for example, the moment of inertia as defined above. If the nucleus were rigid, $\mathcal{J}$ would be constant. But a nucleus is not rigid; the nucleons move throughout the nuclear volume, and values for the moments of inertia of deformed nuclei at low spin are smaller than rigid-body values by factors of 2–3. This is due to correlations in the nucleonic motion, particularly to the pairing interaction. But with increasing angular rotation ($\hbar\omega = E_\gamma/2$), there is a gradual, but smooth, rise in $\mathcal{J}$. This occurs because the increase in ω increases the Coriolis interaction on the paired nucleons, weakening the pairing correlations and so increasing the value of $\mathcal{J}$. But since the Coriolis force is also proportional to the j of the particle, it acts most strongly on the high-j particles. Thus on the background of gradually increasing $\mathcal{J}$ there are occasional sharp, irregular increases, where the nucleus finds it energetically more favorable to align a pair of high-j particles rather completely while essentially keeping the pairing correlations among the lower-j nucleons. This process corresponds to a band-crossing between the first band and an excited band with two more aligned particles (and a larger effective moment of inertia). In the rare-earth region, it is the alignment of a pair of $i_{13/2}$ neutrons that causes the first sudden jump in the value of $\mathcal{J}$ at $\hbar\omega \sim 0.25$ MeV (first backbend).

In Fig. 2 the difference in aligned spin, i, for this aligned crossing band with respect to an extrapolated ground-state band is plotted against rotational frequency for three bands. The solid line is for the lowest-energy band in the even-even nucleus ^{162}Yb. The frequency of the crossing is about 0.26 MeV. The dashed lines are for two bands in ^{163}Yb with the additional neutron located in an (predominantly $h_{9/2}$) orbital labeled either E or F. In ^{162}Yb, this pair of states (E,F) is available for the pairing correlations, and a pair of $i_{13/2}$ neutrons can scatter into them; in ^{163}Yb one, either E or F, is blocked by the odd nucleon. The pairing correlations are thereby weaker, and it is easier to unpair and align the $i_{13/2}$ neutrons, so this occurs at a lower rotational frequency, ~0.22 MeV, as seen in Fig. 2. The shift is clear and also occurs in other nearby nuclei. It can be related, through calculations, to the change in the pairing correlations involved, and turns out to correspond to a 20–30% reduction.

But the analysis of such data can be carried even further, showing changes in the first crossing frequency that depend upon the nature of the blocking orbital. These higher order effects are referred to as "quadrupole pairing", and such studies can be extended to additional blocked orbitals and other aligning pairs. There are also other effects, mostly less well understood, but the new "bandcrossing spectroscopy" is just beginning and appears quite exciting.

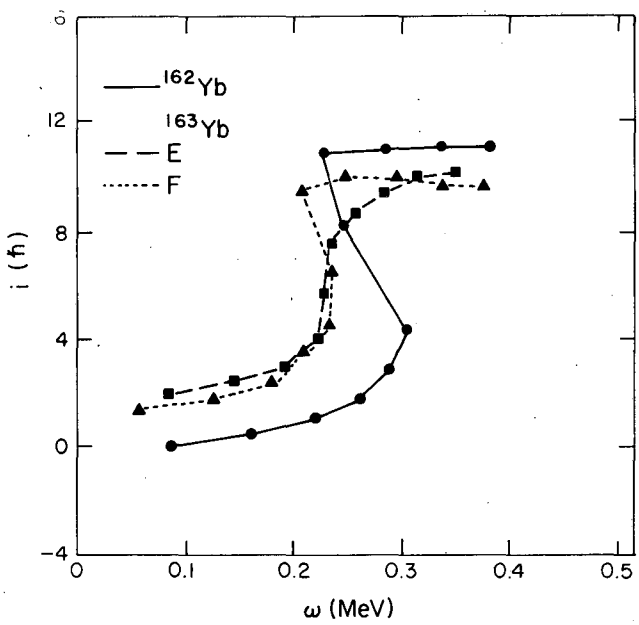

Fig. 2. Aligned spin vs. rotational frequency for yrast sequence in ^{162}Yb and for negative-parity odd quasiparticle bands in ^{163}Yb (states E and F). The crossing frequency is lower with the latter bands

XBL 828-1010

I would like now to go on to still higher spins and rotational frequencies, that is, to the continuum region. The continuum studies, as yet less well developed, are indicating changes in shape and structure at the highest nuclear spins possible, as well as particle alignments from higher shells. As an example of the latter, the de-excitation γ-ray spectra from ^{160,158,156,154}Er all show low-energy peaks around $\hbar\omega \sim 0.25$ MeV that correspond to the known first $i_{13/2}$ neutron backbend. The peak corresponding to the second alignment, of $h_{11/2}$ protons, shows for ^{158}Er and probably for ^{160}Er. It, and possibly a third one (of $h_{9/2}$ neutrons) as well, appears to come at a lower frequency with the lighter Er isotopes, making a narrower and taller group of low-energy peaks in ^{156,154}Er than in ^{158,160}Er. This is plausible, because the decrease in the neutron Fermi level causes it to approach the beginning of the $\nu h_{9/2}$ subshell and because the deformation decreases.

This compression of valence-shell alignments in the lighter Er nuclei leads to a minimum in the spectra around $\hbar\omega \sim 0.5$ MeV and a high-energy peak just above, $\hbar\omega \sim 0.6$ MeV. The minimum suggests that the valence-shell alignments are exhausted by this frequency. The high-energy bump must come then from a new source of angular momentum. The two most likely ones are a change in shape or additional alignments from the next higher shell. The magnitude of deformation required would involve the "superdeformations" that have been suggested and appear in calculations for this region of nuclei, but they are not supposed to occur until higher spins after the proton $i_{13/2}$ and $h_{9/2}$ alignments from the next shell. Also such large deformations should give strong rotational transitions, which, however, do not seem to be observed in γ-γ correlation experiments. So we believe that the higher bump is caused by alignments of the $i_{13/2}$ and $h_{9/2}$ protons. These should be relatively unaffected by the neutron number, and indeed, the high-energy bump appears to be the same in all four nuclei. Thus in the favorable cases of ^{156,154}Er, we can directly see separate regions of particle alignment from the valence shell and now from the next higher shell, even with the relatively primitive, present-day continuum methods.

New experimental developments such as the NaI balls and the still newer BGO-shielded (Compton-suppressed) Ge detector arrays will contribute both toward resolving the continuum and to the detailed spectroscopy of the lower-spin regions.

*Condensed from LBL-15883, Proceedings of the Conference on Nuclear Physics with Heavy Ions, April 1983, Stony Brook, N.Y.

Shell Effects at High Angular Momentum*

M.A. Deleplanque, A.O. Macchiavelli,† R.M. Diamond, F.S. Stephens, E.L. Dines,‡ and J.E. Draper‡

It now appears that the behavior of nuclei at high spins can be largely understood as an interplay between collective and single-particle motion. At spins up to $40\hbar$ where the γ-ray spectra are resolved, the collective and single-particle contributions to the angular momentum can be rather easily separated. Collective rotational motion is characterized by a smooth increase in rotational frequency with spin. The rotational frequency is proportional to the collective E2 transition energy (E_γ), and thus in rotational nuclei there is a strong correlation between the observed γ-ray energies and spins ($E_\gamma \simeq 2I\hbar^2/\mathcal{J}$ Angular momentum can also be built from single-particle motion by aligning the single-particle spin along a common axis, and there is very little or no resulting correlation between γ-ray energy and spin. This latter behavior is generally observed in nuclei near closed shells, but alignments may occur in rotational nuclei, producing local irregularities in the γ-ray energies as a function of spin (backbends).

Above spin $40\hbar$, individual sequences can no longer be seen in the decay of compound nuclei, and it becomes necessary to analyze the unresolved (continuum) γ-ray spectra. This is generally done by measuring average moments of inertia[1] and γ-ray energy correlations (E_γ vs I or E_γ vs E_γ). In favorable cases these can also lead to a separation between the single-particle and the collective contribution to the angular momentum of the system.

Whether the nucleus behaves collectively or not depends very much on shell effects. Near closed shells the shape tends to be spherical, and alignment of single-particle angular momentum is favored. Between closed shells deformations tend to build up, favoring rotational behavior. However, in a single nucleus these tendencies will both occur as a function of spin or rotational frequency. Some frequency regions will be favorable for alignments and others for rotations. It can also happen that a nucleus is so located in N and Z that the large alignments of the major shells tend to be bunched together in frequency. This will produce large effects in the γ-ray spectrum. We believe such effects occur in the light Er nuclei, where the large alignments of the valence shell are bunched together at low frequency and those from the next higher shell produce a broad peak at higher frequencies. To see these effects, we have compared the continuum spectra of Er nuclei in the mass region 154 to 160.

Fig. 1 shows continuum γ-rays deexciting a population of high spin states (selected by a high total γ-ray energy slice) in ^{160,158,156,154}Er, which are the main (4n) products in the ^{40}Ar-induced compound reactions performed at the 88-Inch Cyclotron in Berkeley. The spectra evolve from a rather flat structure in ^{160}Er to a "double bump" in ^{156,154}Er, with ^{158}Er intermediate. A flat spectrum is characteristic of good rotational properties. The peaks around frequencies of 0.28, 0.35, 0.42 MeV correspond to the known first, blocked, and second backbend in ^{160}Er. The low-frequency (<0.5 MeV) part of the spectrum consists of a taller and narrower peak in the lighter Er nuclei, suggesting a compression of those backbend frequencies. This is quite clear in ^{158}Er where the second backbend is known and where a known third discontinuity is seen as a shoulder at ~0.5 MeV. As the neutron Fermi level becomes lower in the lighter Er nuclei, closer to the beginning of the $h_{9/2}$ and $i_{13/2}$ neutron subshells, the neutrons in those orbitals align more easily. At the same time, the lighter Er nuclei become softer and can move more easily towards triaxial shapes. This also means that those alignments will occur at lower frequencies. The trend clearly continues in ^{156}Er where it leaves a "dip" at 0.5 MeV. This occurs after the three main backbends in the valence shell have aligned much of the angular momentum available in that shell, so that the only way to generate

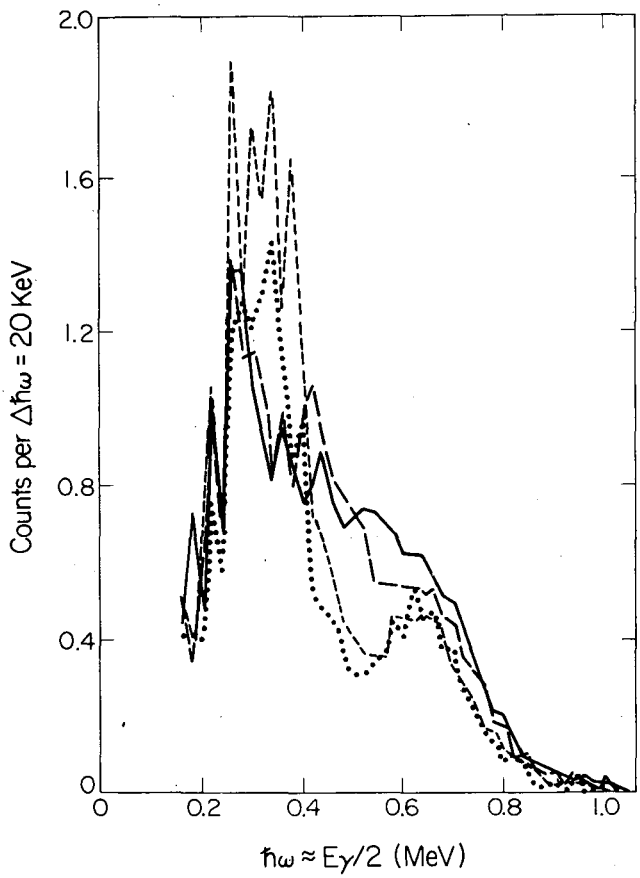

Fig. 1. The γ-ray "isotropic" spectra (after subtraction of a statistical background) as a function of frequency for the following systems: ^{124}Sn + ^{40}Ar (solid line), ^{122}Sn + ^{40}Ar (long dashed line), ^{120}Sn + ^{40}Ar (short dashed line), ^{118}Sn + ^{40}Ar (dotted line).

XBL 834-1544

additional angular momentum is by collective motion. The occurrence of a bump above 0.5 MeV in this nucleus indicates that a new source is contributing angular momentum in that frequency region. The only plausible new source is from the next higher shell. It could contribute either through "superdeformations" or through alignments of high-j orbitals, here essentially $h_{9/2}$, $i_{13/2}$ proton orbitals which are closest to the Fermi level. The former explanation is less likely since strong rotational transitions have not yet been observed in γ-γ correlations, although this cannot be excluded at the highest spins.

Thus, the effects of the valence shell and of the next higher shell are seen directly as two separate bumps in the ^{156}Er spectrum. The same two shells are also seen in ^{154}Er, but the lower bump (valence-shell region) has a noncollective character, as can be seen from the smaller proportion of stretched quadrupole transition (Fig. 2) in that region. In ^{158,160}Er, the neutron Fermi level is higher and the prolate deformation is more stable. In those cases, the neutron alignments are less easy and therefore generated over a wider frequency range than in the lighter Er nuclei. As a consequence, there is no longer a pronounced separation between the two shells. Such major shell effects in the unresolved γ-ray spectrum are also likely to occur in other regions of nuclei, and can provide some important tests of present cranked-shell-model calculations.

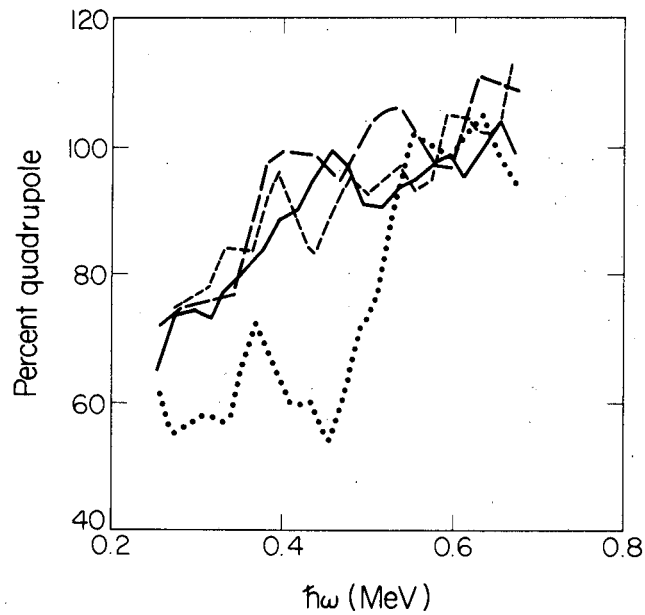

Fig. 2. Percentage of stretched quadrupole transitions as a function of frequency for the spectra of Fig. 1. The systems are represented by the same symbols as in Fig. 1. XBL 834-1543

Footnotes and Reference

*Condensed from Phys. Rev. Lett. **51** (1983) 1854.
†Permanent address: Comisión Nacional de Energía Atómica, Buenos Aires, Argentina
‡Department of Physics, University of California, Davis, CA 95616.

1. M.A. Deleplanque, H.J. Körner, H. Kluge, A.O. Macchiavelli, N. Bendjaballah, R.M. Diamond and F.S. Stephens, Phys. Rev. Lett. **50**, 409 (1983).

Nuclear Moments of Inertia at High Spins*

M.A. Deleplanque

Nuclei at sufficiently high spin fission. This is the main limit to studying nuclear structure at high angular momenta, since in the fission process a lot of angular momentum is tied up in the relative motion of the fragments. The maximum spins that can be produced are around $70\hbar$ and are obtained in the rare earth region, which will therefore be discussed here. At those high spins, the level density is high, and the lifetimes of statistical transitions and of collective E2 transitions are comparable, resulting in many different decay paths for the nucleus. The corresponding γ-ray spectrum is therefore unresolved. A statistical component can be recognized and subtracted, leaving the "yrast-like" part which contains most of the nuclear structure information.

It turns out that this yrast-like part of a continuum γ-ray spectrum shows naturally how angular momentum is generated as a function of frequency. In rotational nuclei, the rotational frequency is $\omega = dE/dI \sim E_\gamma/2$, half the collective E2 transition energy. The height of the spectrum for a rotor is proportional to $dN/dE_\gamma = dI/4d\omega$. $dI/d\omega$ is a dynamic (second derivative of energy with spin) moment of inertia. It contains both alignments and collective effects and is therefore an *effective* moment of inertia $\mathcal{J}^{(2)}_{\text{eff}}$. It shows how much angular momentum is generated at each frequency. If the collective moment of inertia $\mathcal{J}^{(2)}_{\text{band}}(\omega)$ is measured (from γ-γ correlation experiments) for the same system, the collective and aligned (Δi) contributions to the increase of angular momentum ΔI in a frequency interval $\Delta\omega$ can be separated: $\Delta i/\Delta I = 1 - \mathcal{J}^{(2)}_{\text{band}}/\mathcal{J}^{(2)}_{\text{eff}}$. This is at present the only way to extract such detailed information at the highest spin states where discrete lines cannot be resolved.

Previous studies of continuum spectra have suggested that many nuclei have a rotational behavior at high spins (frequencies), even if they do not near their ground state, so that the above considerations could apply to many of them at high frequencies.

It is especially interesting that many nuclear properties including $\mathcal{J}^{(2)}_{\text{eff}}$ and $\mathcal{J}^{(2)}_{\text{band}}$ can also be calculated as a function of rotational frequency with the so-called cranking model. The frequency is then a parameter: for axially symmetric nuclei, for example, the nuclear potential is rotated with a frequency ω either around the symmetry axis or around an axis perpendicular to the symmetry axis. The measured values represent an average over many decay paths, and will probably be smeared out, compared to the theoretical values which represent an average over a few paths lowest in energy. Nevertheless, these measurements will provide important tests to the cranked-shell-model calculations.

Fig. 1 shows an example of the spectra obtained in several Er nuclei. They are plotted in units of the moment of inertia $\mathcal{J}^{(2)}_{\text{eff}}$. The high-energy part of the spectra has been corrected[1] for incomplete feeding at these frequencies.

At a frequency above the known low-spin discrete lines, the spectrum of ^{160}Er shows three peaks which are three known backbends in the valence shell. There are peaks because in a backbend several transitions pile up at the same energy (frequency). Another way to view them is to say that alignments generate a lot of angular momentum ($dI/d\omega$ is high) in that frequency region. $\mathcal{J}^{(2)}_{\text{eff}}$ rises at the highest ($\hbar\omega > 0.6$ MeV) frequencies. This rise is accompanied by a decrease in $\mathcal{J}^{(2)}_{\text{band}}$, which suggests it is due to alignment effects. The comparison[1] with the $\mathcal{J}^{(2)}_{\text{eff}}$ spectrum of its isotone ^{162}Yb further suggests that this is a proton alignment of $h_{9/2}$, $i_{13/2}$ orbitals from the next higher major shell which come down to the Fermi level around $\hbar\omega \simeq 0.6$ MeV for Er nuclei.

The $\mathcal{J}^{(2)}_{\text{eff}}$ spectra of ^{158,156}Er can be understood if the evolution of the properties of ^{160}Er with changes in Fermi level and shape is considered. As

the neutron Fermi level goes down, it comes closer to the highly aligned $\Omega = 1/2$ components of the intruder $i_{13/2}$ neutron valence subshell, and in addition the nucleus becomes less deformed. Both of these make the valence shell backbends (hole backbends) easier: in the lower frequency region, the valence backbends are compressed in frequency, producing a taller and narrower peak in the lighter nuclei. At high frequencies, the spectra are more similar. This could be expected for proton alignments since these nuclei have the same proton number, and the next higher shell might not be so sensitive to softness as the valence shell. However the values of $\mathcal{J}^{(2)}_{eff}$ are higher for ^{156}Er. This could result from the fact that ^{156}Er is softer than the heavier Er nuclei, and the population of highly aligned proton orbitals could trigger a change towards superdeformed shapes more easily in that nucleus. The cranking model calculations[2,3] indeed show the same trends, although they differ somewhat from the experimental results if the detailed behavior of a given nucleus is considered.

These studies have considerably enriched our knowledge of high spin properties of the nucleus. In particular, they suggest that single-particle effects may be identified at high spins. Only qualitative trends can be measured with such methods. More quantitative spectroscopy will require resolving the spectra. This will be possible up to spins around $50\hbar$ in the near future, thanks to high resolution high-efficiency γ-ray detectors now becoming available.

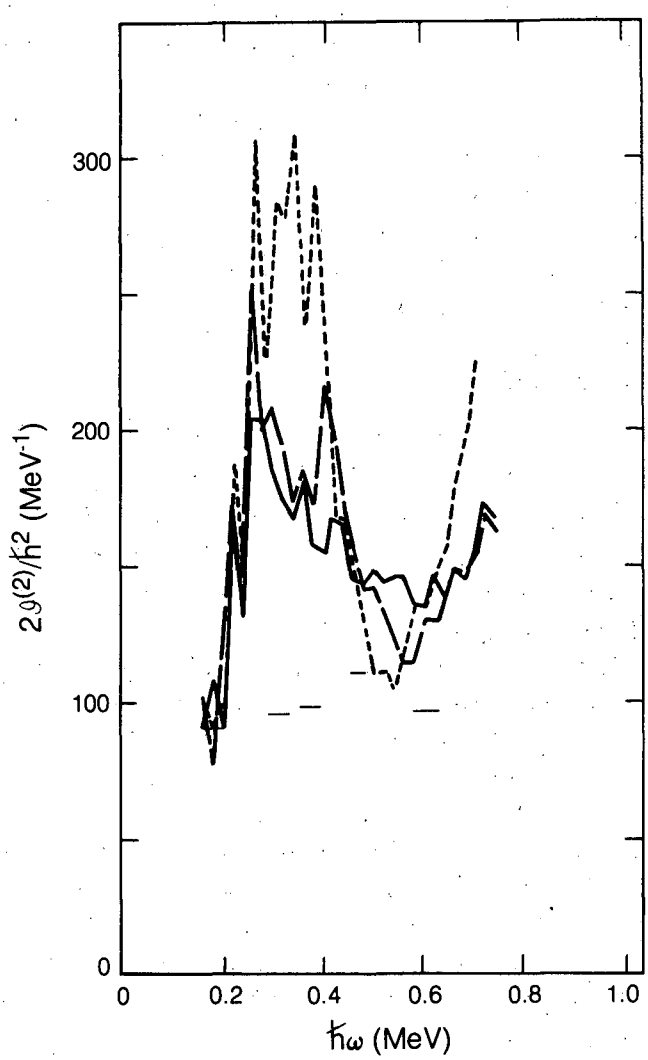

Fig. 1. Plot of $\mathcal{J}^{(2)}_{eff}$ (thick lines) as a function of frequency for the systems ^{124}Sn + ^{40}Ar (solid line), ^{122}Sn + ^{40}Ar (long-dashed line), ^{120}Sn + ^{40}Ar (short-dashed line). In each spectrum, the last point corresponds to 25% feeding (correction of a factor of 4). The thin solid lines are values of $\mathcal{J}^{(2)}_{band}$ for ^{124}Sn + ^{40}Ar.

XBL 8311-646

Footnote and References

*Parts of talks given at Oak Ridge, U.S.A. and Suzhou, China.

1. M.A. Deleplanque, H.J. Körner, H. Kluge, A.O. Macchiavelli, N. Bendjaballah, R.M. Diamond and F.S. Stephens, Phys. Rev. Lett. **50**, 409(1983).
2. T. Bengtsson and I. Ragnarsson, Phys. Lett. **115B**, 431 (1982).
3. T. Bengtsson and I. Ragnarsson, Physica Scripta **T5**, 165 (1983).

Transient Magnetic Fields for Large Z Atoms Recoiling Through Gadolinium*

O. Häusser,† H.R. Andrews,† D. Horn,† M.A. Lone,† P. Taras,‡ P. Skensved,§ R.M. Diamond, M.A. Deleplanque, E.L. Dines, A. Macchiavelli, F.S. Stephens

The g-factors of a large class of collective nuclear states are presently of considerable interest because they depend on how the total angular momenta are composed of collective and single-particle contributions. Because of the short mean lifetimes of these states ($\tau \lesssim 1$ ps), large magnetic fields, $B \gtrsim 10$ kT, are required to accurately measure these g-factors. In heavier nuclei the largest magnetic fields observed so far are when fast, heavy recoils decelerate in foils of polarized, ferromagnetic Gd. Compared to the more commonly used Fe (Z = 26), Gd (Z = 64) has the added advantages of a larger Coulomb barrier and a longer ion-solid interaction time associated with the smaller stopping power dE/dx of Gd.

We have utilized Coulomb excitation of the $\frac{5}{2}^-$ first excited state in ^{207}Pb, whose g-factor is well known, to calibrate the transient field (TF) for Z = 82 recoils in ferromagnetic Gd at 77 K over a wide range of velocities, $2.4\ v_0 \leqslant v \leqslant 10.2\ v_0$ (v_0 is the Bohr velocity c/α). At Chalk River ^{58}Ni beams of 222 and 230 MeV were used, and at LBL a 610 MeV ^{136}Xe beam from the SuperHILAC was used. These beams bombarded triple-layered foils, consisting of a $\sim$1 mg/cm^2 thick target layer (97% enriched ^{207}Pb, natural Th or U) evaporated onto rolled and annealed Gd, and an $\sim$12 mg/cm^2 thick Cu layer evaporated onto the back of the Gd. Intimate mechanical contact of the Cu backing with a 0.8 mm thick, liquid-N_2 cooled Cu plate resulted in target temperatures of $\simeq$ 80 K, well below the Curie temperature for Gd (293 K).

Beam particles scattered at backward angles between 160° and 125° were detected in an annular avalanche detector. Gamma rays coincident with the particles were observed in two large-volume (85–100 cm^3) detectors. They were placed 9.5 cm from the target at $\Theta_\gamma \simeq \pm 65°$, near the maximum of the logarithmic slope, $S = -(dW/d\Theta_\gamma)/W$, of the γ-ray angular distribution for E2 transitions.

For each γ-ray transition Coulomb excited in the ^{207}Pb, ^{238}U, or ^{232}Th target, four intensities (two detectors at $\pm\Theta_\gamma$, two directions of the polarizing field, ↑ and ↓) were combined in the usual way to deduce the TF yield effect $\epsilon = (Y\uparrow - Y\downarrow)/(Y\uparrow + Y\downarrow)$. The measured ϵ values were converted to those of an idealized point detector, and these yield effects were then compared to computer calculations. In a first step of the analysis the TF B(v,z) was assumed to be constant over the velocity interval of each measurement. These values of $\langle B \rangle$ for the ^{207}Pb case are shown in Fig. 1. They are consistent with a nearly constant TF of $\sim$6 kT at velocities between 4 v_0 and 10 v_0.

In a second step the TF was represented by a smooth empirical parameterization of the velocity dependence,

$$B(v,Z) = aZ\ v/v_0 \exp(-\beta v/v_0) \qquad (1)$$

From the χ^2 plot in Fig. 1 a value $\beta(Z=82) = 0.13 \pm 0.03$ is obtained, in good agreement with the best-fit value obtained earlier for ^{169}Tm, $\beta(Z=69) = 0.135$. For a fixed $\beta = 0.135$ we obtain $a(Z=82) = 28.0 \pm 2.6$ T, which is similar to the Tm value, $a(Z=69) = 29.0 \pm 1.8$ T. In the quoted error, contributions from counting statistics, from the 5.6% error in the g-factor, and from a 5% uncertainty in the areal density and magnetization of the Gd foil have been added in quadrature.

From Fig. 1 it can be seen that the transient field in Gd first increases with increasing recoil velocity, and then assumes a nearly constant value of 6.2 KT for $v \geqslant 5.5\ v_0$. This (not universally expected) result indicates that still higher fields will not be available from this system to measure moments of very short-lived states.

The precession measurements in ^{207}Pb, ^{232}Th and ^{238}U have been combined with the results of other recent experiments to examine the atomic number dependence of the transient field. We find a roughly linear increase of the transient field with Z of the recoil. Finally, using simple estimates for the single-vacancy lifetimes and for the cross sections for electron capture and loss, the observed transient fields for Pb recoils were interpreted as arising from single ns electrons in Gd. These calculations indicate a dominant contribution to the transient field from the 4s shell.

Footnotes

*Condensed from Nucl. Phys. **A412**, 141 (1984) in press.

†Atomic Energy of Canada Limited, Chalk River Nuclear Laboratories, Chalk River, Ontario, Canada K0J 1J0.

‡Laboratoire de Physique Nucléaire, Université de Montréal, Montréal, P.Q. Canada H3C 3J7.

§Queen's University, Kingston, Ontario, Canada K7L 3N6

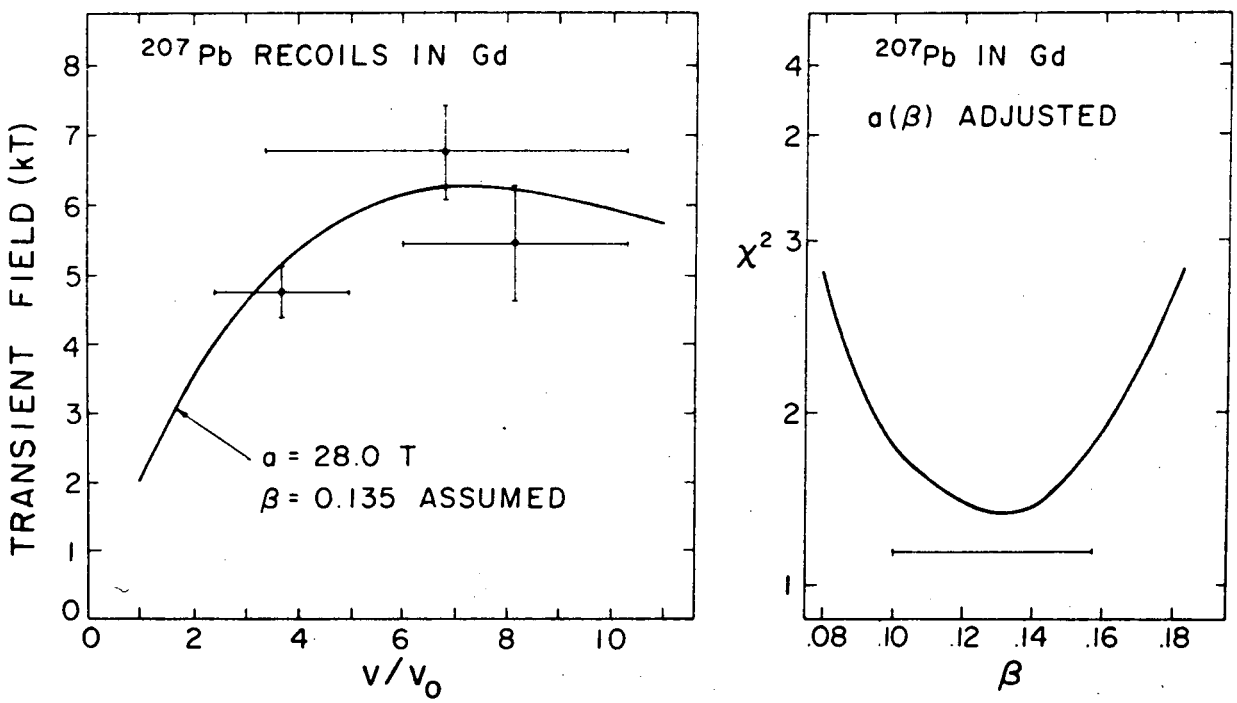

Fig. 1. On the left the TF for ^{207}Pb recoils in Gd is shown versus the recoil velocity. The horizontal bars indicate the velocity intervals relevant for each measurement. The solid line represents a best fit to the data using equation (1) to parametrize the TF. On the right χ^2 is shown versus the parameter β of equation (1).

XBL 8312-2473

Evidence for Reduced Neutron Pairing Correlations in ^{165}Yb*

*C. Schuck,† N. Bendjaballah,‡ R.M. Diamond, Y. Ellis-Akovali,§ K.H. Lindenberger,** J.O. Newton,†† F.S. Stephens, J.D. Garrett,‡‡ and B. Herskind‡‡*

Three rotational sequences in ^{165}Yb have been extended to high spins by using the ^{130}Te(^{40}Ar, 5n) and ^{150}Nd(^{20}Ne, 5n) reactions with beams from the 88-Inch Cyclotron. In this rare-earth region, two band crossings have been established at angular frequencies $\hbar\omega = E_\gamma/2$ of 0.27 and 0.41 MeV in the yrast sequence of the N=90 even-even isotones ^{158}Er and ^{160}Yb. These crossings are interpreted as the alignment of a pair of $i_{13/2}$ quasineutrons and a pair of $h_{11/2}$ quasiprotons. In ^{165}Yb (N=95), which has a somewhat larger deformation, the quasiproton crossing is delayed to a higher rotational frequency. As a result, the rotational sequences based on a specific neutron configuration can be studied to higher frequency than in the lighter, less deformed nuclei.

In this experiment γ-γ coincidences were obtained from an array of five Ge(Li) detectors, four of them set at 153°. An additional coincidence was required with one or more of five 7.6 × 7.6 cm NaI detectors used as a multiplicity filter. Angular distribution measurements were obtained from the fifth Ge(Li) detector positioned alternatively at 0° and at 87°. The extension of these bands to higher spins is based on the relative intensities of the transitions in the γ-γ coincidence data and results in the level scheme of Fig. 1.

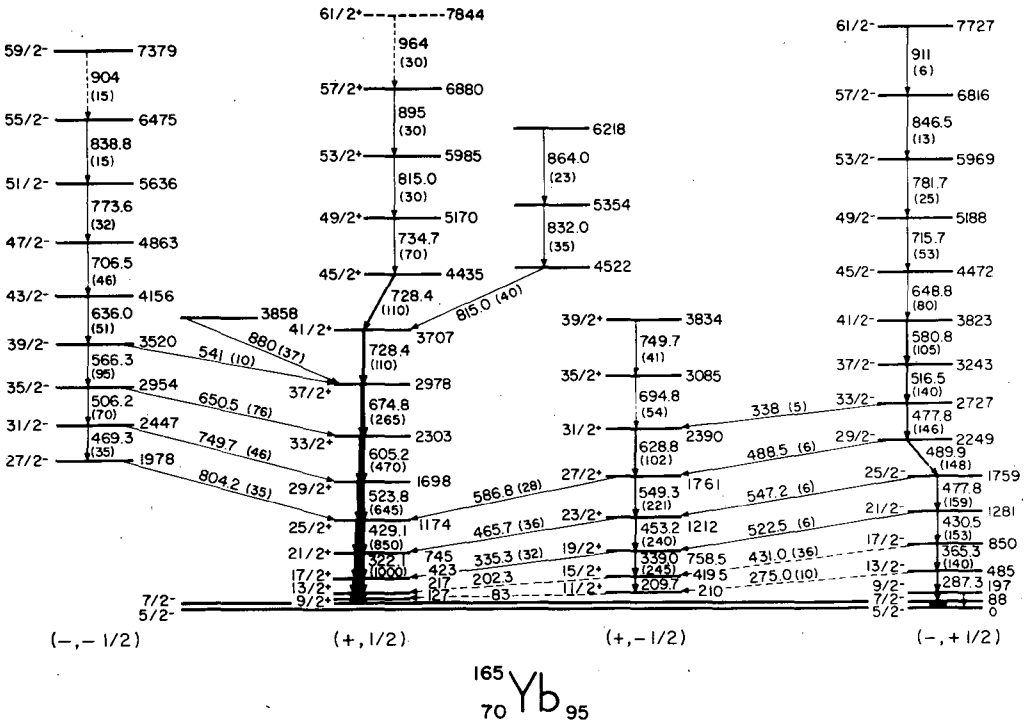

Fig. 1. Level scheme of ^{165}Yb populated by the ^{150}Nd (^{20}Ne,5n) and the ^{130}Te (^{40}Ar,5n) reactions. The numbers between parentheses are the relative intensities of the γ transitions obtained with the ^{20}Ne reaction.

XBL 841-409

The component of the total angular momentum aligned with the rotation is presented in Fig. 2 as a function of the angular frequency $\hbar\omega$ for four rotational sequences in ^{165}Yb together with similar values for the yrast sequence of the neighboring even-even isotopes ^{164}Yb and ^{166}Yb. For $\hbar\omega > 0.28$ MeV in the negative-parity bands of ^{165}Yb and after the blocked band crossing at $\hbar\omega \sim 0.36$ MeV in the positive-parity band, I_x is observed to increase linearly with the frequency.

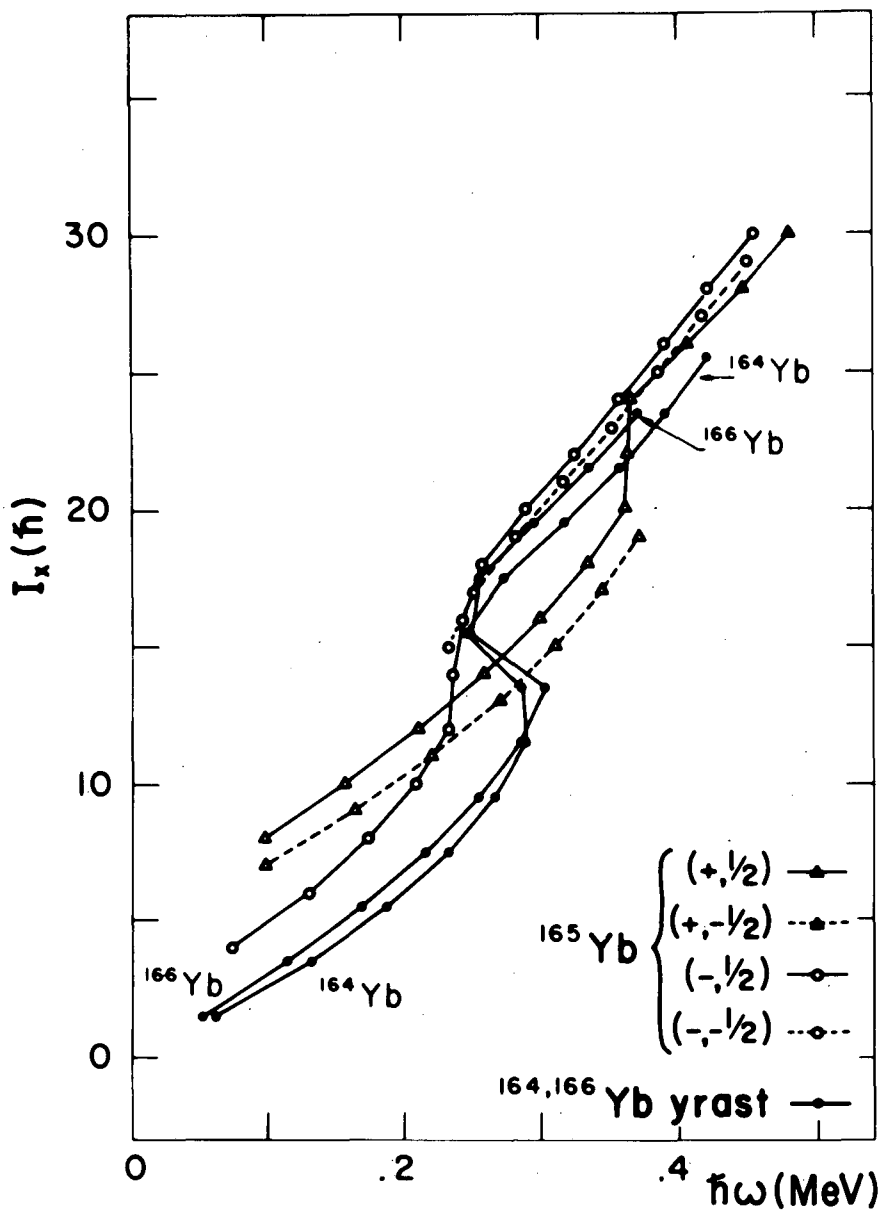

Fig. 2 Plot of I_x vs. $\hbar\omega$ for four rotational bands in ^{165}Yb and the yrast sequences in ^{164,166}Yb. XBL 841-410

The kinematic moments of inertia, $\mathcal{J}^{(i)}/\hbar^2 = I_x/\hbar\omega$ are presented as a function of the frequency in Fig. 3a. At large rotational frequencies ($\hbar\omega > 0.3$ MeV) the $\mathcal{J}^{(1)}$ values for the seniority three (V = 3) sequences in ^{165}Yb are only slightly frequency dependent. In the frequency region where such data exist for the V=2 yrast sequences in ^{164,166}Yb, the $\mathcal{J}^{(1)}$ values are slightly smaller than those of the V=3 configurations. However, all $\mathcal{J}^{(1)}$ values, if extrapolated, seem to converge at the largest rotational frequencies to values close to 65 MeV^{-1}. The dynamic moments of inertia, $\mathcal{J}^{(2)}_{band}/\hbar^2 = dI_x/\hbar d\omega$, are shown as a function of the frequency in Fig. 3b. They are much more sensitive to changes in the local structure than $\mathcal{J}^{(1)}/\hbar^2$, but are nearly constant for the negative-parity states for $0.36 < \hbar\omega < 0.44$.

From these analyses a striking feature that emerges is the nearly constant value of $\mathcal{J}^{(1)}$ above $\hbar\omega = 0.36$ for all three configurations in ^{165}Yb. Two other mathematically equivalent ways to say this are $\mathcal{J}^{(2)}_{band}$ is nearly equal to $\mathcal{J}^{(1)}$ and the I_x vs. $\hbar\omega$ curve is approximately straight with an intercept near zero. The value of $\mathcal{J}^{(1)}/\hbar^2 \sim 65$ MeV^{-1} found at large frequencies is nearly as large as the deformed rigid-rotor value, 73 MeV^{-1}. To understand this behavior we can first consider the properties of a system with no pairing correlations, because the three quasi-neutrons and high rotational frequency are expected to result in a strong reduction of pairing. With no pairing (neutron or proton), $\mathcal{J}^{(1)}$ should average to the deformed rigid-rotor value, but should not be constant due to the occurrence of particle alignments

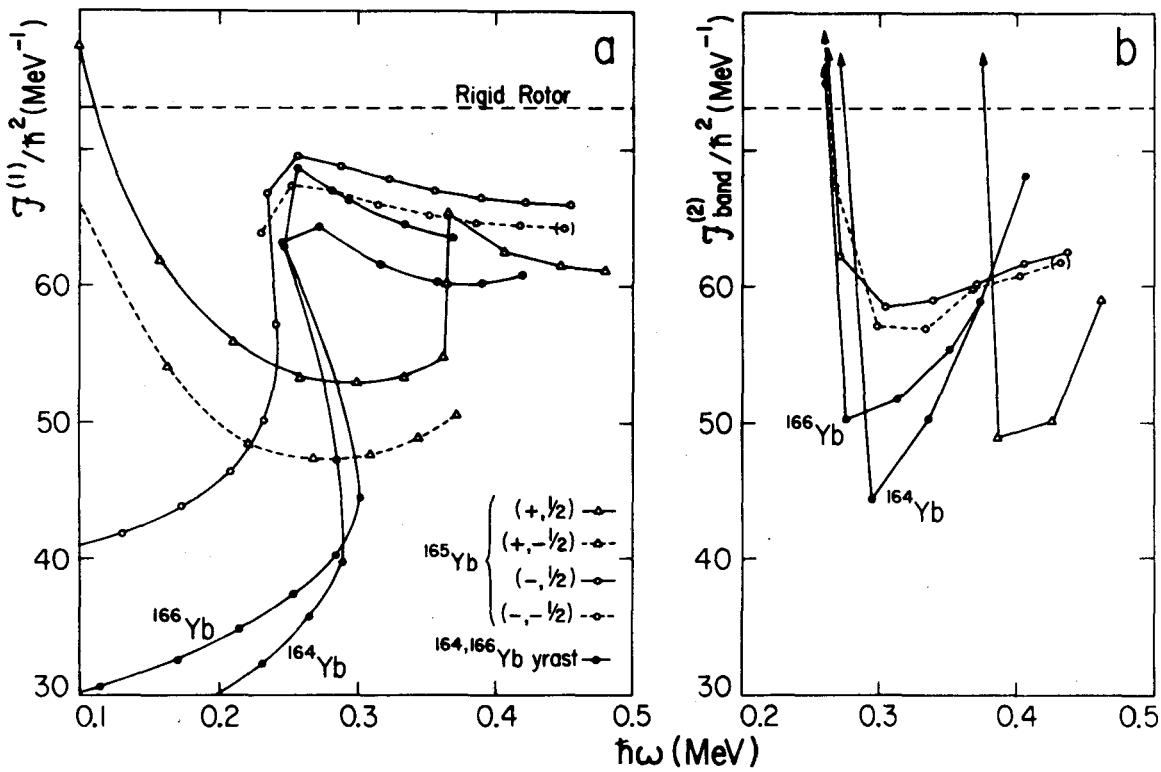

Fig. 3. (a) Plot of $\mathcal{J}^{(1)}$ vs. $\hbar\omega$ for four rotational bands in ^{165}Yb and the yrast bands in ^{164,166}Yb
(b) Plot of $\mathcal{J}^{(2)}_b$ vs. $\hbar\omega$ for three bands in ^{165}Yb and the yrast bands in ^{164,166}Yb XBL 841-411

which cause jumps in $\mathcal{J}^{(1)}$. All Cranked Shell-Model (C.S.M.) calculations of high-spin nuclear behavior predict that part of the angular momentum will continue to come in these sudden alignments, leaving significantly less available for the collective motion. Between alignments, $\mathcal{J}^{(2)}_{\text{band}}$ should therefore be less than $\mathcal{J}^{(1)}$ (around 1/2 to 2/3 on average), causing $\mathcal{J}^{(1)}$ to drop slowly. Thus, $\mathcal{J}^{(1)}$ is expected to oscillate around the rigid-rotor value.

This described behavior is not very similar to that observed. However, there are no quasi-protons in the observed bands of ^{165}Yb, so that the proton pairing correlations are almost surely not quenched. This means that the protons will contribute less angular momentum at a given frequency, resulting in an $\mathcal{J}^{(1)}$ lower than the rigid-body value (as observed). It also means that the proton pairing will be continuously reduced by the Coriolis interaction (Coriolis anti-pairing) as $\hbar\omega$ increases. This will, by itself, contribute to an increasing $\mathcal{J}^{(2)}_{\text{band}}$ value, and together with the decreasing $\mathcal{J}^{(2)}_{\text{band}}$ expected after the (neutron) alignments, could give a nearly constant $\mathcal{J}^{(2)}_{\text{band}}$ as observed. If so, this is a somewhat accidental cancellation of two opposite tendencies. But other examples are now known where $\mathcal{J}^{(2)}_{\text{band}}$ is even more constant over a larger range and where $\mathcal{J}^{(2)}_{\text{band}} \approx \mathcal{J}^{(1)}$. Thus, there may be more fundamental reasons for this behavior but these are not apparent in present C.S.M. calculations. The above discussion requires that the neutron pairing be rather low, but gives no quantitative measure of it.

There are other features about the high-spin states in ^{165}Yb for $\hbar\omega$ = 0.3–0.5 MeV that suggest that the neutron pairing correlations are being substantially reduced, although the experiments performed so far do not rule out the possibility that part of the effects are due to a shape change. Furthermore, because of this and the difficulty in separating the changes in neuton and proton pairing, it does not seem possible to be quantitative about the decrease in neutron pairing from these data. But future experiments (observation of the next few states) and better calculations that simultaneously take into account changes with pairing and deformation may make that possible.

We would like to thank Thomas Døssing for enlightening advice and comments.

Footnotes

*Condensed from LBL-17281

†Centre de Spectrometrie Nucléaire et de Spectrometrie de Masse, 91406 Orsay, France.

‡C.S.T.N. University of Alger, B.P. 1017, Alger, Algeria.

§Nuclear Data Project, Oak Ridge National Laboratory, Oak Ridge, TN, 37830, U.S.A.

**Hahn Meitner Institute, Berlin, W-Germany.

††Australian National University, Canberra, Australia.

‡‡The Niels Bohr Institute, University of Copenhagen, DK 2100 Copenhagen, Denmark.

E2 Properties of the Ground-State Band in ^{248}Cm*

*T. Czosnyka,†§ D. Cline§, L. Hasselgren,‡§ C.Y. Wu,§ R.M. Diamond, H. Kluge, C. Roulet, E.K. Hulet,** R.W. Lougheed,** C. Baktash††*

The transuranic nucleus ^{248}Cm was Coulomb excited using 641 MeV ^{136}Xe from the LBL SuperHILAC and 260 MeV ^{58}Ni projectiles from the Tandem Van der Graaff at Brookhaven National Laboratory. The ground band was observed to spin 22$^+$. The transition energies derived from the present data are in agreement with those obtained from Coulomb excitation of ^{248}Cm by ^{208}Pb ions.[1] These energies lead to a monotonic increase in the moment of inertia of the yrast states as a function of the transition energy or, as in the usual backbending plot, of the square of the rotational frequency. The initial

approximately linear increase in the moment of inertia is thought to result from the Coriolis anti-pairing, the gradual reduction of the pairing correlations among the nucleons with an increase in angular momentum. However, the rise (beyond spin $14\hbar$) above a line extrapolated from the lower-spin-values provides evidence which, while not conclusive, is consistent with the rotation-alignment by the Coriolis force of a pair of high-j nucleons, probably $i_{13/2}$ protons and/or $j_{15/2}$ neutrons, as suggested in ref. 1. The gentleness of this "upbend" implies appreciable mixing of the ground and the intersecting bands in the neighborhood of the band crossing, suggesting that the mixing matrix elements between the intersecting bands are non-negligible. The behavior of the level energies can be reproduced by postulating that the bands intersect around spin 20^+ and that the strength of the interaction between the bands is $\approx$ 200 keV.

The E2 matrix elements of the ground-band states involved in the Coulomb excitation process have been extracted from the data in a model-independent manner using a new least-squares search code. As shown in Fig. 1 the transition E2 matrix elements are in agreement with the spheroidal rigid-rotor model within the indicated errors. The static quadrupole moments derived from the data are consistent with an intrinsic quadrupole moment $0.7^{+2.3}_{-0.4}$ times the value derived from the B(E2: $0_1^+ \rightarrow 2_1^+$) assuming the prolate spheroidal rigid-rotor model. This is consistent with the prolate shape expected for the ground band of ^{248}Cm. The measured B(E2) and static quadrupole moments show no observable influences due to the octupole, β or γ vibrational bands, and these bands were not excited in our studies. Also, if there is one or more band crossings of the ground band in the spin range observed in the present experiments, the E2 properties of the interacting band must not be significantly different from those of the ground band within the indicated experimental errors.

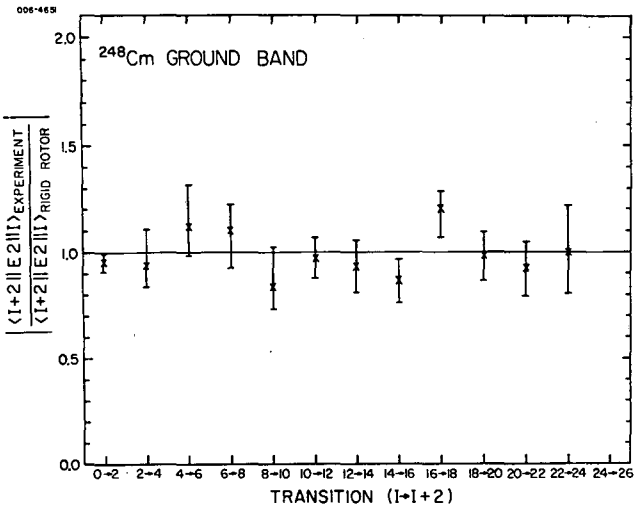

Fig. 1. Ratios of the transition matrix elements, extracted from the present data, to the matrix elements derived from the known B(E2: $0_1^+ \rightarrow 2_1^+$), assuming the spheroidal rigid-rotor relation.

XBL 841-6

Footnotes and Reference

*Condensed from paper to be published in Nucl. Phys.

†Permanent address: ZXXV, Institute of Nuclear Research, 05-400 Swierk, Poland.

‡Permanent address: Institute of Physics, University of Uppsala, Box 530, S-751 Uppsala, Sweden.

§Nuclear Structure Research Laboratory, University of Rochester, Rochester, New York 14627

**Lawrence Livermore Laboratory, Livermore, California 94550.

††Brookhaven National Laboratory, Upton, New York 11973.

1. R.B. Piercey, J.H. Hamilton, A.V. Ramayya, H. Emling, P. Fuchs, E. Grosse, D. Schwalm, H.J. Wollersheim, N. Trautmann, A. Faessler, and M. Ploszajczak, Phys. Rev. Lett. **46**, 415 (1981).

Future Directions for High-Spin Studies*

F.S. Stephens

I want to consider some future directions for experimental high-spin studies, concentrating mainly on the region above I $\sim 30\hbar$, where the γ-ray spectra are currently unresolvable. The 4π NaI balls offer a means to exploit the temperature effects recently shown to exist in such spectra. Large arrays of Compton-suppressed Ge detectors, on the other hand, lead to higher effective resolution as it becomes possible to study triple and quadruple coincident events. We are presently building in Berkeley a detector system that combines both approaches, and I want to describe that briefly.

An overall view of this device is shown in Fig. 1. It consists of an inner, approximately 4π, ball of bismuth germanate, (BGO), surrounded by 21 Compton-suppressed Ge detectors which view the source through small holes in the ball. The Ge detectors are arranged in three rings of seven each, one in the median plane of the ball, and the other two above and below that plane. The BGO ball has 44 elements arranged in three concentric cylinders. (The phototubes, etc. that attach to these elements at the top and bottom of Fig. 1 are not shown.) The elements are about 5 cm thick, giving an overall effi-

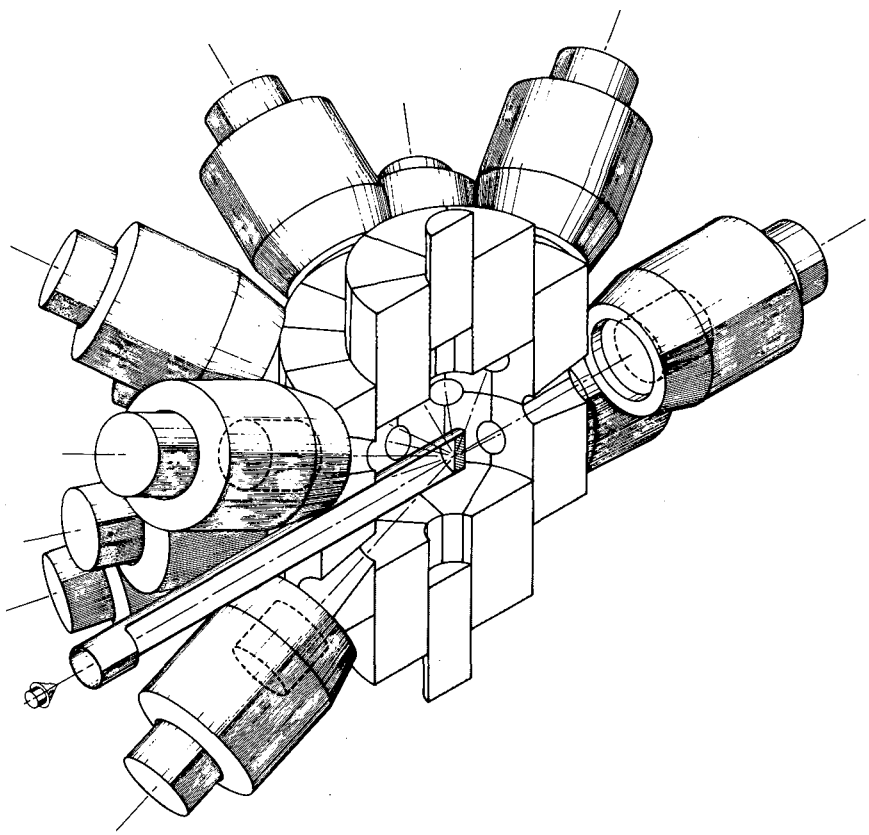

Fig. 1. Perspective view of the High Resolution Ball system currently under construction. XBL 819-2051

ciency of 80% for energies around 1 MeV, not much different from the NaI balls. On the other hand, for multiplicities as high as 30, the resolution in multiplicity will be ~50%, twice that of the NaI balls. At lower multiplicities, of course, it approaches the NaI ball. Thus this device gives an energy-spin cut twice as large as that for the NaI balls but at the same time we have the power of a Ge array far larger than any now existing. An analysis of the performance of the Ge array is given in Table I. In the top section the improved quality due to the Compton suppression is shown. The analysis is for 20% Ge detectors, which have peak (full energy)-to-total ratios around 0.15. In a coincidence arrangement, the probability of obtaining a useful event (full energy-full energy) is only $0.15^2 \simeq 2\%$. That means 98% of all the events give no information, and serve only to obscure the good 2%. For triple or quadruple coincidences the situation is hopelessly bad. Using a prototype of our cylindrical BGO Compton suppressors (whose walls are 3 cm thick), we find we can achieve peak-to-total ratios of about 0.5. A coincident event thus has 25% probability of being useful, an improvement of more than a factor of ten. Furthermore, a triple event has 13% chance to be composed of three full energy peaks, and a quadruple event, a 6% chance to involve four full energies. This last figure is more than 100 times better than a quadruple event with no Compton suppression, and is even three times better than a double coincidence with no Compton suppression. Thus the quality of the events from our array will be 10 to 100 times better than those from an array without Compton suppression.

The lower part of Table I shows the quantity of events that will be produced by this array. We start with an event rate (rate of forming compound nuclei) of 10^5 per second (this is a rate we use routinely in current experiments) and an average multiplicity of 20 (also a normal value). Then we can evaluate rates coming out of various arrays. Listed are the counts per second, and below that the

TABLE I Analysis of the performance expected for HRB.

Ge	20% (of 1.33MeV c.f. 3×3 in. NaI)			
	1 Ge	Ge × Ge	Ge^3	Ge^4
Peak/Total	0.15	0.022	0.0034	0.0005
Compton Supp. Peak/Total	0.5	0.25	0.13	0.06
Improvement	×3	×10	×30	×100

10^5 Triggers/sec $M_\gamma = 20$	Counts per second Days to collect 2.5×10^8 events		
	Ge × Ge	Ge^3	Ge^4
5 Detectors	230	3.3	0.02
17 cm	13	2.4 yr	345 yr
5 Detectors	870	25	0.35
12 cm	3.3	116	23 yr
21 Detectors	11000	2200	280
12 cm	0.26	1.3	10

number of days to collect 2.5×10^8 events, a number which corresponds to the best current experiments. The first line in the lower part of Table I gives rates for the best Compton-suppressed array so far used, 5 detectors located 17 cm away from the target. The estimate is that it takes 13 days to collect 2.5×10^8 double events, and years to collect that many triples or higher. Such an experiment was run at the Copenhagen tandem accelerator,[1] and it did, in fact, take about two weeks. In the next lower line of Table I, the effect of the solid angle is emphasized. Bringing those detectors in to 12 cm (impossible in the experiment due to the large NaI Compton suppressors), would produce a factor of ~ 4 in the double rate, and change the experiment from the "heroic" class to the "normal" class. The expected performance of our array is shown in the bottom line of Table I. The doubles rate is ~ 50 times the previous one and the "classic" experiment can be done in a quarter of a day. For the first time in nuclear physics, triple Ge coincidence experiments become really feasible, and 2.5×10^8 such events can be accumulated in a little over a day. Quadruples will be accumulated about the rate of doubles in the "classic" experiment, an improvement of more than 10^4 over quadruples in that experiment. Thus while the NaI balls will explore for the first time the temperature effects on high spin states, this ball will explore for the first time what can be done with high quality triple and quadruple coincidence data. I will mention a few possibilities we see now for such data.

First, consider the usual experiment to identify high spin states. For a collective nucleus, there are normally ~ 10 bands appreciably populated at the highest spins, and one must find a "clean" line rather high up in a band (above known branchings) to serve as a coincident gate in looking for higher unknown members of that band (or branch). The limit (apart from present-day statistics) comes when no sufficiently clean line can be found, and one cannot be sure if weak observed lines are band members or not. An obvious use of triple coincidences is to set double gates in a band, thereby greatly increasing the purity of the observed spectrum. A rough estimate shows that about 10 times more bands can be resolved using triple coincidences than with doubles. This should push the spin limit up by $\sim 6\text{-}10\hbar$ on average.

A more general and exciting overall approach to this problem is to make triple (or quadruple) correlation studies. Here one looks for sets of three or four γ-ray energies that occur more frequently than would be expected statistically. The existing subtraction methods can easily be expanded to three or four dimensions in order to subtract out the uncorrelated events. What will we learn from a triple correlation plot? It is not so easy to answer that question. At a simple level, it is a way to extend the known high spin bands or sequences. This is essentially the method discussed in the previous paragraph, but with an uncorrelated background subtracted and a systematic look at all sets of three γ-rays, rather than preselecting two. To take a more pragmatic view, we saw almost no structure in one dimensional Ge spectra from the high spin regions of these heavy-ion fusion reactions, but there is a lot of structure in the two dimensional correlation plots. These structures are broader than individual coincidence pairs would be. In a triple correlation plot, we can expand these interesting regions out along a third dimension. This seems to be one of our best hopes to resolve features from individual bands or sequences at very high spins. Once we can get down to resolving sets of individual γ-rays, I am confident they can be put together into level schemes. The challenge here will be to handle the very large data arrays and learn methods to extract the information we want. If we can do that, this is the way to much higher effective resolving power.

Footnote and Reference

*Presented at the Conference on High Angular Momentum Properties of Nuclei, Oak Ridge, TN, November 2-4, 1982.

1. B. Herskind, private communication, 1982.

Polarization Studies

Separation of Projectile and Ejectile Spin-Orbit Distortions in an $\ell = 0$ (d,^{3}He) Reaction*

*J.D. Brown,† J.M. Barnwell,‡ S. Roman,‡ H.E. Conzett, D. Eversheim, R.M. Larimer, J. Birchall,§ C. Lapointe,§ J.S.C. McKee,§ N.M. Clarke,** R.J. Griffiths,** J.S. Hanspal,** R.A. McCulloch***

The distorted wave Born approximation (DWBA) is used extensively in the analysis of single nucleon transfer reactions. Although experimental differential cross-section angular distributions are seldom irreproducible by the DWBA, it has been frequently reported that the DWBA predictions for polarizations are far from satisfactory.

Improvements to the "fitting" of the experimental data may occur by choosing different entrance and/or exit channel optical potentials. Therefore in the case of a poor reproduction of observable quantities it would be advantageous to differentiate between the inadequacies of a particular optical model potential set used in the DWBA calculation and the limitations of the DWBA theory. It is necessary to ascertain the shortcomings of the DWBA, as it is widely used to extract spectroscopic factors in nuclear reactions and to assign spins and parities of nuclear states.

If it is possible to identify observables which are dependent on some terms in the optical potential, then the effectiveness of these particular terms in reproducing the data could be investigated. For polarization observables the value of the orbital angular momentum transfer is the precursor for identifying terms in the optical potential which play the dominant role in producing the observable. For a reaction where the orbital angular momentum transfer, ℓ_{tr}, is non-zero, the polarization effects originate primarily in the central potential,[1,2] whereas if the ℓ_{tr} is zero and D-state effects are neglected, the spin-orbit potentials are the only ones which contribute to the polarization observables.[3,4]

Johnson[5,6] has produced a formalism that enables the separation of the spin dependent distortions in the entrance and exit channels when the ℓ_{tr} is zero. Combinations of the polarization and analyzing power in a single nucleon transfer reaction yield two quantities which are dependent upon the spin-orbit potential in the entrance and exit channel. This theory can be applied to investigate the problems associated with the predictions of polarization data in terms of the spin-orbit potential of one or the other channel.

In an $\ell_{tr} = 0$ (d,^{3}He) reaction initiated by polarized deuterons, the analyzing power, A_y, in the absence of D-state considerations, is given by

$$A_y = (\frac{2}{3})S_h + S_d \qquad (1)$$

where S_h and S_d are terms proportional to the ^{3}He and deuteron spin-orbit potential, respectively. If the deuteron beam is unpolarized then the polarization, p_y, of the outgoing ^{3}He particles is written as

$$p_y = S_h + S_d \qquad (2)$$

Inspection of equations 1 and 2 yields the formalism for the construction of S_d and S_h from the analyzing power and polarization, namely

$$S_h = 3p_y - 3A_y = 3p_y - 2\sqrt{3}\, iT_{11}$$

$$S_d = 3A_y - 2p_y = 2\sqrt{3}\, iT_{11} - 2p_y \qquad (3)$$

where iT_{11} is the vector analyzing power expressed in a spherical co-ordinate system. In this way the ^{3}He and deuteron spin-orbit distortions are now

separated, and experimental angular distributions can be obtained by measuring the analyzing power and polarization in an $\ell_{tr} = 0$ (d, ^{3}He) reaction. If use is made of the "polarization-asymmetry theorem"[7], then the polarization in a (d, ^{3}He) reaction is equal to the analyzing power in the inverse (^{3}He,d) reaction at the same center of mass energy and angle. Thus, experimentally the polarization data are best obtained by measuring the analyzing power of the exact inverse reaction.

Data were taken at Birmingham for the ^{30}Si($^3\vec{\text{He}}$, ^{3}He)^{30}Si and ^{30}Si($^3\vec{\text{He}}$,d)^{31}P reactions at 33 MeV. Data for the ^{31}P($\vec{\text{d}}$, ^{3}He)^{30}Si reaction together with the deuteron elastic scattering were taken simultaneously at the the 88-Inch Cyclotron using a 35 MeV vector polarized deuteron beam.

The ($\vec{\text{d}}$,^{3}He) and ($^3\vec{\text{He}}$,d) analyzing powers measured at the same center of mass angle were combined in the way prescribed by equation 3, producing the angular distribution of S_d and S_h. S_d and S_h are opposite in sign and are of equal magnitude. This observation implies that the deuteron and ^{3}He spin-orbit potentials play equally important roles in determining the polarization observables.

An optical model study of the ^{3}He elastic scattering data revealed that the spin-orbit potential with a radial variation that is sharply peaked at the nuclear surface is preferred. A "forced fit" with a large spin-orbit diffuseness could not reproduce the elastic scattering analyzing power data as well as a potential with a small diffuseness. The method for choosing deuteron optical potentials was to perform "one-shot" optical model and DWBA calculations and to compare the predictions with the data. This was justified by the satisfactory quality of the fits to the experimental observables including S_d.

Experimental angular distributions of the quantities S_d and S_h indicate that there is no predominance of the entrance or exit channel spin-orbit distortion over the other. However, DWBA predictions reproduce the trend of S_d reasonably well, whereas predictions for S_h are only appreciable when the D-state component of the ^{3}He wave function is included in the calculation. The result of the removal of one or the other of the spin-orbit potentials in the calculation is in agreement with theoretical expectations for S-state only calculations.

It appears that by using the "conventional" derivative Woods-Saxon potential form factor a satisfactory fit to S_h is very difficult to find, indicating perhaps that a different potential form factor may prove to be required in order to reproduce the data for S_h. Calculations with different form factors have not been attempted in detail. In spite of the difficulties encountered with the description of the spin separated quantities S_d and S_h, the present work has clearly proven the usefulness of this approach in the study of the role of nuclear distortion in the mechanism of the (d,^{3}He) one-nucleon transfer reaction.

Footnotes and References

*Condensed from LBL-16965, submitted to Nucl. Phys. A.

†Indiana University Cyclotron Facility, Bloomington, IN 47405.

‡Physics Department, University of Birmingham, Birmingham, England.

§Cyclotron Laboratory, University of Manitoba, Winnipeg, Manitoba R3T 2N2, Canada.

**Physics Department, Kings College, University of London, England.

1. T.J. Yule and W. Haeberli, Phys. Rev. Lett. **19**, 756 (1967).
2. T.J. Yule and W. Haeberli, Nucl. Phys. **A117**, 1 (1968).
3. L.J.B. Goldfarb and R.C. Johnson, Nucl. Phys. **21**, 462 (1960).
4. R.C. Johnson, Nucl. Phys. **A90**, 289 (1967).
5. R.C. Johnson, Nucl. Phys. **35**, 654 (1962).
6. R.C. Johnson, private communication.
7. N. Austern, "Direct Nuclear Reaction Theory" (J. Wiley, New York, 1970).

Spin-Polarization Observables at the $J=\frac{3}{2}^+$ Resonance in the Reactions $^3H(d,n)^4He$ and $^3He(d,p)^4He$*

H.E. Conzett

The charge-symmetric reactions $^3H(d,n)^4He$ and $^3He(d,p)^4He$ have an extensive history of both experimental and theoretical study.[1] In particular, it was early shown that at the near-threshold s-wave $J=\frac{3}{2}^+$ resonance, these reactions could serve as analyzers of low energy tensor-polarized deuterons and as sources of polarized nucleons from unpolarized incident deuterons.[2,3] Later studies examined the effects of including a $J=\frac{1}{2}^+$ reaction amplitude[4] and, in addition, calculations of some polarization-transfer coefficients were made.[5] More recently it was noted,[6] for the case of the single non-zero $J=\frac{3}{2}^+$ reaction amplitude, that the cartesian component $A_{yy}(\Theta)$ of the deuteron tensor analyzing power was a constant,

$$A_{yy}(\Theta) = -\left(\frac{1}{2}\right)^{1/2} T_{20}(\Theta) + \left(\frac{1}{3}\right)^{1/2} T_{22}(\Theta) = \frac{1}{2},$$

which was implicit in the earlier expressions for the spherical components of the tensor analyzing powers.[4,5] Also, a very recent investigation showed that the $^3H(d,n)^4He$ fusion reaction rate could be enhanced by a factor of $\frac{3}{2}$ if the fusion plasma consisted of both polarized deuterons and tritons, forming exclusively the channel-spin $s = \frac{3}{2}$ and $J=\frac{3}{2}^+$ state.[7] This result follows simply from the statistical weights of the quartet $s=\frac{3}{2}$ and doublet $s=\frac{1}{2}$ initial states, with the assumption of the single $J=\frac{3}{2}^+$ reaction amplitude.

It is this latter result that motivates this paper, since this result should be seen in the expression for the cross section with deuteron polarization components p_{zz}, $p_z(1)$ and triton (or ^3He) polarization $p_z(1/2)$,

$$I(\Theta) = I_0(\Theta)(1+\frac{1}{2}p_{zz}A_{zz}+\frac{3}{2}p_z(1)p_z(1/2)C_{z,z}),$$

where $I_0(\Theta)$ is the cross section with unpolarized participants, A_{zz} is a tensor analyzing-power component, and $C_{z,z}$ is a spin-correlation coefficient.[8,9]

So, for $p_{zz} = p_z(1) = p_z(1/2) = 1$,

$$I(\Theta) = I_0(\Theta)(1+\frac{1}{2}A_{zz}+\frac{3}{2}C_{z,z}). \qquad (1)$$

Although $A_{zz} = \sqrt{2}\, T_{20} = -\frac{1}{2}(3\cos^2\Theta - 1)$ was available from the previous work,[4,5] $C_{z,z}$ and other spin-correlation and polarization-transfer coefficients were not. This work provides the values of these remaining polarization observables.

All of the polarization observables for this system, with the spin structure $1 + \frac{1}{2} \rightarrow \frac{1}{2} + 0$, have been tabulated[8,9] in terms of the elements of the transition matrix M between the initial and final spin states, $\chi_f = M\,\chi_i$. Here $M \equiv [M_{\gamma,\alpha\beta}]$, where α, β, γ label the magnetic substates of the initial state spin-1, spin-$\frac{1}{2}$, and final state spin-$\frac{1}{2}$ particles, respectively. This is the uncoupled representation. Partial-wave expansions of the transition matrix elements are more readily available in the coupled (channel-spin) representation $\chi_f = K\Phi_i$ with $K \equiv [K_{s'\nu' s\nu}]$, where $s,\nu(s',\nu')$ are the initial (final) state channel-spin and its substates and Φ_i is the set of initial-state channel-spin functions. Since here $\chi_f = M\chi_i = K\Phi_i$, the transformation between the elements of M and K is the same as that between the spin-functions χ_i and Φ_i. The procedure, then, is to obtain the K-matrix elements from the partial wave expansions and transform these to the M-matrix elements, from which the polarization observables are calculated. The M-matrix elements obtained are:

$$M_{\frac{1}{2},1\frac{1}{2}} = \left(\frac{\pi}{5}\right)^{1/2} UY_2^1(\Theta) = \frac{(-iA-D)}{\sqrt{2}}$$

$$M_{\frac{1}{2},0\frac{1}{2}} = \left(\frac{4\pi}{15}\right)^{1/2} UY_2^0(\Theta) = F$$

$$M_{\frac{1}{2},-1\frac{1}{2}} = \left(\frac{\pi}{5}\right)^{1/2} UY_2^{-1}(\Theta) = \frac{(-iA+D)}{\sqrt{2}} \quad (2)$$

$$M_{\frac{1}{2},1-\frac{1}{2}} = \left(\frac{2\pi}{15}\right)^{1/2} UY_2^0(\Theta) = \frac{(-B-C)}{\sqrt{2}}$$

$$M_{\frac{1}{2},0-\frac{1}{2}} = \left(\frac{2\pi}{5}\right)^{1/2} UY_2^{-1}(\Theta) = E$$

$$M_{\frac{1}{2},-1-\frac{1}{2}} = \left(\frac{4\pi}{5}\right)^{1/2} UY_2^{-2}(\Theta) = \frac{(-B+C)}{\sqrt{2}}$$

The right hand side of Eqs. (2) is the M-matrix representation in which the calculated polarization observables are tabulated.[8,9] From (2)

$$\begin{array}{ll} A=0 & D=E=-N(3\sin\Theta\cos\Theta) \\ B=N & F=-N(3\cos^2\Theta-1), \\ C=N(3\cos^2\Theta-2) & \text{with } N=-U/2\sqrt{3} \end{array} \quad (3)$$

Using Eqs. (3), the tabulated polarization observables have the following values:

$\vec{1} + \frac{\vec{1}}{2} \rightarrow \frac{1}{2} + 0$ observables:

$$A_y(1) = A_y(1/2) = p^{y'} = 0$$

$$A_{yy} = \frac{3}{4}C_{y,y} = \frac{1}{2}$$

$$A_{xy} = \frac{3}{2}C_{z,x} = \frac{3}{2}C_{x,z} = -\frac{3}{2}\sin\Theta\cos\Theta$$

$$A_{xx} = -\frac{3}{2}C_{z,z} = \frac{1}{2}(3\cos^2\Theta-2) \quad (4)$$

$$A_{zz} = -\frac{3}{2}C_{x,x} = -\frac{1}{2}(3\cos^2\Theta-1)$$

$$C_{xy,x} = C_{yz,x} = C_{xz,y} = C_{xx,y} = 0$$

$$C_{yy,y} = C_{zz,y} = C_{xy,z} = C_{yz,z} = 0$$

$\vec{1} + \frac{1}{2} \rightarrow \frac{\vec{1}}{2} + 0$ observables:

$$K_x^{x'} = -\frac{1}{3}(3\cos^2\Theta-1) \quad K_y^{y'} = -\frac{2}{3}$$

$$K_z^{x'} = K_x^{z'} = \sin\Theta\cos\Theta \quad K_z^{z'} = \frac{1}{3}(3\cos^2\Theta-2)$$

$$K_{xy}^{x'} = K_{yz}^{x'} = K_{xz}^{y'} = K_{xx}^{y'} = 0 \quad (5)$$

$$K_{yy}^{y'} = K_{zz}^{y'} = K_{xy}^{z'} = K_{yz}^{z'} = 0$$

$1 + \frac{\vec{1}}{2} \rightarrow \frac{\vec{1}}{2} + 0$ observables:

$$K_x^{x'} = -\frac{1}{3}(3\cos^2\Theta-1) \quad K_z^{z'} = \frac{1}{3}(3\cos^2\Theta-2)$$

$$K_y^{y'} = -\frac{2}{3} \qquad K_z^{x'} = K_x^{z'} = \sin\Theta\cos\Theta \ .$$

Since Ohlsen[5,8] describes the final-state particles in their own cm helicity frame, his $K_z^{x'}$ and $K_z^{z'}$ are related to those of (5) by a rotation through the angle Θ around the y-axis. With the values (4) of A_{zz} and $C_{z,z}$, integration of Eq. (1) over the 4π solid angle give $\sigma = \frac{3}{2}\sigma_0$.

Footnote and References

*Condensed from invited paper, 10th International Conference on Few Body Problems in Physics, Karlsruhe, Germany, August 21-27, 1983, LBL-16383.

1. F. Ajzenberg-Selove, Nucl. Phys. **A320**, 1 (1979).
2. A. Galonsky *et al.*, Phys Rev. Lett. **8**, 349 (1959).
3. L.J. B. Goldfarb, Nucl. Phys. **12**, 657 (1959).
4. L.C. McIntyre and W. Haeberli, Nucl. Phys. **A91**, 369 (1967).
5. Gerald G. Ohlsen, Phys. Rev. **164**, 1268 (1967).
6. F. Seiler, Nucl. Phys. **A286**, 1 (1977).
7. R.M. Kulsrud *et al.*, Phys. Rev. Lett. **17**, 1248 (1982).

8. Gerald G. Ohlsen, Rep. Prog. Phys **35**, 717 (1972).

9. P.W. Keaton, Jr. *et al.*, Ann. Phys. **85**, 152 (1974).

Insensitivity in Some Tests of Time-Reversal Invariance*

H.E. Conzett

Among the various tests of time-reversal invariance (TRI), the polarization-analyzing power theorem has the virtue that it follows directly from TRI. The theorem states that the spin-polarization (P) of a final-state particle in a (binary) nuclear reaction is equal to the analyzing power (A) for that polarized particle incident in the inverse reaction. Since elastic scattering is its own inverse process, until recently it has been used in essentially all of the tests of TRI that use the polarization-analyzing power equality. It is now clear that all of these previous P-A comparisons fail as adequate tests of TRI either because of a lack of sensitivity to T-symmetry violation or a lack of experimental precision.

The majority of P-A comparisons have been made in pp elastic scattering, the older ones at energies between 142 and 635 MeV before the advent of accelerated polarized beams. More recently, a comparison was made at 6 GeV/c. Two more accurate comparisons have been made in p-nucleus elastic scattering, p-^{3}He and p-^{13}C. Bystricky, Lehar, and Winternitz[1] have recently shown that the older pp results do not, in fact, establish TRI in that region of nucleon-nucleon scattering; and I have found that none of the other three comparisons was accurate enough to provide a significant test of TRI, because the equality between P and A depends on the equality of the two possible spin-flip probabilitites. It is now known from measurements of the depolarization in 6 GeV/c pp scattering and in p-nucleus elastic scattering that the spin-flip probabilities are very small, leading to $P - A \simeq 0$ even if the probabilities are not equal, as required by TRI.

It is now clear that tests of TRI in elastic scattering, using the P-A equality, should be made through measurements where the spin-flip probability is expected or known to be large. Even better, more stringent and conclusive tests are provided by P-A comparisons in a reaction and its inverse, since the testing of TRI is not then limited to the spin-flip cross sections. Additionally, large spin-flip probabilities are common to many reactions which are suitable for these tests of TRI.

Footnote and Reference

*Abstract of paper contributed to the International Conference on Nuclear Physics, Florence, Italy, August 29-September 3, 1983, LBL-16020A.

1. J. Bystricky, F. Lehar, and P. Winternitz, J. Physique, to be published.

Scattering of Polarized Protons from ^{24}Mg, ^{27}Al, ^{32}S and Anomalies in the Giant-Resonance Regions of ^{25}Al, ^{28}Si, and ^{33}Cl*

R. Roy,† C.R. Lamontagne,† R.J. Slobodrian,† J. Arvieux,‡ J. Birchall,§ and H.E. Conzett

Differential cross-section and analyzing power angular distributions have been measured for the elastic scattering of polarized protons on ^{24}Mg, ^{27}Al and ^{32}S between 13 and 27 MeV. An optical model analysis has been performed, and the spin-orbit potentials display significant variations in the giant resonance region of ^{25}Al, ^{28}Si and ^{33}Cl. The ^{24}Mg and ^{32}S data have been examined in a phase-shift analysis.

Footnotes

*Abstract of LBL-16403, submitted to Nuclear Physics A.

†Laboratoire de Physique Nucléaire, Université Laval, Québec, Canada G1K7P4.

‡Laboratoire National Saturne, CEN Saclay, 91191, Gif-sur-Yvette, France.

§Cyclotron Laboratory, University of Manitoba, Winnipeg, Manitoba, R3T 2N2, Canada.

Time-Reversal Asymmetry: Polarization and Analyzing Power in Nuclear Reactions*

C. Rioux, R. Roy,† R.J. Slobodrian,† and H.E. Conzett

Measurements of the proton polarization in the reactions ^{7}Li(^{3}He, $\vec{p}$)^{9}Be and ^{9}Be(^{3}He, $\vec{p}$)^{11}B and of the analyzing powers in the inverse reactions, initiated by polarized protons at the same center-of-mass energies, show significant differences. This implies the failure of the polarization-analyzing-power theorem and, *prima facie*, of time-reversal invariance in these reactions. The reaction ^{2}H(^{3}He, $\vec{p}$)^{4}He and its inverse have also been investigated and show smaller differences. A discussion of the instrumental asymmetries is presented.

Footnotes

*Abstract of Nuclear Physics **A394**, 428 (1983).

†Laboratoire de Physique Nucléaire, Université Laval, Québec, Canada G1K7P4.

Elastic and Inelastic Scattering of Polarized Protons from ^{6}Li

D. Rowley, C.H. Poppe,* F.S. Dietrich,* H.E. Conzett, D. Eversheim, and C. Rioux*

As part of an effort to systematically test the predictions of nuclear reaction models based on complex, density-dependent nucleon-nucleon interactions, we have measured analyzing powers of polarized protons scattered from ^{6}Li. Angular distributions of protons corresponding to the ground and first-excited (3+, T = 0) states of ^{6}Li were measured at incident energies of 25, 35, and 45 MeV.

The elastic scattering data have been analyzed with a microscopically-derived potential using a ground-state density consistent with electron scattering measurements and effective two-body interactions as input, as well as with a standard phenomenological potential.[1] The calculations with the microscopic potential (central potential from ref. 2; spin-orbit interaction from ref. 3) are compared in the upper portion of Fig. 1 (solid curve) with the present analyzing power measurements and with previously measured differential cross sections[1] at 35 MeV.

In contrast to the excellent results obtained in heavier nuclei with the same type of model,[4] the agreement with the data is poor, particularly for the analyzing powers. The phenomenological model also yields poor results for the analyzing powers. The dashed curve shows that the agreement can be significantly improved by multiplying the real central optical potential by an L-dependent factor $1 + c(-1)^L$. This modification is motivated by resonating group calculations[5] and simulates[6] exchange processes other than the single-nucleon knockout mechanism that is already approximated in the microscopic optical potential. The magnitude of c is small (<0.1), as predicted by the resonating-group calculations[5] for ^{6}Li.

The analyzing powers calculated in a distorted-wave Born approximation with a microscopic transition form factor for the inelastic transition are also in striking disagreement with the measurements, as shown in the lower part of Fig. 1. The disagreement becomes more pronounced with increasing energy. The transition form factors were calculated with the central interaction of ref. 7 and a spin-orbit interaction from ref. 3, and a transition density determined by electron scattering. The results are similar for either a microscopic distorting potential (solid curve), or a phenomenological one (dashed curve).

The results of this experiment suggest that an improved treatment of exchange processes is required for nucleon scattering from very light nuclei.

Footnote and References

*Lawrence Livermore National Laboratory

1. K.H. Bray *et al.*, Nucl. Phys. **A189**, 35 (1972).
2. J.D. Jeukenne, A. Lejeune, and C. Mahaux, Phys. Rev. **C16**, 80 (1977).
3. G. Bertsch *et al.*, Nucl. Phys. **A284**, 399 (1977).
4. S.H. Mellema *et al.*, Phys. Rev. **C28**, 2267 (1983).
5. D.J. Stubeda *et al.*, Phys. Rev. **C17**, 447 (1978).
6. F.K. Vosniakos *et al.*, Nucl. Phys. **A332**, 157 (1979).
7. F.A. Brieva and J.R. Rook, Nucl. Phys. **A291**, 299 (1977).

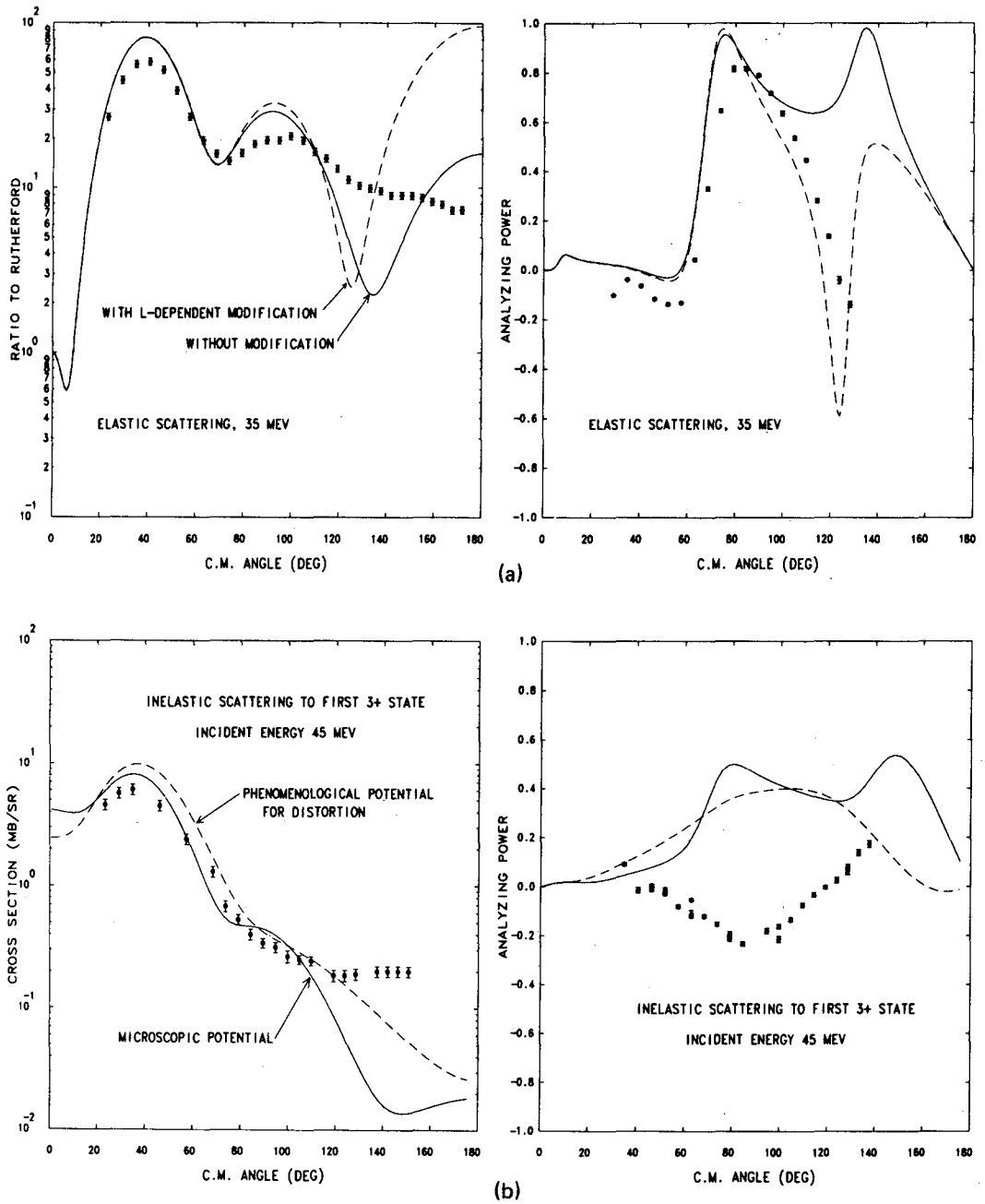

Fig. 1. (a) Differential cross sections and analyzing powers in ^{6}Li(p,p)^{6}Li elastic scattering at 35 MeV. The calculated curves are described in the text. (b) Differential cross sections and analyzing powers in the inelastic transition ^{6}Li(p,p′) ^{6}Li(2.184 MeV, 3^+, T = 0) at 45.4 MeV. The calculated curves are described in the text. XBL 842-591

Damped Collisions and Transfer Reactions

Compound Nucleus Decay Via the Emission of Large Fragments*

L.G. Sobotka, M.L. Padgett, G.J. Wozniak, G. Guarino,† A.J. Pacheco,‡ L.G. Moretto, Y. Chan, R.G. Stokstad, I. Tserruya,§ and S. Wald

We have obtained experimental evidence for the emission of complex nuclei from helium through fluorine by compound nuclei produced in the reaction 90 MeV ^{3}He + ^{nat}Ag. ^{3}He was used since it is desirable to have a projectile with low velocity to minimize preequilibrium losses but massive enough to bring in sufficient energy. In addition, the mass of the projectile should be sufficiently smaller than those of the complex fragments of interest to rule out the ambiguity of projectile fragmentation or multinucleon transfer.

To determine the existence of an isotropically emitting source and its velocity, the laboratory energy spectra were transformed into invariant cross-section plots in velocity space. Two conclusions were drawn from these invariant cross-section plots. First, for all elements there is an angular region in the backward hemisphere where only a single component is observed, which can be characterized by c.m. emission. This angular region increases and extends to more forward angles as the ejectile mass increases. Second, there is a component of non-c.m. emissions that results in harder energy (or velocity) spectra at forward angles.

The energy spectra of the equilibrium component in the c.m. system have Coulomb-like mean energies which increase as the charge of the fragment increases. The most interesting feature in the energy spectra of the equilibrium component is the evolution from a Maxwellian shape for α-particles or Li ions through a more symmetric shape for B or C to a symmetric shape for the heaviest ejectiles, as predicted in ref. 1. At forward angles, our data show the presence of a nonequilibrium exponential tail.

The experimental yields of the equilibrium component are shown in Fig. 1. To minimize contributions from sources other than the compound nucleus, we have plotted the yields only for the most backward angle (171°). These yields drop precipitously in going from Z = 2 to Z = 3, after which they decrease more slowly. The one exception is the enhanced Z = 6 yield.

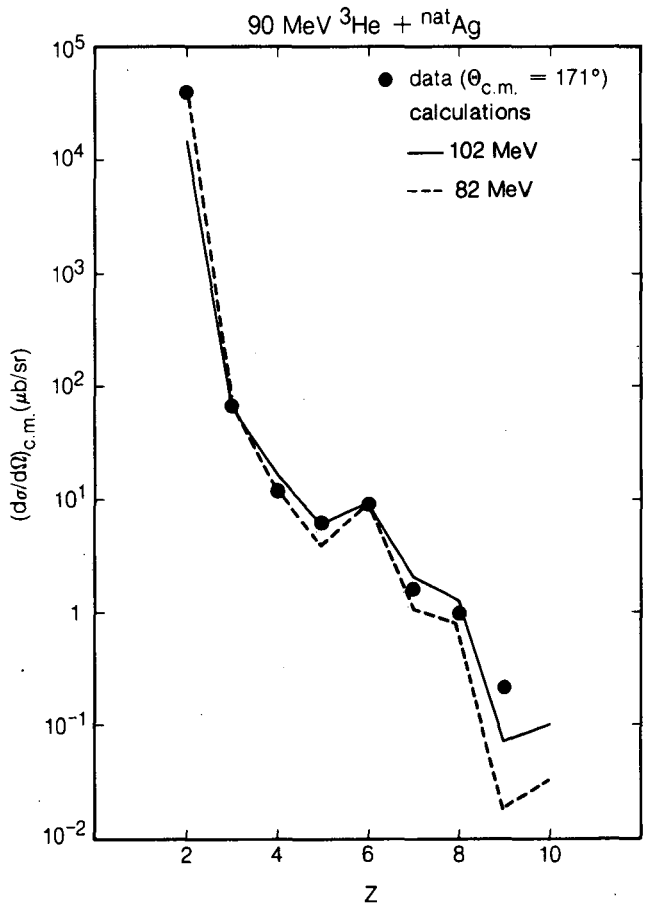

Fig. 1. Experimental (circles) and theoretical yields versus ejectile atomic number (Z). XBL 836-392

Regardless of whether the transition state approach or an evaporation formalism is employed, the yield from an equilibrium statistical emission process should be roughly proportional to a factor $\exp[-B_Z/T_Z]$, where B_Z is the emission barrier for fragment Z and T_Z is the temperature at the barrier.[1,2] A compound nucleus excitation energy (E*) of 102 MeV (the value for full momentum transfer) was assumed. The theoretical ejectile yields, which include isotope and ground state spin considerations, were calculated as a ratio of Γ_Z/Γ_6 and have been normalized to the data at Z = 6 in Fig. 1. The agreement between the data (circles) and this simple equilibrium statistical calculation (solid line) is exceptionally good for Z = 3–9. The calculation underpredicts the α-particle yield because it only takes into account first chance emission, whereas substantial amounts of higher chance α-emission occur. The agreement depicted in Fig. 1 does indicate that an equilibrated process is responsible for the emission of these complex fragments.

The angular distributions in the center of mass are shown in Fig. 2. From ~100° to 170° the angular distributions change from flat to backward peaked as the ejectile mass increases. Such an increase in anisotropy with increasing particle mass is well understood from angular momentum considerations and discussed in some detail in ref. 1. These angular distributions, which for the heaviest elements have a minimum at ~90°, are consistent with an equilibrium process for the complex fragments observed in the backward hemisphere.

In summary, we have observed the emission of large fragments (He to F) from the reaction 90 MeV ^{3}He + ^{nat}Ag. Various aspects of these data suggest that these complex fragments are emitted from an equilibrated compound nucleus. At backward angles the fragment energies are Coulomb-like. A single source with the c.m. velocity is observed in the invariant cross-section plots. As the charge of the ejectile increases, the yield decreases as predicted for an equilibrium statistical process, the angular distributions evolve from flat to backward peaked, and the energy spectra evolve from Maxwellian to Gaussian.

Footnotes and References

*Condensed from LBL-15696

†Permanent address: Universitá Degli Studi di Bari, 70100 Bari, Italy.

‡Permanent address: Comisión Nacional de Energía Atómica, Buenos Aires, Argentina.

§Permanent address: Weizmann Institute of Science, Rehovot 76100, Israel.

1. L.G. Moretto, Nucl. Phys. **A247**, 211 (1975).
2. W.J. Świątecki LBL-11403 (to be published, Australian J. of Phys.).

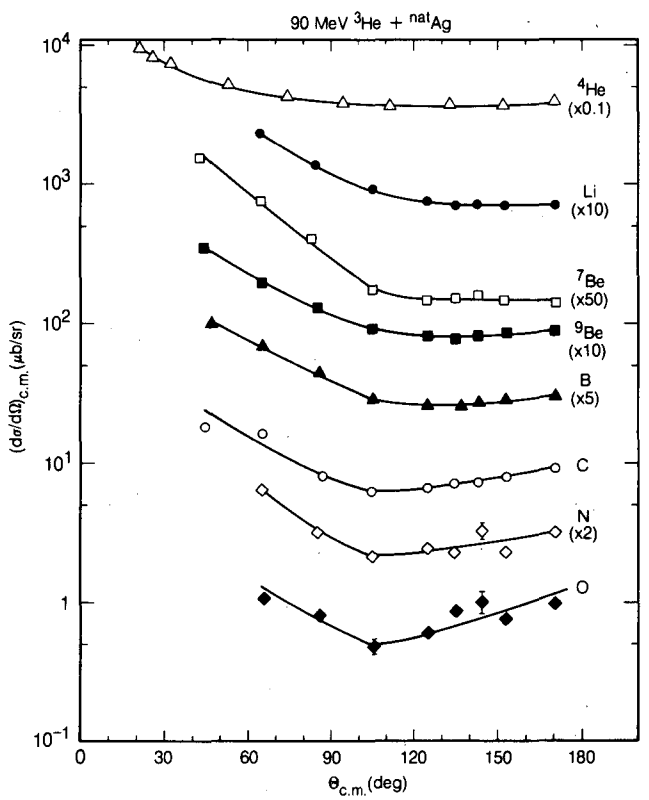

Fig. 2. Angular distributions in the c.m. system for various ejectiles. The curves through the data points are to guide the eye. Statistical error bars are only shown when they exceed the size of the data point.

XBL 836-393

Complex Nuclei Emission In Compound Nucleus and Deep-Inelastic Reactions*

G.J. Wozniak

Nuclei at large excitation energies can emit with low probability complex nuclei (Li, Be, B, C, N and O). These rare decay channels have been observed in the reaction $^{3}He + {}^{nat}Ag$ at four bombarding energies (50, 70, 90 and 130 MeV). Inclusive energy spectra have been measured from 20–170° in the laboratory and invariant cross section plots constructed. These plots show two components: a low energy equilibrium component present at all angles and a higher energy component present at forward angles. At all bombarding energies the fragment energies of the low energy component are Coulomb-like. Furthermore, as the charge of the ejectile increases, the yield decreases nearly exponentially, the angular distributions evolve from flat to backward peaked, and the energy spectra evolve from Maxwellian to Gaussian (see Fig. 1).

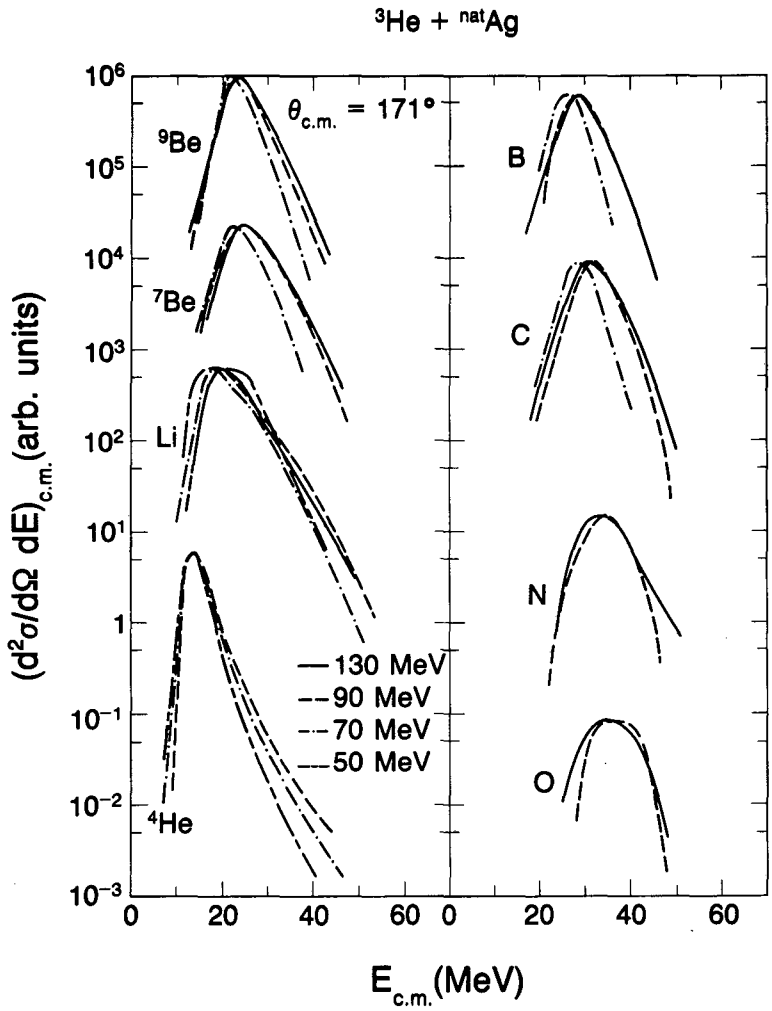

Fig. 1. Energy spectra ($\Theta_{c.m.} = 171°$) for complex nuclei emitted from the $^{3}He + {}^{nat}Ag$ reaction at several beam energies. XBL 838-3031

A search for the emission of complex nuclei in the deep-inelastic reaction 484 MeV ^{56}Fe + ^{nat}Ag has also been undertaken. Because of the expected low yield of complex nuclei from this reaction and the need for coincidence data, large solid angle detection systems were employed. Complex nuclei were measured in the reaction plane on both sides of the beam axis in the backward hemisphere. A comparison of singles and coincidence data from a preliminary analysis indicates that the bulk of the complex nuclei are emitted from the fully accelerated deep-inelastic fragments.

*Invited talk presented at the Symposium on Current Trends in Heavy Ion Reaction Studies at the American Chemical Society National Meeting, Aug. 29 – Sept. 2, 1983, Washington, D.C.

Excitation Function for ^{3}He + ^{nat}Ag

M.L. Padgett, L.G. Sobotka, G.J. Wozniak, G. Guarino, A.J. Pacheco,† L.G. Moretto, Y. Chan, R.G. Stokstad, I. Tserruya,‡ and S. Wald*

Complex fragment emission from the compound nucleus formed in the reaction of ^{3}He on ^{nat}Ag has been studied at bombarding energies of 45, 50, 60, 70, 90[1] and 130 MeV. The ^{3}He beam was produced by the LBL 88-Inch Cyclotron and the energy spectra of alphas, Li, ^{7}Be, ^{9}Be, B, C, N, O, F and Ne were obtained using standard gas ΔE–solid state E telescopes (in some cases the alpha spectra were obtained with separate solid-state telescopes).

Fig. 1 shows the partial differential cross section of these particles at 170° as a function of beam energy. By looking at the most backward angle data, one can study the relative yield of the fragments emitted from the compound nucleus, since this angular region is free of other components.[1] The yields of all products decrease with decreasing beam energy or correspondingly as the excitation of the compound nucleus decreases. Furthermore, the yields of the heavier products decrease more rapidly than those of the lighter products with decreasing beam energy.

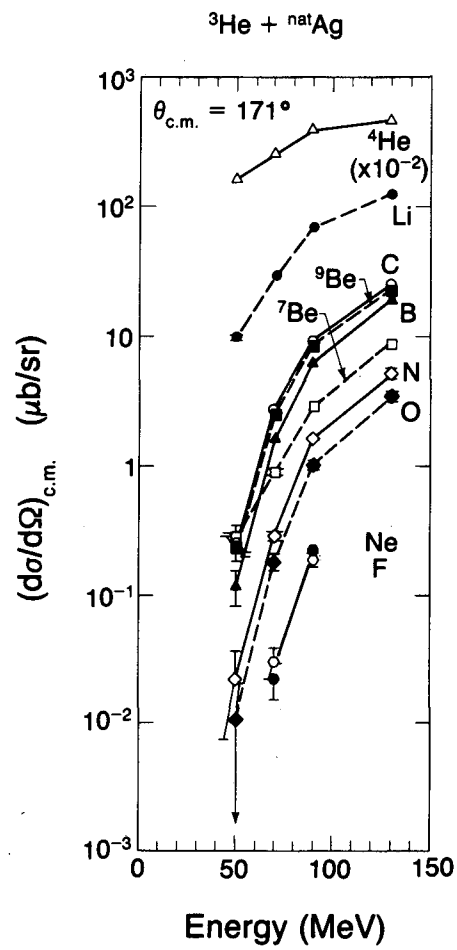

Fig. 1. Yield at 170° versus beam energy for various ejectiles from the ^{3}He + Au system in the center of mass. The curves through the data points are to guide the eye. XBL 838-3025

The yield from an equilibrium statistical emission process is roughly proportional to a factor $\exp[-B_Z/T_Z]$, where B_Z is the emission barrier for fragment Z and T_Z is the temperature at the barrier. Since B_Z increases and T_Z decreases as the atomic number of the fragment increases, emission probability decreases with [increasing] atomic number. As both the beam energy and the ratio of the total excitation energy to the Coulomb barrier decrease this effect becomes stronger, causing the yields of the heavier fragments to decrease faster than the lighter ones with decreasing beam energy.

Footnotes and References

*Permanent address: Universitá Degli Studi di Bari, 70100 Bari, Italy.
†Comisión Nacional de Energia Atómica, Buenos Aires, Argentina.
‡Weizmann Institute of Science, Rehovot 76100, Israel

1. L.G. Sobotka *et al.* LBL-15696.

Bridging the Gap between Evaporation and Fission

L.G. Sobotka, R.J. McDonald, C. Signarbieux, G.J. Wozniak, M.L.Padgett, H.H. Gu,† Z.Q. Yao, †Z.H. Liu, ‡L.G. Moretto*

In a recent experiment we have utilized reverse kinematics to measure the product charge distribution from Z = 1 to symmetry for the reactions ^{93}Nb + ^{12}C and ^{93}Nb + ^{9}Be. The reverse kinematics has several important advantages over light ion bombardments. These advantages include: 1) the focusing of the reaction yield into a forward cone, 2) large fragment energies, which allow for the determination of fragment charge from $1 \leqslant Z \leqslant$ symmetry and 3) improved sensitivity to the velocity of the emission source.

The last of these advantages is illustrated in Fig. 1. This figure compares the mean energies of the fragments as a function of charge to several estimates of these energies from a Monte Carlo simulation code. The solid line shows the expected velocities based on full momentum transfer and Coulomb emission energies. The dashed lines show the sensitivity of this simulation to a variation of ±10% in the Coulomb energies, while the dotted lines show a similar percentage variation in the center of mass velocity. The comparison clearly illustrates the sensitivity of the fragment energies to the velocity of the source and the insensitivity to the exact Coulomb parameters. The agreement between the data and

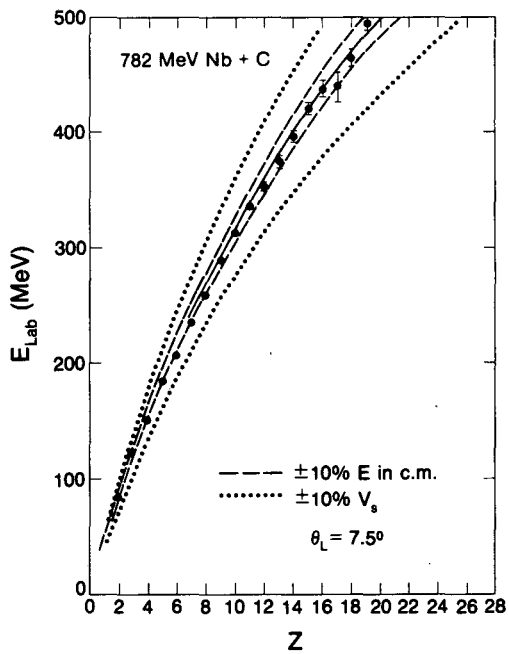

Fig. 1. Laboratory energies as a function of atomic number for the reaction 782 MeV Nb+C. The solid, dashed and dotted lines are calculations (see text). The data and calculations are for Θ_{lab} = 7.5°.

XBL 8311-7390

the calculations indicates that these large fragments are being emitted from complete momentum transfer reactions.

The cross sections for the production of fragments with $1 \leqslant Z \leqslant 19$ are shown in Fig. 2. The yields drop exponentially from Z =1 to Z = 10, however from Z = 10 to 19 (near symmetry) the yield is almost constant. This behavior can be understood on the basis of the potential energy surface of the critical decay shape (saddle point) as a function of asymmetry.[1] It is interesting that the data do not agree with a power law dependence ($A^{\sim -2.5}$) that has had some success in reproducing the mass yields in higher energy reactions.[2]

Footnotes and References

*Permanent address: CEN, Saclay

†Permanent address: Shanghai, Peoples Republic of China

‡Permanent address: Institute of Atomic Energy, Beijing, Peoples Republic of China

1. L.G. Moretto Nucl. Phys. **A247**, 211 (1975).
2. J.E. Finn, Phys. Rev. Lett. **49**, 1321 (1982).

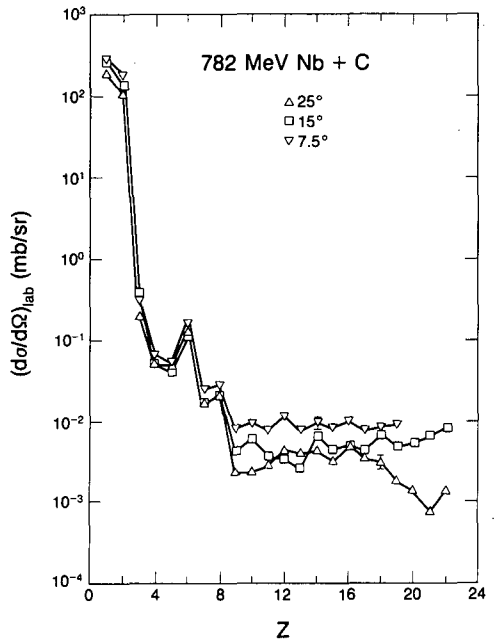

Fig. 2. Laboratory cross sections as a function of atomic number. Statistical errors are indicated when they exceed the size of the symbol. XBL 8312-7488

Incomplete and Complete Fusion at Intermediate Energies

W. Loveland, K. Aleklett,† Wing Kot, Li Wenxin,‡ D.J. Morrissey,§ T.T. Sugihara,* and G.T. Seaborg*

We have begun a radiochemical study of the variation of complete and incomplete fusion processes with increasing projectile energy in the reaction of intermediate energy heavy ions with neutron-rich rare earth nuclei. (These nuclei have been selected to minimize fission and to lead to products suitable for detection by radiochemical techniques.) Specifically, we have measured the yields, differential range spectra and angular distributions for near and trans-target residues produced in the interaction of 137 MeV (8.6 MeV/nucleon) and 307 MeV (19.1 MeV/nucleon) ^{16}O (at the LBL 88-Inch Cyclotron), 418 MeV (34.8 MeV/nucleon) ^{12}C (at the Michigan State University superconducting cyclotron) and 1032 MeV (86 MeV/nucleon) ^{12}C (at the CERN SC synchrocyclotron) with ^{150}Nd, ^{154}Sm and ^{176}Yb. From these measured distributions, we have deduced isobaric yields and invariant velocity spectra.

To help understand the trends in the data, we compare the data to predictions of a "low-energy" model, the generalized sum rule model of Wilczynski *et al.*[1] This model predicts the primary residue cross sections due to complete and incomplete fusion. We have added to this model the dynamics of the semiclassical DWBA calculation of Toepffer[2] to allow us to calculate primary fragment excitation energies, velocities, etc. To model the deexcitation of the primary fragments, we have used the DFF code of McGaughey and Morrissey.[3]

In Fig. 1a, we show the preliminary isobaric yield distribution for the reaction of 137 MeV (8.6 MeV/nucleon) ^{16}O with ^{154}Sm. The integrated total residue cross section is ~1300 mb which is in good agreement with the track detector studies of Zebelman and Miller[4] who found σ_{CF} = 1260 ± 200 mb with $\sigma_{fission}$ = 40 mb for this reaction.

Also shown in Fig. 1a is the isobaric yield distribution predicted by the sum rule model. The predicted distribution agrees reasonably well with the measured distribution except for the yields of the lightest fragments which are overestimated in the model calculation. This is not serious since one can easily show that such fragments result from small

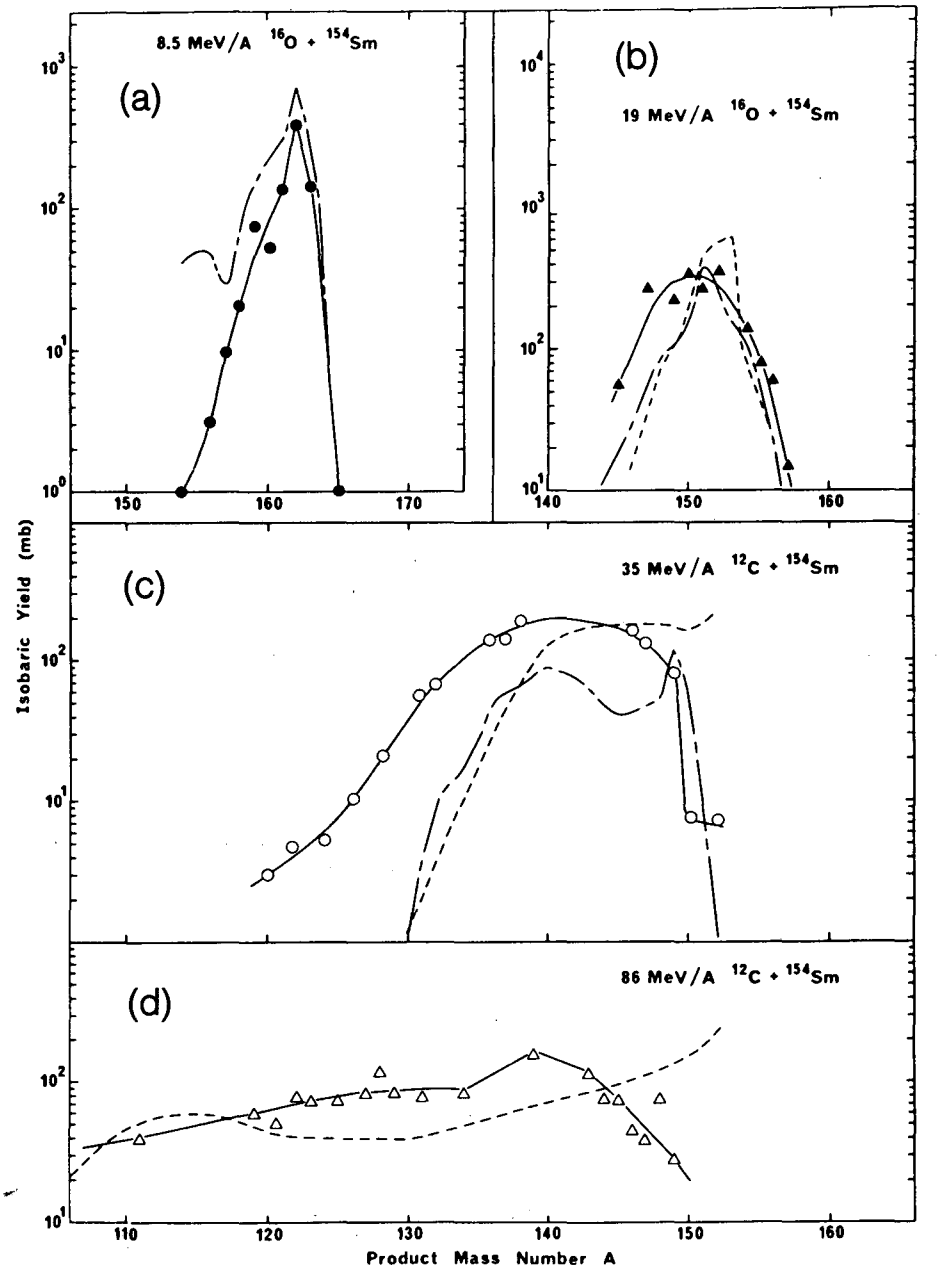

Fig. 1. Comparison of measured isobaric yield distributions (solid curve) with those predicted by the sum rule model (long line-dashed curve) and the firestreak model (dashed curve). XBL 846-8473

mass transfers – (^{16}O, ^{12}C), (^{16}O, ^{14}C) – which in the sum rule model result from the highest *l*-waves in the entrance channel. The magnitudes of the predicted cross sections are thus subject to any uncertainties or inaccuracies in the r_0 values in the calculation. A few selected invariant velocity spectra are shown in Fig. 2a, along with indications of the mean fragment velocities predicted by the sum rule model. Once again, the model appears to represent the gross features of the data adequately. Using the velocity spectra for all the nuclides as a guide, one can estimate that ~93% of the residue cross section at this energy results from full momentum transfer events.

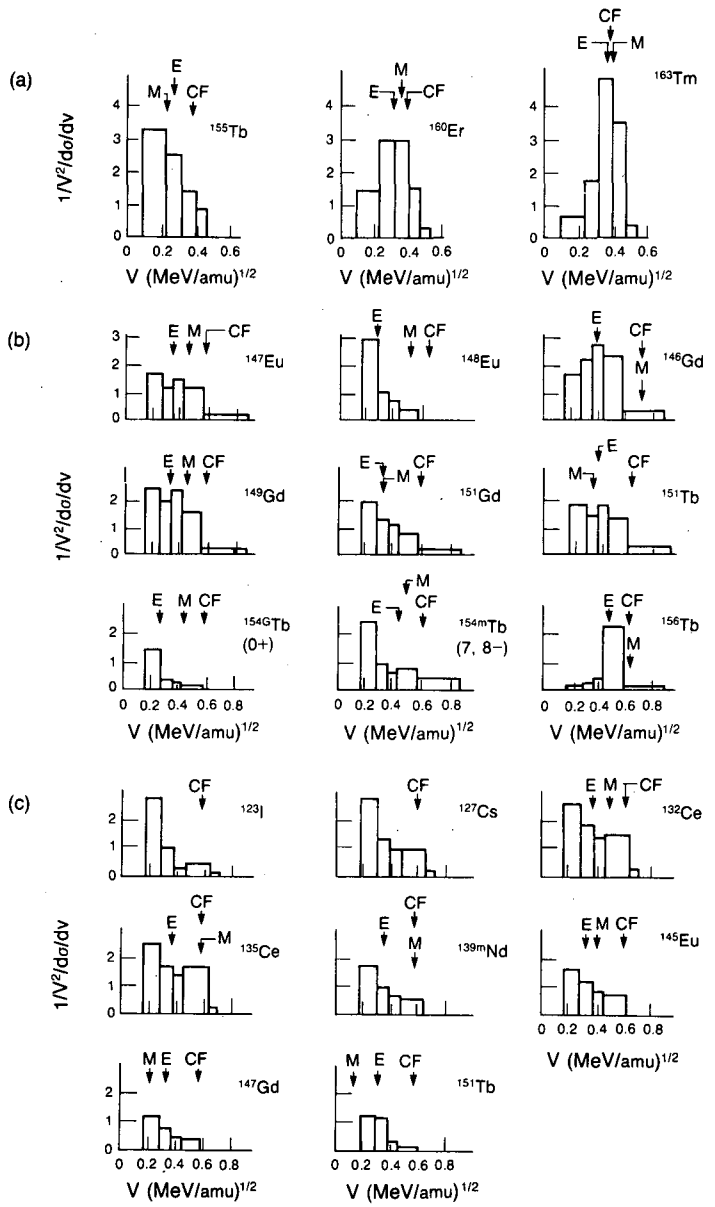

Fig. 2. Measured invariant velocity spectra for residues from the reaction of a) 137 MeV ^{16}O, b) 307 MeV ^{16}O, c) 418 MeV ^{12}C with ^{154}Sm. The arrows indicate the mean residue velocity such that CF corresponds to complete fusion, E the mean measured velocity, and M the average velocity as calculated by the sum rule model.

XBL 8311-669

The predicted and measured isobaric yield distributions for the reaction of 307 MeV ^{16}O with ^{154}Sm are shown in Fig. 1b. The sum of the measured residue yields is ~1460 mb. Comparison of the reaction yield surface with that for the reaction of 307 MeV ^{16}O with ^{176}Yb (i.e., comparison of systems with targets and compound nuclei of similar N/Z) shows that maximum yields are found at the same ΔN and ΔZ relative to the target and compound nuclei. The measured distribution is considerably broader than the calculated distribution in Fig. 1b. The sharp peak in the calculated distribution can be attenuated by truncating the l-distribution in the entrance channel at l=103, thus eliminating the small (p or d) transfer reactions. The invariant velocity spectra (shown in Fig. 2b) show further evidence for the failure of the sum rule model to correctly describe the experimental data at this energy and indicate substantial probability for the occurrence of incomplete fusion processes. Although the velocities of residues near the center of the isobaric yield distribution are described adequately, there are substantial problems in describing the nuclei on the edges of the yield distribution. Further support for the idea that considerable incomplete fusion is occurring at this projectile energy comes from the angular distribution data which shows most distributions to peak at angles between 0° and the heavy fragment complement of the grazing angle. Only the heaviest fragments show angular distributions peaking at 0° in accordance with their large velocities. From the velocity spectra, one can deduce that ~35% of the residues result from complete fusion events.

In Fig. 1c we show the calculated and measured isobaric yield for the reaction of 418 MeV (34.8 MeV/nucleon) ^{12}C with ^{154}Sm. In Fig. 2c we show the invariant velocity spectra for this reaction. The range distributions clearly show the residues of interest to stop in approximately the third foil of the stack. Transforming these range distributions into invariant velocity distributions reveals the dominance of low velocity residues. Only a tiny fraction of the residue events is due to complete fusion. The sum rule model consistently overestimates the magnitude of the average residue velocity.

The failure of the sum rule model at the higher bombarding energies can be understood in terms of the fact that the same range of entrance channel partial waves leads to complete fusion, α transfer, etc., regardless of the incident projectile energy. Thus, a configuration in which the nuclei are barely touching will lead to complete fusion at 8.5 and 35 MeV/nucleon projectile energy. This is simply unrealistic given the difference in projectile trajectories at low and intermediate energies.

Footnotes and References

*Oregon State University, Corvallis, OR 97331
†Studsvik Science Research Laboratory, S-611 82 Nyköping, Sweden
‡Institute of Modern Physics, Lanzhou, China.
§State University, E. Lansing, MI 48824

1. J. Wilczynski, K. Siwek-Wilczynska, J. van Driel, S. Gonggrijp, D.C.J.M. Hageman, R.V.F. Janssens, J. Lukasiak, and R.H. Siemssen, Phys. Rev. Lett. **45**, 606 (1980).
2. C. Toepffer, Z. Physik **253**, 78 (1972).
3. P.L. McGaughey, LBL-15325, November 1982.
4. A.M. Zebelman and J.M. Miller, Phys. Rev. Lett. **30**, 27 (1973).

Angular Momentum Transfer and Alignment for ^{208}Pb- and ^{197}Au-Induced Reactions

G.J. Wozniak, A.J. Pacheco, G. Guarino,† J.H. Gu, R.J. McDonald, L.G. Sobotka, and L.G. Moretto*

During the last several years, the magnitude and alignment of the angular momentum transferred into intrinsic spin during a deep-inelastic collision has been studied utilizing continuum γ-ray techniques. Near-symmetric systems with total masses in the range of $A_p + A_T = 273–341$ have been investigated (see Table Ia).[1,2] In the present work, we extend these studies to heavier systems with total masses for $A_p + A_T = 362–416$ (see Table Ib). To keep the total angular momentum of the dinuclear system similar to that of previous studies and to reduce the tendency of the heavier nuclei to undergo sequential fission, bombarding energies of ~7.5 MeV/nucleon were employed.

In Fig. 1 are shown the in-plane (solid symbols) and out-of-plane (open symbols) γ-ray multiplicities (M_γ) as a function of Q-value for six heavy systems. M_γ rises steeply with increasingly negative Q-values and levels off at ~−200 MeV. This trend is very similar to that observed for lighter systems[1,2] and indicates that orbital angular momentum is being converted into fragment intrinsic spin. Larger values of M_γ are observed for reactions involving ^{197}Au or ^{165}Ho and smaller values for reactions involving ^{208}Pb.

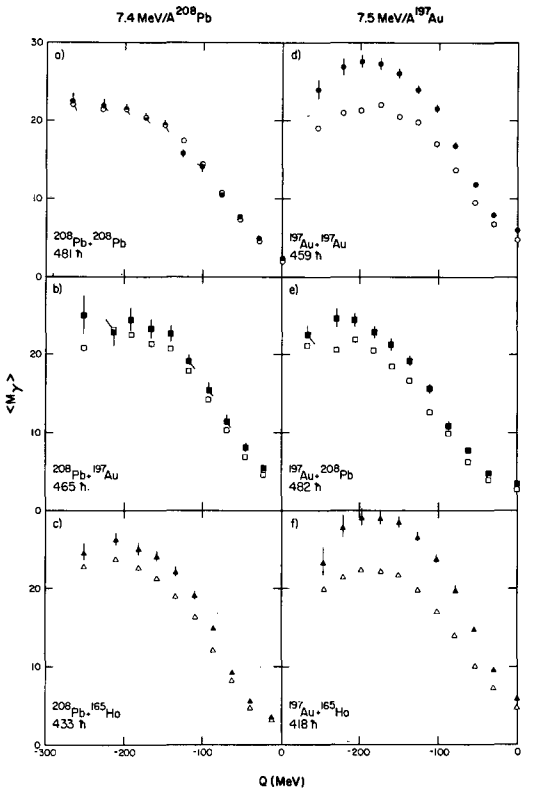

Fig. 1. In-plane (solid symbols) and out-of-plane (open symbols) γ-ray multiplicities (M_γ) as a function of Q-value for six heavy systems. The target and projectile plus ℓ_{max} are indicated in the lower left hand corner of each box. XBL 835-2604

In Fig. 2 are shown the γ-ray anisotropy (A_γ) as a function of Q-value for six heavy systems and two windows on the γ-ray energy. For γ-rays with E_γ = 0.6−1.2 MeV sizable anisotropies are observed for the ^{197}Au + ^{197}Au and ^{197}Au + ^{165}Ho systems. Reduced anisotropies are observed when ^{208}Pb is substituted for a ^{197}Au or ^{165}Ho nucleus and essentially isotropy is observed for the ^{208}Pb + ^{208}Pb system.

For lighter systems ($A_p + A_T$ = 273–341), A_γ increases from near unity for Q = 0 MeV to values substantially greater than unity at Q = −150 MeV. This has been interpreted as an increase in the alignment of the intrinsic spin with increasing Q-value. For these heavier systems, A_γ is rather independent of Q-value. For the Pb + Pb system a γ-ray anisotropy of unity for all Q-values may indicate that the intrinsic spin is never aligned. However, the sizable values of A_γ observed for the ^{197}Au + ^{197}Au and ^{197}Au + ^{165}Ho systems indicate that even at small Q-values the transferred spin is aligned. In addition, it seems that the temperatures are too low to strongly excite the collective depolarizing modes.

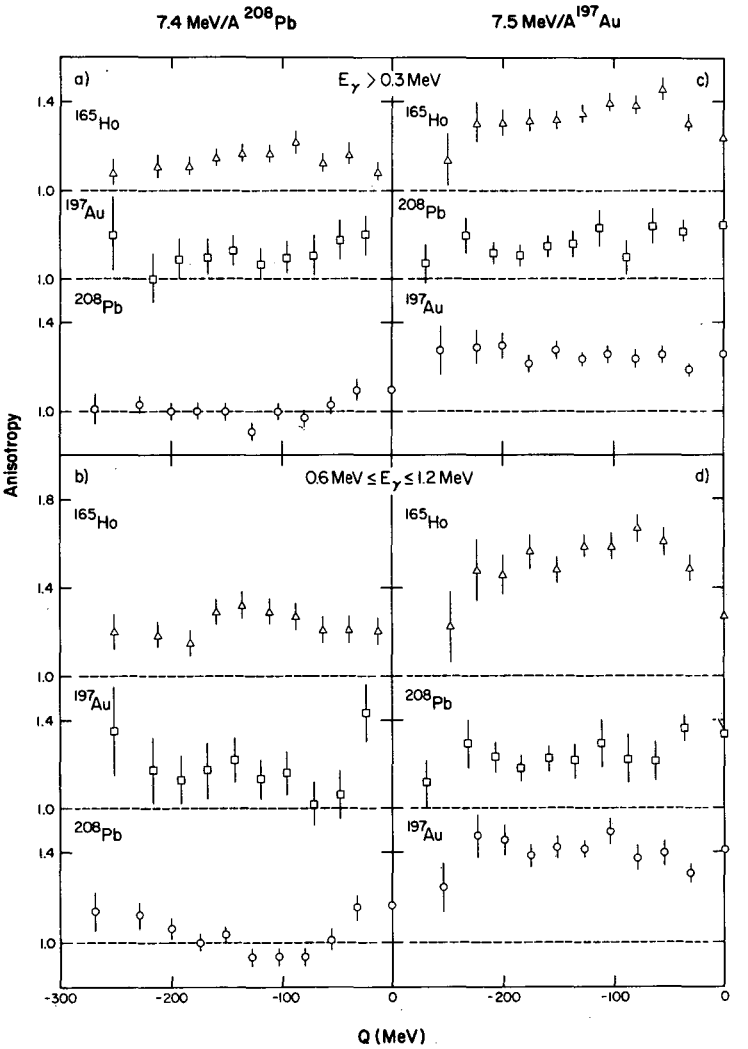

Fig. 2. γ-ray anisotropy as a function of Q-value for six heavy systems and two windows in γ-ray energy.

XBL 835-2603

TABLE I

	Projectile	Target	$A_p + A_T$	Beam energy (MeV/nucleon)	ℓ_{max} ($\hbar$)
a)	^{165}Ho	^{176}Yb	341	8.5	516
	^{165}Ho	^{165}Ho	330	8.5	505
	^{165}Ho	^{148}Sm	313	8.5	471
	^{165}Ho	^{nat}Ag	273	8.5	392
b)	^{197}Au	^{197}Au	394	7.5	459
	^{197}Au	^{208}Pb	405	7.5	472
	^{197}Au	^{165}Ho	362	7.3	418
	^{208}Pb	^{208}Pb	416	7.4	481
	^{208}Pb	^{197}Au	405	7.4	465
	^{208}Pb	^{165}Ho	373	7.4	433

References

1. R.J. McDonald *et al.*, Nucl. Phys. **A273**, 54 (1982).
2. A.J. Pacheco *et al.*, Nucl. Phys. **A397**, 313 (1983).

*Comisión Nacional de Energia Atómica, Buenos Aires, Argentina.

†Permanent address: Universitá Degli Studi di Bari, 70100 Bari, Italy.

Coincidence Measurements of Fusion-Like Residues in the $^{16}O + ^{40}Ca$ Reaction at $E^{Lab}_{^{16}O} = 313$ MeV

A. Budzanowski, Y. Chan, R.G. Stokstad, I. Tserruya,† S. Wald, and M. Blann‡*

Recent measurements of the velocities of the products of light heavy ion induced reactions[1,2] in the region of masses where the evaporation residues of the compound nucleus are expected have revealed a significant decrease of the mean velocity as compared to the predictions of the fusion-evaporation model. This so-called velocity shift of the fusion-like residues (FLR) was shown to appear at projectile energies higher than 8 MeV/nucleon and to increase almost linearly with increasing value of the relative velocity of the colliding nuclei at the top of the Coulomb barrier.[2]

Several models, e.g., incomplete fusion, Fermi jets, pre-equilibrium emission and emission from a moving hot source, can be invoked in order to explain the observed shift. The distinction between these various models cannot be made on the basis of the single velocity spectra of FLR alone. It was hoped that a coincidence experiment, in which correlations between the velocities of FLR and the energies of the accompanying light ejectiles would be measured for various angles of light particle emission, could help in explaining the mechanism causing the observed velocity shift.

In the present investigation, coincidences between α-particles and FLR emitted in the ^{16}O + ^{40}Ca reaction were measured at $E^{Lab}_{^{16}O}$ = 313 MeV. The experiment was performed in the 60″ scattering chamber using the ^{16}O beam from the 88-Inch Cyclotron. The velocities and masses of FLR were measured with the time of flight spectrometer mounted on the side window of the scattering chamber in the vertical plane at an angle of −15° with respect to the beam direction. The start signal was obtained from a channel-plate detector with a thin carbon conversion foil, about 84 $\mu g/cm^2$, tilted at an angle of 45° to the 1.4 m flight path. As a stop detector, a 900 mm^2, 100μm-thick silicon surface barrier detector was used. The target was natural calcium with a thickness of 400 $\mu g/cm^2$. Alpha particles were detected by five counter telescopes placed in the horizontal plane at the angles −5°, +5°, +15°, +30° and +115° with respect to the beam (+ and − signs denote the left and right side of the beam looking along beam direction).

In Fig. 1 velocity spectra of FLR, both singles and in coincidence with α-particles emitted at 5° and 115°, are shown. The arrow indicates the value of the center of mass velocity. We note a substantial shift of the mean velocity in the coincidence distribution compared to the singles distribution depending on the angle of emission and the energy of the accompanying alpha particles. In Fig. 2 α-particle spectra at 5°, both singles and in coincidence with FLR, are shown. The inclusive spectrum is rather structureless, whereas the coincidence spectrum seems to contain two distinct groups, the low energy evaporation part peaked around 37 MeV and the high energy part peaked at 80 MeV. The high energy part can be attributed to the fast absorptive break-up process of the ^{16}O projectile, e.g., ^{12}C fusing with ^{40}Ca and α out, or ^{8}Be fusing and ^{8}Be out, which subsequently decays into two α particles. Studies of the FLR velocity distributions gated by α particles emitted at 5° in the energy range from 0-50 MeV (LW for lower window) and in the energy range from 50-120 MeV (HW for higher window) were also performed. A shift of 7% was obtained for the mean velocity of the coincidence relative to the singles for

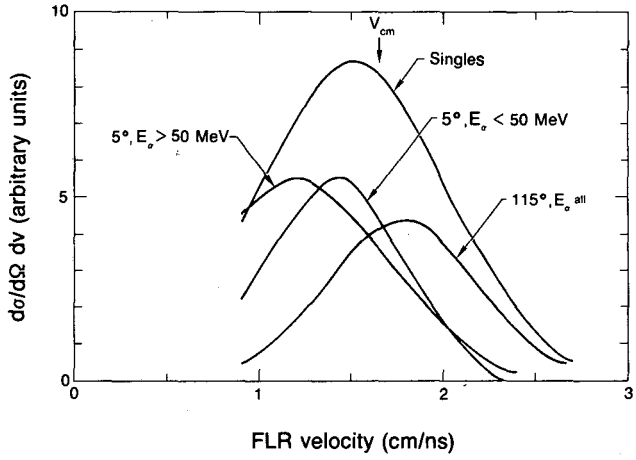

Fig. 1. Fusion-like residue velocity spectra at 15°: solid line – singles spectrum; dotted line – in coincidence with α particles at 115°; dashed line – in coincidence with α particles at 5° and α energies 50-120 MeV; dot-dashed line – in coincidence with α particles at 5° and α energies 0-50 MeV.

XBL 8312-6912

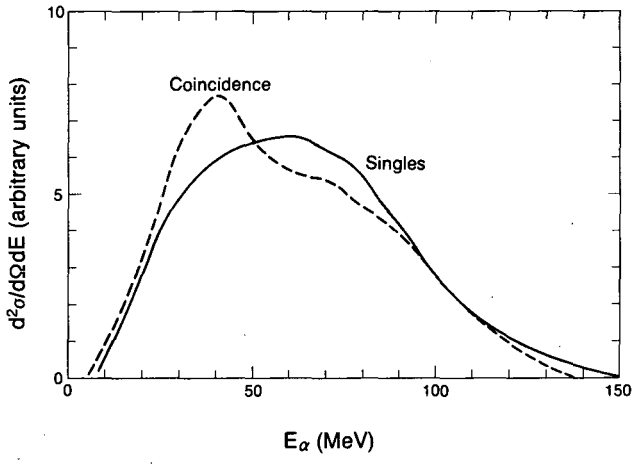

Fig. 2. Alpha particle spectra at 5°: solid line – singles spectrum; dashed line – in coincidence with fusion-like residues. XBL 8312-6913

the LW distribution. This shift can be explained as a biasing of the FLR velocity distribution by the detection of α particles evaporated from the ensemble of the excited nuclei. The same explanation can be given for the velocity distributions measured in coincidence with α-particles emitted at 115°. However the shift of 22% of the mean velocity of the HW distribution against the singles velocity, which amounts to 43% with respect to the center of mass velocity, cannot be explained by the emission of one primary alpha particle with the beam velocity. In order to explain such a large shift it is necessary to assume that a significant number of α-particles detected at forward angles are due to the decay of some heavier ejectile, such as ^{8}Be emitted in the process of incomplete fusion of ^{16}O. A simple equation for the ratio of the mean coincidence FLR velocity $\overline{V}_C$ to the CM velocity V_{CM} can be written:

$$\overline{V}_C/V_{CM} = (.81\sigma_\alpha + .58\cdot 2\sigma_{^8Be})/(\sigma_\alpha + 2\sigma_{^8Be}) \quad (1)$$

where σ_α and $\sigma_{^8Be}$ are cross sections for α and ^{8}Be emission at 5° respectively, .81 and .58 are ratios of velocities of ^{52}Fe and ^{48}Cr (originating from ^{12}C and ^{8}Be fusion, respectively) to the CM velocity. Using eq. (1) together with the present experimental data on $\overline{V}_C/V_{CM}$, a lower limit on the ratio $\sigma_{^8Be}/\sigma_\alpha$ at 5° equal to 0.32 can be deduced. Thus at least 64% of the fast ($E_\alpha > 50$ MeV) alpha particles emitted at 5° are due to ^{8}Be transfer. It should be mentioned in support of the above conclusion that the overlap model of transfer reactions proposed recently by Harvey and Homeyer[3] predicts values of the cross section for ^{8}Be fusion channel comparable to that of the ^{12}C fusion channel for the ^{16}O + ^{40}Ca collision at 300 MeV.

Footnotes and References

*Permanent address: Institute of Nuclear Physics, Krakow, Poland.
†Weizmann Institute, Rehovot, Israel
‡Lawrence Livermore National Laboratory

1. H. Morgenstern *et al.*, Phys. Lett., **113B**, 463 (1982).
2. Y. Chan *et al.*, Phys. Rev. **C27**, 447 (1983).
3. B.G. Harvey and H. Homeyer, LBL-16882 (1983) and this report.

Velocity Distributions of Fusion-like Products for Medium Mass Heavy-Ion Systems

Y. Chan, C. Albiston, M. Bantel, P. Countryman, D. DiGregorio,† H. Homeyer,‡ R. Stokstad, S. Wald, S.H. Zhou,§ Z.Y. Zhou,** A. Budzanowski,†† K. Grotowski,‡‡ and R. Planeta‡‡*

The velocity of compound nuclei prior to their decay can be determined by studying the invariant velocity distribution of the final residues.[1] Thus, by comparing the differences between the empirically measured parent emitter velocity, V_{obs}, to that expected for complete fusion, $V_{c.m.}$, one can learn about the relative importance of incomplete fusion (or massive transfer) processes.

Following the results reported previously[2] for ^{16}O beams, a series of measurements on a wider range of projectile and target masses was initiated at the 88-Inch Cyclotron. Time-of-flight techniques were used to measure the velocities directly. Reactions between ^{14}N, ^{16}O, ^{19}F, ^{20}Ne, ^{24}Mg projectiles and ^{24}Mg, ^{26}Mg, ^{27}Al, ^{28}Si, ^{40}Ca, ^{58,60}Ni targets have been studied in the bombarding energy range of 7–20 MeV/nucleon (Table I).

The invariant velocity spectra of the residues can be expressed as:[1,3]

$$\frac{1}{v^2}\frac{d^2\sigma_A}{dv\,d\Omega} \propto \left[\exp\left(-\frac{(v - V_p\cos\Theta)^2 + V_p\sin^2\Theta}{2S_A^2}\right)\right]$$

$$\left[\frac{\sqrt{(v - V_p\cos\Theta)^2 + V_p^2\sin^2\Theta}}{V\sin\Theta}\right]^{n_A}$$

where v, V_p and Θ are the residue velocity, parent emitter velocity, and detection angle, respectively, in the laboratory frame. The width parameter S_A reflects the dynamics of the decay process, and n_A, a parameter characterizing the anisotropy of the angular distribution in the emitter frame, varies from 0 in the weak coupling limit to 1 in the strong coupling limit. The differences found in the velocity centroids by treating n_A as a free parameter were found to be quite small for the higher mass residues. The present results were obtained by assuming $n_A = 0$, in which case the quantity of interest R ($\equiv V_{obs}/V_{c.m.}$) is equal to $\langle v\rangle/(V_{c.m.}\cos\Theta)$. Here $\langle v\rangle$ is the empirical centroid of the invariant velocity spectrum at angle Θ.

A. Global behavior

Fig. 1a shows the mass-averaged velocity ratio plotted versus the local relative velocity of the reactants at the barrier, $V_{loc} \equiv [2(E_{cm} - V_C)/\mu]^{1/2}$. All results here correspond to values of the mass asymmetry $A \equiv (A_T - A_P)/(A_T + A_P)$ that are larger than zero. The deviation of $\langle R\rangle$ from the nominal value of 1.0 (complete fusion) increases with increasing bombarding energy, an expected behavior, since incomplete fusion processes should become more prominent at higher bombarding energies. It is also of interest to expand the comparison and include results from other linear momentum transfer measurements[4,5,6,7] at high bombarding energies for fissile systems (Fig. 1b). Even though there are certainly variations among the data, the deviation from complete fusion exhibits an approximately linear decrease with increasing relative velocity over a surprisingly wide range. The deviation from complete fusion appears to have a threshold of about 5 MeV/ nucleon above the barrier.

We have also plotted the same data versus the effective fissility x_{eff}, as has been suggested by Świątecki[8] (Fig. 2). This parameter is proportional to the ratio of the Coulomb-plus-centrifugal force to the attractive nuclear surface force at the point of contact. It is interesting to note that the threshold for deviation from complete fusion in this case appears at $x_{eff} \simeq 35$, which is very close to the well known criterion value of 33 where an extra-push is required for heavy systems to fuse.[9]

B. Projectile and target dependence

It is possible that break-up thresholds of the projectile might play a role in the incomplete fusion mechanism. To see how this is reflected in our data, Fig. 3a shows the excitation functions for different projectiles (^{14}N, ^{16}O, and ^{20}Ne) on the same Ca target. Within errors there are no drastic differences between these reactions and in fact for ^{14}N + Ca, where the projectile is not an alpha nucleus and has a low threshold for proton emission, the excitation function shows at least as strong a fall-off as for ^{16}O and ^{20}Ne projectiles. This may imply that particle thresholds of the projectile alone cannot predetermine the fraction of momentum loss in a fusionlike event, but that other dynamical factors can be of equal importance.

There are reasons to expect, however, that the velocity shift should depend on the mass asymmetry of the system for small asymmetries. To investigate this, Fig. 3b shows a comparison of the ^{20}Ne + ^{26}Mg and the ^{14}N + Ca reactions (corresponding to A = 0.13 and 0.48). It is quite clear that the former reaction, which is more symmetric with respect to the projectile and target masses, exhibits a much smaller velocity shift at a comparable value of V_{loc}. This is because, for more symmetric systems, stripping-like and pick-up-like processes can contribute to residue production with comparable probability, reducing the net average velocity shift (but broadening the distribution). In fact, for identical projectile and target nuclei, the average parent velocity is the same as the center-of-mass velocity. In this case, the centroid approach is no longer sensitive to the underlying reaction mechanism.

C. Relative cross sections

The deduction of cross sections for different processes from the inclusive residue velocity spectra alone is quite difficult as one does not know *a priori* the number and velocities of parent emitters that may be present. The spectra are broad and featureless at high bombarding energies making fitting procedures with multiple peaks less reliable. Fig. 4 shows such an attempt for the ^{19}F + Ca reaction at 184 MeV. The spectra are fitted by a complete fusion component obtained from an evaporation model calculation, LILITA,[1] and another Gaussian component whose center, width, and height are allowed to vary. Typical results obtained indicate that about 20% of the fusionlike cross sections in fact are not coming from a complete momentum transfer process. Preliminary studies show that these numbers are larger than what one would have expected from, for instance, the standard Wilczynski sum rule model.[10]

In summary, the present experimental method is well adapted for measurements of the amount of linear momentum that is transferred in a fusionlike process for medium mass heavy-ion systems. It is quite efficient for studying systematics and provides a complementary approach to the more conventional method of studying the fast light ejectiles.

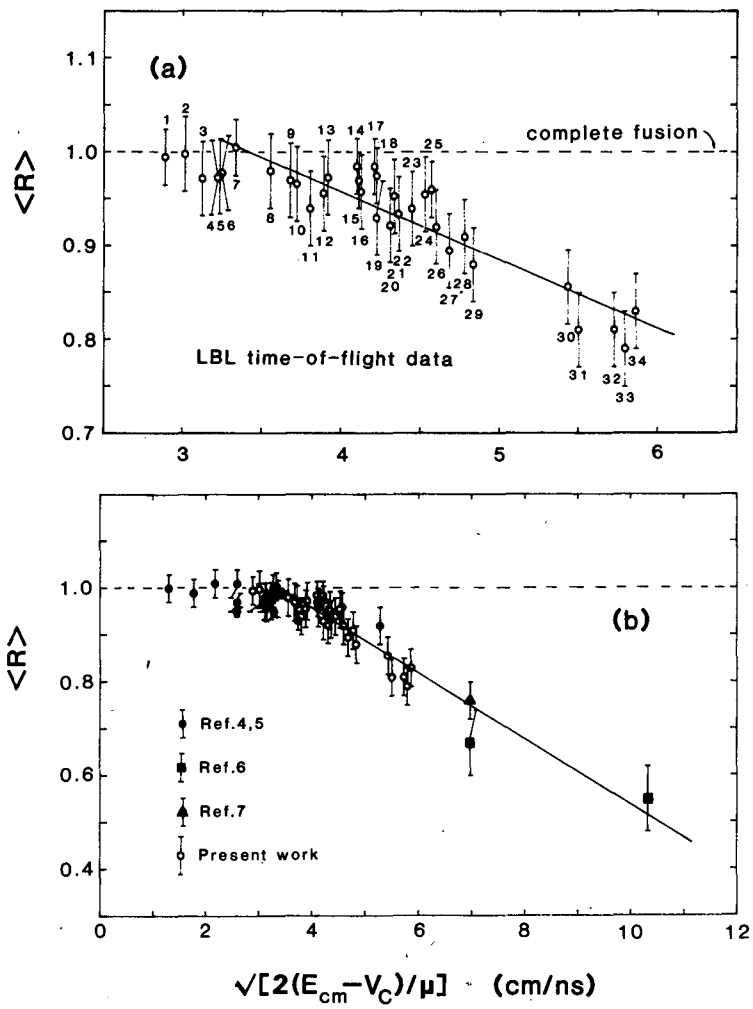

Fig. 1. (a) Systematics of the average parent emitter velocity, expressed as a ratio R to the velocity corresponding to complete fusion. (b) Comparison including results from other linear momentum transfer measurements (refs. 4–7). XBL 8312-2515

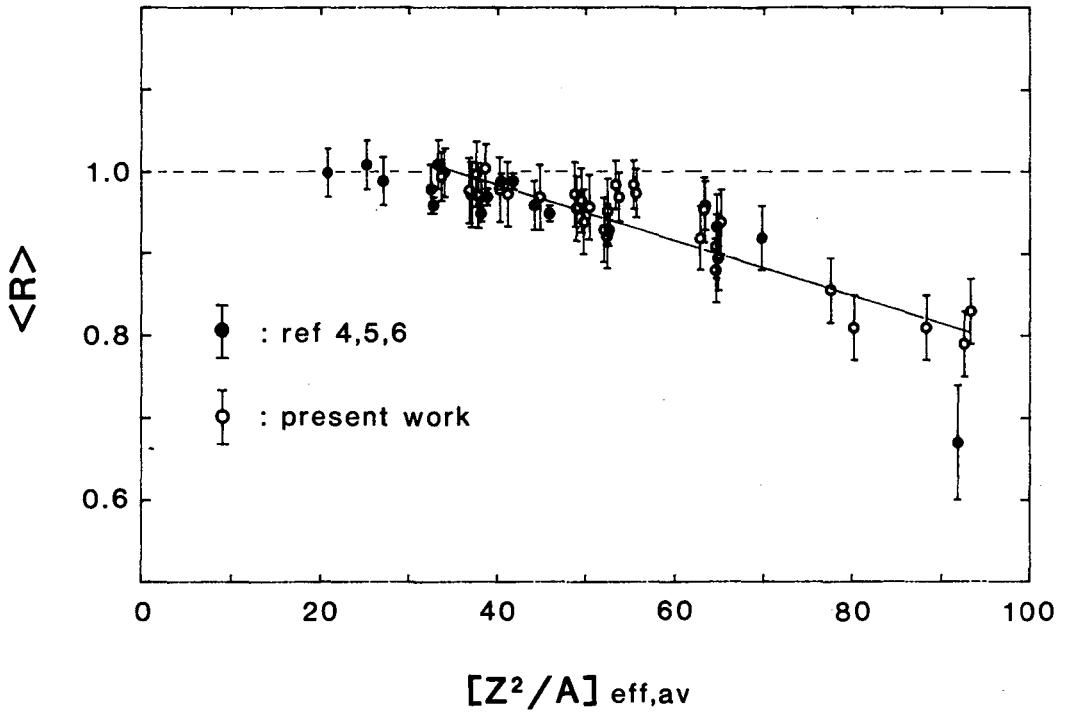

Fig. 2. Systematics of the ratio R plotted against the effective fissility (ref. 9). XBL 8312-2516

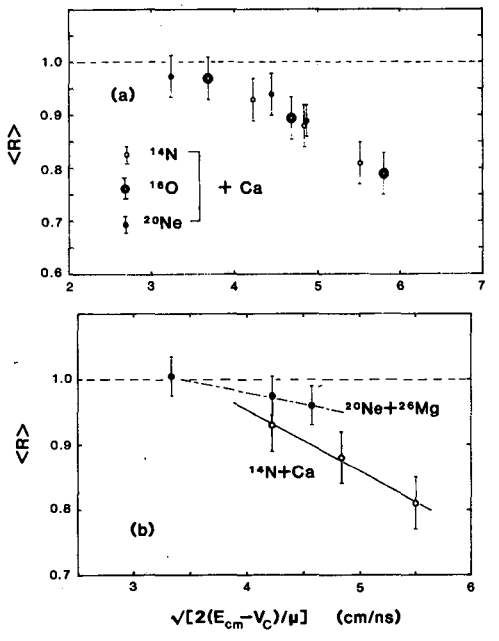

Fig. 3. Comparison of velocity shifts as a function of bombarding energy for (a) different projectiles on the same target and (b) systems with different mass asymmetry in the entrance channel. XBL 8312-2517

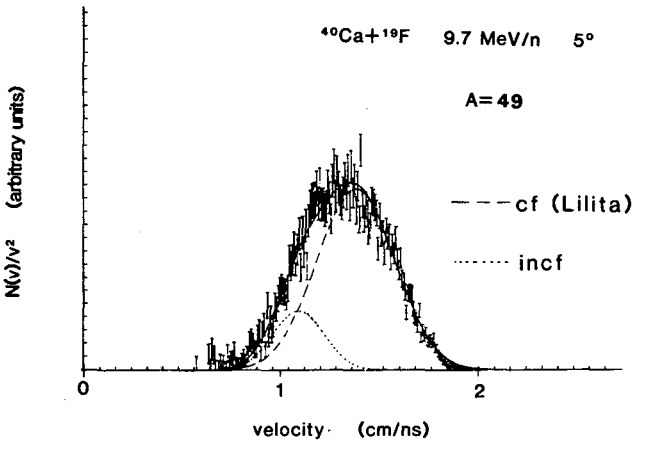

Fig. 4. Relative ratio for complete and incomplete fusion contributions to the velocity spectrum from peak shape fitting. The complete fusion component is calculated by the evaporation code, LILITA.[1]

XBL 8312-2518

Table I.

A summary of reactions studied in this work. The velocity ratio (see text) has been averaged over the higher portion of the residue masses. Errors are preliminary and include systematic errors.

	E_{Lab} (MeV/nucleon)	V_{loc} (cm/ns)	<R> (%)	Reaction
1	6.3	2.89	99.5 ± 3.	$^{24}Mg + ^{24}Mg$
2	7.2	3.02	99.8 ± 4.	$^{19}F + ^{58}Ni$
3	7.2	3.13	97.2 ± 4.	$^{19}F + ^{40}Ca$
4	7.2	3.22	97.3 ± 4.	$^{19}F + ^{28}Si$
5	7.7	3.24	97.4 ± 4.	$^{20}Ne + ^{40}Ca$
6	7.2	3.25	97.8 ± 4.	$^{19}F + ^{27}Al$
7	7.5	3.34	100.5 ± 3.	$^{20}Ne + ^{26}Mg$
8	8.8	3.56	98.0 ± 4.	$^{16}O + ^{27}Al$
9	8.8	3.68	97.0 ± 4.	$^{16}O + ^{40}Ca$
10	9.7	3.73	96.6 ± 4.	$^{19}F + ^{58}Ni$
11	9.7	3.81	94.0 ± 4.	$^{19}F + ^{40}Ca$
12	9.7	3.89	95.6 ± 4.	$^{19}F + ^{28}Si$
13	9.7	3.92	97.3 ± 4.	$^{19}F + ^{27}Al$
14	10.4	4.10	98.5 ± 3.	$^{22}Ne + ^{24}Mg$
15	10.4	4.11	97.0 ± 3.	$^{22}Ne + ^{26}Mg$
16	11.4	4.13	95.8 ± 4.	$^{14}N + ^{58}Ni$
17	11.0	4.21	98.5 ± 3.	$^{20}Ne + ^{24}Mg$
18	11.0	4.23	97.5 ± 3.	$^{20}Ne + ^{26}Mg$
19	11.4	4.23	93.0 ± 4.	$^{14}N + ^{40}Ca$
20	11.4	4.31	92.2 ± 4.	$^{14}N + ^{28}Si$
21	11.4	4.34	95.3 ± 4.	$^{14}N + ^{27}Al$
22	12.5	4.36	93.4 ± 4.	$^{20}Ne + ^{58}Ni$
23	12.5	4.45	94.0 ± 4.	$^{20}Ne + ^{40}Ca$
24	12.5	4.53	95.5 ± 4.	$^{20}Ne + ^{27}Al$
25	12.6	4.57	96.0 ± 3.	$^{20}Ne + ^{26}Mg$
26	13.6	4.60	92.0 ± 4.	$^{16}O + ^{60}Ni$
27	13.6	4.68	89.5 ± 4.	$^{16}O + ^{40}Ca$
28	13.6	4.78	91.0 ± 4.	$^{16}O + ^{27}Al$
29	14.3	4.84	88.0 ± 4.	$^{14}N + ^{40}Ca$
30	17.9	5.43	85.6 ± 4.	$^{14}N + ^{58}Ni$
31	17.9	5.50	81.0 ± 4.	$^{14}N + ^{40}Ca$
32	19.6	5.73	81.0 ± 4.	$^{16}O + ^{27}Al$
33	19.6	5.80	79.0 ± 4.	$^{16}O + ^{40}Ca$
34	19.6	5.87	83.0 ± 4.	$^{16}O + ^{60}Ni$

Footnotes and References

*Stanford University
†TANDAR, Buenos Aires
‡Hahn-Meitner Institute, Berlin, Germany
§Institute of Atomic Energy Beijing, Peoples Republic of China
**Nanking Univ. Peoples Republic of China
††Institute for Nuclear Physics, Cracow, Poland

‡‡Jagellonian University, Cracow, Poland

1. J. Gomez del Campo *et al.*, Phys. Rev. **C19**, 2170 (1979).
2. Y. Chan *et al.*, Phys. Rev. **C27**, 447 (1983).
3. H. Morgenstern *et al.*, Z. Phys. A, **313**, 39 (1983).
4. V.E. Viola, Jr., *et al.*, Phys. Rev. **C26**, 178 (1982) and references therein.
5. E. Duek *et al.*, Z. Phys. A, **307**, 221 (1982) and references therein.
6. J. Galin *et al.*, Phys. Rev. Lett., **48**, 1787 (1982).
7. G. Nebbia *et al.*, Z. Phys. A, **311**, 247 (1983).
8. W.J. Świątecki, private communication.
9. W.J. Świątecki, Nucl. Phys. **A376**, 275 (1982); H. Sann *et al.*, Phys. Rev. Lett. **47**, 1248 (1981).
10. J. Wilczynski *et al.*, Phys. Rev. Lett., **45**, 606 (1980).

Excitation Functions for Fragments Produced in the ^{20}Ne + ^{197}Au Reaction

H. Homeyer, C. Albiston, M. Bantel, K. Van Bibber,† Y.D. Chan, P. Countryman,† R.G. Stokstad, S. Wald*

In order to test absolute predictions of the overlap model[1] excitation functions for fragments produced in the ^{20}Ne + ^{197}Au reaction were measured over the energy range from the Coulomb barrier to 220 MeV. This is the region where the cross sections show the most dramatic changes. The experiments were carried out at the 88-Inch Cyclotron at bombarding energies of 108, 112, 124, 150, 175 and 220 MeV. Angular distributions for projectile-like fragments and fission residues were measured with a triple ΔE-E telescope. Mass and charge analyzed spectra were obtained at the precise angles for each energy by measurement of time of flight between a thin (12 μm) ΔE detector close to the target and an E detector at a distance of 60 cm away from the ΔE element. In the analysis of the angle-integrated isotopic yields, it is assumed that the different isotopes of a single charge have the same angular distribution.

The observation of increasing energy thresholds for more massive transfers is very well reproduced by the overlap model, as are the elemental cross sections. However, there are marked differences in excitation functions for separated isotopes (see Fig. 1) that cannot be fully explained by the model in its present stage. Effects of cluster binding energies and two-step processes such as particle pickup from the target will have to be taken into account. The measured fission cross section (see Fig. 1), which arises

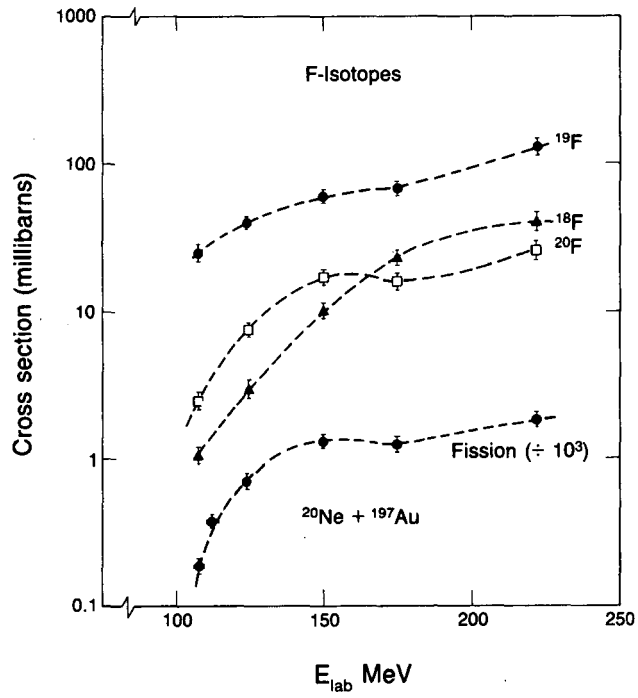

Fig. 1. Excitation functions for fission and for the fluorine isotopes produced in the ^{20}Ne + ^{197}Au reactions. XBL 8312-6914

from fusion and from sequential fission induced by massive transfer reactions, should help to supply more accurate parameters for the fusion cross sections that are needed in the model.

*Hahn-Meitner Institut, Berlin.
†Stanford University.

1. B.G. Harvey and H. Homeyer, LBL-16882 (1983) and this report.

Production of Neutron Rich Bi Isotopes by Transfer Reactions*

*K. Eskola,† P. Eskola,‡ M.M. Fowler,§ H. Ohm,§ E.N. Treher,** J.B. Wilhelmy,§ D. Lee, and G.T. Seaborg*

Production of neutron rich Bi isotopes was investigated by irradiating Hg, Tl, and Pb targets with ^{18}O ions in the 5–10 MeV/nucleon range. Following irradiation, bismuth was chemically separated and the yields of $^{211-213}Bi$ isotopes were determined via α-emitting Po daughters. Effective residual transfers of ^{3-5}H to ^{208}Pb, $^{7,8}He$ to ^{205}Tl and ^{8}Li to ^{204}Hg were observed. Cross sections generally peaked in the 7–8 MeV/nucleon region and ranged from a high of 2 mb for ^{3}H absorption to 4 nb for ^{8}He absorption. Total α- and β-decay branches of the $J^{\pi} = 9^{-}$, 25 min isomer of ^{212}Bi were measured to be 67% and 33%, respectively, $3.2 \pm 0.2\%$ of the decays being associated with β-delayed α-particle emission. Production yields for the $J^{\pi} = 1^{-}$ ground state and 9^{-} and 15^{-} isomeric levels for ^{212}Bi were extracted. The ratio of isomeric states to the ground state increased by more than two orders of magnitude over the energy range studied (Fig. 1). However, the maximum value of the cross section ratio $\sigma(J^{\pi} = 15^{-})/\sigma(J^{\pi} = 9^{-})$ was only 0.04, implying a low angular momentum transfer. The observed relatively high cross sections, modest angular momentum transfer, and broad excitation functions indicate that quasielastic transfer processes provide a viable method for reaching neutron-rich nuclides in the heavy element region.

Footnotes

*Condensed from paper submitted to Phys. Rev.
†Department of Physics, University of Helsinki, Finland.
‡Department of Theoretical Physics, University of Helsinki, Finland.
§Los Alamos National Laboratory.
**Squibb Institute for Medical Research, New Brunswick, NJ.

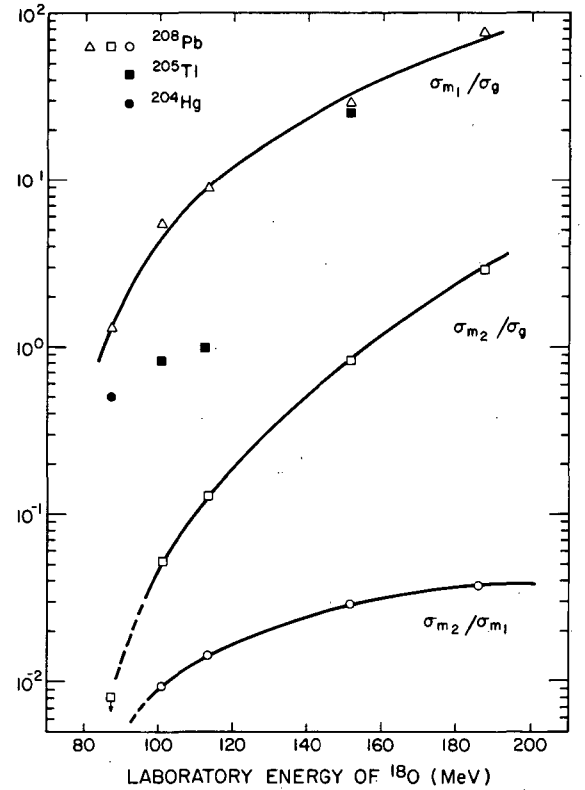

Fig. 1. The experimental isomer ratios for the $J^{\pi} = 9^{-}$ (M_1) and $J^{\pi} = 15^{-}$ (M_2) states of ^{212}Bi plotted as a function of the ^{18}O projectile energy. The points, joined by eye-guiding lines, are associated with bombardments of ^{208}Pb targets. The individual points relate to ^{205}Tl (□) and ^{204}Hg (•) targets, and measured values of the ratio σ_{m_i}/σ_g. XBL 8311-6903

Excitation Functions for Production of Heavy Actinides from Reactions of ^{40}Ca and ^{48}Ca with ^{248}Cm

*D. Lee, K. Moody, K. Gregorich, R. Welch, G.T. Seaborg, H. von Gunten,**
D.C. Hoffman,† M. Fowler,† W.R. Daniels,† G.S.I. Mainz Collaboration‡

Measurements of cross sections for production of isotopes of U through Fm have now been extended to reactions of ^{40}Ca and ^{48}Ca projectiles on ^{248}Cm targets. Experiments were conducted with ^{48}Ca at the Super HILAC at LBL and with ^{40}Ca and ^{48}Ca at the Unilac accelerator at the Gesellschaft für Schwerionenforschung (GSI) in Germany. Excitation functions for production of heavy actinides from reactions of ^{48}Ca ions with incident energies on target of 239, 263, 288 and 318 MeV and ^{40}Ca ions of 234, 259, and 294 MeV were measured using off-line radiochemical techniques. Results for Bk through Fm isotopes are presented here.

A comparison of mass-yield curves for ^{40}Ca and ^{48}Ca ions at an energy of 5–10% above the Coulomb barrier is shown in Fig. 1. The peaks of the mass distributions for Bk, Cf, Es, and Fm are all some 2 to 3 mass units larger for ^{48}Ca than for ^{40}Ca. In general, the Q-values calculated[1] for these actinide products are positive for ^{40}Ca reactions and negative for ^{48}Ca reactions. The excitation functions for production of Es and Fm isotopes from reactions of ^{248}Cm with ^{48}Ca and ^{40}Ca are shown in Fig.s 2 and 3, respectively. In general, the maxima are about 20 MeV over the Coulomb barrier for ^{48}Ca, consistent with calculations[1] showing that the Q-values are negative by 10–12 MeV for these Es and Fm isotopes. In the case of ^{40}Ca reactions, the Q-values are positive by 6–20 MeV and indeed the excitation functions are quite flat, showing no real maxima. It is rather surprising that the cross sections do not drop off much more sharply as the bombarding energy is increased to 50 MeV over the Coulomb barrier. Obviously this projectile kinetic energy does not appear as excitation energy, E_x, of the actinide products whose fission barriers are only 5 to 6 MeV. More work is needed in order to understand the reaction mechanism and energy dissipation. However, these results are most encouraging for production of new neutron-rich isotopes of heavy elements for study.

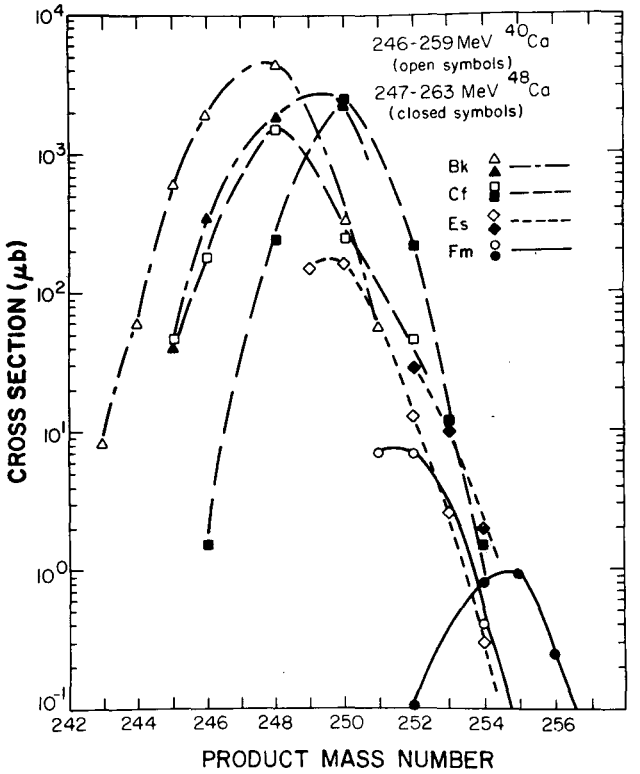

Fig. 1. Comparison of actinide yields from ^{40}Ca and ^{48}Ca reactions with ^{248}Cm. (Projectile energies in the center of the target are from about 1.05 to 1.11 of the Coulomb barrier energy.) XBL-8311-721Y

Footnotes and Reference

*Universität Bern, Switzerland
†Los Alamos National Laboratory
‡W. Brückle, M. Brügger, H. Gäggeler, M. Schädel, K. Sümmerer, G. Wirth: Gesellschaft für

Schwerionenforschung (GSI); Th. Blaich, G. Herrmann, J.V. Kratz, M Lerch, N. Trautmann: Universität Mainz, Germany

1. D.C. Hoffman and M.M. Hoffman, Los Alamos National Laboratory Report LA-UR-824 1982.

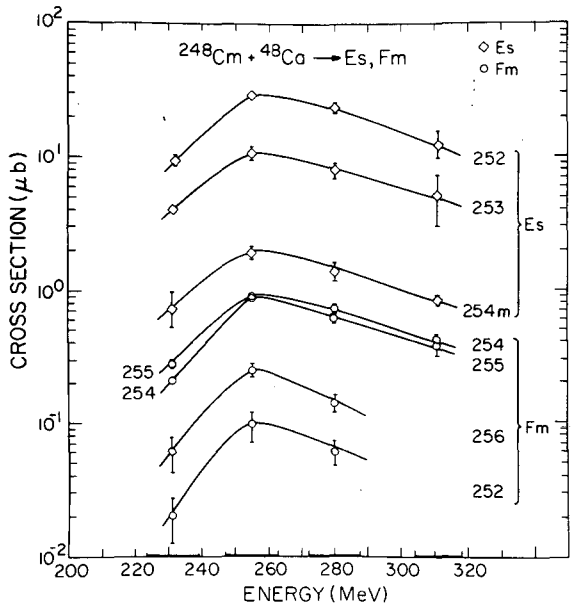

Fig. 2. E_x for Es and Fm from ^{48}Ca + ^{248}Cm. (Yields were determined from added tracer except for the 272–288 MeV bombardment, for which a yield of 50 ± 25% was estimated.) XBL-8311-722Y

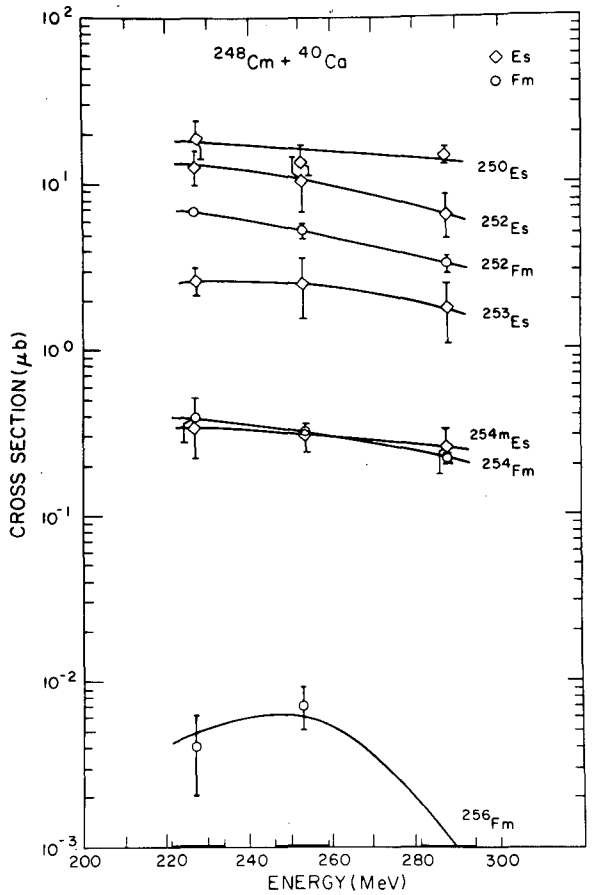

Fig. 3. Same as Fig. 2 for ^{40}Ca + ^{248}Cm. XBL-8311-723Y

Alpha Particle Emission from the Reaction 484 MeV ^{56}Fe + ^{nat}Ag

L.G. Sobotka, G.J. Wozniak, G. Guarino, R.J. McDonald, J.H. Gu,† Z.Q. Yao,† and L.G. Moretto*

In a recent experiment a natural Ag target was bombarded by 484 MeV ^{56}Fe from the SuperHILAC. A gas ΔE- solid state E telescope was positioned in the new 60 inch scattering chamber near the classical grazing angle (Θ_{lab} = 20°) to detect the projectile-like fragment. The α-particles were also detected by a gas ΔE- solid state E telescope. The design of these light particle detectors is described in ref. 1. In brief, these counters consist of 5 solid state stopping detectors in an arc with a common gas ΔE section. In the present experiment the α-particles were detected at a total of 15 angles (60°, 70°, 80°, 90°, 100°, 120°, 130°, 140°, 150°, 160°, 195°, 205°, 215°, 225°, 235°), as measured clockwise from the beam direction.

In Fig. 1 contour plots of the Galilean invariant cross section are shown for α-particles detected both in singles (upper) and in coincidence with a heavy fragment (Z = 14–38) at 25° (lower). The solid lines are levels of constant cross section as determined by interpolation between measurements spaced 10° apart. The dashed lines involved interpolations over greater distances. The singles plot is shown for

reference and to verify that our calibrations are correct. One should note that the detection of a heavy ion at 25° introduces a strong asymmetry about the beam axis in the backward hemisphere. We can immediately conclude from this that there is a strong non-center-of-mass component.

The average kinematics for three different exit channel asymmetries is shown in Fig. 1 (lower). The pronounced change in the velocity vectors over such a wide range of asymmetries washed out the features of the emission pattern expected for fragment emission. For this reason and in order to determine if the contribution from the various possible components changes with the exit channel asymmetry, these data have been divided into 5 asymmetry (Z) bins. The spectra, plotted in histograms as a function of Z bin and angle, are shown in Fig. 2.

Examining the data as a function of Z of any fixed angle, one is again forced to the conclusion that a c.m. component cannot be dominant. This is evident because prescission emission would not be sensitive to the exit channel masses, yet the data do exhibit a strong and systematic change with the Z of the detected fragment.

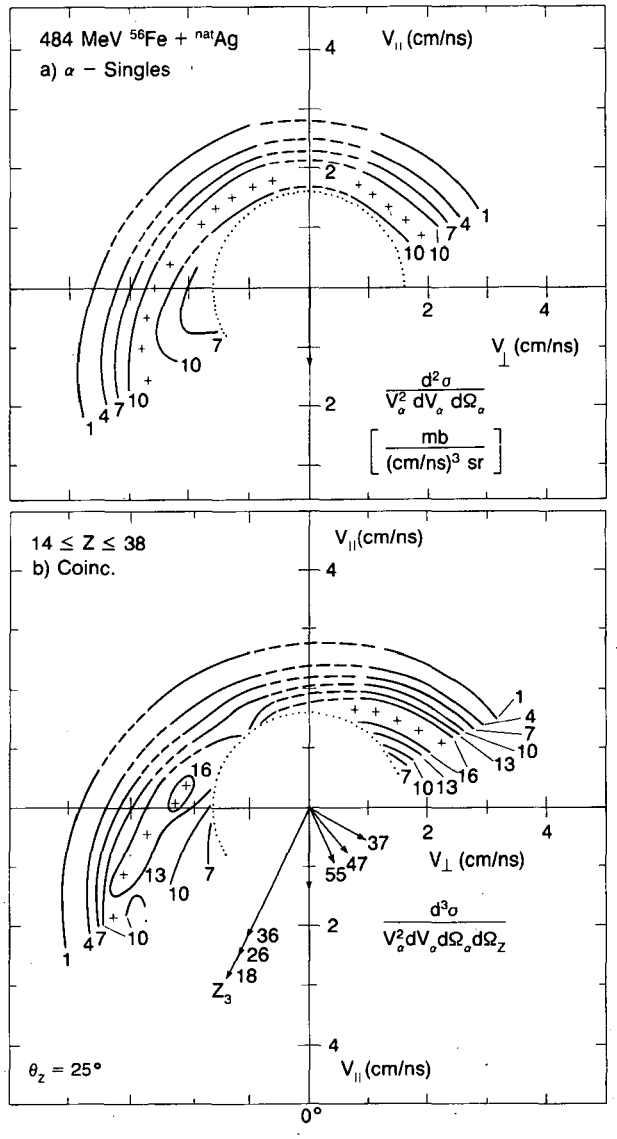

Fig. 1. Contour plots of the Galilean invariant cross section for angles (upper) and coincidence (lower).
XBL 838-3099

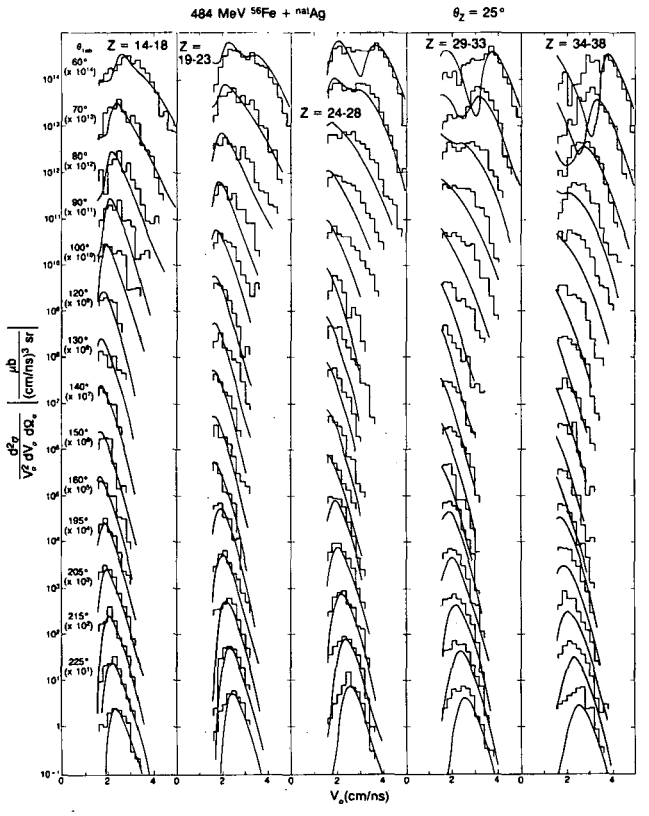

Fig. 2. Comparison between the data (histograms) and simulation (solid lines) as a function of charge asymmetry and angle. XBL 8312-2528A

The data shown in Fig. 2 are compared to a Monte Carlo simulation of α-particle emission from the two fully accelerated fragments. The simulated spectra are shown as the solid lines in Fig. 2. For the most asymmetric bins ($14 \leqslant Z_3 \leqslant 18$ and $19 \leqslant Z_3 \leqslant 23$) the simulation reproduces the data remarkable well. However, for more symmetric bins the discrepancy increases. This discrepancy is most noticeable in the region near 130°.

From this comparison we conclude that while no source other than emission from the fully accelerated fragments is required to reproduce the data for the most asymmetric exit channels, a significant additional component is required for the symmetric products.

Footnotes and Reference

*Present address: Universitá Degli Studi di Bari, 70100 Bari, Italy.

†Present address: Shanghai, Peoples Republic of China

1. R.J. McDonald, LBL Annual Report (1983).

Identification of Complete Charge Transfer Reactions for ^{20}Ne + ^{197}Au with the Plastic Box*

*S. Wald, C.R. Albiston, M. Bantel, Y.D. Chan, B.G. Harvey, M.J. Murphy,† I. Tserruya,‡ R.G. Stokstad, P.J. Countryman,§ K. Van Bibber,§ H. Homeyer***

The inclusive products of heavy-ion reactions at bombarding energies above 10 MeV per nucleon in general result from several competing mechanisms.[1] Experimental methods that isolate and identify one or more of these mechanisms are able to make important contributions to the understanding of heavy-ion reactions. To illustrate how this new detector is used, consider the inclusive reaction ^{20}Ne + ^{197}Au $\rightarrow$ ^{12}C + X. The ^{12}C ejectiles at forward angles might be produced by any of the following mechanisms: (i) transfer leading to a bound state of the ejectile: (^{20}Ne, ^{12}C); (ii) complete charge transfer followed by neutron decay: (^{20}Ne, ^{13}C*), ^{13}C* $\rightarrow$ ^{12}C + n; (iii) transfer followed by charged-particle decay: (^{20}Ne, ^{16}O*), ^{16}O* $\rightarrow$ ^{12}C + α; (iv) inelastic scattering followed by sequential decay: (^{20}Ne, ^{20}Ne*), ^{20}Ne* $\rightarrow$ ^{12}C + 2α; (v) direct fragmentation: ^{20}Ne $\rightarrow$ ^{12}C + ^{8}Be.

The last three mechanisms produce at least one additional light charged particle, normally energetic and kinematically correlated with the projectile-like fragment. A 4π detector that observes the associated light charged particles in coincidence with a projectile-like fragment, but that is insensitive to fission fragments, neutrons and gamma rays, can discriminate mechanisms such as (iii) – (v) from (i) and (ii). We refer to the former loosely as breakup reactions and to the latter as complete charge transfer reactions. We describe here the first application, for low and intermediate bombarding energies, of a 4π electronic charged-particle detector, the "Plastic Box", to distinguish between transfer and breakup reactions.[2]

We have studied reactions of the system ^{20}Ne + ^{197}Au at 220 and 341 MeV with this detector; measurements were made at Θ_{lab} = 15° and 20° at the lower energy, and at 8° and 16° at the higher energy.

Fig. 1 shows the relative and absolute magnitudes of complete charge transfer reactions at both 220 and at 341 MeV. The fraction of complete charge transfer events, defined as $N(Z,0)/\sum_{S\geqslant 0} N(Z,S)$ where S is the number of scintillator walls detecting a charged particle, diminishes with increasing bombarding energy and, in general, with increasing transferred charged ΔZ. The most important feature of these data is that substantial probability ($\gtrsim$17%) persists for transfer reactions with ΔZ at least as

large as 7, i.e., for the transfer of ~14 amu, even at a bombarding energy of 17 MeV per nucleon.

Energy spectra for ^{16}O and ^{17}O ejectiles are shown, as an example, in Figs. 2a and 2b for inclusive, S=0, and S=1 reactions. The shapes of the energy spectra for the transfer and breakup reactions in the oxygen isotopes differ in detail. The transfer component lies at somewhat higher energies and, at this particular angle, appears to be narrower in width. These characteristics may be analyzed and compared with predictions of reaction models.[3] It is more useful here, however, to examine the characteristics of the different reaction products in a general way. This is done by determining the first three moments of each spectrum, the mean <E>, the standard deviation $\sigma = (\langle E^2\rangle - \langle E\rangle^2)^{1/2}$ and the skewness γ_1, defined here by

$$\gamma_1 = \frac{\langle (E - \langle E\rangle)^3\rangle}{\sigma^3} .$$

The advantage of this procedure is that it involves neither arbitrary decisions on which portions of the spectrum to emphasize nor assumptions about the reaction mechanism.

The values of the moments are presented in Fig. 3. As in the case of the oxygen isotopes, the mean energy for the S=1 component is lower. This is

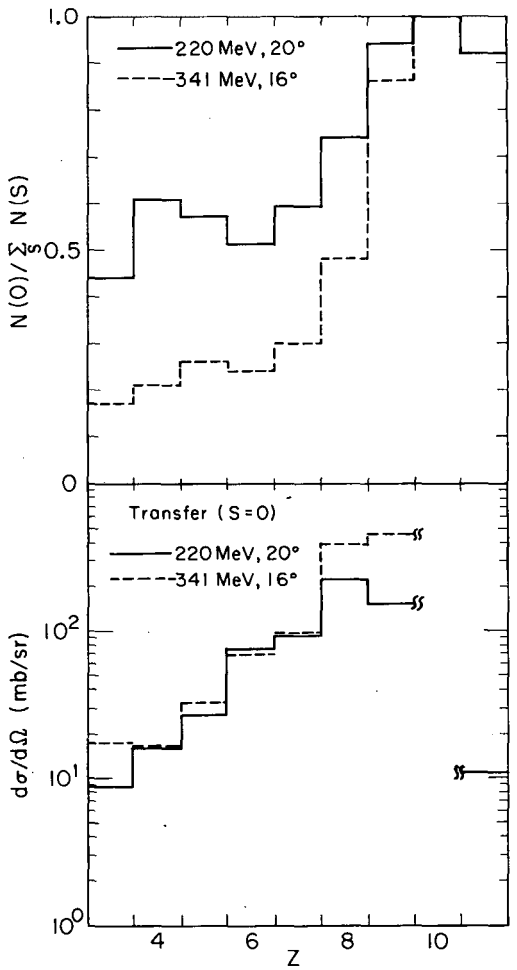

Fig. 1. a.) The probability for complete charge transfer, i.e., that no wall detects a charged particle when an ejectile of atomic number Z is observed in the solid state telescope.
b.) Absolute differential cross sections for complete charge transfer (S=0). The uncertainty is ±15%.
XBL 839-4004

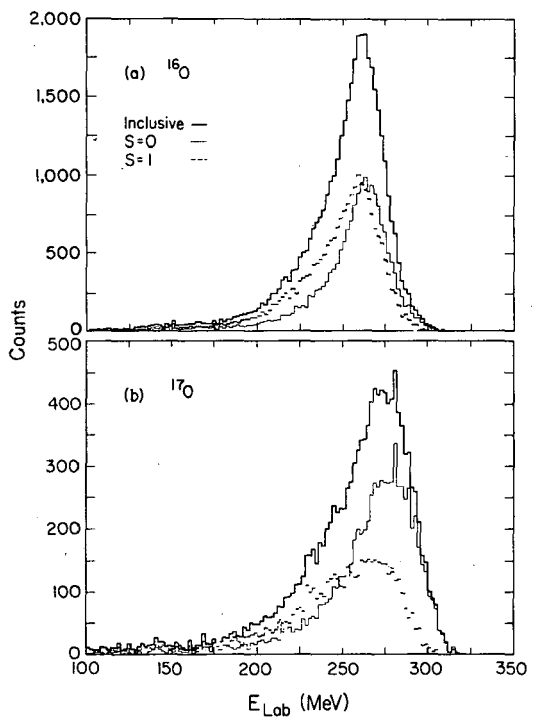

Fig. 2. Energy spectra of oxygen ions produced at 341 MeV and Θ = 16° for inclusive reactions (heavy line), complete charge transfer (fine line) and for S=1 (broken line) a) for ^{16}O, b) for ^{17}O. XBL 8311-769

observed at 8° as well and reflects the loss of kinetic energy associated with the liberation of an additional particle.

The energy widths (Fig. 3b) show a more complex behavior. The transfer (S=0) component is narrower than the breakup (S=1) component for masses close to the projectile (as predicted in ref. 3), but for the lighter ejectiles the opposite is true. At 8°, however, the transfer component is broader than the breakup component for all ejectiles except fluorine. The largest widths at 8° occur for the oxygen isotopes, whereas at 16° the carbon and nitrogen isotopes are the broadest. It is clear that the second moment shows a strong angle dependence.

The skewness (Fig. 3c) indicates a trend toward spectra that are symmetric about the mean as more charge is lost from the projectile. (A spectrum that is symmetric about the mean has a skewness of zero; a low energy tail gives a negative skewness, as seen in Fig. 2). With few exceptions, the breakup spectra are more symmetric than the corresponding transfer spectra.

An interesting and striking feature of this global comparison in Fig. 3 is the overall similarity of the trends shown by the moments for transfer and breakup as a function of fragment mass. This feature is present at all angles and at both bombarding energies. An explanation for this similarity is suggested directly by a closer examination of the information from the scintillators. The thicknesses of the scintillators are such that alpha particles and protons with beam velocity normally will penetrate the first element of the wall and thus can be identified. Analysis of the scintillator signals shows that most of the associated charged particles are alpha particles or protons. This implies that when, for example, ^{7}Be is detected with S=1, either four or five units of charge were captured by the target. The most likely process responsible for this is transfer followed by charged-particle decay of the primary beam-like product (item iii above).[4] This subsequent emission of a light-charged particle apparently does not alter drastically the gross characteristics of the secondary products.

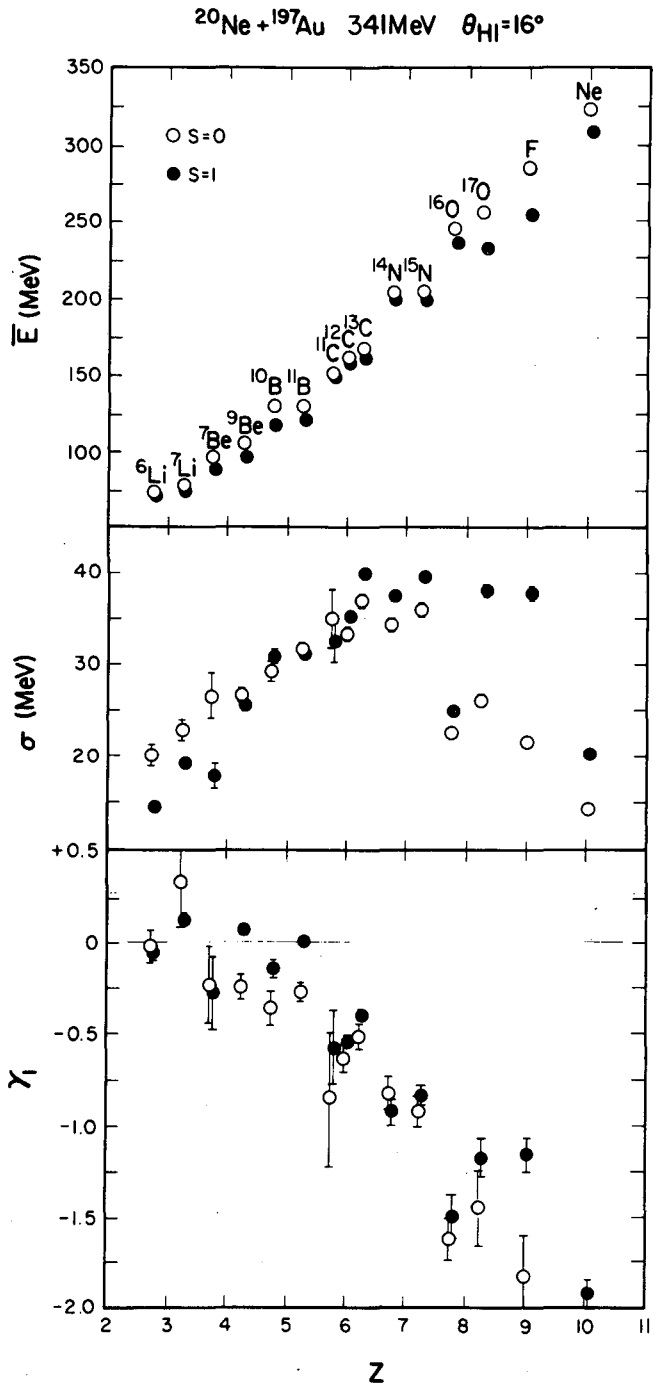

Fig. 3. Moments of the energy spectra for ejectiles observed in the telescope. Solid points are for spectra with S=1, open points for S=0. Upper: the mean energy; middle: the standard deviation; and bottom: the skewness. XBL 8311-770

In summary:

1) The quasi-elastic reaction products more than two charge units removed from the projectile are frequently accompanied by one or more additional charged particles.
2) Significant cross section still exists, however, for the complete transfer of large amounts of charge from the projectile to the target, leaving the projectile remnant in a particle-bound state.
3) The moments of the transfer and breakup spectra, while exhibiting some differences, behave in a remarkably similar manner.
4) The associated charged particles in the case of breakup are predominantly alpha particles or protons, and not large fragments. These results provide further evidence in favor of the importance of two-body transfer reactions in the *primary* state of the reaction, even for energies up to 20 MeV per nucleon.[1,4]

Footnotes and References

*Condensed from LBL-16899
†Present address: Nuclear Structure Laboratory, University of Washington, Seattle, Washington.
‡Permanent address: Weizmann Institute of Science, Department of Physics, Rehovot - 7600, Israel.
§High Energy Physics Laboratory and Department of Physics, Stanford University, Stanford, CA 94305
**Permanent address: Hahn-Meitner-Institut, Berlin.

1. M.J. Murphy *et al.*, Phys. Lett. **120B**, 319 (1983).
2. K. Van Bibber *et al.*, This report. 397 (1983).
3. K.W. McVoy and M.C. Nemes, Z. Physik, **A295**, 177 (1980); B.G. Harvey and M. Murphy, Phys. Lett. **130B**, 373 (1983). B.G. Harvey and H. Homeyer, This report;
4. H. Homeyer *et al.*, Phys. Rev. **C26**, 1335 (1982); R.K. Bhowmik *et al.*, Nucl. Phys. **A390**, 117 (1982).

Transfer Reactions with Very Heavy Ions

A.O Macchiavelli, M.A. Deleplanque, R.M. Diamond, F.S. Stephens, E.L. Dines,† J.E. Draper†*

One- and two-nucleon transfer reactions with light ions (e.g., (t,p), (d,p), etc.) have been widely used to obtain information about single-particle aspects and residual interactions in nuclei.[1] Light heavy ions have similarly been used to study nuclei near closed shells[2a] but only recently applied to deformed nuclei when the selective population of high-j orbitals in ^{167,169,171}Er was observed, using C and O projectiles.[2b] Here we consider transfer reactions with very heavy ions ($A \gtrsim 40$), which add the interesting feature of strong collective excitations to the transfer process.

In the last few years several studies have been devoted to transfer reactions with very heavy ions. H. Siekmann *et al*[3] studied proton transfer reactions induced by ^{86}Kr on ^{88}Sr, ^{90}Zr, ^{92}Mo. G. Himmele *et al*[4] reported results on neutron transfer in ^{184}W + ^{238}U. W. von Oertzen *et al*[5] have discussed pairing effects in quasi-elastic neutron transfer in the reaction ^{120}Sn + ^{112}Sn. In the present work we have tried to extend to transfer reactions the studies of M. Guidry *et al*[6] on Coulomb-nuclear interference by using particle-particle-γ coincidence techniques.

We used the ^{132}Xe beam from the SuperHILAC to bombard $\simeq$0.5 mg/cm^2 self supporting targets of ^{154}Sm, ^{176}Yb, and ^{171}Yb at $\frac{E_{cm}}{V_{Coulomb}} \simeq 1.1$ to look for one- and two-neutron transfers. The experimental arrangement consisted of two large solid-angle position-sensitive gas avalanche detectors (PSAD's) in coincidence with 2 Ge(Li) detectors placed 180° from the PSAD's. A particle-particle-γ coincidence was required as a master gate. This technique combines intermediate resolution in the heavy ion to define the "classical trajectory" of the collision and

the high resolution possible with γ-rays to identify products and states populated in the reaction process. The different timing characteristics of distant and close collisions allowed their clean separation. Fig. 1 shows the Ge(Li) spectrum for close-collision events with the ^{171}Yb target. Both one neutron pick-up and stripping reactions are clearly seen. In Table I we summarize the results of the present work.

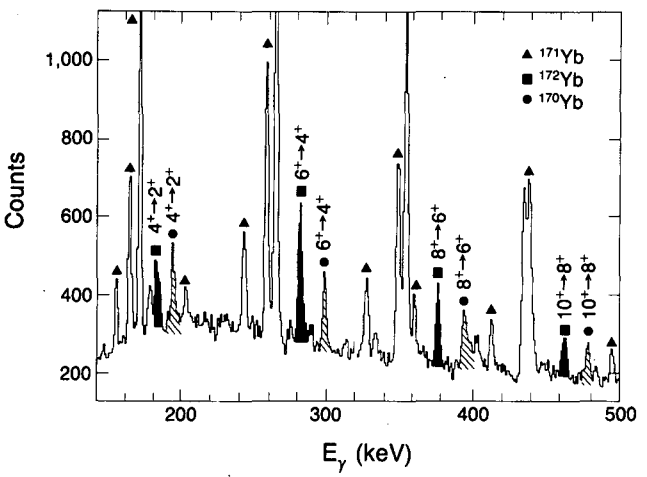

Fig. 1. Ge(Li) spectrum in coincidence with close-collision events for the ^{132}Xe + ^{171}Yb run. Transfer lines are clearly seen. XBL 841-10014

Table I

Reaction	ΔN	Q_{gg}(MeV)	$P_{\Delta N}$(%)
^{132}Xe + ^{154}Sm	0	0	22 *1*
	+1 n	−1.52	7 *1*
	+2n	1.14	3.5 *0.5*
	−2n	−2.49	0.7 *0.3*
^{132}Xe + ^{176}Yb	0	0	21 *1*
	+1 n	−0.43	3.8 *0.6*
	+2 n	2.29	2.0 *0.3*
^{132}Xe + ^{171}Yb	0	0	35 *2*
	+1 n	−0.17	3.0 *0.5*
	−1 n	−0.92	≃3 *1*[a]

a)Larger uncertainty due to ^{172}Yb impurity in the target.

For heavy ions we can define a distance of closest approach

$$D(\Theta) = \frac{n}{k}\left(1 + \frac{1}{\sin\Theta/2}\right) .$$

The transfer probabilities as a function of D(Θ) are presented in Fig. 2 for the different reactions. All the cases show an exponential behavior, i.e.,

$$P_{\Delta N}(\Theta) \propto \exp\left(-KD(\Theta)\right) \qquad K = 2\sqrt{2mB_{eff}}$$

characteristic of a barrier penetration model.[7] The values of K for the 1n cases are in reasonable agreement with the values calculated using the appropriate binding energies. On the other hand, it is expected in either sequential or direct transfer of two neutrons that $K_{2n} \simeq 2K_{1n}$. This fact is clearly not observed in this experiment nor in the previous results of references 3 and 4. Therefore it is possible that these 2n reactions proceed via intermediate states of higher excitation energy, $E_x \simeq 6$ MeV, thereby changing the effective binding energy of the transferred particles. At any distance D(Θ) we can define an enhancement factor,

$$EF(D) = \frac{P_{2n}(D)}{P_{1n}^2(D)}$$

from Fig. 2. We find EF ~ 5–30. An interesting interpretation of this enhancement factor is to relate it to the pairing interaction. One expects pairing to enhance 2n transfers both in a single (true pair)- and a two (sequential)-step process. [1,8] However, as discussed previously, above the Coulomb barrier 2n transfer probably proceeds via states of higher excitation energy. Due to the smaller effective barrier the probability for 2n transfer is in this case larger than that expected for a cold transfer.

We are currently analyzing the probabilities as a function of spin; these may be sensitive to the spatial localization of the wave functions involved in the transfer.

Footnotes and References

*Permanent Address: Comisión Nacional de Energía Atómica, Buenos Aires, Argentina.

†Permanent Address: Department of Physics, University of California, Davis, CA 95616.

1. B. Elbek and P. Tjøm, Adv. in Nucl. Phys. **3**, 259 (1969); R. Broglia, O. Hansen, and C. Riedel, Adv. in Nucl. Phys. **6**, 287 (1973).
2. a) S. Kahana and A. Baltz, Adv. in Nucl. Phys. **9** (1977); b) P. Bond *et al*, Phys. Rev. Lett. **46**, 24 (1981).
3. H. Siekmann *et al*, Z. Phys. A. **307**, 113 (1982).
4. G. Himmele *et al*, Nucl. Phys. **A404**, 401 (1983).
5. W. von Oertzen, *et al*, Z. Phys. **A313**, 189 (1983).
6. M. Guidry *et al*, Phys. Rev. Lett. **40**, 1016 (1978).
7. G. Breit and M.E. Ebel, Phys. Rev. **103**, 679 (1956).
8. H. Weiss, Phys. Rev. **19C**, 834 (1979); U. Götz *et al*, Phys. Rep. **16C**, 115 (1975).

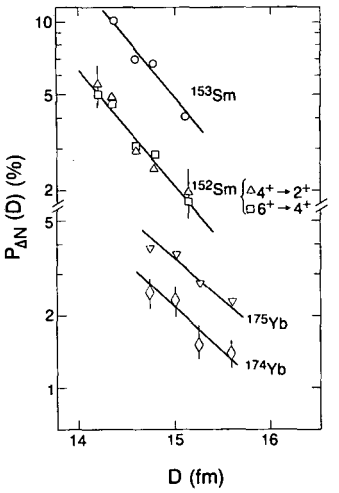

Fig. 2. Probabilities for transferring one and two neutrons as a function of the distance between the two nuclei. XBL 843-10125

Below-Target Transfers in the ^{136}Xe + ^{249}Cf Reaction

K.E. Gregorich, K.J. Moody, R.B. Welch, W. Kot, D. Lee and G.T. Seaborg

Over the past several years much effort has gone into the study of the deep-inelastic transfer reaction mechanism. It was hoped that this mechanism could be used to produce new elements and new isotopes of known elements. It has been shown that the deep-inelastic mechanism is of little use in producing new heavy elements[1] and that the best area of production of new isotopes, especially in very heavy ion bombardments,[2] is in the region near the target (or projectile) with fewer protons and more neutrons than the target (or projectile).[3] Nearly all studies with very heavy ions on actinide targets have used the most neutron rich targets available. With these neutron rich targets, the products with fewer protons and more neutrons than the target are beyond the neutron rich side of known nuclides, and most have predicted half lives of about one minute or less.[4] Because of these short half lives, most of the yields of nuclides with fewer protons and more neutrons than the target have not been measured. In the present experiments a ^{249}Cf target was used. ^{249}Cf is relatively neutron deficient and many of the neutron rich below-target nuclides are observable. These bombardments were carried out in order to measure the yields of nuclides with $87 < Z < 103$ with special emphasis on the neutron rich Am and Bk isotopes.

A target consisting of .825 mg/cm^2 of ^{249}Cf as Cf_2O_3 on a 1.8 mg/cm^2 Be backing was produced by the molecular plating procedure.[5] It was bombarded by 8.5 MeV/nucleon ^{136}Xe ions at the SuperHILAC in the High Level Cave, and the recoiling products were stopped in a 25 mg/cm^2 gold foil. At the end of bombardment the gold foil was transported to the chemistry lab for processing. The short-lived americium isotopes were separated from all other elements in a procedure which involved a HDEHP/HNO_3 extraction chromatography column,[6] a 13 M HCl cation exchange column, and a LaF_3 co-precipitation. The time from the end of bombardment to the

availability of the finished chemical fraction was < 35 min. The short lived Bk isotopes were separated in a similar procedure. The long lived Am and Bk isotopes were produced in a long bombardment and were separated from all other elements in a procedure involving an ammonium α-hydroxyisobutyrate cation exchange column and a 13 M HCl cation exchange column.

In Fig. 1 the cross sections for the production of Bk and Am isotopes are presented along with the cross sections for analogous transfer products from the $^{136}Xe + ^{248}Cm$ reaction. It should be noted that the $^{136}Xe + ^{248}Cm$ results are from a slightly lower energy bombardment. As can been seen from Fig. 1, the yields of products with one less proton than the target are comparable, and we have measured the neutron rich side of the one proton out yield distribution in the $^{136}Xe + ^{249}Cf$ reaction. The peak of the three proton out distribution of isotopes from the $^{136}Xe + ^{248}Cm$ reaction is not clearly shown because the cross section for ^{240}Np is the yield for only half of an isomer pair. It appears, however, from the relative heights of the distribution, that the Am yields from the $^{136}Xe + ^{249}Cf$ reaction peak about two or three mass numbers heavier than do the corresponding Np yields from the $^{136}Xe + ^{248}Cm$ reaction. A possible explanation for these results is that in the one Z out products, the neutron deficient nuclides may be formed by a direct interaction (direct transfer of a proton and possibly some neutrons to the projectile). This direct interaction would not allow a large amount of energy and N/Z equilibration and therefore would not be very sensitive to the position of beta stability. On the other hand, the yields of the three proton out products must be due to a much "deeper" interaction where there is much more equilibration of energy and N/Z and therefore the yields peak nearer to beta stability.

References

1. M. Schädel *et al.*, Phys. Rev. Lett. **41**, 469 (1978).
2. K.J. Moody, Ph.D. thesis, LBL-16249 (1983).
3. K. Rykaczewski *et al.*, Z. Physik A **309**, 273 (1983).
4. H.K. Klapdor, J. Metzinger, T. Oda, to be published.
5. D.C. Aumann, G. Mullen; NIM **115**, 75 (1974); G. Mullen, D.G. Aumann; NIM **128**, 425 (1975).
6. E.P. Horwitz, C.A.A. Bloomquist, D.J. Henderson, JINC **31**, 1149 (1968); E.P. Horwitz, C.A.A. Bloomquist, D.J. Henderson, D.E. Nelson, JINC **31**, 3255 (1969).

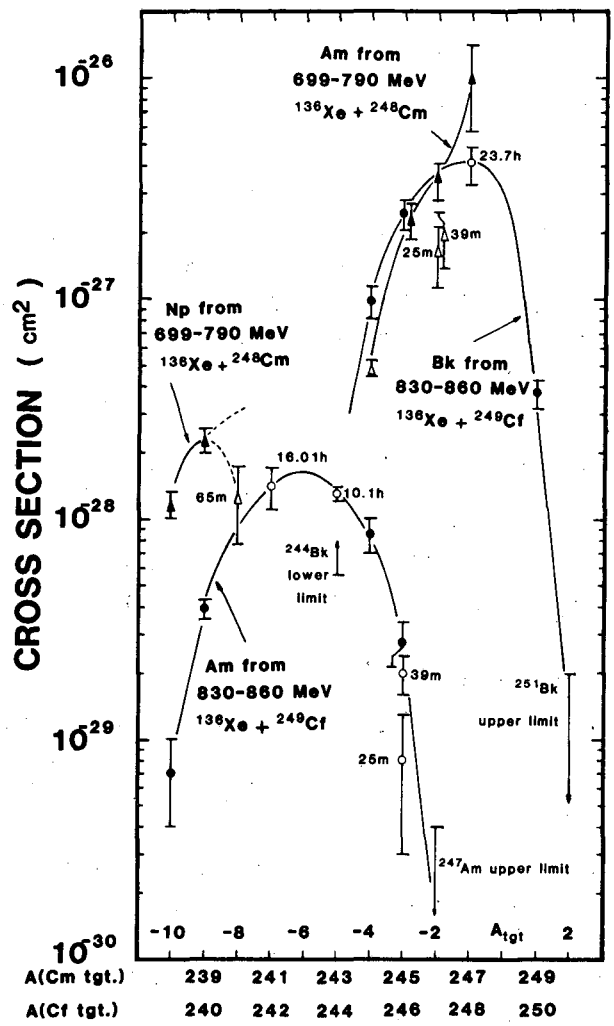

Fig. 1. A comparison of analogous target-like transfer products for $Z_T - 1$ and $Z_T - 3$ from 699–790 MeV $^{136}Xe + ^{248}Cm$ and from 860–890 MeV $^{136}Xe + ^{249}Cf$. Open points indicate the cross section for one half of an isomer pair. XBL 8311-720

Mass Distributions in the Reaction of 240 MeV ^{12}C with ^{197}Au

H. Kudo, K.J. Moody,† and G.T. Seaborg*

It is interesting to study how the reaction mechanisms in heavy ion induced reactions vary with incident projectile energy, especially for energies near the nuclear Fermi energy. Very little radiochemical work has been published on reaction systems in the energy region between low energy heavy ion reactions (a few MeV/nucleon) and high energy heavy ion reactions (hundreds of MeV/nucleon or more). In our work, we have examined the mass distribution of 20 MeV/nucleon ^{12}C + ^{197}Au using radiochemical methods.

The gold targets were self-supporting foils of 5.16 mg/cm^2 thickness, mounted between two pieces of 6.24 mg/cm^2 aluminum foil to completely collect both forward and backward recoil products. These targets were irradiated with an average beam current of 20 nanoamperes of 240 MeV $^{12}C^{5+}$. Each run produced 3 to 10 chemical fractions. These samples were counted for gamma rays with Ge(Li) detectors equipped with pulse height analyzers. The gamma ray count rates as a function of time were analyzed to give end-of-bombardment activities and nuclidic cross sections. Whenever possible, the activities were corrected for precursor decay before the cross section calculation.

The cross sections of about 250 nuclides were determined. They are plotted in Fig. 1a. Many of the fission products determined were members of the same mass chain, so charge dispersions could be obtained. The most probable atomic number Z_p is well reproduced with the linear equation $Z_p = 0.417 A + 1.4$. The Gaussian charge dispersions for all fission products were found to have similar values of the width parameter, $2\sigma^2 = 1.6$. This width included fission reactions. Fig. 2 shows a cumulative, scaled charge dispersion for all measured fission products.

The cross sections of target-like products are plotted in the form of charge dispersion in Fig. 3. For A = 196 to 199, the charge dispersions have two components. The low Z quasi-elastic component is described with a width parameter of 0.6. The high Z "deep-inelastic" component has $2\sigma^2 = 1.1$. The charge dispersions for A = 200 to 204 can be described with a single Gaussian function with a width of 1.6, similar to the fission products. The most probable charge of "deep-inelastic" products from A = 198 to 202 remains constant at $Z_p = 82$; this is due, in part, to the effect of the 82 proton shell on the transfer process and on the fission survival probability of the primary reaction products.

The charge-dispersion-corrected mass distribution of the 20 MeV/nucleon ^{12}C + ^{197}Au reaction is shown in Fig. 1b. A Gaussian fit to the fission distribution from A = 71 to 145 has a width parameter of 38 mass units. This, too, is considerably wider than that obtained from lower energy heavy ion induced fission. The integral of this Gaussian gives a fission cross section of 1700 mb. This is considerably larger than the predicted fusion cross section of 967 mb.[1] We feel that the width of the charge and mass distributions for fission products is due to the large variety of fissioning systems produced in the reaction, and the wide range of angular momenta for these systems. An ALICE[2] calculation, including pre-equilibrium processes, reproduced the total fission cross section very well, independent of the initial exciton number, which was varied from 12 to 20.

The ALICE calculation was less successful at reproducing the charge distributions of target-like products. The experimental cross sections of Tl, Pb and Bi isotopes were 1 to 2 orders of magnitude larger than those predicted by the calculation. The trend of the experimental cross sections falls off from the target Z; the trend of the calculation is for the cross sections to fall off from the compound nucleus Z. The polonium cross sections are in agreement with ALICE calculation, except for ^{202}Po and ^{204}Po, which are too large. We attribute this to the de-excitation of primary products near the compound nucleus (A,Z) by the emission of high energy, non-

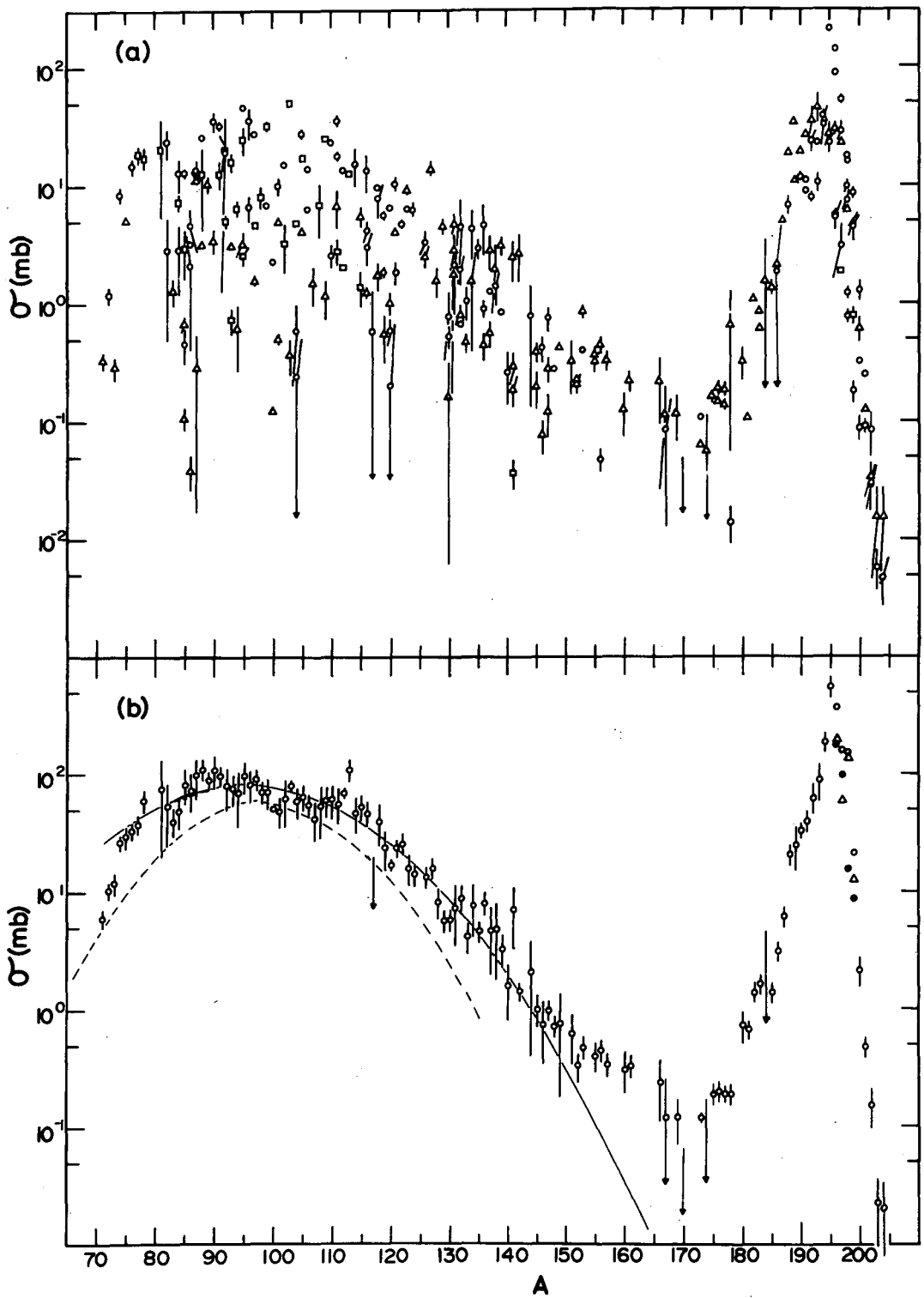

Fig. 1. Cross sections from the reaction of 240 MeV ^{12}C with ^{197}Au. (a) Individual cross sections. Circles denote independent cross sections, triangles denote partially cumulative cross sections from β^+ or EC decay, and squares denotes partially cumulative cross sections from β^-decay. (b) The charge-dispersion-corrected mass distribution. The full curve is a result of Gaussian fitting the fission products. The dashed curve is from Blann,[3] describing the fission distribution of 112 MeV ^{12}C + ^{197}Au. XBL 839-11650

equilibrium nucleons.

The total cross section for the production of target-like products is roughly 1700 mb, giving a total reaction cross section of 3.4 b, in good agreement with the calculated 3.3 b.[1]

Footnotes and References

*Department of Chemistry, Faculty of Science, Niigata University, Niigata, Japan

†Gesellschaft für Schwerionenforschung mbH, Postfach 11 05 41. 6100 Darmstadt 11, West Germany.

1. W.W. Wilcke, J.R. Birkelund, H.J. Wollersheim, A.D. Hover, J.R. Huizenga, W.U. Schröder, and L.E. Tubbs, At. Nucl. Data Tables **25**, (1980).
2. F. Plasil, Oak Ridge National Laboratory Report TM-6054 (1977).
3. H.M. Blann, Phys. Rev. **123**, 1356 (1961).

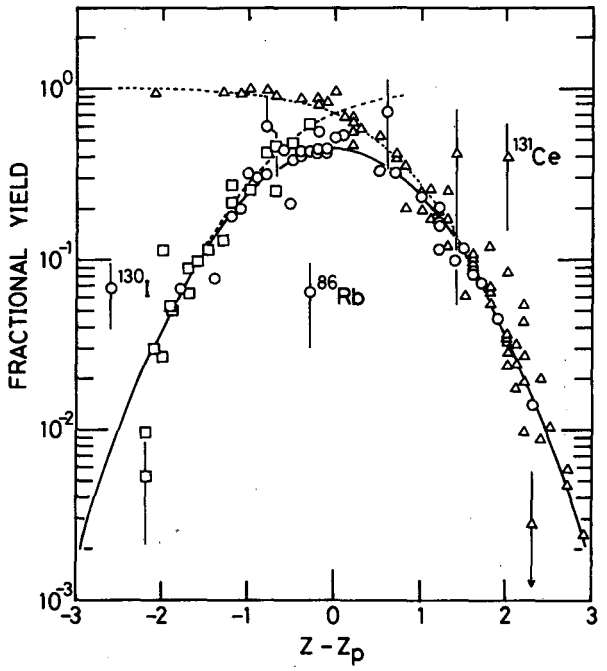

Fig. 2. The cumulative charge dispersion of the fission products. XBL 839-11649

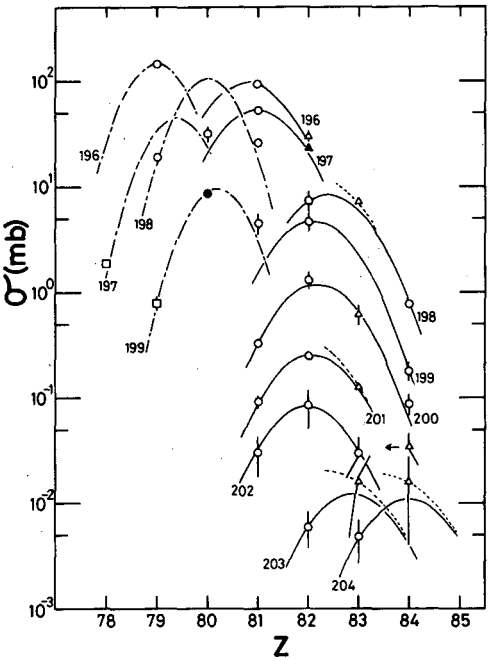

Fig. 3. The charge dispersions of target-like products for A = 196 to A = 204. XBL 839-11648

Transfer Reaction Cross Sections from the Interactions of ^{20}Ne and ^{22}Ne with ^{232}Th

S. Tanaka, K.J. Moody and G.T. Seaborg*

There has recently been a lot of interest in the possibility of synthesizing new neutron-rich actinide and transactinide nuclides in transfer reactions of light heavy ions (A ≤ 40) with actinide targets.[1,2,3] In these reactions, the complicated way in which the energy and angular momentum states in the primary products are originally populated and then undergo deexcitation by the emission of particles or photons

or by fission makes the extremes of the cross section distributions of the evaporation residues hard to theoretically predict. In order to pick the optimum projectile/target/reaction energy combination to make a particular nuclide, it is important to systematize the reaction product cross sections in the known regions of nuclear mass and charge.

We have bombarded an electroplated 1 mg/cm^2 ^{232}Th target with ^{20}Ne and ^{22}Ne and chemically isolated the reaction products, concentrating on those elements with one, two and three more protons than the target, at energies not far in excess of the calculated Coulomb barrier at 105 MeV. The decays of the product nuclides were observed via the emitted gamma rays with a Ge(Li) detector. The cross sections for the formation of these nuclides were determined, and are given in Table I. Fig. 1 shows a plot of the isotopic distributions of protactinium, uranium and neptunium from one of the experiments.

Comparison of the data from ^{22}Ne and ^{20}Ne irradiations of ^{232}Th at the same energy excess over the Coulomb barrier shows that, in the neptunium isotopes, the peak cross section is shifted by two mass units to neutron excess for ^{22}Ne-induced reactions. This is similar to the result obtained in ref. 1 for similar transfers from ^{20}Ne and ^{22}Ne to ^{248}Cm. The width of the mass distributions for neptunium (FWHM = 2.5 units) is also similar to those arising from Ne + ^{248}Cm. It is our feeling that, since the ground state Q values and Coulomb potentials of reactions between Ne and ^{232}Th and between Ne and ^{248}Cm are dominated by changes in the mass and charge of the projectiles, and since the fission barriers of the products of interest are roughly the same in both systems, it is not surprising that the cross sections for similar transfers are very nearly the same.

Fig. 2 shows the behavior of the cross sections for the production of the protactinium isotopes with projectile energy for ^{20}Ne + ^{232}Th. The increase in the product cross sections with projectile energy is very nearly the same for these nuclides, showing that the peak in the distributions is roughly independent of projectile energy. The ^{233}Pa cross section remains roughly constant, due to the fact that ^{233}Pa is fed by ^{233}Th ($t_{1/2}$ = 22 min) during the bombardment, and the neutron pick-up cross section is not as energy dependent as those involving charge transfer. Surprisingly, the neutron-rich ^{234g}Pa cross section is the most sharply increasing with energy. We propose that this is due to an increase in the fraction of the reaction cross section going to form ^{234}Pa which results in the high spin (4+) ground state, and a corresponding decrease in the fraction which forms the unobserved $J^{\pi} = 0^-$ isomer. By all indications, the primary reaction products which survive fission to become the observed target-like products are formed with very little excitation energy or angular momentum.

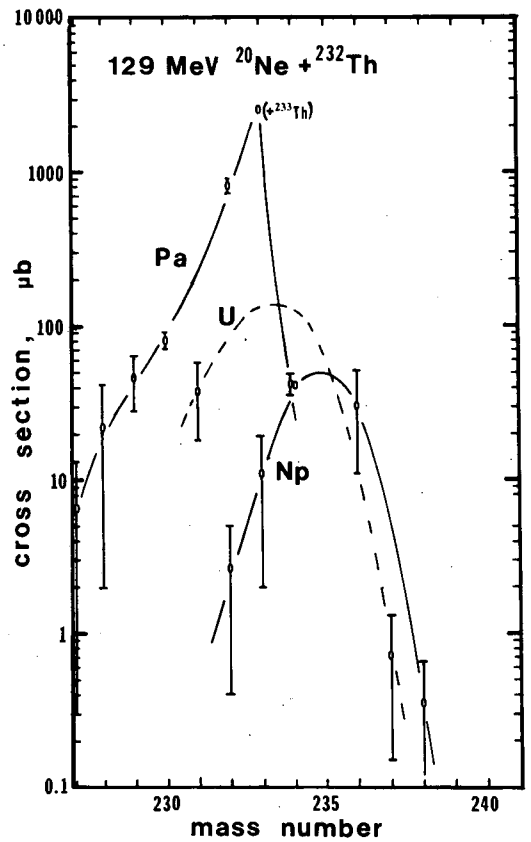

Fig. 1. Product cross sections from the reaction of 129 MeV ^{20}Ne with ^{232}Th. Cross sections for nuclides of the same element are connected to guide the eye. XBL 839-11839

Table I Measured Cross Sections (mb)

Nuclide	114 MeV ^{22}Ne	114 MeV ^{20}Ne	129 MeV ^{20}Ne
^{227}Pa			$(6.9 \pm 6.6)10^{-3}$
^{228}Pa		$(1.6 \pm 1.3)10^{-3}$	$(2.2 \pm 2.0)10^{-2}$
^{229}Pa	$(5.1 \pm 2.2)10^{-3}$	$(2.9 \pm 1.6)10^{-2}$	$(4.6 \pm 1.8)10^{-2}$
^{230}Pa	$(1.2 \pm 0.8)10^{-2}$	$(3.7 \pm 0.6)10^{-2}$	$(8.1 \pm 0.9)10^{-2}$
^{232}Pa	$(1.08 \pm 0.12)10^{-1}$	$(3.7 \pm 0.5)10^{-1}$	$(8.1 \pm 0.9)10^{-1}$
^{233}Pa	(1.29 ± 0.09)	(2.8 ± 0.1)	(2.6 ± 0.1)
^{234g}Pa	$(1.98 \pm 0.22)10^{-2}$	$(1.1 \pm 0.1)10^{-2}$	$(4.2 \pm 0.6)10^{-2}$
^{231}U		$(2.2 \pm 1.6)10^{-2}$	$(3.8 \pm 2.0)10^{-2}$
^{237}U	$(1.0 \pm 0.7)10^{-2}$	$(1.7 \pm 1.5)10^{-3}$	$(7.3 \pm 5.8)10^{-4}$
^{239}U	$(1.0 \pm 0.8)10^{-2}$		
^{240}U	$(3.1 \pm 2.7)10^{-3}$		
^{232}Np			$(2.7 \pm 2.3)10^{-3}$
^{233}Np		$(5.0 \pm 4.6)10^{-3}$	$(1.1 \pm 0.9)10^{-2}$
^{234}Np	$(9.3 \pm 7.3)10^{-4}$	$(3.2 \pm 0.2)10^{-2}$	$(4.2 \pm 0.2)10^{-2}$
^{236m}Np	$(9.2 \pm 4.7)10^{-3}$	$(3.7 \pm 2.2)10^{-2}$	$(3.1 \pm 2.0)10^{-2}$
^{238}Np	$(1.04 \pm 0.16)10^{-2}$	$(1.9 \pm 1.5)10^{-4}$	$(3.6 \pm 3.0)10^{-4}$
^{239}Np	$(1.6 \pm 1.3)10^{-3}$		

Footnote and References

*University of Tokyo, Nuclear Engineering Research Laboratory, The Faculty of Engineering, Tokai-Mura, Naka-Gun, Ibaraki-Prefecture, Japan.

1. D. Lee, H.R. von Gunten, B. Jacak, M. Nurmia, Y.-F. Liu, C. Luo, G.T. Seaborg and D.C. Hoffman, Phys. Rev. **C25**, 286 (1982).
2. D. Lee, K.J. Moody, M.J. Nurmia, G.T. Seaborg, H.R. von Gunten and D.C. Hoffman, Phys. Rev. **C27**, 2656 (1983).
3. M. Schädel, R.W. Lougheed, J.H. Landrum, J.F. Wild, R.J. Dougan, A.D. Hoover, E.K. Hulet, G.R. Bethune, A. Ghiorso, M.J. Nurmia, L.P. Somerville, K.J. Moody, and G.T. Seaborg, Annual Report of the Nuclear Chemistry Division, Lawrence Livermore National Laboratory (1982), p. 100.

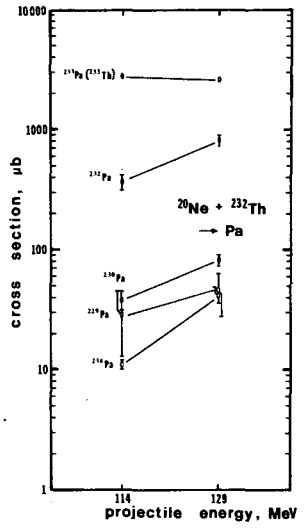

Fig. 2. Excitation functions for the protactinium isotopes produced in the bombardment of ^{232}Th with ^{20}Ne. XBL 839-11843

Relativistic Nuclear Collisions

Heavy Target Fragmentation and the Energy Dependence of Nucleus-Nucleus Total Reaction Cross Sections*

W. Loveland,† C.P. Oertel,† D.J. Morrissey, P.L. McGaughey, G.T. Seaborg, and K. Aleklett‡

Over the past several years, we have been pointing out that the integrated isobaric yields from target fragment mass distributions are lower limits on the total reaction cross section, σ_R, and can be used to study the variation of σ_R with projectile energy in nucleus-nucleus collisions. During the past year, we have reanalyzed some of our previous measurements of Au and Ta target fragment mass distributions to yield more accurate estimates of σ_R, and we have finished the analysis of the target fragment mass distribution in the interaction of 3 GeV ^{12}C with ^{181}Ta. We have used these analyses as well as others as the basis for a study of the energy variation of σ_R with projectile energy.

To integrate the isobaric yields in a target fragment mass distribution to give a lower limit for the total reaction cross section, $\sigma_R^<$, certain assumptions must be made. First, we assume that with the exception of fission fragments, the multiplicity of all fragments with $A \geqslant 60$ is unity. (We can correct for the effects of fission [multiplicity = 2] using published values of the fission cross section or by assuming that all fragments contributing to any central "bump" in the mass yield curve, especially at low and intermediate projectile energies, are fission fragments.) For fragments with $A > A_{tgt}/2$, this assumption of unit multiplicity for non-fission fragments is obviously valid. The yields of such fragments typically amount to ~75% of the geometrical reaction cross section. For fragments with $60 \leqslant A \leqslant A_{tgt}/2$ it is numerically possible to have fragment multiplicities of 2 or more. However, studies[1] of such processes in the reaction of 11.5 GeV protons with ^{238}U have shown that these binary reactions are rare. We do not choose to integrate the yields below A = 60 because the work of Warwick *et al.*[2] showed large multiplicities of A = 20 – 40 fragments in relativistic nuclear collisions.

In Fig. 1 we show the results of all reactions involving Au and Ta nuclei that we have studied. We also show appropriately scaled results derived from the isobaric yield data of Kaufman *et al.*[3] for the reaction of 4.8 GeV ^{12}C + ^{197}Au. In this radiochemical work, a somewhat different approach to integrating the measured nuclidic cross sections to give isobaric yields was taken. It is gratifying to note the agreement between our data and that of Kaufman *et al.* We also show (after appropriate conversion) the data of Buenerd *et al.*,[4] Grabez *et al.*[5] and Videbaek *et al.*[6]

Certain features of Fig. 1 deserve further comment. At a projectile energy (lab) of 86 MeV/nucleon, the results of three measurements are shown. They are the lower limit on σ_R as measured using track detectors by Grabez et al.[5], the lower limit on σ_R deduced from radiochemical data (this work) and the true value of σ_R as deduced by optical model analysis of elastic scattering.[4] What is interesting is that the two "lower limits" are greater than the "true value," and similar to data at other energies. At a projectile energy of 2.1 GeV/nucleon, there is some disagreement between the two radiochemical measurements although both measurements lie within two standard deviations of the mean of the two measurements. The data are consistent with an invariant value of $\sigma_R^<$ from 15 – 2100 MeV/nucleon but are better described by a dip in $\sigma_R^<$ in the region of 100 – 400 MeV/nucleon. (A Student's t-test would indicate that the mean of the data points at 235, 360 and 377 MeV/nucleon is statistically significantly different (5% rejection level) from the mean of the other data points from 17 –

2100 MeV/nucleon.

It is interesting to compare the observed energy dependence of $\sigma_R^<$ with theoretical expectations for σ_R. In Fig. 1 we show the energy dependence of the true ^{20}Ne + ^{181}Ta total reaction cross section as predicted by the microscopic theory of DeVries and Peng.[7] These microscopic calculations, based on Glauber theory, predict that the transparency in nucleus-nucleus collisions is due to a large impact parameter "translucent" region, corresponding to interactions involving the surface regions of the colliding nuclei. With a heavy nucleus such as Ta, most collisions involve the central densities of projectile and target. Thus, transparency effects are predicted to be small. Indeed, the calculations predict a generally invariant value of σ_R from 20 – 2100 MeV/nucleon with a very small dip in σ_R near 100 – 400 MeV/nucleon.

We also show in Fig. 1 the values of σ_R predicted by a high energy double folding optical potential approximation by Townsend *et al.*[8] who consider it more accurate than the DeVries and Peng calculation. The predicted values of σ_R are considerably fewer than those of DeVries and Peng and show a decrease in σ_R from 50 – 500 MeV/nucleon. The significance of the agreement between the predictions of ref. 8 and the magnitude of $\sigma_R^<$ is difficult to assess. Normally one would expect $\sigma_R^<$ to be somewhat less than σ_R and the agreement between the predicted value of σ_R and the measured value of $\sigma_R^<$ would indicate a problem. However, the situation is clouded by the agreement between two measurements of $\sigma_R^<$ at 86 MeV/nucleon and the measurement of σ_R by Buenerd *et al.*

Footnotes and References

*Condensed from LBL-16931

†Oregon State University, Corvallis, OR 97331

‡Studsvik Science Research Laboratory, S-611 82 Nyköping, Sweden

1. B.D. Wilkins, S.B. Kaufman, E.P. Steinberg, J.A. Urbon and D.J. Henderson, Phys. Rev. Lett. **43**, 1080 (1979).
2. A.I. Warwick, H.H. Wieman, H.H. Gutbrod, M.R. Maier, J. Peter, H.G. Ritter, H. Stelzer, F. Weik, M. Freedman, D.J. Henderson, S.B. Kaufman, E.P. Steinberg and B.D. Wilkins, Phys. Rev. **C27**, 1083 (1983).
3. S.B. Kaufman, E.P. Steinberg, B.D. Wilkins and D.J. Henderson, Phys. Rev. **C22**, 1897 (1980).
4. M. Buenerd, J. Pinston, J. Cole, C. Guet, D. Lebrun, J.M. Loiseaux, P. Martin, E. Monnand, J. Mougey, H. Nifenecker, R. Ost, P. Perrin, Ch. Ristori, P. De Saintignon, F. Schussler, L. Carlén, H.Å. Gustaffson, B. Jakobsson, T. Johansson, G. Jönsson, J. Krumlinde, I. Otterlund, H. Ryde, B. Schroder, G. Tibell, J.B. Bondorf and O.B. Nielsen, Phys. Lett. **102B**, 242 (1981).
5. B. Grabez, R. Beckman, P. Vater and R. Brandt, Nucl. Instr. Meth. (to be published).
6. F. Videbaek, R.B. Goldstein, L. Grodzins, S.G. Steadman, T.A. Belote and J.D. Garrett, Phys. Rev. **C15**, 954 (1977).
7. R.M. DeVries and J.C. Peng, Phys. Rev. **C22**, 1055 (1980).
8. L.W. Townsend, J.W. Wilson and H.B. Bidasaria, Can. J. Phys. **60**, 1514 (1982); see also NASA Technical Paper **2138**, April, 1983.

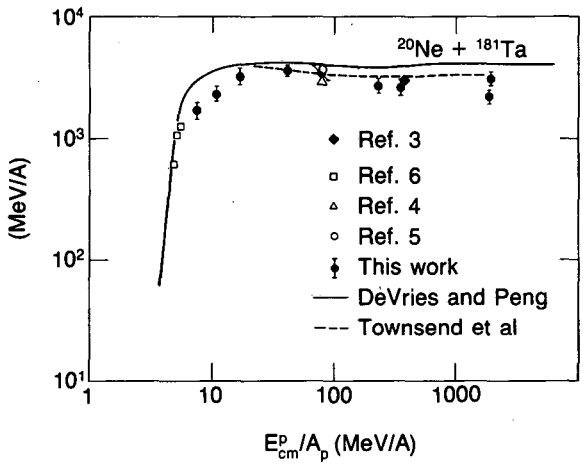

Fig. 1. The variation of the deduced lower limits of the total reaction cross section, $\sigma_R^<$, as a function of the projectile energy. Also shown are other measurements of σ_R and two optical model calculations of σ_R. XBL 836-953A

The ^{139}La + ^{139}La Reaction at 245 MeV/nucleon*

Li Wenxin,[†] *W. Loveland,*[‡] *K. Aleklett,*[§] *and G.T. Seaborg*

The target fragment isobaric yield distribution was measured for the reaction of ^{139}La + ^{139}La at a projectile energy of 245 MeV/nucleon using the Bevalac. A La metal target of thickness 402 mg/cm^2 was irradiated with a ^{139}La beam for ~2 days with a total particle fluence of 5.7 x 10^{11} ions. (The irradiation was the experiment of Schroeder *et al.* who generously gave us their target at the conclusion of the experiment). Following irradiation the target was cut in half, with one half being analyzed by direct γ-ray spectroscopy, while the other half was separated into 4 chemical fractions prior to counting. The chemical yields were determined by normalization to the unseparated foil yields.

Seventy-four different target fragment yields were measured and, using techniques described previously,[1] the target fragment isobaric yield distribution was deduced from these data. This distribution (shown in Fig. 1) exhibits two features not previously observed in rare earth target fragment mass distributions. First, the large bump in the distribution (centered at A ~60) presumably is due to fission of a La-like species. The cross section associated with this bump is ~450 mb, which is quite large compared to observations made of p-La collisions[2] at similar energies (where $\sigma_f \lesssim 1$ mb). The second unusual feature of the distribution is the magnitude of the total integrated residues cross section which is ~3.3 b, i.e., about 60% of the total reaction cross section as calculated by the soft-spheres model[3]. In all of our previous experience[4], the measured total integrated residue cross section is ~85-90% of the soft spheres estimate of the total reaction cross section.

In an attempt to understand the physics of this reaction, we have used the nuclear firestreak model to predict the fragment mass distribution for this reaction. The version of this model used to predict the primary target fragment distributions has been described previously.[5] Deexcitation of the primary fragments was calculated using our version[5] of the DFF code with liquid drop model fission barriers for the rare earth nuclei. If we assume a_f/a_n is 1.05, which is appropriate for the interaction of relativistic heavy ions with other rare earth nuclei or for p-La collisions, the model fails to predict any significant fission cross section and generally fails to reproduce the general character of the mass distribution (see Fig. 1).

Thus, we conclude that two unexpected features occur in the ^{139}La + ^{139}La reaction at 245 MeV/nucleon. They are: (a) an enhanced fissionability of the La-like fragment and (b) a significant fraction of the events (~40%) leading to either a total nuclear disintegration with no target fragments of A>40 being produced or an inelastic scattering with little energy deposit in the target-like-fragment.

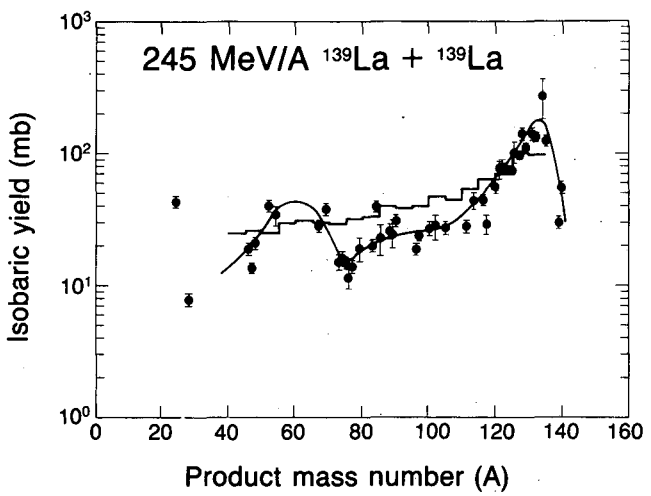

Fig. 1. Target fragment isobaric yields vs. fragment mass number A for the interaction of 245 MeV/nucleon ^{139}La with ^{139}La. The solid curve is to guide the eye through the data while the histogram shows the target fragment yield distribution as predicted by the nuclear firestreak model.

XBL 8311-668

Footnotes and References

*Condensed from LBL-17328
†Institute of Modern Physics, Lanzhou, People's Republic of China
‡Oregon State University, Corvallis, OR 97331
§Studsvik Science Research Laboratory, S-611 82 Nyköping, Sweden

1. D.J. Morrissey, W. Loveland, M. de Saint-Simon, and G.T. Seaborg, Phys. Rev. **C23**, 1044 (1981).
2. G. Anderson *et al.*, Z. Phys. **A293**, 241 (1979).
3. P.J. Karol, Phys. Rev. **C11**, 1203 (1975).
4. W. Loveland, C.P. Oertel, D.J. Morrissey, P.L. McGaughey, G.T. Seaborg and K. Aleklett, Phys. Rev. C (submitted for publication).
5. P.L. McGaughey, LBL-15325, November, 1982.

Au Target Fragmentation in Intermediate Energy Heavy Ion Reactions*

W. Loveland,† K. Aleklett,‡ P.L. McGaughey, K.J. Moody, R.M. McFarland, R.H. Kraus, Jr., and G.T. Seaborg*

In recent years, we have been engaged in a set of general survey measurements of target fragmentation in intermediate energy heavy ion reactions. In previous Annual Reports, we have discussed the kinematic properties of the target fragments from the reaction of 12 – 84 MeV/nucleon heavy ions with ^{197}Au. During the past year, we have completed our analysis of the target fragment yields from these reactions. In Fig. 1 we show the isobaric yield distributions for the systems studied in this survey.

In attempting to do more than qualitatively comment on the changes in the shapes of the yield distributions, one is faced with the lack of quantitative theoretical predictions about the character of these distributions in this projectile energy region. This is in sharp contrast with the situation at projectile energies of 250 MeV/nucleon or more, where two distinctly different models do a reasonable job of quantitatively describing the shapes of the distribution of products with $A>60$.[1,2] The two models in question, the intranuclear cascade model of Yariv and Fraenkel[3] and the nuclear fire streak model[4] contain assumptions that might be expected to be invalid at the lowest projectile energies studied in this work. Nonetheless, because projectile fragmentation data suggest that the two highest energies in this study might be characterized as "high energy" behavior, we thought it might be instructive to compare the predictions of these models with our data.

Upon comparing the predictions of the intranuclear cascade model of Yariv and Fraenkel with the data (Fig. 1), one observes that the model significantly underestimates the magnitude of the fission and deep spallation cross sections, apparently through an underestimation of the energy deposited by the projectile in the target nucleus. This discrepancy between the data and the calculations gets worse as the projectile energy decreases. Such results are not unexpected, since at the projectile energies in question the wavelength of the nucleons in the projectile is not negligible with respect to the internucleon spacing in the target. Thus, collective phenomena in which significant portions of the projectile are captured by the target are expected to become increasingly important as the projectile energy decreases, and these phenomena are not included in the intranuclear cascade model.

The comparison of the predictions of the nuclear firestreak model and the data (Fig. 1) is quite interesting. Perhaps because the firestreak model emphasizes the collective aspects of the reactions, it appears to do a better job than the cascade model in describing the data. It even appears to do a reasonable job of describing the 18.4 MeV/nucleon data.

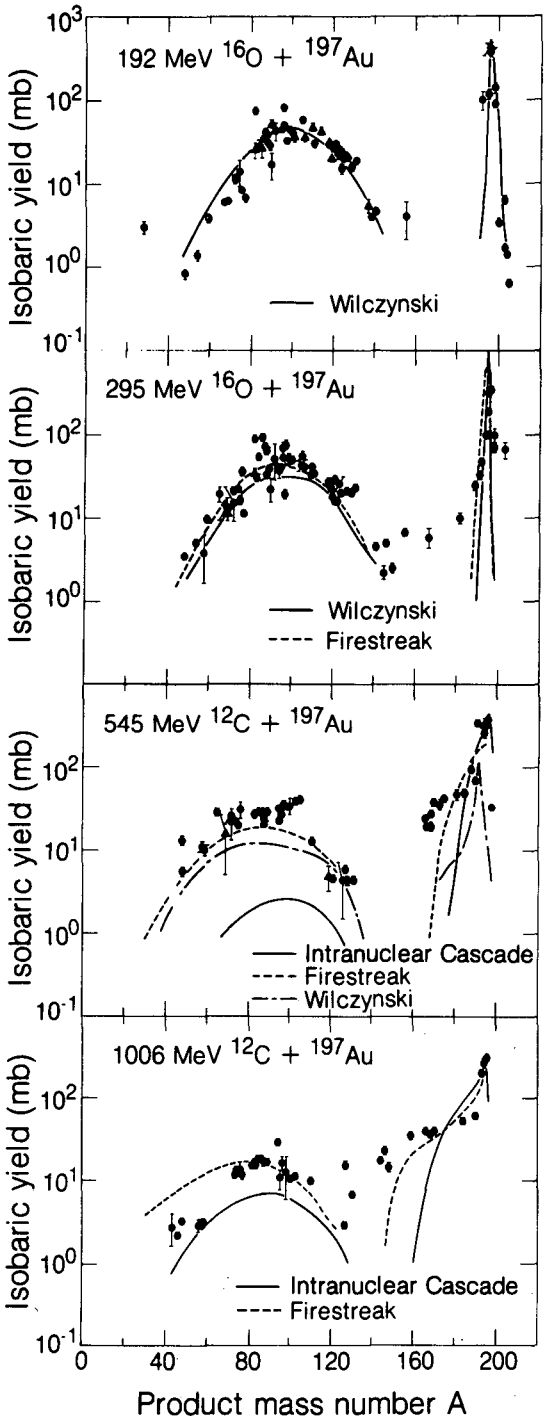

Fig. 1. The fragment isobaric yield distributions for the cases studied in this work along with the distributions predicted by various theoretical models of nucleus-nucleus collisions. XBL 839-11811

Neither the cascade nor the firestreak model predicts the production of fragments in the mass region between the fission fragments and the near-target species. Since both models (and the associated fragment deexcitation code) correctly predict the yields of these species in higher energy reactions, it would appear that the production of these fragments in intermediate energy heavy ion reactions is not fully understood.

To describe the fragment yields from a "low energy viewpoint," we use the generalized sum rule model of Wilczynski *et al.*[5] to calculate the cross sections for various complete and incomplete fusion reactions. The parameters of the calculation (T, Δ_p etc.) were the same as used by Wilczynski *et al.* The excitation energy of each of the many resulting products was assumed to be the "optimal" excitation energy as calculated using a semi-classical DWBA of Toepffer[6] as used by Hubert *et al.*[7] to calculate the yields of transfer products in low energy reactions. The deexcitation of each primary fragment was calculated using the same DFF code used in the cascade and firestreak calculations.[4] The agreement between the calculated and measured fragment yields (Fig. 1) for the reaction of 12.0 MeV/nucleon ^{16}O with ^{197}Au seems excellent. Satisfactory agreement between the calculations and the data is also seen at 18.4 MeV/nucleon projectile energy but when the projectile energy is raised to 45.4 MeV/nucleon there appears to be a significant difference between measured and calculated distributions. This discrepancy may be due to the fact that the only way in which the projectile energy enters into the model is the calculation of the projectile wavelength (i.e., there is no change in the character of the interaction with increasing projectile energy).

Thus it would seem that the nuclear firestreak model shows the most promise for understanding the general trends in the fragment mass distributions in the intermediate energy region.

Bertsch[8] and Bertsch and Siemens[9] have proposed that the light (A<60) fragments from these reactions could be produced in a nuclear phase transition caused by a mechanical instability of nuclear matter. One signature for the occurrence of this

process would be a lower threshold for the production of light fragments in nucleus-nucleus as compared to p-nucleus collisions. In Fig. 2 we show the available data on excitation functions for light fragment production in NN and pN collisions. The data are generally qualitatively consistent with the Bertsch-Siemens hypothesis although the data do not permit quantitative evaluation of these ideas.

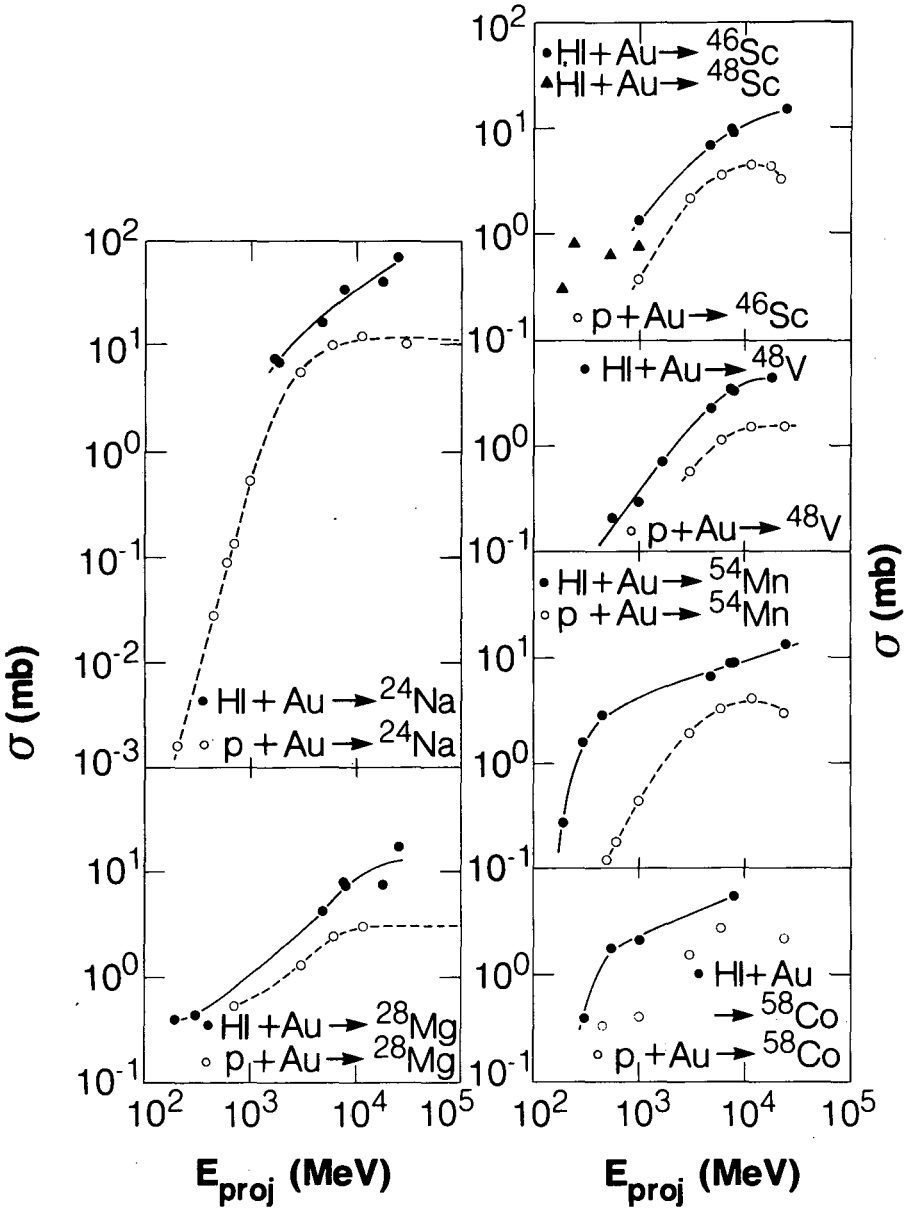

Fig.2. Excitation functions for production of various light fragments from proton-Au and nucleus-Au collisions.
XBL 8310-889

Footnotes and References

*Condensed from LBL-16280
†Oregon State University, Corvallis, OR 97331
‡Studsvik Science Research Laboratory, S-611 82 Nyköping, Sweden

1. D.J. Morrissey, W. Loveland, M. de Saint Simon, and G.T. Seaborg, Phys. Rev. **C21**, 1783 (1980).
2. P.L. McGaughey, LBL-15325, November, 1982.
3. Y. Yariv and Z. Fraenkel, Phys. Rev. **C20**, 2227 (1979).
4. W.D. Myers, Nucl. Phys. **A296**, 177 (1978); see also ref. 2 where the implementation of this model for the calculation of target fragment distributions is described.
5. J. Wilczynski, K. Siwek-Wilczynska, J. van Driel, S. Gonggrijp, D.C.J.M. Hageman, R.V.F. Janssens, J. Lukasiak, and R.H. Siemssen, Phys. Rev. Lett. **45**, 606 (1980).
6. C.Toepffer, Z Physik **253**, 78 (1972).
7. F. Hubert, H. Delagrange, and A. Fleury, Nucl. Phys. **A228**, 415 (1974).
8. G.F. Bertsch, Nucl. Phys. **A400**, 221c (1983).
9. G. Bertsch and P.J. Siemens, Phys. Lett. **B126**, 9 (1983).

Target Fragment Angular Distributions for the Interaction of 86 MeV/nucleon ^{12}C with ^{197}Au

R.H. Kraus, Jr., W. Loveland,* K. Aleklett,† P.L. McGaughey, T.T. Sugihara,* G.T. Seaborg, T. Lund,‡ Y. Morita, E. Hagebø,§ and I.R. Haldorsen§*

Target fragment angular distributions were measured using radiochemical techniques for 69 different fragments ($44 \lesssim A \lesssim 196$) from the interaction of 86 MeV/nucleon ^{12}C with ^{197}Au. The angular distributions in the laboratory system are forward-peaked with some distributions also showing a backward peak (Fig. 1). The shapes of the laboratory system distributions were compared with the predictions of the nuclear firestreak model[1,2] (the histograms in Fig. 1). The measured angular distributions differ markedly from the predictions of the firestreak model in most cases. This discrepancy could be due to overestimation of the transferred longitudinal momentum by the firestreak model, the assumption of isotropic angular distributions for fission and particle emission in the moving frame, and incorrect assumptions about how the lightest fragments ($A<60$) are produced. Recent hydrodynamical model calculations[3] would seem to indicate that ~20% of the total reaction cross section for this reaction should involve events in which the target fragments move sidewise to the beam. No evidence is seen for this phenomenon.

The laboratory frame angular distributions were transformed into the frame of the moving target nucleus after the primary reaction had taken place (and prior to fission or particle emission) using three different assumptions about $\eta_{\parallel}$, the ratio of the moving frame velocity to that recoil velocity given the system by fission or particle emission (Fig. 2). The three assumptions about $\eta_{\parallel}$ were: (a) $\eta_{\parallel}$ as given by the thick target–thick catcher recoil studies; (b) $\eta_{\parallel}$ as given by thin target studies; (c) the value of $\eta_{\parallel}$ needed to symmetrize the moving frame angular distribution about 90°. The resulting light fragment distributions showed an asymmetry in the moving frame indicative of their production in a fast process without the establishment of statistical equilibrium. Some years ago Moretto[4] suggested a mechanism for the production of these fragments by very asymmetric fission. Recently evidence has been presented[5] showing this mechanism to be operative

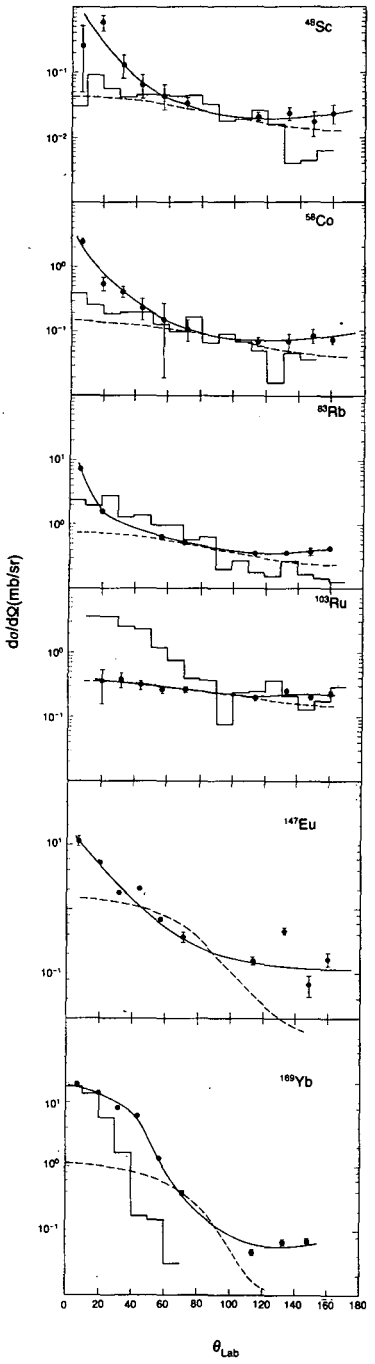

Fig 1. Measured target fragment angular distributions from the interaction of 86 MeV/nucleon ^{12}C with ^{197}Au. The solid lines are to guide the eye through the data, the histograms represent predictions of the nuclear firestreak model, while the dashed lines represent the two-step model predictions with b/a = 0 and $\eta_{\parallel}$ taken from ref. 7.

XBL 8311-671

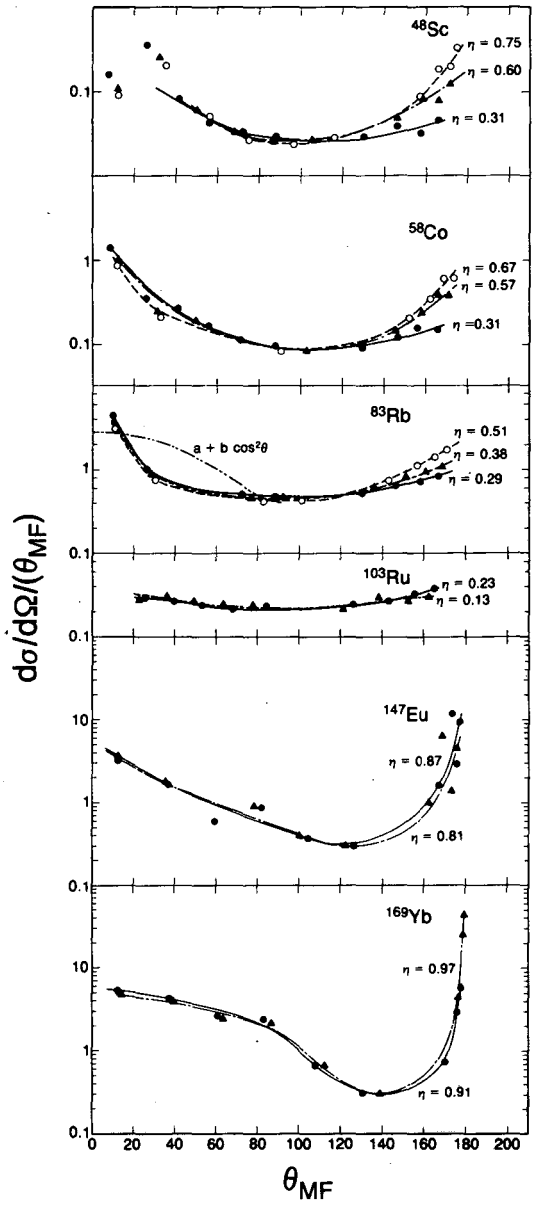

Fig 2. Angular distributions of V, the kick given the primary target fragment by fission or particle emission, in the moving frame for fragments shown in Fig. 1. The solid points (solid line) result from using thick target recoil data for $\eta_{\parallel}$, solid triangles represent $\eta_{\parallel}$ from thin target data, while the open circles (dashed line) are a "best fit" to the data. For ^{95}Zr and ^{103}Ru, the thin target data are the best fit. For ^{147}Eu and ^{169}Yb there are no "best fit" curves since no choice of $\eta_{\parallel}$ seemed to symmetrize the distributions.

XBL 8311-672

in the reaction of 90 MeV ^{3}He with Ag. The above observation about the light fragment distributions along with the fact that neither $\frac{d\sigma}{d\omega}(7°)/\frac{d\sigma}{d\omega}(114°)$ nor $\frac{d\sigma}{d\omega}(160°)/\frac{d\sigma}{d\omega}(114°)$ increased with increasing fragment mass number suggest that this mechanism is not a dominant one in this reaction. The fission fragment angular distributions in the moving frame were compared to standard formulas for such distributions[6] and a crude "ball-park" estimate of the "average" fissioning system angular momentum of $J = 40 - 50\hbar$ was obtained. It was not possible to find a moving frame in which the heavy fragment distributions were symmetric about 90°.

Footnotes and References

*Oregon State University, Corvallis, OR 97331
†Studsvik Science Research Laboratory, S-611 82 Nyköping, Sweden
‡Philipps Universität, D-3550 Marburg, Federal Republic of Germany
§University of Oslo, Blindern, N-Oslo 3, Norway

1. W.D. Myers, Nucl. Phys. **A296**, 177 (1978).
2. P.L. McGaughey, LBL-15325, November, 1982.
3. G.Buchwald, G. Graebner, J. Theis, J.A. Maruhn, W. Greiner and H. Stöcker, Phys. Rev. **C28**, 1119 (1983).
4. L.G. Moretto, Nucl. Phys. **A247**, 211 (1975).
5. L.G. Sobotka, M.L. Padgett, G.J. Wozniak, G. Guarino, A.J. Pacheco, L.G. Moretto, Y. Chan, R.G. Stokstad, I. Tserruya and S. Wald, LBL-15696, July, 1983.
6. J.R. Huizenga, A.N. Behkami and L.G. Moretto, Phys. Rev. **177**, 1826 (1969).
7. W. Loveland, K. Aleklett, P.L. McGaughey, K.J. Moody, R.M. McFarland, R.H. Kraus, Jr., and G.T. Seaborg, Phys. Rev. C (submitted for publication).

First Results from a Repeat Experiment on the Mean Free Path of Projectile Fragments from 1.88 GeV/nucleon ^{56}Fe – Emulsion Interactions*

Y.J. Karant, H.H. Heckman, and E.M. Friedlander

In this experiment we used three different stacks denoted symbolically by *2 Fe*, *Long Fe*, and *3 Fe*; each stack was made of 600 μm thick pellicles of Ilford G-5 research emulsion. The number of pellicles and dimensions of these stacks are, respectively, 42 pellicles of size 7.5 × 12 cm^2, 63 pellicles of size 10 × 23 cm^2, and 50 pellicles of size 7.5 × 25.5 cm^2, where the dimensions have been rounded to the nearest 0.5 cm. In all cases the primary particles entered the stacks normal to one end and parallel to the long dimension. Stack *2 Fe* was the stack used for our previous investigation. We have done further scanning in stack *2 Fe*, as well as in stacks *Long Fe* and *3 Fe*. The mean free paths (MFPs) of projectile fragments (PFs) of charge $\geqslant 3$ are reported from stack *3 Fe* only, while He PFs are reported from all three stacks.

The reason for this charge selection is that for stack *3 Fe* we had calibration beams of C and Ar present in the same emulsion batch, exposed at essentially the same time, and processed with the emulsion that we used for track following. Hence, we can verify with known charges our charge measurement methods that depend on delta-ray parameters of the track structure over a wide range of charge. By comparison, our published results for the *2 Fe* stack were dependent on the known primary Fe tracks and one very good candidate for the track of an 0 PF, where the 0 was identified by its alternative method using lacunarity, which can be internally self

calibrated; however, since we have not yet calibrated charges from Li to B in stack *Long Fe*, nor have we charge measured our new data in stack *2 Fe*, we only analyzed He PFs from these stacks. Direct measurements under several conditions have shown that visual identification of He PFs is better than 99% reliable.

The simplest first step to compare the two experiments is to change the actual stack length in all cases to that of stack *2 Fe*, i.e., 12 cm; this can be accomplished easily in the data analysis programs by ignoring all tracks that have a starting coordinate beyond 12 cm and by terminating all other tracks at 12 cm, so that interactions beyond 12 cm are ignored. This is what we have actually done. Under this cut, we have a total of 754 PF interactions to use, as compared to the 730 that we previously had from Fe-initiated processes.

While there are many ways to examine the MFP data for the presence of an anomalously short component, one of the most direct is to plot the MFP parameter Λ^* as a function of the distance after emission of the PF and thereby determine if the data agree with our previous observations. In this analysis we assume the same scaling law for the MFP as a function of charge that we used in the previous analysis of the LBL data:

$$\lambda(Z) = \Lambda Z^{-b}$$

where we assign $\Lambda = 32$ cm and $b = 0.43$.

A basic quantity to plot is the ratio R of the measured Λ^* to its expectation Λ; this permits experiments with different scanning efficiencies, interaction definitions, or other systematic differences to be compared. To compute Λ^* one sums all the measured path length $S_N(Z)$ of particles of charge Z, multiplies it by Z^b, adds this to the charge weighted path length of the other charges, and divides the whole by the number N of interactions observed, i.e.,

$$\Lambda^* = \frac{\sum_Z S_N(Z) Z^b}{\sum_Z N(Z)} .$$

Unlike our previous experiment, a systematic scan was also done on all He PFs from extranuclear cascades initiated by Fe primaries. To keep consistency with the 12 cm stack cut used for PFs of charge $\geqslant 3$, we present in Fig. 1 our first results for He PFs under the same cut. Under this cut, we have 1161 He PF interactions. We compute the observed MFP λ^* unscaled by any charge weight factor, i.e.,

$$\lambda^* = \frac{S_N}{N}$$

where S_N is the total path length within the bin of both interacting and noninteracting He PF tracks, and N is the number of observed interactions within the bin. We have already measured the MFP at 2 GeV/nucleon of primary ^{4}He and primary ^{3}He, the only isotopes expected to have any reasonable population in He PFs. We observed 1010 ^{4}He interactions with a MFP of 21.85 cm and 445 interactions of ^{3}He with a MFP of 19.50 cm. Based on PF cross sections, we expect 75% of the He PFs to be ^{4}He and 25% to be ^{3}He. Using this mix, we would expect a He MFP of 21.26 cm; to be on the conservative side,

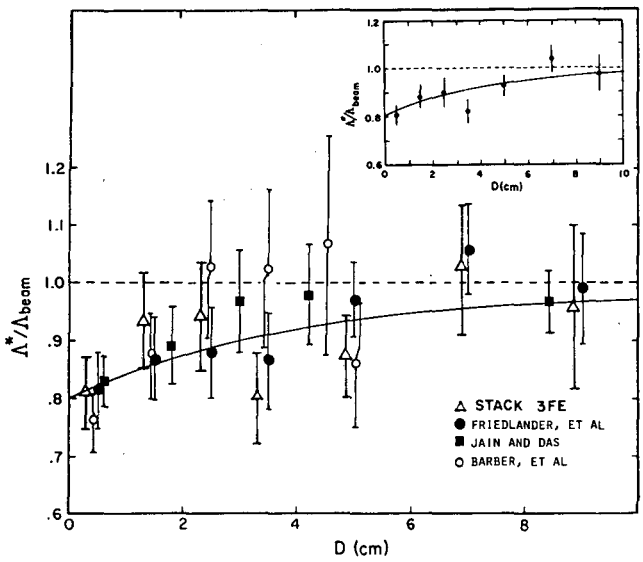

Fig. 1. The ratio of Λ^*/Λ is plotted as a function of distance after emission. The straight line at 1 represents the null hypothesis of a normal PF MFP, while the curve represents the hypothesis of 6% anomalons with a fixed MFP of 2.5 cm independent of PF charge. Insert: the points are the results of combining the data of ref. 1 with the data of this report, while the straight line and curve are the same as in the main figure. XBL 8312-2597

we take the expected value of the He PF MFP to be 21 cm. Even though there is a slight difference between the measured MFPs of the two He isotopes, over a 10 cm interval the MFP of the mix should stay essentially constant at its expectation value.

We plot in Fig. 2 the ratio R of our measured He PF MFP, λ^*, to its expectation value of 21 cm, against the distance D after emission of a He PF, along with a curve representing a 2.5% 2.5 cm component. As is evident by visual inspection, the data agree rather well with such a curve. By combining the first three distance bins, we observe a MFP of 18.9 cm with 513 interactions, which is 2.3 SD away from the expected value of 21 cm.

In conclusion, our new data on PFs in the charge interval from Li to Fe from 1.88 GeV/nucleon ^{56}Fe primaries agree with our previous results. In addition, we have made a systematic examination of the MFP of He PFs as a function of distance after emission and find that these too appear to have anomalons present. However, the inclusive effect in He PFs is weaker and will require further analysis and data for elucidation.

Footnote and Reference

*Based on paper presented at Sixth High Energy Heavy Ion Study and Second Workshop on Anomalons, LBL, June 28 – July 1, 1983.

1. E.M. Friedlander, *et al*, Phys. Rev. C **27**, 1489 (1983).

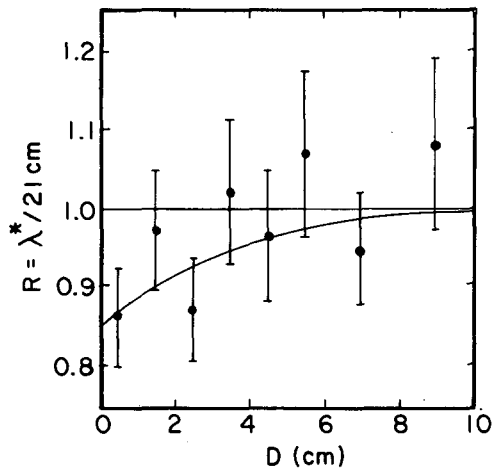

Fig. 2. A plot of the ratio of the observed He PF MFP from this experiment to its expectation value of 21 cm; the ratio is plotted against the distance after emission of the PFs; straight line, the expected dependence under the null hypothesis of normal PFs; curve, the expected dependence under the hypothesis that 2.5% of the He PFs are anomalons with a 2.5 cm MFP. XBL 8312-2596

Evidence Against "Anomalon" Production in High-Energy Heavy Ion Collisions*

J.D. Stevenson,† J.A. Musser and S.W. Barwick

Recent experiments[1-6] have claimed that a small fraction of projectile fragments in relativistic nucleus-nucleus collisions have properties very different from normal nuclei. Measurements of the mean free path of secondary projectile fragments measured in nuclear emulsion within a few centimeters of their point of formation were observed to be shorter than those of primary nuclei of the same charge. Measurements of the mean free path of secondary projectile fragments as a function of distance from their formation point indicated the existence of a small component of projectile fragments with anomalously short mean free paths.

We present here the result of an electronic experiment to measure projectile fragment mean free paths. The detector is a fifteen element telescope consisting of a trigger scintillator followed by fourteen Čerenkov detectors ranging in thickness from 3.5 mm to 1.27 cm. The detectors were in the following order: a trigger scintillator (0.65 cm thick), 6

Čerenkov counters (each 0.35 cm thick), 5 Čerenkov counters (0.65 cm each), 2 Čerenkov counters (1.27 cm each), and a final Čerenkov counter (0.65 cm). Each paddle was connected by a lucite light guide to a 3″ diameter (RCA 4900) photomultiplier tube. The paddles were placed with their faces in contact so as to form a solid segmented stack. The Čerenkov counters were made of Nuclear Enterprise Pilot 425 (lucite with a waveshifter additive), which has a threshold energy of E_{thresh} = 310 MeV/nucleon.

Interactions can be seen clearly in the sample event shown in Fig. 1. The first interaction occurs near the boundary between detectors two and three and is a loss of four charge units. The second interaction is in detector number twelve. In order to study interactions of secondaries at long distances it is necessary to form the secondary near the front of the detector. We did this by using the third detector element as an inelastic trigger, requiring that its signal correspond to a fragment with charge Z within the range $9 \leqslant Z \leqslant 17.5$. The lower level on the trigger was used to eliminate secondaries with charge too low to analyze reliably.

Interactions were found by fitting the 15 signals for each event with successively higher numbers of interactions until a good fit was achieved. Signals from detectors in which interactions were assumed to occur were excluded from the fit and signals between interactions were fit with their average value.

In order to fully utilize the statistics of this experiment it was necessary to merge results from several secondary charges with different mean free paths. The procedure used to do this was to divide the individual mean free paths $\lambda(x,Z)$ by their average value $\lambda_{AV}(Z)$ for each charge. The quantity $\lambda(x,Z)/\lambda_{AV}(Z)$ can then be averaged over several charges. Fig. 2 shows the result of this procedure for secondary charges Z in the interval $13 \leqslant Z \leqslant 17$. The data points are fit reasonably well by the straight line, no anomalon hypothesis, (χ^2 = 9.87, for 9 degrees of freedom). An anomalon abundance of 2% or more can be ruled out if they have interaction lengths between 0.4 and 3 cm. The previous results with the plastic track detector CR-39 should be directly comparable to our lucite result. The CR-39 result of Tincknell *et al.*[5] is clearly outside our limits. The smaller anomalon abundance (1.2%) claim of Heinrich *et al.*[4] is a bad fit to our data (85% CL) but cannot be definitively ruled out. A comparison to emulsion experiments is obviously difficult. This experiment easily rules out anomalons being produced in lucite with the same abundance and mean free path reported in emulsion.

One possible problem with previous results[4,5] is that they depend on calculations of the mean free path of primary nuclei. We have compared measured primary mean free paths of ^{20}Ne and ^{40}Ar(λ_{Ne} = 12.9 ± 0.2 cm, λ_{Ar} = 9.6 ± 0.15 cm) with calculations (λ_{Ne} = 14.39 cm, λ_{Ar} = 9.94 cm) based on the procedure used in ref. 5. The measured mean free paths are systematically shorter (11% for ^{20}Ne) than the calculated values. Reducing the calculated mean free paths in previous results[4,5] would reduce the statistical significance of their conclusions.

Footnotes and References

*Condensed from a paper submitted to Phys. Rev. Letters.

†Also at Space Sciences Laboratory

1. E.M. Friedlander, G.W. Gimpel, H.H. Heckman, Y.J. Karant, B. Judek and E. Ganssauge, Phys. Rev. Lett. **45**, 1084 (1980).
2. P.L. Jain and G. Das, Phys. Rev. Lett. **48**, 305 (1982).
3. H.B. Barber, P.S. Freier and C.J. Waddington, Phys. Rev. Lett. **48**, 856 (1982).
4. W. Heinrich, H. Drechsel, W. Trakowski, J. Beer, C. Brechtmann, C. Dreute, R. Rudat, S. Sonntag, E.V. Benton, R.M. Cassou, R.P. Henke, Univ. of Siegen Preprint SI-83-11 (1983); *Proc. Intl. Conf. on Nucleus-Nucleus Collisions*, Michigan State Univ., Sept. 27–30, 1982; Sixth High Energy Heavy Ion Study, LBL Berkeley, June 28–July 1, 1983.
5. M.L. Tincknell, P.B. Price, and S. Perlmutter Phys. Rev. Lett. **51**, 1948 (1983).

6. E.M. Friedlander, R.W. Gimpel, H.H. Heckman, Y.J. Karant, B. Judek and E. Ganssauge, Phys. Rev. C 27, 1489 (1983).

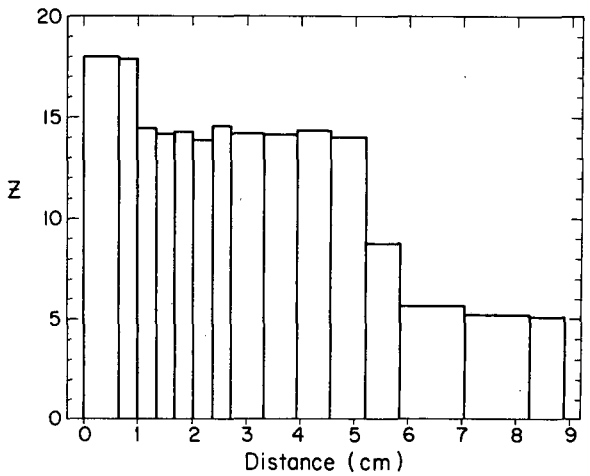

Fig. 1. A bar plot of signals from a sample event. The bar width is the detector thickness and the bar height is the signal in charge units. Two interactions can be identified by the abrupt change in signal.

XBL 8312-4304

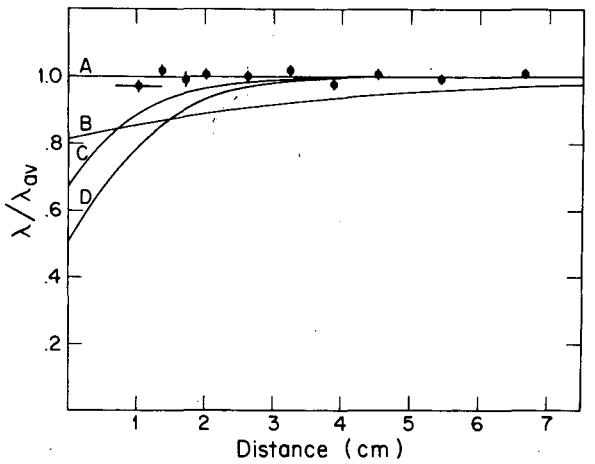

Fig. 2. A plot of the projectile fragment mean free path as a function of distance from the fragments' formation point. The individual values have been divided by their average in order to combine data from several secondary charges (see text). The calculated curves are A – no anomalons; b – 3% anomalons, λ_{anom} = 7 mm; C – 6% anomalons, λ_{anom} = 7 mm; and D – 6% anomalons, λ_{anom} = 2.5 cm.

XBL 8312-4306

Observation of Anomalons in CR-39 Track Detectors

*M.L. Tincknell and P.B. Price**

We have observed fragments of 1.85 GeV/nucleon ^{40}Ar in CR-39 etched track detector, and we find anomalously short mean free paths (mfp's) of secondary nuclei with $11 \leqslant Z \leqslant 17$ in the first 2 cm after their production, at ~3 standard deviations.[1] This confirms previous reports of this "anomalon" effect in nuclear emulsion in a new detector with dissimilar potential systematic errors.

We exposed a stack of 0.064 cm thick sheets of CR-39 to an Ar beam from the Bevalac. After the sheets were etched, tracks from the Ar and its fragments appeared as conical pits of ~35 μm diameter. The track diameters are a simple monotonic function of (Z/β), and since changes in β due to ionization and nuclear collisions are negligibly small, we were able to identify the nuclear charges with resolution ~0.25e by measurement of a single diameter. Only charges $Z \geqslant 10$ record tracks in CR-39 (DOP), and we can sample these charges only every ~ 600 μm along the path of the particle.

We isolated the fragments of Ar interactions near the front of the stack by superimposing and aligning pairs of the transparent CR-39 sheets which were originally 5 sheets apart during the exposure. We scanned at the interface between these sheets for changes between the upstream and downstream diameters, indicating an Ar interaction in the 5 sheet interval. The observable fragments we found were propagated downstream in 1 cm jumps, and interactions of these secondaries were further localized to within 0.25 cm by a binary search of sheets in the 1 cm intervals.

We followed 1530 secondaries with $11 \leqslant Z \leqslant 17$, and we found 612 interactions of these secondaries within ~6 cm downstream of their primary interactions. While measuring, we referred to an upstream sheet beneath the sheet being measured to ensure that we were following the secondaries correctly. A sample of 246 events was completely remeasured, and only 5 disagreements were found.

The mfp of any charge species can be estimated over any distance interval by $\lambda = (\Sigma_i l_i)/n$ or by $\lambda = -D/\ln(1-n/N)$, where λ is the mfp, l_i are pathlengths of interacting and noninteracting particles, D is the width of the interval, n is the number of interactions, and N is the total flux. We find agreement between values calculated with a Bradt-Peters expression using parameters by Westfall *et al.*,[2] our measurements of primary Ne, Ar, and Fe, and the downstream λ values of our pooled secondaries with $11 \leqslant Z \leqslant 17$.

Using a charge-weighting derived from the empirical relation $\lambda = \Lambda Z^{-b}$, we define a parameter $\Lambda^* = (\Sigma_i l_i Z^{+b})/n$ which pools the various secondary charges into a single mfp statistic. The normalization value $\Lambda_{th} = 52.25$ cm, and the power b = 0.58 were calculated with a Bradt-Peters formula for Ar fragments in CR-39. We find a clear depression of ~15% in Λ^* in the first 2 cm after the primary interactions, as depicted in the figure. Dividing the data into 2 bins, from 0.18 to 2.14 cm, and 2.14 to 6.30 cm, we have respectively 284 and 328 secondary interactions, and Λ^* values of 44.36 ± 3.1 and 52.93 ± 2.9, giving a 2.7 S.D. difference. An F-test gives a probability of $<4 \times 10^{-2}$ for these observations under the null hypothesis of normal exponential interaction behavior, independent of calculated parameters.

We have divided the data into even and odd charges, and find no differences in the anomalous behavior, within statistics. We also divided the data into secondary interactions with large and small ΔZ, and find the anomaly only in the large ΔZ group. A least-squares fit to the data for a fraction of anomalons α, and an anomalous mfp λ_a, gives $\alpha = 0.036 \pm 0.015$, $\lambda_a = 1.0$ (+0.85, −0.50) cm. Comparison to the emulsion results can be used to test an "inflated nucleus" model of anomalon interactions. We find that anomalons do not interact as inflated nuclei with large geometrical cross sections, and that anomalous interactions with AgBr nuclei in emulsion are enhanced over those with HCO.

In conclusion, we confirm the observations of anomalously short mean free paths of secondary projectile fragments, first seen in nuclear emulsion, with CR-39 etched track detector. We intend to repeat these experiments with an Fe beam, and to attempt to distinguish the anomalon lifetime and interaction cross section in a separate stack with ~1 cm air gaps between the CR-39 sheets.

Footnote and Reference

*Also at Space Sciences Laboratory

1. M.L. Tincknell, P.B. Price, and S. Perlmutter, Phys. Rev. Lett. **51**, 1948 (1983).
2. G.D. Westfall, L.W. Wilson, P.J. Lindstrom, H.J. Crawford, D.E Greiner, and H.H. Heckman, Phys. Rev. **C19**, 1309 (1979).

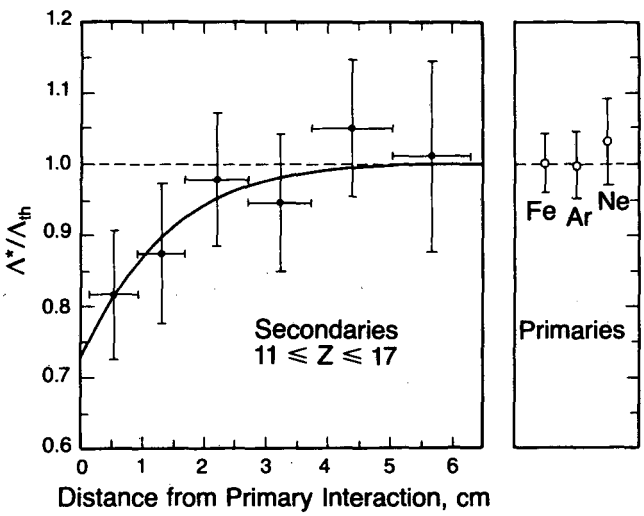

Fig. 1. Λ^* vs distance from primary interactions for secondaries with $11 \leqslant Z \leqslant 17$; and Λ^* for primary Ne, Ar, and Fe. Horizontal bars are bin widths and vertical bars are 1σ statistical error limits.

XBL 8312-4305

Search for Short-Lived Anomalons in Projectile Fragmentation*

H.A. Gustafsson, H.H. Gutbrod,† B. Kolb,† B. Ludewigt,‡ A. M. Poskanzer, T. Renner, H. Riedesel,§ H.G. Ritter,† A.I. Warwick,† and H.H. Wieman†

Nuclear emulsion studies[1,2] suggest that fragmentation products from relativistic heavy-ion collisions have anomalously large reaction cross sections and that these anomalons disappear over the first few centimeters of their track in emulsions. If these anomalons exist, their disappearance could be due either to depletion by a very large reaction cross section, or to decay with a mean lifetime of about 10^{-11} sec and with only somewhat enhanced cross section. We have conducted an experiment to test this decay model and the design of our counter experiment, shown in Fig. 1, was based on the published information from the above mentioned emulsion studies.

The experiment was performed at the Bevalac by bombarding alternately a solid (20 mm thick) and a dilute (ten 2-mm slabs each separated by 20 mm) Cu target with a beam of 1.7 GeV/nucleon ^{56}Fe ions. The produced projectile fragments were detected within a cone of $\pm 1°$ opening angle 5.5 m downstream in ΔE plastic scintillators. The existence of short-lived anomalons that decay within a few centimeters should, because of the greater number of interactions in the solid target before decay than in the dilute one, move yields from the upper part of the energy-loss spectrum to the lower part. This change in the shape of the measured ΔE spectra should, when the ratio is taken of the yields in the ΔE spectra for solid and dilute target, show up as a line with negative slope.

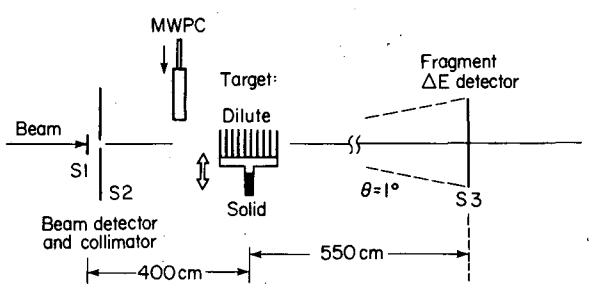

Fig. 1. Schematic view of the experimental layout, S1 and S2 being the beam-defining scintillators. The multiwire chamber MWPC was used for focusing the beam and then retracted. S3 represents the ΔE detectors. XBL 831-1137

To determine the sensitivity to the various proposed decay scenarios[2,3] a Monte Carlo simulation of the experiment was done. The experimental results as well as the results from the Monte Carlo simulations are shown in Fig. 2.

Our experiment rules out the proposed decay model[2,3] in which the disappearance of the anomalons' short mean free path is due to decay. Our data are consistent both with the nonexistence of anomalons and with the disappearance of the short-mean-free path effect due to reactions. If 100% of the projectile fragments are anomalons, then our data indicate that their mean lifetime must be at least 5×10^{-11} sec.

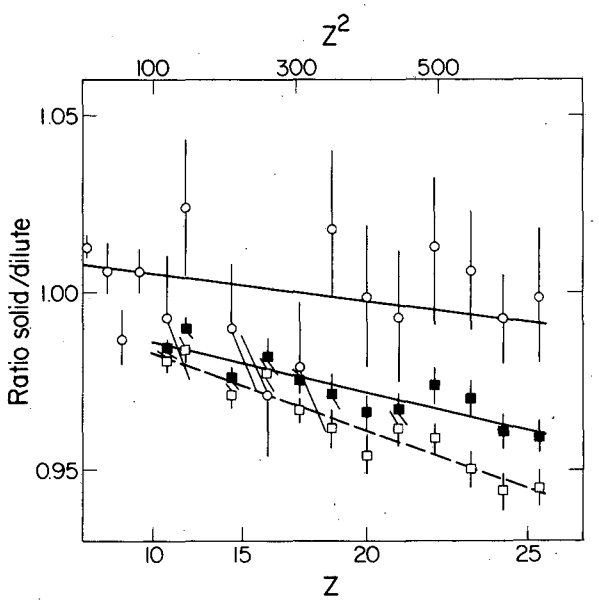

Fig. 2. The ratio of yields in the ΔE spectra produced by solid/dilute targets. Open circles show the data. Open and filled squares show the Monte Carlo simulations based on the parameters taken from refs. 2 and 3. XBL 833-1294

Footnotes and References

*Condensed from Phys. Rev. Lett. **51**, 363 (1983).
†Gesellschaft für Schwerionenforschung, Darmstadt, West Germany.
‡Universität Münster, Münster, West Germany.
§Present address: Max-Planck-Institut für Kernphysik, Heidelberg, West Germany.

1. E.M. Friedlander *et al.*, Phys. Rev. Lett. **45**, 1084 (1980).
2. H.B. Barber *et al.*, Phys. Rev. Lett. **48**, 856 (1982).
3. Y. Karant, private communication.

Radiochemical Search for Anomalons

G.Dersch, K. Aleklett,† R. Beckman,* R. Brandt,* E.M. Friedlander, W. Loveland,‡ T. Lund,* P.L. McGaughey, N.T. Porile,§ G.T. Seaborg, and R.M. Weiner**

We have initiated a radiochemical search for anomalons aimed at demonstrating the existence of anomalons using a nonemulsion or track detector technique. The experiment is similar to one used by Rossi in 1941 to detect the decay of the muon. Two identical copper blocks, 1 cm thick and 8 cm in diameter, are irradiated by relativistic projectiles in two different configurations. In configuration I, the blocks are touching one another while in configuration II, the blocks are separated by 10 cm of air. It is assumed that when the relativistic projectiles interact with the first block of each pair, projectile fragments are created which in turn interact with other nuclei in the first and second blocks. Particular attention is given to those interactions in which ^{24}Na and ^{28}Mg target fragments are generated by the interaction of the beam nuclei and projectile fragments with the Cu nuclei. (The threshold for the production of such fragments from Cu is ~1GeV/nucleon). What is measured is the ratio of ^{24}Na or ^{28}Mg produced in the second block relative to the first block, R, in the two configurations of the Cu blocks, i.e., R_I and R_{II}. With beam spots ~2.5 cm in diameter and opening angles of 1 GeV/nucleon projectile fragment cones of $<12°$, the loss of projectile fragments in configuration II by "missing" the second block becomes negligible; hence, any difference between R_I and R_{II} is assigned to decay in flight of some of the fragments in the longer flight path.

Measurements of R_I and R_{II} have been made for the interaction of 24 GeV protons, 0.9 GeV/nucleon and 1.8 GeV/nucleon ^{40}Ar, and 2.1 GeV/nucleon ^{12}C with the Cu blocks. If we define $Q = R_{II}/R_I$, we would expect Q=1 in the absence of "decay effects" (as well as the absence of anomalons). For the aforementioned beams, the measured values of Q are 1.02 ± 0.03, 1.035 ± 0.024, 1.074 ± 0.03 and 1.03 ± 0.02, respectively.

We will repeat the measurement with 1.8 GeV/nucleon ^{40}Ar to ascertain the magnitude of any systematic errors in the measurement and to understand if Q=1.07 is a meaningful deviation from Q=1 for this type of experiment.

Footnotes

*Philipps Universität, D3550 Marburg, Federal Republic of Germany
†Studsvik Science Research Laboratory, S-611 82 Nyköping, Sweden
‡Oregon State University, Corvallis, OR 97331
§Purdue University, W. Lafayette, IN 47901

Search for Relativistic Projectile Fragments with Charges of 4/3, 5/3, 7/3, and 8/3*

M.A. Bloomer,† E.M. Friedlander, H.H. Heckman, and Y.J. Karant

Recent speculation on the cause of the anomalously short reaction mean free paths of projectile fragmentation products (PF's) produced from relativistic heavy-ion (RHI) collisions with emulsion nuclei has led to the suggestion that nuclei with bound third-integral charges might be present among the PF's. We were thus motivated to search for such fractional charges among the $1 \leqslant Z \leqslant 3$ PF's produced by the interactions of 1.88 GeV/nucleon ^{56}Fe nuclei in G-5 nuclear emulsion.

In an earlier paper[1] we described in detail how to measure the nuclear charge of $1 \leqslant Z \leqslant 3$ PF's of RHI collisions in nuclear emulsion. Specifically, measurements based on the lacunarity, i.e., fractional transparency, of the linear track structure of such ionization tracks will easily yield a precision of σ = 0.05 charge units for Z = 1 and Z = 2, and about σ = 0.07 charge units for Z = 3.

We show in Fig. 1 a plot of the charge distribution for 1179, $1 \leqslant Z \leqslant 3$, PF's of all generations (data from three observers). No corrections of any kind have been made to these data. Recall that

$$Z = k_0\sqrt{-\ln L},$$

where L = lacunarity and k_0 = normalization constant.

The salient feature of Fig. 1 is that all charge measurements for each PF are narrowly distributed around their integer means, and, with the possible exception of the set of measurements scattered around Z = 2.33, there is no indication that PF's of third-integral charge are produced with the same relative abundance as reported for anomalons to date, i.e., 2–6% for $3 \leqslant Z \leqslant 26$.

More rigorous tests for fractional charges were made on a total of 15 tracks (see Fig. 1) whose charges differed from unit charges Z = 1, 2 and 3 by more than 3σ. After i) making improved statistical estimates of the charges of these tracks, ii) eliminating events exhibiting high $p_\perp$ (production angles in excess of 6°) and iii) eliminating slow, Z = 1 fragments that emulated relativistic Z = 2 PF's, as determined by multiple scattering measurements and kinetic analysis of their interactions, we found that none of the 15 candidate events were compatible with beam-velocity, fractionally charged PF's.

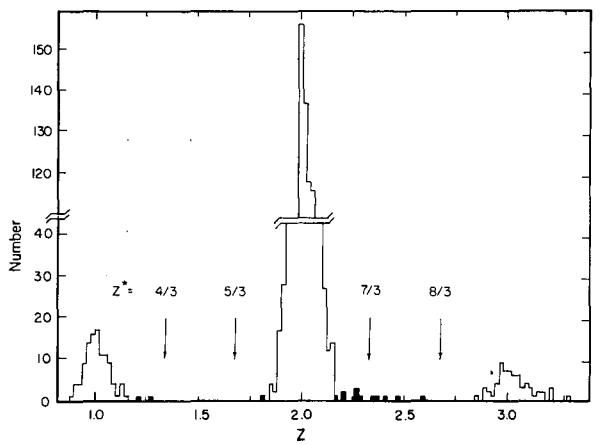

Fig. 1. Charge distribution of $1 \leqslant Z \leqslant 3$ projectile fragments from the extra-nuclear cascade of interactions from a ^{56}Fe beam, all generations and all observers. The blackened squares are those measurements which lie outside intervals of $\pm 3\sigma_Z$ centered around the integer means Z = 1.0, 2.0 and 3.0.

XBL 838-10928

Therefore, we conclude that we observed in 1179 charge measurements no PF's with Z* = 4/3, 5/3, 7/3, or 8/3. This puts an upper limit of 3×10^{-3} at a confidence level of 99.9% on the relative number of such PF's with a charge differing from an integer by 1/3 charge units. This upper limit is strictly true only if the relative occurrence of fractionally charged PF's is independent of charge. Our result is in agreement with a similar fractional charge search recently carried out by Price *et al.*[2] on

$10 \leqslant Z \leqslant 18$ PF's from the cascade of interactions produced by a 1.85 GeV/nucleon ^{40}Ar beam incident on CR-39 plastic detector.

Footnotes and References

*Based on LBL-16487, submitted to Physics Letters B.

†Massachusetts Institute of Technology, Cambridge, MA.

1. M.A. Bloomer, H.H. Heckman and Y.J. Karant, NIM **215**, 247 (1983).
2. P.B. Price, M.L. Tincknell, G. Tarlé, S.P. Ahlen, K.A. Frankel, and S. Perlmutter, Phys. Rev. Lett. **50**, 566 (1983).

Search for Fractional Charges Produced in Heavy-Ion Collisions at 1.8 GeV/nucleon

M.A. Lindgren, D.C. Joyce,* P.C. Abrams,* R.W. Bland,*† R.T. Johnson,* T.D.Knoop,* M.H. Savage,* M.H. Scholz,* B.A. Young,* C.L. Hodges,‡ A.A. Hahn,§ G.L. Shaw,§ K.S. Lackner,**H.G. Pugh, R. Slansky††*

Searches for fractionally charged particles have been made in many kinds of elementary-particle interactions, including searches at e^+e^- and hadron storage rings.[1] These experiments typically look for tracks with ionization below the minimum for singly charged particles. They have seen no evidence for fractional charges.

With the high-energy beams of heavy nuclei available at the Bevalac, it is possible to search for fractional charge produced in interactions involving huge numbers of quarks and large hadronic volumes.[2] Processes that involve heavy nuclei might yield fractional charge by mechanisms not possible in elementary-particle interactions.[3,4] That is, where it is difficult to separate a particle with fractional charge from the remaining colored fragment in the vacuum, the separation process may be greatly enhanced in the environment of a quark-gluon sea created in a heavy-ion collision.

The experiment is done in two steps. The first stage is a scheme to collect and concentrate fractional charges produced in heavy-ion collisions at the Bevalac. In the second stage, the target and concentrated materials from the Bevalac exposure are brought to one of the existing experiments designed to look for free fractional charge in bulk material. These include magnetic levitometers,[5] Van de Graaff charge spectrometers,[6] and droplet experiments.[7,8] In this paper we report the details of the initial Bevalac exposure, and then describe the analysis of this exposure with the San Francisco State University automated Millikan apparatus. Other analyses of the Bevalac materials will be reported elsewhere.

A total of 3×10^{10} Fe ions of 1.8 GeV/nucleon kinetic energy were incident on a target configuration consisting of a number of heavy materials (mainly Pb). Within a 30° cone behind the target were 26 five-gallon tanks of carbon tetrachloride. The layout of the tanks and the composition of the target are described more completely in Fig. 1. Each tank had a thin central wire maintained at a potential of ± 90 V with respect to its inside wall. Fractionally charged particles that stop in the tank form fractionally charged atoms or molecules which drift to the wire[9] and are trapped there by the image charge, since no subsequent reaction can make them natural.

The choice of fully ionized Fe was made to optimize the energy per nucleon, atomic number, and intensity of the beam. The Pb target was selected to optimize the probability of a central collision. Since following the nuclear collision, fractional charge may be part of a nuclear fragment, the total collection configuration was designed to stop both low- and high-charge fragments. Most high-charge

fragments (Z>6) are expected to stop in the target, while most low-charge fragments pass through the target plates into the tanks. The stopping efficiency of the tanks was estimated with use of Monte Carlo techniques and the Bethe-Bloch formula. We find, for a large range of mass and reasonable momentum distributions for the produced particles, that about 1% of all particles with charge e/3 and about 8% of those with charge 4e/3 are stopped in each of the forward tanks. The collection efficiencies of the other tanks decrease with production angle and distance from the target.

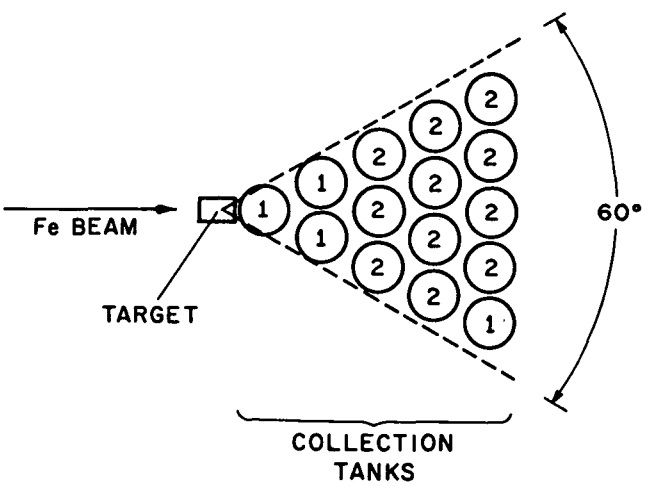

Fig. 1. Schematic top view of the experimental setup at the Bevalac showing the target configuration and the stopping tanks of CCl_4. Some of the five-gallon tanks are arranged in a double layer as denoted by the 2. The 26 central collection wires included Au, In, Cu, Nb, and W wires, each maintained at +90 V or −90 V with respect to the inside wall of its tank. The target configuration consisted of 22 Pb and 9 In (interspersed) wafers 1/8 in. thick and 3 cm in diameter. Near the middle of the target there were some Cu plates, totaling 1/8 in. in thickness, 10 g of Hg, and several hundred steel balls, each with a mass of about 0.1 m. The Fe beam was 1.5 cm in diameter and was accurately maintained in the center of the target. XBL 842-739

We now turn to the analysis of some of these samples by the automated Millikan technique.[7] One sample was prepared from the 36-μm-diam. central gold wires from two of the forward tanks, one of each polarity. Each wire was passed twenty times through a small drop of mercury in a capillary tube in order to remove the surface layer of the wire. These two drops were combined to form sample A. In this process the fractional charge is transferred to the mercury with an unknown efficiency. As this efficiency could be small, a second sample B was prepared by dissolving the gold wires in some mercury from the target assembly. Thus sample B combines collection from the target and the tank.

The measuring apparatus is a modification of the Millikan oil-drop experiment in which small drops are introduced one at a time into a measuring chamber by a piezoelectric drop ejector. The drop's drift velocity in a switched electric field is measured by timing the passage of an image of the illuminated drop over a series of slits. The measured velocity of a typical drop as a function of time is shown in Fig. 2. The field switches from positive to negative at slit 39. The change is velocity seen at this point corresponds to a charge on the drop of 14e. The field returns to its original polarity at slit 74, and the velocity returns to nearly its original value. A change in charge during the measurement can be detected by comparing the final velocity with the original one. Drops which change charge during the measurement are identified in this way and rejected. The occurrence of such charge changes is less than one per 1000 drops.

Drops with substantial residual charge are further analyzed to ensure that their charge measurements are not erroneous. Limits are placed on the initial and final transverse positions, the charge change, the χ^2 of the velocity fit, and the drop radius such that 5% of all drops would fail any one cut. These limits remove twenty drops which compose a fairly flat distribution of residual charges between 0.2 e and 0.8e. The radius limit is particularly significant since most disturbances that affect the charge

determination also affect the radius determination. Under good running conditions the radius is constant to 0.1%. The radius test rejects drops which have radii about 0.7% too big or too small.

To ensure objectivity in the analysis, $\pm e/3$ is added at random intervals to a drop's measured charge. There are 236 of these test events, of which 197 remain in the sample after all limits have been applied. The test events are identified as such and removed from the sample only at the end of the analysis.

Drops can be measured at a rate of 1 sec^{-1}, and 5 μg of mercury can be measured in an hour of good running. The charge on a 6-μm-diam mercury drop is measured to an accuracy of about 3.5% of e. To keep the charge on the drops near zero, a bias wire is inserted into a column of water which is in contact with the mercury drop in the drop ejector's tip. The potential of this wire (a few volts) is adjusted by the computer. Drops with charge between -16 e and $+16$ e are accepted.

A total of 500 μg of mercury was measured, 200μg from sample A and 300 μg from sample B. A histogram of residual charge for both samples, a total of 260,000 drops, is shown in Fig. 3. The residual charge is the charge in excess of an integral value. The charge measurement is calibrated directly from the integral-charge peaks by assuming that the peak to peak separation is e. There are no measurements near fraction-charge values of e/3 or 2e/3.

A limit on the fractional-charge production rate can be set for sample A by noting that 200 μg is 2% of the mercury bead used to rinse the gold wire and by using the calculated 1% capture efficiency of the tanks for particles of charge $\pm 3/3$. If the efficiency in transferring fractional charges from the gold wires to the mercury in sample A is 100%, then we obtained a production limit of less than 5×10^{-7} fractionally charged particles per collision with 95% confidence. If the fractional charges were not removed by the mercury rinse and remained on the gold wire, then the fractional charges from the two tanks are concentrated instead in sample B. We

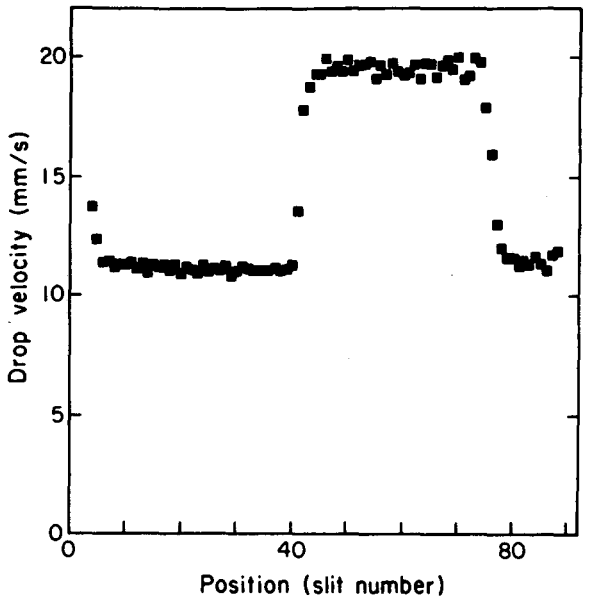

Fig. 2. Drift velocity as a function of position for a typical mercury drop. Reversals of the electric field occur at slits 39 and 74. XBL 842-740

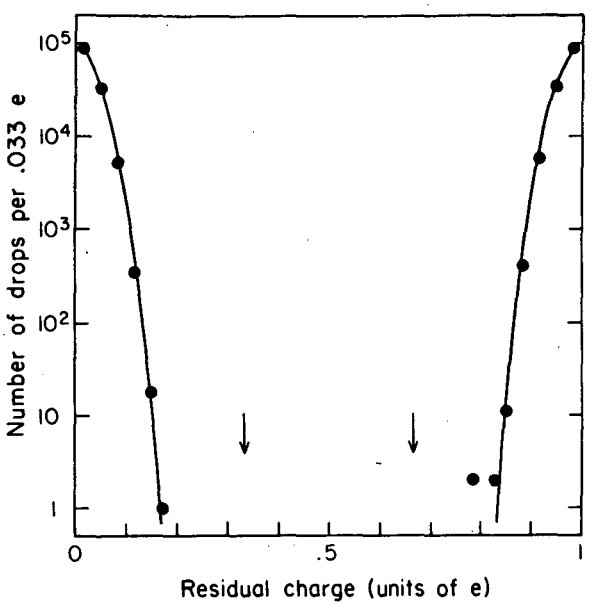

Fig. 3. Combined distribution of residual charge for samples A and B. The arrows indicate the positions where measurements of drops containing 1/3-integer charges would fall. The curve shown is a Gaussian with standard deviation of 0.035e. XBL 842-741

measured approximately 0.02% of sample B. Thus, assuming that the mercury rinse did not remove the fractional charges, the 95% confidence level on the production rate is less than $5 - 50^{-5}$ fractionally charged particles per collision. (More restrictive limits apply if the produced particles have total charge greater than e/3, for then the stopping efficiency is greater.)

Sample B is also used to set the limit on the production of high-Z fractionally charged nuclear fragments, all of which would be stopped in the portion of the target covered by the beam. The mercury measured from sample B corresponds to 1×10^{-6} of the target, which gives a production limit of less than 1×10^{-4} fractional charges per collision with 95% confidence.

In summary, we have carried out a first-generation experiment to detect fractionally charged particles produced in Fe-Pb nuclear collisions at 1.8 GeV/nucleon incident beam energy. We detect no 1/3-integrally charged particles. We can rule out production of fractional charges in the target at the rate of one per 1×10^4 collisions, or under certain assumptions, to one per 2.0×10^6 collisions.

Footnotes and References

*Physics and Astronomy Department, San Francisco State University, San Francisco, California 94132
†Current address: Laboratoire de Physique Nucléaire des Hautes Energies, Ecole Polytechnique, Route de Saclay, F-01128 Palaiseau, France.
‡Physics and Astronomy Department, San Francisco State University, San Francisco, California 94132, and Physics Department, University of California, Riverside, California 92521
§Physics Department, University of California, Irvine, California 92717
**Stanford Linear Accelerator Center, Stanford, California 94305
††Theoretical Division, Los Alamos National Laboratory, Los Alamos, New Mexico 97545

1. J.M. Weiss *et al.*, Phys. Lett. **101B**, 439 (1981); W. Bartel et al., Z. Phys. C **6**, 295 (1980); J. Napolitano *et al.*, Phys. Rev. D **25**, 2837 (1982); C.W. Fabian *et al.*, Nucl. Phys. **B101**, 349 (1975); M. Basile *et al.*, Nuovo Cimento **40**, 41 (1977).

2. An experiment performed at the Bevalac by P.B. Price *et al*, Phys. Rev. Lett. **50**, 556 (1983), set a limit that less than 1 in 300 of the fragments produced in 1.81-GeV/nucleon argon collisions in a plastic track detector have fractional charge.

3. R. Slansky, T. Goldman, and G.L. Shaw, Phys. Rev. Lett. **47**, 887 (1981).

4. G.L. Shaw and R. Slansky, Phys. Rev. Lett. **50**, 1967 (1983).

5. G.S. LaRue, J.D. Phillips, and W.M. Fairbank, Phys. Rev. Lett. **46**, 967 (1981); M. Marinelli and G. Morpurgo, Phys. Rep. **85**, 161 (1982); D. Liebowitz, M. Binder, and K.O.H. Ziock, Phys. Rev. Lett. **50**, 1640 (1983).

6. K.H. Change *et al.*, to be published; D. Elmore, private communication; R. McKeown, private communication.

7. C.L. Hodges *et al.*, Phys. Rev. Lett. **47**, 1651 (1981); P.C. Abrams *et al.*, in **Novel Results in Particle Physics**, edited by R.S. Panvini *et al.*, AIP Conference Proceedings No. 93 (American Institute of Physics, New York, (1982), p. 15; D. Joyce *et al.*, Phys. Rev. Lett. **51**, 731 (1983).

8. G. Hirsch, R. Hagstrom, and C.D. Hendricks, Lawrence Berkeley Laboratory Report No. LBL-13636, 1981 (unpublished).

9. A.O. Allen, M.P. de Haas, and A. Hummel, J. Chem. Phys. **64**, 2587 (1976).

Two-Particle Correlations Observed with the Plastic Ball Detector

H. Wieman, H.H. Gutbrod,* H.A. Gustafsson, B. Kolb,* H. Löhner,† B. Ludewigt,* A.M. Poskanzer, T. Renner, H. Riedesel,‡ H.G. Ritter,* A. Warwick,* and F. Weik§*

Three different categories of two-particle correlations are being investigated in the analysis of the Plastic Ball data. The first category, which has already received the most attention by others in the field of relativistic heavy ions, is source size determination using Hanbury-Brown, Twiss type interferometry. Two-pion correlations have been measured for this purpose with a streamer chamber[1] and with a magnetic spectrometer.[2] Source size measurements have also been made with proton-proton correlations[3] following the calculations of Koonin,[4] which include Coulomb and nuclear forces in addition to strictly interference effects. In this category of two-particle correlations, the relative velocities are quite low. For protons the kinetic energy in the center of mass of the pair is on the order of 0.5 MeV.

The second category of two-particle correlations deals with low energy nuclear cluster formation, the kinetic energy in the center of mass of the pair being in the region 1 MeV to 10 MeV. Here one observes nuclear composites – the formation and decay of particle-unstable isotopes and levels such as ^{5}Li.

The third category addresses higher energies, 100 MeV or more in the center of mass of the pair. In this energy region the possibility exists for seeing baryon resonances. For example, delta decay might be observed via π^+-p correlations or dibaryon resonances by π^+-d correlations.[5]

Here we shall be reporting only on preliminary results obtained in the first two categories. So far source sizes and cross sections have not been extracted, since we have mainly been exploring, looking for those areas where the unique features of the Plastic Ball can best be exploited. The most obvious advantage of the Plastic Ball for two-particle correlation measurements is its large solid angle ($\sim 4\pi$) and rapid data collection, which allow better statistics than are easily obtained with other devices. On the other hand, the relatively coarse angular resolution (3.5° to 7°) and the limited energy resolution impose restrictions on the types of correlations that can be measured. The studies described here have been limited to the possible two-particle combinations of p, d, t, ^{3}He, and ^{4}He with low relative velocities. Particles included in the analysis were stopped in the Ball detector (laboratory angle 10° to 160°) where particle type and energy could be determined. As work progresses the correlations will be compared for various projectile target combinations, but to date our efforts have been concentrated on Ca + Ca at 400 MeV/nucleon, the system for which we have the largest data set. These data were recorded using a central collision trigger.

The correlation function F(Δp) has been generated in a manner similar to that used in two-particle interferometry studies.[3]

$$F(\Delta p) = nN_s(\Delta p)/N_d(\Delta p)$$

where $N_s(\Delta p)$ is the number of pairs per unit, Δp taken from the same event, and $N_d(\Delta p)$ are the number of pairs per unit, Δp constructed from different events. The momentum Δp is the particle momentum in the center of mass of the pair. The factor n is chosen arbitrarily such that $F(\Delta p) \simeq 1$ at large Δp. This correlation function is closely related to the R correlation function used by Koonin: $F(\Delta p) - 1 \simeq R(\Delta p)$. F(Δp) is greater than 1 for positive correlations. The particle momentum in the center of mass (Δp) was chosen for this analysis for two reasons. First, this choice is consistent with the variable used in other source size determinations ($\Delta p \simeq |\vec{p}_1 - \vec{p}_2|/2$ for pairs of like mass particles). Second, Δp is easily related (nonrelativistically) to Q values and excitation energies (E_x) of clusters formed from the pair, i.e.,

$$\Delta p = \left[2 \frac{m_1 m_2}{m_1 + m_2} (E_x - Q) \right]^{1/2} .$$

The resulting correlation function for proton-proton pairs is shown in Fig. 1. The expected enhancement in the measured correlation function is clearly observed, but it is truncated below ~20 MeV/c, the peak in Koonin's predicted value. Also the peak is broader than predicted. Both of these distortions can be blamed on the finite angle subtended by a Plastic Ball detector module. This distortion, however, is not a serious problem for a source size analysis, since the plastic ball distortion may be folded into Koonin's predictions for comparison with our measurements.

We have found that p-p is not the only two-particle system to show correlations at low Δp. A number of other two-particle systems exhibit stronger correlations, some positive, some negative. The most striking examples appear in Figs. 2 and 3. As shown, there is a strong enhancement in the p-^{4}He system at a Δp value corresponding to the decay of the ^{5}Li ground state. Likewise, d-^{4}He has a peak that apparently comes from the decay of the lowest excited levels of ^{6}Li. For the d-d system, on the other hand, there is a negative correlation. At low relative velocity deuterons appear to coalesce into excited states of ^{4}He that decay by another channel. The observed depression in the d-d correlation function extends up to Δp = 150 MeV/c. This is well beyond the Δp = 55 MeV/c instrumental cutoff imposed by the finite angular size of the detectors in the Plastic Ball. The d-d system may be contrasted with the p-t system, which couples to slightly lower values of ^{4}He excitation. In this case there is evidence again of a positive correlation at low Δp. A summary of observed correlations is shown in Table I along with the Q value for the various pairings of the particles. The Q value seems to be important for lithium and beryllium; positive correlations are only observed when the pairs couple to the ground state or lowest excited states of the composite.

The results obtained so far show that the Plastic Ball with its large solid angle can be a useful tool for measuring two-particle correlations. The present effort will continue along two lines. First, work will continue towards extracting source size information from proton-proton correlations. The second line of effort will be devoted to extracting relative cross sections for the formation of the particle-unstable isotopes and levels that we have observed. These can then be compared with phase space models such as Fai and Randrup's[6] which predict yields of unstable as well as stable clusters.

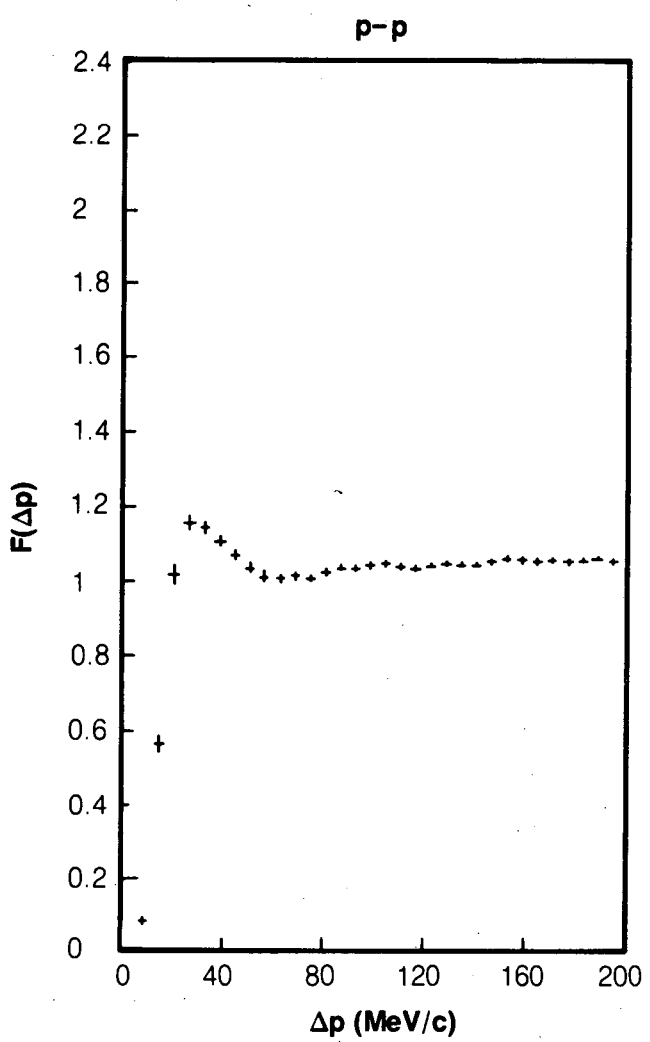

Fig. 1. p-p two-particle correlation function as a function of the particle momentum in the center of mass of the pair. Values of F(Δp) greater than 1 indicate a positive correlation. XBL 835-268

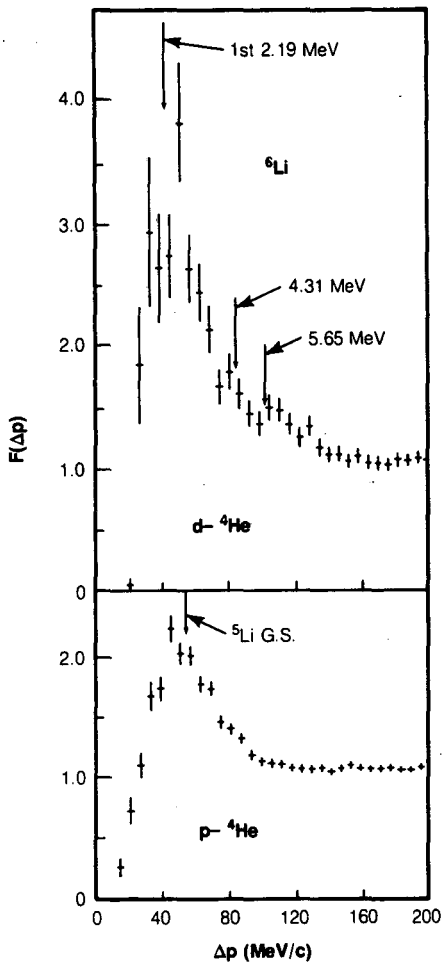

Fig. 2. Two-particle correlation functions for d-^{4}He coupling to ^{6}Li and p-^{4}He coupling to ^{5}Li. Position of levels known to decay to the pair particles are indicated. XBL 835-270

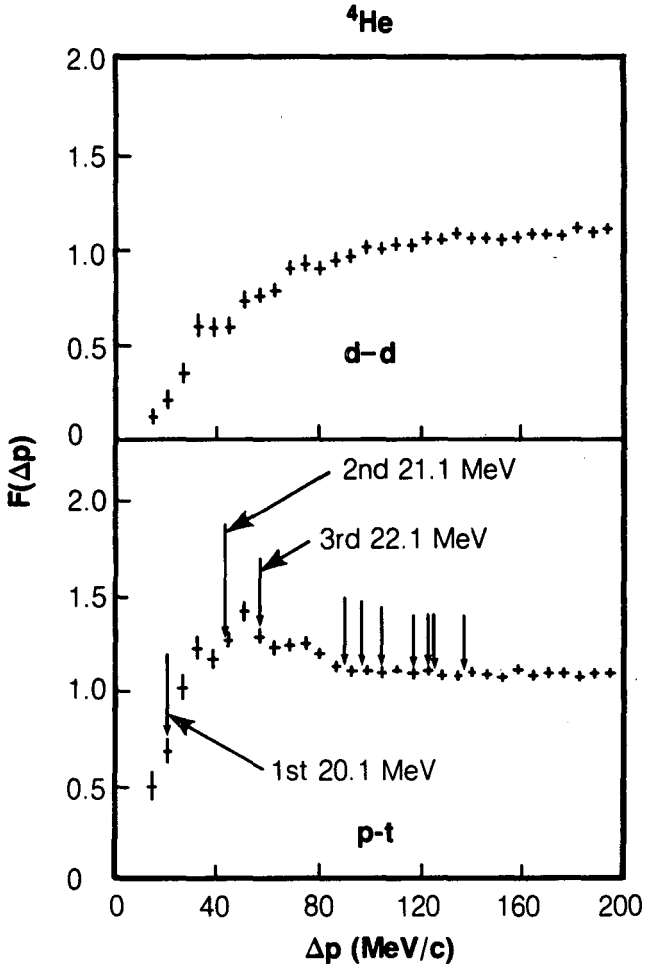

Fig. 3. Two-particle correlation functions for d-d p-t both coupling to ^{4}He. Correlations are shown as a function of the particle momentum in the center of mass of the pair. Position of some ^{4}He excited states are indicated in the p-t system. XBL 835-267

Footnotes and References

*Gesellschaft für Schwerionenforschung, Darmstadt, West Germany.

†Universität Münster, Münster, West Germany.

‡Present address: Max Planck Institut für Kernphysik, Heidelberg, West Germany.

§Present address: Toledo Corp. Köln, West Germany

1. J.J. Lu, *et al.*, Phys. Rev. Lett. **46**, 898 (1981).
2. J.A. Bistirlich, *et al.*, LBL-13366, 146 (1982).
3. F. Zarbakhsh, *et al.*, Phys. Rev. Lett. **46**, 1268 (1981).
4. S.E. Koonin, Phys. Lett. **70B**, 43 (1977).
5. T. Siemiarczuk, J. Stepaniak, private communication, 1983.
6. J. Randrup, G. Fai, Phys. Lett. **115B**, 281 (1982).

Table I

Two-Particle Correlations
Low Δp

^{4}He					^{8}Be −0.09 pos.
^{3}He				^{6}Be 11.5 −	^{7}Be 1.6 pos.
	isotope Q Corr.				
t			^{6}He 12.3 ~pos.	^{6}Li 15.8 −	^{7}Li 2.5 pos.
d		^{4}He 23.8 neg.	^{5}He 16.7 −	^{5}Li 16.4 −	^{6}Li 1.47 pos.
p	^{2}He − pos.	^{3}He 5.5 neg.	^{4}He 19.8 pos.	^{4}Li −2.9 pos.	^{5}Li −2.0 pos.
	p	d	t	^{3}He	^{4}He

Angular Correlations Between Target and Projectile Fragments Emitted from ^{238}U + Ag(Br) Collisions at 0.85 GeV/nucleon*

H.H. Heckman, E.M. Friedlander and Y.J. Karant

Our examination of inelastic nuclear interactions of ~1 GeV/nucleon ^{238}U in research emulsions revealed a large range of target/projectile multiplicities, from simple binary fission to complete disintegration of both the uranium projectile and the target nucleus into nucleons and light nuclear fragments.[1] A particular class of U-reactions that we have begun to study are those that exhibit the classical target/projectile fragment topologies, selected by the criteria that at least 10 target- and 10 projectile-related fragments are produced in the reaction. Such reactions, when observed in emulsion, are identified with collisions of the incident uranium ions with the heavy component, Ag(Br), of the emulsion.

A 4 × 11 × 1 cm^3 ILFORD emulsion stack irradiated by 0.96 GeV/nucleon ^{238}U nuclei has been scanned over the beam profile for a distance of 1 cm from the entrance surface of the stack. Of a total of 399 interactions detected in the interval 0.85±0.10

GeV/nucleon, 52 fulfilled the selection criteria. Of these, 19 events were deemed unsatisfactory for measurement owing to obscuration by nearby beam tracks and/or the proximity, i.e., $\lesssim 40\mu m$, of the event to either the top or bottom surface of the emulsion pellicle.

This report describes the status of our measurements on the angular distributions of i) target fragments whose rates of ionization correspond to Z = 1 particles having energies < 100 MeV/nucleon and ii) projectile fragments, $Z \geqslant 2$, emitted within a forward 15–20° cone. All emission angles were determined by measuring the xyz coordinates of two points along each track separated by distances up to ~1 mm, depending on the energy, i.e., multiple scattering, and direction of the emitted particle. From these measurements we have obtained the distributions of space – and azimuthal – angles of the target and projectile fragments i) relative to the incident beam vector or ii) relative to their respective angular "center-of-gravity." The c.g. of angles conceptually identifies the vector of the "jet" axis for each class of fragment.

Fig. 1 defines the coordinate systems (lab frame) we have used. a) is the "beam" system, where $\underline{i}$ is along the beam axis, with $\underline{k} = \underline{i} \times \underline{j}$ being normal to the beam-emulsion plane. b) is the "jet" system, where the $\underline{i}$ axis is directed along the angular c.g. (the jet axis) of either the target or projectile fragments, with $\underline{k}' = \underline{i}' \times \underline{i}$. The space angles Θ (Θ') and azimuthal angles Φ (Φ') are indicated in their respective systems.

We define the "center-of-gravity" of n fragments to be:

$$\text{i) in azimuth: } \langle\Phi\rangle = \tan^{-1}\left(\frac{\Sigma \sin \Phi_i}{\Sigma \cos \Phi_i}\right)$$

and ii) in space: $\langle\cos\Theta\rangle = \frac{1}{n}\,\Sigma\, \underline{r}_i \cdot \underline{i}$, where $\underline{r}_i$ is the unit vector of the ith fragment.

The data on the differences between the c.g. azimuthal angles of the target and projectile ($Z \geqslant 2$) fragments in the beam coordinate system, $\Delta\Phi = \langle\Phi\rangle_{TF} - \langle\Phi\rangle_{PF}$, based on 28 events, show a

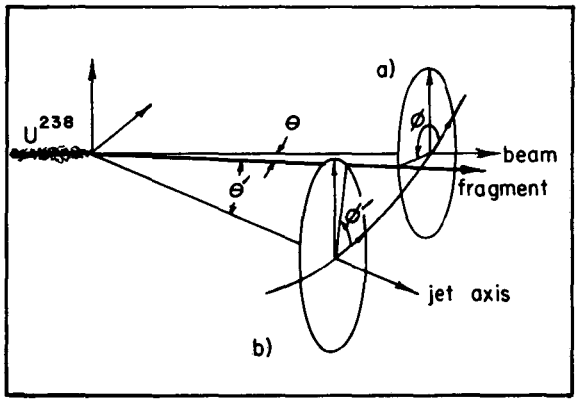

Fig. 1. Coordinate systems: a) Beam system, b) "Jet"system. XBL 8312-2598

strong back to back correlation; all values of $\Delta\Phi$ are greater than 90°, with a mean difference $\Delta\Phi = (149 \pm 4)°$ and dispersion D = 23°. These data are compared with those derived from a Monte Carlo (M.C.) simulation of each event assuming the target fragments are uniformly distribution in azimuth. This simulation removes the bias (spurious asymmetry) inherent to choosing the empirical center of gravity as the angular origin. The calculated distribution $\Delta\Phi = \langle\Phi\rangle_{TF} - \langle\Phi\rangle_{M.C.}$ has a mean $\Delta\Phi = (101 \pm 11)°$ and $D = (56 \pm 8)°$, compatible with that expected for a uniform distribution, namely 90° and 52°, respectively.

The verification that the asymmetries used to identify the c.g. of the azimuthal angle go beyond the above mentioned bias is that the angular distribution of all (643) target fragments measured relative to the c.g. angle $\langle\Phi\rangle$ on an event-by-event basis exhibits a stronger correlation with $\langle\Phi\rangle$, i.e., a peaking towards 0°, than does the M.C. (isotropic) simulation of the data. In this case, the dispersion of the distributions are $D_{exp} = (73 \pm 2)°$ and $D_{M.C.} = (91 \pm 3°)$, the ratio of the variances giving a $P(<F) \sim 10^{-6}$.

These azimuthal correlations imply significant correlations in the angles of emission of the fragments. In Fig. 2 we show the angular distribution of the target fragments in their "jet" frame, where

$\cos\Theta' = 0$ is the jet axis, Fig. 1b. A plot of $\ln\left(\frac{1}{N}\frac{dN}{d\cos\Theta'}\right)$ vs $\cos\Theta'$ reveals a forward-peaked distribution, the linear relationship indicated being characteristic of a Boltzmann energy distribution. For a Boltzmann distribution the ratio of $\beta_{\parallel}$, the longitudinal velocity, to β_0, the characteristic velocity $\left(\propto\sqrt{T_0\,[\mathrm{Temp}]}\right)$ of the emitting system, is $\mathrm{erf}\,(\beta_{\parallel}/\beta_0) = \frac{1 - F/B}{1 + F/B}$ (see ref. 2). For the observed value of $F/B = 4.3 \pm 0.6$, $\beta_{\parallel}/\beta_0 \approx 0.6$, i.e., the translational energy $T_{\parallel} \approx 0.4T_0$.

Based on our present data, the "jet" direction of the target fragments is also peaked forward, with an average value of $\langle\cos\Theta\rangle \approx 0.6$. The average emission angle of projectile fragments in the same events is $\langle\cos\Theta\rangle = 0.9986$ (3°). These angles are incompatible with "bounce-off" (elastic) collisions of the U + Ag(Br) system before break-up, although they are compatible with two-body kinematics provided the excitation energies are about 50 MeV/nucleon.

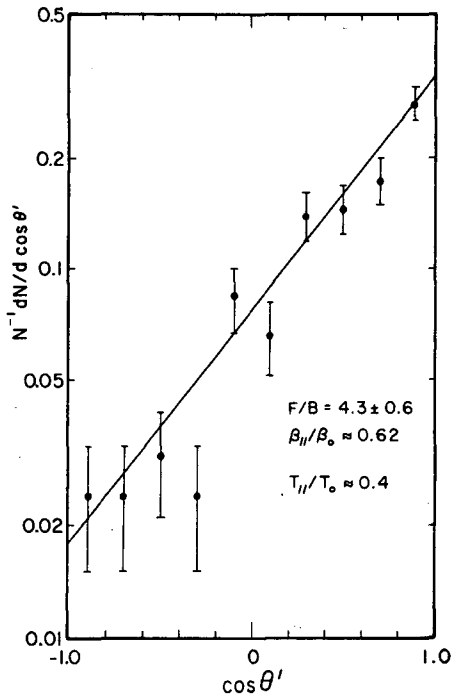

Fig. 2. Angular distribution of targets in the "jet" system. XBL 8312-2595

Footnote and References

*Based on paper presented at Sixth High Energy Heavy Ion Study and Second Workshop on Anomalons, LBL, June 28 – July 1, 1983.

1. E.M. Friedlander, H.H. Heckman and Y.J. Karant, Phys. Rev. **C27**, 2436 (1983).
2. H.H. Heckman, *et al.*, Phys. Rev. **C17**, 1651 (1978).

Spectator-Velocity Pions from Heavy Ions*

J. Ridout, D. Murphy, H.M.A. Radi, and J.O. Rasmussen

The focus of this paper is on pions in the velocity regions of target and projectile, where strong spectral features appear.

Our main studies have been in the projectile-velocity and center-of-mass regions, measuring pions near 0° in a magnetic spectrometer. We have made only a modest beginning to study pions in the target-velocity region by searching for stopped pions from emulsion interactions of 1.8 Gev/nucleon Fe ions. In this latter work we are indebted to Dr. Harry Heckman for invaluable assistance in generously making available his emulsions and microscopes and in directing his scanners in the anomalon studies to flag apparent slow pions, so that undergraduate research student James Ridout could further study the slow pions by tracing them to their stopping point and to a possible star. Fig. 1 shows a photomicrograph of a stopped π^- event initiated by

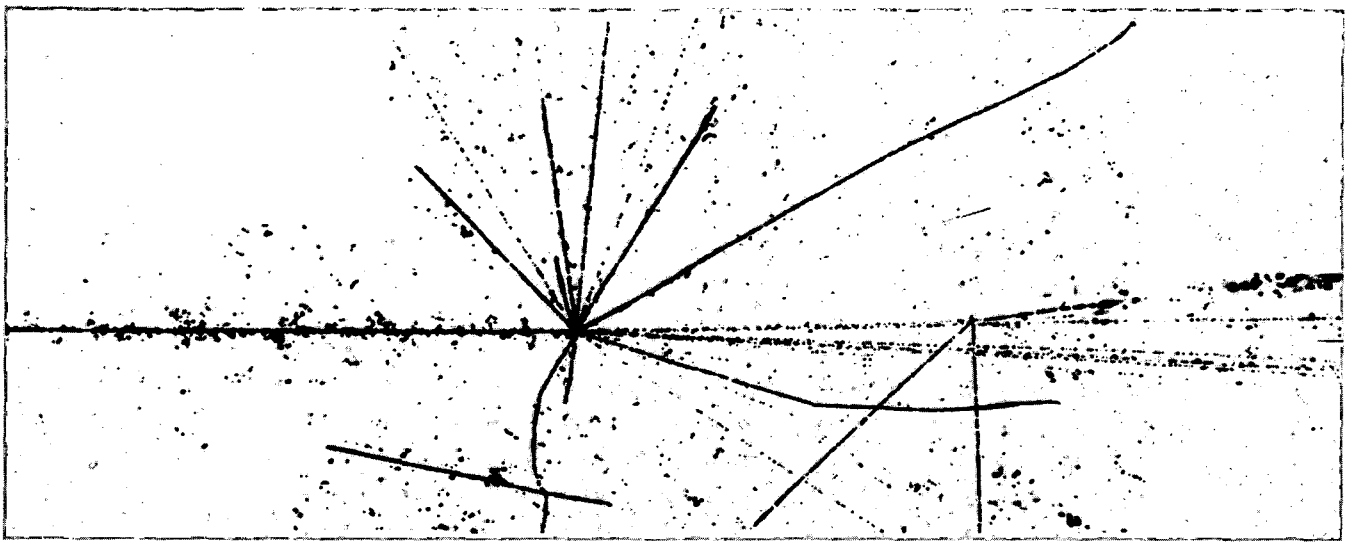

Fig. 1. Photomicrograph of a stopped π^- event initiated by 1.8 Gev/nucleon ^{40}Ar ion in emulsion. The argon ion enters from the left, and the pion wanders downward, forming a "star" at the end. XBB 802-1770

an ^{40}Ar beam from earlier work of Heckman and colleagues. Seeing this picture on the wall by Heckman's office had much to do with inspiring us to look for more such events.

From early on it became clear that we were dealing with a Coulomb effect of spectator fragments. In some of the earliest, and now classic, studies[1-2] on the Bevalac, Drs. Harry Heckman, Douglas Greiner, Peter Lindstrom, and their collaborators showed that GeV-energy heavy ions often fragmented, with the spectator pieces continuing on with velocities in a narrow distribution about the projectile velocity. Thus, our observaton of a prominent π^- peak near beam velocity and a π^+ depression in the cross section there evidently was a result of Coulomb forces from the projectile spectator fragments. We shall discuss the theory in more detail in a later section.

The target counterpart of the beam-velocity pions we studied are pions of one to a few MeV in the laboratory. At these low energies there is a good chance that the pions will stop in the emulsion stack. After stopping, the π^+ undergoes decay to a muon, which in turn decays to a positron. This succession of decays leaves a very characteristic identification. After stopping, the π^- will cascade down through Bohr orbits of an atom of the stopping medium and from a low orbit will undergo a nuclear disintegration in which usually one or more energetic particles emerge to form a "star". Of course, some of the time the pion's rest mass of 140 MeV can be carried off by neutrons and gamma rays and be missed in emulsions. Scanners can often recognize the characteristic multiple-scattering or meandering nature of a slow-pion track. This meandering makes the problem of energy determination a little greater, since one must try to estimate the track length of a wandering track.

Stopped pion emulsion studies with cosmic rays were published long ago by Friedlander and his collaborators.[3] One aspect they found remarkable was the presence of π^+ at sub-barrier energies in numbers greater than would be expected for simple quantum mechanical tunneling. More extensive work has been reported by Kostanashvili and others.[4-6] She has presented work for emulsions irradiated with protons at 660 MeV and 9 GeV and with π^- at 60 GeV.

The projectiles for our work were ^{56}Fe ions of kinetic energy 1.8 Gev/nucleon incident upon Ilford G5 emulsion stacks of pellicles either 25 cm $\times$ 7 cm $\times$ 600 microns or 12 cm $\times$ 7 cm $\times$ 600 microns.

In all, we examined 105 pions. Of these, only 15 proved acceptable in that they originated in an Fe-produced star and they stopped in the emulsion with a recognizable signature. This total is made up of 9 π^- and 6 π^+. For each pion accepted, the Fe "star" from which it emerged was examined in order to decide whether a heavy emulsion nucleus (Br or Ag) was involved. Ten of the 15 events were determined to involve heavy targets due to the presence of more than eight target-assocated fragments ($N_h > 8$). The remaining five events may involve either heavy or light target collisions. For each of the heavy-target events we attempted to estimate the residual target charge, Z_{eff}, by determining the total charge that emerged from each collision and subtracting this value from the sum of the atomic number of Fe and the average of the atomic numbers of Br and Ag.

Our pion energy distributions are shown in Figs. 2 and 3, along with the Kostanashvili *et al.*[6] data. Fig. 2 refers to heavy-target events and Fig. 3 to undetermined-target events. It is difficult to draw conclusions from our few events. It does seem that we have less suppression of π^+ relative to π^- compared to the Georgian work. This is qualitatively understandable, since the initiating proton and pion projectiles of their work would not be as likely to disintegrate Ag and Br to the extent that Fe ions would. For central collisions, where there is but little residual target charge, the ratio of the two charged pions could approach unity, though one would expect some excess of negative pions, since the neutron-to-proton ratios of projectile and targets exceed one.

In Fig. 4 we present the result of the estimates of the charge of target residues. Each pion event we accept is shown, with its abscissa the residue charge and its ordinate the pion energy. In parentheses by the data points is given the polar angle of emission with respect to the beam direction. The letter relates to the azimuthal correlation with the emission of evaporated particles from the target. The letter H denotes that the pion was emitted in the azimuthal quadrant with the highest multiplicity of evaporation tracks; the letter L, the lowest; and the letter A, one of the two adjacent quadrants. Only one π^+ is

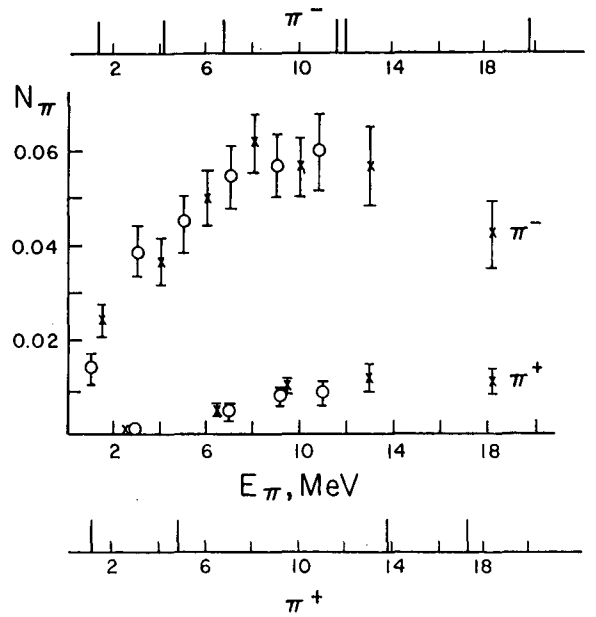

Fig. 2. Kinetic energy distribution of stopped π^- (above) and π^+ (below) from Fe ions on heavy (Ag or Br) atoms. (Each bar represents one pion). The middle graph is for comparison from work of Reference 6 for three projectiles: 660 MeV protons (○), 9 GeV protons (X), and 60 GeV negative pions (○).
XBL 841-61

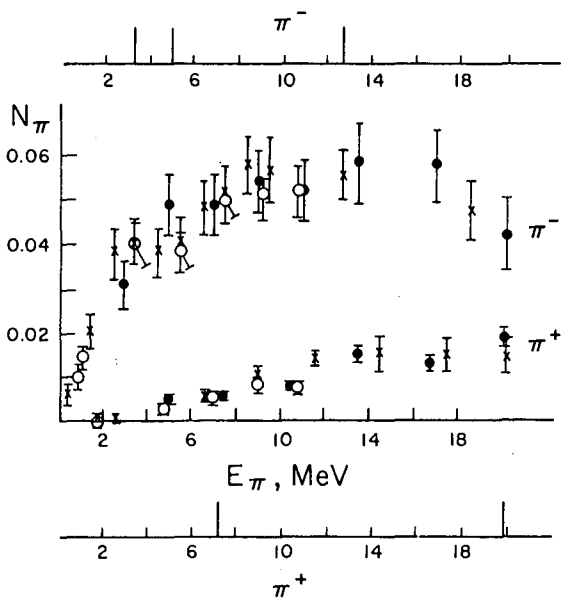

Fig. 3. Same as Figure 2 except emulsion target nuclei are undetermined. XBL 841-62

actually "sub-barrier," namely, the lowest dot of Z_{eff} of 9. It may be that the residual charge is really lower due to uncertainties in our estimates. Again, the statistics are clearly insufficient for many conclusions, but there does seem to be a tendency for the π^- to be the most abundant for residual charges greater than 29, and the energies of the π^- are lower than the lone π^+ in this region.

Footnote and References

*Condensed from LBL-15283, paper presented by J.O. Rasmussen at the Nuclear Physics Conference, Cairo, Egypt, December 1982.

1. D.E. Greiner *et al.*, Phys. Rev. Lett. **35**, 152 (1975).
2. P.J. Lindstrom *et al.*, LBL-3650 (1975) unpublished.
3. E.M. Friedlander, Phys. Lett. **2**, 38 (1962).
4. N.I. Kostanashvili *et al.*, Sov. J. Nucl. Phys. **6**, 385 (1968).
5. N.I. Kostanashvili *et al.*, Sov. J. Nucl. Phys. **13**, 715 (1971).
6. N.I. Kostanashvili *et al.*, Sov. J. Nucl. Phys. **16**, 542 (1973).

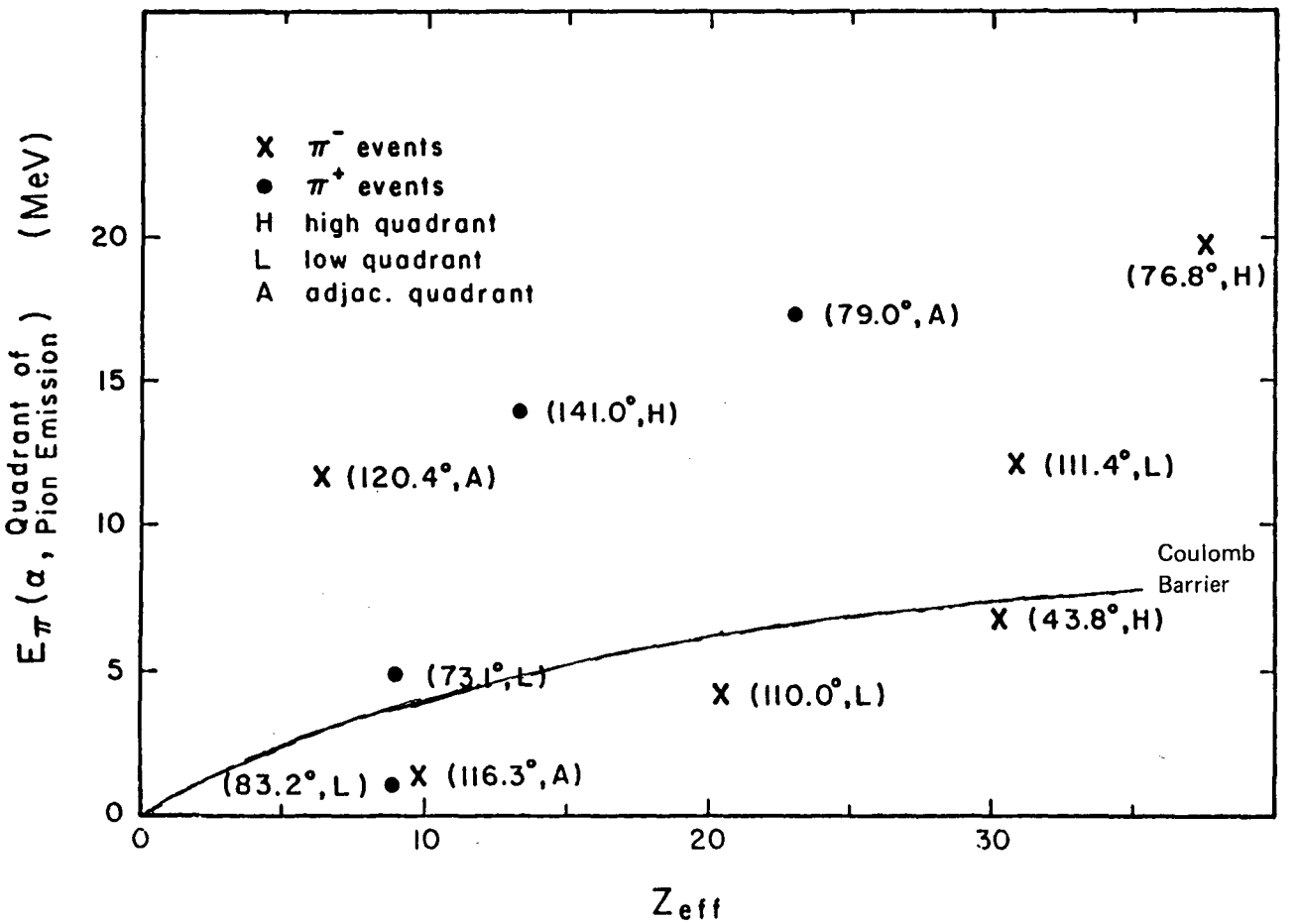

Fig. 4. Plot of our pion energies vs. estimated target residual charge Z_{eff}. The associated polar angle α and the azimuthal quadrant are indicated in parentheses. See text for azimuthal correlation explanation. XBL 841-63

Interaction of 4.22 GeV and 7.54 GeV ^{20}Ne with Cu*

K.H. Hicks,† T.E. Ward, H. Bowman, J.G. Ingersoll, J.O. Rasmussen, J.P. Sullivan,‡ M. Koike, and J. Peter

The cross sections of 15 products produced in the relativistic heavy ion reactions of 211 and 377 MeV/nucleon ^{20}Ne ions with Cu were measured using activation techniques. The isobaric mass yield curves measured in this study compare well with previous results of relativistic heavy ion- and proton-induced Cu spallation, after taking into account the increased absolute total reaction cross section of ^{20}Ne. The target fragmentation yields resulting from peripheral collisions were compared with abrasion-ablation model calculations. Central collision processes were examined by comparing light mass ^{7}Be yields.

Two copper targets were irradiated with 4.22 GeV (211 MeV/nucleon) and 7.54 GeV (377 MeV/nucleon) ^{20}Ne ions in the external beam of the Bevalac. The production cross sections measured in the present study are listed in Table I. The uncertainties in these measurements are 12–20%. Recoil loss effects of target fragments can be neglected from the thick target yields and low mass beam velocity projectile fragments such as ^{7}Be, which have ranges in Cu of $\geqslant$ 30 g/cm^2 at the energies used in this study, and can be assumed to escape completely. The thick-target yields of products near the target were corrected for secondary production processes in the manner outlined by Cumming and coworkers[1-3] for target thicknesses of 2–2000 mg/cm^2. The corrections amount to a 5% reduction in the thick target yield of ^{54}Mn and increase with mass number to about 20% for ^{60}Co and 35% for ^{65}Zn. The error in these corrections is estimated to be of the order of 20% of the reduction and would amount to increased errors of a few percent or less for the thick target error values. The low-mass products ^{7}Be and ^{24}Na were corrected approximately 30% and 15%, respectively, to obtain their zero-thickness yields.

In Fig. 1 are plotted the cross sections or, in the case of ^{14}N, the relative yields for the cobalt isotopes. The four Co distributions have the same shape within experimental errors, although the absolute cross sections vary. Such behavior is expected from concepts of factorization as detailed by Cumming *et al.*[1-3]

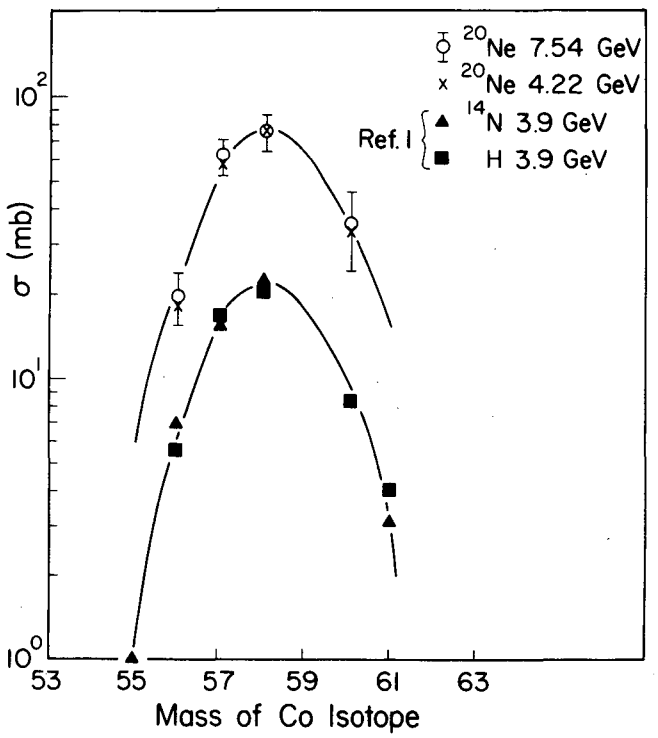

Fig. 1. Comparison of the mass yields of Co isotopes observed in the reaction of 4.22 GeV and 7.54 GeV (open circles) ^{20}Ne with Cu. Results from ref. 1 of 3.9 GeV ^{14}N (triangles) and ^{1}H (boxes) are also shown. The ^{14}N results are normalized relative to the ^{1}H. Photo courtesy of Indiana University Cyclotron Facility. XBL 841-260

In Table I and Fig. 2 are listed and shown the isobaric yields for 4.22 and 7.54 GeV ^{20}Ne interactions with Cu. The uncertainties of the linear portions of the plots are typically 20%. Linear regression analysis of the fitted line indicates that the slopes of the two lines are quite similar, 7.355%/u and 7.515%/u for 4.22 GeV and 7.54 GeV, respectively, with equal correlation coefficients of 0.956. These results compare well with other RHI and proton-induced Cu spallation studies[1-3] as expected from concepts of limiting fragmentation (energy independence) at energies greater than a few GeV.

The cross sections for production of heavy fragments produced in the peripheral collisions were compared with the calculations of Oliveira, Donangelo, and Rasmussen,[4-5] where the reaction was treated as a two-stage process: abrasion or fragmentation followed by ablation or evaporation. The preliminary comparisons showed the need for a frictional spectator interaction process (FSI) between the abraded nucleons and the spectator (target or projectile) fragments. The calculations were performed by the Cu + Ar reaction at 80 GeV.[3] The general trend of the data was well reproduced by the calculations, although the absolute values were a factor of 2 lower than the data. A comparison of the theory to the results of this investigation and other RHI- or proton-induced Cu spallation studies can be made by normalizing to the independent yield of ^{54}Mn. This is a necessary procedure for purposes of comparison, since the absolute yields differ by large geometric factors, whereas the relative yields of the spallation curve are only affected by small changes at these energies. Clearly, the FSI calculation better reproduces the mass yield ratios for the products near the target, where the total primary yield distribution is altered due to the increased energy deposited by a nucleon undergoing FSI. Ultimately, it is the increased average energy deposited in the FSI process which alters the number of nucleons removed in the interaction. Since this energy is typically 20–40 MeV, the most dramatic effect will occur for those product yields near the target (See Fig. 3).

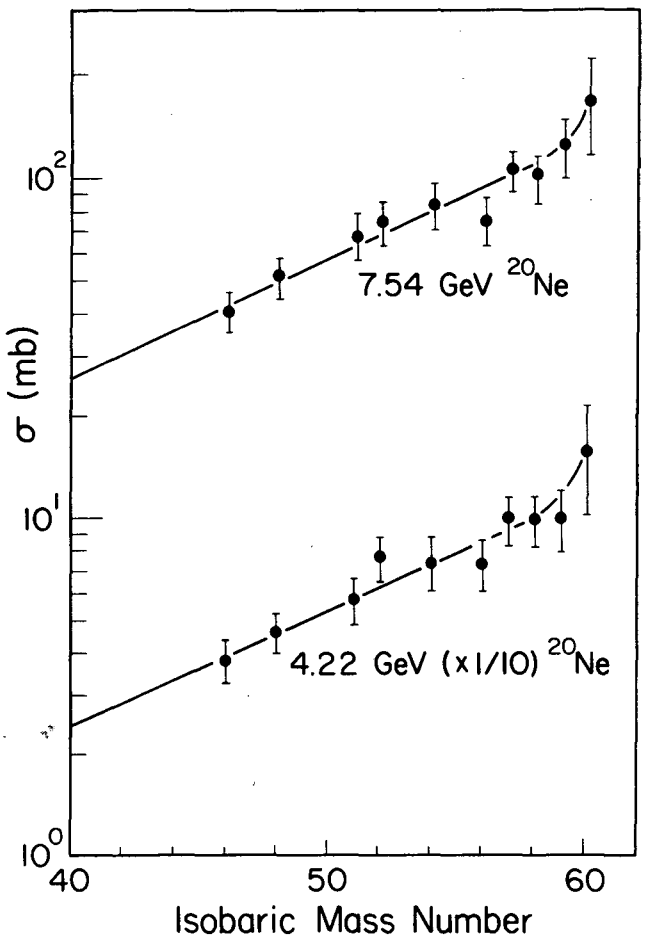

Fig. 2. Isobaric mass yield curves for the spallation of Cu with 4.22 GeV and 7.54 GeV ^{20}Ne. The points represent the zero target thickness yields. The exponential lines represent a best fit to the data as discussed in the text. Photo courtesy of Indiana University Cyclotron Facility. XBL 841-261

TABLE I. Absolute cross sections of long-lived radionuclides produced in the interaction of 4.22 GeV and 7.54 GeV ^{20}Ne with Cu targets.

		Cross section (mb)[b] 4.22 GeV			Cross section (mb)[b] 7.54 GeV		
Nuclide	Type of yield[a]	3.255 g/cm^2	0 g/cm^2	Isobaric yield	2.046 g/cm^2	0 g/cm^2	Isobaric yield
^{7}Be	I	53.0 ± 9.3	70.8		71.2 ± 10.9	92.9	
^{22}Na	C^+	42.2 ± 9.7	49.1		43.6 ± 9.2	50.7	
^{46}Sc	I	15.3 ± 2.3	15.3	38.3	16.2 ± 2.3	16.2	40.5
^{47}Ca	C^-	1.2 ± 0.2	1.2		1.3 ± 0.2	1.3	
^{48}V	C^+	24.0 ± 2.8	24.0	46.2	27.0 ± 3.1	27.0	51.9
^{51}Cr	C^+	52.0 ± 8.0	52.0	57.8	61.0 ± 8.6	61.0	67.8
^{52}Mn	C^+	22.5 ± 2.6	22.5	77.6	21.8 ± 2.5	21.8	75.2
^{54}Mn	I	46.0 ± 7.3	43.9	74.4	51.8 ± 7.7	49.5	83.9
^{56}Co	C^+	20.8 ± 2.9	18.9	72.7	21.1 ± 2.8	19.2	73.9
^{56}Ni	C^+	0.20 ± 0.3	0.18		0.36 ± 0.5	0.33	
^{57}Co	C^+	67.0 ± 10.6	58.3	100.5	71.9 ± 10.2	62.5	107.8
^{58}Co	I	89.7 ± 12.6	74.8	99.7	91.3 ± 12.2	76.1	101.5
^{59}Fe	C^-	5.4 ± 1.0	4.5	100.0	6.8 ± 1.1	5.6	124.4
^{60}Co	I	51.7 ± 14.9	41.4	159.0	55.0 ± 13.8	44.0	169.2
^{65}Zn	C^+	9.3 ± 3.0	6.2		10.2 ± 3.0	6.8	

[a]Independent (I), cumulative positron (C^+), and cumulative negatron (C^-).
[b]See text for explanation of zero target yields. The total uncertainties are estimated to be the same as the thick target errors.

Footnotes and References

*Condensed from Phys. Rev. C **26**, 2016 (1982).

†Present address: Nuclear Physics Laboratory, University of Colorado, Box 446, Boulder, CO 80309.

‡Present address: Cyclotron Laboratory, Texas AM University, College Station, TX 77843.

1. J.B. Cumming, P.E. Haustein, R.W. Stoenner, L. Mausner, and R.A. Naumann, Phys. Rev. C **10**, 739 (1974).
2. J.B. Cumming, R.W. Stoenner, and P.E. Haustein, Phys. Rev. C **14**, 1554 (1976).
3. J.B. Cumming, P.E. Haustein, T.J. Ruth, and G.J. Virtes, Phys. Rev. C **17**, 1632 (1978).
4. L.F. Oliveira, R. Donangelo, and J.O. Rasmussen, Phys. Rev. C **19**, 826 (1979).
5. L.F. Oliveira, thesis, LBL-8561, 1978 (unpublished).

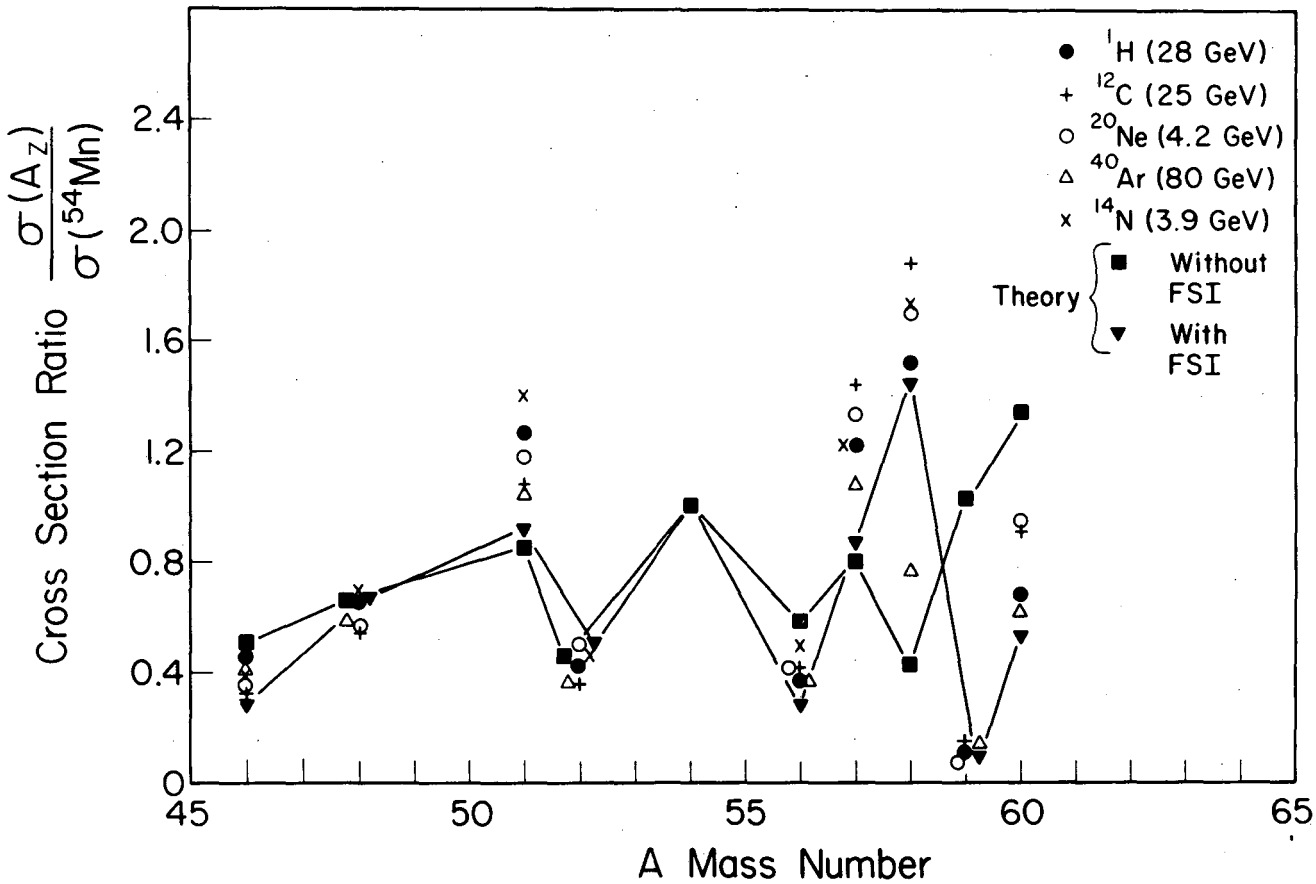

Fig. 3. Comparison between the relative proton-induced and RHI Cu spallation yields and the abrasion-ablation model calculations of Oliveira, Donangelo, and Rasmussen (refs. 4 and 5) with and without a frictional spectator interaction (FSI). The data are normalized to the independent yield of ^{54}Mn, effectively cancelling out large differences in the absolute yields due to geometric factors. Photo courtesy of Indiana University Cyclotron Facility. XBL 841-262

Charged Particle Multiplicity Distributions in the Reaction ^{139}La + ^{139}La at 1 GeV/nucleon

G. Odyniec, D. Bangert, R. Brockmann,† A. Dacal,‡ J.W. Harris,† M. Maier,* M. Ortiz,‡ H.G. Pugh, W. Rauch,* R.E. Renfordt,§ A. Sandoval,† R. Stock,† H. Stroebele,† D. Schall,§ and K.L. Wolf***

There is considerable interest in studying charged-particle production in heavy ion collisions.[1] In this report we present preliminary results of the study of production and accompanying nuclear disintegration in the reaction ^{139}La + ^{139}La at 1 GeV/nucleon for two trigger modes. These

correspond to impact parameters b < 6.76 fm (central trigger) and b < 11.9 fm (minimum bias trigger) in the geometrical model. The experiment was performed at the Bevalac using the Steamer Chamber Facility. Over 5300 pictures were accumulated for the different trigger modes. The techniques and experimental procedure have been described in ref. 2. A typical central-collision picture is shown in Fig. 1. Up to now only a small part of the data has been analyzed. The results presented below are based on 388 events for the central trigger and 202 events for minimum bias. Scanning was done twice with an efficiency better than 97%. Fig. 2 shows the total positive charged particle multiplicity distribution for the central (continuous line) and the minimum bias trigger (dotted line) respectively. The negative pion multiplicity distributions for both trigger conditions are shown in Fig. 3. The mean multiplicity values for these distributions (corrected for scanning efficiency) are displayed in Table I.

Table I

	minimum bias trigger	central trigger
$\langle n_{\pi^-} \rangle$	5.1	7.3
$\langle n_{tot^+} \rangle$	67.6	88.1

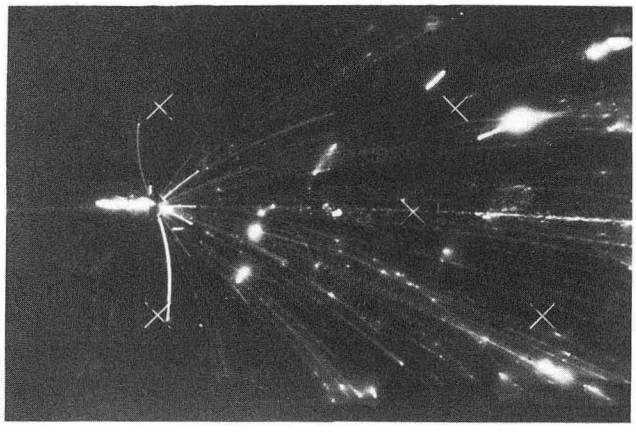

Fig. 1. Central $^{139}La+^{139}La$ collision at 1 GeV/nucleon. BBC 830-10386

We have found that in many interactions large fragments of the projectile survive the collision and appear as heavy fragments. This creates the need to identify their charge from the streamer chamber picture. We have observed that as the fragment's charge increases a larger number of high energy delta rays are produced that connect the ground and high voltage electrodes, creating a characteristic pattern.

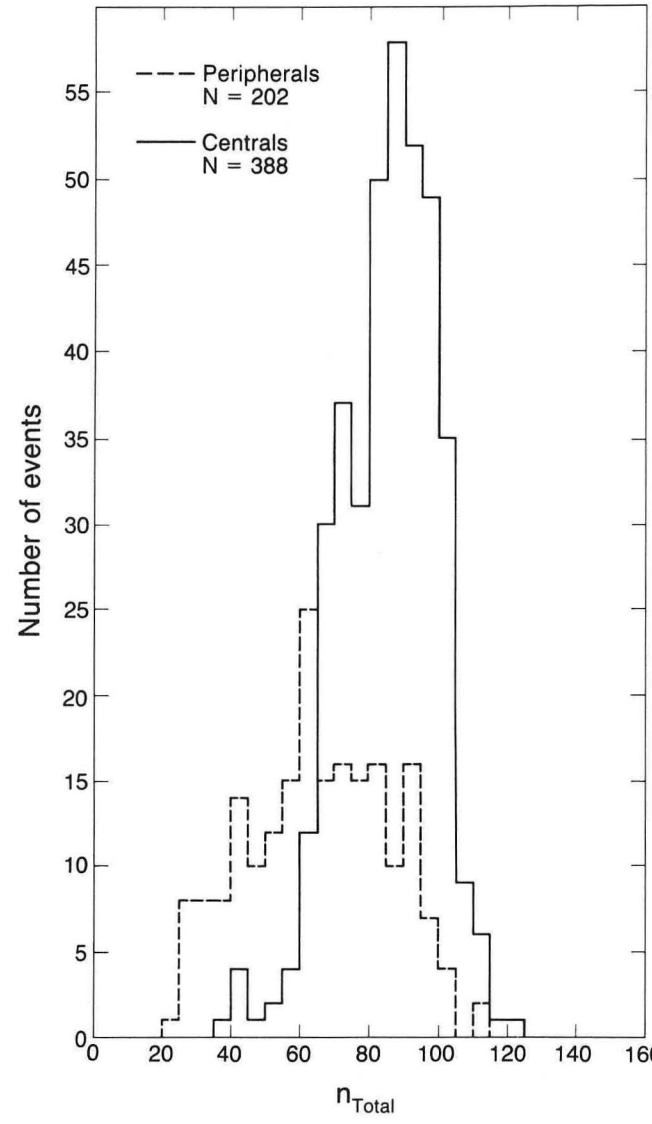

Fig. 2. Total positive charge multiplicity distribution for central (continuous line) and minimum bias (dashed line) trigger for the reaction La+La at 1 GeV/nucleon. XBL 830-6931

This effect can be used to do charge identification if it has enough of a dynamic range and charge resolution. From our previous experiments we have used Ne, Ar, Ca and La beams at the same energy to calibrate the Z dependence of the number of high energy delta rays per unit length identifiable in the streamer chamber pictures. This dependence is linear at these energies for the charge range studied (Fig. 4).

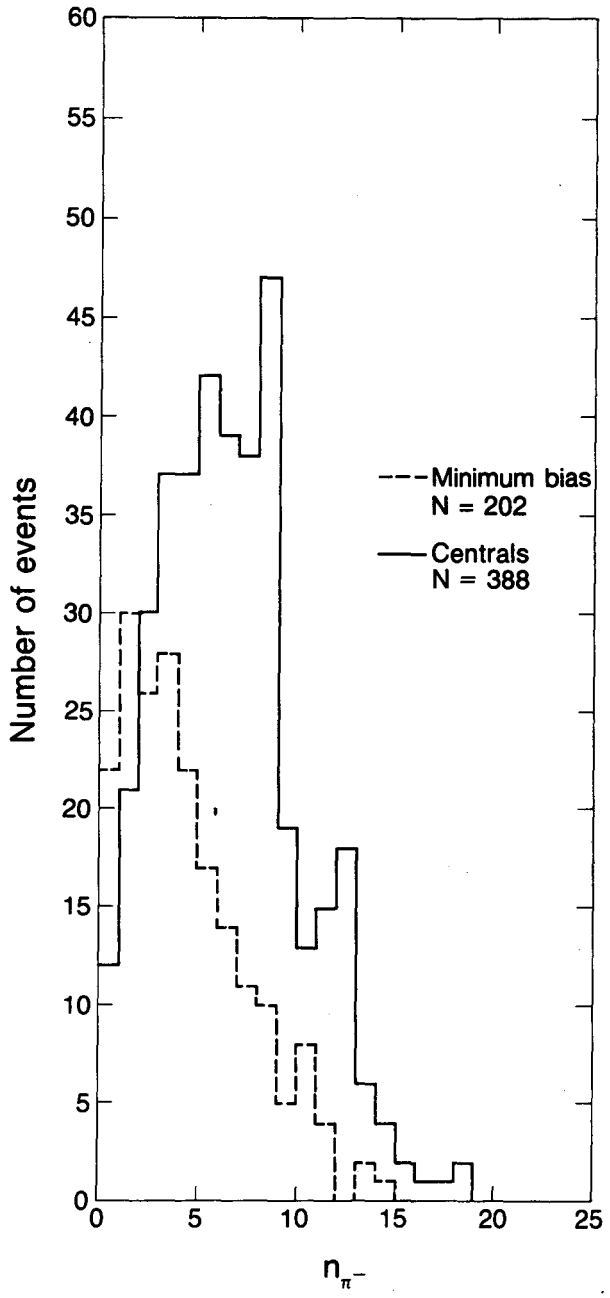

Fig. 3. Negative pion multiplicity distribution for central (continuous line) and minimum bias (dashed line) trigger for the reaction La+La at 1 GeV/nucleon. XBL 830-6932

Footnotes and References

*University of Marburg, 3550 Marburg, West Germany

†Gesellschaft für Schwerionenforschung, 6100 Darmstadt, West Germany

‡Instituto de Fisica, UNAM, Mexico D.F., Mexico.

§University of Heidelberg, 6900 Heidelberg, West Germany

**Texas A&M University, College Station, Texas 77843.

1. A.Sandoval *et al.* Nucl. Phys. **A400**, 365 (1983), and references there.
2. K. Van Bibber and A. Sandoval, LBL-12883 (1981).

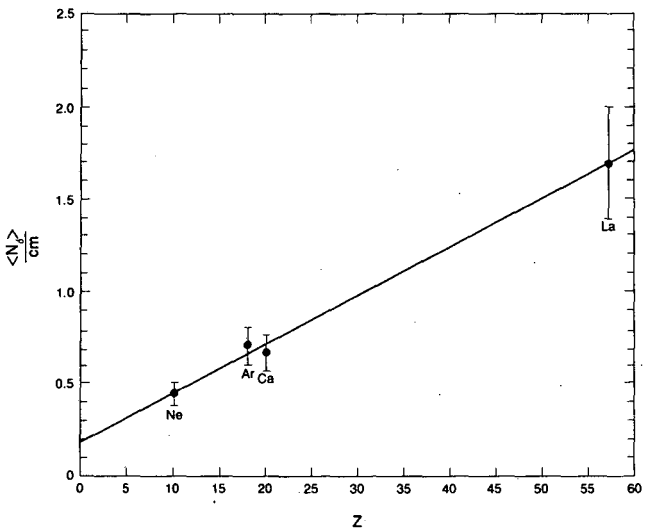

Fig. 4. Dependence of the number of delta-rays per unit length on the charge of the fragment at an energy of 1 GeV/nucleon. XBL 830-6933

Uranium Fragmentation at 900 MeV/nucleon

D.E. Greiner, T.J.M. Symons, H. Crawford, P.J. Lindstrom, H. Gould, J. Kidd,† and W. Schimmerling*

The acceleration of ^{238}U to relativistic energies at the Bevalac has opened a new area of study.[1,2] Very little is known experimentally about the physics of such highly charged energetic particles. In order to begin to study the reactions in this realm the basic questions about reaction rates and modes of fragmentation must be answered.

During an experiment to measure the equilibrium charge distributions of relativistic uranium in matter, a few hours of beam time was devoted to the first measurements of the nuclear cross sections of uranium on targets of various elements. The goal of the experiment was to measure the target mass dependence of the reaction and fission cross sections and to obtain some information on the probability of very central collisions. Such information tests the geometric models of the reaction mechanism and also provides necessary information for the design of future experiments.

Apparatus and Analysis

The uranium ions were injected into the Bevatron at charge state +68 from the SuperHILAC. The beam was accelerated to 962 MeV/nucleon, extracted and delivered to the experimental area. The ions then left the vacuum chamber through a 55 mg/cm^2 window and struck the experimental apparatus shown in Fig.1a.

Two 1 mm thick by 4.6 cm diameter position sensitive solid state detectors (D1, D2) were used to identify the beam charge and position before the target. These detectors assured us that fragments made in the window and the air of the cave were not used in the cross section determinations. The position determination required that the beam particles selected for reaction measurements were centered on the targets. Behind the target there was a solid state detector telescope (D3–10) consisting of two 1 mm thick by 4.6 cm diameter detectors and seven 5 mm thick by 7.6 cm diameter detectors to determine type of reaction which had taken place. Detector spacing was typically 8-9 mm, the target was 2 cm behind the second PSI and 12.5 cm in front of the D3-10 telescope. All particles produced in the target traveling within 10.4 degrees of the beam direction must hit the D3 detector. Targets ranged from CH_2 to Pb.

Data was collected whenever D1 and D2 were in coincidence and above one half of the normal beam pulse height. The signals from the detectors were amplified and then digitized using LeCroy 2259 peak sensing analog to digital units in CAMAC. Data was routed through the standard Heavy Ion Spectrometer System of data collection and diagnostics.[3]

In Fig. 1b is shown the pulse height spectrum in D3 when D1 and D2 record a $_{92}U$ beam particle centered on a Cu target. Basic to understanding the features of this data is the fact that at the energy used in this experiment the projectile fragments are moving at a velocity very close to the beam velocity. Because the projectile fragments move forward in a narrow cone, the detectors downstream of the target record the total energy loss of all projectile fragments from the reaction. Thus the signal is proportional to the *sum* of the charges squared of the fragments. Since our trigger scheme accepts un-interacted events, we have the known charge of the beam to calibrate the energy seen in the detectors. A useful variable is the effective charge of the particle or particles after the reaction. Because de/dx is proportional to Z^2 at constant velocity, the square root of the energy deposit is proportional to the charge of the particle. We define the effective charge, Z^*, as the square root of the energy deposit normalized so that the Z^* of the beam is 92. In our case there are frequently more than one particle present, however, Z^* is usually dominated by one or two particles. For instance, a $Z^* = 20$ event could be produced by: one $Z = 20$ particle, two $Z = 14.1$ particles, one $Z = 18$ + 76 protons, 100 alpha particles, 400 protons, etc.

Because we have only 92 charges available it is clear that only cases where one or two multiply charged particles dominate the signal are possible. At the higher Z^* regions the leading charges dominate more fully due to the Z^2 dependence of dE/dx.

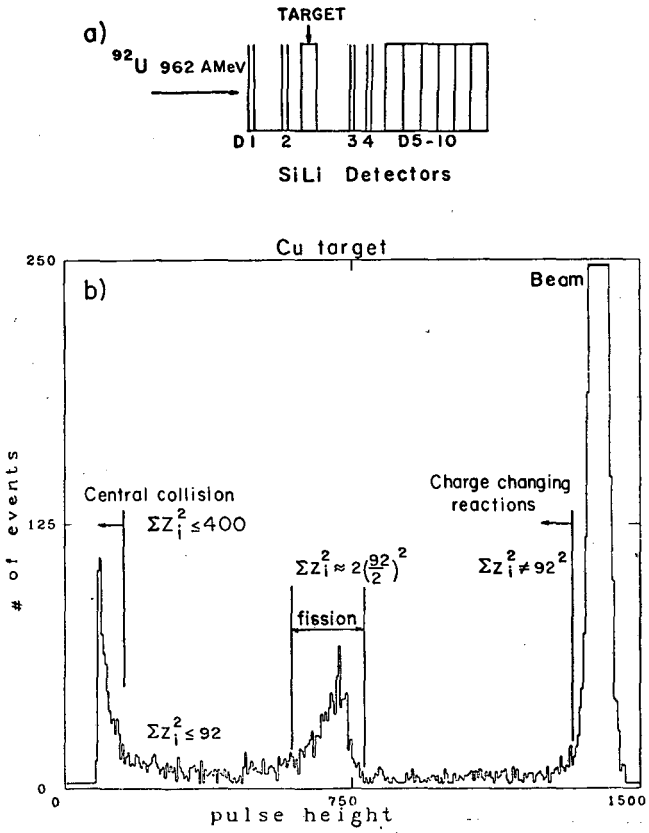

Fig. 1. a) Experimental apparatus: Detectors D1-4 are 1.02 mm thick, position sensitive solid state detectors with resistive read out. Detectors D5-10 are 4.72 mm thickness solid state detectors. The detectors downstream of the target subtend an opening angle of 60°.
b) Typical pulse height spectrum for detector D3 with the Cu target in place. The features common to all targets are: the large peak of un-interacted beam, the fission peak near dE/dx = half of the beam value and the destruction peak occurring at low dE/dx indicating loss of most of the highly charged particles in the forward direction. The cuts to determine the charge-changing, fission, destruction, and total destruction cross sections are shown. XBL 839-11829

With these considerations in mind let us turn to Fig. 2. Here we have plotted the Z^* spectra approximately equal numbers of reactions produced in the various targets. The spectrum from the hydrogen target was obtained by subtracting an appropriate number of carbon target events from the CH_2 date. We have cut off the Z^* scale at $Z^* = 86$ to avoid confusion with the tails of the un-interacted beam signals. The qualitative change in the nature of the signal is striking as the target mass increases. First, the peak at about $Z^* = 65$, is a clear indication that fission has taken place because two particles of about Z = 46 would have a Z^* of 65. This semi-raw data then shows us in a qualitative fashion that the reaction of uranium with hydrogen is dominated by fission and that the fission process becomes less and less prominent as the target mass increases. Also we see that there is a drastic increase of low Z^* events as the target mass increases to such an extent that this feature competes with fission as the most favored topology in the reaction. These low Z^* events are naturally interpreted as violent events where the bulk to the projectile is broken up in the reaction. The probability of catastrophic collisions is of more than passing interest, such events are the first place where one expects new phenomena to be exhibited due to the possibilities of high nuclear temperatures and densities. In a longer report we will quantify the reaction modes we have shown here.

Charge-Changing Cross Section

At the right of the graph in Fig. 1b is the peak produced by the un-interacted beam which defines the signal produced by the detector for Z = 92. The difference in the integrated beam flux before and after the target measures the cross section for charge-change (after suitable subtraction of target out contributions). Due to the fact that this experiment is insensitive to neutron removal, we quote the charge changing cross section which is a lower limit to the actual reaction cross section. The analysis methods are essentially the same as those used in an earlier experiment described in ref. 4. One further target (Si) is made available by looking at the decrease of beam flux in the telescope itself.

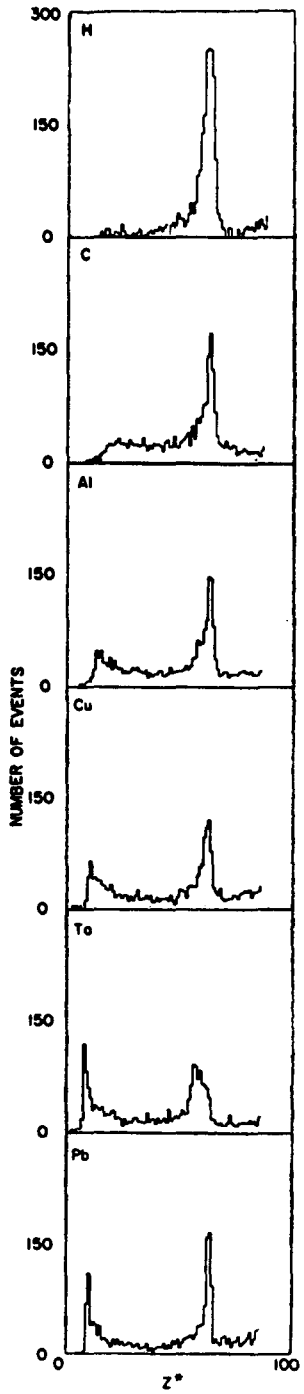

Fig. 2. Effective charge of fragments after the target. Samples show equal numbers of reactions with the H target values obtained by subtraction of C from CH_2. Interesting features include: the predominance of fission indicated by the peak at $Z^* = 65$ and the growth of the central collision component at the low Z^* in the heavier targets. XBL 839-11825

The charge-changing cross sections present a problem when one seeks to compare with theory because they are not usually calculated. We know that the unobserved neutron removal component of the cross section is appreciable from the fact that up to 12 neutrons can be removed from the uranium and still produce a nucleus long-lived enough to appear as Z = 92 in our detectors. However, something can be learned by the following chain of reasoning: First, in Fig. 3, we compare the data to the standard geometrical overlap model. The overlap model has the following form:

$$\sigma = \pi R_0^2 (A_t^{1/3} + A_b^{1/3} - \delta)^2$$

where we take $R_0 = 1.4 \times 10^{-13}$ and $\delta = 1.0$ which are values found to fit heavy ion reactions in the region of Ab = 12 – 56.[5] The fit is quite poor. The overprediction at low target masses is probably due to nuclear transparency effects. At target masses above 40 amu the underprediction may be explained by the fact that Coulomb processes become significant. Further insight is found by comparing with the soft-spheres model of Karol.[6] This model uses tapered nuclear density distributions and should account for the transparency effect; however Coulomb effects are specifically ignored. In applying this model we have allowed the nucleon-nucleon cross section input parameter to be variable. The resultant best fit value of 20 mb is an effective nucleon-nucleon cross section for the charge-changing portion of the reaction cross section. The open triangles in Fig. 3 show the agreement is good up to a target mass of 40 amu. The discrepancy above 40 amu target mass may be due to Coulomb effects, however, the data is not statistically significant to extract a Z^2 deviation. The difference between our effective nucleon-nucleon cross section and the experimental value of 40 mb for this energy range may be interpreted as being due to the lack of observation of the neutron removal contribution to the reaction cross section. If this interpretation is true, then the reaction cross section is larger than the charge-changing cross sections reported here by 13% for a hydrogen target to 6% on the lead target.

Because the energy loss in the detectors is appreciable, the silicon target measurement is available as a function of beam energy. The energy dependence of the charge-changing cross section of uranium on silicon is negligible at the level of our statistics over the range 150 – 962 MeV/nucleon (Fig. 4). This behavior would be expected if the reaction is primarily determined by geometrical effects as we have concluded above from the success of the Glauber approach for the lighter targets.

Fission Cross Section

The peak at half the beam pulse height is caused by the events where fission of the uranium took place (Fig. 1). When fission takes place the fragment charges are both close to half the uranium charge, thus we expect to see a signal $(Z/2)^2 + (Z/2)^2 = Z^2/2$. The asymmetric events broaden the peak out and a small component of Z = 1, 2 fragments shift the peak slightly toward lower pulse heights. The fission cross sections were calculated by integrating the events in the area of the fission peaks, subtracting background from target out and also subtracting the continuum produced by fragmentation events that produce a single highly charged fragment. The continuum was estimated by smoothly connecting the continuum areas on each side of the fission peak. The fission cross section of ^{238}U when bombarded with 1 GeV protons has been measured previously using emulsion techniques by Bochagov *et al.*[7] Their value of 1.4±.1 barns agrees quite well with our value of 1.3±.1. Thus we have some corroboration to engender confidence in our method of extracting the fission portion of the reaction.

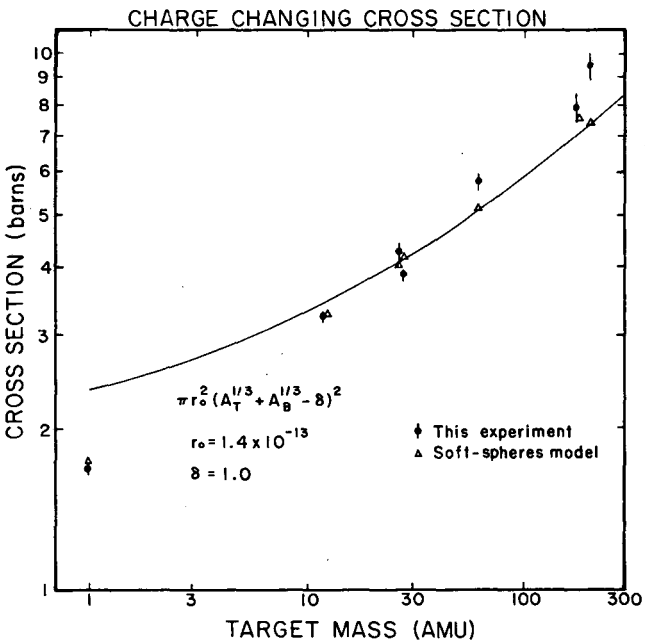

Fig. 3. The charge-changing cross section (•) plotted as a function of target mass. The solid curve is the best fit of the geometrical model which assumes that the nuclei are black disks and a certain overlap is required for interaction. A Glauber[7] reaction cross section calculation is shown as the (Δ) points.

XBL 8311-4645

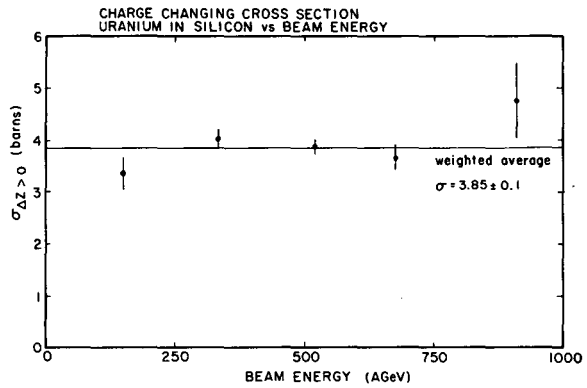

Fig. 4. Cross section, dZ > 1, for various energies of the ^{238}U as it penetrates the detector stack. There is no statistically significant evidence for energy variation of this cross section over the energy range observed.

XBL 839-11826

Footnotes and References

*Space Sciences Laboratory, UCB.

†Naval Research Laboratory, Washington D.C. 20375.

1. H.H. Heckman, Y.J. Karant, and F.M. Friedlander, Science **217**, 1137 (1982).
2. E.M. Friedlander, H.H. Heckman, Y.J. Karant, Phys. Rev. **C27**, 2436 (1983).

3. *Data Acquisition at the Bevalac, an example: The HISS Facility* C. McParland, to be published in IEEE Transactions on Nuclear Science Topical Conference on Computerized Data-Acquisition Systems in Particle and Nuclear Physics, Oct. 1983.
4. G.D. Westfall, Lance W. Wilson, P.J. Lindstrom, H.J. Crawford, D.F. Greiner, H.H. Heckman, Phys. Rev. **C19**, 1309 (1979).
5. H.H. Heckman, D. E. Greiner, P.J. Lindstrom, and H. Shwe, Phys. Rev. **C17**, 1735 (1978).
6. Paul J. Karol, Phys. Rev. **C11**, 1203 (1975).
7. B.A. Bochagov *et al.*, Sov. J. Nucl. Phys. **28(2)**, 291 (1978).

Charge Distributions of 962 and 430 MeV/nucleon U in Matter

H.J. Crawford, H. Gould, D.E. Greiner, P.J. Lindstrom, and T.J.M. Symons*

We present charge state distributions for 962 and 430 MeV/nucleon U ions passing through target foils of CH_2, Cu and Ta. Charge distributions for various target thickness are used to determine single electron capture and stripping cross sections.

The number of electrons localized on an ion traversing matter, i.e., its charge state Q, fluctuates due to its interaction with the electrons and nuclei of the matter. Very fast ions spend most of their time in matter fully stripped of electrons while very slow ions may have their full complement of electrons, or more. Slow and fast are relative terms with the scale being set by the velocities associated with electron orbitals for the ion and the matter traversed. The probability of an ion having a charge Q in matter depends on the ion's velocity, the composition of the matter and on the initial Q of the ion when it entered the matter. For sufficiently deep penetration of the matter the dependence on initial Q disappears and an equilibrium occurs in which the probability of a given Q becomes independent of position in the matter.

The equilibrium charge state distribution for relativistic heavy ions is of interest in studying cosmic ray propagation, in investigations of energy loss in matter, and in design of heavy ion accelerator and beam transport systems. We have measured the charge state distribution for 430 MeV/nucleon and 962 MeV/nucleon U ions as a function of target charge and thickness for beams delivered from the Bevalac.

The experimental setup is shown in Fig. 1. U ions were accelerated in charge state Q = +68 (i.e., ions having 24 electrons still attached) and delivered through a high vacuum beam line to a focus in the target area of the Beam 40 Zero Degree Spectrometer. There they were passed through thick free standing foils of C, Mylar, CH_2, Cu or Ta.

We show in Fig. 2 the charge state distributions emerging from foils of thickness from 0.65 to 650 mg/cm^2. Note that equilibrium is reached in the last two foils whose thicknesses are 380 and 640 mg/cm^2.

The equilibrium charge state distributions are shown for various targets for 962 and 430 MeV/nucleon U in Fig. 3. This shows that Ta is the most efficient stripper for the 962 MeV/nucleon beam, but that Cu is more efficient at 430 MeV/nucleon.

*Space Sciences Laboratory, Univ. of Calif., Berkeley, Calif.

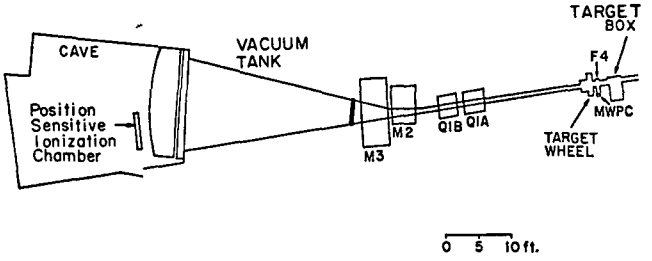

Fig. 1. Diagram of experimental setup.

XBL 8311-4672

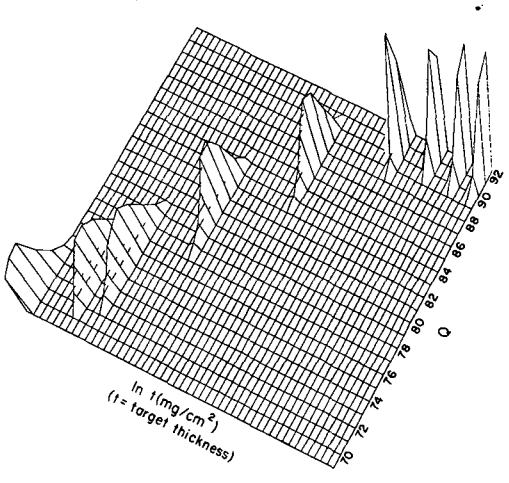

Fig. 2. Charge state distribution as a function of target thickness for C, CH_2 and Mylar targets.

XBL 8311-4642

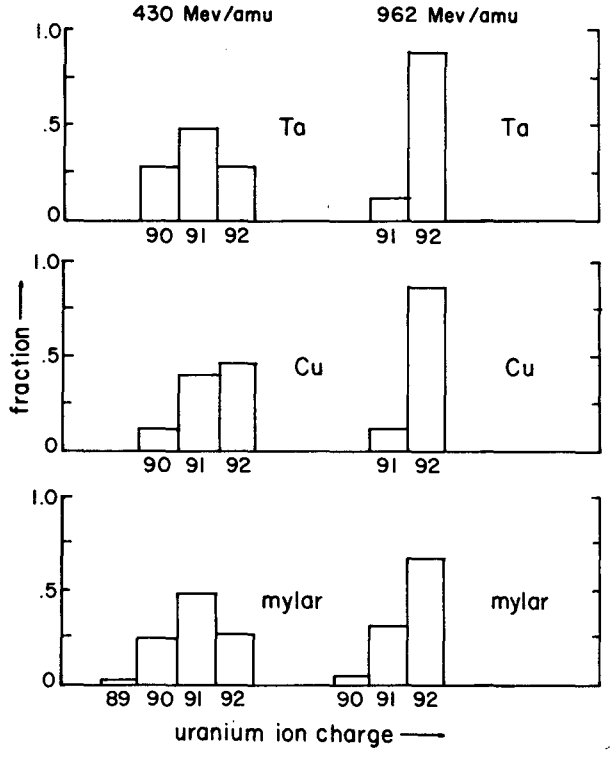

Fig. 3. Equilibrium charge state distributions for 962 and 430 MeV/nucleon U beams in Mylar, Cu and Ta targets.

XBL 835-9640

Particle-Gamma Coincidence Measurements in ^{12}C + ^{12}C and ^{12}C + Pb Collisions at 2.1 GeV/nucleon Incident Energy, First Results – γ-Ray Spectrum

G. Roche, J. Carroll,† C.C. Chang,‡ T. Hallman,§ P.N. Kirk,** R. Koontz, G. Krebs,** L. Madansky,§ T. Mulera,† H. Pugh, L. Schroeder, J. Vicente**

High-energy γ-rays are mainly produced through π° decay in relativistic heavy ion collisions at incident energies in the range 1–2 GeV/nucleon. Other possible contributions are: nucleus-nucleus bremsstrahlung, η-meson production, and $\Delta(1232)$ decay. Up to now, only a few experimental studies have been done on this subject.[1-3] More recently, γ-ray measurements have been performed to study projectile fragments having an anomalously short interaction length, i.e., the so-called anomalons.[4-8] Liss, *et al.*[9] have searched for single delayed gammas as an eventual decay process. Their negative result does not completely rule out a possible electromagnetic decay of an anomalous state, because their

measurement was done at 940 MeV/nucleon, an energy at which it has been suggested[7] that the effect could have disappeared.

We have undertaken a different approach to the study of anomalous fragments. The study is done in the target fragmentation region, where we look for singly charged anomalous fragments through particle-gamma coincidence measurements. On the theoretical side, Frederiksson, *et al.*[10] suggest the existence of a possible six-quark deuteron state that we estimated could produce a γ-ray around 200–300 MeV. Our experimental method consists then in looking for any sharp line or bump in the γ-ray spectra in coincidence with particles and, ultimately, looking for any signal in the particle-gamma invariant mass distribution. We present here the experimental setup and preliminary results on the measured gamma-ray spectrum.

The experimental configuration is shown in Fig. 1. The multiwire proportional chambers WC2 and WC3 were used for beam alignment and the ionization chamber IC for beam intensity measurement. Photons and charged particles produced in the target T were detected in a thick NaI crystal system and two ΔE-E telescopes TEL2 and TEL3. The detector system NaI consists of a plastic scintillator V used as a charged particle veto, a 1″ thick NaI crystal in which the shower is generated, a plastic scintillator C, which detects the γ-ray conversion, and two 5″ thick NaI crystals in which the shower deposits the rest of its energy. The signal from the annular plastic scintillator H was used off-line as a veto to better select the showers emitted around the central axis of the system. The neutron contamination is less than ~1%, and the overall resolution was determined to be ~30% at 130 MeV (for minimum ionizing cosmic rays). The telescope TEL2 consists of two 1-mm thick silicon detectors with a 3-in thick NaI crystal, and TEL3 consists of five identical elements made with a plastic scintillator (0.5 inch) and a 5-in NaI crystal. The overall resolutions for TEL2 and TEL3 are, respectively, ~10 MeV at 50 MeV and 7 MeV at 100 MeV, for protons. The angles between the beam direction and the detector axes are 41° for TEL2, 45° for TEL3, and 124° for NaI, and the azimuthal angles between TEL2/TEL3 and NaI are, respectively, 168/127°.

Gamma-ray spectra have been extracted off-line for both C and Pb targets, both TEL2·NaI and TEL3·NaI coincidence requirements, and the four following conditions:

Condition 1: anything in the particle telescopes satisfying the coincidence requirement,

Condition 2: same as 1 plus a little higher energy threshold in the particle telescopes,

Condition 3: protons in the particle telescopes (20–120 MeV for TEL2, 40–200 MeV for TEL3),

Condition 4: deuterons in the particle telescopes, (30–180 MeV for TEL2, 60–300 MeV for TEL3).

The most inclusive γ-ray measured cross sections are those under condition 1. For conditions 3 and 4, the energy spectra of the charged particles were also extracted, and the invariant mass distributions computed on an event-by-event base. Fig. 2 shows an example of γ-ray spectrum obtained under condition 1, for a Pb target and detectors TEL2·NaI. The solid line is an exponential fit of the spectrum above 90 MeV to the form, $A \exp(-E_\gamma/T)$, where A and T are the parameters. Table 1 gives the values of T for our data. These numbers do not seem to depend much on the type of condition, except perhaps for condition 4, where we have a lower value for Pb and a higher one for C (with large errors). They are consistent with Budiansky, *et al.*[3] measurements at 2 GeV/nucleon incident energy (central trigger), from which one obtains:

$$T = 173 \text{ MeV for Ar + Pb} \rightarrow \gamma\ (30°)$$
$$T = 70 \text{ MeV for Ar + Pb} \rightarrow \gamma\ (90°)$$

Finally, there are no obvious sharp lines or bumps in our γ-ray spectra or mass distributions so far obtained. More data are in the final stage of analysis, which should allow us to draw stronger conclusions very soon.

Table 1

Tgt	Condition	T(MeV) TEL2·NaI	TEL3·NaI
Pb	1	63.9 ± 4.1	62.5 ±3.0
	2	62.9 ± 4.3	63.1 ±2.8
	3	59.9 ±10.0	65.2 ±4.4
	4	55.7 ±10.0	50.8 ±5.8
C	1	88.9 ±14.9	72.5 ± 5.6
	2	79.0 ±12.7	70.7 ± 6.5
	3		73.8 ± 7.6
	4		98.5 ±19.1

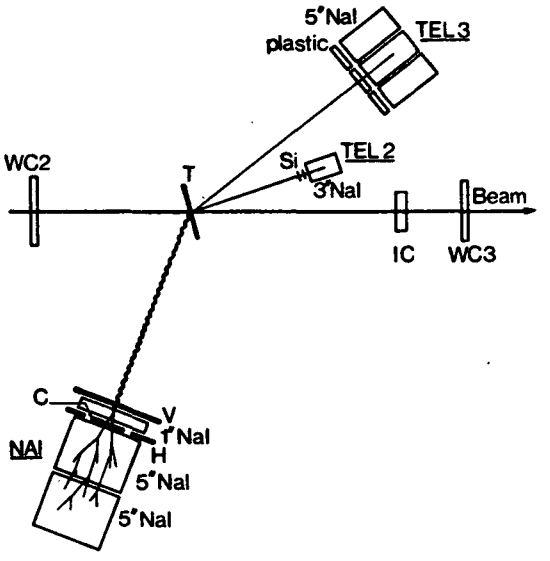

Fig. 1. Experimental setup. XBL 8312-2567

Footnotes and References

*Université de Clermont-Ferrand, IN2P3, France.
†University of California, Los Angeles, CA 90024.
‡University of Maryland, College Park, MD 20742.
§Johns Hopkins University, Baltimore, MD 21218.
**Louisiana State University Baton Rouge, LA 70803.

1. W. Dejarnette, *et al.*, Phys. Lett. **94B**, 327 (1980).
2. T. Hallman, *et al.*, unpublished.
3. M.P. Budiansky, *et al.*, Phys. Rev. Lett. **49**, 361 (1982).
4. B. Judek, Can. J. Phys. **46**, 343 (1968).
5. B. Judek, Can. J. Phys. **50**, 2082 (1972).
6. E.M. Friedlander, *et al.*, Phys. Rev. Lett. **45**, 1084 (1980).
7. P.L. Jain, *et al.*, Phys. Rev. Lett. **48**, 305 (1982).
8. H.B. Barber, *et al.*, Phys. Rev. Lett. **48**, 856 (1982).
9. T.M. Liss, *et al.*, Phys. Rev. Lett. **49**, 775 (1982).
10. S. Frederiksson, *et al.*, 5th High Energy Heavy Ion Study, May 18–22, (1981), LBL-12652, UC-34, CONF-8105104.

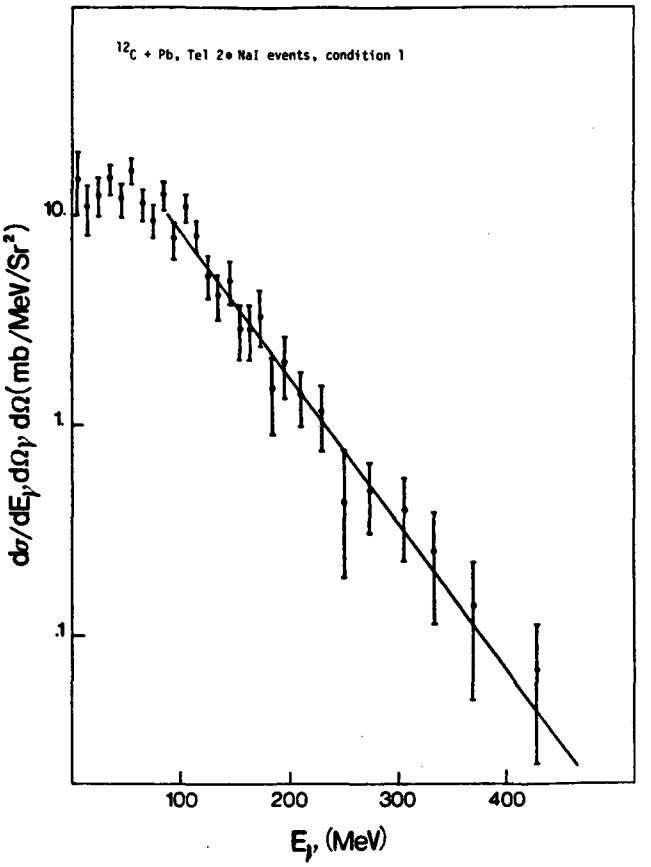

Fig. 2. A γ-ray spectrum. XBL 8312-2568

Inclusive Measurements of Pions and Light Fragments in 800 MeV/nucleon $^{139}_{57}$La + $^{139}_{57}$La Collisions

X. Bai, H. Hamagaki,† O. Hashimoto,† K. Kimura,‡ T. Kobayashi,† Y. Miake,§ S. Nagamiya,§ G. Shapiro, Y. Shida** and I. Tanihata***

With the upgraded Bevalac it has now become possible to study high energy heavy ion collisions with projectiles as heavy as uranium. Measurements of inclusive spectra of pions and light fragments are expected to provide valuable information about reaction mechanisms, as they have already done in the case of lighter mass projectiles such as C, Ne and Ar.[1] Up to now no clear evidence for collective phenomena have been detected in these experiments. A possible reason is that the sizes of the nuclei involved in these processes have been too small. With much heavier projectiles such as La or U, we may increase our chance for observing nuclear collective phenomena.

The 800 MeV/nucleon La beam was accelerated at the upgraded Bevalac. The beam intensity on the target was as high as 10^6 particles/spill. A magnetic spectrometer was used to measure negative pions in the momentum range above 150 MeV/c and light fragments between 400 MeV/c and 2000 MeV/c at laboratory angles of 15, 20, 40, 60, 80 and 90°. The experimental set up was the same as that described in ref. 1 except that the spectrometer was modified so that it could handle events with higher multiplicities. In addition, two sets of ΔE-E counter telescopes were installed to detect protons and deuterons in the momentum range from 350 MeV/c to 700 MeV/c at laboratory angles between 80° and 120°.

In Fig. 1 we show a proton energy distribution at 90° c.m. for the La + La reaction together with the C + C, Ne + NaF and Ar + KCl reactions. We will briefly mention three interesting points:

(1) The slope parameter in the case of La (~82 MeV) is slightly larger than that for Ar (~79 MeV). In the light mass system, we note that the heavier the projectile and the target masses are, the less steep is the slope of 90° c.m. spectra. This tendency holds for La, but the difference in the slope parameter between La + La and Ar + KCl seems to be small.

(2) In the 90° c.m. proton spectrum shown in Fig. 1, the shoulder structure of the spectrum in the low energy region, which is common to a lighter mass system, appears less distinct in La + La. The exponential slope seems to extend down to very small kinetic energy in contrast to the lighter nucleus case. Our interpretation of this result is that the system may be more equilibrated because of the larger number of collisions made by the proton before it comes out of the reaction region.

(3) The slope parameter of the pion spectrum for La seems to be somewhat steeper (~57 MeV) than that for Ar (~66 MeV). This may again be related to the increase in the average number of collisions in larger systems.

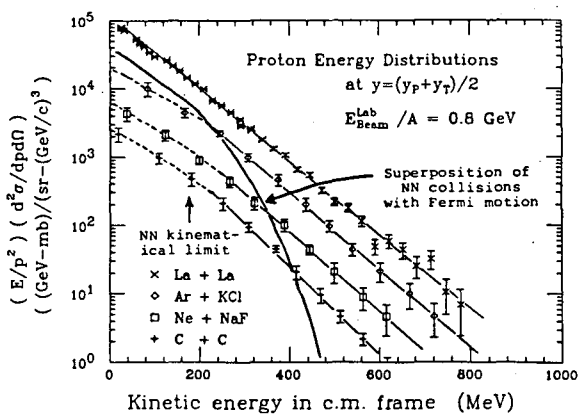

Fig. 1. Proton energy distribution at 90° c.m. in 800 MeV/nucleon La + La collisions together with C + C, Ne + NaF and Ar + KCl collisions. XBL 841-27

Footnotes and Reference

*Institute of Atomic Energy, Beijing, China
†Institute for Nuclear Study, University of Tokyo, Tanashi, Tokyo 188 Japan and LBL
‡Department of Physics, Kyushu University, Fukuoka, Japan
§Department of Physics, University of Tokyo, Hongo, Tokyo, Japan
**Institute for Nuclear Study, University of Tokyo, Tanashi, Tokyo 188 Japan

1. S. Nagamiya, M.C. Lemaire, E. Moeller, S. Schnetzer, G. Shapiro, H. Steiner and I. Tanihata, Phys. Rev. **C24**, 971 (1981).

Measurement of High P_T Light Fragments at 90° C.M. in 800 MeV/nucleon ^{12}C + ^{12}C Collisions

X.X. Bai, H. Hamagaki,† O. Hashimoto,† S. Kadota,† K. Kimura,‡ Y. Miake,§ S. Nagamiya,§ K. Omata,** Y. Shida,** I. Tanihata,† and N. Yoshikawa***

The study of emission of light fragments at 90° c.m. is an interesting subject for various reasons. For example, in p + A collisions protons emitted at 90° c.m. cannot have an energy greater than $E_{max} \approx$ 517 MeV from a simple consideration of kinematics. The emission of protons at 90° c.m. having kinetic energy above 517 MeV is possible only in nucleus-nucleus collisions. Detailed studies of such high p_T protons will enable us to probe short range correlations, cluster scatterings and high temperature phase in high energy heavy ion reactions.

In the past, the proton energy distribution at 90° c.m. in 800 MeV ^{12}C + ^{12}C collisions has been measured for proton energies up to 700 MeV.[1] The spectrum shows a "shoulder-arm" shape with a turning point between the shoulder and arm located at $E_p^{c.m.} \sim 200$ MeV. Above that energy the spectrum shape approaches an exponential,

$$E\,(d^3\sigma/dp^3) \propto \exp\,(-E_p^{c.m.}/E_0)\ , \qquad (1)$$

with $E_0 \approx 68$ MeV. In the present experiment, we have extended the previous measurements to $E_p^{c.m.} \approx 1100$ MeV, where the cross section is four orders of magnitude lower than that at $E_p^{c.m.} = 700$ MeV.

A layout of the experimental setup is shown in Fig. 1. The Heavy Ion Spectrometer System (HISS) at the Bevalac was used. We report measurements of inclusive spectra by the A-arm shown in Fig. 1. The A-arm consists of a small scintillator (TA1) and two sets of multi-wire proportional chambers (WCA1, WCA2) inside the magnet, and two sets of drift chambers (DC1, DC2) and two scintillator hodoscopes (TA2, TA3) outside the magnet. Particle identification was almost perfect up to $p_{lab} \approx 4$ GeV/c. The momentum resolution was typically ~6% at $p_{Lab} \sim 3$ GeV/c.

Fig. 2 shows the observed proton energy spectra at 90° c.m. in 800 MeV/nucleon ^{12}C + ^{12}C collisions. Open circles indicate the present results,

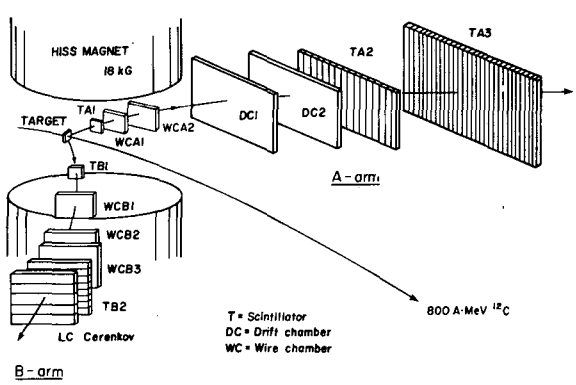

Fig. 1. Layout of the experimental setup.

XBL 8210-1240

whereas closed circles show the data reported in ref. 1. These data span a range of invariant cross sections over eight orders of magnitude. The solid line in Fig. 2 shows the previous fit[1] with an exponential shape given by Eq. (1). Clearly, the data show a smooth inward deviation from this exponential in the high-energy region above ~700 MeV. It is noted that the slope of the spectrum in the high energy region is quite similar to that for negative pions.[1] The dot-dashed curve in Fig. 2 shows the phase-space calculation by Knoll,[2,3] and the dashed curve shows the cascade calculation using the code of Cugnon.[4] The cascade calculation gives a reasonable fit in the low-energy region, while it gives a steeper slope than the data in the high-energy region. The phase-space calculation explains the data very well in the high-energy region, although the fit is not good in the low-energy region. These results may suggest that some coherent mechanism other than random multiple nucleon-nucleon collisions is important in describing proton emission in the high-p_T region.

Deuteron and triton spectra at 90° c.m. are shown in Fig. 3. Deuteron cross sections cover about 7 orders of magnitude and triton about 5 orders. In both cases we have tried to compare the data with squares and cubes of the observed proton cross sections, respectively, as expected from a coalescence model.[5,6] Amazingly, for such large orders of magnitudes the cross sections satisfy the coalescence relation of

$$[E\,(d^3\sigma/dp^3)]_A = C_A\,[E\,(d^3\sigma/dp^3)]_p^A \qquad (2)$$

$$\text{for } \vec{p}_A = A\cdot\vec{p}_p\ .$$

We may conclude that both the deuteron and triton are formed through final state interactions among nucleons over a wide range of kinetic energy. It should also be noted that the slopes of the spectra are not necessarily related directly to the temperature of the system at which these composite particles are created.

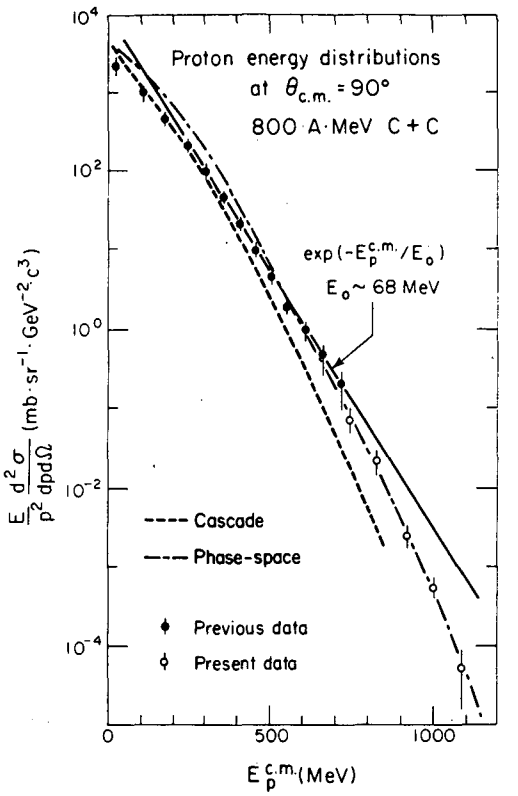

Fig. 2. Proton energy distribution measured at 90° c.m. in 800 MeV/nucleon ^{12}C + ^{12}C collisions. Data are compared with the phase-space model (dot-dashed curve) and the cascade model (dashed curve). XBL 839-872A

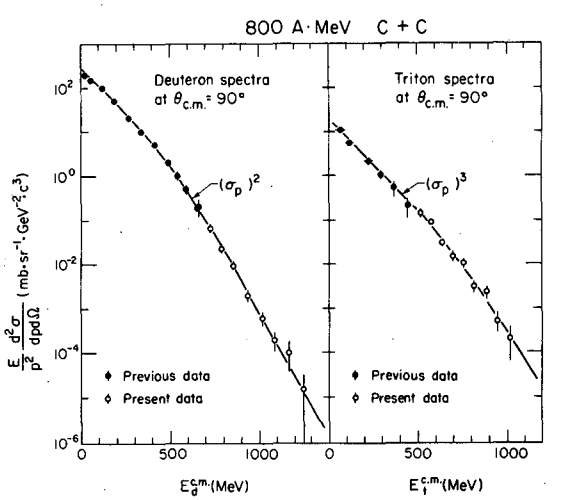

Fig. 3. Deuteron and triton spectra measured at 90° c.m. in 800 MeV/nucleon ^{12}C + ^{12}C collisions, as compared with squares and the cubes, respectively, of the observed proton spectra. XBL 839-871

Footnotes and References

*Present address: Institute of Atomic Energy, P.O. Box 275, Beijing, People's Republic of China.
†Institute for Nuclear Study, University of Tokyo, Tanashi, Tokyo 188 Japan and LBL
‡Present address: Department of Physics, Kyushu University, Hakozaki, Higashiku, Fukuoka-shi, 812, Japan.
§Present address: Department of Physics, University of Tokyo, Hongo, Bunkyo-ku, Tokyo, 113, Japan.
**Institute for Nuclear Study, University of Tokyo, Tanashi, Tokyo 188 Japan

1. S. Nagamiya, M.-C. Lemaire, E. Moeller, S. Schnetzer, G. Shapiro, H. Steiner, and I. Tanihata, Phys. Rev. C **24**, 971 (1981).
2. J. Knoll, Phys. Rev. C **20**, 773 (1979).
3. The calculation by the phase-space model was done by J. Knoll, private communication (1983).
4. J. Cugnon, T. Mizutani, and J. Vandermeulen, Nucl. Phys. **A352**, 505 (1981).
5. H.H. Gutbrod, A. Sandoval, P.J. Johansen, A.M. Poskanzer, J. Gosset, W.G. Meyer, G.D. Westfall, and R. Stock, Phys. Rev. Lett **37**, 667 (1978).
6. M.-C. Lemaire, S. Nagamiya, S. Schnetzer, H. Steiner, and I. Tanihata, Phys. Lett. **85B**, 38 (1979).

The Production of Negative Pions at $\Theta_{c.m.} = 90°$ from the 246 MeV/nucleon $^{139}La + ^{139}La$ Reaction

G.F. Krebs, J.-F. Gilot,* P.N. Kirk,* L.S. Schroeder, J. Miller, H.G. Pugh, G. Roche,† J. Vicente,† W. Benenson,‡ K. Beard,‡ H. van der Pflicht,‡ B. Sherill,‡ and J.W. Harris§*

The pion production cross section for the inclusive reaction La + La $\rightarrow \pi^- + X$ was measured at an incident energy of 246 MeV/nucleon for pions produced at 90° in the center-of-mass (c.m.)

The primary goal of this experiment was to test the theoretical prediction of a pionic instability effect related to pion condensation.[1] In this theory Gyulassy predicts that a new phase of pionic instability might be created in nucleus-nucleus collisions at 2 $m_\pi c$ at 90° c.m. So far pion production cross sections have been measured at incident energies of 400, 800 and 2100 MeV/nucleon.[2,3] At these energies the cross section for incoherent pion production is much larger than the predicted excess of pions from a condensate and would obscure any possible signal. Recently, a measurement of the pion production cross section was made at an incident energy of 183 MeV/nucleon with a target-projectile system of A = 20 where no effect was observed.[4] However, in his paper Gyulassy stresses the importance of using the heaviest target-projectile combination possible. In order to see the proposed effect we have used a beam energy below the pion production threshold of 290 MeV in N-N collisions with a high intensity heavy beam, ^{139}La.

The cross sections were measured with the two-armed spectrometer system (TASS) at the Bevalac. The TASS system has been fully described elsewhere.[5] Only the front arm of TASS was used with two additional multi-wire proportional chambers added. A La beam of charge state +29 with a circulating energy of 255 MeV/nucleon was brought to a focus on a 400 mg/cm^2 La target. The average energy of the beam at the center of target was 246 MeV/nucleon. Mounted 1 cm upstream of the target was a wire chamber which allowed the beam to be centered on target. To reduce the uncertainty in the beam energy due to ionization (dE/dx), the target and wire chamber were mounted inside a vacuum box, and the wire chamber was removed from the beam during data collection. An 800 MeV/nucleon Ne beam was utilized to measure the

cross section from the inclusive reaction Ne + NaF $\rightarrow \pi^- + X$ as a check on the TASS system and our overall normalization. We found our measured pion cross section from this reaction to be in excellent agreement with the results of Lemaire *et al.*[6], at the same energy and production angle. The number of La ions incident on the target was determined using an ion chamber. A ^{11}C activation study was carried out as well, where the total cross section for the reaction $^{139}La + {}^{12}C \rightarrow {}^{11}C$ was scaled as $A^{2/3}$ to simulate the La target.[7] We found the results of the two La calibration procedures to be consistent with each other to ± 10%. Typically we obtained 3×10^7 La ions/pulse at our target. The overall error in the absolute value of the cross sections presented here is estimated to be ± 20%.

Fig. 1 shows preliminary results for the inclusive pion production cross section at 90° ± 4° c.m. For the angular and magnetic field settings used in this experiment the TASS system was capable of measuring pions from 50 to 550 MeV (c.m.). However, no pions were detected past 365 MeV (c.m.). The solid line is a least mean square fit to the expression exp $(-T^{\pi}_{c.m.}/T_0)$. The slope parameter is $T_0 = 32 \pm 4$ MeV. The dashed line is the excess pion cross section predicted at $E_{c.m.} = 2m_{\pi}c$ by the theory of Gyulassy.[1] We see no evidence of a bump or change of slope due to pion condensation which would support the theoretical prediction of Gyulassy. The data taken will be compared to the existing theoretical models such as the intranuclear cascade model of Cugnon.[8] Further analysis will also compare the 90° c.m. data to 50° c.m. data taken during this experiment to check for isotropy.

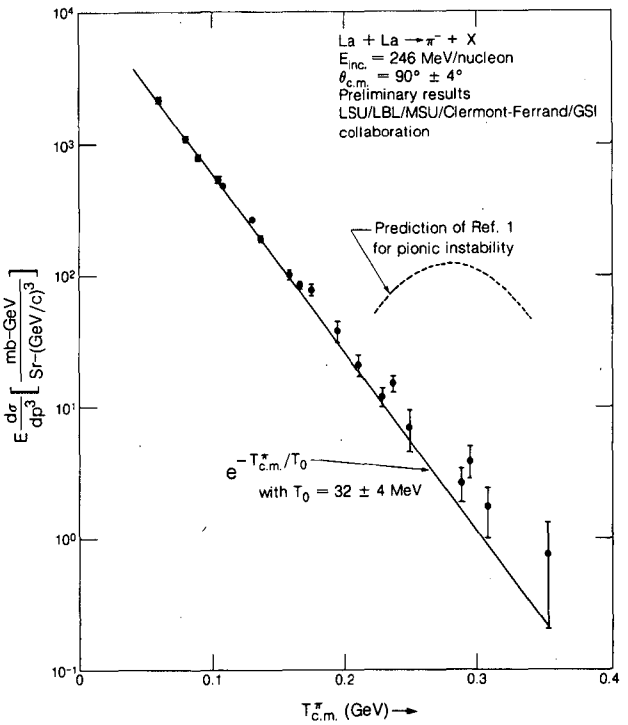

Fig. 1. The invariant cross section vs. the c.m. kinetic energy for the La + La $\rightarrow \pi^- + X$ inclusive reaction at 90° c.m. The incident energy is 246 MeV/nucleon. T_0 is the inverse slope parameter when the cross section is parameterized by exp $(-T^{\pi}_{c.m.}/T_0)$. A least square fit using this parameterization is shown as a solid line. The dashed curve is the expected cross section for pionic instability as calculated in ref. 1. Error bars are statistical in origin. XBL 8312-6860

Footnotes and References

*Department of Physics and Astronomy, Louisiana State University, Baton Rouge, Louisiana 70803.
†Université de Clermont II - IN2P3 - Ferrand, Clermont-Ferrand, France, 63170.
‡Michigan State University, East Lansing, Michigan, 48824.
§Gesellschaft für Schwerionenforschung, D-6100, Darmstadt, Germany.

1. M. Gyulassy, Nucl. Phys. **A354**, 375 (1981).
2. S. Nagamiya, M.-C. Lemaire, E. Moeller, S. Schnetzer, G. Shapiro, H. Steiner, I. Tanihata, Phys. Rev. **C24**, 971 (1981).
3. I. Tanihata, S. Nagamiya, O. Chamberlain, M.-C. Lemaire, S. Schnetzer, G. Shapiro, H. Steiner, Phys. Lett. **878**, 349 (1979).
4. S. Nagamiya, H. Hamagaki, P. Hecking, S. Kadota, R. Lombard, Y. Miake, E. Moeller, S. Schnetzer, H. Steiner, I. Tanihata, S. Bohrman, J. Knoll, Phys. Rev. Lett **48**, 1789, (1982).

5. R. Treuhaft, LBL-14677 July 1982. Also R. Treuhaft, J.V. Geaga, J.W. Harris, R. Koontz, H.G. Pugh, G. Roche, L.S. Schroeder, C.L. Ruiz, J. Engelage, P.N. Kirk, G.F. Krebs, LBL-14910, submitted to Phys. Rev. C, Nov. (1983).
6. M.-C. Lemaire, S. Nagamiya, O. Chamberlain, G. Shapiro, S. Schnetzer, H. Steiner, I. Tanihata, LBL-8463.
7. A.R. Smith, J.B. McCaslin, J.V. Geaga, Phys. Rev. **C28**, 1614 (1983).
8. J. Cugnon, D. Kinet, J. Vandermeulen, Nucl. Phys. **A 379**, 533 (1982).

Subthreshold K^- Production in Nucleus-Nucleus Collisions*

A. Shor,† J. Carroll,‡ E. Barasch,§ S. Abachi,‡ V. Perez-Mendez, T. Mulera, P. Fischer, G. Igo,‡ S. Trentalange,‡ K. Ganezer,‡ F. Kazeminzhad‡

We previously reported the observation of copious production of K^- in the reaction $^{28}Si + ^{28}Si$ at 2.1 GeV/nucleon.[1] As we pointed out, this bombarding energy is below threshold for K^- production in simple nucleon-nucleon collisions and the production rate is too copious to be explained by such trivial mechanisms as internal nuclear (Fermi) momentum or secondary and tertiary collisions of nucleons and produced π's and Δ's. The enhanced K^- production is an indication of multi-nucleon processes occurring in relativistic nucleus-nucleus collisions.

We have recently measured the momentum distribution of these subthreshold K^- using a secondary beam line as a magnetic spectrometer. Particle identification was achieved using multiple measurements of TOF and dE/dx and by using two sets of threshold Čerenkov counters. Preliminary results of this measurement are shown in Fig. 1 where we plot the K^- invariant production cross section as a function of the kaon kinetic energy in the Si-Si center of mass frame.

The data are consistent with an exponential distribution in energy with a slope parameter of about 80 MeV. This may indicate a thermal source at mid-rapidity, though it is difficult to imagine equilibration occurring in a system as small as ^{28}Si.

These data, though preliminary, enable us to rule out two possible multi-nucleon mechanisms as being responsible for the enhanced sub-threshold K^- production. The first of these is the ϕ-bremsstrahlung model of K.-H. Müller.[2] This model predicts a sharp peaking of the kaon distribution at mid-rapidity. Also ruled out is the possibility that the K^- originate from $K\bar{K}$ condensation. Such condensation is predicted to give rise to structure in the K^- spectrum which is not observed.

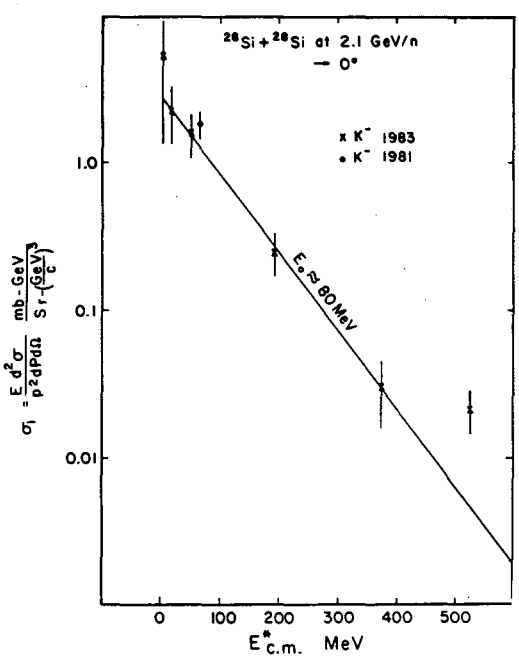

Fig. 1. Energy distribution in the c.m. system of the K^- produced in Si-Si collisions. The line drawn is fitted to the first six points (χ^2 = 0.43/degree of freedom). XBL 8311-4576

Footnotes and References

*Condensed from LBL-16175 (1983), a talk presented at the Sixth High Energy Heavy Ion Study and Second Workshop on Anomalons, LBL June 28 – July 1, 1983 and Phys. Rev. Lett. in preparation.

†LBL and UCLA, Los Angeles, CA 90024
‡UCLA, Los Angeles, CA 90024
§UC Davis, Davis CA 95616

1. A. Shor *et al.*, Phys. Rev. Lett. **48**, 159 (1982).
2. K.-H. Müller, Nucl. Phys. **A395** (1983)

Charge, Mass and Energy Measured in the Plastic Ball

H.-A. Gustafsson, H.H. Gutbrod, B. Kolb,* H. Löhner,† B. Ludewigt,* A.M. Poskanzer, T. Renner, H. Riedesel,‡ H.G. Ritter,* A. Warwick,* F. Weik,*§ H. Wieman**

In relativistic nuclear collisions the multiplicity of charged particles reflects the violence of the reaction and, presumably, the impact parameter. Furthermore, the total transverse energy in a collision might be a signature of compression. Both quantities are global features that can be measured in the Plastic Ball. The total mass in an event in light charge fragments can be detected (with assumptions made in certain kinematic regions) through particle identification. In addition, the neutron detection efficiency is quite high because of the large thickness of the plastic scintillator in the Plastic Ball. Here we present several global quantities for the reaction of 400 MeV/nucleon Nb + Nb.

In Fig. 1 the total charge measured, plotted as a function of charged particle multiplicity (MC), is seen to increase linearly and for some events reaches the initial number of protons in the event (note that the production of a π^- can increase the measured charge by two units). In Fig. 2 the total mass of charged particles is plotted as a function of MC. This curve reaches values of approximately 70 per cent of the initial mass of the system. The dotted line indicates the mass when the neutral particles (which have no ΔE signal in the Plastic Ball) are added in. The missing masses, especially at lower multiplicities are in fragments that are either not detectable or identifiable with the Plastic Ball/Wall. Fig. 3 shows the total kinetic energy and total transverse kinetic energy in the c.m. system as a function of MC. For some events as much as 24 GeV lab kinetic energy or 9 GeV in the c.m. system is detected. Of this as much as two-thirds can go into transverse kinetic energy. It is these events that may be thermalized and for which temperatures can be extracted.

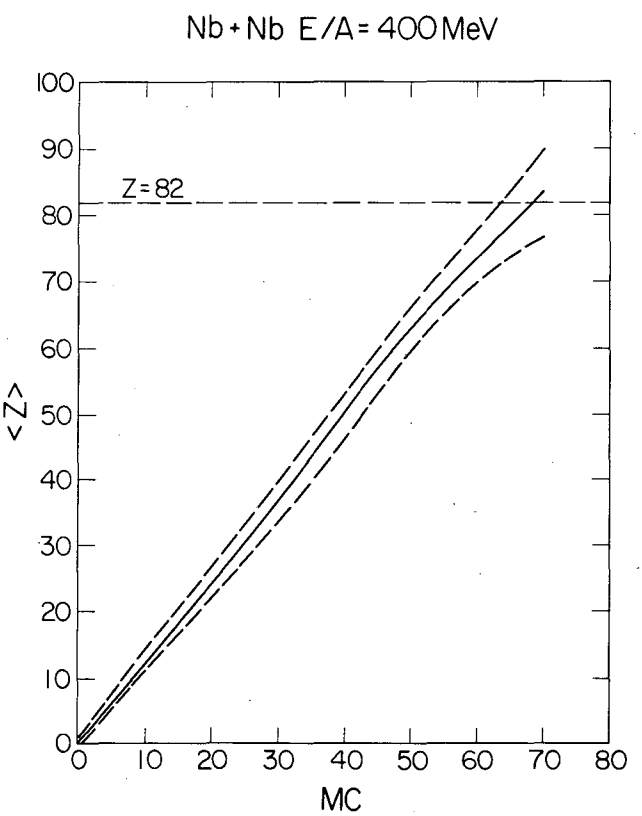

Fig. 1. Average charge as a function of charged particle multiplicity. XBL 831-1158

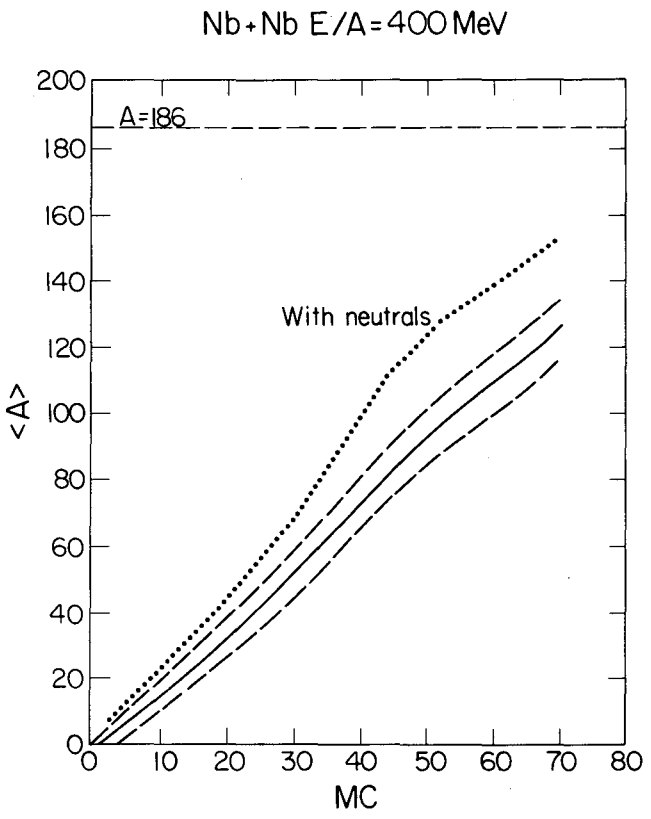

Fig. 2. Average mass as a function of charged particle multiplicity. XBL 831-1159

Footnotes

*Gesellschaft für Schwerionenforschung, Darmstadt, West Germany.

†Universität Münster, Münster, West Germany.

‡Present address: Max-Planck-Institut für Kernphysik, Heidelberg, West Germany.

§Present address: Toledo Corp., Köln, West Germany.

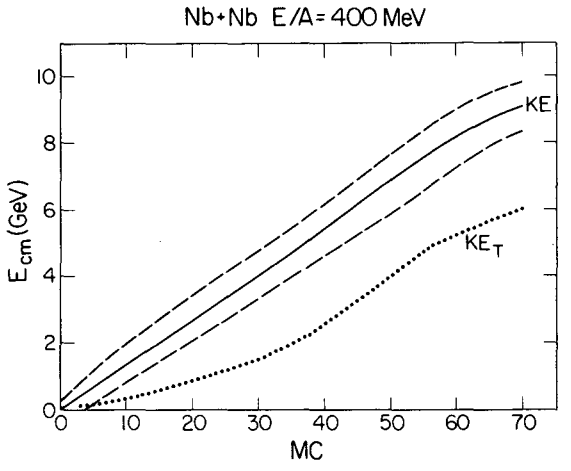

Fig. 3. Average c.m. kinetic energy as a function of charged particle multiplicity. XBL 831-1163

Thermalization in High Energy Nuclear Collisions

H.-A. Gustafsson, H.H. Gutbrod, B. Kolb,* H. Löhner,† B. Ludewigt,* A.M. Poskanzer, T. Renner, H. Riedesel,‡ H.G. Ritter,* A. Warwick* and H. Wieman**

One of the major questions in high energy nuclear physics is whether thermal equilibrium can be reached or whether nuclei already become transparent at Bevalac energies.

In Fig. 1 the ratio of the average momentum components, perpendicular ($p_\perp$) and longitudinal ($p_\parallel$), in the center-of-mass is shown as a function of the detected fraction of all projectile and target charges N_Z/Z. Assuming a correlation between the impact parameter and the charged-particle multiplicity, the increase of R with N_Z/Z can be partly understood as due to a decrease of spectator or leading particle contributions. A ratio of 1, which corresponds to isotropic events on the average, is reached only for the Nb + Nb system at 400 MeV/nucleon, whereas at higher energies and for the smaller Ca + Ca system the projectile is not fully stopped by the target nucleus.

Since proton spectra at Θ_{cm} = 90° are not disturbed by spectator contributions, they were used to extract temperature parameters by fitting with a relativistic Maxwell-Boltzmann distribution. The resulting T_0 values increase with the charged-particle multiplicity M_c (Fig. 2) for Ca + Ca as well as for Nb +

Nb, indicating the system is approaching equilibrium. From the two figures we conclude that equilibrium is not reached for the smaller system but might be established for the heavier one at the highest M_c. The analysis of a system even heavier than Nb + Nb would show whether T_0 increases further as a function of M_c for higher M_c values.

Footnotes and References

*Gesellschaft für Schwerionenforschung, Darmstadt, West Germany.

†Universität Münster, Münster, West Germany.

‡Present address: Max-Planck-Institut für Kernphysik, Heidelberg, West Germany.

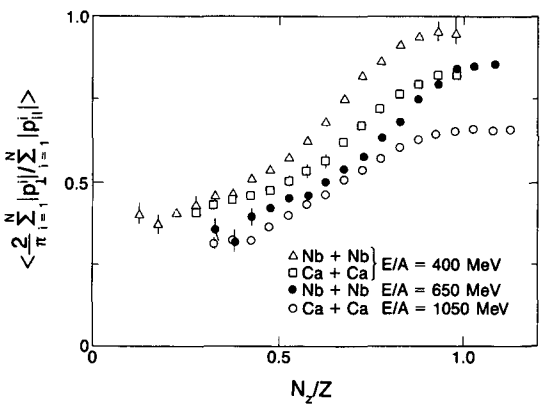

Fig. 1. Ratio of the average perpendicular to longitudinal momentum as a function of the detected fraction of all charges in the system, N_Z/Z.

XBL 8312-7397

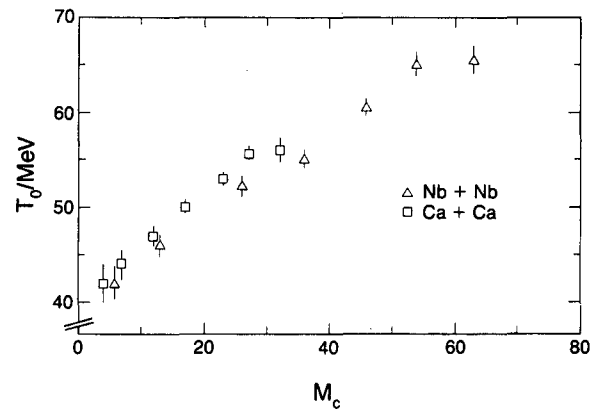

Fig. 2. Extracted temperature parameters T_0 as function of charged-particle multiplicity. The error bars indicate the statistical errors only. The relative errors of the T_0 values for the same system at different multiplicities are mainly statistical, but the absolute errors can be up to ±20%. XBL 8312-7396

Pion Spectra from the Interaction of Intermediate and Heavy Nuclear Systems

R. Brockmann, D. Bangert,† A. Dacal,‡ J.W. Harris,* M. Maier,† G. Odyniec, M. Ortiz,‡ H.G. Pugh, W. Rauch,† A. Sandoval,§ R.E. Renfordt,§ R. Stock,* H. Stroebele,* and D. Schall§*

Very preliminary results are available on the pion spectra for 2.1 GeV/nucleon Ca + Ca and 1.0 GeV/nucleon La + La.

In the Ca+Ca reaction the angular distribution and energy spectra are qualitatively the same as in the previously measured Ar + KCl reaction at 1.8 GeV/nucleon, the negative pion temperature as extracted from the $p_\perp$-spectra is T = 74.3 ± 1. MeV (Fig.1).

In the La + La reaction it turns out that the pions are equilibrated, within statistics, and no forward - backward enhancement is observed in the angular distribution(Fig.2). This is in contrast to our observation in the Ar + KCl reaction at 1.2 GeV/nucleon where a substantial anisotropy in the pion emission has been observed.

The heavier systems obviously reach a higher degree of equilibration than lighter systems at the same energy.

From the $p_\perp$-distribution we extracted a preliminary value for the temperature of approximately $T = 55 \pm 5$ MeV.

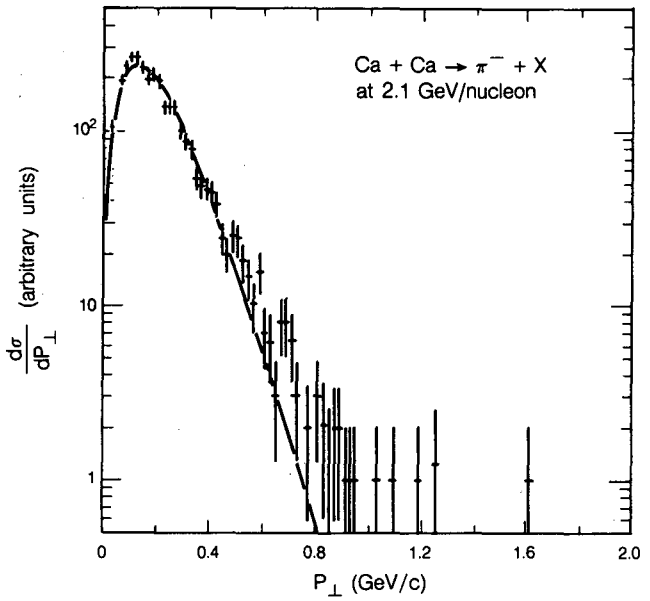

Fig. 1. Transverse momentum spectrum of the π^- created in central collisions of ^{40}Ca + Ca at 2.1 GeV/nucleon. The extracted pion temperature is 74.3 MeV. XBL 8312-6929

Footnotes

*Gesellschaft für Schwerionenforschung, 6100 Darmstadt, West Germany

†University of Marburg, 3550 Marburg, West Germany

‡Instituto de Fisica, UNAM, Mexico D.F., Mexico.

§University of Heidelberg, 6900 Heidelberg, West Germany

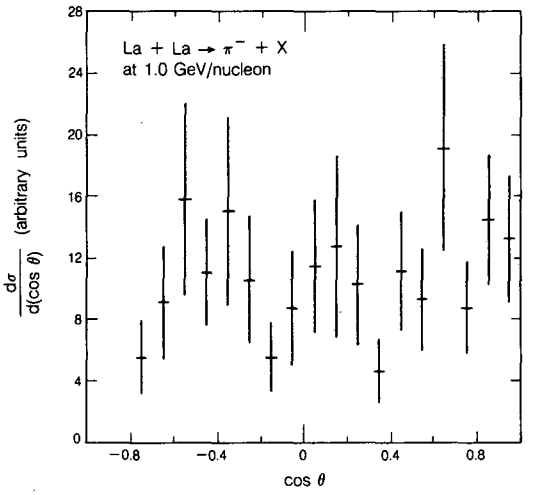

Fig. 2. The c.m. angular distribution of negative pions produced in central collisions in the reaction ^{139}La + ^{139}La at 1 GeV/nucleon. XBL 8312-6930

Momentum Flow in the 800 MeV/nucleon Ar + Pb Reaction

R.E. Renfordt, D. Bangert,† R. Brockmann,‡ J.W. Harris,‡ M. Maier,‡ G. Odyniec, H.G. Pugh, A. Sandoval,‡ R. Stock,‡ H. Stroebele,‡ D. Schall,* L.S. Schroeder, K. Tittel,* and K.L. Wolf§*

Central collisions of 800 MeV/nucleon ^{40}Ar + Pb have been studied in the streamer chamber at the Bevalac in terms of the azimuthally rotated flux tensor approach suggested by Danielewicz and Gyulassy[1] in an attempt to identify possible signatures of the flow of nuclear matter.

The particle identification and details about the central trigger have been described previously [2,3]. Significant experimental biases were found only for particles near target rapidity due to target absorption and composite particle ambiguities. Therefore, the tensor analysis was restricted to particles in the

forward hemisphere of the participant center-of-mass system which was computed event-by-event from particles with transverse momentum $p_\perp > 270$ MeV/c (corresponding to the maximum Fermi momentum of nucleons in the nucleus). Five hundred events were analyzed.

The data are compared to events generated by the intranuclear cascade code [4] and an isotropic particle emission Monte Carlo routine. Both types of theoretical events were subjected to a Monte Carlo "filter" procedure simulating experimental biases. Furthermore, to alleviate biases due to the unobserved neutrons and those bound in clusters, only the momentum carried by the protons are included in the analysis. The impact parameter (b) range imposed by the hardware trigger in the experiment corresponds to $0 < b < 5.5$ fm when the geometrical model is associated with the observed trigger cross section. In order to select on even smaller impact parameters than imposed by the trigger, the total charged-particle multiplicity M was used. The relationship between M and impact parameter b was studied using the results of the cascade code and is shown in Fig. 1a. The multiplicity M is observed to increase with decreasing impact parameter over the range of the hardware trigger.

A straightforward view of the event shape in momentum space can be seen directly from the mean transverse to longitudinal momentum ratio R per event (equation 2 in ref. 2):

$$R = \frac{2}{\pi} \frac{<p_\perp>}{<p_\parallel>} . \qquad (1)$$

R is shown as a function of M for 4 multiplicity bins in Fig. 1b. Also displayed in Fig. 1b are results from cascade and isotropic Monte Carlo events. The data are isotropic for the two higher multiplicity bins, but deviate toward excess longitudinal momentum for the two lower bins. On the other hand, the cascade events have a significant excess of longitudinal momentum for all multiplicities and thus all impact parameters.

In order to elaborate on the flux pattern of the events in momentum space a more complicated flux tensor analysis was performed (equation 3 in ref. 2). To eliminate fluctuations due to the limited number of particles per event, the procedure of azimuthal rotation[1] of the events was used. In this approach the azimuthal orientation of the major axis (E_3) of the flux tensor is computed event by event. Each event is then rotated about the beam direction in order to align the azimuthal orientation of all events. This is analogous to aligning the "reaction planes" of all events. For each multiplicity-selected subset of the data the events are added together to yield a single momentum flux tensor.

The deflection angle Θ, primary aspect ratio $R'_{32} = Q_3/Q_2$ of the major-to-secondary axes and secondary aspect ratio $R'_{21} = Q_2/Q_1$ of the secondary-to-minor axes of the flux tensors are plotted in Fig. 1c,d,e as a function of multiplicity for the data, cascade, and isotropic Monte Carlo. The isotropic Monte Carlo is essentially independent of the multiplicity with $R'_{32} = 1.5$, $R'_{21} = 1.1$ and $\Theta = 60$. These values correspond to the limiting values for a spherical flux distribution with the same multiplicity per event and number of events in each sample as found in the data. The values for R'_{32} and R'_{21} observed in the data are in agreement with both the isotropic Monte Carlo results and with the values found in ref. 1 for a spherical distribution with mean particle multiplicity of 40. Only for the lower multiplicities are the data prolate and oriented along the beam direction. The cascade results are consistently oriented more in the forward direction than the data but have nearly spherical shapes at the highest multiplicities as can be seen in Fig. 1d and 1e.

After the phi rotation was applied to each event as described above, the momenta of all particles (without any cuts) were projected onto the plane spanned by the main axis of the flux tensor and the beam. Shown on linear contour plots in Fig. 2 is $p_\perp$ "in-plane" as a function of rapidity for the data, cascade and isotropic Monte Carlo. A small but finite enhancement in the population density is observed in the data asymmetric to the beam axis as displayed in Fig. 2a. This enhancement is observed for all momenta, whereas the cascade events displayed in Fig. 2b exhibit an anisotropy only for the larger

momenta at small angles. As a comparison, an analogous contour plot projected in the plane perpendicular to the "reaction" plane, i.e. "out-of-plane" is indeed symmetric with respect to the beam direction as would be expected and is shown for the data, cascade and isotropic Monte Carlo in Figs. 2c-e, respectively.

In summary, the global variables "R-ratio", "flux-angle" and "aspect-ratio" were used along with the newly-introduced technique of azimuthal rotation to analyze semi-exclusive data of central collisions of 800 MeV/nucleon Ar + Pb. For high multiplicities, which were shown to correspond to small impact parameters, the data approach a thermal isotropic distribution. For larger impact parameters (lower multiplicity subsamples) a finite deflection of the flux tensor is observed after azimuthal rotation of the flux tensor. This deflection is also observed in the contour plots of $p_\perp$ as a function of rapidity of the azimuthally rotated data sample. The event shapes for the larger impact parameters are prolate. There is no indication from these data for oblate event shapes which would be created in very central collisions by enhanced particle emission at 90 degrees in the c.m. as predicted by the one fluid hydrodynamical model[5]. Furthermore, there is a significant difference between the data and the intranuclear cascade model in that the cascade events are consistently oriented closer to the beam direction than the data, particularly at larger impact parameters. Finally, if one wishes to identify the sideward enhancement in momentum flux observed in the data for the larger impact parameters with the sideward flow of nuclear matter predicted by the one-fluid hydrodynamical models, the results from hydrodynamics must be subjected to identical analysis procedures as in the experiment to ensure that the systematic biases introduced by the procedure, experimental apparatus, and finite particle numbers are the same in both cases.

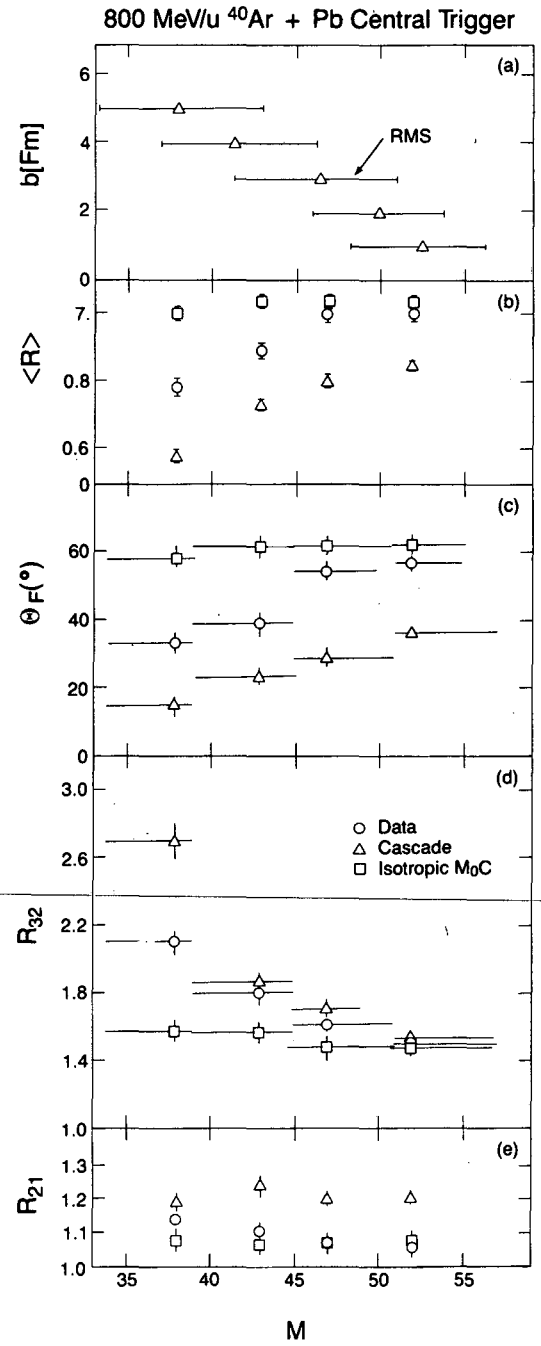

Fig. 1. a.) Correlation between impact parameter b and total multiplicity M in the Cascade calculation. b. – e.) After the phi rotation described in the text the following variables are plotted as a function of total charged multiplicity M each for data, Cascade and isotropic Monte Carlo : b.) R-ratio (see equation 1) . c.) Flux angle Θ. d.) Aspect ratio $R'_{32} = Q_3/Q_2$. e.) Aspect ratio $R'_{21} = Q_2/Q_1$. XBL 841-10019

Footnotes and References

*University of Heidelberg, 6900 Heidelberg, West Germany

†University of Marburg, 3550 Marburg, West Germany
‡Gesellschaft für Schwerionenforschung, 6100 Darmstadt, West Germany
§Texas A&M University, College Station, Texas, USA

1. P. Danielewicz and M. Gyulassy, LBL 15721 (1983).
2. H. Stroebele *et al.*, Phys. Rev. **C27**, 1349 (1983)
3. A. Sandoval *et al.*, Phys. Rev. Lett. **45**, 874 (1980). J. W. Harris *et al.*, Phys. Rev. Lett. **47**, 229 (1981).
4. J. Cugnon *et al.*, Nucl. Phys. **A379**, 553 (1982).
5. J. Kapusta and D. Strottmann, Phys. Rev. **C23**, 1282 (1981).

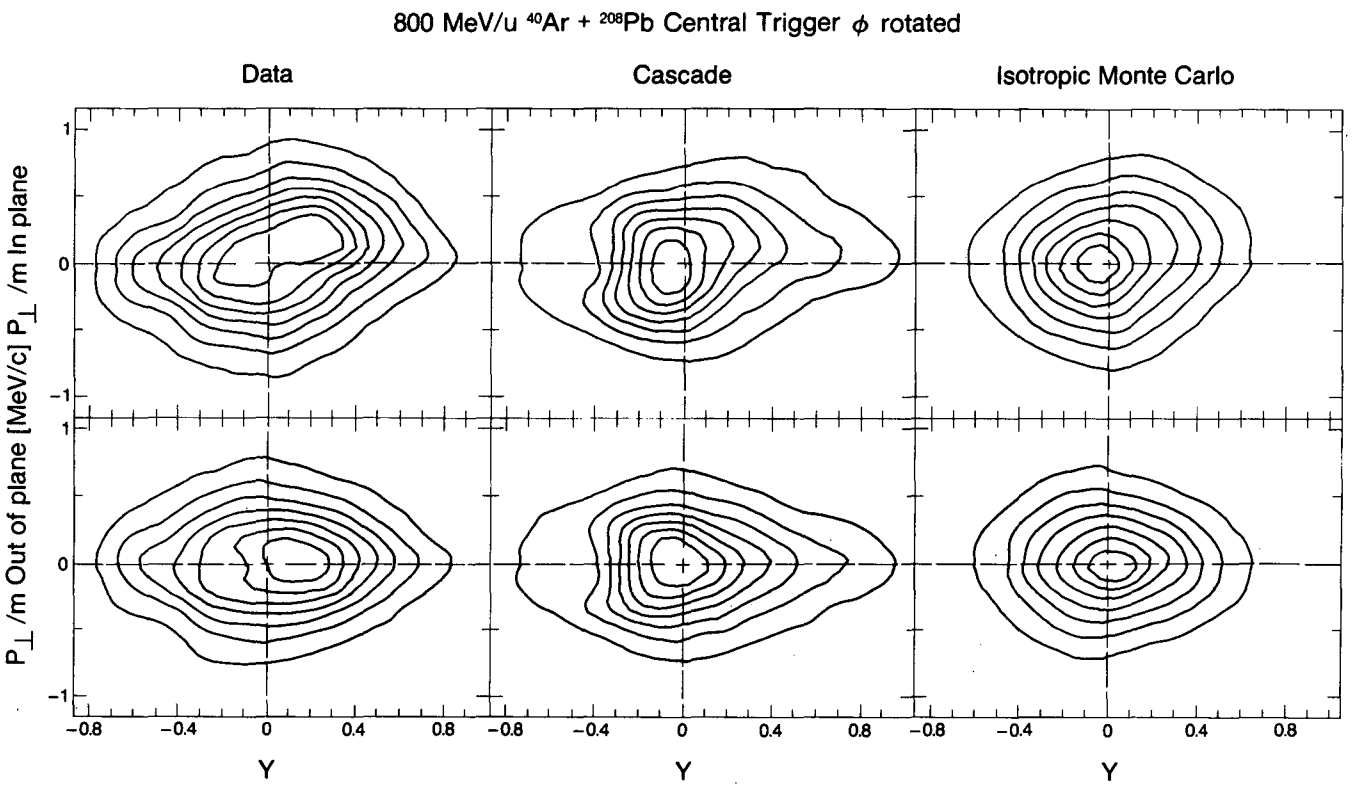

Fig. 2. After the phi rotation described in the text the momenta of all particles (no cuts) of our data set are projected onto the reaction plane as defined by the main axis of the momentum flux tensor and the beam axis. The linear contour plot shows $p_\perp$ (normalized to the mass of the particle) within this "reaction" plane as a function of rapidity for the data (a), Cascade events (b), and isotropic Monte Carlo (c). For comparison, $p_\perp$ in the plane perpendicular to the "reaction plane" vs rapidity is also shown in the lower half of the figure for the data (c), Cascade (d), and isotropic Monte Carlo (c) events. XBL 841-10020

PART IV: THEORY

Static Nuclear Properties

An Update on Droplet Model Charge Distributions*

W.D. Myers and K.-H. Schmidt†

The Droplet Model predictions for nuclear density distributions differ from those of the Liquid Drop Model in two important ways. The most important difference is that the equivalent sharp radii of the neutron and proton distributions are determined by minimizing the macroscopic energy of the system. This procedure results in a prediction that light nuclei are squeezed slightly by the surface tension and that most nuclei have a neutron skin because the neutron distribution is slightly larger than the proton distribution for neutron excess nuclei. The other difference is the prediction of a small amount of bulk redistribution under the influence of the repulsive Coulomb force.

The most dramatic effect of the new features that are included in the Droplet Model is the accurate prediction that isotope shifts in the nuclear charge radii should be about half as large as the Liquid Drop Model would predict. This can be seen very clearly in Fig. 1.

Here, the measured RMS radii have been coverted to equivalent sharp radii by the approximate procedure of multiplying by (R_D/RMS_D), where R_D is the Droplet Model predicted equivalent sharp radius, and RMS_D is the Droplet Model prediction for the RMS radius with all the diffuseness, deformation and redistribution effects included. A straight line has then been fitted to isotopic sequences and the slope of this line ΔR_n (multiplied by $A^{2/3}$) has been plotted against the Z value for the sequence. The Liquid Drop model would predict that this quantity should always have the constant value 1/3 r_0 (as is indicated by the dotted line in the figure). The data are seen to cluster about the dashed line representing the Droplet Model prediction. The solid horizontal line at $\Delta R_n * A^{2/3} = 0$ corresponds to the idea that charge radii depend only on the value of Z, as has sometimes been advocated.

We have extended the usual Droplet Model predictions of charge moments to include deformation and redistribution contributions. When compared with the measured values the accuracy obtainable by this method seems to be about 0.01 fm (or 10 am), which corresponds to 0.2% in the RMS radius for a heavy nucleus. This is almost as good as the 0.1% accuracy (1 MeV out of 1000 MeV) that can be obtained for the binding energy, when the macroscopic approach is supplemented by shell corrections.

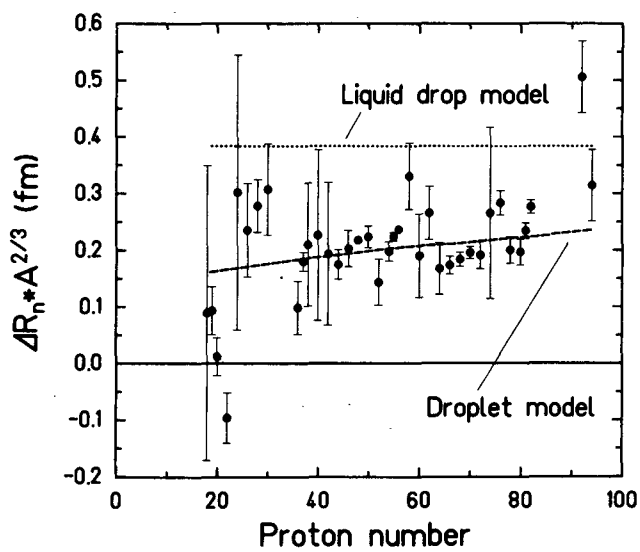

Fig. 1. The slope ΔR_n of the equivalent sharp charge radius versus neutron number multipled by $A^{2/3}$ is plotted against the charge number of the isotopic sequence being considered. The dashed line is the Droplet Model prediction, and the dotted line is the Liquid Drop Model prediction. XBL 834-9062

Footnotes
*Condensed from LBL-15446

†Gesellschaft für Schwerionenforschung D-6300 Darmstadt 11, West Germany

Combining the Droplet Model and the Yukawa-plus-Exponential Macroscopic Model*

P. Möller† and W.D. Myers

Motivated by the excellent agreement between the measured values of nuclear masses and the predictions of the Yukawa-plus-Exponential Macroscopic Model (YPEMM)[1] (even for masses far from stability that were not included in the database from which the model parameters were originally determined), we have undertaken to incorporate the essential features of this approach into the Droplet Model.[2] In spite of its success in fitting measured masses (and fission barriers) the YPEMM lacks certain physical features such as compressibility, Coulomb redistribution and the neutron skin. These omissions prevent this approach from being able to accurately predict the change in size of the proton distribution as one moves along isotopic sequences, and raise questions about its reliability for the prediction of nuclear properties far from stability.

The most important features of the YPEMM that are being added to the Droplet Model are the exact calculation of Coulomb energies for diffuse charge distributions, and the use of a folding integral for representing the effect of the finite range of the nuclear force on the size and shape dependence of the surface energy. The reference database is being extended to include more recently determined nuclear masses, and also the nuclear charge radii and isotope shifts.

Footnotes and References

*Work in progress
†Permanent address: Department of Mathematical Physics, Lund University, P.O. Box 725, S-22007, Lund, Sweden

1. P. Möller and J.R. Nix, Nucl. Phys, **A361**, 117 (1981).
2. W.D. Myers, *Droplet Model of Atomic Nuclei* (IFI/Plenum Data Co., New York, 1977).

Note on Nuclear Disintegration Widths*

W.J. Świątecki

Symmetric expressions for fission and neutron (or other particle) emission widths are derived by applying uniformly the canonical version of the transition-state method to all cases. This treatment should provide a conceptually cleaner set of baseline formulae, against which one may more readily ascertain the advantages of refinements, such as the inclusion of shell effects, deformations or the singling out of special treatment of selected degrees of freedom.

*Condensed from Australian Journal of Physics **36**, 641 (1983).

The Surface Energy of Multi-Component Systems*

W.D. Myers, W.J. Świątecki and C.S. Wang†

For a sufficiently large system, such as a homogenous fluid or a heavy atomic nucleus, the total energy of the system may be approximated as a sum of a volume energy (proportional to the volume V of the system) and a surface-layer energy. (For a recent formulation of this method see ref. 1). The surface-layer energy is approximately proportional to the area S of the surface bounding the system. The *surface-energy coefficient* γ (i.e., the surface energy per unit area of a flat surface) may be defined as the following limit

$$\gamma = \lim_{S/V \to 0} \frac{E - E_{ref}}{S} , \qquad (1)$$

where E is the actual energy of the system, E_{ref} is a reference energy taken to represent the volume contribution, and the limit is taken for a large system for which the ratio S/V tends to zero.

It may come as a surprise that, in the case of multi-component systems (such as nuclei consisting of neutrons and protons), there exist two sensible and commonly used definitions of the reference energy E_{ref} which, when inserted in Eq. (1), can lead to widely different values of γ. For example, in the case of a model of the nuclear surface of a type used in astrophysical as well as nuclear applications,[2] the two definitions lead to two values of γ whose magnitudes diverge with increasing neutron excess. In the model in question the ratio of the two values of γ reaches 2.7 at the point of "neutron drip" (where the neutrons become unbound). Beyond this point, when the nucleus becomes immersed in a neutron gas, the ratio of the (interfacial) surface energies increases further, reaching a value of the order of 10 close to the point of proton drip! How can this be and what does it mean? Which value of γ should one use in practice, e.g., in astrophysical applications?

Consider for definiteness a large fluid system consisting of two components. For example, we may think of a large fictitious nucleus consisting of N neutrons and Z uncharged protons, with N + Z = A. Assume the nucleus to be sufficiently large, so that a well-defined distinction can be made between the bulk region (where the neutron, proton and total densities are essentially constant and equal to ρ_m, ρ_p and ρ), and a surface region, where the densities fall off to zero. The first definition of γ, which we will refer to as the e-definition, γ_e, is based on subtracting from E in Eq. (1) the energy that the total number of particles, A, would have under bulk conditions. Thus, if we denote by e the energy per particle in the bulk, the reference energy is

$$E_e = eA . \qquad (2)$$

In the second definition, γ_μ, one introduces, in place of the energy per particle in the bulk, the chemical potentials (i.e., the separation energies) of the neutrons and protons as well as the pressure p inside the system. As the nucleus becomes larger and larger, these chemical potentials tend to definite limits, the chemical potentials μ_n, μ_p of infinite nuclear matter characterized by a neutron density ρ_n and a proton density ρ_p. The reference energy is now taken as

$$E_\mu = \mu_n N + \mu_p Z - pV , \qquad (3)$$

where V is the volume of the system, defined by A/ρ. The physical meaning of E_μ is that it would be (the negative of) the energy needed to disassemble into its constituents a very large nucleus, under the assumption that the chemical potentials (separation energies) remained at their asymptotic, nuclear matter values μ_n, μ_p. In this way one again hopes to isolate the surface corrections, which make the actual separation energies decrease as the surface energy comes into play.

Using these reference energies it is possible to show that the difference between the two values of γ

is given by,

$$\gamma_e - \gamma_\mu = \frac{1}{2}\,\rho\,(1-\delta^2)\,(\partial e/\partial\delta)\,t\ , \qquad (4)$$

where $\delta = (\rho_n - \rho_z)/\rho$ and t is the neutron skin thickness. All the symbols on the right of Eq. (4) refer to quantities evaluated in the limit $S/V \rightarrow 0$, i.e., for semi-infinite matter. Thus the difference (like the surface energy coefficients themselves) is a constant characteristic of the (semi-infinite) matter being considered.

Because of the substantial difference in value of the two surface energy coefficients, it is absolutely essential to match the definitions of surface and reference energies when formulating macroscopic descriptions of nuclei for the purpose of predicting masses or fission barriers, or for use in astrophysics applications.

Footnotes and References

*Condensed from LBL-16947, in preparation.

†Permanent address: Department of Technical Physics, Peking Unversity, Beijing 100871, People's Republic of China.

1. J. Blocki *et al.*, Ann. Phys. (NY) **132,** 53 (1981).
2. F.D. Mackie and G. Baym, Nucl. Phys. **A285,** 332 (1977).

On the Coulomb Sum Rule in the Relativistic Nuclear Many-Body Problem*

T. Matsui

In the non-relativistic quantum many-body theory, the Coulomb sum rule gives a simple and very useful relation between the static two-body correlation function and the inelastic electron scattering cross section integrated over the energy loss.[1] Recently a relativistic extension of the non-relativistic Coulomb sum rule has been made by Walecka.[2] For a point-like Dirac nucleon it is written as

$$S(q) \equiv \int_0^\infty d\omega\, W_{Coul}\,(q^2,\omega)$$

$$= Z + \iint e^{-i\mathbf{q}\cdot\mathbf{x}} g(\mathbf{x},\mathbf{y})\, e^{i\mathbf{q}\cdot\mathbf{y}} d\mathbf{x}d\mathbf{y} \qquad (1)$$

where $W_{Coul}\,(q^2,\omega)$ is the Coulomb response function for transferred energy-momentum $(\omega,\mathbf{q})$, Z is the total charge of the system, and $g(\mathbf{x},\mathbf{y})$ is the relativistic proton two-body correlation function defined by the ground state expectation value of a product of proton Dirac spinor $\Psi_\alpha(\mathbf{x})$;

$$g(\mathbf{x},\mathbf{y}) \equiv \langle\Psi_\alpha^+(\mathbf{x})\,\Psi_\beta^+(\mathbf{y})\,\Psi_\beta(\mathbf{y})\,\Psi_\alpha(\mathbf{x})\rangle$$

$$- \langle\Psi_\alpha^+(\mathbf{x})\,\Psi_\alpha(\mathbf{x})\rangle\langle\Psi_\beta^+(\mathbf{y})\Psi_\beta(\mathbf{y})\rangle \qquad (2)$$

As one sees from the above expression, the relativistic Coulomb sum rule involves an integral of the Coulomb response function over the entire positive energy region as in the non-relativistic one. Thus it has remained an open problem whether the sum rule value is really exhausted, as commonly assumed, in the *space-like* momentum transfer ($\omega < q$) region, which can be reached by the electron scattering.

We studied the relativistic Coulomb sum rule by focusing on the distribution of the sum rule value over two different kinematical regions, i.e., *space-like* vs. *time-like* ($\omega > q$) momentum transfer regions. After the analysis of the lowest order Coulomb response function in the relativistic mean-field theory,[2,3] we observed the remarkable upshot that the sum rule value of the *Fermi-sea* nucleons is not

exhausted in the *space-like* momentum transfer region, and *only half* of the total charge of the system is visible by the inclusive electron scattering at the extreme momentum transfer limit ($q \rightarrow \infty$). The result is shown in Fig. 1 where the sum rule values normalized by the total charge of the system Z are plotted. The *space-like* component of the sum rule value strongly depends on the effective mass M* of the baryon, while the total sum rule value remains very close to the nonrelativistic result. The remaining part of the sum rule value is found in the *time-like* momentum transfer region, mixed with the contribution from the *Dirac sea* nucleons, i.e., the *vacuum polarization* of baryon field. We also made a calculation which includes the anomalous magnetic moments of nucleons and again found a considerable difference between the total sum rule value of the *Fermi sea* nucleons, which was previously computed in ref. 2, and its *space-like* visible part. This result implies that the Coulomb sum rule should be used with a particular caution to analyze deep inelastic electron scattering from nuclei.

Footnote and References

*Condensed from Phys. Lett. **132B**, 260 (1983).

1. A.L. Fetter and J.P. Walecka, "Quantum Theory of Many Particle Systems," (McGraw-Hill Book Co., N.Y., 1971).
2. J.D. Walecka, Stanford University preprint ITP-721 (1982); Nucl. Phys. A in press.
3. J.D. Walecka, Ann., of Phys. **83**, 491 (1974).

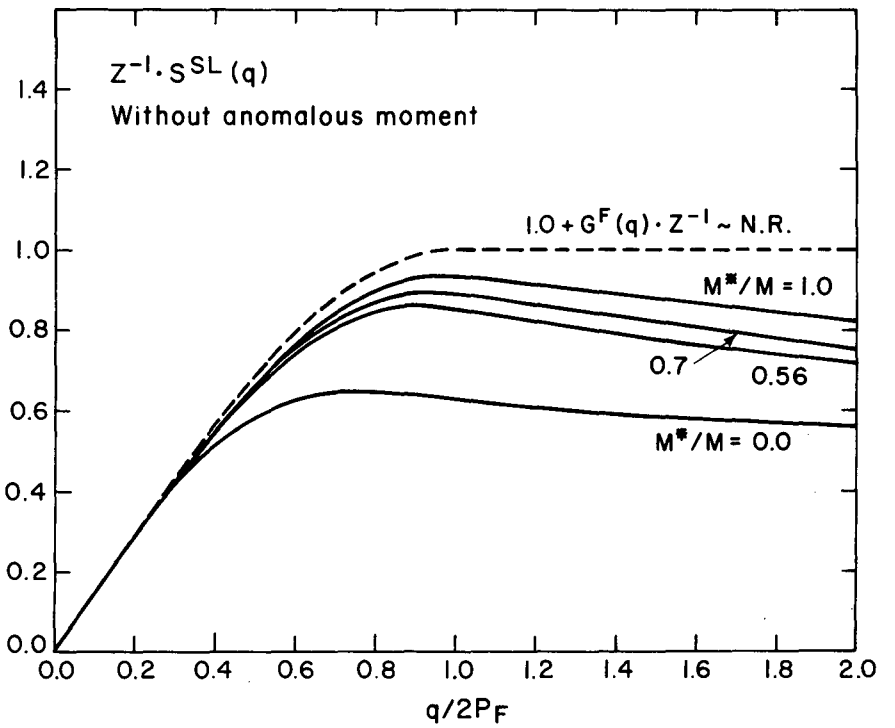

Fig. 1. Space-like components of the Coulomb sum rule value are represented by solid lines for several different values of effective baryon mass M*. The total sum rule value of the Fermi sea nucleons (dashed line) does not depend much on the effective baryon mass and appears very close to the nonrelativistic result.

XBL 835-202

Dynamical Evolution of Angular Momentum in Damped Nuclear Reactions: I. Accumulation of Angular Momentum by Nucleon Transfer

T. Døssing and J. Randrup

The exploration of damped reactions between atomic nuclei has been a central theme in nuclear physics during the last decade. Through this period steady improvements in instrumentation have permitted increasingly detailed data-taking and thus paved the way for an ever better understanding of those processes. The experimental data can be briefly, and roughly, characterized by stating that the multivariate distribution of the observables resembles that of a transport process, with the kinetic energy loss TKEL playing the role of the generalized time parameter.

An important goal in the theory of nuclear dynamics is to understand the observed transport phenomena in terms of the basic microscopic processes in the system. For this purpose a model was developed in which the dissipative mechanism responsible for the transport process is the transfer of nucleons between the two reacting nuclides.[1]

Until now, most efforts to confront that theory with data have concentrated on the evolution of the charge and mass distribution with energy loss, and overall good agreement has been obtained for a variety of features.

While this success lends strong support to the theory, it is important to broaden the contact with experiment by considering also other aspects of the data. Therefore we have undertaken a comprehensive study of the angular momentum variables which represent six additional observables (three for each fragment spin) and thus provide a rich testing ground for the theory.

First we derive the equations of motion for the mean values $\langle \vec{s}^F \rangle$, F = A,B of the six spin variables and their associated covariances, $\overleftrightarrow{\sigma}^{FG}$. In order to fully include the so called tilting mode (in which the two nuclides rotate in the same sense around the dinuclear axis) it is essential to work in a coordinate system which is aligned with the fluctuating direction of the orbital angular momentum $\vec{L}$, as well as with the dinuclear axis $\hat{R}$. This feature introduces additional terms in the dynamical equations which are essential for ensuring the proper asymptotic approach to the statistical limit. It is also of importance to transform from the internally defined dynamical coordinate system to an external coordinate system in order to obtain quantities amenable to experimental measurement.

Observables other than the fragment spins are also discussed, in particular the relative fragment motion. This enables us to calculate not only the fluctuations in scattering angle and energy loss, but also the correlation between this latter quantity and the spin observables. This feature in turn makes it possible to calculate differential cross sections for specified energy losses in accordance with standard presentations of the data. This is accomplished by calculating the appropriate conditional mean values and covariances for a specific impact parameter and then subsequently adding up contributions from all impact parameters to a specified energy loss.

A major part of the work consists in a detailed discussion of the characteristic features of the dynamical evolution of the spin distribution in the course of a nuclear reaction. For a given total angular momentum $\vec{J}$ of the dinucleus, the state of lowest energy corresponds to a rigid rotation in which the entire system turns as a whole. Relative to this yrast mode of motion the dinucleus can have intrinsic

rotational excitations which carry no net angular momentum. They are 1) the two degenerate "wriggling" modes, where the two nuclides rotate in the same sense around an axis perpendicular to the dinuclear axis $\hat{R}$, 2) the "tilting" mode where they rotate in the same sense around $\hat{R}$ (which implies that $\vec{J}$ has a component along $\hat{R}$). These three are referred to as positive modes. In the three negative modes the two nuclides rotate in the opposite sense: 3) the two "bending" modes perpendicular to $\hat{R}$ and 4) the "twisting" mode along $\hat{R}$.

For a symmetric collision, the dynamical evolution of positive and negative modes decouple and the general features of the spin evolution can be understood in terms of the behavior of the relaxation times for these various normal rotational modes of the dinucleus. They are shown in Fig. 1. The relaxation times for the three negative modes are generally larger than those for the "wriggling" modes due to the relative smallness of the neck radius (or, more precisely, the average off-axis displacement of the transferred nucleons): $c^2_{ave} \ll R^2$. Therefore the dinucleus will relax relatively fast towards a "rolling" situation (where the wriggling modes have decayed) while the subsequent approach to "sticking" is much slower, and usually not reached within the reaction time. The tilting relaxation time is fairly complicated but typically this mode is excited only relatively little.

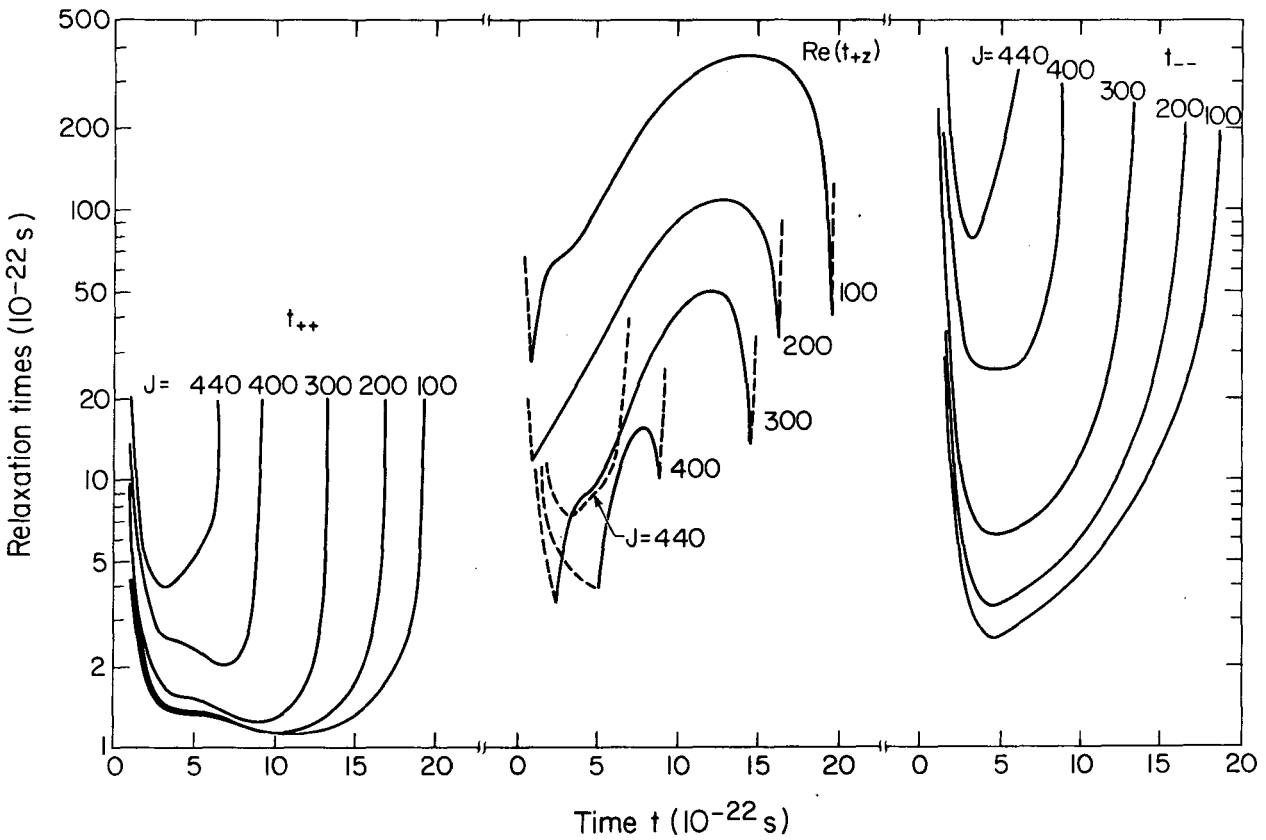

Fig. 1. Calculated local relaxation times for the reaction 1400 MeV ^{165}Ho + ^{165}Ho for various values of the total angular momentum J. The relaxation times for the two positive perpendicular modes (wriggling) are denoted t_{++}, while the one of the positive longitudinal mode (tilting) is denoted t_{+z}. The relaxation time for the three negative modes (bending and twisting) is denoted t_{--}. XBL 841-23

Due to the predominance of the positive spin excitations in the dinucleus the two fragments will emerge with spins tending to be positively correlated. In general the degree of relaxation of the various dinuclear rotational modes can be probed by studying the fragment spin-spin correlations. A particularly powerful tool for this is the double fission process which is given special consideration in the following investigation.[2]

Several illustrative applications of the theory are discussed. The time evolution of the dinuclear geometry is found to be rather similar to that of the Time-Dependent Hartree Fock and the Coherent Surface Excitation models. Detailed discussions are given of the cases 1400 MeV Ho + Ho and 610 MeV Kr + Bi which have been experimentally studied.

A pictorial impression of the evolution of the dinuclear geometry can be gained from Fig. 2. Equiprobability contours of the in-plane spin distributions for the two nuclides are superimposed. One notes how the fairly peripheral collision ($J = 440\ \hbar$) the window grows wider and the isotropic negative modes are more readily excited; the distribution also tracks the turning dinuclear axis better. These features are even more apparent for $J = 100\ \hbar$.

The investigation is concluded with a discussion of other models addressing angular momentum in damped nuclear reactions.

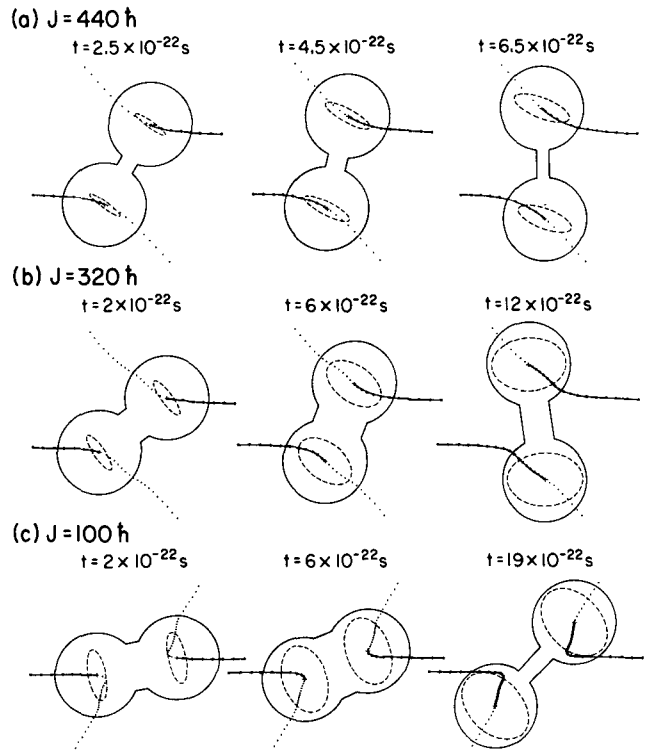

Fig. 2. For three different values of the total angular momentum J, the dinuclear complex produced in the reaction 1400 MeV ^{165}Ho + ^{165}Ho is shown at three different points in time: shortly after the neck has opened, at the time of closest approach, and just before the neck collapses. (The actual times indicated are measured from the time of nuclei approach to a surface separation of s = 4 fm.) The dots indicate past and future locations of the nuclear centers at intervals of 10^{-22} sec. The dashed ellipses indicate the one-sigma contours of the in-plane distribution of the nuclear angular momenta $\vec{S}^A$ and $\vec{S}^B$ scaled so that one fm corresponds to two $\hbar$ (the nuclides have a radius of 6.3 fm). XBL 836-2647

References

1. J. Randrup, Nucl. Phys. **A327**, 490 (1978); **A383**, 468 (1982).
2. Following contribution.

Dynamical Evolution of Angular Momentum in Damped Nuclear Reactions: II. Observation of Angular Momentum through Sequential Decay

T. Døssing and J. Randrup

The angular momentum built up in the fragment nuclei during a damped nuclear reaction is subsequently lost through decay. Since the decay is very fast, the only way to learn about the angular momentum accumulated in the nuclei is to observe the sequential decay products. The present investigation aims at providing precise methods for calculating properties of the sequential decay on the basis of primary spin distributions in the fragments, especially applied to the spin distributions calculated with the transfer induced transport theory.

γ-multiplicity experiments provide information about the spin magnitude distribution, while angular correlation experiments provide information about the directional distribution of the spin vector. The moments of the directional distribution are the statistical tensors, the polarization, the alignment, asymmetry etc. The first few terms in an expansion of the angular correlation on spherical harmonics contain the lowest order tensors of even order.

The angular distribution coefficient of second order, multiplied by the corresponding angular distribution coefficients,

$$B_2(S) = \frac{3\langle H^2\rangle - S(S+1)}{(S+1)(2S+3)}$$

is a function of the second moment of the distribution of helicity H of the decay. This way of expressing the angular correlation is general and displays the relation between the statistical tensor components and the angular correlation of sequential decay.

Fig. 1 shows the fission probability and the 2nd and 4th order angular distribution coefficients for fission as functions of angular momentum for three different excitation energies in the nucleus $^{208}_{84}$Po, which is a typical nucleus produced in reactions with $^{208}_{82}$Pb as target or projectile. In the calculation, fission delayed by the emission of one or more neutrons is

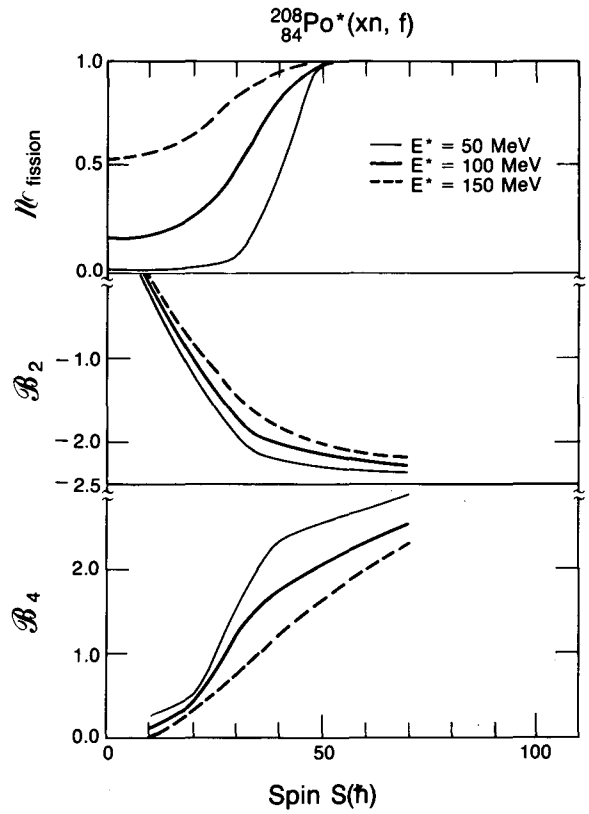

Fig. 1. Fission probability (top), second (middle) and fourth order angular distribution coefficient (bottom) for fission of the nucleus $^{208}_{84}$Po as functions of angular momentum for the excitation energies E = 50, 100 and 150 MeV. The parameters entering the calculation – neutron separation energy, fission barrier, deformation of the saddle shapes – are all given by the liquid drop model with the Lysekil parameters. XBL 844-10400

taken into account, both with respect to the change of the fissility of the nucleus, the temperature, the magnitude of the spin, and the dealignment caused by the neutrons. We test the calculated properties of the sequential fission by comparing calculated and experimental angular distributions for nuclei formed in fusion reactions in which case the distribution of the spin magnitude and the statistical tensors are known.

Some of the results of our comparison between data and theoretical results based on transfer induced transport are given in Figs. 2 and 3, which show γ-multiplicity data and fission data, respectively. These figures display the current status of our comparison to data.

The rather large spin magnitude dispersion seems to be well reproduced. About 20% of this dispersion is due to the positive correlations of the spins between the two nuclei. The main discrepancy between the theory and data occurs for the smallest total kinetic energy losses where the comparison to data suggests that the average spin vector is increasing too rapidly with increasing TKEL. For medium energy losses there is a good agreement with data, and for the highest energy losses the average spin vector is slightly too small.

A separate discussion is made for double fission angular correlations which contain information about the spin-spin correlations. When correlations are present between the spins of the two reaction

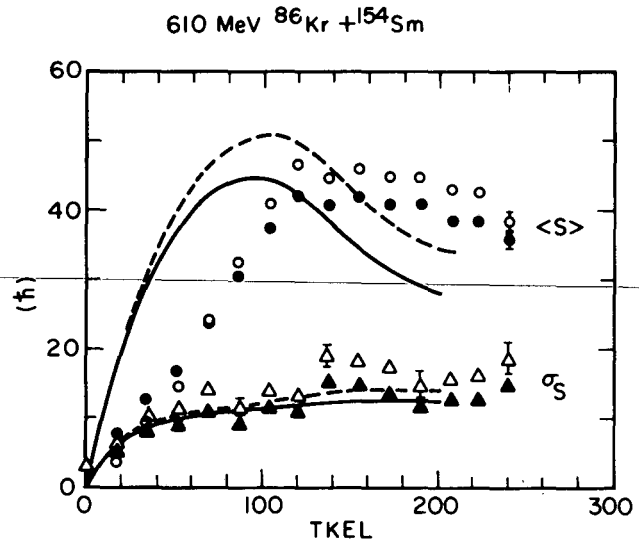

Fig. 2. Average spin magnitude <S> and dispersion σ_S as functions of TKEL for the reaction 610 MeV ^{86}Kr + ^{154}Sm. The dashed lines correspond to the spin distributions in the nuclei right after the collision, and the full curves are corrected for neutron emission prior to the emission of γ-rays. The data points are extracted from the γ-multiplicity data of ref. 1 using the following relation between spin magnitude moments and γ multiplicity moments: $\langle S\rangle = 2(\langle M_\gamma\rangle - 3)$ (open circles), $\langle S\rangle = 1.6\ \langle M_\gamma\rangle$ (full circles), $\sigma_S = 2\ \sigma_{M_\gamma}$ (open triangles), $\sigma_S = 1.6\ \sigma_{M_\gamma}$ (filled triangles). XBL 841-7502

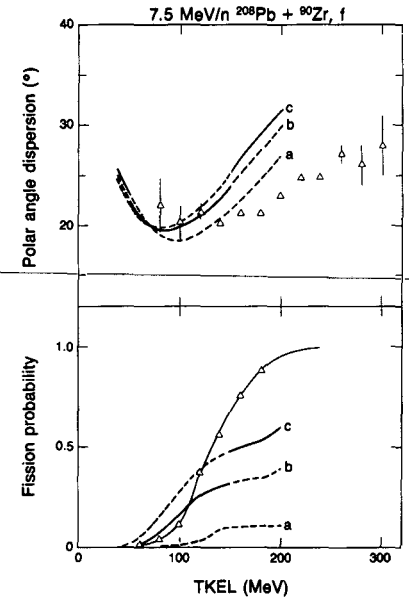

Fig. 3. Polar angle dispersion (top) and fission probability (bottom) as functions of TKEL for fission of the heavy nucleus produced in the reaction of 7.5 MeV/nucleon ^{208}Pb + ^{90}Zr. The curves labeled a, b, and c are calculated with the theoretical values for the average mass and charge of the heavy nucleus, corresponding to small, medium and maximum TKEL, respectively, and the curves are fully drawn in that region of TKEL where they apply. The data are from ref. 2. XBL 8311-7316A

product nuclei the detection of fission from one nucleus in a direction out of the reaction plane biases the angular distribution of fission products from the other nucleus and that breaks the reflection symmetry with respect to the reaction plane. The Nuclear Exchange Transport Theory predicts a substantial symmetry breaking (up to a factor of three) while a statistical model, which yields much smaller covariances, predicts only a 20% effect.

We are currently pursuing the confrontation with the data; although there appears to be rather good overall agreement with a variety of observables, the significance of certain discrepancies still needs to be carefully ascertained.

References

1. P.R. Christensen, *et al.*, Nucl. Phys. **A390**, 336 (1982).
2. D. v. Harrach *et al.*, Phys. Rev. Lett. **42** 1728 (1979).

Dissipative Resistance Against Changes in the Mass Asymmetry Degree of Freedom in Macroscopic Nuclear Dynamics: The Completed Wall-and-Window Formula

J. Randrup and W.J. Świątecki

The wall formula and the wall-and-window formula for the dissipation of collective energies in macroscopic nuclear dynamics have been used for some time in discussions of fission and nucleus-nucleus collisions.[1,2] The wall formula applies in the "mononuclear" regime, when the nuclear shape has no constrictions, the wall-and-window formula in the opposite limit, when the nucleus consists of two (or more) pieces communicating through a small neck. The conventional wall-and-window formula consists of a part associated with the rate of deformation of the two fragments and a part associated with their relative motion. It does not, however, address itself to the asymmetry degree of freedom, i.e., to the rate of change of the relative sizes of the two pieces. We have remedied this deficiency by analyzing the relation of the dissipation formulae to the transport treatment of deep inelastic reactions.[3] The relevant dissipation coefficient in the asymmetry degree of freedom turns out to be essentially the reciprocal of the "mobility coefficient" for mass transfer in ref. 3. This leads to the following "completed wall-and-window formula" for the rate of dissipation of collective energy in a system consisting of two pieces, 1 and 2, which are in relative motion and whose relative sizes are changing by virtue of a flow of matter through a small window of area a:

$$-\frac{dE}{dt} = \rho v \oint_1 d\sigma\,(\dot{n} - D_1)^2 + \rho v \oint_2 d\sigma\,(\dot{n} - D_2)^2 + \frac{1}{4}\rho v\,(2\dot{z}^2 + \dot{y}^2)a + \frac{16}{9}\frac{\rho v}{a}\dot{V}_1^2 \qquad (1)$$

In the above, the first line is the conventional wall-and-window formula and the second line is the new term. The nuclear mass density is denoted by ρ, the mean speed of the nucleons is v and $\dot{n}$ is the normal velocity of an element $d\sigma$ of the nuclear surface. The quantity D (D_1 or D_2) is the normal component at $d\sigma$ of a drift velocity impressed on the nucleons by the presence of translational and rotational components in the velocity field $\dot{n}$ describing the fragment deformations. (The drifts D_1, D_2 ensure linear and angular momentum conservation.) The relative

motion of the two fragments has components $\dot{z}$ along the normal to the window and $\dot{y}$ in the plane of the window. In the last term, $\dot{V}_1$ is the rate of change of the volume of fragment 1. The appearance of the window area *a* in the *denominator* shows that the dissipation in the mass-asymmetry degree of freedom dominates when the window is small, leading to an effective freezing of mass transfer between the nuclei. Such a term is essential for the ability of a dynamical model of nuclear collisions to describe the existence of deep-inelastic reactions. We have verified that without it such reactions would be altogether absent, the mass flow being far too rapid. We are in the process of studying the degree of quantitative agreement with experiments that may be obtained when the completed wall-and-window formula is used in dynamical model studies.

References

1. J. Blocki *et al*, Ann. of Phys. **113**. 330 (1978).
2. A.J. Sierk and J.R. Nix, Phys. Rev. **C21**, 982 (1980).
3. J. Randrup, Nucl. Phys. **A327**, 490 (1979).

Dynamics of Nucleus-Nucleus Collisions

J. Blocki and W.J. Świątecki*

The generalization of the wall-and-window dissipation formula, devised recently by J. Randrup and W.J. Świątecki (see contribution to this report), has been incorporated in our numerical computer program for following the dynamics of nucleus-nucleus collisions and fission. Extensive studies are in progress. Some of the current results include estimates of sticking times for various non-fusion reactions, in particular as regards dependence on the target and projectile masses and the collision energies. Table I gives a sample of our results to date. For each pair of values A_1, A_2 the atomic number Z of the system was taken as the sum of the atomic number $Z_1(\beta)$, $Z_2(\beta)$ specifying the valley of β-stability for A_1 and A_2. The last two columns give the final fragment masses after scission. Owing largely to the new term in the generalized wall-and-window formula (which strongly inhibits mass transfer between the two nuclei) the final masses usually show relatively little mass drift, reminiscent of a deep-inelastic reaction. The sticking times range from about 2×10^{-21} s to 2×10^{-20} s. For a given system the sticking time increases by something like a factor of two when the energy is raised from zero to 50 MeV over the Coulomb barrier. The value 1.6×10^{-21} s for $A_1 = A_2 = 240$ seems consistent with a recent estimate of $1\text{–}1.5 \times 10^{-21}$ s based on an analysis of positron and γ-ray spectra associated with U + U collisions (ref. 1).

Footnote and Reference

*Institute for Nuclear Research, D5-400, Swierk, Poland.

1. H. Backe *et al.*, Phys. Rev. Lett. **50**, 1838 (1983).

Table I

Initial A_1	Initial A_2	C.M. Collision Energy above Coulomb Barrier (MeV)	Sticking Time in 10^{-22} s	Final A_1	Final A_2
80	80	0	∞ (Fusion)	–	–
80	160	0	74	88.7	151.3
		10	119	93.5	146.5
		20	135	94.7	145.3
		50	166	96.9	143.1
80	240	0	77	96.3	223.7
		10	104	103.6	216.4
		20	110	105.0	215.0
		50	121	106.7	213.3
160	160	0	24	160	160
		10	38	160	160
		20	43	160	160
		50	54	160	160
160	240	0	20	161.9	238.1
		10	29	163.3	236.7
		20	34	163.9	236.1
		50	42	165.1	234.9
240	240	0	16	240	240
		10	22	240	240
		20	24	240	240
		50	29	240	240
48	248	0	213	96.3	199.7
		10	235	96.8	199.2

A Simple Model for Fermi Jets

K. Möhring, W.J. Świątecki and M. Zielińska-Pfabé†*

Fermi jets or PEPs (promptly emitted particles) are nucleons predicted to be ejected (through the back sides of two colliding nuclei) in the early stages of a collision, before the relative velocity of the nuclei has fallen below a certain threshold value (corresponding to about 1/2 MeV/nucleon).[1,2] The prediction is based on elementary aspects of the addition of the Fermi velocities of the nucleons to the relative motion of the nuclei. An experimental confirmation of Fermi jets could open up a fascinating field of investigations, in which a nucleus, instead of being irradiated by a beam of nucleons from an accelerator, is, in effect, illuminated "from inside" by a flash of neutrons and protons originating in the vicinity of the contact point with the collision partner.

The presence of high-energy ("pre-equilibrium") tails in the energy spectra of nucleons produced in nucleus-nucleus reactions has been known for a long time, but the relation to the Fermi jetting mechanism remains unclear. Part of the reason has to do with the cumbersome nature of the calculations necessary to characterize the properties of the Fermi jets, requiring numerical computer studies involving time integrations over the poorly understood time evolution of the collision dynamics.

In a recent study of these questions we have developed a rudimentary model of Fermi jetting, resulting in theoretical predictions that are often expressible by closed algebraic formulae. Apart from the numerical applications, of which two are illustrated in what follows, the model has brought out the fact that, through an appropriate change of the time integration variable, the question of the time evolution of the collision can be by-passed. In this way, the predictions of the model become, to a certain extent, independent of this aspect of the theory.

Our idealized model represents the nucleus-nucleus collision as the conventional coming together of two sharp-surfaced potential wells filled with Fermi gases of nucleons. After contact, a window opens up between the nuclei; its area, a(t), is a (complicated) function of time. Through this window time-dependent fluxes of particles (calculable elementarily in terms of the instantaneous motions of the Fermi gases, and proportional to the window area) begin to irradiate the two potential wells. A (small) fraction of these nucleons have velocities high enough to escape through the back sides of the collision partners and produce the Fermi jets. The remainder of the fluxes is captured in the receptor potential wells and is assumed to cause a slowing down of the relative motion of the nuclei according to the standard window-friction mechanism.[3] The first-order equation of motion for this slowing down sets up a proportionality relation between the decrement of relative velocity, dv, and the corresponding time interval dt, the factor of proportionality containing, naturally, the window area a(t). Conversely, dt is proportional to dv *divided* by a(t). It follows that when the Fermi jetting, which at each instant is *directly* proportional to a(t), is integrated over time, and the integration variable is changed from dt to dv, the unknown window-area function a(t) cancels out and the result is an elementary integral over v, independent of the time evolution of the collision dynamics.

Since the jetting fluxes as well as the window friction contain no adjustable parameters, the final answers to all calculations with the above idealized model come out as absolute magnitudes, with no adjustable parameters.

As an example we give the formula for the predicted total number of particles, ΔA, jetted through the projectile (A_p) and the target (A_t), as a function of the relative velocity, v, at the moment of contact in a head-on collision:

$$\Delta A = A_{red} \left[F(\nu) - F(\nu_e - 1) \right], \qquad (1)$$

where

$$A_{red} = A_t A_p/(A_t + A_p)$$

and

$$F(x) = (1 - \nu_e^2)^2 \ln x + \frac{8}{3}(1 - \nu_e^2)x$$

$$+ (1 + \nu_e^2)x^2 - \frac{1}{12}x^4 \ .$$

In the above, ν is the velocity v in units of the Fermi velocity v_F and ν_e is the nucleon "escape velocity" (also in units of v_F), given by

$$\nu_e = \left(\frac{E_F + S}{E_F}\right)^{1/2} ,$$

where E_F is the Fermi energy and S is the neutron separation energy in the case of neutron jetting or the proton separation energy augmented by the proton Coulomb barrier in the case of proton jetting. (In the illustrative examples described below, we adopted a nominal value S=10 MeV and disregarded the effect of the electric forces on the proton trajectories.)

Fig. 1 shows ΔA divided by the reduced mass, as suggested by Eq. (1). A typical value at X=4 is ΔA=6. The abscissa X is proportional to the relative velocity at contact. The solid curve represents the calculations for head-on collisions. The crosses are averages over that range of impact parameters which would lead to fusion followed by particle evaporation according to the estimates of ref. 4.

Fig. 2 shows how the emission of Fermi jets would decrease the velocity of a compound nucleus resulting from a compound nucleus reaction. The "relative velocity anomaly", $\Delta u/u$, where u is the velocity that the compound nucleus would have in the absence of Fermi jets, is plotted against the relative velocity variable X, as in Fig. 1. Experimental data are taken from ref. 5.

We are proceeding with more detailed calculations of angular and energy spectra of the jetted particles. At the moment our tentative conclusions are as follows:

1. The absolute number of the jetted particles are only small to moderate fractions of the particles

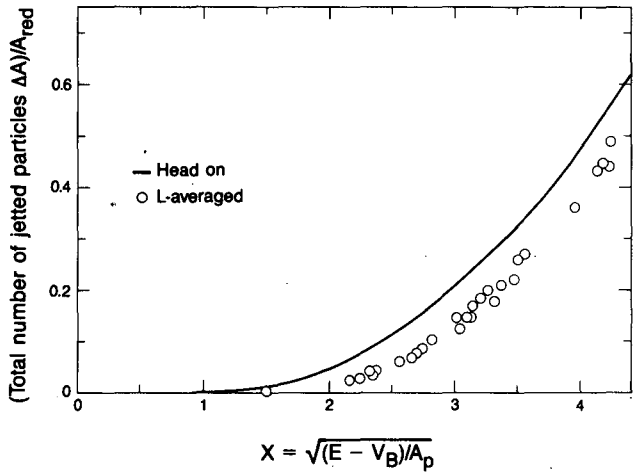

Fig. 1. The total number of jetted particles, divided by A_{red}, as a function of a variable X, proportional to the relative velocity at contact. (E is the bombarding energy and V_B the Coulomb barrier in the laboratory frame.) XBL 842-10036

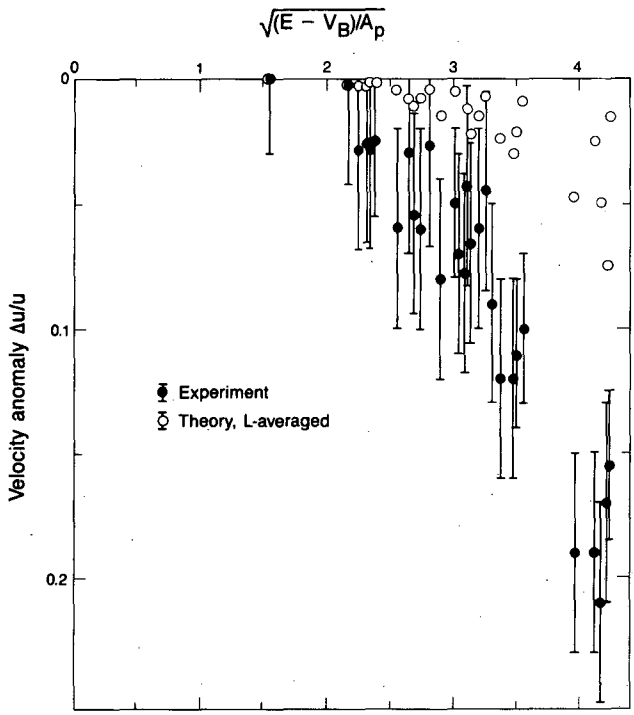

Fig. 2. The contribution of the Fermi jetting to the relative anomaly in the laboratory velocity of compound-nucleus evaporation residues is shown by crosses. The data are from ref. 5. XBL 842-10035

emitted by the standard post-fusion evaporation mechanism, but the energy and angular distributions of the jets have characteristic features that should help in their identification.

2. The observed velocity anomalies in compound-nucleus reactions are most likely due, in large measure, to a mechanism other than Fermi jets.[6] The jetting contribution should, however, be taken into account in a quantitative analysis of the anomalies.

Footnotes and References

*Permanent address: Hahn Meitner Institut für Kernforschung Berlin, Germany.

†Permanent address: Department of Physics, Smith College, Clark Science Center, Northampton, Mass. 01063.

1. J.P. Bondorf, J. de Phys. **C5**, 195 (1976); J.P. Bondorf *et al.*, Nucl. Phys. **A333**, 285 (1980).
2. M.Robel, Ph.D. thesis, LBL-8181 (1979), unpublished.
3. J. Blocki *et al.*, Annals of Phys. **113**, 330 (1978).
4. S. Bjørnholm and W.J. Swiątecki, Nucl. Phys. **A391**, 471 (1982).
5. Yuen-Dat Chan *et al.*, private communication, 1983.
6. B.G. Harvey and H. Homeyer, LBL-16882, November 1983.

An Overlap Model for Fragment Yields in Heavy Ion Reactions*

B.G. Harvey and H. Homeyer†

We have developed a theoretical model for the calculation of projectile fragment cross sections in low and intermediate energy heavy ion reactions. Its basic assumption[1,2] is that the nucleons to be removed from the heavy ion projectile must overlap spatially with the target nucleus. The distance of closest approach $R_i(i)$ during the collision is therefore $R_1 + R_2 - H(i)$ where H(i) is the height of a spherical cap in the projectile R_1 which contains the nucleons to be removed to leave the ith ejectile.

The cross section for the formation of a given ejectile depends upon the product of two probabilities $p_\ell(E,i)$ and P(i). The first has its maximum value for the partial wave corresponding exactly to $R_i(i)$ and decreases from lower and higher partial waves. The second expresses the relative probability for projectile breakup into the ejectile (i) and a residue which may or may not be captured by the target nucleus. The P(i) are calculated from the fragmentation model of Friedman[3] which uses approximate wave functions and spectroscopic factors to obtain the relative breakup probabilities from the appropriate separation energies.

The $p_\ell(E,i)$ varies around its maximum value as:

$$p_\ell(E,i) = \frac{\ell - \ell_0(i) + \sigma_\ell}{\sigma_\ell^2} \exp - \left[\frac{\ell - \ell_0(i) + \sigma_\ell}{\sigma_\ell} \right] : \ell > \ell_0(i) - \sigma_\ell$$

$$= 0 : \ell \leqslant \ell_0(i) - \sigma_\ell \qquad (1)$$

Here $\ell_0(i)$ is the partial wave corresponding to $R_i(i)$ and σ_ℓ is a width parameter in ℓ-space corresponding to a fixed width σ_R in R-space.

The complete fusion (CF) process must be treated separately. We use an energy dependent fusion radius of the form:

$$R(CF) = 0.95(R_1 + R_2) \left(\frac{V_B}{E_{CM}} \right)^{1/2} \qquad (2)$$

where V_B is the combined Coulomb plus nuclear potential evaluated at $(R_1 + R_2)$ by the method of Wilczynski.[4] The energy dependent critical angular momentum for CF is therefore:

$$\ell_0(CF) = V_{rel}\, R(CF) A_1 A_2/(A_1 + A_2) \qquad (3)$$

where V_{rel} is the projectile target relative velocity for a Coulomb trajectory at $(R_1 + R_2)$ where contact first occurs. The $p_\ell(E,CF)$ is calculated with a smooth cutoff from:

$$p_\ell(E,CF) = \left[\ell_0(CF)(1 + \exp\frac{\ell - \ell_0(CF)}{\Delta} \right]^{-1} . \qquad (4)$$

With $\Delta = 2\hbar$ and $P(CF) = 1$, these equations reproduce the prediction for CF of $^{20}Ne + {}^{197}Au$ obtained with the function model of Gross and Kalinowski,[5] which in turn agree well with experimental CF cross sections for various systems and energies.

The constraint that each partial wave must contribute to the complete and incomplete fusion channel is expressed by the $N_\ell(E)$ values obtained from the sum rule of Wilczynski *et al.*[6]

$$N_\ell(E) = \left[\sum_i p_\ell(E,i) P(i) \right]^{-1} . \qquad (5)$$

The cross sections are then given by:

$$\sigma(E,i) = \Pi\lambda_2 P(i) \sum_{\ell=0}^{\ell_{max}(E)} (2\ell+1) N_\ell(E) p_\ell(E,i). \qquad (6)$$

The sum is carried up to the partial wave $\ell_{max}(E)$ which corresponds to the radius $(R_1 + R_2)$.

Fig. 1 shows a comparison of the model with experimental results[7,8] for $^{20}Ne + {}^{197}Au$. The data have been corrected for the formation and decay of excited primary ejectiles in sequential decay processes such as $^{20}Ne \rightarrow {}^{16}O^* \rightarrow {}^{12}C + \alpha$. Thus the experimental and calculated cross sections of Fig. 1 both represent the primary yields of the various elements. The calculated Z=2 yield includes the ^4He that comes from the particle-unstable nuclei ^5He, ^5Li, ^8Be and ^9B.

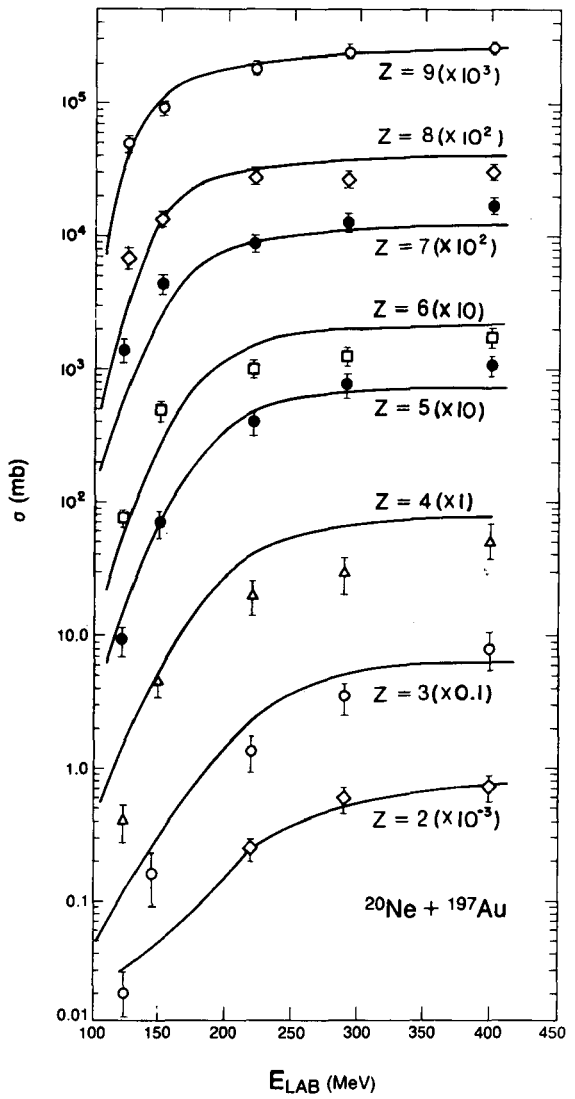

Fig. 1. Comparison of experimental and calculated excitation functions for primary element yields from $^{20}Ne + {}^{197}Au$. XBL 8311-4018Y

Fig. 2 shows the contributions of complete and incomplete fusion to linear momentum transfer measured by the angular correlation of fission fragments from $^{20}Ne + {}^{197}Au$ at 290 MeV.[9] For carbon isotopes, only one half of the calculated cross section was used, since at this beam energy the most probable excitation of the residual nucleus following

transfer of eight nucleons lies just at the fission barrier. In the calculation, the effect of ^{8}Be formation (a large part of the Z=4 yield) appears explicitly.

As Figs. 1 and 2 show, the agreement of the model with the experimental results is excellent.

Footnotes and References

*Condensed from LBL-16882; submitted to Phys. Rev. Lett.

†Permanent address: Hahn-Meitner Institut, Berlin.

1. B.G. Harvey and M.J. Murphy, Phys. Lett. **130B**, 373 (1983).
2. G.D. Westfall *et al.*, Phys. Rev. Lett. **37**, 1202 (1976).
3. W.A. Friedman, Phys. Rev. **C27**, 569 (1983).
4. J. Wilczynski and K. Siwek-Wilczynska, Phys. Lett. **55B**, 270 (1973).
5. D.H.E. Gross and H. Kalinowski, Phys. Rep. **45**, 177 (1978).
6. J. Wilczynski *et al.*, Phys. Rev. Lett. **45**, 606 (1980).
7. Ch. Egelhaaf *et al*, Nucl. Phys. **A405**, 397 (1983).
8. S. Wald *et al.*, to be published; H. Homeyer *et al.*, this Annual Report, to be published.
9. J.R. Huizenga *et al.*, Phys. Rev. **C28**, 1853 (1983).

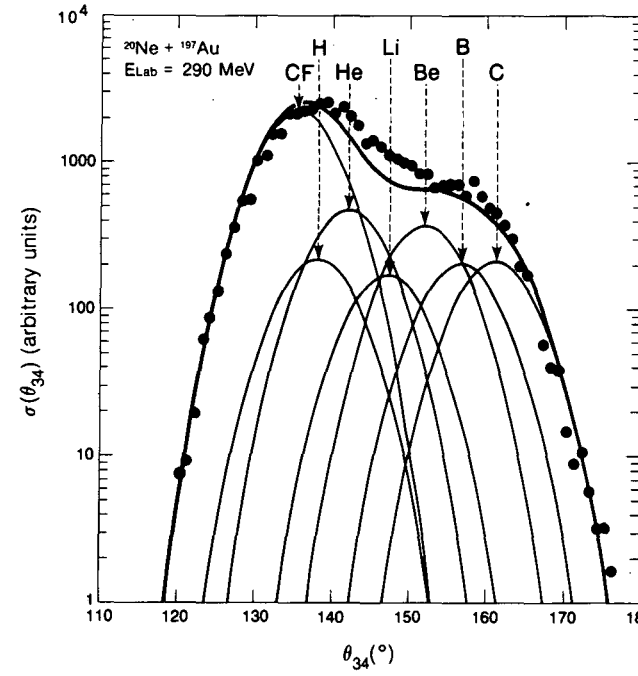

Fig. 2. Comparison of experimental and calculated fission product angular correlations for ^{20}Ne + ^{197}Au at 290 MeV. An angular width of 10.4° was assumed for all channels. The thin lines represent the individual contributions of the complete and incomplete fusion channels. The thick line is their sum.

XBL 8311-4017Y

Monte Carlo Studies of Alpha-Accompanied Fission*

H.M.A. Radi,† J.O. Rasmussen, R. Donangelo,‡ L.F. Canto,‡ and L.F. Oliveira‡

To compare with the wealth of new data[1] on alpha-accompanied fission of ^{236}U*, we have made new trajectory calculations. Initial conditions for several parameters were selected from Gaussian distributions by the Monte Carlo method, and about 15,000 trajectories were run for alpha source at the electrostatic saddle point. Momentum and energy are fully conserved in the three-body problem, though the usual point charge approximation without nuclear forces was used. A principal difference of our work from earlier work is that we constrained the spatial and momentum distribution initially to satisfy the minimum uncertainty relation of a Gaussian wave packet for the alpha particle. The main calculations center the alpha source at the electrostatic saddle. General agreement with experiment is remarkable, including even the appearance of low-energy secondary peaks at large angles. Effects

of shifting the source from the saddle point toward either fragment are studied. Both the satellite peak phenomena and the angular distribution indicate the need for a small shift of source toward the light fragment.

In Fig. 1 we plot the initial distributions of several parameters. The top curve is the distribution of D, the fission fragment separation distance at scission. Both the actual histogram and the Gaussian fit are shown. The middle curve gives the distribution of d, the location of the saddle with respect to light fragment; it is computed from each random choice of D and is not separately chosen. The lowest curve gives the off-axis distribution of the initial alpha position, both histogram and computer-smoothed curve shown. The most probable values of D, d, and R_C are 21.9 fm, 9.07 fm, and about 1.2 fm, respectively. The standard deviations (from the Gaussian fit) of D and d are σ_D = 1 fm and σ_d = 1.04, respectively.

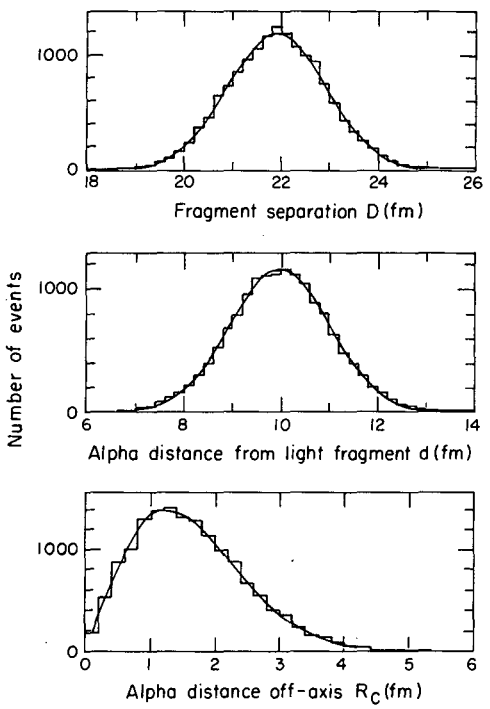

Fig. 1. Initial probability distributions of some parameters. The top curve is the distribution for fragment separation distance D. The middle curve is the x-separation d between alpha and light fragment. The lowest curve is the off-axis distance distribution for the alpha. XBL 821-4418

Our Fig. 2 is analogous to Fig. 3 of Guet *et al.*,[1] giving alpha energy distributions for fixed angles, the interval being ±2.5° from the stated angle. The angle is measured from the direction of the light fragment. We show the event number histograms and computer-fitted Gaussians. One should bear in mind that our Monte Carlo calculation is for fixed mass asymmetry, and their presentation of data in their Fig. 3 is for all asymmetries. For the angles 68° through 88° we get fairly good unskewed Gaussian fits. For 93° and larger angles we see a secondary peak develop at lower energies. In their Fig. 3 data the secondary peak at lower energies is manifested at both large and small angles. Guet *et al.*[2] in their own Monte Carlo study have stated that the low-energy component at small angles comes from trajectories starting near the light fragment heading toward the heavy fragment and backscattering from it.

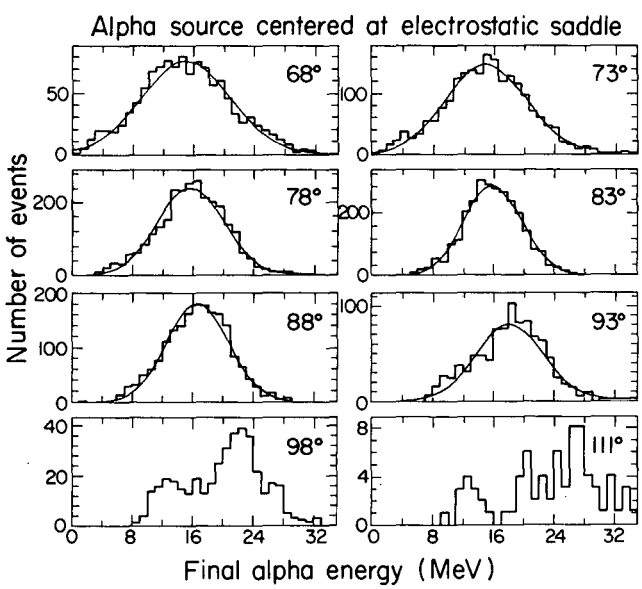

Fig. 2. Final alpha energy distributions for fixed angles 2.5° of the labeled angle $\Theta_{\alpha L}$, the angle between alpha and light fragment final velocity vectors. Alpha source entered at electrostatic saddle point. XBL 821-4414

As one sees from Fig. 3, our theoretical all-energy angular distribution (histogram) perfectly matches the Guet *et al.* data[1] (dots) around the maximum. However, the match is less good in the wings of the curve. Our Fig. 3 is analogous to their Fig. 9. However, note that their Fig. 9 counts only alphas $E_\alpha > 7.5$ MeV, and this would seem to affect mainly small angle data as can be seen from Fig. 3. Taking their cut-off into account makes for greater disagreement with our points. However, in our final section we explore shifting the alpha source position and see that a shift toward the light fragment acts to correct this angular distribution mismatch.

Our Fig. 4 shows energy distributions at fixed angles for the shift in the initial alpha wave packet from the electrostatic saddle by a 1.5 fm toward light fragment. Fig. 4 is analogous to Fig. 2 for the saddle-point center. In Fig. 4 we see that the shift toward the light fragment does not produce any clear double-peaking, but there is a pronounced broadening and shift to lower energy for small angles.

We present in Fig. 5 separate angular distribution plots for the shifted cases. The position shift toward light fragment moves the peak of the angular distribution toward larger angles and vice versa. A small admixture of light-shifted component could improve the angular distribution of Fig. 2. We conclude that an alpha source distribution somewhat

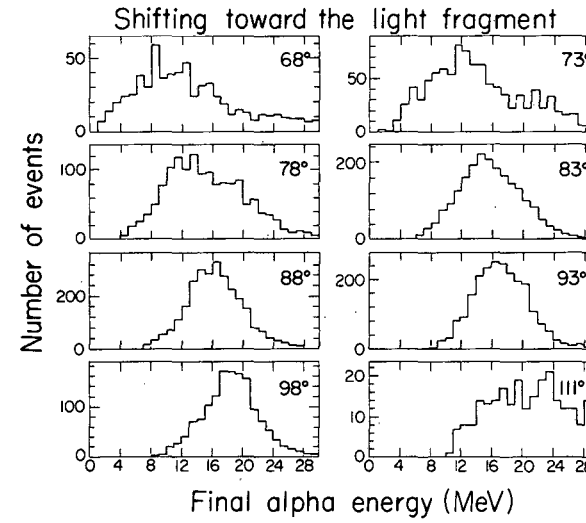

Fig. 4. Same as Fig. 2 except that alpha source is shifted from saddle toward light fragment.

XBL 821-4423

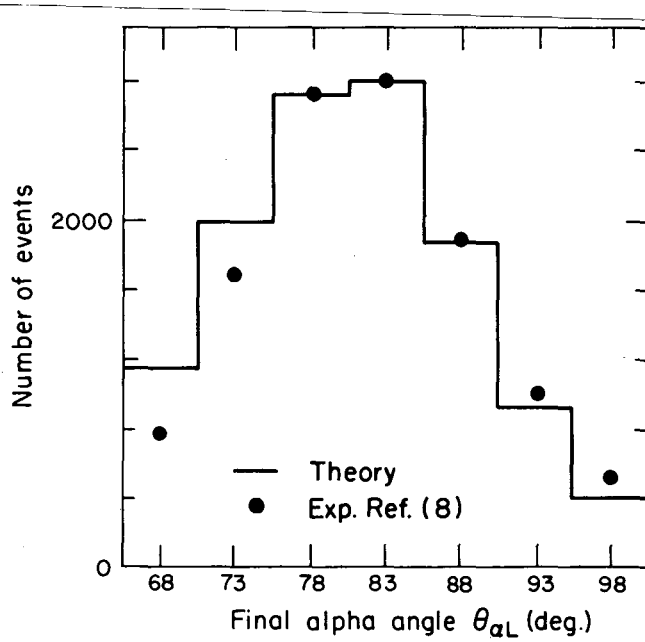

Fig. 3. Final alpha angular distribution (histogram: theory–all energies; dot: experiment of ref. 8–energies > 7.5 MeV). XBL 821-4425

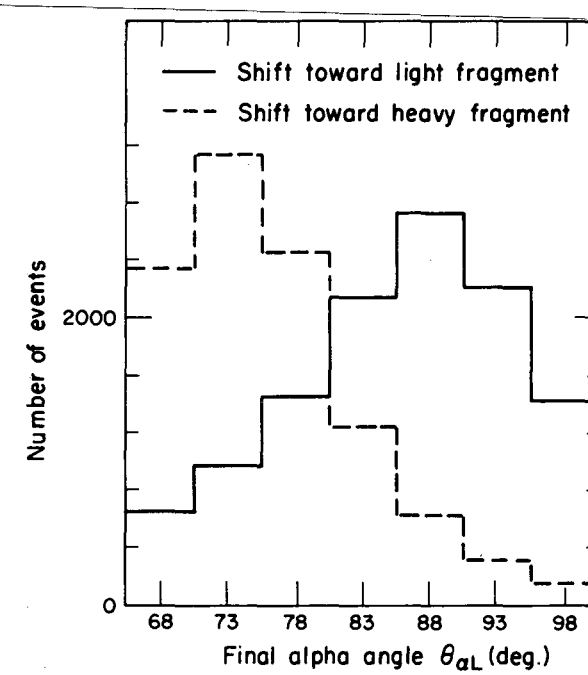

Fig. 5. Final alpha angular distributions (all energies) for the two source-shift cases. XBL 821-4406

shifted from saddle toward light fragment might give optimum agreement with experiment down to fine details of satellite structure.

We believe that our calculations and those of ref. 2 show the adequacy of Monte Carlo work based on the dominant monopole-monopole Coulomb interaction. The refinements of the higher moment interactions explored by Carjan and Leroux[3] remain to be more fully taken into account, but they will require a greater attention to dynamics of large-amplitude nuclear vibrations. Likewise, nuclear forces in the calculations could alter trajectories grazing one of the fragments. It is not always clear from earlier trajectory papers whether energy and momentum were strictly conserved, as here, or whether the alpha moved in the field of the unperturbed fission fragments. It is hard to say how much difference it makes to take the recoil terms into account.

Without much more study of varying parameters of initial conditions, it is hard to say how uniquely fixed are the conditions in parameter space. We used a theoretical value of 13 MeV for scission-point fission kinetic energy. It seems unlikely that substantial departures from this value could be compensated by other parameters.

A future goal might well be to formulate a dynamic model for the initial conditions of alpha and fission fragments and to extend to fragments other than alphas. We hope our work constitutes a step toward these goals.

Footnotes and References

*Condensed from LBL-13901

†LBL and Physics Department, Kuwait University, Kuwait

‡Universidade Federal do Rio de Janeiro, Brazil.

1. C. Guet, C. Signarbieux, P. Perrin, H. Nifenecker, M. Asghar, F. Caitucolli, and B. Leroux, Nucl. Phys. **A314**, 1 (1979).
2. C. Guet, H. Nifenecker, C. Signarbieux, and M. Asghar, Proc. Int. Symp. on Phys. and Chem. of Fission, Jülich, May 1979. IAEA Report SM-241/F13.
3. N. Carjan and B. Leroux, Phys. Rev. C **22**, 2008 (1980).

Feedback and Self-Regulation in Energy and Mass Exchange Between Heavy Ions*

L.G. Moretto

I would like to consider here two apparently unrelated aspects of heavy ion reactions: the energy partition between fragments on the one hand, and the lack of mass drift on the other.

The former aspect is that the dissipated energy is divided between the fragments proportionally to their masses. This feature is characteristic of thermal equilibrium between the two fragments. Experiment shows that such a thermal-like energy partition is present even at the smallest energy losses and thus at the shortest interaction times.[1-3] Just about any mechanism that may be involved in the energy transfer process tends to deposit approximately equal energy in the two fragments, irrespective of the mass asymmetry. So, how does the system succeed in equilibrating so quickly?

The problem with the second aspect resides in the lack of drift toward symmetry of the mass distributions as a function of Q-value (time) when such a drift is predicted by the potential energy gradient as a function of mass asymmetry.[4] In fact, this drift is indeed observed and in the correct direction, but only when the relative motion of the fragments is exhausted. It seems fairly safe to conclude that the

mass drift is controlled by something else besides the potential energy.

Let us assume that particle transfer alone is responsible for energy dissipation. Let us also assume that the particle fluxes are temperature-dependent. Since particle exchange deposits nearly the same amount of energy in each fragment, if the system is asymmetric, the lighter fragment must grow hotter. This temperature gradient creates an imbalance in the particle fluxes, the large fragment receiving more nucleons than it gives away. Since the *energy deposition on each fragment is proportional to the number of nucleons that land on it,* more energy will now be deposited on the heavy fragment in an attempt to correct the temperature gradient. Therefore we see here a feedback effect that leads to a self-regulation in the energy partition. The initially generated thermal imbalance redirects the energy depsition toward the large fragment and controls the thermal gradient *at the expense of the mass of the light fragment.*

Let us consider two objects moving *tangent* to one another with a window open between them which allows for particle transfer. Let $\Phi(T)$ be the particle flux and $\Phi_E(T)$ be the energy flux exclusive of the relative motion. Also let the energy temperature relation be given by $E = Nf(T)$, and the nucleon mass $m = 1$.

Particle conservation gives the first equation,

$$\frac{dN}{dt} = \Phi(T_2) - \Phi(T_1). \qquad (1)$$

Notice that in the absence of an external driving force

$$\frac{dN_1}{dt} < 0 \text{ if } T_2 > T_1 .$$

From momentum conservation we have:

$$\frac{dp_i}{dt} = -V_1\Phi(T_i) - V_2\Phi(T_2) = N_1\frac{dV_1}{dt} + V_1\frac{dN_1}{dt}$$

$$N_1\frac{dV_1}{dt} = -(V_1+V_2)\Phi(T_2);$$

$$N_2\frac{dV_2}{dt} = -(V_1 + V_2)\Phi(T_1).$$

Finally:

$$\frac{d\ln V}{dt} = -\left(\frac{\Phi(T_2)}{N_1} + \frac{\Phi(T_1)}{N_2}\right);$$

$$V = V_1 + V_2 \qquad (2)$$

From energy conservation we have

$$\frac{dE_1}{dt} = \Phi_E(T_2) - \Phi_E(T_1) + \frac{1}{2}\Phi(T_2)V^2 . \qquad (3)$$

In order to obtain an equation for the temperature we can use

$$E = N\,f(T); \quad \frac{dE}{dt} = f(T)\frac{dN}{dt} + N\frac{df(T)}{dT}\frac{dT}{dt}$$

$$= f(T)\frac{dN}{dt} + c_v\frac{dT}{dt}$$

where c_v is the heat capacity.

Solving for dT/dt we have

$$\frac{dT_1}{dt} = \frac{1}{c_{v,1}}\Big[\Phi_E(T_2) - \Phi_E(T_1)$$

$$- f(T_1)\Big\{\Phi(T_2) - \Phi(T_1)\Big\} + \frac{1}{2}\Phi(T_2)V^2\Big] \qquad (4)$$

$$\frac{dT_2}{dt} = \frac{1}{c_{v,2}}\Big[\Phi_E(T_1) - \Phi_E(T_2)$$

$$- f(T_2)\Big\{\Phi(T_1) - \Phi(T_2)\Big\} + \frac{1}{2}\Phi(T_1)V^2\Big] . \qquad (5)$$

The last two equations show the feedback quite clearly. If, for instance, $T_1 > T_2$, the last term of eq. (5) will increase the value of dT_2/dt provided that there is a nonzero relative velocity.

Let us consider the case of two finite nuclei constituted of classical gases. The natural units are defined as

$$n_1 + n_2 = 1 \quad n_1 - n_2 = r$$

$$n_1 = \frac{1+r}{2}; \quad n_2 = \frac{1-r}{2} .$$

The equations in dimensionless form are:

$$\frac{dr}{d\tau} = 2\left(\sqrt{T_2} - \sqrt{T_1}\, e^{-\Delta/T_1}\right) \tag{6}$$

$$\frac{d\ \ln v}{d\tau} = -2\left(\frac{\sqrt{T_2}}{1+r} + \frac{\sqrt{T_1}}{1-r}\, e^{-\Delta/T_1}\right) \tag{7}$$

$$\frac{dT_1}{d\tau} = \frac{4}{3(1+r)}\left[\sqrt{T_2}\left(2T_2 + \Delta - \frac{3}{2}T_1\right) - \sqrt{T_1}\, T_1\left(\frac{1}{2} + \frac{\Delta}{T_1}\right)e^{-\Delta/T_1} + \frac{1}{2}\sqrt{T_2}\, v^2\right] \tag{8}$$

$$\frac{dT_2}{d\tau} = \frac{4}{3(1-r)}\left[\sqrt{T_1}\, e^{-\Delta/T_1}\left(2T_1 + \Delta - \frac{3}{2}T_2\right) - \sqrt{T_2}\, T_2\left(\frac{1}{2} + \frac{\Delta}{T_2}\right) + \frac{1}{2}\sqrt{T_1}\, v^2\right] . \tag{9}$$

Notice that the potential gradient Δ can be made to depend on r. Also notice that there exists a stationary state for T_1, T_2 that is not an equilibrium state in general. On the other hand, there is no stationary state for r. Let us consider first the case for $\Delta = 0$. In Fig. 1 a case is studied for an initial asymmetry of 1:3 ($r = -0.5$). The temperatures T_1, T_2 and their ratio are shown as a function of time τ. Both T_1 and T_2 initially increase, T_1 rising faster than T_2 until the feedback effect contains the differential rise and brings the two temperatures together. Simultaneously, the asymmetry grows larger and eventually saturates at a new larger value. The quantity Q is defined as $Q = \frac{E_1/E_2}{(E_1/E_2)eq}$. At the beginning it takes the value 3 due to the equal energy deposition and to the mass ratio, 1:3. However, the feedback effect rapidly reduces the value of this quantity to its equilibrium limit, namely 1. In Fig. 2 we see the effect of the interplay between the dynamical drift towards greater asymmetry and the static driving force towards symmetry. One observes an initial compliance of the system to the potential energy, the

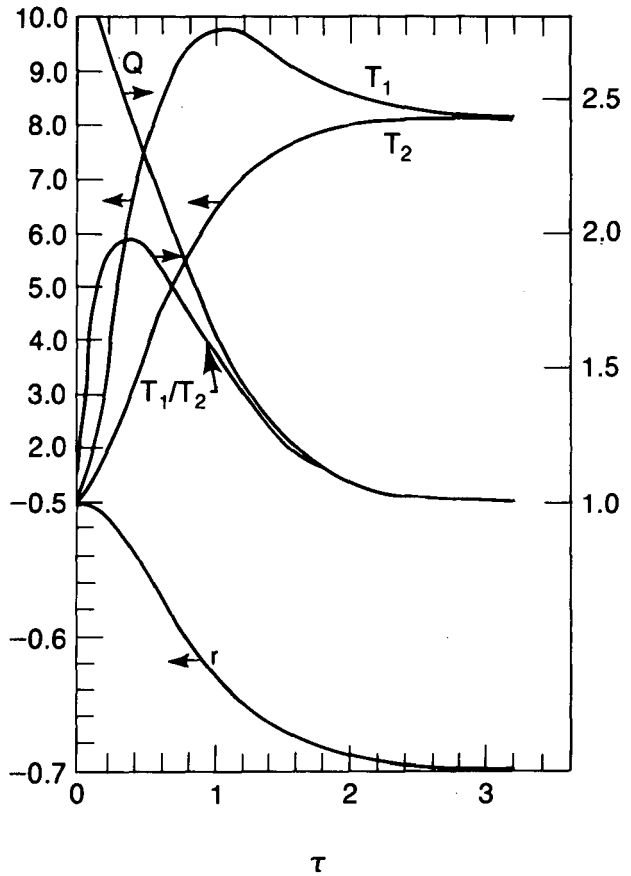

Fig. 1. Dependence of T_1, T_2, T_1/T_2 and $Q = \frac{E_1/E_2}{A_1/A_2}$ as well as of r upon time. XBL 844-10428

onset of the dynamical effect which counteracts the potential as soon as the temperature gradient is established, and the final drift towards symmetry once the kinetic energy in the relative motion has been dissipated. In Fig. 3 we can observe the dependence of the mass asymmetry upon energy. Again one can comment on the general ability of the dynamical effect to counteract the drift towards symmetry over the entire range of energy losses. Only when all the energy is dissipated can the system finally drift toward asymmetry.

Footnote and References

*Condensed from the proceedings of the 21st International Winter Meeting on Nuclear Physics, Bormio, Italy, January 1983.

1. B. Tamain, R. Chechik, H. Fuchs, F. Hanappe,

M. Morjean, C. Ngø, J. Péter, Nucl. Phys. **A330**, 253 (1979).

2. Y. Eyal, A. Gavron, I. Tserruya, Z. Fraenkel, Y. Isen, S. Wald, R. Bass, J.R. Gould, G. Kreyling, R. Renfort, K. Stelzer, R. Zitzmann, A. Gobbi, U. Lynen, H. Stelzer, I. Rode, R. Bock, Phys. Rev. Lett. **41**, 625 (1978).
3. D. Hilscher, J.R. Birkelund, A.D. Hoover, W.U. Schröder, W.W. Wilke, J.R. Huizenga, A. Mignerey, K.C. Wolf, H.F. Breuer, V.I. Viola, Phys. Rev. **C20**, 576 (1979).
4. For the abundant literature on the mass distributios see for instance: W.U. Schröder, J.R. Huizenga, Ann. Rev. Nucl. Sci. **27**, 465 (1977); M. Lefort and G. Ngø, Ann. Phys. (N.Y.) **3**, 5 (1978); L.G. Moretto, R.P. Schmitt, Rep. Prog. Phys. **44**, 543 (1981).

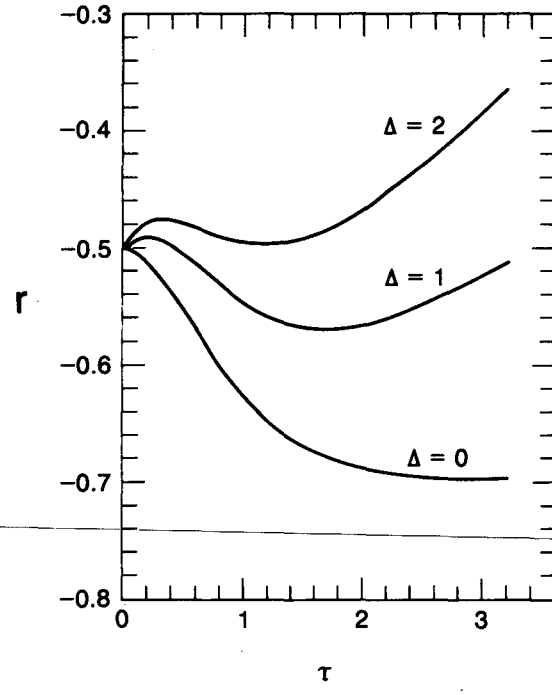

Fig. 2. Dependence of the mass asymmetry r upon time for different values of the driving force Δ.
XBL 844-10427

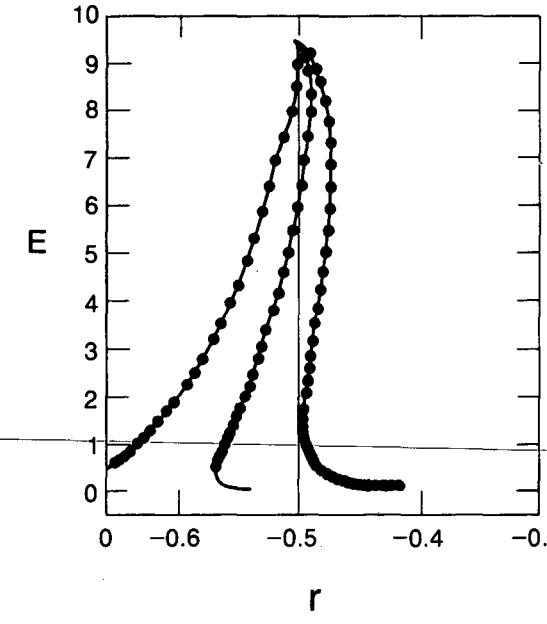

Fig. 3. Dependence of the mass asymmetry r upon time for different value of Δ. XBL 844-10425

A Feedback Process Controlling Energy Partition and Mass Exchange Between Heavy Ions*

L.G. Moretto,[†] *E.G. Lanza*[‡]

In a previous contribution we have shown the possible relation between the interfragment thermalization and the lack of the expected mass drift toward symmetry. In this work we show that both effects can be explained in terms of particle exchange with Fermi fluxes. In order to perform some relevant calculation, we apply the model described in the previous report to two Fermi gases separated by a barrier.

The one-way particle flux is given by:

$$\Phi(T) = K\left[\frac{\pi^2}{12}T^2 + T(\mu - B)\ln(1 + \exp\frac{\mu - B}{T}) + T^2\int_{(B-\mu)/T}^{0}\frac{z}{1+e^z}dz\right].$$

The corresponding energy flux, exclusive of the damped energy, is given by

$$\Phi_E(T) = K\left[\frac{3}{2}\zeta(3)T^3 + \frac{\pi^2}{12}T^2(2\mu - B) + T\mu(\mu - B)\ln(1 + \exp\frac{\mu - B}{T}) + T^2(2\mu - B)\int_{(B-\mu)/T}^{0}\frac{z}{1+e^z}dz + T^3\int_{(B-\mu)/T}^{0}\frac{z^2}{1+e^z}dz\right]$$

where μ is the chemical potential, $\zeta(3)$ is the zeta function of argument 3, B is the barrier height and T is the temperature. Relevant limits for small and large values of the quantity $(\mu-B)/T$ are easily obtained.

A calculation performed for an asymmetric system (A_1 = 50, A_2 = 150) at 300 MeV center of mass energy is shown in Fig. 1 for the following values of $\mu-B$: 0.5 MeV, 10 MeV, 20 MeV, 30 MeV and 40 MeV. The temperature dependence of the one-sided flux goes from very great at the lower range of this interval, to minimal at the upper range. The upper part of Fig. 1 shows the temperature ratio T_1/T_2 as a function of kinetic energy. For very low barriers (e.g., $\mu-B$ = 40 MeV) the temperature ratio goes rapidly up to $\sqrt{3}$ consistently with equal energy deposition, and weakly declines thereafter. The effect of thermal conductivity is visible in the very late decline associated with the largest energy losses. In this regime there is little self-regulation and a very slow thermalization. For a barrier very close to the Fermi surface, the result is dramatically different. The initial rise in temperature ratio is quickly controlled by the feedback effect and kept within a narrow range above unity throughout the Q-value range. In this case we see that the feedback effect is present and that it leads to a very nearly thermalized energy partition even at moderately low energy losses.

The lower part of Fig. 1 shows the dependence of the mass of the light fragment upon energy loss. For low barrier values the mass remains fixed near 50 for most of the Q-value range. Only very late in the collision does one observe a decrease in mass as a late and slow response of the system to a great temperature gradient. For barriers near the Fermi

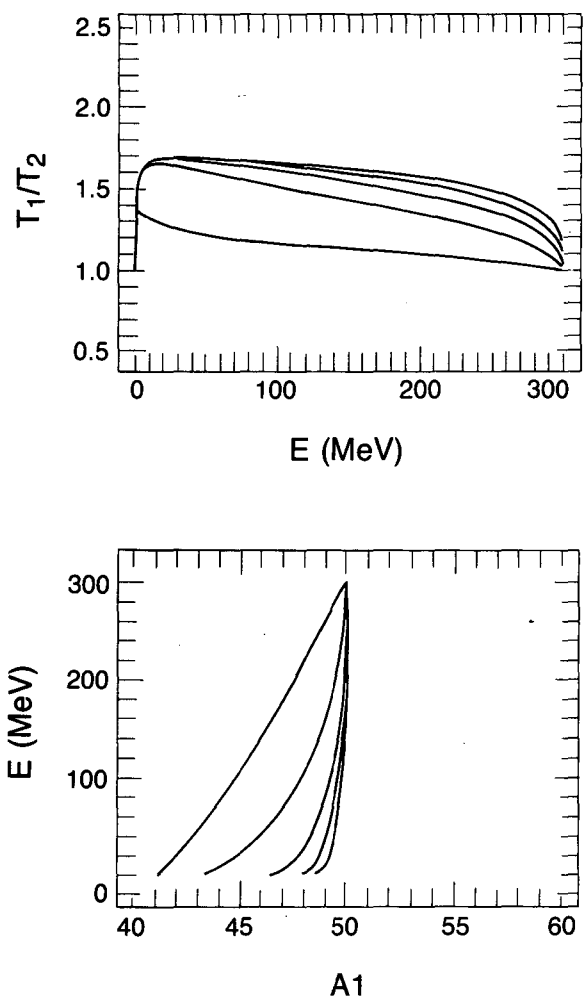

Fig. 1. Top: Temperature ratio vs. total kinetic energy loss for a set of values of $\mu-B$ (see text).

XBL 844-10430

Bottom: Light fragment mass vs. kinetic energy for the same value of $\mu-B$ from right to left.

XBL 844-10431

surface the fluxes become substantially imbalanced at once, and the light fragment loses mass steadily throughout the Q-value range. This calculation quantitatively verifies our expectation. When the barrier is close to the Fermi surface, the temperature dependence of the fluxes is sufficiently strong to set a strong feedback effect in motion leading to a fine control of the temperature gradient on one hand and to a steady mass loss suffered by the light fragment on the other.

In Fig. 2 the effect of a progressively greater driving force toward symmetry is studied. The curves shown represent the light fragment mass as a function of kinetic energy for the following driving forces: 0, 0.5, 1.0, 1.5, 2.0 MeV/nucleon, the lower Fermi surface being 0.5 MeV above the barrier. For nonzero driving forces we observe an initial tendency of the system to move toward symmetry. This tendency is readily controlled and even inverted by the feedback process as soon as a temperature gradient is established. Only very late in the collision, when lack of energy in the relative motion prevents the feedback process from operating, can the system follow the driving force toward symmetry once again. In the inset of Fig. 2 the pre-evaporation light fragment mass vs Q-value for the reaction Kr + Er shows a behavior that is not unlike that predicted by this theory.

The response of the system to a driving force depends rather strongly on the difference between average chemical potential and the barrier $\bar{\mu} - B$. Large values of $\bar{\mu} - B$ lead to a small mass drift when observed against energy loss. The reason is that the energy loss rate depends upon the sum of the one-way fluxes while the drift depends on their difference. In Fig. 3 such an effect is illustrated. The relation between energy loss and light fragment mass is shown for $\bar{\mu} - B = 50, 25, 10, 0.5$ MeV with a driving force of 1.5 MeV. The systematic increase of the mobility with decreasing $\bar{\mu} - B$ is readily seen at small energy losses. However, at the smallest values of $\bar{\mu} - B$ the increased mobility is compensated by the feedback effect which, as was already seen in Fig. 2, stabilizes the mass near the entrance channel value. Consequently, while a small mass drift could be consistent with either large or small $\bar{\mu} - B$, the near thermalization of the dissipated energy is consistent only with a small value of $\bar{\mu} - B$.

Footnotes and References

*Condensed from LBL-16373

†LBL and Max-Planck-Institut für Kernphysik, Heidelberg.

‡Max-Planck-Institut für Kernphysik, Heidelberg.

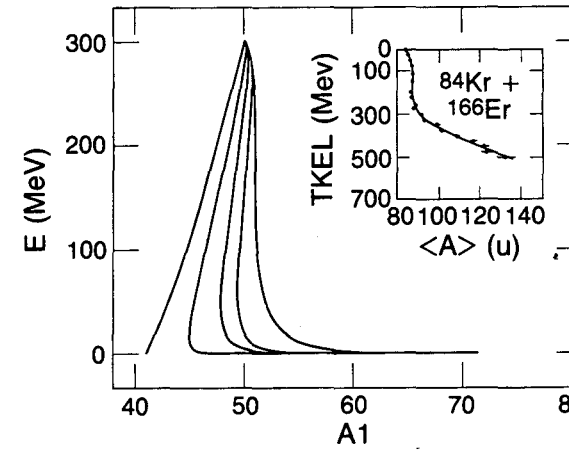

Fig. 2. Light fragment mass vs. kinetic energy for different driving forces (see text). The inset shows the experimental pre-evaporation mass in the reaction $^{84}Kr + ^{166}Er$. XBL 844-10426

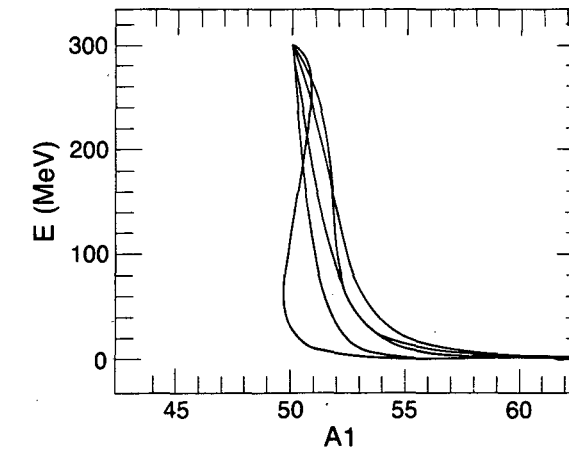

Fig. 3. Light fragment mass vs. kinetic energy for different values of $\mu - B$ and a fixed driving force. XBL 844-10429

New Statistical and Non-Statistical Effects in Deep Inelastic Heavy Ion Collisions*

L.G. Moretto

The physics of deep inelastic heavy ion collisions is briefly reviewed in the light of the experimental capabilities offered by large Tandem Accelerators. Three aspects are selected for illustration. The first is the problem posed by the angular distributions. The role of quantal fluctuations (diffraction) and of dynamical fluctuations is discussed. The possibility of extracting angular momentum fluctuations from the angular distribution width is pointed out, as well as the way to compare such results with those obtained from gamma-ray multiplicities or angular distributions. The likely sources of angular momentum fluctuations are discussed. The second problem is that of energy dissipation and partition. The experimental evidence for thermal equilibrium is reviewed and experiments to test thermal equilibrium through the measurement of the variance in the energy distribution are suggested. The correlation between energy loss and the mass variance is reviewed in terms of the mass transfer mechanism. Possible ways to determine the mass of the transferred particle are illustrated. The third problem considered is the experimental lack of mass drift in the mass distributions vs. Q-value when it is expected on the basis of potential energy considerations. This problem is associated with the fast fragment thermalization and explained in terms of a feed-back effect associated with the temperature gradient that developes between two colliding nuclei of different mass.

*Presented at the International Symposium on Nuclear Physics at Large Tandem Accelerators, Legnaro-Padova, Italy, March 15–17, 1983. Condensed from LBL-16371.

The Phenomenology of Deep-Inelastic Processes*

L.G. Moretto

The field of heavy-ion deep-inelastic reactions is reviewed with particular attention to the experimental picture. The most important degrees of freedom involved in the process are identified and illustrated with relevant experiments. Energy dissipation and mass transfer are discussed in terms of particles and/or phonons exchanged in the process. The equilibration of the fragment neutron-to-proton ratios is inspected for evidence of giant isovector resonances. The angular momentum effects are observed in the fragment angular distributions and the angular momentum transfer is inferred from the magnitude and alignment of the fragments' spins. The possible sources of light particles accompanying the deep-inelastic reactions are discussed. The use of the sequentially emitted particles as angular momentum probes is illustrated. The significance and uses of a thermalized component emitted by the dinucleus is reviewed. The possible presence of Fermi jets in the prompt component is shown to be critical to the justification of the one-body theories.

*Presented at the International Conference on Heavy Ion Physics and Nuclear Physics, Catania, Italy, March 21–26, 1983. Condensed from LBL-16372.

Statistical Properties of Deep Inelastic Reactions*

L.G. Moretto

The multifaceted aspects of deep-inelastic heavy-ion collisions are discussed in terms of the statistical equilibrium limit. It is shown that a "conditional" statistical equilibrium, where a number of degrees of freedom are thermalized while others are still relaxing, prevails in most of these reactions. The individual degrees of freedom that have been explored experimentally are considered in their statistical equilibrium limit, and the extent to which they appear to be thermalized is discussed. The interaction between degrees of freedom on their way towards equilibrium is shown to create complex feedback phenomena that may lead to self-regulation. A possible example of self-regulation is shown for the process of energy partition between fragments promoted by particle exchange.

*Presented at the International Conference on Nuclear Physics, Florence, Italy, August 29 – September 3, 1983. Condensed from LBL-16390.

High Energy Collisions

Effect of Fluctuations on Global Analysis of Fluid Dynamical Calculations for High-Energy Nuclear Collisions*

L.P. Csernai,† G. Fái,‡ and J. Randrup

Recent experimental developments promise to give us a better insight into the dynamics of high-energy nuclear collisions. A major objective of those efforts is to determine whether collective-flow effects can be identified and distinguished from expectations based on intranuclear cascade calculations. However, one expects, and recent studies confirm, that the formation of composite fragments, the finiteness of the multiplicity, and the statistical fluctuations in the final states affect the event analysis in important ways. In the present work we wish to elucidate this situation by analyzing events generated theoretically using fluid-dynamical results[1] in conjunction with the statistical simulation model by Fái and Randrup.[2]

Our starting point is a series of detailed three-dimensional fluid-dynamical calculations. From these results we extract certain gross features that are used to give an approximate characterization of the final state of the fluid dynamical stage of the collision in terms of a few sources, usually one participant source and two spectator sources. These sources are then subsequently treated in two alternative ways:

i) *In the first*, each source is described as a grand canonical ensemble so that the mean fragment abundancies and spectral distributions can be calculated from the associated partition functions. Having determined the grand canonical parameters, we can then calculate directly the associated flow tensor and subsequently the global parameter of interest, namely the flow angle Θ, the aspect ratio $R_{1/3}$, etc.

ii) *In the alternative treatment* of the sources, we use the explosion-evaporation model of ref. 2 to generate statistically a number of actual events and make the flow analysis for each event separately, as is done experimentally. We then proceed to compare the two sets of results and achieve an impression of the effects arising from composite fragment formation, finite multiplicity, and statistical fluctuations.

In Fig. 1 we compare the resulting fluid-dynamical and statistically generated flow diagrams (flow angle Θ versus aspect ratio $R_{1/3}$) in the collision ^{93}Nb + ^{93}Nb at 400 MeV/nucleon. The continuous curves represent the fluid-dynamical expectation with three different species selections: 1) protons only; 2) all hydrogen and helium fragments, i.e., p, d, t, ^{3}He, α; and 3) all fragments, including neutrons. In the fluid-dynamical description a given impact parameter yields a well-defined point in the flow diagram (in the actual generation of the figures the impact parameters s/s_{max} = 0.1, 0.3, 0.5, 0.7 have been used). Nevertheless, at each impact parameter we included the full fluid-dynamical curve to guide the eye. As should be expected, exclusion of the heavier fragments leads to more spherical events. Since the fluid-dynamical description does not include the secondary evaporation-type deexcitation of the spectators, we terminated the continuous lines for selections 1 and 2 at the impact parameters where the spectators no longer explode, thereby leading to the fluid-dynamical treatment of one source only, which, by definition, results in complete sphericity.

In the figure a sample of ten statistically generated events are displayed as dots (if $\Theta \leqslant \pi/2$) or crosses ($\Theta > \pi/2$, $\pi - \Theta$ plotted) for each impact parameter considered. It is immediately clear that fluctuations play an important role here: the spread of the points is very large and they follow only very

loosely the fluid-dynamical expectation. (As a word of caution we stress that the employed parameterization of the fluid-dynamical results was meant for intermediate and large impact parameters, so that good correspondence should not be expected for central collisions.)

When comparing selections 1), 2), and 3), one should remember that the flow tensor, although ideally coalescence invariant, depends on the specific species selection which must always be made in a real experiment. Thus, in contrast to naive expectations, the observed flow tensor is *not* coalescence invariant, as is clearly borne out by Fig. 1. Due to the final evaporation there is an observable shift for light fragments (selections 1 and 2) toward more elongated emission patterns compared to fluid-dynamical expectations. The fluctuations associated with these selections are also considerably larger than those of selection 3. Especially the fluctuation of the flow angle Θ is very large for small impact parameters, because the events are rather close to spherical.

In conclusion, we have shown that the total flow tensor (selection 3) is fairly close to the fluid-dynamical expectation. However, in the experimental situation, where only light fragments are considered, the measured flow tensor depends strongly on the cut-off on the fragment mass considered. It is very important to take account of this fact when comparing experimental and theoretical results.

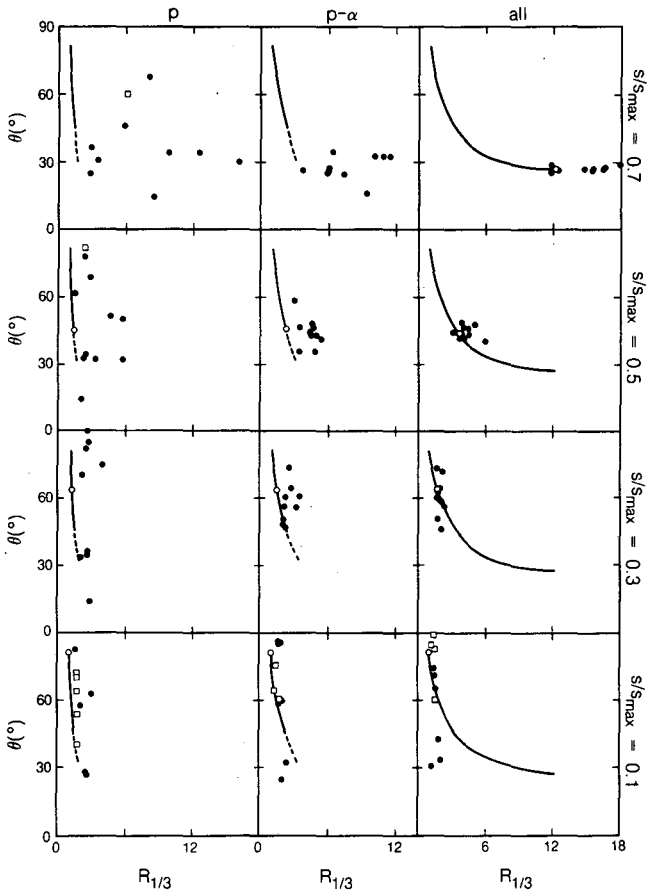

Fig. 1. Fluid-dynamical (continuous curves with open circles) and statistically generated (dots if $\Theta < \pi/2$ and open squares if $\Theta > \pi/2$) flow diagrams: flow angle Θ versus the aspect ratio $R_{1/3}$ of the flow tensor for the reaction $^{93}Nb + ^{93}Nb$ at 400 MeV/nucleon energy. Four different impact parameters s = 0.1, 0.3, 0.5, 0.7 s_{max} and three different fragment species selections (p, p-α, all fragments) are shown. At each impact parameter the full fluid-dynamical curve is plotted. Both the fluid-dynamical expectation and the statistically generated flow tensor depend strongly on the species selection.

XBL 8311-774

Footnotes and References

*Condensed from LBL-16440

†Central Research Institute for Physics, Budapest, Hungary

‡R. Eötvös University, Budapest, Hungary

1. L.P. Csernai, H. Stöcker, P.R. Subramanian, G. Graebner, A. Rosenhauer, G. Buchwald, J.A. Maruhn, W. Greiner, Phys. Rev. **C28** (1983) in press
2. G. Fái, J. Randrup, Nucl. Phys. **A404**, 551 (1983).

Global Event Analysis as a Tool to Study the Nuclear Matter Equation of State*

H. Stöcker, G. Buchwald, G. Graebner, J. Haruhn, W. Greiner, K. Frankel, M. Gyulassy

We compared intranuclear cascade calculations with fluid dynamic calculations to the expected global characteristics of nuclear collisions. The kinetic flow tensor[1] was computed in both cases. The most significant finding was the sensitivity of the energy dependence of the kinetic flow ratio R_{13} to the equation of state. Cascade calculations give R_{13} independent of energy. However, in the energy range $E_{lab} \sim 100 - 1000$ MeV/nucleon fluid calculations predict a strong energy dependence of that ratio. In addition that "excitation" curve can easily distinguish between nuclear compressibility moduli K = 200 and 400 MeV. Thus, we proposed that an experimental determination of that excitation function could help constrain the nuclear matter equation of state. A variety of background effects were also considered and suggestions for their removal made.

Footnote and Reference

*Condensed from Michigan State University preprint MSU-409 (1983).

1. M. Gyulassy, K. Frankel, H. Stöcker, Phys. Lett. **110B**, 185 (1983).

Jacobian-Free Global Event Analysis*

P. Danielewicz and M. Gyulassy

We show that the conventional global event analysis using the sphericity tensor is biased against shapes with degenerate radii and vanishing flow angles for multiplicities $M < 100$. The general sphericity matrix[1] is given by

$$S_{ij} = \sum_{\nu=1}^{M} \omega_\nu \, p_i(\nu) \, p_j(\nu) \qquad (1)$$

where i,j = 1,2,3 refer to a Cartesian coordinate system with the 3-axis pointed along the beam direction, and ω_ν are weight factors. The measurement of S requires the determination of the momenta $\mathbf{p}(\nu)$ of M particles in each event.

For a given M particle distribution ρ_M associated with a fixed reaction plane, the probability to find the matrix elements of S between T_{ij} and $T_{ij} + dT_{ij}$ is

$$\Phi_M(T) = \int d\mathbf{p}(1), \ldots, \int d\mathbf{p}(M)$$
$$\rho_M(\mathbf{p}(1), \ldots, \mathbf{p}(M)) \prod_{i \geq j} \delta(S_{ij} - T_{ij}). \qquad (2)$$

In the limit $N \to \infty$, the central limit theorem assures that $\Phi_M(T)$ will be of a Gaussian form, strongly peaked around average $\langle S_{ij} \rangle$ that depend only on the single-particle distribution associated with the reaction plane. Experimentally, however, we have no control on the reaction plane. On the event by event basis the geometrical content of S is exhibited by the diagonalization:

$$S = \Lambda F \Lambda^+ , \qquad (3)$$

where $F = \mathrm{diag}\,(f_1, f_2, f_3)$ is the diagonal matrix of eigenvalues ordered such that $0 \leq f_1 \leq f_2 \leq f_3$ and

$$\Lambda = R_x(\Phi) R_y(\Theta) R_z(X) \qquad (4)$$

is a product of the orthogonal rotation matrices. The angle Θ is the angle of most rapid collective matter flow, while Φ is an estimate of the reaction plane. With (3) S characterizes an event in the momentum space as an oriented ellipsoid with radii

$\sqrt{f_i}$. The transformation of the variables from S_{ij} to (f_i, Θ, Φ, X) necessarily brings in a Jacobian factor J (f_i, Θ) that multiplies (2)

$$J(t_i,\Theta) = \left| \frac{\partial^6 [\, \Lambda F \Lambda^+ \,]}{\partial^6 [\, f_i, \Theta, \Phi, X \,]} \right|$$

$$= \sin\Theta\,(f_3 - f_i)(f_3 - f_2)(f_2 - f_1)\,. \qquad (5)$$

The Jacobian expresses the vanishing of the phase space for small flow angles and shapes with degenerate radii. For multiplicities M < 100 the Jacobian strongly distorts the event shape and orientation. The finite multiplicity distortions are indicated in Fig. 1. The knowledge of the Jacobian (5) allows one to construct "corrected" distributions with the effects of the Jacobian removed. For example, for a 2-dimensional distribution in the aspect ratios $r_{32} = f_3/f_2$ and $r_{21} = f_2/f_1$, $d^2N/dr_{32}dr_{21}$, the Jacobian-free distribution is

$$\frac{d^2N}{dr_{32}dr_{21}} = \frac{(1 + r_{21} + r_{21}r_{23})^6}{r_{21}^2(r_{32}-1)(r_{21}-1)(r_{32}r_{21}-1)} \frac{d^2N}{dr_{32}dr_{21}}\,, \qquad (6)$$

and for the degenerate shapes the distributions are compared in Fig. 2.

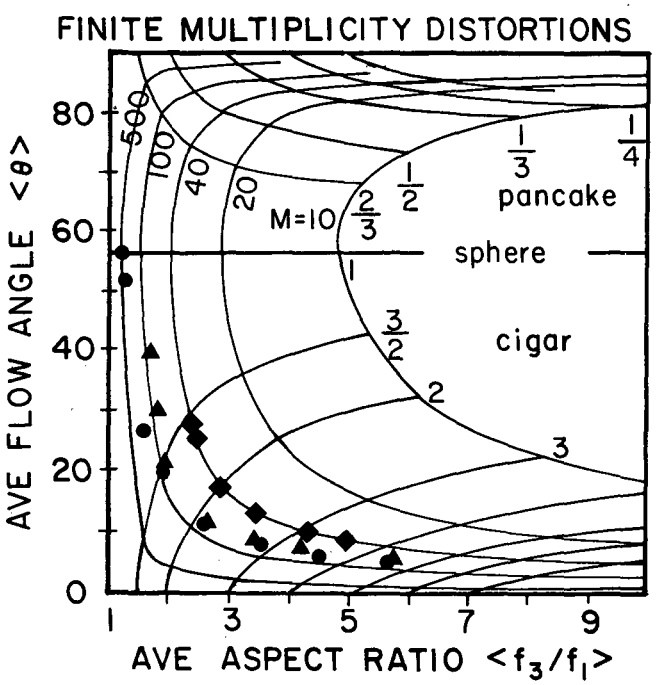

Fig. 1. Average polar angle and aspect ratio f_3/f_1 for events sampled from shapes along the beam axis, with different multiplicities M. The sphere is mapped onto the <Θ> = 57° line. The diamonds, triangles and dots correspond to the intranuclear calculations of ref. 1. XBL 832-8003

Footnotes and References

*Condensed from Phys. Lett. **129B**, 283 (1983) and LBL-15721.

1. M. Gyulassy *et al.*, Phys. Lett. **110B**, 185 (1982).

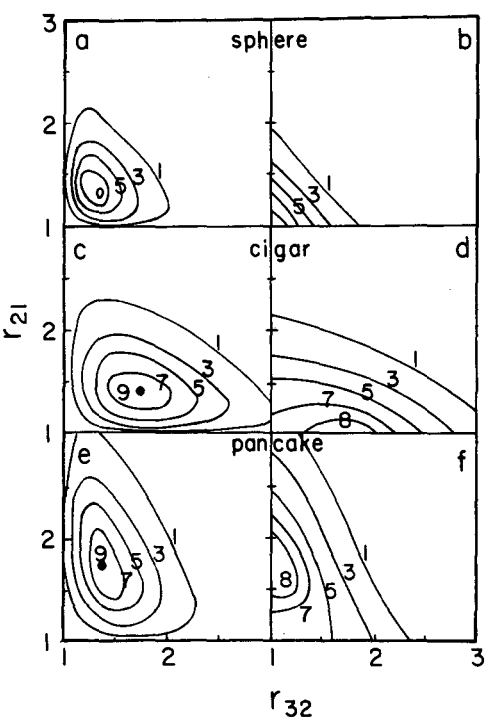

Fig. 2. Double differential distributions of aspect ratios r_{32} and r_{21} (a, c, e) compared with the Jacobian-free distribution (b, d, f) for degenerate shapes and multiplicity 40. XBL 832-8004

Non-Binary Effects in High-Energy Nuclear Collisions

K.C. Chung, R. Donangelo, S.B. Duarts, T. Kodama, R.A.M.S. Nazareth, J. Randrup

The intra-nuclear cascade model (INC) is being used extensively in studies of high-energy nuclear collisions. It is based on the assumption of sequential binary interactions between elementary hadrons. However, particularly during the early compressional stage, the dynamical conditions are often such that simultaneous interactions between several particles are expected. We have undertaken a study to elucidate this problem.

To this end we consider a model system of nucleons which interact via a static two-body potential. We then solve the corresponding coupled classical equations of motion for a nucleus-nucleus collision. The results are compared with the corresponding intra-nuclear cascade results. These are obtained by letting two nucleons scatter at their closest approach according to the deflection function dictated by the chosen two-body interaction. We define dynamical clusters according to whether nucleons are within interaction range of each other. During the high-density stage many of the nucleons appear in clusters. During the expansions, the INC clusters again disintegrate, of course, but those of the exact solution largely remain forever. The angular distribution becomes more forward peaked while the rapidity distribution widens. We also find that the temperature in the system, as measured by the mean transverse kinetic energy per nucleon, is larger when the many-body effect is included.

Quantum Theory of Nonequilibrium Processes*

P. Danielewicz

Green's function techniques for nonequilibrium quantum processes are developed, with numerous possible nuclear applications. The techniques utilizing the single-particle Green's functions and self-energies, are closely related to the standard nuclear ground-state methods, and in fact reduce to these for the ground-state problem. Another standard limit of the theory is the thermodynamic equilibrium, in which limit the utilized Green's functions reduce to the temperature Green's functions. In their full generality, the Green's function techniques are devised for studying the time and space evolution of a nonequilibrium many-body system, and therefore are appropriate for the space-time evolution of a reaction of heavy nuclei. Various interactions can be summed up systematically and allow one to go beyond the mean-field approach to the nuclear collisions.

As a first application of the theory, the problem of equilibration in nuclear matter has been studied. The two-body collisions have been included, and the accomplished calculations correspond to a nuclear collision with the beam energy E_{lab}/nucleon = 400 MeV. One of the most amazing results emerged as a lowering of the scattering rates from the classical expectations. When the interaction strength is increased, the scattering rates do not increase arbitrarily but exhibit a saturating behavior (see Fig. 1). The value at the saturation is about equal to the temperature of the system.

Further applications of the theory will include a study of the equation of state, scattering rates, and their interrelation in dense excited nuclear matter, and a study of the transport coefficients for nuclear matter and their variation with temperature and density.

*Based on LBL-15436 and LBL-15437, Ann. Phys. in press.

Fig. 1. Rates Γ from quantum evolutions, averaged over momentum distributions close to equilibrium, plotted vs. averaged Γ from Boltzmann equation, when the multiplication constant in the potential is varied. Long-dashed line corresponds to a Hartree-Fock initial state, solid to correlated initial states. Short-dashed line $\langle\Gamma\rangle = \langle\Gamma\rangle_{\text{Boltzmann}}$ serves as a guide to the eye. The arrow locates the values corresponding to the multiplication constant in the potential equal to 1. XBL 8210-4840

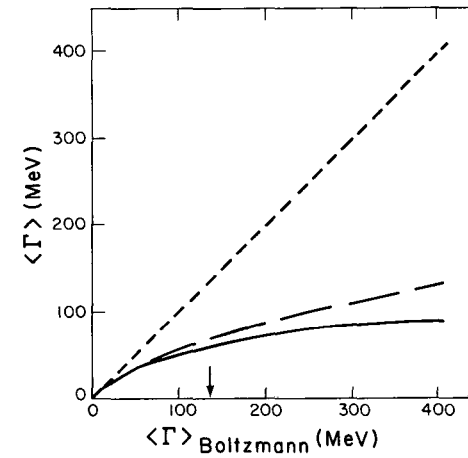

Quark-Gluon Plasma Evolution in Scaling Hydrodynamics*

M. Gyulassy and T. Matsui

Recently a new hydrodynamic theory has been proposed by Bjorken[1] and others[2] to describe the space-time evolution of the matter produced in ultrarelativistic central nuclear collisions, incorporating the inside-outside cascade picture of secondary particle formation. Based on this theory, we studied the relation between the rapidity density dN/dy of produced particles and the maximum energy density ϵ_0 attained in the central rapidity region. In the case of the isentropic (i.e., without entropy production) expansion described by a single equation of state, $p = c_0^2\epsilon$, we found

$$\epsilon_0 = \left[\frac{k}{\tau_0 A_\perp}\frac{dN}{dy}\right]^{1+c_0^2}$$

where k is the constant, $\tau_0 \sim 1$ fm/c is the time when the system starts to expand hydrodynamically, $A_\perp$ is the transverse area of the reaction zone, and c_0 is the sound velocity. For a Stefan-Boltzmann gas with $\epsilon = aT^4$, $c_0 = 1/\sqrt{3}$ and $k = 3/a^{1/4}$.

This result differs from the earlier estimate of ϵ_0 by Bjorken[1] in the point that we have included the effect of the energy loss, along the longitudinal expansion, due to the work done by the pressure acting on the neighboring cells. Thus our new estimate of the initial energy density for a given rapidity density exceeds Bjorken's previous estimate. We also considered the case when the system undergoes a first order phase transition from a quark-gluon plasma to a hadron gas through an isentropic path. This was done by making use of the MIT bag equation of state for a quark-gluon plasma phase and the Shuryak resonance gas equation of state for a hadron gas phase. The result is plotted in Fig. 1 by two dashed lines which correspond to two different choices of parameters. The solid dots on these curves indicate the critical energy density which is required to complete the phase transition to the plasma phase. For comparison we show a result for viscous expansion along the path of maximum entropy production by the solid curve, which coincides with Bjorken's result. The data for the reduced rapidity density from $p\bar{p}$ collider events[3] and from a Si + Ag JACEE event[4] are also shown. From this analysis we infer that the energy density can reach well above the critical value in heavy ion collisions at cosmic-ray energies.

Footnote and References

*Condensed from LBL-15947, Phys. Rev. **D** in press.

1. J.D. Bjorken, Phys. Rev. **D27**, 140 (1983).
2. K. Kajantie, L. McLerran, Phys. Lett. **121B**, 415 (1982).
3. UA5 Collaboration, Phys Lett. **107B**, 310 (1981); UA1 Collaboration, CERN-EP/82-125 Rev. (1982) preprint.
4. T.H. Burkett *et al.*, Phys. Rev. Lett. **50**, 2062 (1983).

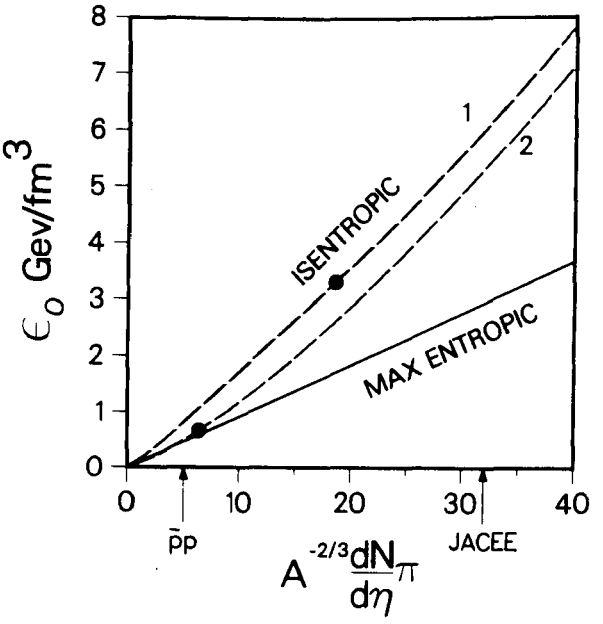

Fig. 1. Initial energy density versus reduced final pion multiplicity in the scaling domain. Curves explained in text. XBL 838-10935

Deflagrations and Detonations in Quark-Gluon Plasmas*

M. Gyulassy, K. Kajantie, H. Kurki-Suonio, L. McLerran

Quantum chromodynamics predicts the transition from nuclear matter to a quark gluon plasma when energy densities exceed a few GeV/fm^3. The rehadronization of that plasma is studied in terms of relativistic combustion theory. We study the consequences of a first order transition as illustrated by the Bag Model. Applying the hydrodynamic equations with that equation of state we first derive conditions under which one dimensional deflagration and detonation solutions can exist. We find that detonations require extreme supercooling conditions which are not likely to be reached in nuclear collisions. On the other hand, simple surface deflagrations cannot tolerate the moderate supercooling which is expected to occur. Therefore, we consider new bubble solutions as illustrated in Fig. 1. The space-time evolution of deflagration and detonation bubbles is shown. We consider the conversion of the plasma with energy density ϵ_2 to hadronic matter with energy density ϵ_0. Numerical estimates again show that detonation bubbles require unreasonably extreme supercooling. However, deflagration bubbles can occur readily for the conditions expected in nuclear collisions. This is the main result of this work.

We also consider observable consequences of such explosive processes. We identify large transverse energy density $dE_\perp/dy$, and multiplicity density, dN/dy, fluctuations coupled with large local circularity, dc/dy, as probable signatures. In addition, medium range correlations on a rapidity interval $\Delta y \sim 2 \ln R$ are expected. The observations of such signatures could help identify the production of this speculative new form of matter in ultrarelativistic nuclear collisions.

Footnote

*Condensed from LBL-16277 (1983) submitted to Nucl. Phys. B.

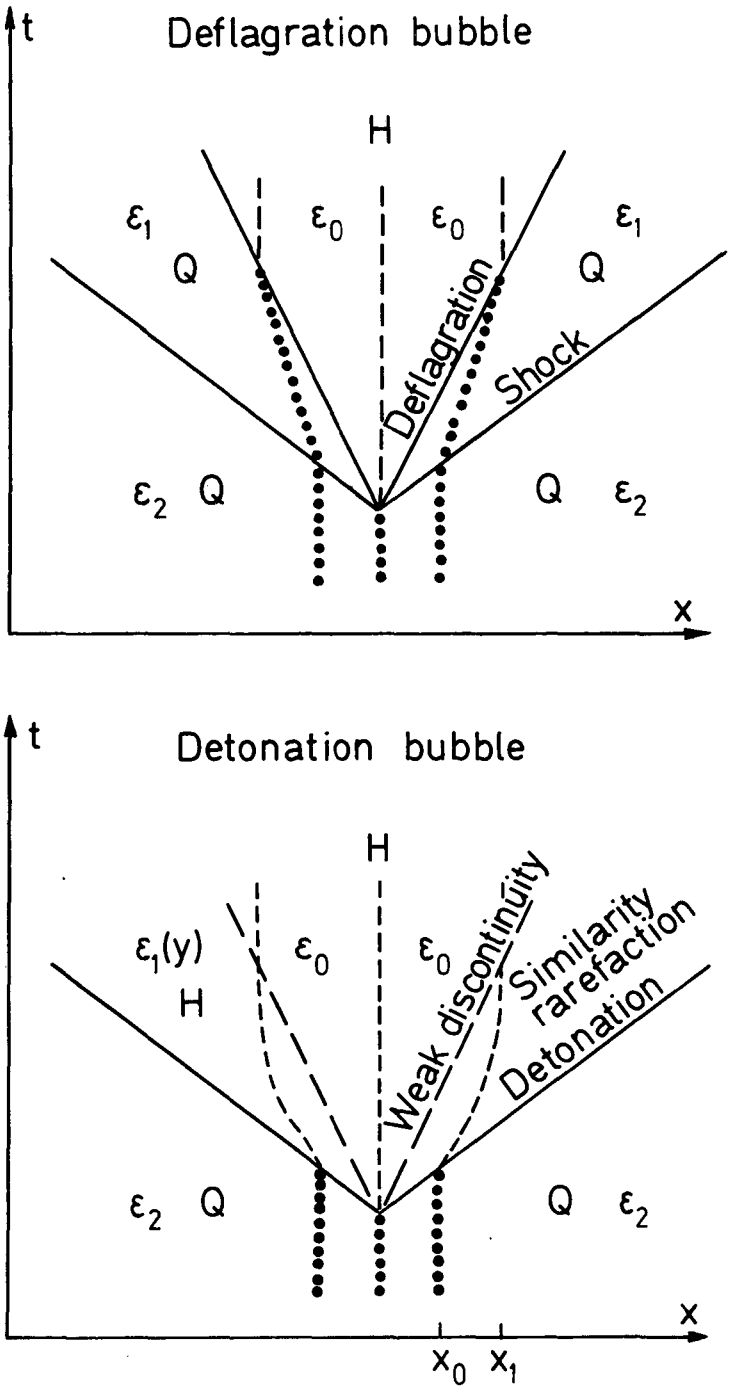

Fig. 1. Space-time growth of hadron bubble via deflagration front following precompression shock. Paths of quarks and hadrons are indicated by dotted and dashed lines, respectively. The solution is symmetric and scale invariant. XBL 836-10332

Creation of a $q\bar{q}$ Pair in a Chromoelectric Flux Tube*

N.K. Glendenning, and T. Matsui

In a classic paper on quantum electrodynamics, Schwinger derived, among other things, the persistence of the vacuum against e^+e^- creation in a uniform external electric field.[1] It is implicit in his derivation that the mutual interaction of the pair is neglected and that the energy stored in the external field is large compared to $2m_e$. His explicit formula for the rate per unit volume that a e^+e^- pair will be created in the uniform field of strength ϵ is,

$$p = \frac{(e\epsilon)^2}{4\pi^3} \sum_{n=1}^{\infty} \frac{1}{n^2} \exp(-\pi m_e^2 n/e\epsilon) \qquad (1)$$

where e is the electron charge and m_e its mass. Recently a number of authors have applied this result to hadronic production in high-energy e^+e^- annihilation.[2-4] In the annihilation event, a tube of color flux is supposed to be formed connecting a rapidly receding quark and antiquark. In this uniform color field a virtual $q\bar{q}$ pair may tunnel to a real state causing the tube to fission and thus creating mesons. The mass of the created quark appears explicitly in (1), thus giving different production rates for K and π.

However, there are essential differences between the QED and QCD processes of pair creation. While it is true in QED that Schwinger's approximations can be rendered as innocuous as one pleases because the external field is at the disposition of the experimenter, this is not true for QCD. The lines of color flux in QCD are believed to be confined to a narrow tube connecting opposite color charges. We adopt this picture quite literally. A virtual pair in such a field will generate a color field of the *same* strength as that in which they were born. Thus the mutual interaction is not negligible. Indeed, if it were negligible, as has been tacitly assumed in earlier work,[2] it would be inconsistent to assume that pair creation causes the fission of a color tube. It is precisely because the field is equal and oppositely directed to the original field that the region between the created pair is devoid of color flux and causes fission. Moreover, the energy of created pairs in a jet need not be negligible in comparison with the energy of the jet. Fortunately, in contrast with QED, the confinement of the color field allows us to account precisely for the mutual interaction and energy conservation (in the idealization of a uniform field in the tube). This we now do.

Suppose that a virtual pair appears spontaneously at some point in the flux tube. The quark and antiquark of this pair can have any combination of momenta, spins, flavors, and colors if they carry as a whole the same quantum numbers as the vacuum from which they emerge. This means that the spin, flavor, color change, and momenta of each component of the pair should be opposite. Let the magnitude of the transverse momentum be denoted by p_T. (We shall use longitudinal to denote the orientation of the tube and transverse to denote an orthogonal direction.) First we calculate the probability that each component will tunnel from the virtual state to a real state having the same energy as the original. The longitudinal momentum of each component at the point where the virtual pair first appears must satisfy

$$p_L^2 + p_T^2 + m^2 = 0 \qquad (2)$$

or

$$p_L = iE_T \equiv i(p_T^2 + m^2)^{1/2} \qquad (3)$$

As they move apart in the field of the tube their mutual interaction produces a field equal in magnitude but opposite in direction to the field in the tube, thus destroying the field between. After they have each moved a distance r in opposite directions from the point of first appearance, the energy balance reads

$$2\left(p_L^2(r) + p_T^2 + m^2\right)^{1/2} = 2\sigma r \qquad (4)$$

The right side is the energy of the field of the tube that is destroyed when the quark and antiquark each moves a distance r. The string constant, σ, is the energy per unit length stored in the field, and its value, deduced from Regge trajectories, is about 1 GeV/fm. The longitudinal momentum is therefore

$$p_L(r) = i\left(E_T^2 - (\sigma r)^2\right)^{1/2}, \quad E_T = \left(p_T^2 + m^2\right)^{1/2} \qquad (5)$$

The action of both quarks integrated from the initial point to the point where they materialize given by $p_L(r) = 0$ is

$$\text{Action} = 2\int_0^{E_T/\sigma} |p_L|\,dr = \frac{\pi E_T^2}{2\sigma} \qquad (6)$$

The probability that a virtual pair can tunnel to a real state in the field of the tube, with each component having transverse momentum, p_T, is therefore

$$P(p_T) = |e^{-\text{Action}}|^2 = \exp(-E_T^2/\sigma) \qquad (7)$$

Knowing the correct tunneling probability from a virtual to a real state we can now calculate the probability that a pair will actually be created. Following Casher *et al.*, we compute the vacuum persistence probability, which is the probability that no such tunneling event for any spin, flavor, or transverse momentum has occurred at any point r in the tube at any time t during the existence of the tube,

$$<0_+|0_->^2 = \prod_{\text{flavor}}\prod_{\text{spin}}\prod_{p_T}\prod_{r}\prod_{t}[1 - P(p_T)] \qquad (8)$$

$$= \exp\left\{\sum\sum\sum\sum\sum \ln[1 - P(p_T)]\right\}$$

Let $L_xL_yL_zT$ be the space-time region of the tube in which no such event is supposed to have occurred. Let z be the longitudinal direction. Divide it into cells of length equal to that required for the materialization of a pair, which is according to (5),

$$\Delta z = 2\,E_T/\sigma \qquad (9)$$

The time interval T is divided into cells according to the frequency with which such tunneling attempts can occur in accordance with the uncertainty principle,

$$\Delta t = \frac{2\pi}{\omega} = \frac{2\pi}{2E_T} = \frac{\pi}{E_T} \qquad (10)$$

Since $P(p_T)$ is independent of r, t, and spin, we obtain

$$|<0_+|0_->|^2 = \exp\left\{\gamma\frac{L_z}{\Delta z}\frac{T}{\Delta t}\sum_f\int\frac{p_T dp_T d\Phi}{\left[\frac{2\pi}{L_x}\right]\left[\frac{2\pi}{L_y}\right]}\ln[1 - P(p_T)]\right\} \qquad (11)$$

$$= \exp(-L_xL_yL_z\,Tp)$$

where

$$p = -\gamma\frac{\sigma}{8\pi^2}\sum_{\text{flavor}}\int_{m_f^2}^{\infty} dE_T^2 \ln[1 - P(p_T)]$$

$$= \frac{\sigma^2}{4\pi^3}\sum_{\text{flavor}}\sum_{n=1}^{\infty}\frac{1}{n^2}\exp\left(-\pi m_f^2 n/\sigma\right) \qquad (12)$$

In the above $\gamma = 2$ is the spin degeneracy.

The above p may be interpreted as the rate at which a $q\bar{q}$ pair having opposite color charges g/2 are created per unit volume inside the tube containing the color field. Of course, it is independent of position in the tube and of time.

It is important to note that Casher *et al.* have demonstrated that Schwinger's exact QED treatment of the approximate problem (noninteracting e^+e^- pairs) is precisely obtained by a WKB calculation of the tunneling probability from a virtual to a real state and the subsequent calculation of the persistence probability. This is reassuring because otherwise one would not have been sure that the enumeration of tunneling events employed above, involving the equality in the uncertainty relation (10) and the materialization distance (9) would have

yielded the exact numerical factor in (12).

Now we wish to compare our new result (12), which does include the mutual interaction of the created pair, with the problem solved by Schwinger and Casher *et al.* To do this, we adopt the *abelian* version of Gauss' law used by Casher *et al.* to relate the color field strength ϵ the cross section of the flux tube, A, and the quark charge g/2,

$$\epsilon A = g/2 \ . \tag{13}$$

They also assume that the string tension is related to the energy density $\frac{1}{2}\epsilon^2$ by

$$\sigma = \frac{1}{2}\epsilon^2 A \tag{14}$$

(This would be modified by the addition of the term BA on the right if one assumed that the flux is confined by an external pressure B.) These relations imply

$$\sigma = g\epsilon/4 \ . \tag{15}$$

Substituting into (12) our result reads

$$P = \frac{(g\epsilon)^2}{64\pi^3} \sum_f \sum_{n=1}^{\infty} \frac{1}{n^2} \exp(-4\pi m_f^2 n/g\epsilon) \tag{16}$$

This has precisely the same form as Schwinger's formula (1) but differs in the numerical constants. This can be understood easily, because if the mutual interaction of the pair is neglected in QED the geometry of the constant external field is the same as that of the flux tube *whether or not* the mutual interaction is included in QCD.

As an additional note, if one conjectures that the color field is confined by an external pressure, B, then

$$\sigma = \frac{1}{2}\epsilon^2 A + BA = \frac{1}{8}\frac{g^2}{A} + BA \rightarrow (g/2)\epsilon \tag{17}$$

where the final result corresponds to the equilibrium value of A.

In view of our derivation of the probability for creation of interacting pairs in a flux tube, it becomes clear how the substitution procedure $e\,\epsilon \rightarrow \sigma$ employed in refs. 3 and 4 in Schwinger's formula, which neglects the mutual interaction, nonetheless yields our results (12).

In summary, we have derived the probability per unit four volume for creation of a quark antiquark pair in a chromoelectric flux tube. Our result differs from Schwinger's because we are able to take into account the mutual interaction of the pair and strict energy conservation. While neglect of these in QED are justified for macroscopic electric fields, they are not justified in QCD. It is remarkable that with the assumption of confinement of the color field it is possible to solve a problem in QCD that has remained intractable in QED. It is of course precisely the confinement of color that allows an easy solution.

Footnote and References

*Condensed from LBL 15957

1. J. Schwinger, Phys. Rev. **82** (1951) 664; E. Brezin and C. Itzykson, Phys. Rev. **D2** 1191 (1970).
2. A. Casher, H. Neuberger, and S. Nussinov, Phys. Rev. **D20** 179 (1979).
3. E.G. Gurvich, Phys. Lett. **87B** 386 (1979).
4. B. Andersson, G. Gustafson, T. Sjøstrand, Z. Phys. **C6** 235 (1980).

Achieving Maximum Baryon Densities*

M. Gyulassy

In continuing work on nuclear stopping power in the energy range $E_{lab} \sim 10$ GeV/nucleon, calculations were made of the energy and baryon densities that could be achieved in uranium-uranium collisions. Results are shown in Fig. 1. Simple uncertainty principle estimates[1] give the minimum stopping distance of a nucleon with rapidity y as

$$D_{min} \sim (1 - 2)\tau_0 \cosh y \quad . \qquad (1)$$

When D_{min} exceeds the Lorentz-contracted nuclear radius R/cosh y then transparency sets in. In Fig. 1 this condition is reached for uranium-uranium collisions when the kinetic energy exceeds $E_{max} \sim 12$ GeV/nucleon as shown by the shaded vertical line. For $E < E_{max}$ shock waves can develop. For a Bag Model equation of state for the quark-gluon plasma produced in the shock zone, the baryon density reached is indicated by the solid line labeled plasma combustion. Notice that below a minimum energy $E_{min} \sim 2$ GeV/nucleon a plasma cannot be created because insufficient energy is available to melt the non-perturbative vacuum, which in this model has an energy density $B \approx 0.15$ GeV/nucleon. Thus, we conclude that there may exist a narrow window in energy $E_{min} < E < E_{max}$ where shock formation could lead to the production of high baryon density quark-gluon plasmas. The energy density reached could exceed 2 GeV/fm^3 and baryon densities could reach as high as ten times normal nuclear densities.

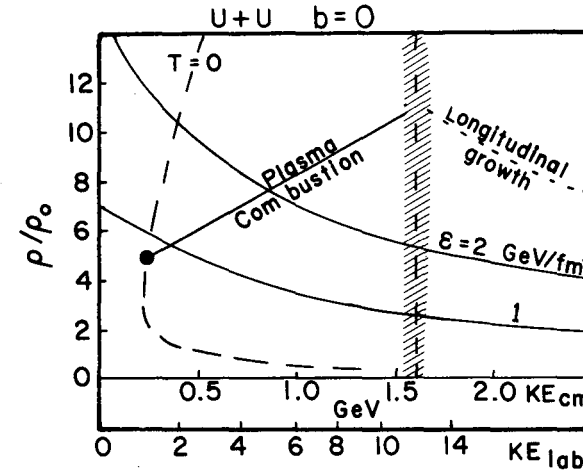

Fig. 1. Baryon density reached in central U+U collisions versus kinetic energy per nucleon. Solid contours indicate energy density. Dashed curve gives threshold for zero temperature plasma production. Shaded line marks onset of nuclear transparency.

XBL 838-10946

*Condensed from LBL-16295 (1983).

Evaporation of Mesons from Quark-Gluon Plasma by Fission of Chromoelectric Flux Tubes*

B. Banerjee,† N.K. Glendenning, and T. Matsui

Lattice gauge solutions of QCD provide fairly convincing theoretical support for the notion that hadrons will dissolve into a quark-gluon plasma at a sufficiently high energy density.[1] If such a plasma is formed in a high-energy hadron-hadron or nucleus-nucleus collision, the high internal pressure af the plasma will cause its rapid disassembly. Therefore, evidence for its prior existence must be found in its decay products. To assess whether signals of the plasma survive the evolution and to identify those

signals, a dynamical description of the disassembly is needed. One facet has been studied by Bjorken, by Kajantie *et al.*, and by Baym *et al.*, who propose a hydrodynamical model for its expansion.[2] As it expands it will cool, and the conditions for condensation back to the hadronic phase will be attained. In this note we address another facet of the disassembly, the formation and radiation of mesons at the surface of the hot plasma. The pre-freezeout radiation, which has also been emphasized in connection with the disassembly of a hadronic fireball,[3] plays two roles. It carries signals of the state of the plasma as it evolves. Second, it is coupled to the hydrodynamical expansion of the plasma, which may be inhibited by the backward radiation pressure. In the extreme, the plasma may evaporate mesons rather than expand collectively as a plasma. Such an extreme scenario was proposed recently by Danos and Rafelsky.[4] However, we shall see that their two-parameter model of evaporation is incompatible with the dynamics of a confining mechanism.

The plasma of almost free quarks, antiquarks, and gluons is viewed as a region of perturbative QCD vacuum embedded in the true nonperturbative vacuum that pervades most of space. Because of the thermal motion, a quark or antiquark may cross the boundary between the two vacua, but it will suffer a strong color interaction with the rest of the plasma and cannot escape alone. However, there are two ways in which such a quark can initiate the evaporation of a meson. As the quark crosses the boundary, a flux tube of chromoelectric field connects it to the plasma, and it will experience an attractive potential that will pull it back unless the tube fissions. The tube can fission through the quantum tunneling to a real state of a virtual $q\bar{q}$ pair in the uniform color field of the tube. The energy and momentum of the meson so formed is then determined by the initial energy and momentum of the leading quark and the space-time position where the $q\bar{q}$ pair creation occurs. This mechanism of hadronization has been commonly used to describe particle production in high-energy e^+e^- annihilation.[5,6] Although in our problem the average momentum of the quarks is not so high ($T \sim 200$ MeV), we expect that the picture will qualitatively describe the fate of the high momentum component of the thermal distribution. The contribution of the low-momentum quarks to this hadronization process is suppressed as will be seen. This supports our idealization of a smooth plasma surface. A second mechanism for hadronization at the plasma surface is the coalescence of a quark-antiquark pair. We shall not further describe this process here, since at the expected plasma temperatures the thermal flux of quarks and antiquarks with specified color charge is small.

Consider a quark (or antiquark) of momentum $\mathbf{k}_0$ that is directed outward with respect to the surface. As the quark passes through the surface, a tube of chromoelectric flux is built up behind it, out of its kinetic energy. The energy per unit length that is stored in the tube is $\sigma = \epsilon^2 A/2$, where ϵ and A are the field strength and cross section of the tube. Gauss' law relates the flux ϵA to the quark charge, g/2 through $\epsilon A = g/2$, yielding

$$\sigma = g\,\epsilon/4 \tag{1}$$

This string constant can also be related to the Regge slope and so is essentially a known parameter, $\sigma = 0.177\ \mathrm{GeV}^2$. We assume that the flux tube that shields its color will connect it to the plasma by the shortest path. The motion of the quark will be governed by the equations expressing the conservation of energy and of momentum parallel to the surface. The string dynamics can be solved analytically both for finite and zero quark mass. Its velocity parallel to the surface remains constant, and its motion perpendicular is illustrated in Fig. 1. It moves a distance E_{z0}/σ before being stopped at time (k_{z0}/σ). Thereafter it is accelerated back into the plasma, unless the string fissions. The color flux tube can fission as the result of the tunneling of a virtual quark-antiquark pair to a real state inside the tube. The field connecting the leading quark to the plasma is then identically cancelled by that connecting the pair. If such a pair is created, say at a distance z′ from the surface of the plasma and at a time t, a meson consisting of the original quark together with the antiquark of the created pair is thus formed.

Its momentum perpendicular to the surface will be that possessed by the leading quark at the time t (see Fig. 1). Its energy will be E_0 less the energy carried back into the plasma by the fragment of string of length z′ and the quark contained in it. Thus, the meson momentum and energy are given by the string dynamics (Fig. 1) and the space-time point where pair creation occurs. For the detailed solution see ref. 7.

The creation of a $q\bar{q}$ pair in the constant color field is similar to the QED process solved by Schwinger[8] more than 30 years ago. His result has been directly transcribed into QCD by several authors who describe hadron production in high-energy e^+e^- annihilation.[5,6]

However, Schwinger's calculation of the production rate of pairs neglects their mutual interaction and their mass in comparison with the energy in the macroscopic external field. These are essential difficulties in QED and the problem has never been solved exactly. While Schwinger's approximations are reasonable in QED, they are very serious in QCD where the field between the created pair is identical to the original field, and the field energy absorbed by the pair in tunneling to a real state is of the same order as the total field energy of the flux tube. We

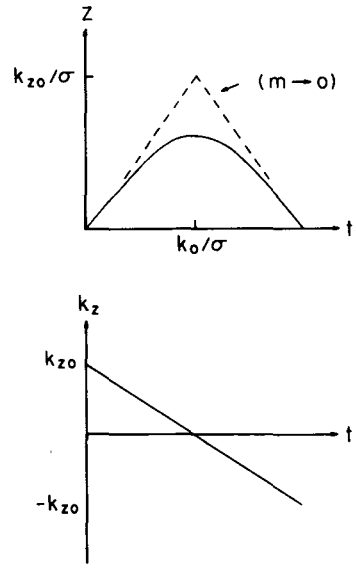

Fig. 1. The solution of the string dynamics showing quark position and momentum normal to the plasma surface as a function of time.

XBL 834-9275

have therefore derived a new result for the rate per unit volume at which $q\bar{q}$ pairs will be created in a color field ϵ, which takes the mutual interaction and strict energy conservation into account. It is very interesting that a problem that has not been solved in 30 years in QED can be solved very easily in QCD in the model of confined color indicated in Fig. 1. The new result is[9]

$$p = \sum_{\text{flavor}} \frac{g\epsilon^2}{64\pi^3} \sum_{n=1}^{\infty} \frac{1}{n^2} \exp\left(-\frac{4\pi^2 m_f^2 n}{g\epsilon}\right) \xrightarrow[m_f=0]{} \frac{\sigma^2}{12\pi} \tag{2}$$

Having calculated the string dynamics (Fig. 1) and the rate per unit volume that a real pair will be formed and that hence the string will fission, we can now calculate the probability that the string will fission at the time t measured from the time that the outward-moving quark crosses the surface and in the interval dt. This is given by

$$dP(t) = pAz(t)\, dt[1 - P(t)] \tag{3}$$

where z(t) is the coordinate of the leading quark at time t and hence the length of the string. Note from Fig. 3 that the scale for both time and distance is controlled by the string tension, σ. Hence according to (3) the parameter that characterizes confinement is, where $\alpha_c = g^2/4\pi$,

$$k_c = \left(\frac{\sigma^2}{pA}\right)^{1/2} = \left(\frac{24\sigma}{\alpha_c}\right)^{1/2} \tag{4}$$

Equation (3) can be integrated analytically for both massive or massless quarks. For pedagogical reasons we exhibit the simpler massless limit in the form of the probability distribution in momentum k_z of the meson produced by a quark of initial momentum k_{z0}. The formula is remarkably simple and instructive

$$\frac{dP}{dk_z} = \frac{k_0}{k_{z0}} \frac{|k_z| - k_{z0}}{k_c^2}$$

$$\exp\left[-\frac{1}{2}\frac{k_0}{k_{z0}}\left(\frac{k_z - k_{z0}}{k_c}\right)^2\right] \qquad (5)$$

which shows that a quark emerging from the plasma with k_{z0} suffers a most probable loss of momentum k_c at the time of fission,

$$\hat{k}_z = k_{z0} - k_c \qquad (6)$$

(see Fig. 2). The integrated probability that a quark of initial momentum k_{z0} will escape in a meson is

$$P_{esc} = 1 - e^{-k_{z0} k_0 / 2k_c^2} \qquad (7)$$

The momentum scale k_c, set by confinement depends on the values of σ and α_c. These parameters must be related through $\mathscr{L}_{QCD}$, but this relationship is unknown. For $\sigma = 0.177\ (\text{GeV})^2$ and for $\alpha_c = 2$ or 0.55,[5,10] we have

$$k_c = \begin{cases} 1.45\ \text{GeV}, & (\alpha_c = 2) \\ 2.78\ \text{GeV}, & (\alpha_c = 0.55) \end{cases}$$

From (7) only quarks from the tail of the thermal distribution with $k \gtrsim k_c$ have an appreciable chance of forming a meson, and the momentum of the meson is shifted downward by k_c from the original quark momentum. Next we calculate the probability that the string will break at the point z' at the time t while the quark is moving outward. This probability is distributed uniformly along the string. Therefore,

$$d^2P(z',t) = pA\, dz'\, dt\, (1 - P(t)) \qquad (8)$$

We fold d^2P with the flux of quarks of momentum $\underset{\sim}{k}_0$ and sum over all such momenta to obtain the number of mesons radiated per unit time per unit surface area of the plasma having normal momentum k_z^M and energy E^M,

$$\frac{d^5N}{dS\, dt\, dk_z^M\, dE^M} = \frac{\gamma}{(2pi)^3}\int d^3k_0 e^{-E_0/T}\frac{k_{z0}}{E_0}\frac{pA}{\sigma^2}$$

$$\left[1 - P(k_z^M)\right]\Theta(E_z - m - (E_{z0}/E_0)E^M) \qquad (9)$$

$$\times\ \Theta(m + (E_{z0}/E_0)E^M - E_{z0})\ \Theta(-k_{zM})\ \Theta(k_z^M - k_{z0})$$

where Θ is the step function $\Theta(+) = 0$, $\Theta(-) = 1$. The degeneracy factor γ is $\gamma = \gamma_c \times \gamma_S \times \gamma_F \times 2 = 24$ where 2 counts quarks and antiquarks. $P(k_z^M)$ means that it is evaluated at the time that yields the momentum k_z^M.

The radiation pressure exerted on the plasma by the radiation of mesons, and the energy flow per unit surface area per unit time carried in the radia-

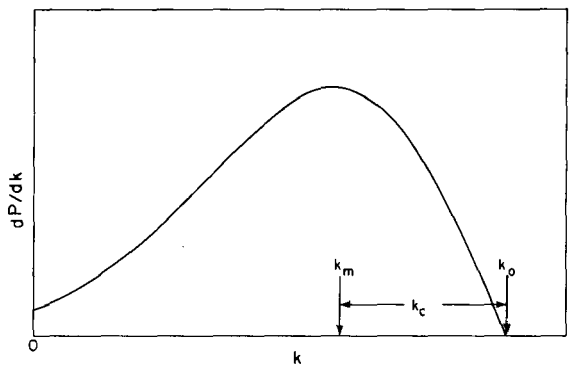

Fig. 2. Momentum distribution of radiated mesons for initial quark momentum $k_{z0} > k_c$. XBL 833-125

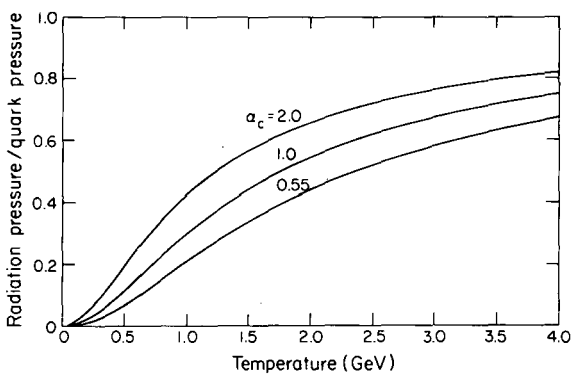

Fig. 3. Pressure acting on the surface of the quark-gluon plasma due to the radiation of mesons as a function of plasma temperature. XBL 833-124

tion follow immediately:

$$P^M = \frac{d^3k}{dS\,dt} = \int_0 dk_z\, k_z \int_{E_\pi} dE^M \frac{d^5N}{dS\,dt\,dk_z\,dE^M} \quad (10)$$

$$\frac{d^3E}{dS\,dt} = \int_0 dk_z \int_{E_\pi} dE^M\, E^M \frac{d^5N}{dS\,dt\,dk_z\,dE^M} \quad (11)$$

where $E_\pi = \sqrt{k_z^2 + m_\pi^2}$.

Fig. 3 shows, as a function of temperature, the ratio of radiation pressure and internal quark pressure. Since this ratio is less than 20% up to T = 500 MeV, we conclude that the radiation due to this process will be a minor perturbation on the collective hydrodynamical disassembly of the plasma.

This conclusion contradicts an assertion made by Danos and Rafelski.[4] Their conclusion, however, is based on a model that does not contain a dynamical description of color confinement but that instead is characterized by two adjustable parameters, a minimum momentum for emission and an efficiency factor defining the fraction of the quark energy carried off by the meson. Fig. 2 contradicts the basis of their model, since they assert that a quark of initial momentum k_0 ($>p_M$) produces a meson of the same momentum.

The flux of mesons that are formed by the fission of the string is given by (9). Many of these, in their rest frame, are more massive than the pion. If the invariant mass M lies in the interval $n < M/m_\pi < n + 1$ it is assumed that the heavy meson will decay into n pions according to phase space distributions. These distributions can be calculated for up to three pion decay. For four or more pion decay modes, a high-energy scaling formula that agrees with the experimentally observed distributions[11] in $e^+e^- \rightarrow q\bar{q} \rightarrow n\pi$ annihilation is used with the irrelevant electromagnetic factors divided out. In terms of the above number distribution in rapidity, dn/dy' as seen in the rest frame of the heavy meson, the pion flux, rapidity distribution, dF/dy, in the rest frame of the plasma surface can be written

$$\frac{dF}{dy} = \int dy_M dM_M \frac{d^2F_M}{dy_M dM_M}\, dy' \frac{dn}{dy'}\, \delta(y - y_M - y')$$

where the flux distribution F_M of heavy mesons follows from (9).

In Fig. 4 this distribution is compared at a plasma temperature of 300 MeV with several other quantities in the comoving frame of the surface. The flux of quarks and antiquarks at the surface is very large but relatively few of them lead to fission events. For those that do, the distribution of heavy mesons is shown (broken strings). Their decay as described above is shown by the pion curve. The number of emitted pions is, for the coupling constant $\alpha_c = 2$, much larger than the number in black-body radiation from a pion gas at the same temperature as the plasma. The peak in the momentum is also shifted down in rapidity as compared to the most probable rapidity of the quarks or of the pion gas.

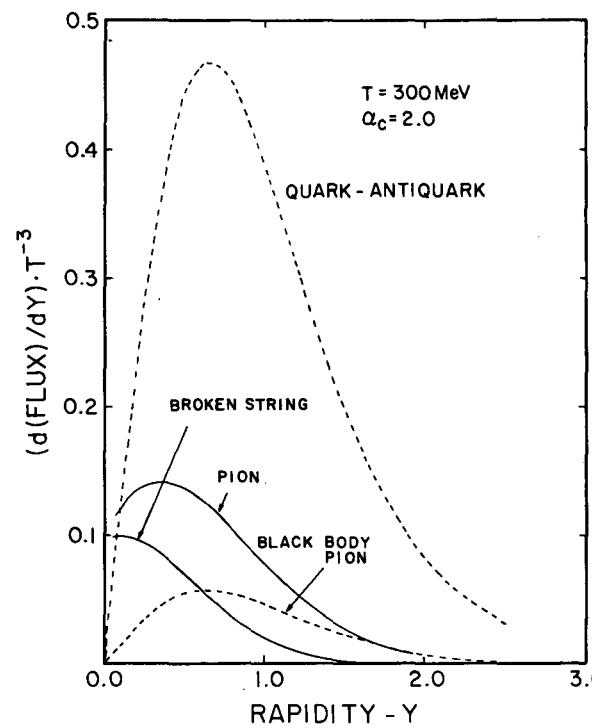

Fig. 4. Rapidity distributions as described in text.

XBL 834-9274

In summary, the hadronization at the surface of a quark-gluon plasma has been studied in the framework of a chromoelectric flux tube model. We find that the radiation pressure is sufficiently small compared to the internal pressure that it can be ignored to first approximation in the hydrodynamical expansion of the plasma. Thus, our solution for meson radiation can be folded with a solution to the hydrodynamical expansion to obtain the spectrum of radiated mesons emitted over the history of the expansion. Of special interest is the distinction between strange and non-strange mesons, which is explicit in the theory through the dependences on the quark masses and the thermal populations in the plasma.

Footnotes and References

*Condensed from LBL-15962 and Phys. Lett. **127B**, 453 (1983).

†Permanent address: Tata Institute for Fundamental Research, Bombay, India

1. L.D. McLerran and B. Svetitsky, Phys. Lett. **98B**, 195 (1981); Phys. Rev. **D24**, 450 (1981); J. Kuti, J. Polonyi, and K. Szlachanyi, Phys. Lett. **98B**, 199 (1981); J. Engels, F. Karsch, I. Montvay, and H. Satz, Phys. Lett. **101B**, 89 (1981); **102B**, 332 (1981).
2. J.D. Bjorken, Phys. Rev. **D27**, 140 (1983); K. Kajantie, R. Raitio, and P.V. Ruuskanen, preprint (Helsinki, 1983); G. Baym, J.-P. Blaizot, W. Czyz, B.L. Friman, and M. Soyeur, preprint (Illinois 1983).
3. N.K. Glendenning and Y. Karant, Phys. Rev. **C21**, 1501 (1980).
4. M. Danos and J. Rafelsky, Phys. Rev. **D27**, 671 (1983).
5. A. Casher, H. Neuberger, and S. Nussinov, Phys. Rev. **D20**, 179 (1979).
6. E.G. Gurvich, Phys. Lett. **87B**, 386 (1979); B. Andersson, G. Gustafson, T. Sjøstrand, Z. Phys. **C6**, 235 (1980).
7. B. Banerjee, N.K. Glendenning, and T. Matsui, Phys. Lett. **127B**, 453 (1983).
8. J. Schwinger, Phys. Rev. **82**, 664 (1951).
9. N.K. Glendenning and T. Matsui, Phys. Rev. D **28** (1983).
10. K. Johnson, Act. Phys. Pol. **B6**, 865 (1975).
11. R. Brandelik, *et al.*, Phys. Lett. **67B**, 358 (1977) and **89B**, 418 (1980).

Charge-Exchange Products of Bevalac Projectiles

John Rasmussen

Here we reexamine some of the earliest Bevalac work, the classic studies of projectile fragmentation by Dr. Harry Heckman's group using a small-angle magnetic spectrometer.[1]

Recall their main finding that there is a substantial production of fragments of all masses lighter than the projectile, such fragments being centered in a narrow region of velocity space around the beam velocity. I want to direct attention here to the rather rare fragments of the same mass number as the projectile but differing in charge by one unit. We shall also keep track, as a frame of reference, of the products that have lost one neutron from the projectile.

From the work of Greiner *et al.*[2] with 2.1 GeV/nucleon ^{16}O and ^{12}C and with 1.05 GeV/nucleon ^{12}C, we see that the isobaric products show abnormally large momentum shifts. For most fragments target factorization holds;[3] that is, the proportion of various fragments is independent of the target, and the only target dependence is through an overall target factor that increases with target mass number. Contrary to this general result, it is evident

that ^{12}N formation from 1.05 GeV/nucleon C has a marked target isospin dependence, as the ratios of Table I attest. The dependence has the sign to be expected; that is, the hydrogen target most effectively drives the projectile toward the higher-charged isobar. This dependence is essentially absent for the 2.1 GeV/nucleon carbon beam, and it is absent for the ^{12}B formation. We defer discussion on the other products. We note that the case with the strongest target isobar effect has the least momentum downshift. It would seem that this case of ^{12}N formation at 1.05 GeV/nucleon is proceeding mainly by simple charge exchange without the formation of a pion in the final state. The other cases, which all have the large momentum downshift, are mainly going by pion formation with capture of one of the final nucleons in the inelastic collision.

Why should ^{12}N and ^{12}B formation show unlike behavior? Examination of their level schemes provides a clue. The nucleus ^{12}N has only one particle-bound state, the 1+ analog state of the giant M1 state in ^{12}C at 15.11 MeV. The collective nature is indicated by the fast beta decay (log ft = 4.1) from the 1+ ground states of ^{12}N and ^{12}B to the ^{12}C ground state. Now the ^{12}B has four additional bound excited states of spins 2+, 2−, 1−, and 0+, ranging up to 2.72 MeV. We can conclude that the lack of target isospin dependence and the somewhat larger cross sections for ^{12}B relative to ^{12}N are due to formation in these excited states.

Deutchman and Townsend[4] have made theoretical calculations of pion production with concurrent formation of a giant M1 excited state in one collision partner. They have estimated that a substantial fraction of pion production, at least at lower beam energies, goes via this process. However, we see that generally of the order of 0.1 mb of cross section goes to the 1+ isobars, and the total charged pion production at 2.1 GeV/nucleon is of the order of a barn.

TABLE I

Cross Section Ratios of Charge Exchange Products to 1-Neutron-Out Product
(From data of P. Lindstrom *et al.*[3])

Beam	Energy	Product	Production Ratio (x 10^3)		
			Target		
			H	^{12}C	^{9}Be
^{16}O	2.1	^{15}C	0.50 ± 0.4	0.93 ± 0.3	1.21 ± 0.3
		^{16}N	0.70[a]	3.00 ± 0.5	1.26 ± 0.4
^{12}C	2.1	^{11}Be	-	-	0.39 ± 0.2
		^{12}B	2.26 ± 0.4	2.24 ± 0.2	3.02 ± 0.3
		^{12}N	1.30 ± 0.4	1.70 ± 0.2	1.24 ± 0.3
^{12}C	1.05	^{11}Be	-	-	0.40 ± 0.3
		^{12}B	2.00 ± 0.5	2.21 ± 0.3	2.08 ± 0.4
		^{12}N	2.12[a]	1.14[a]	0.49 ± 0.3

a) denotes factor of 2 estimate.

Why is the coherence enhancement not realized for the 1+ states in the processes we are examining here? Perhaps it is the bad momentum mismatch that is to blame. When a nucleon-nucleon collision forming a pion (or delta) takes place, the final-state nucleons in their c.m. frame have a total energy that is reduced by at least the rest mass of the pion, or 140 MeV. To form the isobaric product requires that one of these momentum-shifted nucleons be recaptured by the projectile.

Further theoretical work and experiment are called for.

References

1. A.S. Goldhaber and H.H. Heckman, Ann. Revs. Nucl. and Particle Sci.**28**, 161 (1978)
2. D.E. Greiner, P.J. Lindstrom, H.H. Heckman, B. Cork, and F.S. Bieser, Phys. Rev. Lett. **35**, 152 (1975)
3. P.J. Lindstrom, D.E. Greiner, H.H. Heckman, B. Cork, and F.S. Bieser, LBL-3650 (1975) unpublished
4. P.A. Deutchman and L.W. Townsend, Phys. Rev. Lett. **45**, 1622 (1980)

Heavy Ion Pion Production: Spectral Irregularities

John O. Rasmussen

1. The ratio π^-/π^+ near rest velocity in the center-of-mass

Our MSU-Tokyo-Berkeley collaboration made 0° to 30° measurements for both π^- and π^+. The results are reported in two papers by Frankel *et al.*[1] The experimental data show a ratio R(y) that is quite flat with a value 1.5 ± 0.2 around y=0.

Radi and I with collaborators decided to carry out a new Monte Carlo trajectory study on the problem.[2] There are several minor differences we introduced, but probably the most significant is that we introduced pion absorption by the spectator fragments and implicitly by the firecloud, since pions were started from the surface and firecloud charge was neglected at first. This work is described in another report in this volume.

2. The π^-/π^+ ratio near beam velocity

Benenson *et al.*[3] were the first to report the dramatic spectral effects occurring near beam velocity. These effects are thought to be Coulomb effects and have been studied in more detail and reported by Sullivan *et al.*[4] The π^- peak seems to be centered just slightly lower than beam velocity, consistent with the slight slowing of heavy-ion projectile fragments, so abundantly produced at these high energies. In like manner the principal contribution to the width of the peak is thought to be the velocity dispersion of the projectile fragments.[5]

3. Bumps in pion spectra in the center-of-mass region

A puzzle in the pion data from heavy ions is the bump or ridge of extra cross section at very low energy (c.m.) around 15 MeV. This was reported in range telescope work on π^+ for the ^{20}Ne + NaF system by Nakai *et al.*[6] and for the ^{40}Ar + Ca system by Wolf *et al.*[7] The low-energy pion bumps have been observed at E/A of 0.8 and 1.05 GeV but not at 0.4 GeV, and they are not seen in the reaction p + p = π^+ + X.

One rather striking aspect of the low-energy pion bump is that it tends to peak at a $p_\perp$ value of 0.4 to 0.5 $m_\pi c$. The reciprocal of this gives an uncertainty relation size of 2.5 to 2.0 pion Compton wave lengths, or 3.5 to 2.8 fm. Now this is very close to the nuclear size of the neon or argon projectiles or fireclouds they would produce. The relation seems

too remarkable to dismiss as mere coincidence. A fancier way of saying this is that the pion bump profile observed in Fig. 1 and in prior studies is a snapshot of a pion wave function in momentum space. If we perform a 3-dimensional Fourier transform, we get an estimate of the wave function in configuration space. With present data it is not justified to push this analysis too far. Qualitatively, the results are the same as the simple uncertainty relation argument above.

We were prompted to take a new hard look at the curious deeply-bound pionic states which were the subject of a theoretical study by Ericson and Myhrer some years ago.[8] The deeply-bound states come about as follows: the pion optical potential (an expansion from a non-local potential) has static terms that are repulsive and isospin dependent, with a part dependent linearly on the local nuclear density and a part quadratically dependent on the density. The optical potential also has attractive Kisslinger potential terms that have a k^2 dependence just like the kinetic energy term in the Schrödinger equation. The potential has small imaginary components associated with inelastic scattering (linearly dependent on density) and large components associated with true absorption (quadratically dependent.) For π^- and neutron-rich species (or for π^+ and proton-rich species) of ordinary nuclei the attractive Kisslinger term can exceed the kinetic energy term in the nuclear interior. That is, the effective mass is negative there, and it passes through a singularity in the surface region, finally decreasing to its asymptotic value of free pion rest mass of 140 MeV at large distance. The behavior of the wave function near the singularity, where the curvature becomes infinite, poses something of a problem. Mandelzweig, Gal, and Friedman[9] restudied the problem, dropping the repulsive static potential, but looking in great deal at the role of the singularity.

To reexamine these solutions we choose the most up-to-date pion optical potentials, those of Carr, McManus, and Stricker-Bauer (hereafter their published potential set F will be referred to here as the CMS potential.)[10]

To get some orientation on pion orbiting conditions I developed a computer code in BASIC on the Osborne I to solve for eigenvalues of pions in a nuclear optical potential. Deeply-bound states readily occur for the doubled nuclear density expected in interpenetrating heavy nuclei.

4. Speculations on pionic atoms and anomalons

Although I have looked at many double-density solutions in the CMS potential, I will conclude here by showing Ericson-Myhrer inner solutions at rather ordinary nuclear densities. These solutions were made with Prof. Wm McHarris to explore the idea that anomalons might be Ericson-Myhrer solutions of π^- on neutron-rich projectile fragments.

Anomalons are heavy-ion fragments observed in nuclear emulsions to have abnormally short

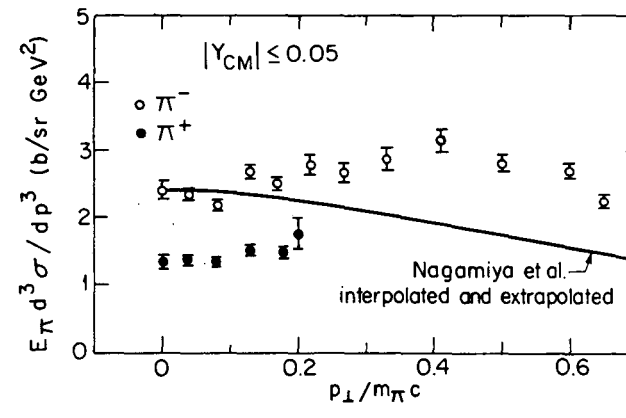

Fig. 1. Pion invariant production cross sections for Ne + NaF at E/A=655 MeV at 90° (c.m.) Data for π^- are shown as open circles and for π^+ as solid dots. The solid line is taken from data of Nagamiya *et al.*[13] The line represents an interpolation in beam energy between their 400 and 800 MeV data and a parabolic (thermal) extrapolation down in pion energy from their lowest points, which would be just on the right-hand margin of our figure. To insure adequate statistics we took the cross section as an average not over a fixed angle (c.m.) but rather over a fixed interval ± 0.05 in rapidity y_{cm}. (From ref. 1)

XBL 8112-12880A

mean-free-paths for interactions in the first 2 or 3 cm of their range. These observations have been made first in cosmic rays and later in exposures at the Berkeley Bevalac and the Dubna synchrophasotron. McHarris and I have described our model[11] of anomalons as pineuts[12] orbiting nuclear fragments, but our quantitative estimates are made by calculating Ericson-Myhrer solutions in their test nucleus ^{34}Na. We, however, use the newer CMS potential and an enhanced local neutron density brought about by the presence of the π^-. It is this local neutron-density build-up that insures attaining a negative effective mass in the nuclear interior, and this effective-density feature is the reason for using the language "orbiting pineuts" to describe our picture of anomalons.

Fig. 2 shows the potentials and eigenvalues for the nodeless π^- solutions for angular momenta 0–4. Also shown is the effective mass behavior. Note that the centrifugal potential of the radial wave equation is negative inside the singularity, and the kinetic energy is also negative.

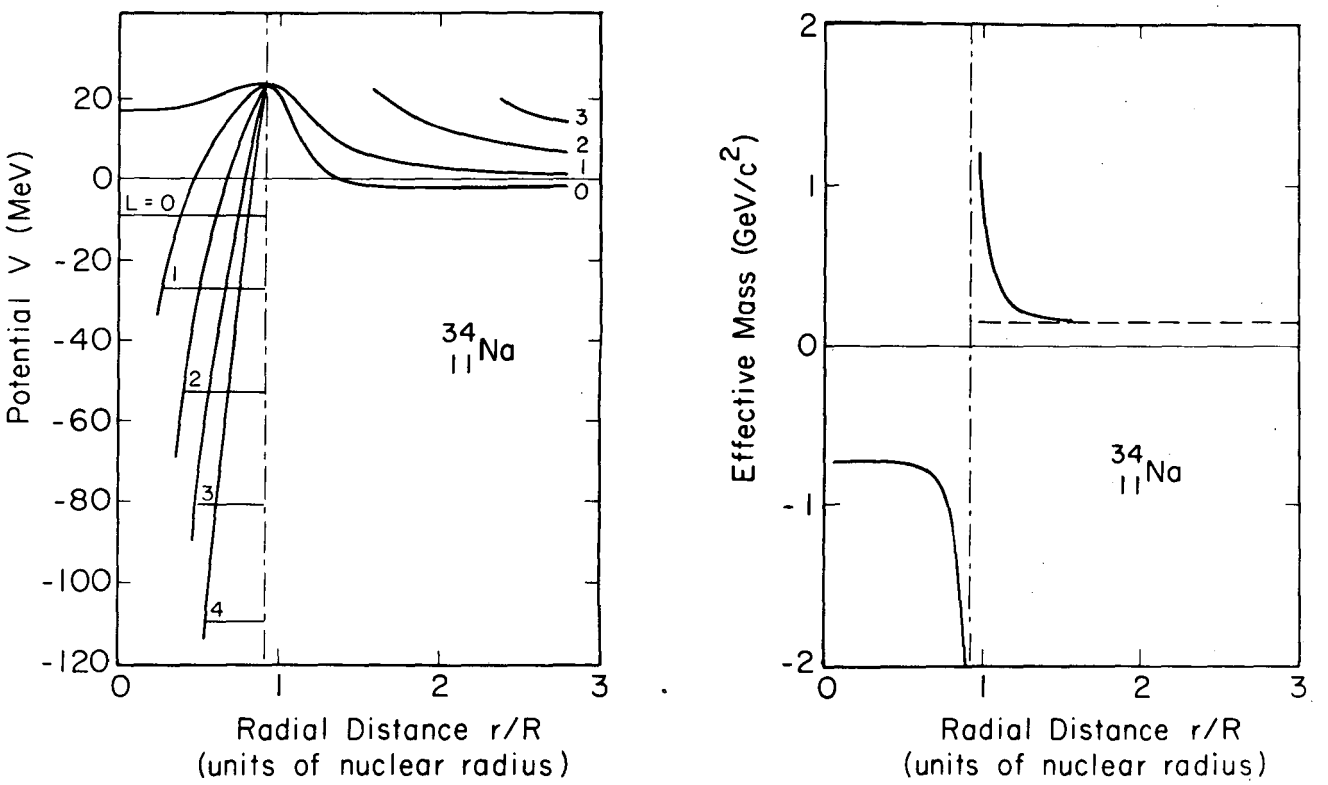

Fig. 2. The left side shows the radial potentials for π^- in neutron-density-enhanced ^{34}Na for L values 0 through 4. The eigenvalues are indicated by horizontal bars at the appropriate energy running between the inner turning point and the mass singularity. The right side shows the effective mass dependence on distance.

XBL 8211-3476A

For the anomalon explanation there is the serious constraint of a long lifetime, i.e., $>10^{-10}$sec. We therefore look to the deepest bound solutions, where all or most channels are closed for the true pion absorption process that involves a π^- converting a proton to a neutron in the close proximity of another nucleon, with the pair of nucleons carrying off the available energy of 140 MeV rest mass energy less the pion binding energy. In the calculations illustrated in Fig. 2 the imaginary parts of the optical potential were therefore set to zero. To furnish an explanation for the mid-rapidity bumps there is no such tight constraint on lifetimes, but we have not paid much attention to the widths given by the CMS potential imaginary parts, since the true absorption will surely be different under firecloud conditions than for normal cold nuclei.

Perhaps it may seem we are overworking the Ericson-Myhrer pionic states to invoke them in explanation for both the mid-rapidity pion bumps and the anomalons. That remains for future experiment and theory to explore.

We would note also that pionic states with two or more pions may gain extra stability from admixtures of Δ pairs, which are predicted to have very strong binding in certain spin-isospin states. The free pineut may have a better chance of being bound with two π^- than with one. Other exotics, such as, the neutral species of two π^- bound to a ^{8}He core might be sought. Even if this anomalon explanation is wrong, it may stimulate the interesting, if difficult, investigation of external pionic atom states in which two π^- are present. Only high energy heavy ion physics offers a realistic opportunity for such studies, which could shed light on the fundamental interaction between two Δ particles in the isospin -3 channel.

Footnote and References

*Condensed from Nucl. Phys. **A400**, 383 (1982).

1. K.A. Frankel *et al.*, Phys. Rev. C **25**, 1102 (1982). Also LBL report in preparation (1982) to be submitted to Phys. Rev. C.
2. H.M.A.Radi *et al.*, LBL-13768 (1982) submitted to Phys. Rev. C
3. W. Benenson *et al.*, Phys. Rev. Lett. **43**, 683 (1979).
4. J.P. Sullivan *et al.*, Phys. Rev. C **25**, 1499 (1982).
5. H.M.A. Radi, J.O. Rasmussen, J.P. Sullivan, K.A. Frankel, and O. Hashimoto, Phys. Rev. C **2**, 1518 (1982).
6. K. Nakai *et al.*, Phys. Rev. C **20**, 2210 (1979).
7. K.L. Wolf *et al.*, Phys. Rev. Lett. **42**, 1448 (1979).
8. T.E.O. Ericson and F. Myhrer, Phys. Lett. **74B**, 163 (1978).
9. V.B. Mandelzweig, A. Gal, and E. Friedman, Ann. Phys. (N.Y.) **124**, 124 (1980).
10. J.A. Carr, H. McManus, and K. Stricker-Bauer, Phys. Rev. C **25**, 952 (1982).
11. W.C. McHarris and J.O. Rasmussen, Physics Lett. **120B**, 49 (1983).
12. The term "pineut" denotes a possible bound species of a π^- bound to a few neutrons and proposed by R. Van Dantzig and J.M. Van der Velden, Netherlands Inst. for Nucl. and High Energy Research NIKHEF, preprint (1981).
13. S. Nagamiya, M.-C. Lemaire, E. Moeller, S. Schnetzer, G. Shapiro, H. Steiner, I. Tanihata, Phys. Rev. C **24** 971 (1981).

Monte Carlo Studies of Pion Distributions from Heavy Ion Collisions*

Hafez M.A. Radi, J.O. Rasmussen, K.A. Frankel, J.P. Sullivan,† and H.C. Song‡

Now after several studies on pion production in heavy ion collisions the general features have been established and qualitatively understood. For example, the measurements of the Coulomb effects on the π^-/π^+ ratio demonstrated by Benenson *et al.*[1] have been investigated by Libbrecht and Koonin,[2] Cugnon and Koonin,[3] and Gyulassy and Kauffmann.[4] In these theoretical studies the pion trajectories were allowed, explicitly or implicitly, to propagate through nuclear matter. Further study of the Coulomb effects was made by Bertsch[5] in explaining the dependence of the π^-/π^+ ratio on the incident bombarding energy. Radi *et al.*[6] formulated the Coulomb effects of spectator fragments on the pion production cross sections near beam velocity in terms of weighted average over various projectile fragments.

Here we shall be mainly concerned with the Coulomb effects on pions that are slower than the beam and projectile in the center-of-mass (c.m.) frame. Frankel *et al.*,[7] in reporting experimental results for ^{40}Ar on calcium at E/A of 1.05 GeV, showed significantly lower π^-/π^+ ratios around zero velocity (c.m.) than were predicted in earlier theoretical studies. The Monte Carlo trajectory calculation of Koonin and Cugnon[3] gave a central ratio of 5.5, whereas experiment gave 1.5. New measurements[8] of the doubly differential cross section for the production of π^- and π^+ from c.m. to beam velocity for Ne on NaF at E/A of 655 MeV have become available. In the present paper we mostly carry out theoretical calculations for the latter system.

In view of disagreements on π^-/π^+ ratios near rest in the center of mass, we decided to carry out new Monte Carlo pion trajectory calculations. Principal differences we wished to test relative to the Cugnon and Koonin work[3] were the following: (1) The pions should originate from the surface, not throughout the collision volume; (2) those trajectories that pass through nuclear matter should be rejected due to pion reabsorption; (3) the pions should be emitted at the time of closest approach, not the late stage of the collisions; and (4) a two-fireball thermal plus first-collision source for initial pion momentum distribution was taken, rather than a single thermal source.

For an average value of the impact parameter ($b = 0.4b_0$, $b_0 = R_P^0 + R_T^0$) for ^{20}Ne + ^{20}Ne at E/A = 655 MeV, we show the results for about 10,000 surviving trajectories (for each type of pion). The scatter plots of Fig. 1 give initial and final velocity distributions for surviving trajectories of π^0, π^-, and π^+, with the abscissa $\hat{v}_\parallel \equiv (\hat{v}_x)$ and ordinate $\hat{v}_\perp \equiv [\hat{v}_y^2 + \hat{v}_z^2]^{1/2}$. Note in the final distributions (upper right plots) the exclusion of π^+ from the velocity region near target and projectile, and note the bunching of π^- in these regions. The distributions are not symmetric in the sign of $\hat{v}_\parallel$, since the Monte Carlo selection of positions on the spherical intersection ring source is only over the range $0 \leq \Theta_\pi \leq \pi/2$ with Θ_π the angle with respect to the z axis. Hence, the negative $\hat{v}_\parallel$ values are more susceptible to nuclear absorption (the trajectory falling within 0.8 of a spectator radius). Of course, the final averaged data must have the symmetry that is forced by identity of target and projectile. Hence, in the final weighted sums of pion cross sections, results are binned by the absolute value $|\hat{v}_\parallel|$. The complete exclusion of π^+ from the regions near target and projectile velocities is a consequence of the classical treatment, and a quantal treatment would bring some π^+ into the classically forbidden region. The upper left two plots are the analogous velocity-plane projections of the initial parameters for *surviving* trajectories of π^- and π^+. Large empty spaces are seen around the projectile and target velocity for π^- (the initial distribution). These holes define the regions of initial conditions leading to π^- absorption and to orbiting trajectories that never converge to a constant velocity.

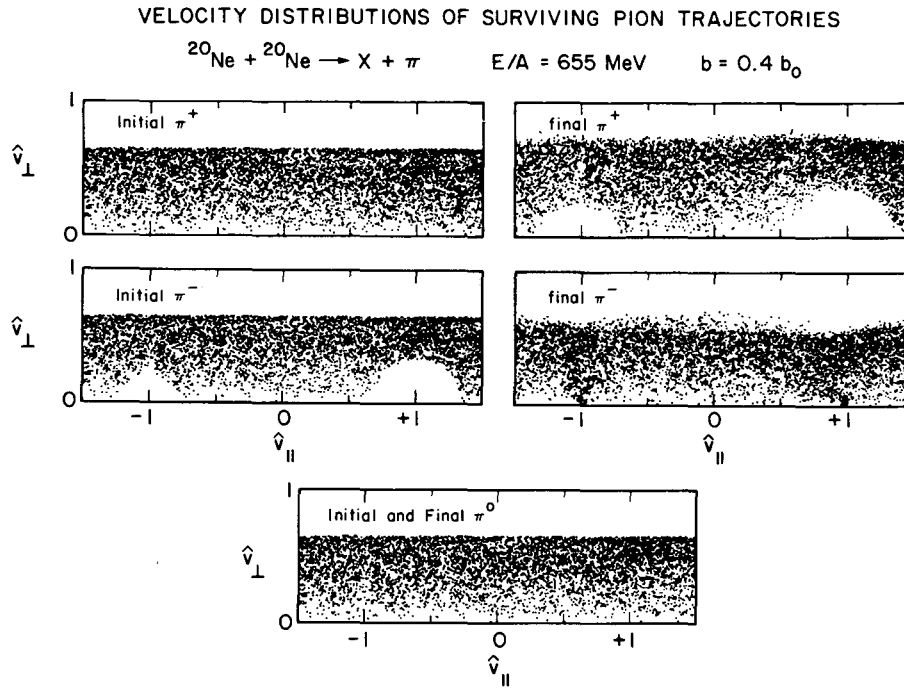

Fig. 1. Scatter plot of Monte Carlo initial and final $\hat{v}_{\parallel}$ and $\hat{v}_{\perp}$ values for trajectories surviving absorption or orbiting capture. Values are shown for one impact parameter $0.4b_0$ for the ^{20}Ne + ^{20}Ne system at 655 MeV/nucleon (see text). XBL 821-7673

In order to compare with pion inclusive data of ^{20}Ne on NaF at E/A of 655 MeV, a detailed two-fireball source function was used to construct the weighting function for the $\simeq$100,000 Coulomb surviving trajectories for each type of pion and for each impact parameter. Thus, they were combined with appropriate weighting for the various impact parameters to yield results to compare with pion inclusive data.

In Fig. 2 are plotted the surviving percentages of trajectories (for about 12,000 trials for each type of pion and for a given impact parameter) as a function of impact parameter.

Fig. 3 compares experiment and theory for π^- at 0°, with the theory being multiplied by an arbitrary factor (different from the one used for the previous three figures) to give matching in the flat region. There is a reasonable agreement with the beam velocity peak in position and width, but the theoretical peak rises somewhat higher above the base than the experimental. Somewhat surprising is a secondary bump near "$\beta_{\parallel}$" of 0.13, evident in both experiment and theory.

Fig. 4 compares experiment and theory for π^+ at 0°. The scale is correct for the data, and the normalization factor applied to the theory is the same as that in Fig. 3 for the π^-.

For the π^+ the theoretical curve is not as flat as the experimental, and the beam velocity mimimum is too low in the theory. We have varied the impact-parameter weighting and can get slightly better agreement for unrealistically strong weighting of central collisions. The more likely explanation of the discrepancy is the neglect of quantum effects. The region of the π^+ beam velocity mimimum will be most sensitive to the neglect of quantum mechanical effects, for those slow-moving pions in the projectile frame spend appreciable time near the projectile and have wavelengths in this frame which are long compared to nuclear dimensions.

Table I summarizes the various factors determining the theoretical π^-/π^+ ratio at the center of mass, and the bottom line gives the corresponding experimental values for comparison.

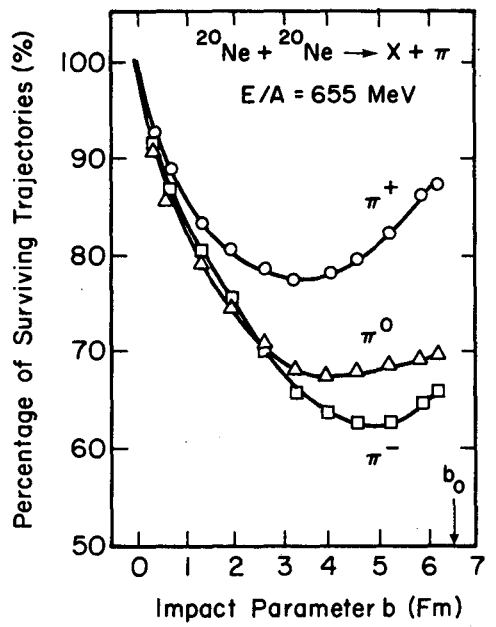

Fig. 2. Plot of the surviving percentage of Monte Carlo trajectories for the three different pion charges as a function of impact parameter. XBL 821-7672

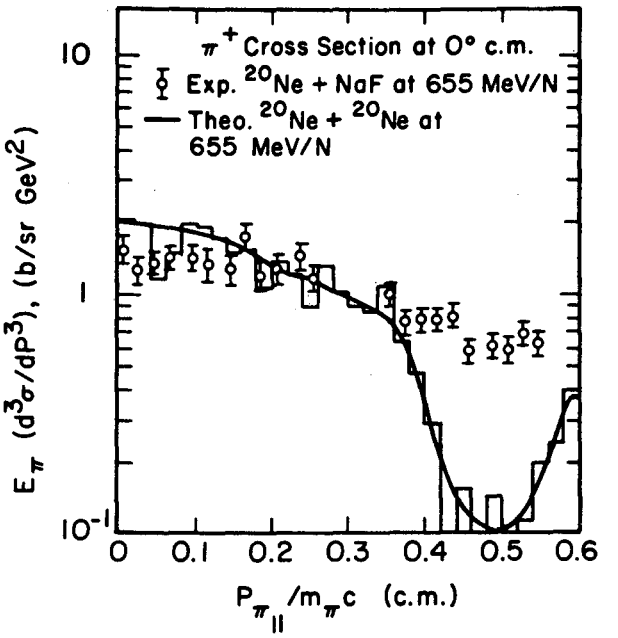

Fig. 4. Same as Fig. 3 except for π^+. The normalization constant for the theory is the same as for Fig. 3. XBL 841-60

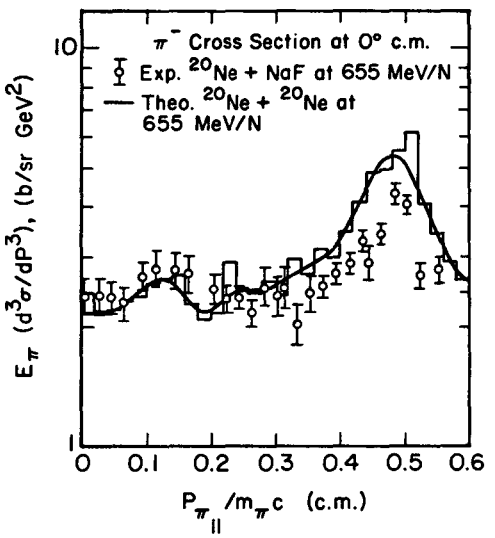

Fig. 3. Cut along 0° for π^-. The theory is shown by both a histogram and a computer-smoothed curve. The width of the cut is β to 0.1c, comparable to experimental resolution. Data are plotted with error bars and the theory has been normalized to the flat portion. XBL 841-59

Footnotes and References

*Condensed from Phys. Rev. **C27**, 606 (1983).

†Present address: Cyclotron Institute, Texas A&M University, College Station, TX77843.

‡Nuclear Physics Research Institute, Academia Sinica, Shanghai People's Republic of China

1. W. Benenson, G. Bertsch, G.M. Crawley, E. Kashy, J.A. Nolen, Jr., H. Bowman, J.G. Ingersoll, J.O. Rasmussen, J. Sullivan, M. Koike, M. Sassao, J. Peter, and T.E. Ward, Phys. Rev. Lett. **43**, 683 (1979).
2. K.G. Libbrecht and S.E. Koonin, Phys. Rev. Lett. **43**, 1581 (1979).
3. J. Cugnon and S.E. Koonin, Nucl. Phys. **A355**, 477 (1981).
4. M. Gyulassy and S.K. Kauffmann, Nucl. Phys. **A362**, 503 (1981).
5. G. Bertsch, Nature **283**, 280 (1980).

6. H.M.A. Radi, J.O. Rasmussen, J.P. Sullivan, K.A. Frankel, and O. Hashimoto, Phys. Rev. C **25**, 1518 (1982); J.O. Rasmussen, H.M.A. Radi, J.P. Sullivan, K.A. Frankel, and O. Hashimoto, Proceedings of the Fifth High Energy Heavy Ion Study, Berkeley, 1981, LBL-12652-UC-34 Conf-8105-104, p. 397.

7. K.A. Frankel, J.A. Bistirlich, R. Bossingham, H.R. Bowman, K.M. Crowe, C.J. Martoff, D. Murphy, J.O. Rasmussen, J.P. Sullivan, W.A. Zajc, J.P. Miller, O. Hashimoto, M. Koike, J. Peter, W. Benenson, G.M. Crawley, E. Kashy, J.A. Nolen, Jr., and J. Quebert, Phys. Rev. C **25**, 1102 (1982); also Phys. Rev. C (to be published).

8. J.P. Sullivan, Ph.D. thesis, University of California, LBL-12546, 1981 (unpublished).

TABLE I. Zero energy (c.m.) π^-/π^+ ratio factors

	^{20}Ne + NaF at 655 MeV/nucleon	^{40}Ar + Ca at 1050 MeV/nucleon
Spectator Coulomb factor	1.40	1.36[a]
Neutron-excess factor	1.083	1.17
Participant Coulomb factor	1.11	1.10
Final product	1.68	1.75
Experimental (ref. 7)	1.76 ± 0.1	1.5 ± 0.2

[a]Calculated by scaling from ^{20}Ne Monte Carlo results.

PART V: INSTRUMENTATION AND TECHNIQUES

General

A Method for Precise Charge Measurements for Relativistic Light Nuclei, $Z \geqslant 3$, in Nuclear Track Emulsion*

M.A. Bloomer,† H.H. Heckman, and Y.J. Karant

A technique for precise charge measurement of particle tracks in nuclear emulsion is described. The method is based on measurements of the lacunarity, i.e., fractional transparency, and/or the fractional opacity in the linear track structure of ionization tracks observed in the developed emulsion. The method yields estimates of charge for relativistic Z = 1 and 2 nuclei to a precision of $\sim \pm 0.05$ charge units, in agreement with Barkas' theoretical model of track structure.[1] The technique is applicable up to Z $\simeq$ 6, but with diminished charge resolution with increasing charge above Z = 3.

For nuclei up to $Z \simeq 6$ the structure of ionization tracks is linear, composed of blobs, i.e., clusters of unresolved grains, gaps, and occasional high-energy delta rays. For a given sensitivity, the primary grain density, g, is assumed to be proportional to the restricted energy-loss rate, $\mathcal{J} = \frac{Z^2}{\beta^2} f(\beta)$,

$$g = K\mathcal{J} \text{ with } K = \text{sensitivity factor.} \qquad (1)$$

Given the observational fact that the gap-length distribution $H(\geqslant \ell)$ in ionization tracks is exponential, then the linear fraction of a track made up of gaps, i.e., the lacunarity, is given by

$$L = -\int_0^\infty \ell \frac{dH}{d\ell} d\ell = \exp(-\alpha g), \qquad (2)$$

where α is the mean grain diameter. From the above relations, the charge of an ionizing particle is given by

$$Z = k_0 \sqrt{-\ln L} \quad , \qquad (3)$$

the proportionality constant k_0 being determined experimentally. Based on the model of Barkas[1] for $\delta L/L$, the expected uncertainty in Z is

$$\delta Z = \frac{k_0^2}{2Z} \left[\frac{2\alpha}{\Lambda} \left(-\frac{1 - L}{L \ln L} - 1 \right) \right]^{1/2}, \qquad (4)$$

where Λ is the length of track segment used for charge measurement.

Equations 3) and 4) show that for $Z \geqslant 4$, charge measurements can be made to an accuracy of $\delta Z \simeq 0.05$ charge units by lacunarity measurements in $\Lambda \leqslant 1$ mm.

To test these predictions we first made charge measurements on tracks of $\sim$2 GeV/nucleon ^{3}He, ^{6}Li, and ^{12}C in G-5 emulsions. The results of these measurements showed that the estimate of Z by the lacunarity method vary linearly with Z in the range $1 \leqslant Z \leqslant 3$. The second test was to measure the charges of a sample of 683 secondary He nuclei emitted from ^{56}Fe interactions at 1.9 GeV/nucleon within the fragmentation cone of $\Theta \lesssim 6°$, using track segments of 1 mm in length. Fig. 1 shows the composite charge spectrum of Z = 2 projectile fragments based on the observations of three scanners, each data set being normalized to $Z \equiv 2.00$. The standard error S_Z varied from 0.042 to 0.057, with a mean of 0.049 (shown in Fig. 1).

We conclude that our measurements of charge for Z = 2 nuclei have demonstrated that the precision of charge estimation by the lacunarity/opacity technique is well accounted for by Barkas' (model-dependent) expression for $\delta L/L$, eq. 4. Although the measurements of lacunarity in this work were carried out visually, the measurements of the integral gap lengths of a track segment are clearly amenable to conventional optical-electronic techniques. The incorporation of such techniques for charge measurement coincident with track following by the observer is the next and essential advance in the development

of this method of charge measurement in emulsion.

Footnotes and References

*Based on M.A. Bloomer, H.H. Heckman and Y.J. Karant, N.I.M., **215**, 247 (1983).
†Massachusetts Institute of Technology, Cambridge, MA.

1. Walter H. Barkas, *Nuclear Research Emulsions*, vol. 1, New York: Academic Press (1963).

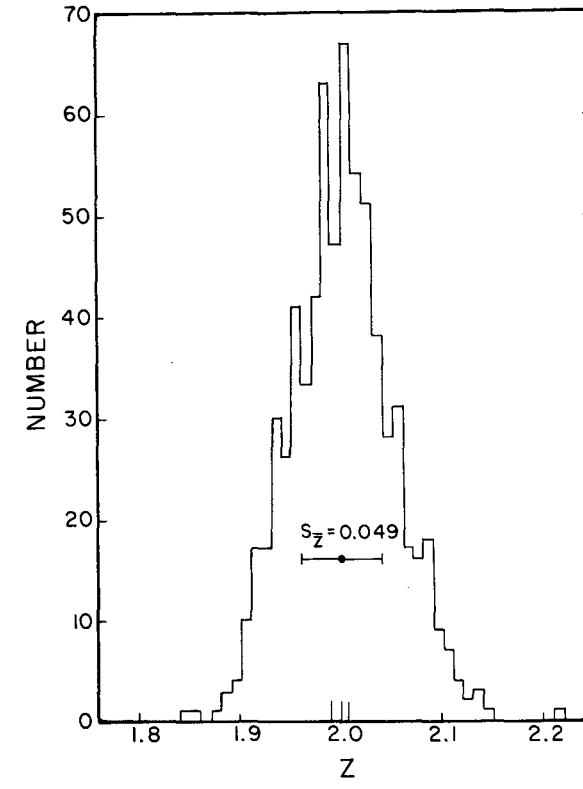

Fig. 1. Distribution of measured charges for Z = 2 projectile fragments from ^{56}Fe at 1.88 GeV/nucleon. The data for each plate are corrected for depth/time gradients and normalized to Z = 2.00. Also shown are the values of $\bar{Z}$ obtained by each observer.
XBL 8212-12046

Development of a New Type of On-Line Mass Analyzer – RIMA

A. Ghiorso, K. Halback, and S. Yashita

For use with heavy ion (H.I.) reactions, we have been constructing a new kind of on-line mass analyzer which, if successful, should have the special properties of high speed and high efficiency. Fundamentally, the principle of operation is based on a very old idea[1] to extract heavy-ion-induced recoils from a stopping gas into vacuum in such a way that they could be reaccelerated as +1 ions to be mass separated magnetically. This system was given the acronym RAMA[2] for Recoil Ion Mass Analyzer and for a few years efforts were devoted to the project with only partial success.

In the late 1970s J.M. Nitschke revived the RAMA idea and succeeded in making it work for recoil nuclei from alpha particle decay; however, when he attempted to use his system for H.I. reaction recoils, he found that beam ionization produced such a high electron density that the recoils were lost quickly by neutralization.

Since it is beam ionization that prevented RAMA from working, we are attempting to solve the problem by drastically reducing the heavy ion beam that traverses the recoil-stopping chamber. This will be done by allowing the beam and recoils to pass through 1 torr of helium in an intense magnetic field (~2 Tesla) for about 30 cm. In the heavy element region, the magnetic rigidity of the beam will be 2–3 times less than that of the recoils so that it can be spatially separated from them. The separated recoils pass through thin windows and come to momentary

rest as +1 ions in a stopping chamber filled with a fraction of an atmosphere of helium.

The positively-charged recoil ions are swept in a few milliseconds by an electric field to a confined space where a high velocity stream of helium can push them through a small orifice into a low pressure ($\sim$1 torr) region created by a high speed pump. At this pressure the mean free path between collisions is still very small and the +1 ions can be directed electrically through a second orifice into a modest vacuum ($\sim 10^{-4}$ torr). A suitable accelerating potential ($\sim$ +30 KV) on this orifice accelerates the ions to ground potential so that they can undergo mass analysis in a suitable magnetic field.

The name RIMA, an acronym for Recoil Ion Mass Analyzer, has been given to this device to differentiate it from its ancestors. A somewhat similar instrument[3] has been completed recently at the University of Jyväskylä in Finland and successfully operated to separate light reaction products produced in proton and helium bombardments. That device does not attempt to avoid beam ionization and as a consequence does not have a high efficiency; but it does work and is the first of its type to do so.

References

1. A. Ghiorso, unpublished work, 1956.
2. Much later this acronym was used by J. Cerny and his group for a different type of on-line mass separator that involved re-ionizing and re-accelerating recoils that had been transported from a target chamber by the helium gas jet method. Its speed and efficiency is orders of magnitude lower than envisioned here.
3. J. Ärje, J. Äystö, P. Taskinen, V. Koponen, A. Hautojärvi, K. Vierinen and K. Valli, Initial Results with the Ion Guide Isotope Separator On-Line (IGISOL), Department of Physics, University of Jyväskylä Nisulankatu 78, SF-40720 Jyväskylä 72, Finland, Research Report No. 13/1983.

A Monopole Search

*F. Beiser, D. Greiner, and R. Hagstrom**

We have begun a project to search for magnetic monopoles in the range of velocities most likely for particles traveling under the influence of Earth's gravity. As Ray Hagstrom has pointed out,[1] this velocity range ($\exp^{-3}$ to $\exp^{-5}$ c) can not be detected with plastic scintillators. Our detector consists of nine planes of lithium-drifted silicon wafers (8 per plane) shown in Fig. 1. Each wafer is 5 mm thick and 5 cm in diameter. The planes are spaced 3 cm apart. The detector array is cooled by a thermoelectric heat pump to -20°C and is insulated with a thermal blanket inside a vacuum cryostat.

Each silicon detector is connected to an amplifier/discriminator circuit board which has the following characteristics:

discriminator threshold:	200 keV (adjustable)
logic output:	differential FCI
analog output:	shaped (1 microsecond)
	200 mv/MeV into 93 ohms
size:	4.5 in $\times$ 4.5 in

All logic outputs are connected to CAMAC hit-pattern registers (LeCroy 4448); the logical OR of all eight wafers in each plane is used to stop gated scalers counting at 100 MHz to measure the time of flight between planes. All analog outputs are processed by 12-bit ADCs (LeCroy 2281) having a common gate.

A monopole signature will be recognized by its constant flight-time between planes in the range of 100 to 10,000 ns, while maintaining a constant rate

of ionization.

Footnote and Reference

*Argonne National Laboratory

1. Proceedings of 1982 Summer Workshop on Proton Decay Experiments Argonne National Laboratory, ANL-HEP-PR 8225

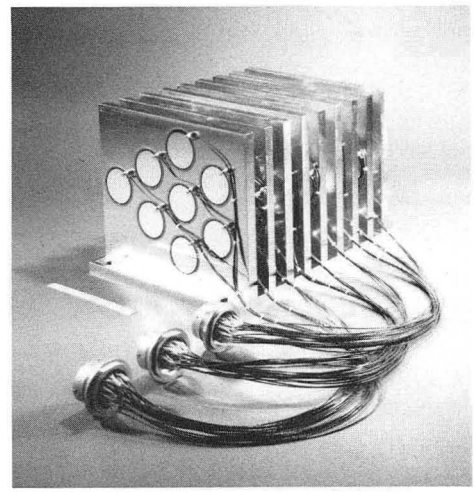

Fig. 1. Silicon detector holder, monopole experiment. BBC 831-603

Mapping the HISS Dipole

C. McParland, F. Bieser*

The principal component of the Bevalac HISS facility is a large super-conducting 3 Tesla dipole. The facility's need for a large magnetic volume spectrometer resulted in a large gap geometry – a 2 meter pole tip diameter and a 1 meter pole gap. Obviously, the field required detailed mapping for effective use as a spectrometer. At very low fields, the dipole yoke iron is unsaturated and fields in this region scale easily. Near the high-end design current, however, iron magnetic saturation effects alter the field substantially and make it impossible to extrapolate fields from lower current maps. As a result, we require a field mapping device which could easily measure many field maps.

The mapping device was designed with several major features in mind. The device would measure field values on a grid which described a closed rectangular solid. The grid would be a regular with the exact measurement intervals adjustable by software. The device would function unattended over the long period of time required to complete a field map. During this time, the progress of the map could be monitored by anyone with access to the HISS VAX computer. Details of the mechanical, electrical, and control design follow.

Mechanical Design

The three orthogonal axes are composed of four vertical posts located just outside the magnet gap, two long beams stretching between pairs of posts, and a cross-beam carrying a moving cart. See Fig. 1. Vertical motion is provided by 1 inch diameter lead screws in each post driven by permanent magnet DC motors through 10:1 reducing right-angle gear boxes. Each screw has an incremental shaft encoder and is driven independently. The cross beam moves back and forth between the two long beams by means of two more 1 inch lead screws with a shaft encoder and PM DC gear motor. The cart which carries the Hall probes shuttles along the cross beam using an 1/2 inch lead screw and a glass scale position encoder such as those used on NC milling machines. All lead screws are made of 310 stainless steel. All beams are extruded aluminum box and all bearings are phosphor-bronze or teflon.

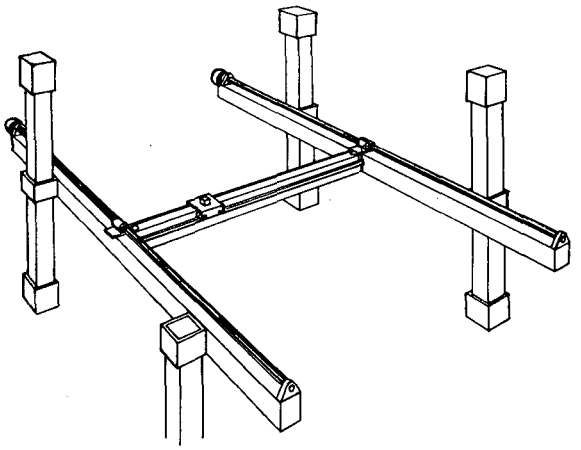

Fig. 1. Hiss magnet mapper. XBL 8312-4710

Electrical/Mechanical Interface

Limit and tilt switches prevent damage to the beams and drive mechanisms due to computer failure, operator error, etc. Each of the six motors is driven by a ±120 VDC power amplifier controlled by a digital to analog converter. Up/down counters fed by the incremental encoders keep track of the position of each axis.

Magnetic Field Measurement

Hall effect probes are cemented to three faces of a precision optical alignment cube. The amplified signals are digitized by very fast 14 bit analog to digital converters. Measurements are taken at each desired grid point when digital comparators determine the probes to be in the exact position (without stopping the motion). The Hall probes are calibrated against an NMR measurement at a low gradient position.

Mapper Control System

The mapper control system consists of an interface chassis with position encoders, motor drive electronics, video display interface, Hall probe ADCs and several miscellaneous control registers. This chassis functions as a peripheral device on an LSI-11 microprocessor. This machine runs the multi-tasking RSX-11S operating system and is connected via a DECNET network to the HISS VAX 11/780.

The LSI-11 fills several functions. As noted above, positioning motors are driven by computer controller DACs. The LSI-11 implements all feedback algorithms for regulating speed and direction of this motion. Motion on each axis consists of a speed up/slow down sequence designed to have the motor reach zero speed precisely at the desired location. In accomplishing this function, the microprocessor must read the location and speed of all six axes and compute how close each axis is to its destination position. At specified distances from its destination, each axis slows down in order not to overshoot the desired destination. If an overshoot does occur, motion is reversed and a new speed up/slow down sequence is started. All motion algorithms were simulated, optimized, and tested on the VAX using the measured response curve for each motor/axis combination. It should be noted that since each Z axis is mechanically independent of all others, the LSI-11 is required for any motion. Without it and its feedback algorithms, small speed variations would drive at least one Z axis faster than all others. When this occurs, internal tilt switches would abort all motion and operator intervention would be required.

In addition to the above algorithms, the LSI-11 provides a means of local manual control for mapper positioning. This has proven invaluable in positioning the field measuring cube in the magnet gap using a surveyor's transit. The microprocessor also drives a continually updating video display of present mapper location, motion commands, and mapper status.

When not in local mode, the LSI-11 is waiting for commands from the VAX control program. As mentioned, communication between processors is accomplished via DECNET. A single VAX process connects to one of three processes running in the LSI-11. This LSI-11 process is responsible for screening VAX commands for legality and advisability. It is capable of rejecting commands which will attempt to map too many points too close together or move the mapper too far in any direction. It also sends a continual string of status messages to keep the VAX monitoring program up to date. The motion and measurement primitive commands

capable of being performed are listed in Table I.

For a summary of VAX display and analysis programs, as well as a list of field maps taken, see Beleal *et al.* in this volume.

*UCB Space Sciences Laboratory, LBL

Table I

command	function
move to x, y, z	move the mapper probe to position x, y, z
measure B(x, y, z)	encode the B field for the x, y, and z hall-effect probes.
report status	report status of all monitored mapper parameters.
map a line in x	record a series of B field values by holding y and z constant and moving x between an upper and lower limit.
map a line in y	similar to above, except hold x and y constant while mapping a line in y.

Status Report on the ECR Ion Source for the 88-Inch Cyclotron

D.J. Clark, Y. Jongen, C.M. Lyneis*

The heavy-ion capability of the 88-Inch Cyclotron at LBL will be significantly upgraded in late 1984 when the Electron Cyclotron Resonance (ECR) ion source now under construction becomes operational.[1,2] The upgraded accelerator system will be capable of higher energy heavy ion beams and improved operational efficiency. The ECR source will strip heavy ions to higher charge states than the conventional internal heavy ion PIG source currently used on the cyclotron, and as a result the maximum energy available from the cyclotron for ions between oxygen and argon will increase by a factor of 2 to 3. Improved operational efficiency will be obtained with the ECR source , since it can be operated continuously without the frequent source changes necessitated by the short lifetime of heavy ion PIG sources.

The projected improvement in the performance of the 88-Inch Cyclotron resulting from the addition of the ECR source is illustrated in Fig. 1. The curves reflect the performance of the ion sources and the energy dependence of the cyclotron beams which is given by

$$\frac{E}{A} = K \frac{Q^2}{A^2}$$

where K is 160, E/A is the energy in MeV per nucleon, Q is the charge and A is the mass in amu. Initial operation for heavy ions with a charge to

mass ratio near 1/2 will be limited to K of 140, which will later increase to 160 as the cyclotron deflector is improved. The present performance with a rapid falloff of energy per nucleon above neon reflects the limitation of the charge states that can be produced by the heavy ion PIG sources.

In an ECR ion source a stabilized magnetic mirror is used to contain a plasma of ions and electrons. The electrons in the plasma are heated with microwave power, which is coupled to the electrons along a magnetic surface where the condition for electron cyclotron resonance is satisfied. The hot electrons strip the ions to high charge states by sequential collisions and the ions are then extracted by biasing the extractor negatively relative to the plasma.

The ECR ion source at LBL is designed for reliable operation, flexibility, and a reasonably short construction time. To meet these criteria the source uses conventional foil-wound solenoid coils and a rare earth sextupole magnet to create the stabilized mirror field. The mirror ratio and location of the field maxima are easily adjusted by changing the current driving the segmented solenoid coils on the main stage. The main source parameters are presented in Table I. In Fig. 2 the source stand, the injection chamber and extraction chamber are shown during preliminary assembly. A horizontal beam line and axial injection line will transport the beam from the ECR ion source to the injection point in the midplane of the cyclotron. A major part of the project involves the construction of the horizontal transport line and upgrading the existing axial beam line by improving the vacuum and installing a new beam optics system. The modifications will increase the transmission from source to extraction to at least 10%.

Injection of the beam into the cyclotron is scheduled for late 1984 with regular operation occurring early in 1985. The ECR ion source and 90 degree analyzing magnet came into initial operation in January 1984. Earlier, a dense cold plasma was produced during successful tests on the injector stage in November 1983. The 90 degree charge state analyzing magnet will be used to measure the performance of the ECR. During the early part of 1984 a major effort to optimize the source performance will be made. At the same time design, fabrication, and procurement for the beam transport system between the analyzing magnet and the center of the cyclotron will be proceeding.

Table 1
ECR Source Parameters

Axial Magnetic Field	
Mirror Ratio	1.3–2.0
Max B on axis	0.42 T
Sextupole Dimensions	
Inner radius (r)	4 cm
Element height (h)	3 cm
Element width (d)	2.8 cm
Length	33 cm
Sextupole Magnetic Field	
Maximum B_{MAG} ($\Theta = 0°$)	0.41 T
Maximum B_{MAG} ($\Theta = 30°$)	0.28 T
$B_{remanent}$ $SmCo_5$	0.94 T
Microwave Power	
Mainstage	3.3 kW at 6.4 GHz
Injector	1.0 kW at 9.2 GHz

Footnote and References

*On leave from Cyclotron Laboratory, Louvain-la-Neuve, Belgium.

1. Proposal to Construct an Electron Cyclotron Resonance Ion Source for the 88-Inch Cyclotron, LBL PUB 5078, September 1982.
2. An ECR Heavy Ion Source for the LBL 88-Inch Cyclotron, D.J. Clark, J.G. Kalnins, and C.M. Lyneis, IEEE Trans. Nucl. Sci. **NS-30, 4**, 2719 (1983).

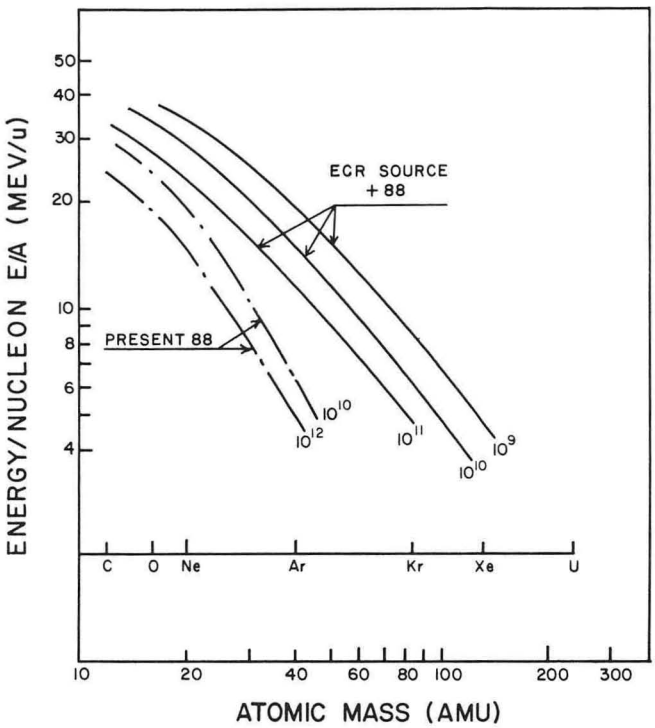

Fig. 1. Energy per nucleon vs mass number for 88-Inch Cyclotron. Cyclotron external beam intensity (particles/sec) is shown for each contour line. Lower curves show performance with present internal PIG source. Upper curves give estimate for injection with the ECR source, assuming a transmission of 4% from source to external beam. XBL 833-8746

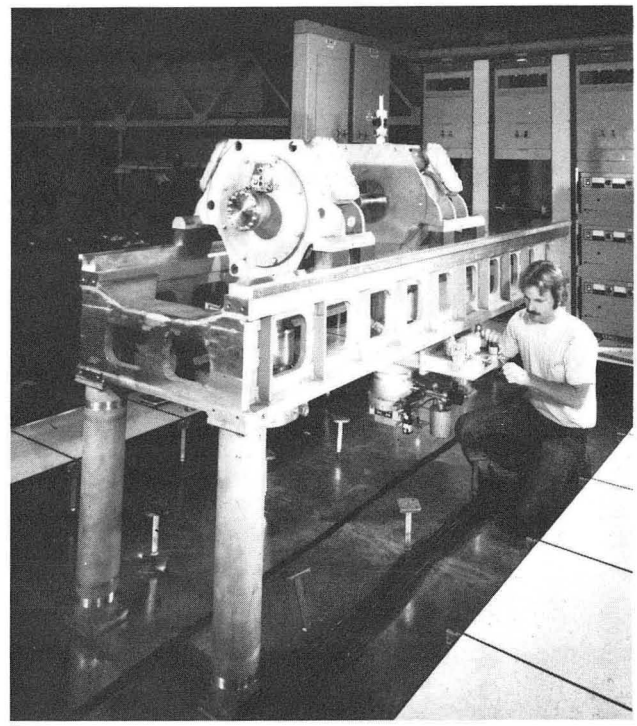

Fig. 2. View of the ECR ion source injection and extraction chambers mounted on the stand during the preliminary assembly. BBC 830-8875

High Charge State Ion Sources*

D.J. Clark

Sources of high charge state positive ions have uses in a variety of research fields. For heavy ion particle accelerators higher charge state particles give greater acceleration per gap and greater bending strength in a magnet. Thus higher energies can be obtained from circular accelerators of a given size, and linear accelerators can be designed with higher energy gain per length using higher charge state ions. In atomic physics the many atomic transitions in highly charged ions supply a wealth of spectroscopy data. High charge state ion beams are also used for charge exchange and crossed beam experiments.

For the sources discussed here bombarding electrons are used to create multiply charged ions. The rate of formation of a high charge state is proportional to the electron beam density and the cross sections. The parameter which determines the charge state obtained is $j\tau$, where j is the electron current density and τ is the ion confinement time. A proportional quantity, often used in plasma physics, is $n\tau$, where n is plasma density. In actual sources the charge state is also limited by charge exchange and recombination. The operating regions of several high charge state sources are shown in Fig. 1 as a

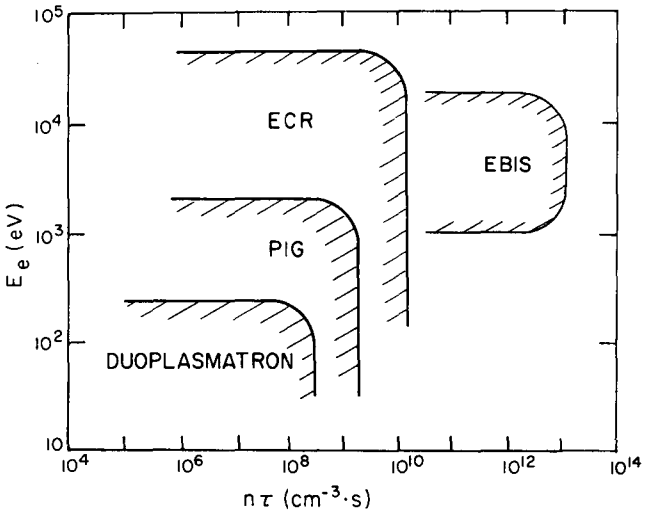

Fig. 1. Operating regions of the most common high charge state ion sources as a function of electron energy (E_e) and $n\tau$. XBL 8211-3261A

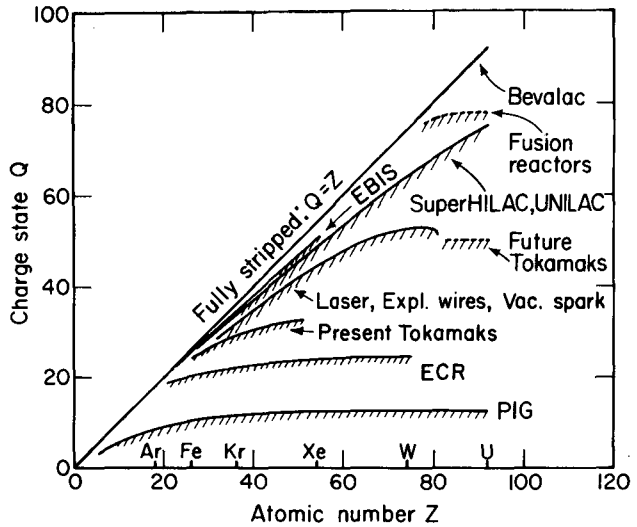

Fig. 2. Charge states produced by ion sources, plasmas and stripped accelerator beams. Upper limits of charge states from each device are shown by lines, solid for present and dotted for future operation. XBL 773-468A

function of electron energy and $n\tau$. The source principally used in present heavy ion cyclotrons and linacs is the PIG. ECR sources are used or planned for several cyclotrons and atomic physics installations. EBIS sources are being used or developed for atomic physics and synchrotron injection. This paper discusses these sources and also short pulse sources such as those based on lasers.

The production of high charge states by electron bombardment can be accomplished either by the use of fast electrons on thermal velocity ions in an ion source or by using fast ions from a first accelerating stage and passing them through a gas or foil stripper. This last method is extensively used in two-stage heavy ion accelerators. The equivalence of fast electrons and fast ions for producing high charge states was discussed by Nagel.[1]

A summary of the charge states available from a variety of ion sources, plasmas, and stripped accelerator beams is shown in Fig. 2. The highest charge states are produced by stripping of beams from high energy accelerators such as the Bevalac, which has recently produced a fully stripped uranium beam through a stripper.[2] These accelerators are of course an expensive way to produce high charge states, and the challenge to the ion source designer is to generate these high charge states with a much less costly ion source. As shown in Fig. 2, the EBIS comes close to producing fully stripped ions up to xenon. Although the ECR source has lower charge states, it has the advantage of higher average beam intensity and 100% duty factor.

During studies of ion-beam fusion the question has arisen of the effectiveness of a plasma for stripping and stopping an ion beam. Calculations of this effect have been done at the Weizmann Institute.[3] The calculation indicates that a plasma stripper would be even more effective than a solid for ions in the energy range of <1 MeV/nucleon, because of the lower cross section for recombination with free electrons in a plasma.

A final method of high charge state ion production is that of recoil target ions produced by fast ion beams hitting a target. In this case the recoil ions are normally of lower charge state than that of the incoming beam, but they have the virtue of having low velocities so that they can be used for low energy atomic physics experiments. An example of this type of experiment is a 19 MeV F^{4+} beam producing $Ar^{1...10+}$ recoils, which are accelerated with a voltage of 200–700 volts, and used for electron capture measurements on gas targets.[4]

We can look forward to continued development of high charge state ion sources in the areas of higher frequency ECR sources, and higher charge state and repetition rate in EBIS sources. Higher power lasers will make higher charge states available.

Footnote and References

*Condensed from LBL-16327 and published in the Proceedings of the 7th Symposium on Ion Sources and Ion Assisted Technology (ISIAT '83) and the 4th International Conference on Ion and Plasma Assisted Techniques, (IPAT '83) Sakyo-ku, Kyoto, Japan, September 12–16, 1983.

1. D.J. Nagel, Beam Foil Spectroscopy, **2**, 961, Ed. I. Sellin and D. Pegg, Plenum Press (1976).
2. Henry Crawford, Harvey Gould, Douglas Greiner, Peter Lindstrom and James Symons, Proceedings of the 6th High Energy Heavy Ion Study and 2nd Workshop on Anomalons, LBL, June 1983.
3. E. Nardi and Z. Zinamon, Phys. Rev. Lett. **49**, 1251 (1982).
4. C.L. Cocke, R. DuBois, T.J. Gray, E. Justiniano and C. Can, Phys. Rev. Lett. **46**, 1671 (1981).

Global Analysis of Relativistic Nuclear Collisions Detected by the Plastic Ball

H.A. Gustafsson, H.H. Gutbrod, B. Kolb,* H. Löhner,† B. Ludewigt,* A.M. Poskanzer, T. Renner, H. Riedesel,‡ H.G. Ritter,* A. Warwick,* F. Weik,*§ and H. Wieman**

Data from 4π detectors like the Plastic Ball are ideally suited to study the event shapes and emission patterns of high energy nuclear collisions. It has been pointed out that event shape analysis might be able to distinguish between predictions of cascade and hydrodynamical models. To do this the sphericity[1,2] analysis used in high energy physics has been proposed.

The sphericity tensor

$$F_{ij} = \sum_{\nu} p_i(\nu)\, p_j(\nu)\, w(\nu)$$

is calculated from the momenta of all measured particles for each event. We use the weight $w(\nu) = 1/(2m)$ as proposed in ref. 2 (kinetic energy flow). The sphericity tensor approximates the event shape by an ellipsoid whose orientation in space and aspect ratios can be calculated by diagonalizing the tensor.

The shapes predicted by hydrodynamical and cascade calculations are quite different. The hydrodynamical model predicts prolate shapes along the beam axis for grazing collisions. With decreasing impact parameter the flow angle increases up to 90 degrees for zero impact parameter events and the shape becomes oblate.[2,3] This behavior is independent of projectile and target mass. Cascade calculations, on the other hand, predict zero flow angles for most systems.[2]

A comparison of experimental data with predictions is only possible if the theory calculates all observed quantities by generating a large number of complete events. Those events have to be filtered with the known experimental acceptance and efficiency of the detector. A big obstacle in extracting information from a flow analysis is fluctuations due to finite particle effects. Recently, Danielewicz and Gyulassy[4] have shown that those distortions strongly depend on multiplicity and that the flow angle, Θ, if properly weighted by the Jacobian ($\sin\Theta$), is much less severely shifted toward higher values than the aspect ratios. The results of the flow analysis of the 400 MeV/nucleon Ca + Ca data can be explained with finite number distortions by assuming prolate shapes along the beam axis.

Heavier symmetric systems are less sensitive to distortions and possibly macroscopic effects can

more easily be detected. As shown in Fig. 1, the Nb + Nb data at 400 MeV/nucleon reach flow angles up to 30 degrees (peak maximum) for the highest multiplicity bins, while predictions from the Yariv-Fraenkel cascades,[5] filtered with the exact acceptance and efficiency of the Plastic Ball, never deviate significantly from 0 degrees even for the highest multiplicity events. The fact that finite flow angles are seen in the data indicates that in those events there exists a plane defined by the flow axis and the beam axis, which will be called the reaction plane. All events can be rotated by the azimuthal angle ϕ determined by the flow analysis so that their individual reaction planes all fall into the x-z plane, with the z-axis being the beam axis. For those rotated events, rapidity plots in the reaction plane[3] can be calculated. The invariant cross sections dp_x/mdy (in plane) and dp_y/mdy (out of plane) can be plotted, where p_x is the projection of the perpendicular momentum into the reaction plane and p_y the projection into the plane perpendicular to the reaction plane. Fig. 2 shows these plots for 400 MeV/nucleon Nb + Nb data and cascade calculations for events with charged particle multiplicities between 40 and 50. The depletion near target rapidities is due to experimental acceptance. The two cascade plots and the out-of-plane data plots are symmetric around the beam axis, while the in-plane data plot is clearly asymmetric. The highest intensity contour, resulting largely from the projectile remnants, indicates a definite deflection. The multiplicity dependence of the outer contour lines seems to follow the trend indicated by the flow angle distributions (Fig. 1). However, the position of the peak from the projectile remnants changes only slightly with multiplicity and corresponds at its maximal sideward position to a momentum transfer of about 50 MeV/c per nucleon. The comparison of the experiment with hydrodynamical calculation[3] is not straightforward because the impact parameter can be related to multiplicity only via cascade calculations. The hydrodynamical prediction for the flow angle seems to be qualitatively in agreement with the measurement, but the very small variation of the deflection of the projectile as a function of multiplicity does not show the behavior predicted by hydrodynamics.

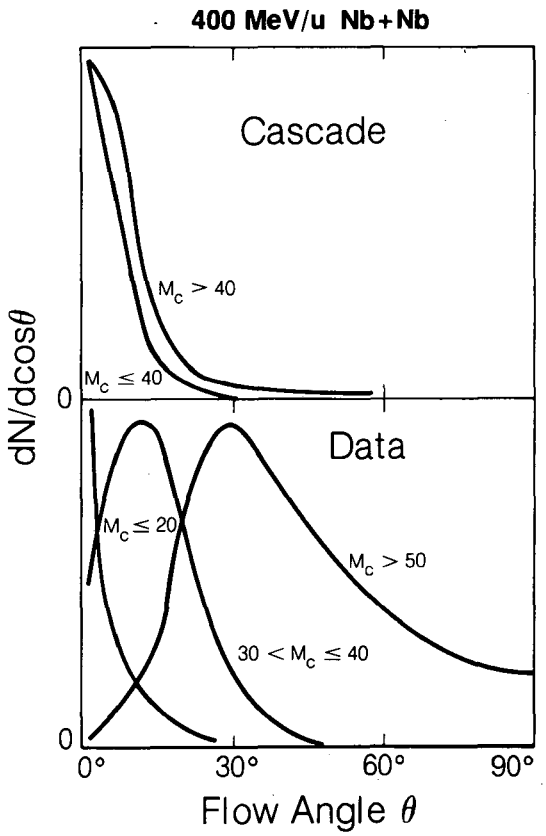

Fig. 1. Frequency distributions of the flow angle Θ for different multiplicity bins (data and cascade calculations). XBL 835-244

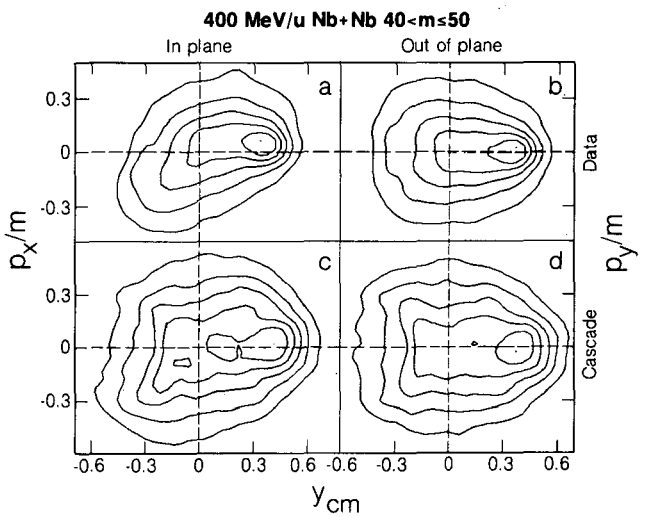

Fig. 2. Contour plots (linear contours) of the projection of the transverse momentum in and out of plane as a function of cm rapidity. XBL 835-243

Footnotes and References

*Gesellschaft für Schwerionenforschung, Darmstadt, West Germany.
†Universität Münster, Münster, West Germany.
‡Present address: Max-Planck-Institut für Kernphysik, Heidelberg, West Germany.
§Present address: Toledo Corp., Köln, West Germany.

1. J. Cugnon, J. Knoll, C. Riedel, and Y. Yariv, Phys. Lett. **109B**, 167 (1982).
2. M. Gyulassy, K.A. Fraenkel, and H. Stöcker, Phys. Lett. **110B**, 185 (1982).
3. H. Stöcker, L.P. Csernai, G. Graebner, G. Buchwald, H. Kruse, R.Y. Cusson, J.A. Maruhn, and W. Greiner, Phys. Rev. **C25**, 1873 (1982).
4. P. Danielewicz and M. Gyulassy, LBL-15721, submitted to Phys. Lett. B.
5. Y. Yariv and Z. Fraenkel, Phys. Rev. **C20**, 2227 (1979).

Minimal-Spanning-Tree Analysis of Plastic Ball Events

H. Löhner, A. Baden, H. Gutbrod,† A.M. Poskanzer, T. Renner, H. Riedesel,‡ H.G. Ritter,† A. Warwick,† H. Wieman†*

One of the goals of relativistic heavy ion collisions is to study nuclear matter in extreme states of high temperature and compression, which might be reached in the participant region of two colliding nuclei. Spectator matter, however, from target and projectile remnants will mask the emission pattern, so that a clean identification of spectator fragments is desirable. Therefore, we have studied the abilities of the cluster algorithm "minimal spanning tree" (MST)[1] by applying it to 4π-exclusive data (Ca + Ca at E/A = 400 MeV/nucleon) from the Plastic Ball.[2] The following analysis was done in the NN-CM system for symmetry reasons. After extensive tests of the algorithm, the analysis should be carried out in the lab system as well and be applied to asymmetric collisions.

The MST algorithm assigns particles of one event to clusters and classifies the event by its cluster number by means of a distance measure d_{ij} between two particles i and j. We took $d_{ij} = \Theta_{ij}/(p_i p_j)$ from ref. 1, where Θ_{ij} is the angle distance between particles i and j, and p_i, p_j are the momenta of i and j. This definition favors leading particles by the inverse momentum weighting. After construction of the "tree" it is cut into subtrees (clusters) at edges (connections between 2 tree elements) which are inconsistently long. This cut is defined from the edge distribution showing a long tail which is cut off from the peak at short edges. Other definitions of d_{ij} were tested, like inverse energy weighting or euclidic distance in the space of rapidity versus transverse momentum. The resulting edge distributions were rather uniform, making a cut definition too ambiguous. Additional parameters are the minimum event multiplicity and the minimum number of particles per cluster, which were set to 5 and 2, respectively. A minimum kinetic energy of 500 MeV per cluster was required in order to avoid too many arbitrarily small clusters. The results are qualitatively insensitive to variations of cuts and parameters within certain limits. Two-cluster events in both the minimum-bias and the central trigger mode[2] of the data have been studied in detail.

Fig. 1 shows for minimum-bias data the rapidity distribution for particles of all events (curve a), for particles assigned to a cluster in 2-cluster events (curve b), for unassigned particles in 2-cluster events (curve c) and the rapidity distribution for the resulting two clusters (dashed line). From this a clear separation into target, projectile, and participant matter at midrapidity can be seen. 80% of projectile (target) clusters are found in a cone around the beam

axis with opening 18° (33°). The cluster quality is very good with a mean n-ticity (see ref. 1) for n = 2 of 0.88. However, the asymmetric structure of curves b and c and the overlapping of the peaks of curve b at midrapidity indicate that the discriminating power of the MST still needs to be improved by finding a more selective distance measure d_{ij}. Fig. 2 shows in the plane of rapidity versus transverse momentum all unassigned particles of 2-cluster events. Looking at angles between 30° and 150°, the contour lines resemble an isotropic emission pattern. For small $P_\perp$ the regions at large $|y_{CM}|$ are distorted obviously due to a wrong cluster assignment and to some extent due to experimental thresholds in the target region.

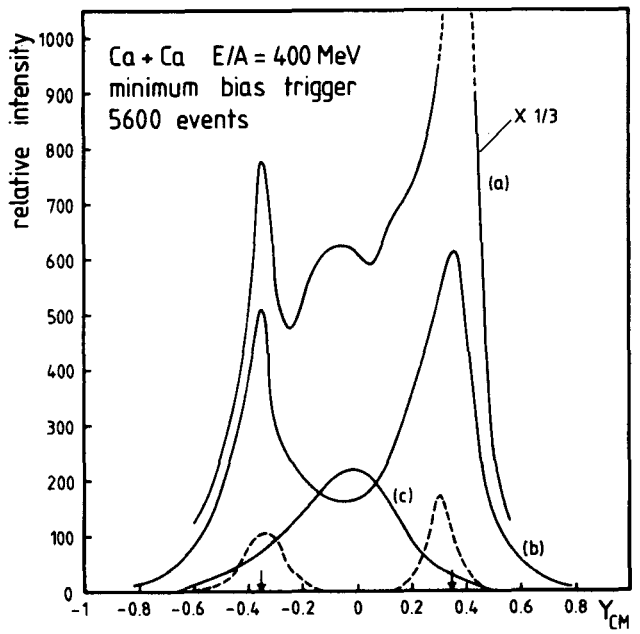

Fig. 1. Rapidity distributions (see text). Arrows indicate the beam and target rapidity in the NN-CM system. XBL 8312-4765

Footnotes and References

*Universität Münster, Münster, West Germany.
†Gesellschaft für Schwerionenforschung, Darmstadt, West Germany.
‡Present address: Max-Planck-Institut für Kernphysik, Heidelberg, West Germany.

1. J. Dorfan, Z. Phys. **C7**, 349 (1981).
2. A. Baden *et al.*, NIM **203**, 189 (1982).

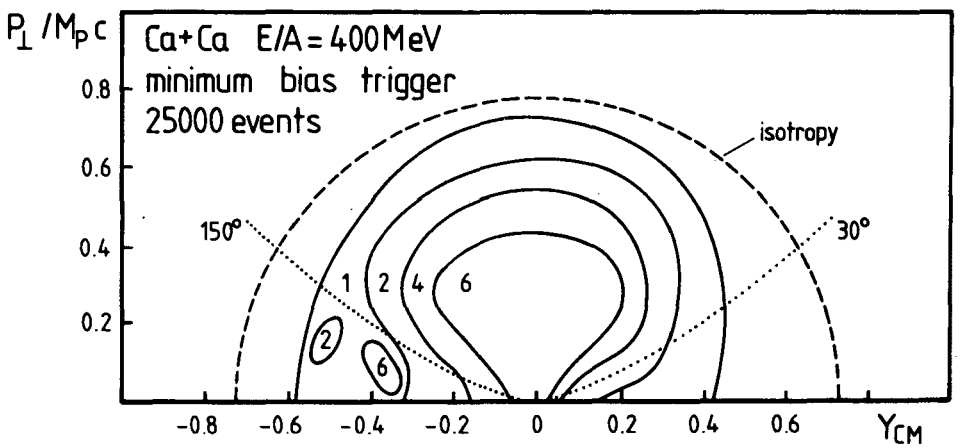

Fig. 2. Rapidity versus normalized transverse momentum for unassigned particles of 2-cluster events. Contour lines are labeled by the relative cross section height. XBL 8312-4764

Enhanced Adhesion of Thin Films by Heavy Ion Bombardment

M. Mendenhall, T. Tombrello,* R.G. Stokstad*

It was discovered recently that thin metallic films can be bonded to insulators, semiconductors and metals by irradiating the surface with energetic ions.[1] The ions have energies sufficiently high that they penetrate well beyond the interface of the two materials and deposit energy at the interface by means of electronic interactions only. The goal of the present research is to discover the nature of the bond between the surfaces and the mechanism for its formation.

Bonding is measured by the "scotch tape" test. A sample thin film (~500 Å) and substrate is irradiated with a beam of heavy ions at a series of spots typically 3 mm in diameter. The dose is varied systematically from spot to spot. Following the bombardment a strip of scotch tape is pressed firmly on the thin film and then pulled away. It is found that the thin film sticks to the tape everywhere except at those spots where the dose exceeded a critical value. The threshold dose varies with the film-substrate combination and with the type and energy of bombarding ion.

Since the bond must be formed as a result of the energy deposited in the surface region it is natural to study the dependence of the threshold dose on the stopping power, $\frac{dE}{dx}$, of the incident ion. To this end initial measurements were done at Caltech with ions from protons to chlorine.[1] Heavier ions at the 88-Inch cyclotron (argon and krypton) and holmium from the SuperHILAC, were then used. The measurements at LBL were made mainly with samples of gold evaporated onto a tantalum substrate.

The dependence of the threshold dose on $\frac{dE}{dx}$ is shown in Fig. 1. The dose and values of $\frac{dE}{dx}$ vary by four and two orders of magnitude, respectively. The straight line is given by the equation Dose = 4.2 x $10^{14} \left(\frac{dE}{dx}\right)^{-1.65}$.

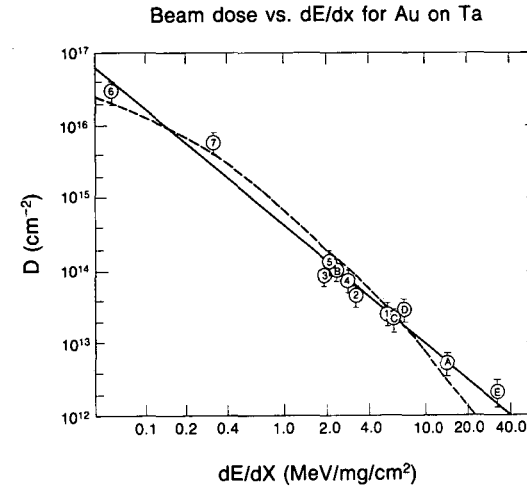

Fig. 1. The threshold dose required to pass the scotch tape test for 500 Å Au films on Ta, versus the energy loss ($\frac{dE}{dx}$) of the bombarding ion at the interface. The values of $\frac{dE}{dx}$ were taken from ref. 3. Table I lists the ions and energies for each data point. The solid curve is a power law fit to the data, $D \propto \left(\frac{dE}{dx}\right)^{-1.65}$. The dashed curve is $\left(\frac{dE}{dx} + Q\right)^{-2}$ where Q corresponds to the liberation of ~70 eV by the increased bonding at the interface. XBL 8312-6916

Initially it was thought that the bonding was due to a displacement or mixing of the atoms of the respective substrates at the interface.[1] This might be a possible mechanism for a system of a metallic thin film on an insulator because the long relaxation time for an electronic disruption in an insulator would provide time to transfer energy into atomic displacement. The short electronic relaxation times for metals, however, would seem to preclude this mechanism for Au or Ta. If bonding does not arise from the interchange or mixing of entire atoms then it must arise from the exchange of electrons at the interface. It has been proposed that a microscopic

area at the interface be regarded as a source of electrons emitted thermionically by the energy deposited by the passing ions.[2] The "current" of electrons across the surface would be responsible for forming the bonds and the threshold dose for the scotch tape test thus should be inversely proportional to this current. Hence,

$$\frac{1}{D_{th}} \propto \Phi^2 e^{-\frac{\Phi}{T}}$$

The temperature is identified with $\frac{dE}{dx} + Q$ where Q is the energy released as a result of the bond formation. In the case of Au on Ta, the work function $\Phi = 0$ and $D \propto \left(\frac{dE}{dx} + Q\right)^{-2}$. The dashed line in Fig. 1 is a fit to the data with a value of Q corresponding to the liberation of 70 eV at the surface.

Further work will be directed toward obtaining systematic data such as in Fig. 1 for systems of a metal on semiconductor and insulator substrates. These systems are already known to require larger doses than metals on metals, which is understandable in terms of the work functions Φ for these substrates.

Table I: Ions and Energies used for irradiation of samples of Au on Ta. The labeling of the entries in the table corresponds to that in Fig. 1. Beams 1–7 are from the Caltech Van de Graaff, A–D from the 88-Inch Cyclotron, and E from the SuperHILAC.

Label	Ion	Energy (MeV)
1	Cl	20
2	Cl	7.2
3	Cl	3.2
4	F	12
5	F	3.7
6	H	1
7	He	1
A	Kr	107
B	O	35
C	Ar	27
D	Ar	87
E	Ho	580

Footnote and References

*California Institute of Technology, Pasadena, California.

1. J.E. Griffith, Y. Qiu and T.A. Tombrello, Nucl. Instr. and Meth. **198**, 27 (1982); M. Mendenhall, Ph. D. Thesis, Calif. Inst. Tech. (1983).
2. T.A. Tombrello, Symposium on Thin Films and Interfaces of the Materials Research Society, Boston, MA, Nov. 14–18, 1983.
3. L.C. Northcliffe and R.F. Schilling, Nucl. Data Tables 7 (1970).

Detectors

Large Solid Angle Bragg-Curve Spectrometer*

R.J. McDonald, L.G. Sobotka, Z.Q. Yao,† G.J. Wozniak, and G. Guarino‡

In 1982, Gruhn *et al.*[1] demonstrated the viability of a gas-filled ionization chamber with the electric field parallel to the particle ionization track. This device was called a Bragg-curve spectrometer (BCS) because the time dependence of the ionization current collected at the anode contains information about the specific ionization along the track (the Bragg curve). For an ion stopping in the active volume (before the Frisch Grid) the total energy (E) can be obtained from the integral of the anode current, the atomic number (Z) is proportional to the maximum current (or Bragg peak), and the ion range (R) is proportional to the total width (in time) of the signal.

One application of a BCS is in the construction of a modular 4π detection array where a compact geometry is required. Such an array, with good E and Z resolution (and possibly some additional position information) would be useful for a wide class of experiments. To obtain close packing, the detector shape of a right circular cone was chosen (see Fig. 1). Charged particles emanating from a point source on the axis of this detector travel along radial paths. In order to maintain the desirable feature of having the particles travel along the field lines, a $1/r^2$ field is required in the detector volume. If the path of ionization deviates from the direction of the electric field lines, or the electron drift velocity is not constant, the ionization current measured at the anode is distorted, affecting both the Bragg peak and range information.

Central to the construction of this detector was the use of computer aided design to produce a printed circuit insert containing a set of equipotentials on the inside of a frustrum of a right circular cone. A Frisch grid made of 38 μm tungsten wire mesh, 16 × 16 per cm, and at a potential of 0 V, follows these electrodes. Its screening inefficiency was calculated to be ~1%. The anode was 1.5 cm behind the Frisch grid. The 3.8 cm diameter window was constructed of 175 $\mu g/cm^2$ aluminized mylar supported by the same wire mesh used for the Frisch grid. This window was capable of supporting 500 torr.

The BCS was placed inside a 152 cm diameter scattering chamber with its window 10 cm from a 0.5 mg/cm^2 Au target and tested with beams of ^{28}Si, ^{56}Fe and ^{86}Kr. Fig. 2 shows a two dimensional plot of the Bragg peak signal versus energy for the Fe + Au reaction. Reaction products in the region Z = 26 to 22 are clearly separated. This corresponds to a charge resolution of ~1.5%. Increasing the solid angle from 1.2 to 83 msr causes a degradation of charge resolution to ~2%. Data for Kr + Au (not shown) give similar results.

Footnotes and Reference

*Condensed from LBL-16434

†Permanent address: Shanghai Institute of Nuclear Research, Shanghai, China.

‡Permanent address: Istituto di Fisica, Universitá Degli Studi di Bari, 70100 Bari, Italy

1. C.R. Gruhn, M. Bini, R. Legrain, R. Loveman, W. Pang, M. Roach. D.K. Scott, A. Shotter, T.J. Symons, J. Wouters and M. Zisman, R. DeVries, Y.C. Peng, and W. Sondheim, Nucl. Instr. and Meth. **196**, 33 (1982).

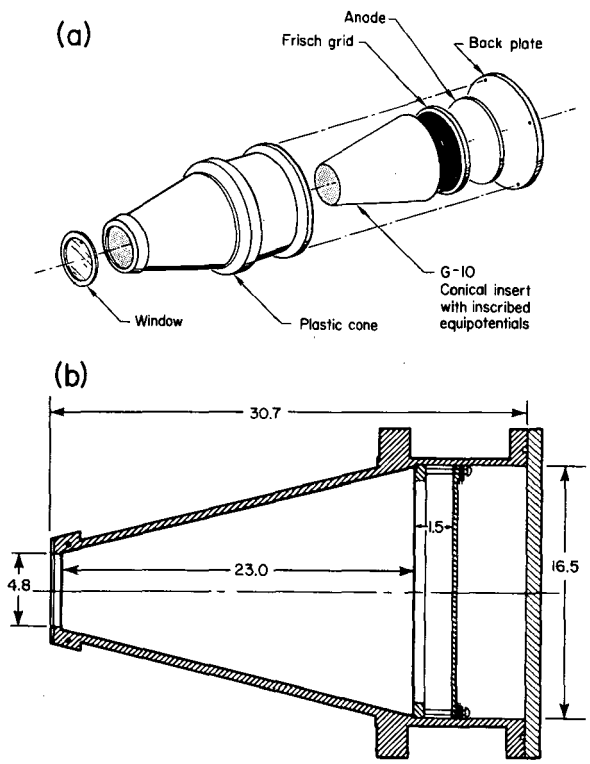

Fig. 1. (a) "Exploded" view of the conical BCS showing its major components. (b) Section of the BCS showing its significant dimensions.

XBL 837-429

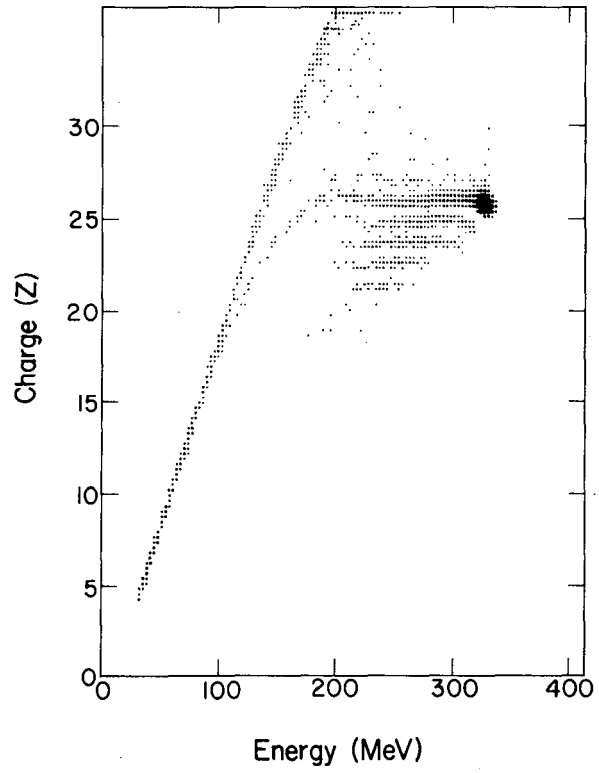

Fig. 2. Two dimensional plot of the linearized Bragg peak as a function of energy for ^{56}Fe ions scattered at 40° from 0.5 mg/cm^2 Au target with a 1.4 msr acceptance angle. The detector window was 175 μg/cm^2 aluminized mylar. XBL 837-426

A Large Solid Angle Ion Chamber

L.G. Sobotka, J.B. Hunter and G.J. Wozniak

We have constructed a large solid angle, segmented anode, position sensitive ion chamber of the double gridded design.[1] The detector (shown in Fig. 1) is designed to function both inside a large scattering chamber and outside a small scattering chamber. This flexibility allows us to use the device in particle-particle coincidence experiments, where the other particle detectors require a large vacuum vessel, and also in particle-γ- or x-ray experiments, where the photon detectors are required to be outside the vacuum vessel but still retain high efficiency. The detector will fit inside the 60″ scattering chambers at the SuperHILAC, the 88-Inch Cyclotron and the low energy beam line (LEBL) at the Bevalac.

In the double gridded design, sense wires positioned between the Frisch grid and the anode parallel to the event track are used to determine one of the position coordinates via a delay line readout. These wires are the radial ones seen in Fig. 2. The other position coordinate is determined by the time difference between the cathode signal (prompt) and an

anode signal (delayed by e^- drift time). Position resolution of $\sim 1°$ in both dimensions has been achieved.

The anode is divided into 3 main sections (see Fig. 2) to obtain dE/dx information. A plot of ΔE_2 vs ΔE_3 is shown in Fig. 3 for the reaction products from 8.5 MeV/nucleon Fe + Ag. This plot is simply the pulse heights of these two anodes with the full solid angle of the detector exposed, (30° in-plane centered at Θ_L = 25° and $\pm 5°$ out-of-plane). No software corrections or gating have been applied. The elastic and quasielastic scattering are clearly visible at large values of ΔE_3. From this plot it can be seen that events with $Z < 30$ are resolvable.

Reference

1. H. Sann *et al.*, Nucl. Instr. Meth., **124**, 509 (1975).

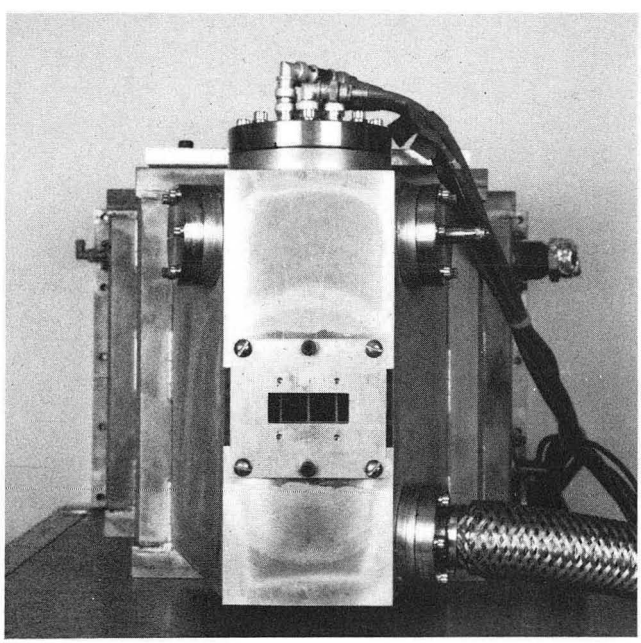

Fig. 1. Photograph of the ion chamber. The recessed, supported entrance window is clearly shown. CBB 830-10125

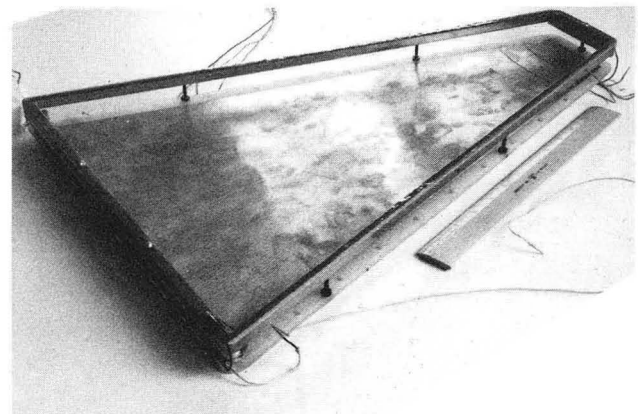

Fig. 2. Photograph of the Frisch grid, Θ-grid and segmented anode package. The Frisch grid is constructed of parallel wires (50 μ Cu-Be, 1 mm spacing). The Θ-grid consist of wires that fan out radially. An LC delay line (8.9 ns per tap, 1 tap = 1°) is attached to the large end of the fan. The anode segments (ΔE_1 = 3 cm, ΔE_2 = 3 cm, ΔE_3 = 47 cm) are seen below the wire planes. CBB 830-10127

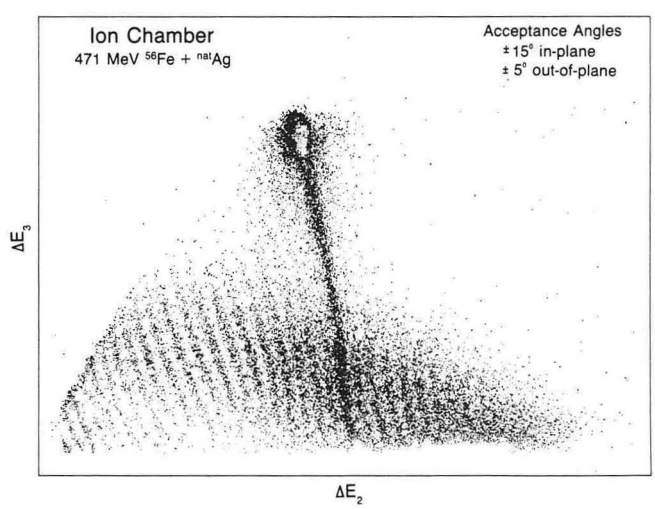

Fig. 3. Data acquired during a recent SuperHILAC run. XBL 8311-3436

A Threshold Čerenkov Counter for Isotopic Identification of High-Energy Heavy Ions*

J. Stevenson,† J. Musser, and P.B. Price†

We have developed an apparatus for isotope identification of heavy-ion projectile fragments with energies from ~330 to 600 MeV/nucleon. The detector uses a Čerenkov intensity measurement in conjunction with a measurement of magnetic rigidity to determine mass. An advantage of this technique is that it allows isotope identification of projectile fragments with higher energies than are possible for "stopping type" detectors. Higher fragment energies allow the use of much thicker targets and, therefore, provide higher sensitivity to rare isotopes.

Fig. 1 shows a schematic of the detector. The detector elements each have a 6″ × 12″ active area with the 12″ dimension being in the focal plane of the spectrometer.

Fig. 2 shows mass histograms for carbon and nitrogen isotopes obtained in a test run performed last year using a 670 MeV/nucleon ^{20}Ne beam and a 30 g/cm^2 Al target.

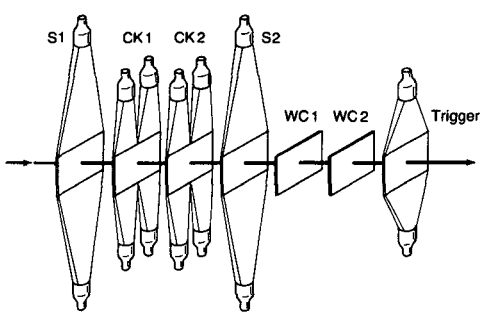

Fig. 1. Exploded view of detector, elements S1 and S2 are 3/8″ thick NE110 scintillators, CK1 and CK2 are 1/2″ thick Pilot 425 Čerenkov counters. WC1 and WC2 are wire chambers, each consisting of a pair of orthogonal planes. The final element in the detector is a 1/4″ thick NE110 scintillator which is used as trigger. XBL 8312-4307

We are now in the process of analyzing data taken this fall from a run in which a 600 MeV/nucleon ^{56}Fe beam and an 8 g/cm^2 Be target were used. A total fluence of ~10^{11} beam particles was obtained, which should be sufficient to allow us to establish the existence of one or two new isotopes for each element with $6 \leqslant Z \leqslant 10$.

Footnotes

*Condensed from a paper published in Nucl. Instr. & Meth. **213**, 285 (1983).

†Also at Space Sciences Laboratory.

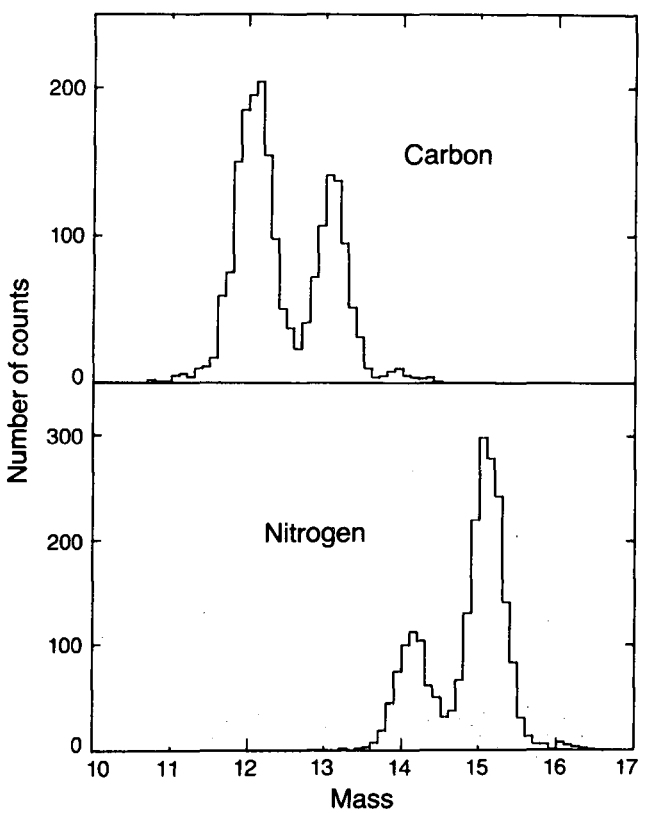

Fig. 2. Isotope histograms for carbon and nitrogen. XBL 8312-4303

HISS Drift Chamber Resolution

D.F. Greiner and F. Bieser

The 1×2 meter prototype drift chambers at HISS have been used in several experiments. Data has been taken for particles with charges 1 to 57. The on-line analysis has shown that the intrinsic resolution of a single cell of the chamber is better than 200 microns. This is seen by comparing the redundant measurements on a single track. The redundancy is due to the fact that successive cells drift the track in opposite directions, thus, for tracks at normal incidence, the sum of the drift distances must add up to a cell width.

The real question about resolution is, "What is the resolution of the chamber over its whole area and over the entire particle charge range?" The answer depends on many factors:

What is the time to distance calibration of a single cell?

Do all cells have the same calibration?

How does the charge of the particle affect the calibration?

Was the system stable over the time of the run?

The first order answer to all the questions is that with a simple linear calibration between time and distance the system resolution is better than 1 millimeter. The fun begins when we try to push significantly below 1 mm.

Bevalac experiment 512H requires the best resolution we can achieve. Our initial approach to the problem is to use the redundancy and get the non-linear part of the calibration in hand. Using a model of the chamber response and fitting it to the data for a pure ^{12}C beam in the chambers we have deduced the TDC to distance calibration shown in Fig. 1. The response becomes nonlinear at about 8 mm of drift. This is due to the weakening of the drift field in the long drift region. This calibration, developed using the data from one cell, fits the data from the thirty or so cells available in the ^{12}C data set. Thus, at the current level of understanding, the cell to cell variations are negligible. After locating the tracks in the 12 planes of the chambers the best fit trajectory is found to be a fitting process. A measure of the resolution is then the difference between the measured values and the fitted trajectory. These differences are shown in Fig. 2 where all data is summed for the 12 planes. The single plane resolution is 355 microns at this time. The variations with charge can now be investigated as well as the position and time dependence.

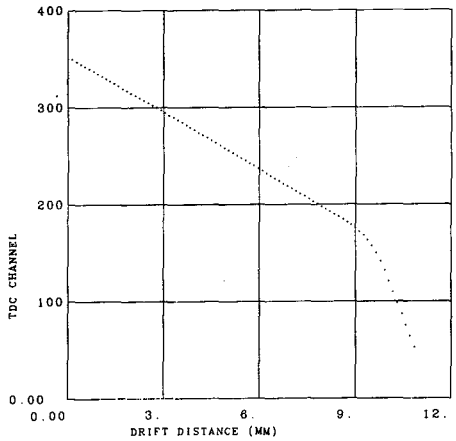

Fig. 1. TDC to Distance Calibration XBL 8311-4674

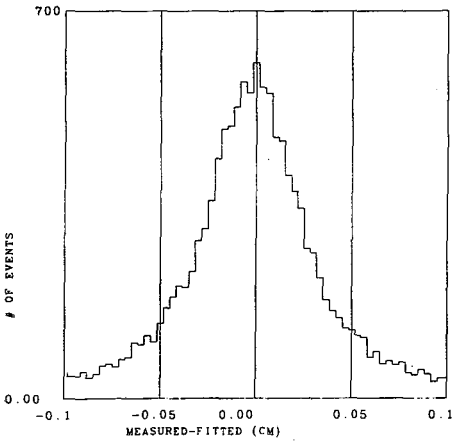

Fig. 2. Single Plane Resolution (Z = 6)

XBL 8311-4675

Multi-Angle Gas and Si Detector Particle Telescope

R.J. McDonald, L.G. Sobotka, and G.J. Wozniak

A simple gas ΔE and multiple Si E detector telescope (called a WEDGE detector) has been constructed, which is particularly suitable for angular distribution studies of light ion emission from fragments following heavy ion reactions. This inexpensive detector was designed to have a low detection threshold, large dynamic range and constant ΔE path length. The detector has been used in studies of complex fragment emission (typically $2 < Z < 10$) following compound nucleus and deep-inelastic heavy ion reactions.

The detector was built in the spirit of the telescope of Fowler and Jarad,[1] where a Frisch gridded ion chamber forms the ΔE element and a Si detector serves as the E detector. The case was formed from pieces of aluminum and G-10 epoxied together vacuum tight and reinforced with screws at points of stress. The back plate supports a thin G-10 grid frame on which a Si detector holder is mounted. This back plate contains gas and signal connectors with the exception of the anode signal connector which is on the detector bottom. Fig. 1 shows the detector separated into its two main sub-assemblies.

Electronically, the top and sides of the case are at ground potential, as is the ring that holds the five Si detectors. The grounded walls provide some focusing of electrons through the grid and into the anode. The ΔE signal was taken from the anode directly into an external preamp located as close to the anode as possible to avoid additional capacitance from a cable. The ΔE signal was processed through standard linear electronics and presented to an ADC. The five Si E detectors were amplified separately, gated and then mixed before being presented to the ADC. A "marker" was generated by each E constant fraction discriminator (CFD). These CFD signals were delayed and their amplitudes adjusted to 2.0, 2.4, 2.8, 3.2, 3.6 and 4.0V and then mixed and presented to an ADC. The firing of multiple Si detectors gave a marker >4V which can be gated away during analysis. A valid event consists of ΔE-E-marker signals.

Fig. 2 shows a plot of ΔE vs E for fragments emitted from the ^{3}He + Ag reaction. Since the yield of He fragments is several orders of magnitude larger

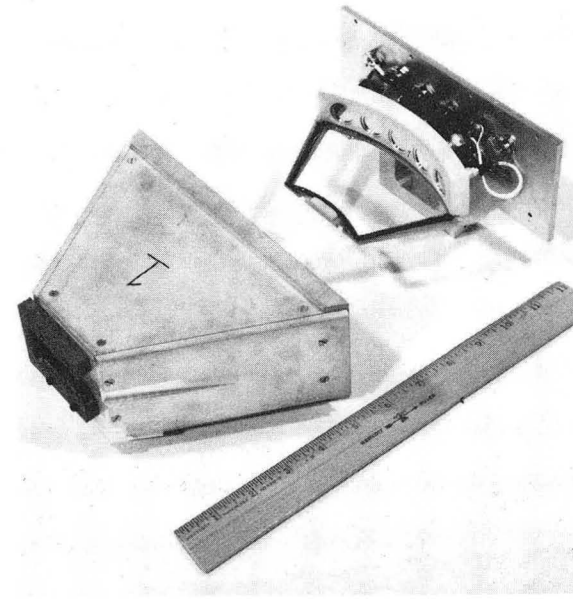

Fig. 1. Photograph of the detector split into its two major components. CBB 833 2554

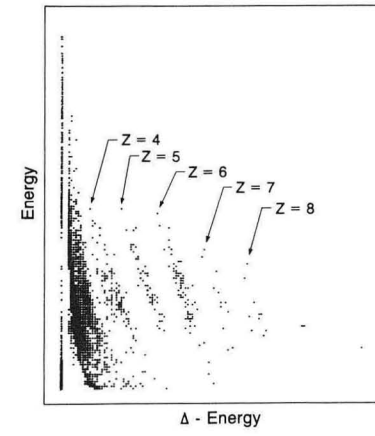

Fig. 2. ΔE vs E plot of complex fragment emission from the ^{3}He + Ag reaction. Zs from 2–8 are labeled. XBL 8311-3435

than that for Z>2, the He intensity spills over into the Z=3 region. Events with Z=4–6 are clearly identifiable in this data. Since the charge and energy resolution demonstrated here were sufficient for our studies, no attempt was made to optimize them.

Please note that sketches giving sufficient detail to build this detector are available from the authors.

Reference

1. M.M. Fowler and R.C. Jared, Nucl. Instr. and Meth. **124**, 341 (1975).

Status of the HISS MUSIC Detector

H.J. Crawford, I. Flores,* F. Bieser, D. Greiner, P. Lindstrom, C. McParland, P. Brady,† C. Castenada,† W. Christie,† J. Romero,† C. Tull†, H. Sann‡*

This note describes the status of a new type of high resolution large area charged particle detector constructed for use at the Bevalac HISS facility. High charge resolution is attained by measuring many samples of the ionization produced along the path of a particle as it traverses 144 cm of P10 gas. A Multiple Sampling Ionization Chamber (MUSIC) detector was selected for use at HISS because it can cover a large area (1M × 1M) at relatively low cost and return individual charge identification for multiple fragments emitted from relativistic heavy ion interactions.

The operation of the detector can best be described by considering the signature of a particle of charge Z_p having speed B_c passing through the 144 cm of gas with negligible change in velocity. An electric field perpendicular to the path of the particle causes the resulting ionization electrons to drift down through a Frisch grid and onto the 72 sense wires which are spaced 2 cm apart. Each of the sense wires collects a sample of the ionization cloud.

The MUSIC box was exposed to 800 MeV/nucleon Ar beam as a test of its resolution. The box was triggered by requiring coincidence between scintillators placed before and after the box, 50 cm above the anode grid, a height corresponding to the center of the box. The electron cloud from a given beam particle was collected on 12 anodes (2–20 cm length, 2–16 cm, 2–12 cm and 6–8 cm) as shown in Fig. 1. The anode length is set externally by connecting the appropriate number of 2 cm spaced wires together. Each anode was connected to a separate electronics channel consisting of a preamp, amplifier, charge coupled device (CCD), and an ADC. Collected charged is shifted onto the CCD at

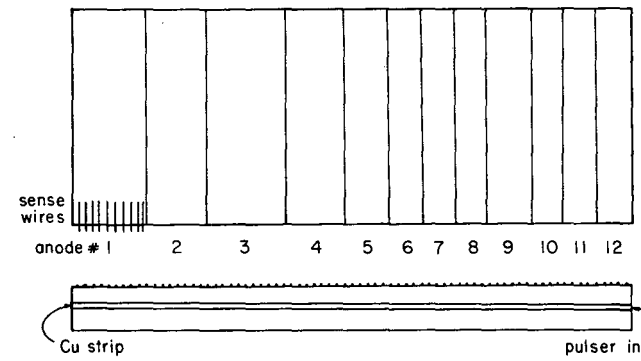

Fig. 1. Schematic of MUSIC detector showing anode pad arrangement used during Ar test run

XBL 8311-4644

10 MHz. The experiment trigger is set to the MUSIC box, and, after a total delay of 25 us to allow drift through 100 cm maximum, used to lower the shift rate to 20 kHz for readout of each CCD bucket.

Fig. 2 shows a typical event on one channel of electronics, the signals from a single anode, plotted as pulse height vs. bucket number for that event. The "TPC" multi-channel waveform digitizers used with the MUSIC Box have been modified in order to improve the charge resolution of the system. The CCDs used to store the waveforms before digitization have both a long term and short term variation in offset voltage (pedestal). These variations cause errors in the reconstructed pulses and thus degrade the pulse height resolution. We have added a 3-word deep First-In-First-Out (FIFO) memory on each digitizer board so that the pedestal before and after each pulse is added to the data stream. The results of this modification can be seen in this figure as the three ADC levels below threshold at the beginning and end of the pulse in this channel. In analysis, these preceding and following background level measurements are used to correct the ADC signals in the real pulse.

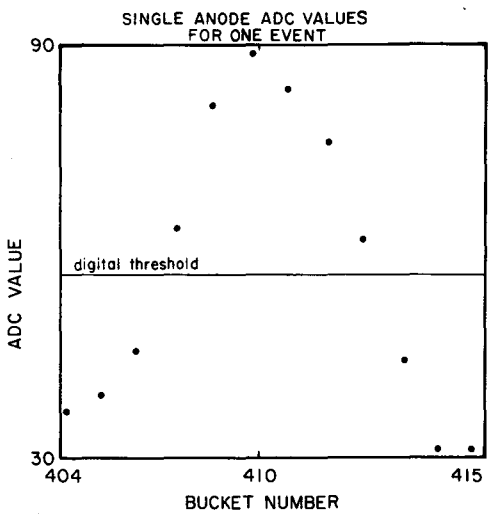

Fig. 2. Example of single event on single anode. Typical event is 11-12 buckets wide. The digital threshold level is set to eliminate low level ADCs from the data stream, preserving only the pre- and post-history background bucket levels.

XBL 8311-4643

A patch board has been added in series with the analog signals from the preamplifiers to allow attenuators to be inserted in order to make better use of the ADC's dynamic range for different beams. By selecting appropriate anode lengths and attenuators we can use a portion of the sense wires for high Z and another portion for low Z fragments. We can now also trim the gain of each channel to simplify data analysis.

Event analysis was performed as follows. Each anode was calibrated with pulser and beam individually. Raw anode signals were corrected for dark current and pedestal offsets. Signals from the longer anodes were compared to the 8 cm anode signals: mean values scaled with anode length; FWHM for each 8 cm anode was 10.5%, for 20 cm anodes it was 8.2%. This is in agreement with predictions that the resolution does not simply scale with anode length for thin detectors. Combining the signals from all anodes gave a resolution of 3% FWHM.

We are in the process of analyzing this data using the sampling methods that lead to this type of detector, namely, sorting anode signals from each event by amplitude and checking the resolution as a function of relative order in the sorted event. We will be taking data with La and U beams in the coming months and expect to attain better than 1% resolution for U and to verify that the particle pair resolution is at least 3 cm.

Footnotes

*UCB Space Sciences Laboratory
†UC Davis
‡Gesellschaft für Schwerionenforschung, Darmstadt (GSI), West Germany

Status of the HISS TOF Wall

M. Baumgartner, H. Crawford,† Ryoichi Wada,‡*

In Fig. 1 we show the layout of the experiment HISS 320. This experiment is designed to capture and analyze all charged projectile fragments produced in the interaction of 2 GeV/nucleon 12C with C, CH, Cu or U targets. Analysis consists of identifying charge, mass and vector momentum for each fragment. This is accomplished through use of a drift chamber system to give trajectories through the magnetic field of the HISS dipole, combined with velocity measurement provided by a time-of-flight scintillator array called the TOF wall. This report describes the present status of the TOF wall system.

The TOF wall consists of 70 pieces. Slats 1 to 40 measured $2 \times 10 \times 300$ cm^3, and slats 41 to 70, $2 \times 10 \times 200$ cm^3. Each slat had on both ends a photomultiplier tube (RCA 8575 or Amperex XP2022). The output signal of every tube was time analyzed with a leading edge discrimination (IRS 620d) whose output was sent as a stop signal to a LeCroy 2228A TDC. The analog signal from a second anode on each tube was passed through an attenuator ($\times$25) into a LeCroy 2280 ADC system.

The raw ADC data were converted into charges as described below. To account for light attenuation in the slats we used the square root of the product of the two ADCs from each slat. Because of saturation in the photomultiplier tubes and scintillator, there was no simple Z^2 dependence of the pulse height in the ADC-product. For that reason the charge was obtained from the ADC-product by using a power law function, which was fitted for each slat to the charge peaks in the ADC-product.

Using leading edge (rather than constant fraction) discriminators for the TOF TDC stop signals leads to a Z-dependent time. Therefore we corrected for that time dependence by an empirical fitted function. The obtained time resolution without any drift chamber trajectory corrections is 350 psec FWHM for charge 6 as shown in Fig. 2.

Because there was a second time of flight wall in the back of the first one, we were able to correlate the two time of flight walls. Requiring that both walls saw the same charge for the fragment we attained the charge resolution, shown in Fig. 3.

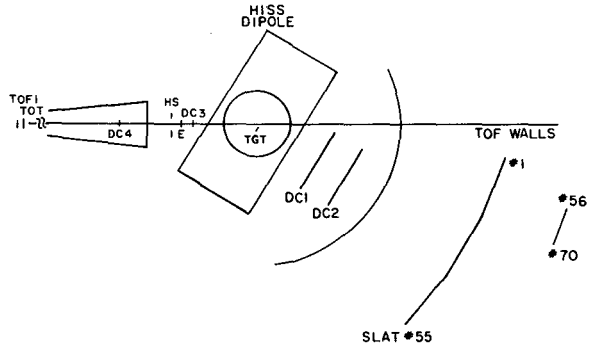

Fig. 1. Layout of the experiment HISS 320.

XBL 8311-4605

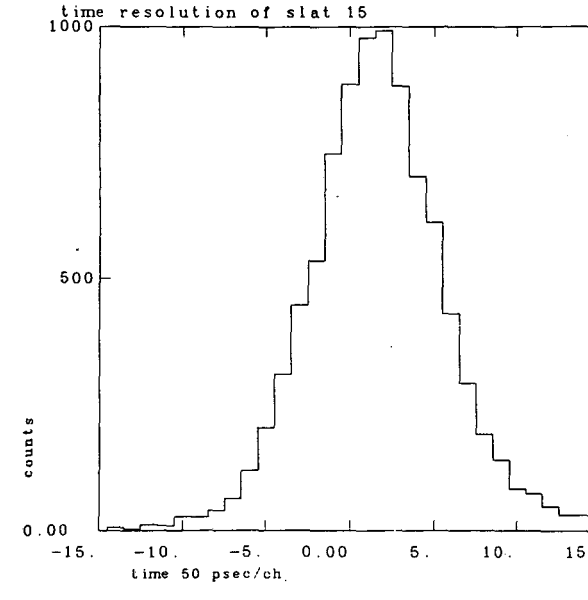

Fig. 2. Time resolution for charge 6 in slat 15. One channel in time corresponds to 50 psec.

XBL 8311-4673

Footnotes

*Accelerator and Fusion Research Division, LBL
†UCB Space Science Laboratory
‡Gesellschaft für Schwerionenforschung, Darmstadt (GSI) and UCB

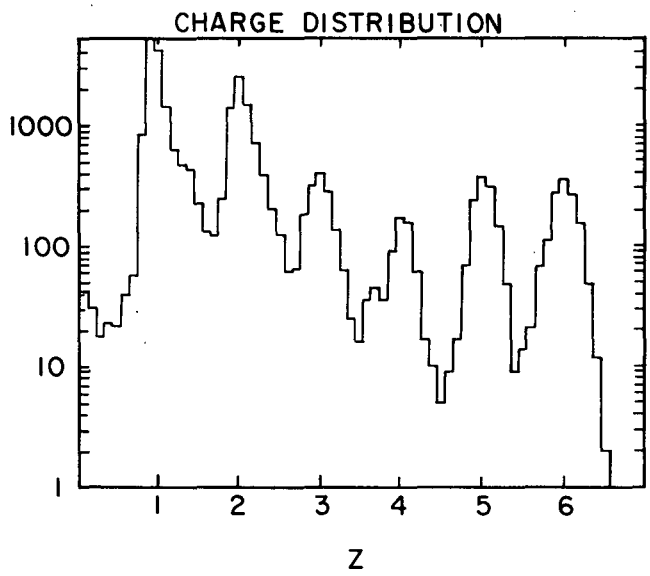

Fig. 3. Charge distribution summed over all slats demanding same charge for fragments in back and front time of flight wall. XBL 8311-4604

A Position-Sensitive "Phoswich" Detector*

M. Bantel, R.G. Stokstad, Y.D. Chan, S. Wald, and P.J. Countryman†

A new type of position-sensitive detector has been designed and tested. It consists of two sheets of plastic scintillator, each 20 cm × 20 cm, arrayed in a "phoswich" configuration. The first sheet, the ΔE element, is 0.5 mm thick and made of Ne 102A, which has a decay time of ~2 ns. The second sheet is 4.5 mm thick and is made of a new scintillator material, NE 115, having a much longer decay time of 225 ns. The signals from the two sheets are separated by using separate charge-to-digital converters (QDC's) with a short 20 ns gate for the first signal and a long 600 ns gate for the second. Thus particle identification is achieved.

The location of an incident particle is determined by comparing the light collected at opposite ends of the scintillator. The amount of light collected in the case of an ideal scintillator with perfectly flat surfaces would be independent of position. Surface irregularities, however, cause some loss of light each time a ray is reflected internally. Thus the amount of light collected will depend on the average number of reflections along the path from source to photocathode and, hence, on the position. A simple model based on this reproduces rather well the position dependence observed for test strips of scintillator.

A sketch of the detector is shown in Fig. 1. Adiabatic light guides of twisted strips connect the edges of the scintillators, beveled at 45° and aluminized to form a 90° mirror. This configuration makes it possible to replace a wall of the plastic box[1] with this prototype detector and thus obtain position information and much improved particle identification.

A test of the detector was made by scattering 60 MeV alpha particles, accelerated by the 88-Inch Cyclotron, from a gold foil. A mask having sixteen holes, 6.2 mm in diameter and spaced ~5 cm apart in a rectangular pattern, was placed in front of the detector at a distance of 25 cm from the target. The detector was operated *in vacuo* in the 60-inch scattering chamber. Fig. 2 shows the locations of the transmitted alpha particles as determined by the light

collected at the edges. The position signal is given by $X = \frac{I_L}{(I_L + I_R)}$ where I_L and I_R denote the intensity of the light collected at the left and right sides, respectively. The y position is defined in a similar manner. The x-y position resolution is ~ 1 cm^2 (FWHM). Note the variation in intensity of the various groups arising from the angular distribution of the scattered alpha particles.

Fig. 3 shows the particle identification obtained for one of the sixteen locations. Protons, deuterons and alpha particles are well resolved. The energy resolution for 60 MeV alpha particles was $\sim$5–6% and the intrinsic time resolution was $\sim$0.6 ns (measured by using one phototube for a start signal and the other for a stop).

Measurements of the light output and decay time of NE 115 were made, since it is a new product and had not been used before. The light output was found to be 35% of anthracene and the decay time to be 225 $\pm$ 20 ns. These values differed from the corresponding specifications supplied by the manufacturer (25% and 375 ns, respectively).

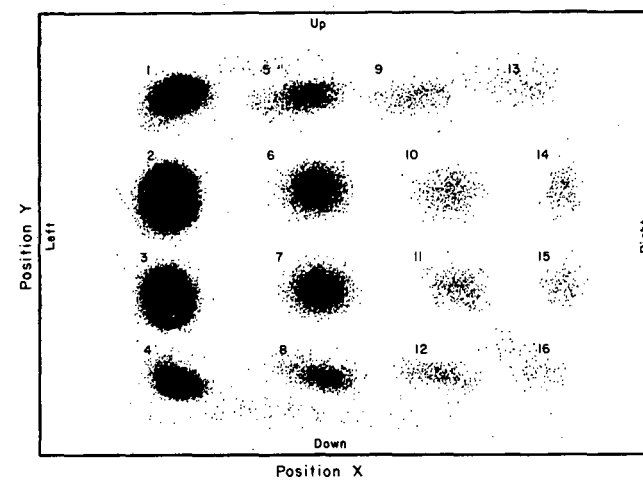

Fig. 2. A two dimensional scatter plot of the position variables x and y. The effect of the mask containing the sixteen holes is evident. Positions 9–16 are beyond the grazing angle for elastic scattering of 60 MeV alpha particles from gold. XBL 8312-6919

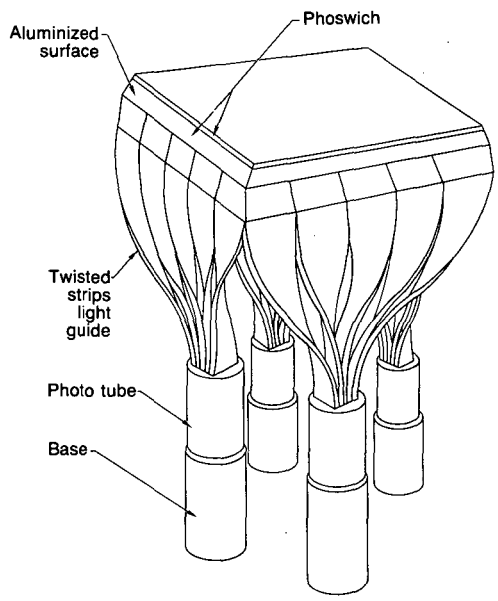

Fig. 1. A sketch of the detector construction. A water-cooled mounting plate attached to the tube bases is not shown. XBL 8312-6917

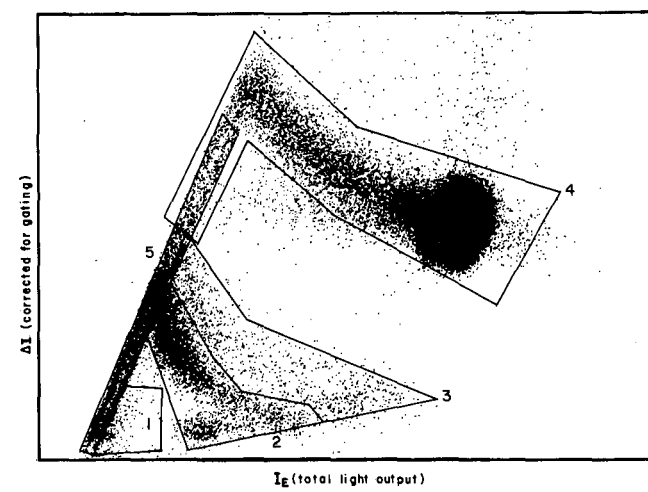

Fig. 3. The light output from the ΔE element vs the total light output for position 3 on the detector. Areas 1) through 5) contain mainly 1) gamma rays and neutrons; 2) protons, 3) deuterium and tritium, 4) alpha particles, 5) low energy particles stopping in the first element. XBL 8312-6918

We expect that this type of detector will find many applications in addition to its use with the plastic box. It has a number of useful features (in addition to its position sensitivity) compared to previous phoswich detectors. First, the fast element is the first element; fast timing is still possible when a particle stops in the first element. Second, because both elements are plastic, which is less expensive than CaF_2 and available in large sizes, much more flexibility is possible in designing the detector for a specific application. A second prototype, consisting of eight phoswich strips, 20 cm × 2.5 cm with a phototube at each end of each strip has been constructed and is under test. This detector, which provides a multi-hit capability will be described at a future date.

Footnotes and References

*Adapted from LBL-17063.

†Stanford University.

1. K. Van Bibber *et al.*, this annual report and LBL-16799.

The Plastic Box

A 4π Detector for Intermediate Energy Heavy Ion Physics*

K. Van Bibber,† P.J. Countryman,† M.J. Murphy,‡
Y.D. Chan, R.G. Stokstad, I. Tserruya,§ S. Wald

A 4π array of plastic scintillator (the Plastic Box) has been constructed and used in conjunction with high resolution solid state detectors. The array is employed principally to discriminate multinucleon transfer reactions from three-body (or more) final states. It should be useful for a broad class of experiments in which a global charged particle anticoincidence is required.

The Plastic Box consists of six walls of plastic scintillator arranged in a 20-cm cube around the target. Two additional walls down-stream back up the heavy ion telescopes, and minimize the missing solid angle around the beam exit (Fig. 1). Each wall consists of an inner (A) and outer (B) element of NE-102 scintillator, each 1 mm thick, and coupled via adiabatic light guides to RCA 8850 and 8575 photomultiplier tubes. The scintillators are wrapped with aluminized mylar 6 microns thick, which adequately screens out any residual light in the scattering chamber, while assisting light transmission down the length of the scintillator. The mylar is sufficiently thick to stop fission fragments but causes negligible energy loss for light charged particles. Light-emitting

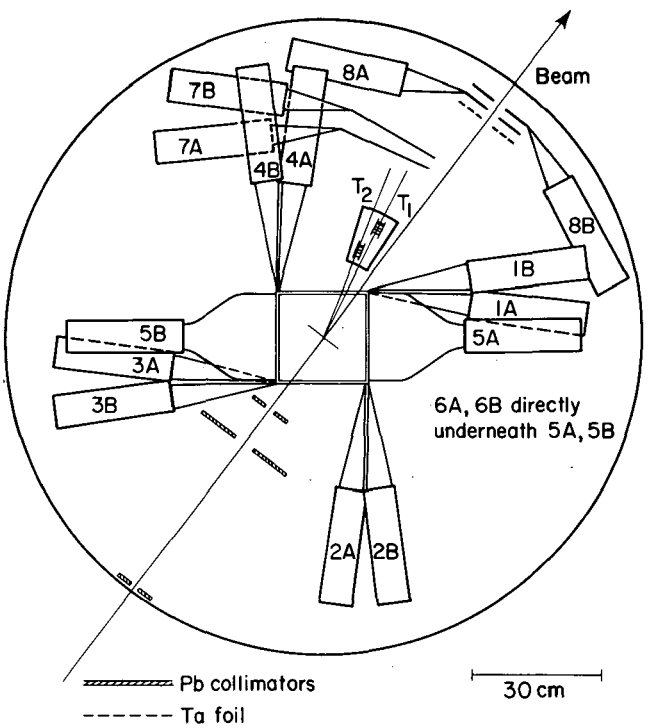

Fig. 1. Schematic top view of the Plastic Box

XBL 834-1475

diodes (LED's) are fixed to the bases of the light guides and, when driven in series with LED's in front of the solid state telescopes, permit the coincidence timing to be adjusted off line. The plastic scintillators are thin in order to minimize their efficiency for neutrons and gamma rays. Making the walls double layered with the inner and outer elements of equal thickness allows us to correct for neutral events to the extent that they do occur.

For typical experiments (i.e., $^{20}Ne + ^{197}Au$;[1] $^{16}O + ^{60}Ni$, ^{208}Pb at 10–20 MeV/nucleon) the elastic scattering rate in the forward scintillators is sufficiently high to necessitate covering scintillator 8A (whose aperture from the target represents a polar angle of 1° around the beam axis) with a thin sheet of tantalum (0.015 cm). This stops elastically scattered beam particles, while allowing fast light particles to penetrate to the scintillator. The same is done with an annular region around the beam exit in 1A to a polar angle of ~8°. Maintaining the scintillator singles rates at $< 10^5$ sec^{-1} with targets typically of ~1 mg/cm^2 limits the beam current to ~1 nA.

Fig. 2 shows the two-dimensional spectra of 2A and 2B from an actual run. In tests where light particles entered a small area and normal to the surface, protons and alphas were easily resolved. Here this separation is considerably degraded. This is due both to the averaging over many angles of incidence (the path length variation in the A wall being a factor of 1.7) and to the position dependence of the light collection efficiency. Events in the middle of the plane (2A·2B) are almost exclusively charged particles; events falling on the horizontal axis ($2A \cdot \overline{2B}$) are both charged particles stopping in A, and neutrons and gamma rays, equal in number to the events which fall on the vertical axis ($\overline{2A} \cdot 2B$), which can be due only to neutrals.

To date, triple-element silicon heavy ion telescopes have been used as the event trigger. The charged particle efficiency of ~100% over the ~4π solid angle of the Plastic Box (while having low neutron and gamma efficiency) thus greatly augments the information from the telescope. For example, we

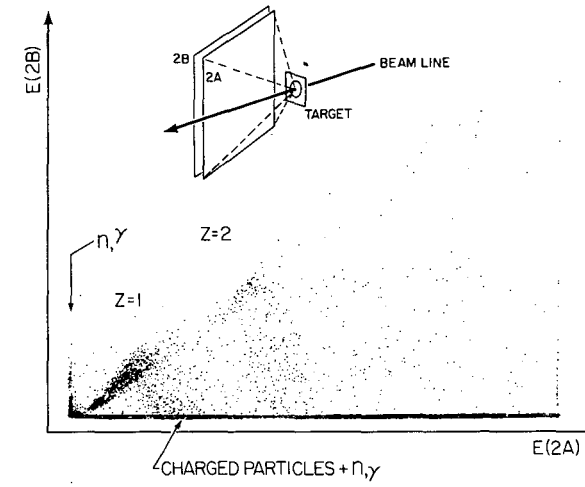

Fig. 2. Plot of scintillator 2A vs. 2B, from data of $^{14}N + ^{197}Au$ at 250 MeV.

XBL 839-577

distinguish transfer reactions such as $^{197}Au(^{20}Ne, ^{12}C)$ leading to particle bound states of the ^{12}C, from other competing reaction pathways, such as transfer followed by statistical decay [$^{197}Au(^{20}Ne, ^{16}O^*)$, $^{16}O^* \rightarrow ^{12}C + \alpha$], by the absence or presence of additional charged particle(s)! This signature is contingent upon the choice of a heavy target (A ~ 200) where charged particle evaporation after transfer will be strongly suppressed in favor of multiple neutron emisson or fission. This consideration furthermore indicates the importance of the array having a low efficiency for neutrons and gamma rays, which could be confused in the analysis with charged particles (α, p, etc) and cause misidentification of projectile transfer and breakup events.

Work on more sophisticated phoswich walls is in progress which will afford good energy, charge and position resolution.[2]

Footnotes and References

*Condensed from LBL-16799.

†High Energy Physics Laboratory and Department of Physics, Stanford University, Stanford, CA 94305

‡Present address: Nuclear Structure Laboratory,

University of Washington, Seattle, Washington.
§Permanent address: Weizmann Institute of Science, Department of Physics, Rehovot - 7600, Israel.

1. S. Wald *et al.*, LBL-16899 and this report.
2. M. Bantel, this report.

Improvements to the Plastic Ball

R. Albrecht, H.-A. Gustafsson, H.H. Gutbrod,* B. Kolb,* H. Löhner,† B. Ludewigt,* A.M. Poskanzer, T. Renner, H. Riedesel,‡ H.G. Ritter,* H. Stelzer,* A. Warwick,* H. Wieman**

After the first round of experiments in 1981, several hardware modifications were made to the Plastic Ball[1] to improve its performance or to facilitate calibration procedures.

Several photomultiplier tubes that were glued to the lucite light guide had broken off, resulting in a reduced light collection efficiency of ~50%. To prevent more of this breakage, a new spring mount was built for each photomultiplier and installed before the new round of experiments in 1982.

For the pulse-shape analysis a fully passive 50Ω 4-way split was introduced, which helped improve the efficiency for π^+ detection. Furthermore, the early AMP-multiconnectors for the 25-fold coaxial ribbon cables had to be modified to prevent the pins from being pushed back. The electronic "Ball boxes" were modified to allow the use of a fast clear on the trigger, which was used beginning in the 1983 experiments.

For the Plastic Wall it became clear that the LED pulser system with its slowly rising pulses was not convenient for an on-line calibration. Therefore, a N_2-Laser system was built that supplies all Wall modules with short pulses of light monitored by a pin diode. Thus, the stability of the Wall in pulse height as well as time can be checked on line. Fig. 1 shows the layout of the Laser system. The adjustment of the light output is obtained via the Laser aperture, while individual light intensity adjustments in each fiber optics channel is made possible by crossed polarization filters.

A further improvement was achieved by integrating into the CAMAC system the CERN-Romulus Processor, which controls all fast TDCs. This added intelligence in the CAMAC reduced the readout time by about 500 μsec. To improve the on- and off-line analysis, the computer system was greatly expanded by the addition of a VAX 11/780 computer.

While the main processing of raw data tapes is still done at the CDC-7600, the generated intermediate tapes are then stored on the large disk space at the VAX 780 for further analysis. The GSI streamer chamber group is the other user of the VAX 780.

In the experiment at 1.05 GeV/nucleon ^{93}Nb + ^{93}Nb the multiplicity of charged particles was so high that the increase in the event length reduced the data acquisition rate to ~20 events per spill. For the planned Au + Au experiments this was an intolerable situation and the front end PDP 11-44 computer was replaced in June 1983 with a more powerful VAX 11/750. This change increased the data acquisition rate by a factor of 3–4.

With the availability of heavy beams at the Bevalac a thin gas detector was designed for use at small angles, called the 0° detector. It features a one-plane avalanche counter for time and position measurement, and a two-stage proportional counter with 3 planes, for position determination as well as dE/dx measurement. The detector is operated at a low pressure of ~2 Torr. Two thin avalanche counters have been built for accurate trajectory measurement of the incident beam.

Footnotes and Reference

*Gesellschaft für Schwerionenforschung, Darmstadt,

West Germany.
†Universität Münster, Münster, West Germany.
‡Present address: Max-Planck-Institut für Kernphysik, Heidelberg, West Germany.

1. A. Baden *et al*, Nucl. Instr. Meth. **203**, 189 (1982).

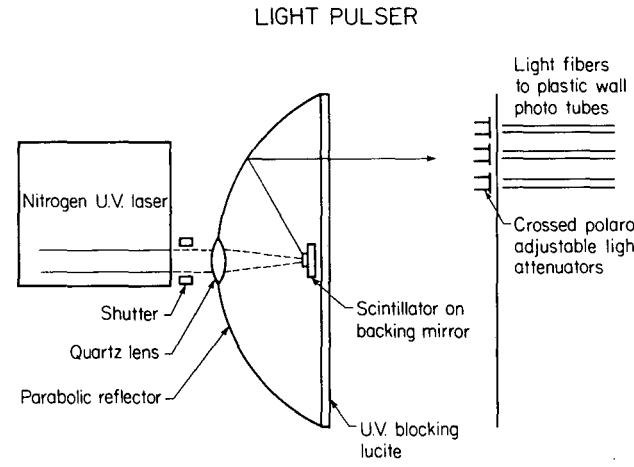

Fig. 1. Schematic view of the Laser-Calibration system. XBL 831-1141

A New Detection System for OASIS

P.A. Wilmarth, J.M. Nitschke, W.D. Zeitz, P.K. Lemmertz*

Heavy ion reactions are commonly used to synthesize exotic nuclei and new isotopes such as neutron-deficient rare earths. These reactions produce a multitude of products making on-line mass separation necessary. The SuperHILAC's mass separator, OASIS,[1] uses an integrated target/ion source combination and is physically located inside the experimental cave. A movable tape system located outside the cave has been added to OASIS for the following reasons: (1) the high background caused by gamma rays and fast neutrons produced in the target is eliminated by placing the detectors outside the cave; (2) the background from long-lived isotopes is removed from the detectors by moving the tape; and (3) detectors can be positioned close to the sample to observe all types of decays with high efficiency.

Isotopes of a single mass are selected by an analyzing slit in the focal plane of the separator and transported to the movable tape located in a shielded room above the cave. The 4 meter long transfer line from the separator to the tape, consisting of an electrostatic mirror and two focusing elements, transports the 50 keV ions in 30 μs (for A = 100) with ~100% efficiency. The mass-separated ions are embedded in computer tape and periodically moved to an array of detectors to observe the decays.

The tape system (Fig. 1) consists of an IBM 729 tape drive modified so that the tape runs through an evacuated detector chamber where the activity is collected and counted. The magnetic tape from the supply reel is guided outside the drive through a differentially pumped vacuum feed-though into the evacuated (10^{-6} TORR) detector chamber, out through a second feed-through and spooled onto the take-up reel. Magnetic tape with a conductivity of 1 to 10 KΩ/□ (Scotch 700) is used to prevent electrostatic charge build-up at the collection point. The transmission from the separator is optimized with a faraday cup located at the collection point, and the spot of collected activity is typically less than 0.25 inch in diameter. The distance from the collection point to the counting position between the detectors is 6.88 inches and the travel time, at a tape speed of 2.86 m/s, is 65 milliseconds.

The tape movement is handled by an Intel 8085 microprocessor-based control computer. The tape usually runs in a stepping mode where the activity is collected for a fixed period of time, then moved to the detectors and counted while the next sample is being collected. Half-life information is obtained by resetting and starting a digital timer when the tape is advanced and time-tagging each decay event as it occurs during the counting interval. The range of half-lives that can be studied is 0.1 s $< T_{1/2} < \infty$ s. In studies of short-lived isotopes where the counting interval is a few seconds or less, the tape can be automatically rewound after ~4000 advances and counting continued without interruption. The tape movement can be externally synchronized if necessary (an example is the synchronization with parasitic beam pulses from the SuperHILAC). Accurate tape positioning is achieved by reading closely spaced magnetic "stripes" written on the tape prior to use. A tape positioning accuracy of ± 1 mm has been obtained thus far, and is being improved.

To fully exploit the tape system, a detection system was designed to observe all known decay modes of neutron-deficient nuclei. In addition to beta–gamma or x-ray–gamma coincidence information, alpha or proton emission (both direct and beta-delayed) is measured along with any coincident photons or betas. The detector arrays "sandwich" the tape front and back as closely as possible for high efficiency counting.

Facing the collection side of the tape is a three element telescope capable of detecting protons, alphas, betas, or photons. Closest to the tape is a 9 micron thick fully-depleted silicon solid-state transmission detector. The middle element consists of a 702 micron thick fully-depleted silicon transmission detector. The third detector is a high purity germanium (HPGe) detector 13 mm thick by 36 mm in diameter. The silicon detectors are at room temperature and are separated from the HPGe detector by a 50 micron Be window. The geometrical efficiency of the telescope is 21% of 4π. The first two elements of the telescope detect and identify protons (0.700 MeV $< E <$ 10.0 MeV) and alphas (2.0 MeV $< E <$ 10.0 MeV). The 702 micron detector and the HPGe detector function as a telescope to measure beta particles (0.200 MeV $< E <$ 10.0 MeV). Gamma ray and x-rays (5 keV $< E <$ 250 keV) are also measured with the HPGe detector. The measured resolution of the HPGe detector for the 59.5 keV line of ^{241}Am is 685 eV FWHM. The HPGe detector has a pulsed optical preamplifier system assuring optimal resolution at all count rates. Energy signals from each detector and fast timing information between the detectors are measured using conventional fast and slow electronics.

Facing the backside of the tape is a large n-type coaxial germanium photon detector. The 52 mm diameter by 56 mm long crystal subtends a solid angle 34% of 4π. The signal from the preamp is split into a high gain channel for x-rays (5 keV $< E <$ 250 keV, resolution of 824 eV FWHM at 59.5 keV) and a low gain channel for gamma rays (5 keV $< E <$ 2500 keV, resolution of 2.10 keV FWHM at 1332 keV). The low gain channel uses a gated integrator to achieve optimal resolution at high count rates.

The energy and fast timing signals for all detectors along with half-life information and a real time "clock" signal are recorded on computer tape in a multiparameter (typically 14 parameters) per event format using the SuperHILAC's data aquisition system. The energy calibration of all detectors is performed with standard sources. Of particular interest is the use of ^{66}Ga to calibrate the beta detector.[2] This standard provides a fast, direct calibration to 4.806 MeV (Fig. 2) using photopeaks. Neutron-deficient Cesium isotopes with known β^+ endpoints were produced on-line to verify the calibration.

The tape transport and detection system described above has been used in three successful on-line experiments to date, results of which are published elsewhere in this report. Continued refinement of the detectors and electronics are underway. This detection system has proven to be a new, powerful tool to study unknown isotopes and exotic decay modes produced in heavy ion reactions.

Footnote and References

*Present address: Hahn-Meitner-Institut für Kernforschung Berlin, West Germany.

1. J.M. Nitschke, Nucl. Instr. Meth. **206**, 341 (1983).
2. R.B. Firestone, *et al.*, Nucl. Instr. Meth. **120**, 199 (1974).

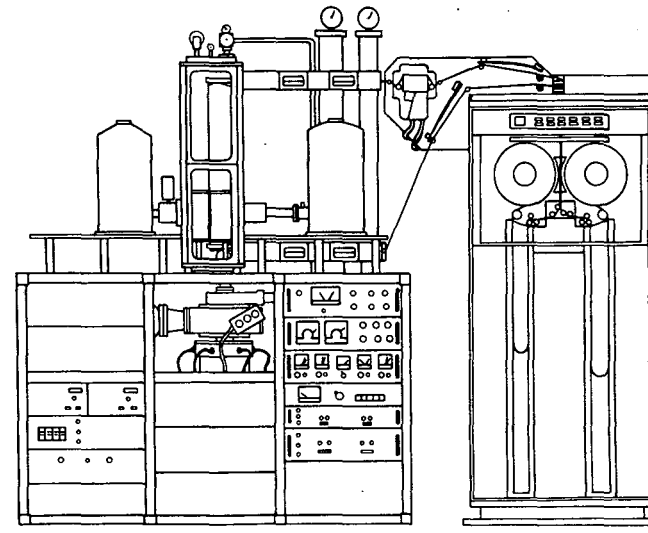

Fig. 1. Schematic representation of the OASIS tape system. XBL 843-1096

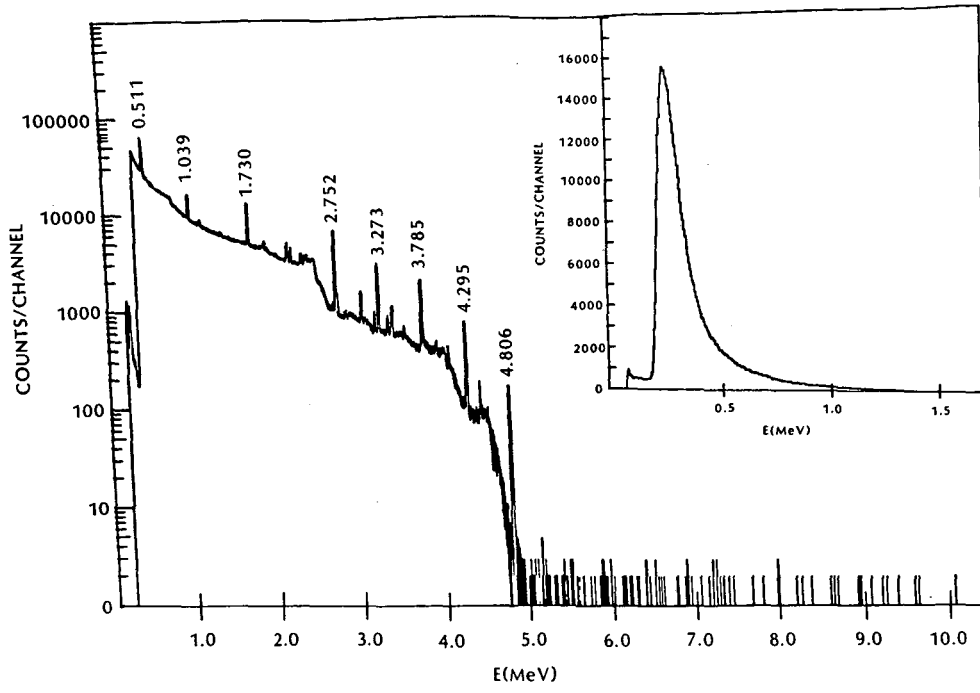

Fig. 2. ^{66}Ga spectra taken with the HPGe detector, and typical ΔE spectra of β^+ particles in the 702-micron detector (see inset). XBL 843-1097

A Forward Scintillator Hodoscope for the Streamer Chamber Facility

R. Brockmann, D. Bangert,† A. Dacal,‡ P. Eitner, J.W. Harris,* W. Hou, M. Maier,† G. Odyniec, M. Ortiz,‡ H.G. Pugh, W. Rauch,† A. Sandoval,§ R.E. Renfordt,* R. Stock,§ H. Stroebele,§ and D. Schall**

At the present time the main effort of our collaboration is to study in detail the interaction of heavy nuclear systems (e.g., ^{139}La + ^{139}La) and isolate collective effects that cannot be explained by binary nucleon-nucleon collisions. Of special interest is also the degree of thermalization and chemical equilibrium between nucleons and deltas and total pion production in these reactions.

Crucial for the analysis of the data is the determination of the impact parameter of the interaction. For heavy nuclei this can be done by measuring the projectile fragments that survive the interaction with essentially the beam velocity (projectile spectators).

To enhance the ability of the Streamer Chamber to detect forward-going fragments a highly segmented hodoscope has been constructed. The hodoscope accepts fragments that are emitted in a forward cone between 0 and 9 degrees. The segmentation of the hodoscope was determined by an extensive Monte Carlo calculation in which the known cross-sections for nuclear fragmentation have been incorporated. The criterium for the segmentation was to maintain a double hit probability below 5%. The hodoscope measures the energy loss (dE/dx) in the 1″ thick scintillators and determines the time of flight between the trigger counter in the Streamer Chamber and the hodoscope.

A prototype hodoscope was tested in the beam. These measurements showed that the required charge and time-of-flight resolution could be met to do charge identification up to Z=20 and together with the measured rigidity in the Streamer Chamber do mass identification for the hydrogen and helium isotopes. These measurements also showed that to cover the dynamical range of the pulse height spectrum from protons to heavy fragments near Fe a dynode read out is necessary.

A schematic view of the hodoscope is shown in Fig. 1. It consists of 384 scintillatior counters, which are divided into 9 subgroups, with an unequal number of channels in each subgroup. Fig. 2 shows 3 of the subunits. The hodoscope can be moved up and down to match the deflection of the charged fragments at different energies for a given magnetic field of the streamer chamber. It can also be rotated by 90 degrees in to a horizontal position to accept cosmic ray particles for calibration. During the run the calibration will be controlled by a laser driven optical system. The hodoscope is assembled and set up behind the Streamer Chamber Magnet (Fig. 3) and the first data will be taken in spring of 1984.

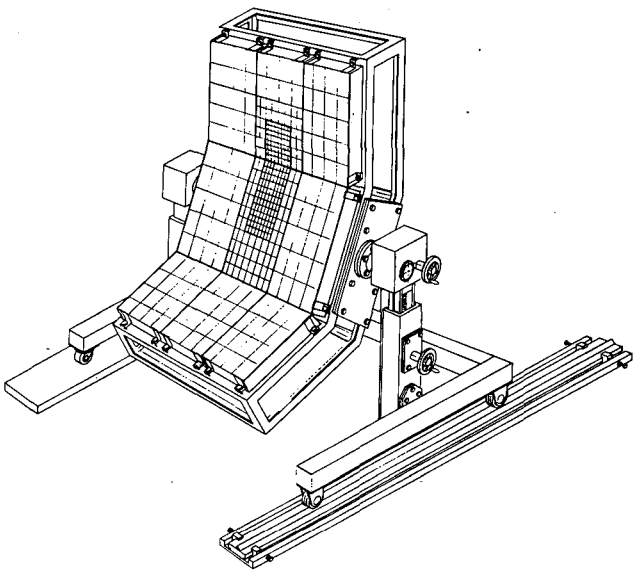

Fig. 1. Schematic view of the forward angle hodoscope. XBL 8312-6923

Footnotes

*Gesellschaft für Schwerionenforschung, 6100 Darmstadt, West Germany
§University of Heidelberg, 6900 Heidelberg, West Germany
†University of Marburg, 3550 Marburg, West Germany
‡Instituto de Física, UNAM, Mexico D.F., Mexico.

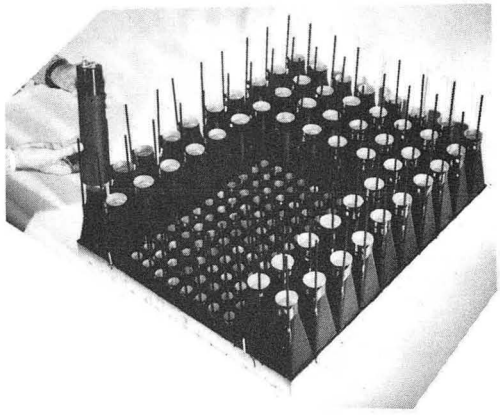

Fig. 2. Two subunits of the hodoscope. The phototubes are air-coupled with an Al cone to the square 1″ thick scintillators mounted on a grid.
CBB 8311-10105

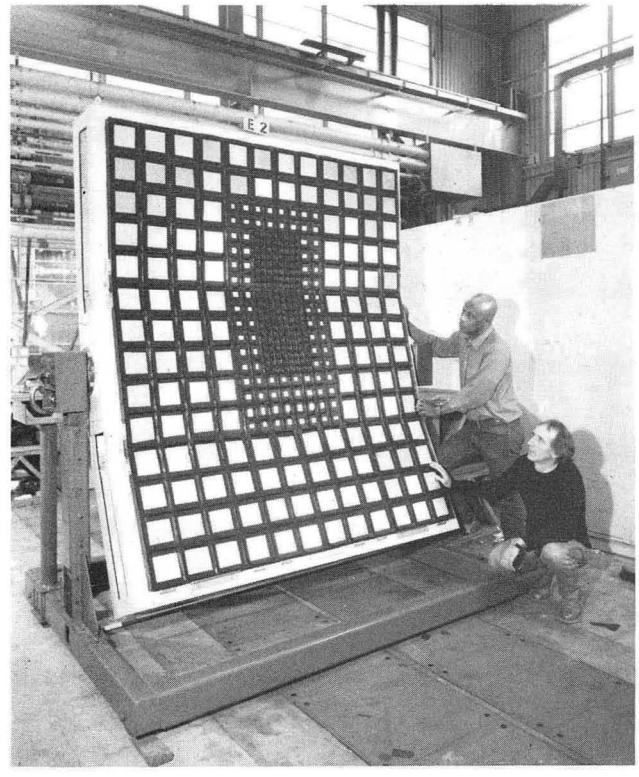

Fig. 3. The hodoscope setup before installation behind the Streamer Chamber. BBC 842-1161

Monitoring System for a Scintillator Hodoscope using an UV Laser

R.E. Renfordt, D. Bangert,† R. Brockmann,‡ P. Eitner, W. Hou, J.W. Harris,‡ M. Maier,† G. Odyniec, H.G. Pugh, W. Rauch,† A. Sandoval,* R. Stock,‡ H. Stroebele,‡ and D. Schall**

A monitoring light pulser system has been developed as part of a forward-angle-hodoscope which operating together with the streamer chamber acts as a hybrid detector to uniquely identify all fast forward emitted reaction products. The monitoring system consists mainly of a pulsed nitrogen laser which illuminates through optical fibers each of the 384 scintillator elements.

By means of a lens system the laser beam is broadened and then coupled to a glass fiber-bundle. The lens system is arranged in such a way as to ensure a homogeneous illumination of the total bundle area. The wavelength of the laser's UV radiation is 337 nm corresponding to a photon energy of 3.68 eV which allows a simulation of the passage of an ionizing particle through the scintillator. The UV light of the laser pulse is absorbed inside of the scintillator and then reemitted according to the characteristic emission spectra of the scintillating material (BC-408) which matches the spectral sensitivity of the subsequent photomultiplier. The scintillator operates as a wavelength shifter resulting in a

conversion of the monochromatic UV laser light to a spectral distribution which is quite similar to the one excited by an incoming charged particle.

This monitoring system allows for a beamless test of the total detector arrangement. Furthermore the time resolution properties of the individual elements of the hodoscope can be checked and a common time zero for all elements can be defined. The stability of the photomultiplier gains can be controlled by analyzing the pulse height during the spill-off time of a running experiment. Using a normalization relative to an additional monitor scintillator, a possible pulse height shift can be corrected.

Footnotes

*University of Heidelberg, 6900 Heidelberg, West Germany
†University of Marburg, 3550 Marburg, West Germany
‡Gesellschaft für Schwerionenforschung, 6100 Darmstadt, West Germany

On Line Streamer Chamber Monitoring System

R.E. Renfordt, D. Bangert,† R. Brockmann,‡ J.W. Harris,‡ G. Odyniec, H.G. Pugh, W. Rauch,† A. Sandoval,‡ M. Maier,† R. Stock,‡ H. Stroebele,‡ and D. Schall**

We have used the Streamer Chamber Facility at the Bevalac for the study of relativistic heavy ion collisions with projectile charges up to Z=57. For such high charges we can no longer assume that the electric field inside the chamber volume will remain constant along the particle trajectories. In order to study the effect of different chamber parameters on these voltage fluctuations and to develop techniques to reduce them as much as possible we have installed a system to monitor variations of the electric field over the chamber volume.

Our system consists of two parts: an UV laser with a focusing optical system and a CCD camera with an LSI 11/23 microcomputer. We use an UV nitrogen laser (Photochem. Res. Ass., Canada) and an RCA charge coupled device (CCD) camera (image array: 512 × 320 pixels with 50 microns resolution and each pixel digitized into 8 bits). The laser light ionizes the streamer chamber gas, this primary ionization is amplified by a factor of 10^8 once the chamber is triggered, making the laser track visible. To monitor the laser output intensity directly, we use a photosensitive PIN diode which is placed in the back of the laser (Fig. 1). The stability of the laser is fairly good. The background (dark picture) of the CCD camera is well known (Fig. 2). For this study, we restrict the area that is actually used on the CCD to the range shown in Figs. 2a and 2b. This guarantees a background stability better than 1.5%. In order to obtain an adequate statistical data sample, it is necessary to collect several hundred laser beam pictures for each setting of the chamber parameters. Fig. 3 shows the light intensity along the chamber for five randomly chosen laser beam shots. Dotted lines denote the background level (dark picture). The structure of streamers deduced from Fig. 3 is the same as that obtained from the normally used Kodak film (SO-143) exposed at the same time. From our studies using the on line monitoring system described above we draw the following conclusions:

1. The light intensity per unit length along the chamber is homogeneous within a few percent for all tested chamber conditions.
2. The average intensity per unit length from one laser shot to another varies by less than 10%.
3. Using this method the streamer chamber parameters (input voltage to the Marx Generator, Marx column gas pressure, main spark-gap gas pressure

and length of the Blumlein transmission line) can be optimized to give the most stable operating condition.

4. The light intensity per unit length varies as the the fourth power of the electric field in the chamber. Because of that, we can detect significant changes of the chamber running conditions during actual data taking with heavy beams. We shall use the system described above during our next run with a Lanthanum beam. We will flash the laser at the same time the chamber is triggered by the standard trigger configuration. This will allow us to detect any inhomogeneities along the chamber resulting in fluctuations of track brightness on film.

Footnotes

*University of Heidelberg, 6900 Heidelberg, W. Germany

† University of Marburg, 3550 Marburg, W. Germany

‡Gesellschaft für Schwerionenforschung, 6100 Darmstadt, W.Germany

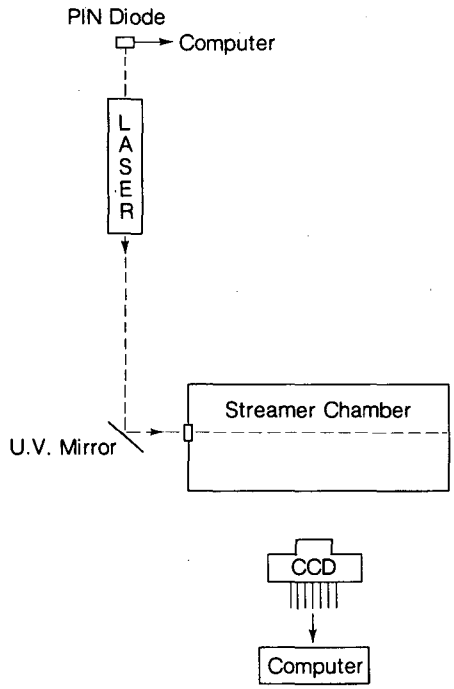

Fig. 1. Experimental setup of on-line monitoring system. XBL 8312-6925

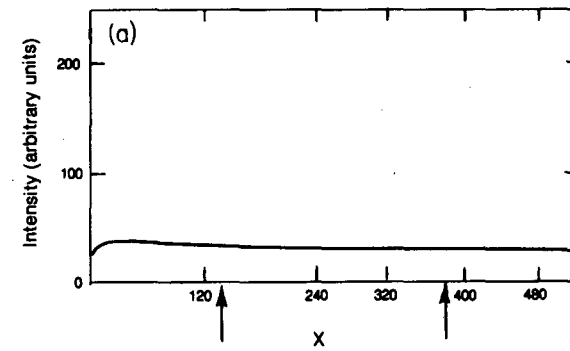

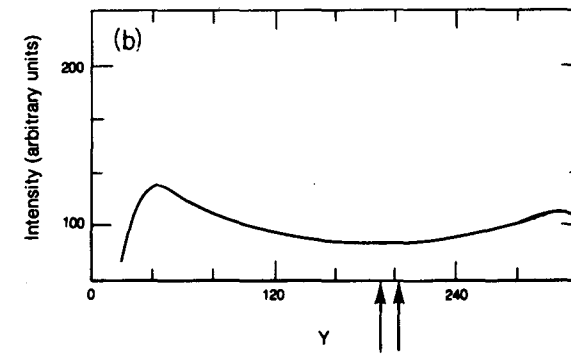

Fig. 2a. CCD background along the X axis. Arrows denote selected range in Y direction.

XBL 8312-6926

Fig. 2b. CCD background along the Y axis. Arrows denote selected range in X direction.

XBL 8312-6928

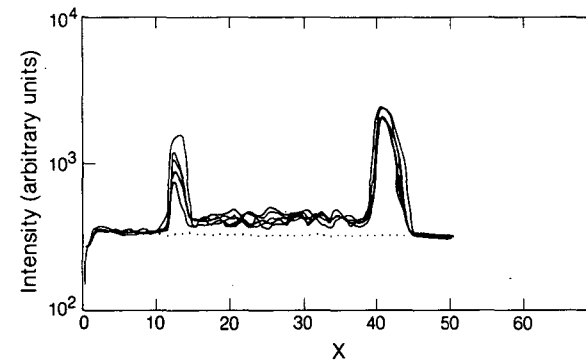

Fig. 3. Laser light intensity along the chamber for five laser beam shots. Dotted line shows the background level. XBL 8312-6927

Computers

WC – A General Purpose Computer Program for Off-Line Analysis

S. Wald

WC is an interactive code for analyzing multiparameter experiments. The code is installed on the MODCOMP computers and handles event-by-event tapes produced by the program, *chaos*. The code is easy to operate, easy to modify and easy to move to another computer.

The program can be used for:

1. Filtering data: producing a new event-by-event tape after selection and modification of events from existing tape or from simulated data.
2. Analyzing data: the program provides subroutines and functions that enable the user to apply complicated tests on each event, increment one-dimensional and two-dimensional spectra, increment scalers, etc. Up to twelve line displays (scatter plots) can be plotted simultaneously. Free-form gates, linearization lines, etc., may be set on these displays. Many operations can be done on the final spectra. This structure enables the user to write an analyzing routine directly from a flow chart without thinking about formats, plots, zeroing scalers, etc.
3. Simulation codes: the program can be used to create simulated events and to analyze them as if they were the measured data.

The above functions are carried out by the user via a single subroutine that can be compiled and linked by itself and then loaded dynamically during run-time. There are procedures for handling the user's favorite subroutine, saving and restoring the setup of the experiment and the spectrum buffer, etc.

The code is written in FORTRAN and is designed to run on minicomputers as well as on big computers. It is segmented so all parts can be overlaid. The PLOT 10 graphic package is used. Drivers are provided to the following graphic devices: the Tektronix 4014, VT100-SELANAR 200P Tektronic emulator, the Digital Tektronix Plotter and the Versatec line printer.

Changing segments of the program or the dimensions of arrays or installating the code on another computer is a relatively trivial task.

Bevalac Software Project Status

C. McParland, M. Bronson, P. Lindstrom*

Several new projects have been undertaken in the area of Bevalac experimental software. One effort has been aimed at increasing the data throughput of the front-end data acquisition machine. A second effort has aimed at making the VAX data analysis interface transportable to the soon-to-arrive NSD Bevalac VAX. A third project has upgraded the LBL GRAFPAC graphics software to allow redirection of graphics output to a number of devices and printers at program run time.

Application of a Large CAMAC-based Buffer Memory to Data Acquisition

There are eight data acquisition machines currently installed at the Bevalac. These systems

consist of a PDP-11(11/34,11/44,11/45) with a number of disk and tape drives, a Micro Programable Branch Driver (MBD), and up to seven CAMAC instrumentation crates. The MBD branch driver is a fast (350 ns cycle) stored program processor that has data paths out to CAMAC as well as into PDP-11 memory. It is downloaded from the PDP-11 and runs asynchronously with the PDP-11 and its RSX-11M operating system.

Our latest attempts to increase data rates have centered on the use of a very large CAMAC-based memory (256K 16-bit words). This device places 256K words of intermediate storage on the CAMAC data bus of one crate. Since it contains an internal address register, data can be stored to sequential memory locations by a simple 1 CAMAC cycle per word sequence. In comparing basic CAMAC cycle times to that of the PDP-11/MBD combination, we found that data can be sent from our present MBD to this large buffer memory faster than to PDP-11 memory. In addition, data moved to this memory via the CAMAC bus, did not contend with any disk or tape data transfers on the UNIBUS. We had observed that this UNIBUS crowding behavior decreased our potential data rate by nearly a factor of two. Therefore, by temporarily directing data back to this CAMAC memory we could increase our instantaneous data rate.

Time savings were not confined solely to hardware. The MBD interface spends a substantial amount of its time checking the consistency and bounds of data buffers written into PDP memory. This has been necessary to insure that the MBD's DMA activity will be confined to the intended data buffers and not write all over the RSX-11M executive (with predictably bad results for all concerned). In the past, with data streaming from CAMAC through the MBD to the PDP-11 memory, these program checks have been performed during the precious one second of live experimental data. Our data rates were thus limited to about 20K words/second. The relatively huge size of the CAMAC buffer memory allows many of the necessary checks to be left until data is transferred to the PDP-11. The result is that during the one second of data collection, a series of fast, simple transfers move data from ADCs and TDCs to the CAMAC buffer memory. The full set of data consistency and buffer length tests are only performed later, during the five second inter-spill gap between data bursts. By using this intermediate buffering scheme, we have increased our data rate to over 100K words/spill.

We have found that by careful control of the data paths used during data acquisition and the use of hardware buffering at the points of maximum congestion, substantial increases in CAMAC system throughput can still be attained. However, it is our belief that data acquisition at these speeds is reaching a fundamental limit. Additional improvements will probably require upgrades to VAX-level computers and Fastbus.

Data Source Routines under VAX/VMS

Development has continued on the creation of software facilities to allow easy access to data on a back end VAX system. This software will be provided on the new NSD machine when it arrives early in 84. Our goal is to create an environment in which people whose computer programming background consists primarily of writing FORTRAN data analysis routines can easily access data from a variety of sources (e.g., "live" data from front end machines running DATACQ, disk files of previously taken data, etc.) This has led to the creation of software tools of general use. Their value lies either in the utility they provide (data rate monitors, spill display programs, etc.) or in their use as templates for special purpose utilities that the physicist can build without further assistance.

Our approach requires a single format in which all data is transmitted – the "counted record" used by the front end data acquisition software (DATACQ). We have built a uniform user interface to data from all sources (e.g., "live" data, data from previous runs, data from monitoring sources, etc.). In the simplest case the user needs only two routines. First a *data open* which makes a connection to a data source on the users behalf. Following this, the user can make repeated calls to a *get buffer* routine which will copy data to a users buffer. The source is

specified in the *data open* as a simple text string. By changing this string, the program can get data from a variety of sources. This makes it extremely simple for the same programs to be used for both online monitoring of a running experiment as well as offline analysis.

We believe this promotes the development of software tools. We have built a generally useful utility for examining data. It will print a data record in different formats allowing a user to quickly check that the data are at least correct in form. It can also search for specific record types and collect frequency and size statistics on those records encountered.

This is an ongoing investment in data monitoring and reduction software that can be useful across many experiments, leading (we hope!) to the stage where a new experiment can have much software ready by just inserting specific procedures into already existing programs.

Graphics Software

The variety of graphics devices that can be connected to any of the VAX analysis machines is overwhelming. This has prompted the adoption of the LBL GRAFPAC software package. One shortcoming of this package has been the inability to redirect graphics output from within a running program. Thus, an analysis program which displays on a graphics screen would be unable to redirect the graphics to a hard copy device. Two solutions were possible: buy hard copy devices for all graphics displays, or enhance GRAFPAC drivers to allow redirection of output. Our choice has been the latter. In making this choice, we wanted to maintain the freedom allowed by the device-independent graphics interface. However, the ability to hard-copy a graphics screen must be available. This enhancement allows us to redirect all graphics to a Versatec printer/plotter without program changes.

Additional enhancements have included the addition of an AED 512 color terminal driver. We have also implemented the GRAFPAC system as a VMS shared image. This has substantially reduced program disk storage requirements and, in some cases, increased program execution speed.

*UCB Space Sciences Laboratory and LBL

Installation Progress of the NSD-Bevalac VAX

*C. McParland**

As reported last year, a new VAX 11/780 has been ordered for installation at the Bevalac. This machine will now make on-line, VAX level processing of experimental data available to all present beam lines. A new building, designated 51H, is being constructed at the Bevalac. This building will house the new computer and the existing Gesellschaft für Schwerionenforschung (GSI) machine. The location has been chosen to minimize cable runs between this facility and the LEBL and TASS experimental areas. The machine will be installed in two steps. The first step will consist of the VAX 11/780 CPU, memory and disks. The initial configuration will include a 204 Mbyte system disk along with two 456 Mbyte user disks. Also included are DECNET links and license for connection to the LBL-DGATE machine. The system is due for delivery in January of 1984.

The second phase includes the purchase and installation of additional devices required for its role as an experimental machine. These devices include a 6250 BPI tape transport, an 80 Mbyte shared disk subsystem, a Versatec printer/plotter, and a line printer. With the addition of these devices, the VAX 11/780 will be very similar to the two VAX systems

presently at the Bevalac (HISS and GSI). Completion is scheduled for late spring of 1984.

All experimental data acquisition and analysis software packages currently installed on both the HISS and GSI VAX 11/780's will be ported to this machine. No significant software development will be required to bring this machine to the current level of the other experimental machines.

*UCB Space Science Laboratory and LBL.

LULU Analysis Program*

H.J. Crawford and P.J. Lindstrom

As we were designing experiments at the Heavy Ion Spectrometer System (HISS)[1] at the Bevalac, it became clear that a new approach to real time data analysis was necessary. Experimental configurations consisting of many different detector types and sizes were envisioned. The primary difficulty with the analysis codes available at that time was that all such codes required a fixed word length event. Since HISS is operated as a facility with many different experiments being performed by different groups of physicists, we felt that it was necessary to provide an analysis code capable of handling arbitrary detector configurations in which each detector may place an arbitrary number of data words into the event stream. The package we constructed to meet our needs is called LULU and it possesses the characteristics shown below.

On- and off-line analysis – raw and preprocessed data

User subroutines

Time functions run through RPN

Graphics device independence

Automatic data statistics

Real time output to other programs

The basic data flow through LULU is shown in Fig. 1. Data is provided from a number of sources in a uniform fashion. It can come as an outline data stream through the route shown at the right: detectors to CAMAC to the Memory Module through an MBD into a PDP 11/45 and onto an intermediate disk. Or it can be loaded onto another disk from

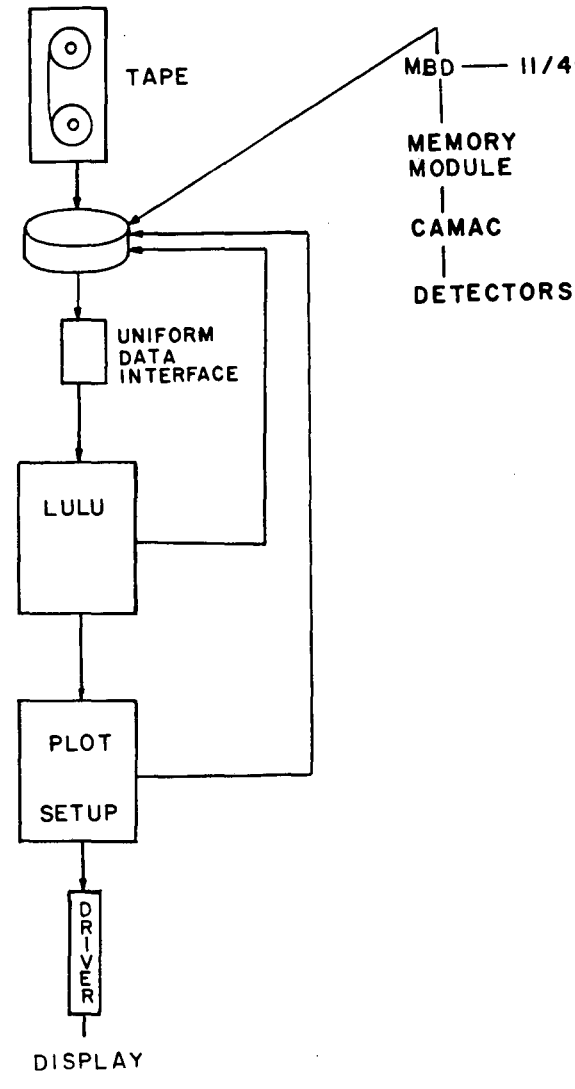

Fig. 1. Data flow through LULU showing both on-line and off-line data sources. XBL 8311-4606

magnetic tape for off-line analysis. LULU is able to read any data that is stored in the form of the Uniform Data Interface.[2]

The program LULU is a housekeeping, sorting and plotting package that operates on word lits generated by a series of user subroutines called ANALYSERS. Analyser output arrays are grouped in a large array called the VALS array as shown in Fig. 2. By executing a series of commands LULU lets you look at raw and digested data, form simple statistics on specified data words, and selectively fill histograms and multidimensional scatter plot arrays from words in the VALS arrays. LULU takes advantage of the very large arrays allowed by the VAX VMS operating system to save every individual data point in a scatter plot rather than forming two dimensional histograms. These saved arrays are then passed to a plot package where they are turned into the appropriate display.

Before presenting a detailed description of the data flow through LULU, we will point out a few of the features that it shares with other analysis programs. Working in LULU it is possible to form up to 100 scatter plots and 100 histograms simultaneously. (The limit of 100 is artificial). These can then be added together, subtracted, normalized, cut, displayed with offsets, scaled with an arbitrary runtime produced function, fit to arbitrary functions and set to graphics, crt or hardcopy devices for viewing and saving. Displays generated from data passing through the complete LULU scheme can be viewed in a continuously updating fashion (useful in debugging detectors) or viewed event by event as well as viewing in the normal fashion when an analysis sequence is completed. Data can be viewed at any intermediate stage in the analysis through the SHOW command, whose subcommands allow the user to select the portion of interest.

The ability to form and save up to 100 multidimensional scatter plots, each having a different dimensionality, gives as much power in the plot package as you have in the main analysis sections of LULU. By selecting variables suspected of being correlated and placing them in groups in the SCAT array, you can then pick any 2 variables, cut on other values in the group or in the event (event structure is built into the SCAT array) and then display these in scatter plots or histograms.

Our analysis program LULU has proven very useful in all stages of experiment analysis, from prerun detector debugging through final data reduction. It has solved our problem of having arbitrary word length events and is easy enough to use that many separate experimenters are now analyzing with LULU. The ability to use the same software for all stages of experiment analysis greatly eases the programming burden. We may even get around to making the graphics elegant someday.

Footnote and References

*Condensed from LBL-16171

1. H.J. Crawford, LBL-15477, 1982.
2. Mark Bronson, *A Uniform Data Interface,* to be published in IEEE Transactions on Nuclear Science Topical Conference of Computer Data Acquisition Systems in Particle and Nuclear Physics, October 1983.

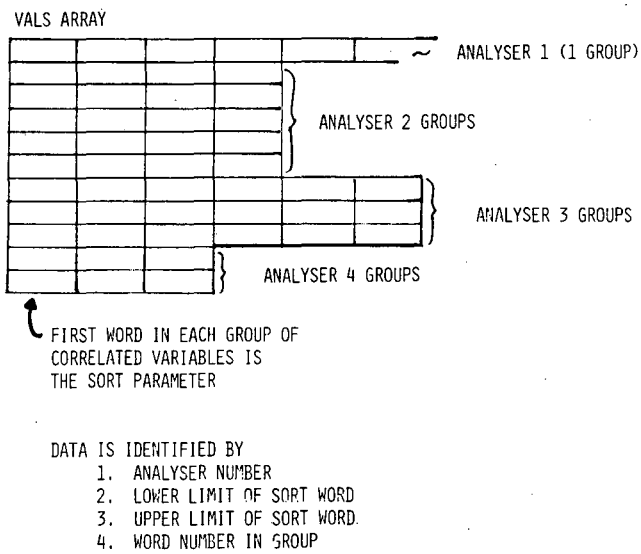

Fig. 2. Structure of the VALS array showing addressing scheme. XBL 8311-4607

Status of HISS Maps

E. Beleal, M. Bronson, C. McParland, D. Olson

In July of 1983, the HISS Group completed mapping five magnetic fields for the following three experiments.

Experiment	Field (in kG)
512H	18.0
512H	20.8
513H	13.0
513H	26.4
517H	22.7

Software control of the Magnet Mapper helped to automate the time consuming mapping procedure. An interactive VAX program called MAPIT (written by E. Beleal) was the command level interface to the Magnet Mapper Controller implemented in an LSI 11-2 by C. McParland. Connection between the LSI 11-2 and the VAX was via DECNET. System control of memory allocations for the Mapper output and a diagnostic program called SHOMAP were contributed by M. Bronson.

The output of program MAPIT consists of one or more files for each plane describing the solid whose surface is being mapped. A minimum of six planes are required to describe this solid. To accommodate mechanically difficult-to-map configurations, it is necessary to break up some of the planes into subplanes. For the five experiments listed above, we mapped identical physical solids with dimensions 210 cm. in X, 280 cm. in Y, 80 cm. in Z. Each mapping consisted of ten files, one each for the bottom and top planes and two for each of the four side planes. The side planes were subdivided at the midpoint to accommodate a reorientation of the rod bearing the three Hall probes. These two files of MAPIT output contain header information plus the raw X, Y and Z components of the Bfield, measured at user stipulated intervals on a grid which in turn describes each plane comprising the mapped surface.

For documentary purposes and as a preliminary consistency check, we are preparing a primer of 3D plots representing the X, Y and Z components of the raw Bfield for each of the five experiments. The accompanying figures, produced by the program SHOMAP show 3d plots for each of the three Bfield components, projected against the XY-bottom plane of the solid mapped in RUN320 (exp 513H).

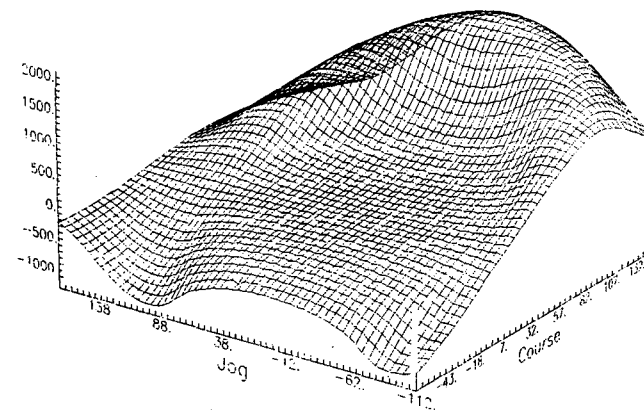

Fig. 1. 3D plot of X component of Bfield for exp 513H. XBL 8312-4684

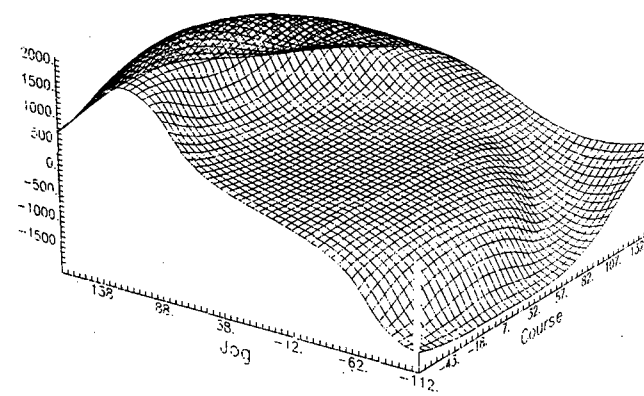

Fig. 2. 3D plot of Y component of Bfield for exp 513H. XBL 8312-4685

Given this raw Magnet Mapper data base for each experiment, the goal is to produce files of Chebycheff coefficients tailored to experimental setups and momentum spreads of interest for subsequent analysis or experiment design programs. Along the way to this goal are many intermediary program steps, requiring precise coordination and yet allowing a high degree of user manipulation.

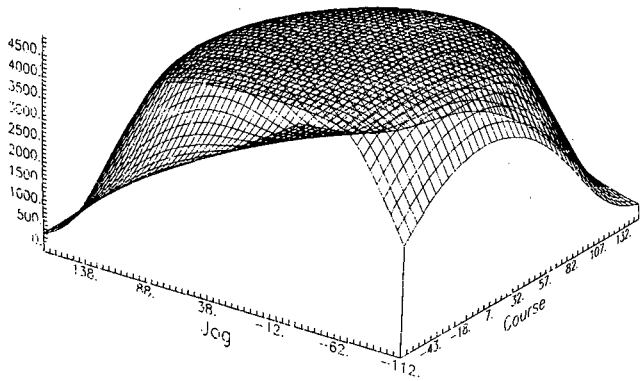

Fig. 3. 3D plot of Z component of Bfield for exp 513H. XBL 8312-4686

ICAMS

A New System for Automated Emulsion Data Acquisition and Analysis*

A.A. Arthur, W.L. Brown, Jr., E.M. Friedlander, H.H. Heckman, R.W. Jones, Y.J. Karant, and A.D. Turney

A general difficulty with visual techniques in high energy physics has been the relatively slow data-taking rate caused by the labor-intensive nature of the experiments and the resulting low statistics of the final data base. On the other hand, visual techniques, and especially research emulsion, have the intrinsic advantages of essentially complete 4π coverage of all charged particles from the target- , mid- , and projectile-rapidity regions. Emulsion has excellent charge resolution, since in one target/detector, charges of minimum ionizing tracks from charge 1 to charge 92 can be determined. With these intrinsic advantages of emulsion, it seemed reasonable to use modern data acquisition and reduction techniques to relieve the labor-intensive functions.

The Interactive Computer Assisted Measurement System (ICAMS) is our answer to this. It is a distributed network system. The system has two major components, the central computer and individual data-taking stations, called Optical Data Stations (ODS). The central computer is a Digital Equipment Corporation PDP 11/23 with a 22-bit address space (of which 1 Mbyte is currently implemented) running under RSX-11M V4.

Each ODS is equipped with a 6512 microprocessor using the Motorola bus and is also equipped with a Creative Micro Systems 9611 arithmetic processor (32 bit floating point unit with higher "slide rule" functions). In addition, a special LBL-designed two-port memory is included, which appears as 512 bytes addressable read-write memory on both the UNIBUS and the Motorola bus. Thus, UNIBUS protocol and arbitration implements the network hardware standard on ICAMS.

The microscope stage is fitted in both axes with incremental encoders and DC servo motors on one millimeter pitch lead screws.

A track ball is provided. Its output is used by the microprocessor either to modify a computer-directed movement or to allow direct position control by the operator. When being used for direct position control the response is nonlinear to both accurate position control and rapid motion when moving substantial distances.

The software implementing ICAMS has several constraints. It must be user friendly to both the end-level scientific user, principally programming for

data analysis in standard PDP FORTRAN-77, and forgiving to a scanner working on an ODS. In fact, to the scanner, the ODS should appear much as constant companion and electronic notebook, reminding the scanner of the current scanning instructions for the experiment in progress and likewise automatically recording the data for later analysis by the physicists. This last step greatly increases the data throughput and reliability, for the previous method of hand-recording data and then entering the data into a computer by either card punch or interactive CRT terminal programs is fully eliminated. Additionally, full advantage must be made of the powered stage control of each ODS, removing the physical tedium of manually turning X and Y crank wheels to follow a track or to return to a specified point in the plate.

Because of the time involved in programming the ODS 6512 in direct assembly language, some other higher level language was desired for general scientific scanner program implementation. On the other hand, the execution speed of assembler programs was desired to implement the direct stage control motion functions. For this reason, it was decided to have two processes time share the 6512 resources; these are the stage control process (written in assembler and fixed EPROM), and the scientific control process, written in a higher level language. Since FORTRAN is not readily available for the 6512 (Apple FORTRAN is in principle available but too cumbersome for many of the applications desired), we selected AIM-65 FORTH, available from Rockwell as a PROM set. This language interfaces directly with assembler routines, has its own structured version of the AIM-65 assembler, and permits high level structures to be implemented, while still executing rapidly enough for real time applications. It is modular and structured; has preexisting 8, 16, and 32 bit word lengths as needed; and has two additional virtues. It is a virtual operating system (unlike RSX but akin to VMS in this respect), and it is extensible. That is, FORTH permits the compiler to be modified from within the compiler to introduce new constructs via the BUILDS and DOES words. Unfortunately, the intrinsic FORTH system only addresses two bytes of disk sector numbers, whereas FILES-11 under RSX addresses four bytes of disk sectors. However, we modified the FORTH PROMs to address the full four bytes implemented under RSX.

The data are then available for analysis by the physicists using FORTRAN-77 programs under RSX, using the non-ODS portion of ICAMS, which also serves as a general purpose computer, text editor, etc. Special data acquisition subroutines are written, of course. These FORTRAN-77 compatible subroutines first parse the appropriate .HED file to determine the pointer into the data file on the disk and then read the data as requested by the physicist-supplied data analysis program.

*Based on LBL-16111, presented to Conference on Real-Time Computer Application in Nuclear and Particle Physics, LBL, May 15–19, 1983.

MONA, the Plastic Ball Data Acquisition System

*B. Kolb**

The addition of new detectors to the Plastic Ball increased the maximum number of parameters in one event to more than 4096, so it became necessary to improve the data acquisition system. In addition, the bus activity in the old PDP 11/44 and the very limited amount of buffer space introduced a large dead time in the system. Measurements of the dead time during the beam spills showed that at least a factor of two improvement in speed should be possible if larger buffers could be used. To provide a system also for the expected addition of several thousand new parameters (when the experiment is

moved to CERN), a new computer with larger address space and independent buses for data acquisition and data logging was purchased. A VAX 11/750 was the reasonable choice because it is compatible with the existing VAX 11/780, provides large physical memory and can accommodate four bus systems. The interface to CAMAC, the MBD (micro programmed branch driver), resides on the UNIBUS, while the tape drivers and the system disk are connected to MASSBUS adaptors.

After a survey of existing software a new driver for the MBD was written, designed specifically for the transfer of large amounts of data with minimal overhead. The existing micro-code for the MBD was modified only in the parts which take care of the communication with the UNIBUS. The experiment code remained essentially unchanged, except for some improvements related to the larger buffer sizes.

The new data acquisition program was already written and tested before the VAX 11/750 was delivered (of course with a simulated input). It consists basically of one process handling the buffers and several command processes which communicate with event flags and data in a global section. There are six buffers of 32K words each which are used in a circular manner. MONA queues two buffers to the MBD-driver which in fact starts the MBD program with the first of the two buffers. The MBD waits for LAMs from CAMAC and then reads out the event into the buffer. As soon as the buffer is almost filled the MBD returned buffer is scanned and checked for consistency. The buffer is then marked to be waiting for logging to tape and disk. The actual transfer to tape and/or disk is started only when the scanning of the buffer reveals a spill-off-event, which means that there will not be any CAMAC activity for some seconds. In this case, or when there is no free buffer, all waiting buffers are queued to the logging devices. When the output is finished the buffers are marked as free. Every time a change in the status of a buffer is detected MONA checks if there are still two buffers queued to the MBD. If there are less than two and there are still free buffers another buffer is queued to the MBD. This ensures that the time required for a buffer change is minimized because the driver immediately starts a new transfer when the previous one has finished. In addition the buffer change takes place when there is no event pending in the MBD because the MBD code checks after each event if there is enough space left for the next event. This is possible now because the maximum event size of about 4k words is small compared to the buffer size of 32k words.

Though each buffer is scanned event by event by MONA this does not slow down the data acquisition because the MBD is already transferring data to the next buffer. Collisions of memory fetches by the VAX and transfers by the MBD are avoided because the bandwidth of the CMI (the internal bus in the VAX 11/750) is much higher than the bandwidth of the UNIBUS. The overhead for QIOs, interrupt handling and buffer housekeeping is reduced through the use of large buffers. First speed measurements showed the new system to be at least a factor of three faster than the old one. In addition the new system is much more reliable and friendly to the user.

*Gesellschaft für Schwerionenforschung, Darmstadt, West Germany.

GAMUT, a Computer Code for Statistical Analysis of γ-Ray Data

R.B. Firestone and E. Browne

GAMUT was written to derive an adopted set of γ-ray energies and intensities from ENSDF decay and/or reaction datasets.[1] Adopted properties in ENSDF are given for each decay mode separately. Values derived from all available information are not in the file. Thus if a specific γ-ray was observed

with a precise energy in β-decay but was crudely measured in alpha decay, both measurements would be present in the ENSDF file. Similarly, the intensity branching ratios of γ-rays deexciting a level may vary between different modes of decay. The Radioactivity Handbook will provide a unique set of adopted γ-ray decay data (which does not explicitly exist in ENSDF) calculated with GAMUT.

Input data to the computer code GAMUT can be supplied with three formats; via a DATATRIEVE (database management system of DEC) procedure from the ENSDF database at LBL, with a special tabular input format, and in a modified ENSDF format. The latter two formats allow the evaluator to include multiple experimental values for each decay mode. GAMUT performs a least-squares fit of experimental γ-ray energies to their associated levels using the following relationship

$$E_{ki} = E_k - E_i + c$$

where E_{ki} is the γ-ray energy, and E_k and E_i are the energies of the initial and final levels. A parameter c adjusts the zero energy for each dataset. Adopted γ-ray energies are then calculated from the above equation using the fitted values of the parameters. Statistical uncertainties are corrected for the corresponding covariances. The uncertainty in the parameter c represents the systematic error consistent with the data. GAMUT adjusts the input data by an iterative chi-square analysis to obtain a new set of energies. First, the experimental uncertainties of the extreme outlying values are increased to improve the fit until a chi-square of 1.0 is achieved. Then the γ-ray energies are recalculated. The errors in the entire dataset are increased by the same factor if the new γ-ray energies still deviate significantly (chi-square > 1) from the input values. Otherwise, only those energies which lie outside a 99.5 percent confidence level are readjusted. This procedure continues until no more changes are required.

γ-ray intensities are averaged by a method similar to those described by Tepel[2] and Lederer[3]. For each level the γ-ray intensities are renormalized to a common scale by an iterative linear regression. Deviations from a weighted average intensity are minimized on each iteration until the process converges for all levels. These final weighted average values represent the best relative γ-ray branchings from each level. Relative intensities for each decay mode are obtained by converting the data to the original decay set scale. Statistical uncertainties are corrected for the covariances, and chi-square analysis is performed to obtain the adopted values. The program may be run interactively and uncertainties in both γ-ray energies and intensities altered by the user during execution.

A summary of adopted γ-ray energies and intensities for decay to ^{231}Pa is shown in Table II. Systematic values given in ENSDF are not used in the averaging process, and questionable values are left to the discretion of the evaluator. Total transition intensities (photons plus conversion electrons) are not averaged with γ-ray photon intensities. However, their energies are used to determine adopted γ-ray energies. Default errors are 1 keV for energies and 20 percent for intensities. "Approximate" intensities are assumed to have 50 percent error, and "upper limits" to span the range from 0 to the limit. When possible, intensities which are not available for one decay mode are calculated from the data of other decay modes. Systematic values are replaced by experimentally derived quantities whenever possible.

References

1. "Evaluated Nuclear Structure Data File", edited and maintained by the National Nuclear Data Center, Brookhaven National Laboratory, on behalf of the International Network for Nuclear Structure Data Evaluation.
2. J.W. Tepel in the summary report of the IAEA Advisory Group Meeting on Nuclear Structure and Decay Data, IAEA Report INDC(NDS)-115/NE (1980), p. 121.
3. C.M. Lederer, NDN Memorandum of 13 April, 1982.

Table I

Final Adopted Level and Gamma Energies for A=231 and Z=91

Level Energy	Gammas Deexciting the Level
9.20*3*	9
58.561*11*	59
77.681*19*	68,78
84.203*9*	26,84
101.389*13*	17,43
102.253*12*	18,93,102
111.636*20*	10
169.4*4*	111
174.156*9*	73,90,116,165,173
183.483*11*	81,82,99,106,125,183
218.217*16*	44,107,117,134,141
247.318*13*	64,136,145,146,163,170,189
317.93*4*	240,309,318
320.191*19*	137,218,236,243,311,320
351.82*4*	250,250,268,274,352
5192.6*9*	4861,4924,4938,4994,5004,5005,5021,5047,5095,5104

Table II: Final Adopted Gamma Energies and Intensities

Gamma Energy	Intensities		
	^{235}Np α Decay	^{231}Th β Decay	^{231}U EC Decay
9.20 *3*	0. ^{S}	0.5 *1* ST	0.42 *8* ST
10.247 *20*	6.0 *12* ST	0.76 *15* ST	0.
17.186 *12*	42. *15* ST	44. *15* ^{T}	1.0 *2* ST
18.050 *12*	15.6 ST	0.17 *17*	0.13 $^{>T}$
25.642 *11*	15.3 *14* ^{S}	14.6 *10*	13.4 *15*
42.828 *14*	0. ^{S}	0.058 *4*	0. ^{S}
44.062 *15*	0.	0.0007 *2*	0.
58.561 *11*	0.6 *2*	0.48 *2*	0.44 *9*
63.834 *12*	0.007 *5* ^{S}	0.023 *2*	0.
68.48 *3*	0. ^{S}	0.0057 *14*	0.0055 *11*
72.766 *12*	0.011 *10* ^{S}	0.251 *15*	0. ^{S}
77.681 *19*	0.	0. ^{S}	0. ^{S}
81.230 *12*	1.48 *9*	0.90 *4*	0.013 *3*
82.094 *12*	0.81 *16* ^{S}	0.49 *9*	0.0074 *19*
84.203 *9*	6.9 *4*	6.6 *3*	6.0 *5*
89.953 *8*	0.04 *4*	0.94 *6*	0. ^{S}
93.05 *3*	0.037 *9*	0.049 *5*	0. ^{S}
99.28 *1*	0.198 *20* ^{S}	0.120 *7*	0.00179 *23* ^{S}
102.253 *12*	0.31 *6*	0.41 *3*	0. ^{S}
105.802 *18*	0.0117 *15* ^{S}	0.0071 *7*	0.000106 *16* ^{S}
106.581 *20*	0.	0.017 *1*	0.
110.8 *4*	0.09 *3*	0.	0.
115.594 *12*	0.00004 *4* ^{S}	0.0010 *2*	0. ^{S}
116.828 *14*	0.	0.0207 *13*	0.
124.922 *12*	0.092 *8*	0.056 *3*	0.00083 *10* ^{S}
134.014 *14*	0.	0.024 *1*	0.
135.681 *17*	0.025 *15* ^{S}	0.078 *5*	0.
136.707 *19*	0.	0.0042 *2*	0.08 *4* ^{S}
140.536 *20*	0.	0.00071 *7*	0.
145.064 *14*	0.0019 *11* ^{S}	0.0058 *4*	0.
145.928 *13*	0.010 *6* ^{S}	0.032 *2*	0.
163.114 *11*	0.05 *3*	0.155 *9*	0.
164.95 *3*	0.00017 *16* ^{S}	0.0039 *4*	0. ^{S}
169.637 *18*	0.00039 *23* ^{S}	0.0012 *1*	0.
174.156 *9*	0.0008 *8*	0.0183 *11*	0. ^{S}
183.483 *11*	0.054 *4*	0.0329 *13*	0.00049 *6* ^{S}
188.756 *12*	0.0010 *6* ^{S}	0.0032 *2*	0.
217.937 *18*	0.	0.040 *3*	0.8 *4*
235.987 *18*	0.	0.0092 *6*	0.18 *9* ^{S}
240.25 *4*	0.	0.00028 *3*	0.
242.510 *22*	0.	0.00084 *8*	0.017 *9* ^{S}
249.57 *4*	0.	0.00078 *8*	0.
250.43 *4*	0.	0.00065 *7*	0.
267.62 *4*	0.	0.00116 *13*	0.
274.14 *4*	0.	0.00003 *1*	0.
308.73 *4*	0.	0.00039 *4*	0.
310.99 *3*	0.	0.0029 *2*	0.06 *3* ^{S}
317.93 *4*	0.	0.00008 *1*	0.
320.190 *19*	0.	0.00011 *1*	0.0022 *11* ^{S}
351.82 *4*	0.	0.00007 *1*	0.
*4806. *7*	0.10 *5*	0.	0. ALPHA
4861.1 *9*	0.7 *1*	0.	0. ALPHA
4923.8 *9*	11.5 *5*	0.	0. ALPHA
4937.7 *10*	0.6 *3*	0.	0. ALPHA
4994.5 *9*	6.3	0.	0. ALPHA
5003.7 *9*	0.25 *25*	0.	0. ALPHA
5004.5 *9*	24. *8*	0.	0. ALPHA
5021.4 *9*	53. *8*	0.	0. ALPHA
5046.6 *9*	1.8 *3*	0.	0. ALPHA
5095.2 *9*	0.2 *1*	0.	0. ALPHA
5104.2 *9*	1.5 *2*	0.	0. ALPHA

systematic energy error = 0.01007 keV
S = systematic value
T = total intensity
> = lower limit
* unplaced transition

PART VI: APPENDICES

Publications Appendix I

ABACHI, S. See SHOR, A. LBL-16175

AL-GHAZI, M.S.A.L. See OKUMUSOGLU, N.T. LBL-15186

ALBISTON, C.R. See WALD, S. LBL-16899

ANDERSON, L., W. Bruckner, E. Moeller, S. Nagamiya, S. Nissen-Meyer, L. Schroeder, G. Shapiro, H. Steiner, LBL-14328
Inclusive Particle Production at Forward Angles From Collisions of Light Relativistic Nuclei, Part I: Nuclear Fragments Phys. Rev. **C28**, 1224 (1983).

ANDERSON, L. See MOELLER, E. LBL-14329

ARTHUR, A.A., W.L. Brown, E.M. Friedlander, H.H. Heckman, R.W. Jones, Y.J. Karant, A.D. Turney, LBL-16111
ICAMS: A New System for Automated Emulsion Data Acquisition and Analysis
Presented at the Conference on Real-Time Computer Application in Nuclear and Particle Physics, Lawrence Berkeley Laboratory, Berkeley, CA, May 15-19, 1983.

ARVIEUX, J. See ROY, R. LBL-16403

AYSTO, J. See WOUTERS, J.M. LBL-13990

BANERJEE, B., N.K. Glendenning, T. Matsui, LBL-15349
Fission of a Chromoelectric Flux Tube and Meson Radiation from a Quark-Gluon Plasma
Phys. Rev. Lett., January 1983

BANERJEE, B., N.K. Glendenning, T. Matsui, LBL-15949
Meson Radiation from Quark-Gluon Plasma by Fission of Chromoelectric Flux Tubes Phys. Lett., April 1983

BANERJEE, B. See GLENDENNING, N.K. LBL-12704

BANERJEE, B. See GLENDENNING, N.K. LBL-15962

BANERJEE, B. See MATSUI, T. LBL-16819

BANTEL, M. See WALD, S. LBL-16899

BARASCH, E. See SHOR, A. LBL-16175

BARNWELL, J.M. See BROWN, J.D. LBL-16965

BAUMGARTNER, M. See SYMONS, T.J.M. LBL-16990

BERMAN, B.L. See OLSON, D.L. LBL-15837

BIRCHALL, J. See BROWN, J.D. LBL-16965

BIRCHALL, J. See OKUMUSOGLU, N.T. LBL-15186

Appendix I Publications

BIRCHALL, J. See ROY, R. LBL-16403

BLOOMER, M.A., E.M. Friedlander, H.H. Heckman, Y.J. Karant, LBL-16487
Search for Relativistic Projectile Fragments with Charges of 4/3, 5/3, 7/3, and 8/3 Phys. Lett. B, August 1983

BLOOMER, M.A., H.H. Heckman, Y.J. Karant, LBL-15246
A Method for Precise Charge Measurements of Relativistic Light Nuclei, $Z < 3$, In Nuclear Track Emulsion
Nuclear Instruments and Methods **215**, 247 (1983).

BOAL, D.H., LBL-16566
The Approach to Chemical Equilibrium in Thermal Models Phys. Rev. C, August 1983

BOAL, D.H., LBL-16538
Fragment Emission and the Lifetime of Pre-equilibrium States Phys. Rev. C, August 1983

BREWER, J.H. See CLAWSON, C.W. LBL-15680

BROCKMANN, R. See RENFORDT, R.E. LBL-16451

BROWN, J.D., J.M. Barnwell, S. Roman, H.E. Conzett, D. Eversheim, R.M. Larimer, J. Birchall, C. Lapointe, J.S.C. McKee, N.M. Clarke, R.J. Griffiths, J.S. Hanspal, R.A. McCulloch, LBL-16965
Separation of Projectile and Ejectile Spin-Orbit Distortions in an ℓ=0 (d, ^{3}He) Reaction
Nucl. Phys. A, November 1983

BROWN, W.L. JR. See ARTHUR, A.A. LBL-16111

BRUCKNER, W. See ANDERSON, L. LBL-14328

BRUCKNER, W. See MOELLER, E. LBL-14329

BUDZANOWSKI, A. See CHAN, Y. LBL-15212

BUDZANOWSKI, A. See STOKSTAD, R.G. LBL-15874

CABLE, M.D., J. Honkanen, R.F. Parry, S.H. Zhou, Z.Y. Zhou, J. Cerny, LBL-15192
Discovery of Beta-Delayed Two-Proton Radioactivity in ^{22}Al and ^{26}P
Presented at the International Workshop XI on Gross Properties of Nuclei and Nuclear Excitation, Hirschegg, Austria, January 17-22, 1983

CABLE, M.D., J. Honkanen, R.F. Parry, S.H. Zhou, Z.Y. Zhou, J. Cerny, LBL-15453
Discovery of Beta-Delayed Two-Proton Radioactivity: ^{22}Al Phys. Rev. Lett. **50**, 404 (1983).

CABLE, M.D., J. Honkanen, R.F. Parry, S.H. Zhou, Z.Y. Zhou, J. Cerny, LBL-15454
Beta-Delayed Proton Decay of the T_z = -2 Isotope, ^{26}P Phys. Lett. **123B**, 25 (1983).

CABLE, MICHAEL DEAN, LBL-15742
Decay of ^{22}Al and ^{26}P: Discovery of Beta-Delayed Two-Proton Radioactivity Ph.D. Thesis, February 1983

CABLE, M.D. See HONKANEN, J. LBL-16606

CABLE, M.D. See NITSCHKE, J.M. LBL-15895

CABLE, M.D. See WOUTERS, J.M. LBL-13990

CARROLL, J. See SHOR, A. LBL-16175

CERNY, J. See CABLE, M.D. LBL-15192

CERNY, J. See CABLE, M.D. LBL-15453

CERNY, J. See CABLE, M.D. LBL-15454

CERNY, J. See HONKANEN, J. LBL-16606

CERNY, J. See WOUTERS, J.M. LBL-13990

CHAN, Y., A. Budzanowski, M. Murphy, R.G. Stokstad, I. Tserruya, S. Wald, LBL-15212
The Onset of Non-equilibrium Phenomena in Fusion-like Processes for ^{16}0 Induced Reactions
Phys. Rev. **C27**, 447 (1983).

CHAN, Y. See SOBOTKA, L.G. LBL-15696

CHAN, Y. See STOKSTAD, R.G. LBL-15874

CHAN, Y.D. See WALD, S. LBL-16899

CHESSIN, S.A., LBL-14262
Pion Production at 180° in Nucleus-Nucleus Collisions Ph.D Thesis, May 1983

CLARK, D.J. LBL-15543
Positive Heavy Ion Sources
To be published as a Chapter in Heavy Ion Science, D.A. Bromley, ed., New York, NY, Plenum Press January 1983

CLARK, D.J., LBL-16327
High Charge State Ion Sources
Presented at the 7th Symposium (1983 International) on Ion Sources and Ion Assisted Technology (ISIAT '83) and the 4th International Conference on Ion and Plasma Assisted Techniques, (IPAT '83), Sakyo-ku, Kyoto, Japan, September 12-16, 1983.

CLARKE, N.M. See BROWN, J.D. LBL-16965

CLAWSON, C.W., K.M. Crowe, S.S. Rosenblum, S.E. Kohn, C.Y. Huang, J.L. Smith, J.H. Brewer, LBL-15680
Low-Temperature Mobility of Positive Muons in Copper Phys. Rev. Lett. **51**, 114 (1983).

Appendix I Publications

CONZETT, H.E., LBL-16383
Spin-Polarization Observables at The J=3/2$^+$ Resonance in The Reactions ^{3}H(d,n)^{4}He and ^{3}He(d,p)^{4}He Presented at the 10th International Conference on Few Body Problems in Physics, Karlsruhe, Germany, August 21-27, 1983.

CONZETT, H.E. See BROWN, J.D. LBL-16965

CONZETT, H.E. See OKUMUSOGLU, N.T. LBL-15186

CONZETT, H.E. See ROY, R. LBL-16403

COUNTRYMAN, P.J. See WALD, S. LBL-16899

CRAWFORD, H.J., LBL-15447
Study of ^{12}C Interactions at HISS
Presented at the Symposium on Detectors in Heavy Ion Physics, Hahn-Meitner Institute für Kernforschung, Berlin, West Germany, October 6-8, 1982

CRAWFORD, H.J., P.J. Lindstrom, LBL-16171
Lulu Analysis Program
Presented at the Conference on Real-Time Computer Application in Nuclear and Particle Physics, Lawrence Berkeley Laboratory, Berkeley, CA, May 15-19, 1983.

CRAWFORD, H.J. See OLSON, D.L. LBL-15837

CRAWFORD, H.J. See SYMONS, T.J.M. LBL-16990

CROWE, K.M. See CLAWSON, C.W. LBL-15680

DANIELEWICZ, P., LBL-15436
Quantum Theory of Nonequilibrium Processes. I Annals of Physics, December 1982

DANIELEWICZ, P., LBL-15437
Quantum Theory of Nonequilibrium Processess. II. Application to Nuclear Collisions
Annals of Physics, December 1982

DANIELEWICZ, P., M. Gyulassy, LBL-15721
Jacobian Free Global Event Analysis Phys. Lett. **129B**, 283 (1983).

DANIELEWICZ, P. See KITAZOE, Y. LBL-16278

DELEPLANQUE, M.A., A.O. Macchiavelli, R.M. Diamond, F.S. Stephens, E.L. Dines, J.E. Draper, LBL-15705
Shell Effects at High Angular Momentum Phys. Rev. Lett., April 1983

DIAMOND, R.M. See DELEPLANQUE, M.A. LBL-15705

DIAMOND, R.M. See WOZNIAK, G.J. LBL-9461

DINES, E.L. See DELEPLANQUE, M.A. LBL-15705

DRAPER, J.E. See DELEPLANQUE, M.A. LBL-15705

DUFOUR, J.P. See SYMONS, T.J.M. LBL-16990

EVERSHEIM, D. See BROWN, J.D. LBL-16965

FAI, G., J. Randrup, LBL-14248
Statistical Simulation of Complete Events in Energetic Nuclear Collisions Nucl. Phys. **A404**, 551 (1983).

FISHER, P. See SHOR, A. LBL-16175

FRANKEL, K. See GYULASSY, M. LBL-15285

FRANKEL, K.A. See RADI, HAFEZ M.A. LBL-13768

FREEDMAN, M. See WARWICK, A.I. LBL-14015

FRIEDLANDER, E.M., H.H. Heckman, Y.J. Karant, LBL-15444
Nuclear Collisions of Uranium Nuclei up to ~1 GeV/Nucleon Phys. Rev. **C27**, 2436 (1983).

FRIEDLANDER, E.M., R.W. Gimpel, H.H. Heckman, Y.J. Karant, B. Judek, E. Ganssauge, LBL-10573
Anomalous Reaction Mean Free Paths of Nuclear Projectile Fragments from Heavy Ion Collisions at 2 AGeV
Phys. Rev. **C27**, 1489 (1983).

FRIEDLANDER, E.M. See ARTHUR, A.A. LBL-16111

FRIEDLANDER, E.M. See BLOOMER, M.A. LBL-16487

FURUTANI, H. See KITAZOE, Y. LBL-16402

GANEZER, K. See SHOR, A. LBL-16175

GANSSAUGE, E. See FRIEDLANDER, E.M. LBL-10573

GHIORSO, A., LBL-16040
Some Reminiscences of the Early Days of Californium
Presented at the Texas Symposium on Particle Induced Desorption Mass Spectrometry Honoring Professor R.D. MacFarlane, College Station, TX, May 15-18, 1983.

GHIORSO, A. See MCFARLAND, R.M. LBL-15529

GIMPEL, R.W. See FRIEDLANDER, E.M. LBL-10573

GIRARD, J. See SYMONS, T.J.M. LBL-16990

GLENDENNING, N.K., B. Banerjee, M. Gyulassy, LBL-12704
Normal and Pion Condensed States in Neutron Star Matter in a Relativistic Field Theory Constrained by Bulk Nuclear Properties I Annals of Physics **149**, 1 (1983).

Appendix I Publications

GLENDENNING, N.K., B. Banerjee, T. Matsui, LBL-15962
Evaporation of Mesons from Quark-Gluon Plasma by Fission of Chromoelectric Flux Tubes
Presented at the International Conference on "High Energy Nuclear Physics," Balatonfüred, Hungary, June 6-11, 1983.

GLENDENNING, N.K., P. Hecking, V. Ruck, LBL-14505
Normal and Pion Condensed States in Neutron Star Matter in a Relativistic Field Theory Constrained by Nuclear Bulk Properties II Annals of Physics **149**, 22 (1983).

GLENDENNING, N.K., T. Matsui, LBL-15957
Creation of $q\bar{q}$ Pair in A Chromoelectric Flux Tube Phys. Lett. **28D**, 2890 (1983).

GLENDENNING, N.K. See BANERJEE, B. LBL-15349

GLENDENNING, N.K. See BANERJEE, B. LBL-15949

GLENDENNING, N.K. See MATSUI, T. LBL-16819

GOODMAN, A.L., J.I. Kapusta, A.Z. Mekjian, LBL-16471
Liquid-gas Phase Instabilities and Droplet Formation in Nuclear Reactions Phys. Rev. C, August 1983

GREINER, D.E. See OLSON, D.L. LBL-15837

GREINER, D.E. See SYMONS, T.J.M. LBL-16990

GRIFFITHS, R.J. See BROWN, J.D. LBL-16965

GROENING, H., K.J. Moody, G.T. Seaborg, LBL-13484
On the Use of Isomer Ratios in ^{44}Sc for Predicting Spin Populations in High Energy Heavy-Ion Nuclear Reactions Nuclear Instruments and Methods **214**, 317 (1983).

GUARINO, G. See SOBOTKA, L.G. LBL-15696

GUSTAFSSON, H.A., H.H. Gutbrod, B. Kolb, B. Ludewigt, A.M. Poskanzer, T. Renner, H. Riedesel, H.G. Ritter, A.I. Warwick, H.H. Wieman, LBL-15791
A Search for Short-Lived Anomalons in Projectile Phys. Rev. Lett. **51**, 363 (1983).

GUSTAFSSON, H.A. See GUTBROD, H.H. LBL-16110

GUSTAFSSON, H.A. See RITTER, H-G. LBL-16469

GUTBROD, H.H., H.A. Gustafsson, B. Kolb, H. Löhner, B. Ludewigt, A.M. Poskanzer, T. Renner, H. Riedesel, H.G. Ritter, A. Warwick, F. Weik, H. Wieman, LBL-16110
4π Data of Relativistic Nuclear Collisions
Presented at the International Topical Meeting on High Energy Nuclear Physics, Balatonfüred, Hungary, June 6-11, 1983

GUTBROD, H.H. See GUSTAFSSON, H.A. LBL-15791

GUTBROD, H.H. See RITTER, H-G. LBL-16469

GUTBROD, H.H. See WARWICK, A.I. LBL-14015

GUTBROD, H.H. See WARWICK, A.I. LBL-16135

GYULASSY, M., LBL-15267
Anomalons, Honey, and Glue in Nuclear Collisions
Invited paper to be presented at NATO Advanced Study Institute, Pearson College, Vancouver Island, B.C., August 23 - September 3, 1982 and to be published in the Plenum Press Proceedings Short-Distance Phenomena in Nuclear Physics, edited by David H. Boal and Richard M. Woloshyn, Plenum Publishing Corporation, pp 237-273 (1983).

GYULASSY, M., LBL-16295
Quark-Gluon Plasma Formation
Presented at the Sixth International Balaton Topical Conference, Balatonfüred, Hungary, June 6-11, 1983.

GYULASSY, M., LBL-16800
Signatures of New Phenomena in Ultrarelativistic Nuclear Collisions
Presented at the Third International Conference on Ultra-Relativistic Nucleus-Nucleus Collisions, Brookhaven National Laboratory, Upton, NY, LBL-September 26-30, 1983 and to be published in Nuclear Physics A. September 26-30, 1983

GYULASSY, M., K. Frankel, E.A. Remler, LBL-15285
Deuteron Formation in Nuclear Collisions Nucl. Phys., November 1982

GYULASSY, M., K. Kajantie, H. Kurki-Suonio, L. Mclerran, LBL-16277
Deflagrations and Detonations as a Mechanism of Hadron Bubble Growth in Supercooled Quark-Gluon Plasmas Nucl. Phys. B, June 1983

GYULASSY, M., T. Matsui, LBL-15947
Quark-Gluon Plasma Evolution in Scaling Hydrodynamics Phys. Rev. D, July 1983

GYULASSY, M. See DANIELEWICZ, P. LBL 15721

GYULASSY, M. See GLENDENNING, N.K. LBL-12704

GYULASSY, M. See KITAZOE, Y. LBL-16278

HANSPAL, J.S. See BROWN, J.D. LBL-16965

HARRIS, J.W. See RENFORDT, R.E. LBL-16451

HARVEY, B., LBL-15565
Are Solitons Already Seen in Heavy Ion Reactions: An Alternative Explanation
Phys. Rev. Lett., February 1983

Appendix I Publications

HARVEY, B.G., H. Homeyer, LBL-16882
An Overlap Model for Fragment Yields in Heavy Ion Reactions Phys. Rev. Lett., November 1983

HARVEY, B.G., M.J. Murphy, LBL-15539 REV.
Dynamics of Heavy Ion Transfer Reactions Phys. Lett. **130B**, 373 (1983).

HARVEY, B.G. See WALD, S. LBL-16899

HAUSTEIN, P.E. See WOUTERS, J.M. LBL-13990

HECKING, P. See GLENDENNING, N.K. LBL-14505

HECKMAN, H.H. See ARTHUR, A.A. LBL-16111

HECKMAN, H.H. See BLOOMER, M.A. LBL-15246

HECKMAN, H.H. See BLOOMER, M.A. LBL-16487

HECKMAN, H.H. See FRIEDLANDER, E.M. LBL-10573

HECKMAN, H.H. See FRIEDLANDER, E.M. LBL-15444

HECKMAN, H.H. See OLSON, D.L. LBL-15837

HENDERSON, D.J. See WARWICK, A.I. LBL-14015

HOMEYER, H. See HARVEY, B.G. LBL-16882

HOMEYER, H. See WALD, S. LBL-16899

HONKANEN, J., M.D. Cable, R.F. Parry, S.H. Zhou, Z.Y. Zhou, J. Cerny, LBL-16606
Beta-Delayed Two-Proton Decay of ^{26}P Phys. Letts. **133B**, 146 (1983).

HONKANEN, J. See CABLE, M.D. LBL-15192

HONKANEN, J. See CABLE, M.D. LBL-15453

HONKANEN, J. See CABLE, M.D. LBL-15454

HUANG, C.Y. See CLAWSON, C.W. LBL-15680

HUBEL, H. See WOZNIAK, G.J. LBL-9461

IGO, G. See SHOR, A. LBL-16175

JACAK, B.V., W. Loveland, P.L. Mcgaughey, D.J. Morrissey, G.T. Seaborg, LBL-15286
Heavy Target Fragment Yields in the Interaction of 28 GeV Protons with ^{238}U
Canadian Journal of Chemistry **61**, 701 (1983).

JONES, R.W. See ARTHUR, A.A. LBL-16111

JUDEK, B. See FRIEDLANDER, E.M. LBL-10573

KAJANTIE, K. See GYULASSY, M. LBL-16277

KAPUSTA, J.I. See GOODMAN, A.L. LBL-16471

KARANT, Y.J. See ARTHUR, A.A. LBL-16111

KARANT, Y.J. See BLOOMER, M.A. LBL-15246

KARANT, Y.J. See BLOOMER, M.A. LBL-16487

KARANT, Y.J. See FRIEDLANDER, E.M. LBL-10573

KARANT, Y.J. See FRIEDLANDER, E.M. LBL-15444

KAUFMAN, S.B. See WARWICK, A.I. LBL-14015

KAUFMAN, S.B. See WARWICK, A.I. LBL-16135

KAZEMINZHAD, F. See SHOR, A. LBL-16175

KITAZOE, Y., M. Gyulassy, P. Danielewicz, H. Toki, Y. Yamamura, M. Sano, LBL-16278
New Cascade Model Calculation of Pion Multiplicity in High-Energy Heavy-Ion Collisions
Phys. Lett. B, July 1983

KITAZOE, Y., M. Sano, Y. Yamamura, H. Furutani, K. Yamamoto, LBL-16402
A Cascade-Model Analysis of Collective Motion in Relativistic Nuclear Collisions
Phys. Rev. C, August 1983

KO, C.M. See RANDRUP, J. LBL-16316

KOHN, S.E. See CLAWSON, C.W. LBL-15680

KOLB, B., LBL-16128
LISA An On- and Off-Line Data Analyzing Program
Presented at the Conference on Real-Time Computer Application in Nuclear and LBL-Particle Physics, Lawrence Berkeley Laboratory, Berkeley, CA, May 15-19, 1983 and to be published in the Proceedings LBL-Particle Physics, Lawrence Berkeley Laboratory, Berkeley, CA, May 15-19, 1983

KOLB, B. See GUSTAFSSON, H.A. LBL-15791

KOLB, B. See GUTBROD, H.H. LBL-16110

KOLB, B. See RITTER, H-G. LBL-16469

KURKI-SUONIO, H. See GYULASSY, M. LBL-16277

LAMONTAGNE, C.R. See ROY, R. LBL-16403

LANZA, E.G. See MORETTO, L.G. LBL-16373

Appendix I Publications

LAPOINTE, C. See BROWN, J.D. LBL-16965

LAPOINTE, C. See OKUMUSOGLU, N.T. LBL-15186

LARIMER, R.M. See BROWN, J.D. LBL-16965

LARIMER, R.M. See OKUMUSOGLU, N.T. LBL-15186

LEE, D. See LIU, Y.-F. LBL-16542

LINDSTROM, P.J. See CRAWFORD, H.J. LBL-16171

LINDSTROM, P.J. See OLSON, D.L. LBL-15837

LINDSTROM, P.J. See SYMONS, T.J.M. LBL-16990

LIU, Y.-F., K.J. Moody, D. Lee, Y. Morita, G.T. Seaborg, H.R. von Gunten, LBL-16542
The Decay of ^{251}Bk Nucl. Phys. A, August 1983

LOVELAND, W. See JACAK, B.V. LBL-15286

LOVELAND, W. See MORITA, Y. LBL-16271

LOHNER, H. See GUTBROD, H.H. LBL-16110

LOHNER, H. See RITTER, H-G. LBL-16469

LUDEWIGT, B. See GUSTAFSSON, H.A. LBL-15791

LUDEWIGT, B. See GUTBROD, H.H. LBL-16110

LUDEWIGT, B. See RITTER, H-G. LBL-16469

MACCHIAVELLI, A.O. See DELEPLANQUE, M.A. LBL-15705

MAIER, M. See RENFORDT, R.E. LBL-16451

MAIER, M.R. See WARWICK, A.I. LBL-14015

MATHEWS, G.J. See WOZNIAK, G.J. LBL-9461

MATSUI, T., LBL-16063
On The Coulomb Sum Rule in The Relativistic Nuclear Many-Body Problem Phys. Lett. **132B**, 260 (1983).

MATSUI, T., B. Banerjee, N.K. Glendenning, LBL-16819
Meson Radiation from Quark-Gluon Plasma
Presented at the Conference on Manifestations of Hadron Substructure in Nuclear Physics, Bloomington, IN, October 19-21, 1983.

MATSUI, T. See BANERJEE, B. LBL-15349

MATSUI, T. See BANERJEE, B. LBL-15949

MATSUI, T. See GLENDENNING, N.K. LBL-15957

MATSUI, T. See GLENDENNING, N.K. LBL-15962

MATSUI, T. See GYULASSY, M. LBL-15947

MCCULLOCH, R.A. See BROWN, J.D. LBL-16965

MCDONALD, R.J. See SOBOTKA, L.G. LBL-14940

MCFARLAND, R.M., A. Ghiorso, G.T. Seaborg, LBL-15529
Recoil Range Studies of Heavy Products of Multinucleon Transfer from $^{18}0$ to ^{245}Cm and ^{249}Cf
Phys. Rev. C, February 1983

MCGAUGHEY, P.L. See JACAK, B.V. LBL-15286

MCGAUGHEY, PATRICK LEE, LBL-15325
Intermediate and High Energy Reactions of Uranium with Neon and Carbon Ph D thesis, November 1982

MCHARRIS, W.C., J.O. Rasmussen, LBL-14075
Anomalons as Pineuts Bound to Nuclear Fragments: A Possible Explanation Phys. Lett. **120B**, 49 (1983).

MCKEE, J.S.C. See BROWN, J.D. LBL-16965

MCKEE, J.S.C. See OKUMUSOGLU, N.T. LBL-15186

MCLERRAN, L. See GYULASSY, M. LBL-16277

MCPARLAND, C., LBL-16148
Data Acquisition at the Bevalac, An Example: The HISS Facility
Presented at the Conference on Real-Time Computer Application in Nuclear and Particle Physics, Lawrence Berkeley Laboratory, Berkeley, CA, May 15-19, 1983.

MEKJIAN, A.Z. See GOODMAN, A.L. LBL-16471

MOELLER, E., L. Anderson, W. Bruckner, S. Nagamiya, S. Nissen-Meyer, L. Schroeder, G. Shapiro, H. Steiner, LBL-14329
Inclusive Particle Production at Forward Angles From Collisions of Light Relativistic Nuclei, Part II: Negative Pions Phys. Rev. **C28**, 1246 (1983).

MOELLER, E. See ANDERSON, L. LBL-14328

MOODY, K.J., LBL-16249
Actinide Production in The Reaction of Heavy Ions with Curium-248 Ph.D. Thesis, July 1983

MOODY, K.J. See GROENING, H. LBL-13484

Appendix I Publications

MOODY, K.J. See LIU, Y.-F. LBL-16542

MORETTO, L.G., LBL-15210
Multifragmentation and the Partition of Angular Momentum, A General Statistical Theory
Nucl. Phys. A, October 1982

MORETTO, L.G., LBL-15211
Energy Equilibration and Anomalous Mass Drift in Heavy Ion Collisions
Z. Phys. A - Atoms and Nuclei **310**, 61 (1983).

MORETTO, L.G., LBL-16371
New Statistical and Non-Statistical Effects in Deep Inelastic Heavy Ion Collisions
Presented at the International Symposium on Nuclear Physics at Large Tandem Accelerators, Legnaro-Padova, Italy, March 15-17, 1983

MORETTO, L.G., LBL-16372
The Phenomenology of Deep-Inelastic Processes
Presented at the International Conference on Heavy Ion Physics and Nuclear Physics, Catania, Italy, March 21-26, 1983.

MORETTO, L.G., LBL-16390
Statistical Properties of Deep Inelastic Reactions
Presented at the International Conference on Nuclear Physics, Florence, Italy, August 29- September 3, 1983

MORETTO, L.G., E.G. Lanza, LBL-16373
A Feedback Process Controlling Energy Partition and Mass Exchange Between Heavy Ions June 1983

MORETTO, L.G. See SOBOTKA, L.G. LBL-14940

MORETTO, L.G. See SOBOTKA, L.G. LBL-15696

MORETTO, L.G. See WOZNIAK, G.J. LBL-9461

MORITA, Y., LBL-16136
Angular Distributions of Target Fragments from The Reactions of 292 MeV - 25.2 GeV ^{12}C with ^{197}Au and ^{238}U Ph.D Thesis, May 1983

MORITA, Y. See LIU, Y.-F. LBL-16542

MORITA, Y., W. Loveland, G.T. Seaborg, LBL-16271
Target Fragment Angular Distributions for the Interaction of 25.2 GeV ^{12}C with ^{197}Au
Phys. Rev. C, June 1983

MORRISSEY, D.J. See JACAK, B.V. LBL-15286

MORRISSEY, D.J. See SOBOTKA, L.G. LBL-14940

MULERA, T. See SHOR, A. LBL-16175

MURPHY, D. See RASMUSSEN, J.O. LBL-15283

MURPHY, M.J., R.G. Stokstad, LBL-15188
REV. Momentum Widths of Heavy-Ion Reaction Products at 27.4 MeV/n Phys. Rev. **C28**, 428 (1983).

MURPHY, M. See CHAN, Y. LBL-15212

MURPHY, M. See STOKSTAD, R.G. LBL-15874

MURPHY, M.J. See HARVEY, B.G. LBL-15539 REV.

MURPHY, M.J. See WALD, S. LBL-16899

MYERS, W.D., K-H. Schmidt, LBL-15446
An Update on Droplet Model Charge Distributions Nucl. Phys. **A410**, 61 (1983).

NAGAMIYA, S. See ANDERSON, L. LBL-14328

NAGAMIYA, S. See MOELLER, E. LBL-14329

NISSEN-MEYER, S. See ANDERSON, L. LBL-14328

NISSEN-MEYER, S. See MOELLER, E. LBL-14329

NITSCHKE, J.M., LBL-15894
The Application of Alpha Spectrometry to The Discovery of New Elements by Heavy-Ion Beam Bombardment Presented at the International Symposium on Alpha Particle and Low Level Measurement, Harwell, England, May 10-13, 1983 and to be published in the Nuclear Instruments and Methods

NITSCHKE, J.M., M.D. Cable, W-D. Zeitz, LBL-15895
New Beta-Delayed Proton Emitters in the Lanthanide Region Zeitschrift für Physik, May 1983

OKUMUSOGLU, N.T., J. Birchall, M.S.A.L. Al-Ghazi, C. Lapointe, J.S.C. Mckee, H.E. Conzett, R.M. Larimer, P. Von Rossen, LBL-15186
The Elastic Scattering of Polarised Protons by ^{40}Ar Nucl. Phys. A, October 1982

OLSON, D.L., B.L. Berman, D.E. Greiner, H.H. Heckman, P.J. Lindstrom, H.J. Crawford, LBL-15837
Factorization of Fragment-Production Cross Sections in Relativistic Heavy-Ion Collisions
Phys. Rev. **C28**, 1602 (1983).

OLSON, D.L. See SYMONS, T.J.M. LBL-16990

PACHECO, A.J. See SOBOTKA, L.G. LBL-14940

PACHECO, A.J. See SOBOTKA, L.G. LBL-15696

PADGETT, M.L. See SOBOTKA, L.G. LBL-15696

Appendix I Publications

PARRY, ROGER FRANKLIN, LBL-15875
Beta Decay Measurements of Neutron Deficient Cesium Isotopes Ph.D Thesis, March 1983

PARRY, R.F. See CABLE, M.D. LBL-15192

PARRY, R.F. See CABLE, M.D. LBL-15453

PARRY, R.F. See CABLE, M.D. LBL-15454

PARRY, R.F. See HONKANEN, J. LBL-16606

PARRY, R.F. See WOUTERS, J.M. LBL-13990

PEREZ-MENDEZ, V. See SHOR, A. LBL-16175

PETER, J. See WARWICK, A.I. LBL-14015

POSKANZER, A.M. See GUSTAFSSON, H.A. LBL-15791

POSKANZER, A.M. See GUTBROD, H.H. LBL-16110

POSKANZER, A.M. See RITTER, H-G. LBL-16469

PUGH, H.G. See RENFORDT, R.E. LBL-16451

RADI, HAFEZ M.A., K.A. Frankel, J.O. Rasmussen, H.C. Song, J.P. Sullivan, LBL-13768
Monte Carlo Studies of Pion Distribution from Heavy Ion Collisions Phys. Rev. **C27**, 606 (1983).

RADI, H.M.A. See RASMUSSEN, J.O. LBL-15283

RANDRUP, J., LBL-15838
Transport Description of Damped Nuclear Reactions
Presented at the Nordic Winter School on Nuclear Physics, Hemsedal, Norway, April 10-20, 1983.

RANDRUP, J., LBL-15877
Statistical Calculation of Complete Events in Medium-Energy Nuclear Collisions
Presented at the Nordic Winter School on Nuclear Physics, Hemsedal, Norway, April 10-20, 1983

RANDRUP, J., C.M. Ko, LBL-16316
Revision of Calculations for Kaon Production in Relativistic Nuclear Collisions Nucl. Phys. A, June 1983

RANDRUP, J. See FAI, G. LBL-14248

RASMUSSEN, J.O., LBL-14956
Heavy Ion Pion Production: Spectral Irregularities
Presented at the International Conference on Nucleus-Nucleus Collisions, Michigan State University, East Lansing, MI, September 26 – October l, 1982, Nucl. Phys. **A400**, 383c (1983).

RASMUSSEN, J.O., LBL-15284
Charge-exchange Products of Bevalac Projectiles
Presented at the Conference on High-Energy Physics with Nuclear Emulsion, Cairo, Egypt, November 22-29, 1982

RASMUSSEN, J.O., J. Ridout, D. Murphy, H.M.A. Radi, LBL-15283
Spectator-Velocity Pions from Heavy Ions Presented at the Conference on High-Energy Physics with Nuclear Emulsion, Cairo, Egypt, November 11-29, 1982

RASMUSSEN, J.O. See MCHARRIS, W.C. LBL-14075

RASMUSSEN, J.O. See RADI, HAFEZ M.A. LBL-13768

REGIMBART, R. See WOZNIAK, G.J. LBL-9461

REMLER, E.A. See GYULASSY, M. LBL-15285

RENFORDT, R.E., R. Brockmann, J.W. Harris, M. Maier, F. Riess, A. Sandoval, R. Stock, H. Ströbele, K.L. Wolf, H.G. Pugh, L.S. Schroeder, N. Schall, K. Tittel, LBL-16451
Search for Flow in the Reaction Ar + Pb
Presented at the Sixth High Energy Heavy Ion Study and Second Workshop on Anomalons, Lawrence Berkeley Laboratory, Berkeley, CA June 28 - July 1, 1983

RENNER, T. See GUSTAFSSON, H.A. LBL-15791

RENNER, T. See GUTBROD, H.H. LBL-16110

RENNER, T.R. See RITTER, H-G. LBL-16469

RIDOUT, J. SeeRASMUSSEN, J.O. LBL-15283

RIEDESEL, H. See GUTBROD, H.H. LBL-16110

RIEDESEL, H. See RITTER, H-G. LBL-16469

RIEDESEL, H. SeeGUSTAFSSON, H.A. LBL-15791

RIESS, F. See RENFORDT, R.E. LBL-16451

RITTER, H-G., H.A. Gustafsson, H.H. Gutbrod, B. Kolb, H. Löhner, B. Ludewigt, A.M. Poskanzer, T.R. Renner, H. Riedesel, A. Warwick, F. Weik, H. Wieman, LBL-16469
Results Obtained Using the Plastic Ball
Presented at the Sixth High Energy Heavy Ion Study and Second Workshop on Anomalons, Lawrence Berkeley Laboratory, Berkeley, CA June 28 - July 1, 1983

RITTER, H.G. See GUSTAFSSON, H.A. LBL-15791

RITTER, H.G. See GUTBROD, H.H. LBL-16110

RITTER, H.G. See WARWICK, A.I. LBL-14015

Appendix I Publications

RITTER, H.G. See WARWICK, A.I. LBL-16135

ROMAN, S. See BROWN, J.D. LBL-16965

ROSENBLUM, S.S. See CLAWSON, C.W. LBL-15680

ROY, R., C.R. Lamontagne, R.J. Slobodrian, J. Arvieux, J. Birchall, H.E. Conzett, LBL-16403
Diffusion des Protons Polarises sur ^{24}Mg, ^{27}Al et ^{32}S et Anomalies Dans la Region des Resonances Geantes de L' ^{25}Al, du ^{28}Si et du ^{33}Cl Nucl. Phys. A, July 1983

RUCK, V. See GLENDENNING, N.K. LBL-14505

SANDOVAL, A. See RENFORDT, R.E. LBL-16451

SANO, M. See KITAZOE, Y. LBL-16278

SANO, M. See KITAZOE, Y. LBL-16402

SCHALL, D. See RENFORDT, R.E. LBL-16451

SCHMIDT, K-H. See MYERS, W.D. LBL-15446

SCHMITT, R.P. See WOZNIAK, G.J. LBL-9461

SCHROEDER, L.S., LBL-16835
High Energy Nuclear Beams at Berkeley - Present and Future Possibilities
Presented at the Third International Conference on Ultra-Relativistic Nucleus-Nucleus Collisions (Quark Matter '83), Brookhaven National Laboratory, Upton, NY, September 26-29, 1983 and to be published in the proceedings

SCHROEDER, L. See ANDERSON, L. LBL-14328

SCHROEDER, L. See MOELLER, E. LBL-14329

SCHROEDER, L.S. See RENFORDT, R.E. LBL-16451

SEABORG, G.T., LBL-15685
Nuclear Reactions and Synthesis of New Transuranium Species
Presented at a workshop on Future Directions in Transplutonium Element Research, Washington, DC, February 28 - March 2, 1983.

SEABORG, G.T. See GROENING, H. LBL-13484

SEABORG, G.T. See JACAK, B.V. LBL-15286

SEABORG, G.T. See LIU, Y.-F. LBL-16542

SEABORG, G.T. See MCFARLAND, R.M. LBL-15529

SEABORG, G.T. See MORITA, Y. LBL-16271

SHAPIRO, G. See ANDERSON, L. LBL-14328

SHAPIRO, G. See MOELLER, E. LBL-14329

SHOR, A., J. Carroll, E. Barasch, S. Abachi, V. Perez-Mendez, T. Mulera, P. Fisher, G. Igo, S. Trentalange, K. Ganezer, F. Kazeminzhad, LBL-16175
Subthreshold K^- Production in Nucleus-Nucleus Collisions
Presented at the Sixth High Energy Heavy Ion Study and Second Workshop on Anomalons, Lawrence Berkeley Laboratory, Berkeley, CA June 28 - July 1, 1983.

SLOBODRIAN, R.J. See ROY, R. LBL-16403

SMITH, J.L. See CLAWSON, C.W. LBL-15680

SOBOTKA, L.G., M.L. Padgett, G.J. Wozniak, G. Guarino, A.J. Pacheco, L.G. Moretto, Y. Chan, R.G. Stokstad, I. Tserruya, S. Wald, LBL-15696
Compound Nucleus Decay Via The Emission of Large Fragments Phys. Rev. Lett., July 1983

SOBOTKA, L.G., R.J. Mcdonald, G.J. Wozniak, D.J. Morrissey, A.J. Pacheco, L.G. Moretto, LBL-14940
Alpha-Particle Emission from The Reaction 1354 MeV ^{165}Ho + ^{181}Ta Phys. Rev. **C28**, 219 (1983).

SONG, H.C. See RADI, HAFEZ M.A. LBL-13768

STEINBERG, E.P. See WARWICK, A.I. LBL-14015

STEINBERG, E.P. See WARWICK, A.I. LBL-16135

STEINER, H. See ANDERSON, L. LBL-14328

STEINER, H. See MOELLER, E. LBL-14329

STELZER, H. See WARWICK, A.I. LBL-14015

STELZER, H. See WARWICK, A.I. LBL-16135

STEPHENS, F.S. See DELEPLANQUE, M.A. LBL-15705

STEPHENS, F.S., LBL-15070
Properties of Nuclei at High Spins
Presented at the Nordic Meeting on Nuclear Physics, Fuglsø, Denmark, August 16-20, 1982 and published in Physica Scripta **T5**, 5 (1983).

STEPHENS, F.S., LBL-15282
Future Directions for High-Spin Studies
Presented at the Conference on High Angular Momentum Properties of Nuclei, Oak Ridge, TN, November 2-4, 1982

STOCK, R. See RENFORDT, R.E. LBL-16451

Appendix I Publications

STOKSTAD, R.G., Y. Chan, M. Murphy, I. Tserruya, S. Wald, A. Budzanowski, LBL-15874
The Onset of Incomplete Momentum Transfer in Fusion-Like Processes
Presented at the Sixth Oaxtepec Symposium, Institute of Physics of the University of Mexico, Mexico City, Mexico, January 4-7, 1983

STOKSTAD, R.G. See CHAN, Y. LBL-15212

STOKSTAD, R.G. See MURPHY, M.J. LBL-15188 REV.

STOKSTAD, R.G. See SOBOTKA, L.G. LBL-15696

STOKSTAD, R.G. See WALD, S. LBL-16899

STROEBELE, H. See RENFORDT, R.E. LBL-16451

SULLIVAN, J.P. See RADI, HAFEZ M.A. LBL-13768

SWIATECKI, W.J., LBL-11403
Note on Nuclear Disintegration Widths Submitted to the Australian Journal of Physics, May 1983

SYMONS, T.J.M., M. Baumgartner, J.P. Dufour, J. Girard, D.E. Greiner, P.J. Lindstrom, D.L. Olson, H.J. Crawford, LBL-16990
Charge-Changing Reactions of Secondary Fragments Produced in High-Energy Heavy Ion Collisions
Phys. Rev. Lett., November 1983

THIERENS, H.M. See WOUTERS, J.M. LBL-13990

TITTEL, K. See RENFORDT, R.E. LBL-16451

TOKI, H. See KITAZOE, Y. LBL-16278

TRENTALANGE, S. See SHOR, A. LBL-16175

TSERRUYA, I. See CHAN, Y. LBL-15212

TSERRUYA, I. See SOBOTKA, L.G. LBL-15696

TSERRUYA, I. See STOKSTAD, R.G. LBL-15874

TSERRUYA, I. See WALD, S. LBL-16899

TURNEY, A.D. See ARTHUR, A.A. LBL-16111

VAN BIBBER, K. See WALD, S. LBL-16899

VON GUNTEN, H.R. See LIU, Y.-F. LBL-16542

VON ROSSEN, P. See OKUMUSOGLU, N.T. LBL-15186

WALD, S., C.R. Albiston, M. Bantel, Y.D. Chan, B.G. Harvey, M.J. Murphy, I. Tserruya, R.G. Stokstad, P.J. Countryman, K. Van Bibber, H. Homeyer, LBL-16899
Identification of Complete Charge Transfer Reactions for $^{20}Ne + ^{197}Au$ with A 4π Detector
Phys. Rev. Lett., November 1983

WALD, S. See CHAN, Y. LBL-15212

WALD, S. See SOBOTKA, L.G. LBL-15696

WALD, S. See STOKSTAD, R.G. LBL-15874

WARWICK, A.I., H.H. Wieman, H.H. Gutbrod, H.G. Ritter, H. Stelzer, F. Weik, S.B. Kaufman, E.P. Steinberg, B.D. Wilkins, LBL-16135
Aspects of Data on the Breakup of Highly Excited Nuclei Presented at the International Topical Meeting on "High Energy Nuclear Physics," Sixth International Balaton Topical Conference, Balatonfüred, LBL-Hungary, June 6-ll, 1983 and the Sixth High Energy Heavy Ion Study and second Workshop on Anomalons, Lawrence Berkeley Laboratory, Berkeley, CA June 28-July 1, 1983

WARWICK, A.I., Wieman, H.H., Gutbrod, H.H., Maier, M.R., Peter, J., Ritter, H.G., Stelzer, H., Weik, F., Freedman, M., Henderson, D.J., Kaufman, S.B., Steinberg, E.P., Wilkins, B.D., LBL-14015
The Breakup of Spectator Residues in Relativistic Nuclear Collisions Phys. Rev. **C27**, 1083 (1983).

WARWICK, A. See GUTBROD, H.H. LBL-16110

WARWICK, A. See RITTER, H-G. LBL-16469

WARWICK, A.I. See GUSTAFSSON, H.A. LBL-15791

WEIK, F. See GUTBROD, H.H. LBL-16110

WEIK, F. See RITTER, H-G. LBL-16469

WEIK, F. See WARWICK, A.I. LBL-14015

WEIK, F. See WARWICK, A.I. LBL-16135

WIEMAN, H. See GUTBROD, H.H. LBL-16110

WIEMAN, H. See RITTER, H-G. LBL-16469

WIEMAN, H.H. See GUSTAFSSON, H.A. LBL-15791

WIEMAN, H.H. See WARWICK, A.I. LBL-14015

WIEMAN, H.H. See WARWICK, A.I. LBL-16135

WILKINS, B.D. See WARWICK, A.I. LBL-14015

WILKINS, B.D. See WARWICK, A.I. LBL-16135

WOLF, K.L. See RENFORDT, R.E. LBL-16451

Appendix I Publications

WOUTERS, J.M., J. Äystö, M.D. Cable, J. Cerny, P.E. Haustein, R.F. Parry, H.M. Thierens, LBL-13990
Beta Decay Energies and Masses of $^{103-105}$ Phys. Rev. **C27**, 1745 (1983).

WOZNIAK, G.J., G.J. Mathews, R.P. Schmitt, R. Regimbart, H. Hübel, R.M. Diamond, L.G. Moretto, LBL-9461
A Study of Charge, Energy and Angular Momentum Transfer in the ^{56}Fe + ^{197}Au and ^{56}Fe + ^{107,109}Ag Reactions at 7.2 and 8.3 Mev/Nucleon Nucl. Phys. **A402**, 322 (1983).

WOZNIAK, G.J. See SOBOTKA, L.G. LBL-14940

WOZNIAK, G.J. See SOBOTKA, L.G. LBL-15696

YAMAMOTO, K. See KITAZOE, Y. LBL-16402

YAMAMURA, Y. See KITAZOE, Y. LBL-16278

YAMAMURA, Y. See KITAZOE, Y. LBL-16402

ZEITZ, W-D. See NITSCHKE, J.M. LBL-15895

ZHOU, S.H. See CABLE, M.D. LBL-15192

ZHOU, S.H. See CABLE, M.D. LBL-15453

ZHOU, S.H. See CABLE, M.D. LBL-15454

ZHOU, S.H. See HONKANEN, J. LBL-16606

ZHOU, Z.Y. See CABLE, M.D. LBL-15192

ZHOU, Z.Y. See CABLE, M.D. LBL-15453

ZHOU, Z.Y. See CABLE, M.D. LBL-15454

ZHOU, Z.Y. See HONKANEN, J. LBL-16606

Decays of ^{22}Al and ^{26}P: Discovery of Beta-delayed Two-proton Radioactivity

Michael Dean Cable

A helium jet system and the ^{24}Mg(^{3}He,p4n)^{22}Al and ^{28}Si(^{3}He,p4n)^{26}P reactions have been used to discover the only known odd-odd, $T_Z = -2$ nuclides, ^{22}Al($t_{1/2}\sim$70ms) and ^{26}P($t_{1/2}\sim$20ms). Observation of beta-delayed protons from each isotope (laboratory energies 7.839±0.015 MeV and 8.149±0.021 MeV for ^{22}Al and 7.269±0.015 MeV and 6.827±0.050 MeV for ^{26}P) established the existence of these nuclides and provided a measurement of the mass excesses of the lowest T = 2 states in their beta decay daughters, ^{22}Mg and ^{26}Si (13.650±0.015 MeV and 5.963±0.015 MeV, respectively). Measurement of these masses confirmed that these T = 2 states were unbound to two-proton emission as had been predicted theoretically.

Subsequent proton-proton coincidence experiments, with a specially constructed three-element (ΔE1, ΔE2, E) semiconductor particle telescope capable of simultaneously identifying and measuring proton energies of two protons, enabled observation of the previously unknown decay mode of beta-delayed two-proton emission for each isotope. Two-proton sum energies observed in the decay of ^{22}Al (laboratory energies 5.636 MeV and 4.139 MeV) correspond to transitions from ^{22}Mg* ($J^{\pi}=4^{+}$, fed by the superallowed beta decay of ^{22}Al) to the ground state ($J^{\pi}=0^{+}$) and first excited state ($J^{\pi}=2^{+}$) of ^{20}Ne. ^{26}P decay produces an observed two-proton sum group (laboratory energy 4.927 MeV) corresponding to the transition from ^{26}Si* ($J^{\pi}=3^{+}$, fed by the superallowed beta decay of ^{26}P) to the ground state ($J^{\pi}=0^{+}$) of ^{24}Mg. Possible mechanisms for two-proton emission are discussed and compared with observed two-proton data. The ^{22}Al decay can not be fully characterized and may consist of components of both ^{2}He and sequential proton emission. The ^{26}P decay observed, however, is spin-parity forbidden to be ^{2}He ($J^{\pi}=0^{+}$) emission and exhibits the expected decay mechanism of sequential emission of two protons.

Beta Decay Measurements of Neutron Deficient Cesium Isotopes

Roger Franklin Parry

The study of nuclei far from beta stability provides information on nuclear binding energies and nuclear structure. However, as one progresses away from the valley of stability, the associated half-lives and production cross-sections decrease with increasing interference from the decays of adjacent nuclei. An experimental solution to these problems was the use of the He-jet fed on-line mass separator, RAMA. This instrument provided a fast and selective technique for the mass separation necessary for the investigation of exotic nuclei. Using this device, a beta decay Q-value study of the neutron deficient cesium isotopes, $^{119\text{-}123}$Cs, was conducted.

Beta decay endpoint energy measurements of the neutron deficient cesium isotopes were done using an energy spectrum shape fitting technique. This was a departure from the typical method of endpoint energy analysis, the Fermi-Kurie plot. A discussion of the shape fitting procedure and its improved features are discussed.

These beta endpoint measurements have led to total decay energies (Q_{EC}) of the neutron deficient $^{119\text{-}123}$Cs isotopes. The total decay energies of ^{122m}Cs (Q_{EC} = 6.95 ± 0.25 MeV) and ^{119}Cs (Q_{EC} = 6.26 ± 0.29 MeV) were new measurements. The total decay energies of ^{123}Cs (Q_{EC} = 4.05 ± 0.18 MeV),

^{122g}Cs (Q_{EC} = 7.05 ± 0.18 MeV), ^{121}Cs (Q_{EC} = 5.21 ± 0.22 MeV), and ^{120}Cs (Q_{EC} = 7.38 ± 0.23 MeV) were measurements with significantly improved uncertainties as compared to the literature. Further, a combination of the energy levels derived from previous literature gamma-gamma coincident measurements and the experimental beta-coincident gamma decay energies has supported an improved level scheme for ^{121}Xe and the proposal of three new energy levels in ^{119}Xe.

Comparison of the experimental cesium mass excesses (determined with our Q_{EC} values and known xenon mass excesses) with both the literature and theoretical predicted values showed general agreement except for ^{120}Cs. This isotope displayed a deviation of ~800 keV in both comparisons with the experimental value. Possible explanations for this deviation are discussed.

Pion Production at 180° in Nucleus-Nucleus Collisions

Stephen Alan Chessin

A survey experiment of pion production at 180° in nucleus-nucleus collisions is presented. Beams of 1.05 GeV/A and 2.1 GeV/A protons, alphas, and carbon were used as well as proton beams of 0.80 GeV, 3.5 GeV, and 4.89 GeV, and argon beams of 1.05 GeV/A and 1.83 GeV/A. This is the first such experiment to use the heavier beams. Targets used ranged from carbon to lead. An in-depth review of the literature, both experimental and theoretical, is also presented. The systematics of the data are discussed, and comparisons are made both with prior experiments and with the predictions of the models reviewed. The cross sections appear consistent with a simple single nucleon-nucleon collision picture, without the need for collective or other exotic effects. Suggestions for future work are made.

Angular Distributions of Target Fragments from The Reactions of 292 MeV – 25.2 GeV ^{12}C with ^{197}Au and ^{238}U

Y. Morita

Angular distributions of target fragments from the reactions of ^{12}C with ^{197}Au and ^{238}U were measured at projectile energies of 292 MeV, 1.0 GeV, 3.0 GeV, 12.0 GeV and 25.2 GeV. The angular distributions of the ^{197}Au target fragments were all forwardly peaked. Extensively forward peaked angular distributions were observed at the non-relativistic projectile energies (292 MeV, 1.0 GeV). No obvious differences were observed in the angular distributions at the different relativistic projectile energies of 3.0 GeV, 12.0 GeV and 25.2 GeV. The characteristic angular distribution pattern from the relativistic projectile energy experiments was also observed in the non-relativistic energy experiments. Maximum degree of forward-peaking in the angular distributions at each projectile energy was observed at the product mass number (A) around 190 from the 292 MeV projectile energy, at A = 180 from 1.0 GeV and

at A = 175 from 3.0 GeV and 12.0 GeV. In general, two different types of angular distributions were observed in the relativistic projectile energy experiments with the ^{238}U target. Isotropic angular distributions were observed for the fission product nuclides. The angular distributions of the fission products at the intermediate (292 MeV) energy showed slightly forward-peaked angular distributions. Because of the long projectile-target interaction time in the primary nuclear reactions, larger momentum was transferred from the projectile to the target nucleus. Steep forward-peaked angular distributions were also observed with the ^{238}U target. The reaction to produce the steep forward-peaked angular distributions with the ^{238}U target was the same as the one operating with the ^{197}Au target at the relativistic projectile energies. An interesting feature of the angular distribution was some favoring of sideward emission at the large angle for the light products from the reaction of 25.2 GeV ^{12}C + ^{238}U in comparison with the 12.0 GeV and 3.0 GeV projectile energy results.

Computations were attempted to estimate the basic properties of the target fragments for the reaction of the 3.0 GeV ^{12}C projectile with the ^{197}Au target using two different assumptions. In the first assumption, proton-proton elastic scattering experimental results were applied and the nucleons of the projectile and target nucleus were treated as completely free nucleons. The computation gave the side peaked angular distributions at all impact parameters. The other assumption was to treat the abraded volume of the target nucleus as a collective volume and to use the nuclear potential energy between the abraded volume and the residual target volume for computations of the recoil energies of the target fragments. The estimated recoil energies of the heavy products based on the second assumption had a trend consistent with the experimental data.

Actinide Production in the Reaction of Heavy Ions with Curium-248

K.J. Moody

Chemical experiments were performed to examine the usefulness of heavy ion transfer reactions in producing new, neutron-rich actinide nuclides. A general quasi-elastic to deep-inelastic mechanism is proposed, and the utility of this method as opposed to other methods (e.g., complete fusion) is discussed.

The relative merits of various techniques of actinide target synthesis are discussed. A description is given of a target system designed to remove the large amounts of heat generated by the passage of a heavy ion beam through matter, thereby maximizing the beam intensity which can be safely used in an experiment. Also described is a general separation scheme for the actinide elements from protactinium (Z=91) to mendelevium (Z=101), and fast specific procedures for plutonium, americium and berkelium.

The cross sections for the production of several nuclides from the bombardment of ^{248}Cm with ^{18}O, ^{86}Kr and ^{136}Xe projectiles at several energies near and below the Coulomb barrier were determined. The results are compared with yields from ^{48}Ca and ^{238}U bombardments of ^{248}Cm. Simple extrapolation of the product yields into unknown regions of charge and mass indicates that the use of heavy ion transfer reactions to produce new, neutron-rich above-target species is limited. The substantial production of neutron-rich below-target species, however, indicates that with very heavy ions like ^{136}Xe and ^{238}U the new species ^{248}Am, ^{249}Am and ^{247}Pu should be produced with large cross section from a ^{248}Cm target.

A preliminary, unsuccessful attempt to isolate ^{247}Pu is outlined. The failure is probably due to the half life of the decay, which is calculated to be less than 3 minutes. The absolute gamma ray intensities from ^{251}Bk decay, necessary for calculating the ^{251}Bk cross section, are also determined.

Monday Seminars

October 4, 1982	P. Schuck ILL, Grenoble	A Boltzmann Equation Approach to the Damping of Giant Resonances in Nuclei
October 11, 1982	R. Klapisch CERN, Geneva	Physics at LEAR
October 12, 1982	H. Homeyer Hahn-Meitner Institute	Decomposition of Reaction Mechanisms between 7.5 and 10 MeV/Nucleon. First results from the Hahn-Meitner Neutron Ball.
October 14, 1982	R.H. Siemssen KVI Groningen	Incomplete Fusion
October 18, 1982	J. De Boer University of Munich	The Sense of Rotation of Colliding Nuclei
October 25, 1982	Peter Ring Technical University of Munich	Giant Resonances in Rapidly Rotating Nuclei
November 8, 1982	Wolf-Dietrich Zeitz LBL/Hahn-Meitner Institute	Perturbed Angular Correlation Measurements at ICKSI
November 15, 1982	Dana Beavis University of California	Pion Interferometry in a Streamer Chamber Experiment at Riverside
November 22, 1982	K. Langanke California Institute of Technology	Resonant Structure in Elastic Cross Sections for Strongly Angular Momentum Mismatched Channels
November 29, 1982	C.D. Zafiratos University of Colorado	The (p,n) Reaction at Intermediate Energies
December 6, 1982	S. Frauendorf Central Institute for Research, Germany	Yrast Spectroscopy: Test Ground for the Interplay between Quasi- particle and Collective Degrees of Freedom
December 13, 1982	K. Gregorich and R. Parry LBL	Experiments with Calcium 48 on Curium 248 and Beta Endpoint Measurements of Neutron Deficient Cesium Isotopes
January 10, 1983	M. Cable and R. Welch LBL	1) Decay of Al^{22} and ^{26}P: Discovery of Beta-Delayed Two Proton Radioactivity 2) Actinide Production and the Reaction of ^{129}Xe and ^{208}Pb with ^{248}Cm
January 17, 1983	John Gunion U.C. Davis	Using The Nucleus as a Probe of Quantum Chromodynamics

Appendix III Seminars

January 24, 1983	L.S. Schroeder LBL	Status of The Tevalac Project
January 31, 1983	Kai Cheng Chung Centro Brasileiro de Pesquisas Fisicas	New Aspects of Intranuclear Cascade Calculation in High Energy Heavy Ion Collisions
February 7, 1983	M. Padgett and P. Wilmarth LBL	Emission of Large Fragments in The Reaction ^{3}He Plus Ag and Further Results from The Superheavy Experiments
February 14, 1983	Prof. W. Mayerhoff Stanford	Atomic Clock for Nuclear Time
February 28, 1983	Dr. S. Brodsky SLAC	Nuclear Chromodynamics
March 7, 1983	E. Dines/J. Musser LBL	A New Approach to Gamma-Ray Continuum Spectra Establishing The Neutron Drip Line from Boron to Neon
March 14, 1983	N. K. Glendenning LBL	Neutron Stars are Giant Hypernuclei
March 21, 1983	Prof. C. Buchanan UCLA	High PT Jets at ISR SFM
March 28, 1983	Prof. John MacDonald Univ. of Alberta	Physics Plans on MARIA
March 28, 1983	Prof. D. Boal Simon Fraiser Univ. Burnaby, B.C.	Nuclear Science in The Early Universe
April 11, 1983	Dr. Kurt Snover Univ. of Washington	Giant Dipole Resonances Built on Excited States
April 14, 1983	R. Barasch and R. Bossingham, LBL	A Test of Weak Interaction Theory in Unpolarized Muon Decay
April 25, 1983	Bent Herskind Neils Bohr Inst. Univ. of Copenhagen	Is There Evidence for Pairing Collapse?
April 29, 1983	Dr. Philip Siemens Texas A & M	The Phenomenology of Nuclear Collisions and the Supernova Bounce

May 2, 1983	C. Albiston and Y. Morita LBL	1) The Plastic Box: A 4π Detector for Transfer Reactions 2) Target Fragment Angular Distribution from Heavy Ion Nuclear Reactions
May 9, 1983	H. Homeyer Hahn-Meitner Institute, Berlin	Particle Transfer and Incomplete Fusion
May 16, 1983	Prof. J.R. Leigh Australian Nat. Univ.	Aspects of Heavy Ion Induced Fission
May 23, 1983	H.G. Ritter GSI/LBL	Results from the Plastic Ball
June 6, 1983	Tony Liss LBL	Sea Level Grand Unification Monopole Search
June 13, 1983	Robert Kenney LBL	Double Beta Decay
June 14, 1983	Dr. Jean-Pierre Dufour CEN/LBL	A System for the Electrostatic Collection of Nuclei and Application to Reactions of 86MeV/nucleon 12C
June 20, 1983	Dr. Joseph Kapusta Univ. of Minnesota	Deuteron and Entropy Production and the Nuclear Liquid-Gas Phase Transition
June 21, 1983	Prof. K. McVoy, Univ. of Wisconsin-Madison	Practical Heavy-Ion Optics in The Near/Far Representation
June 27, 1983	Prof. John Newton Australian Nat. Univ.	Study of Nuclei Up to The Highest Possible Angular Momentum
August 9, 1983	H. R. Schmidt Max-Planck-Inst.	Investigation of the Inelastic of ^{28}Si via (^{4}He, ^{4}Heγ), (^{6}Li, ^{6}Liγ) and (^{12}C, ^{12}Cγ)
September 12, 1983	K. Lackner, SLAC	Search for Fractionally Charged Particles
September 13, 1983	P.J. Carruthers LANL	New Stochastic Dynamics Applied to Particle Physics

Appendix III Seminars

Bevatron Research Meetings

October 5, 1982	H. Stroebele GSI	Charged-Particle Exclusive Analysis for Central Collisions of Ar + KCl and Ar + Pb
October 12, 1982	K. Nakai Univ. of Tokyo	Stopping and Energy Deposition of GeV Particles in Target Nuclei
October 26, 1982	H. Heckman LBL	Survey of Planned Bevalac Experiments Using Visual Detectors
November 2, 1982	M. Gyulassy and A. Poskanzer, LBL	Discussion on Stopping in High Energy Nucleus-Nucleus Collisions
November 9, 1982	B. Price, UC J. Symons, LBL H. G. Ritter, GSI	New Anomalon Experiments Using γ-ray and Plastic Track Detectors, Čerenkov Imaging Techniques, and the Plastic Ball
November 15, 1982	D. Beavis UC Riverside	Pion Interferometry in a Streamer Chamber Experiment
November 23, 1982	H. Matis LANL	The Search for Muon-Number Violating Decays at LAMPF
December 7, 1982	K. Braune, SLAC	High Energy Hadron-Nucleus Interactions
December 15, 1982	J. Alonzo LBL	The State of the Bevalac
January 18, 1983	H. Pugh LBL	Physics Priorities at the Bevalac for the Next Two Years
January 25, 1983	H. Pugh LBL	Physics Priorities at the Bevalac for the Next Two Years – Part II
February 1, 1983	G. Chapline LLL	Can Fractional Charge Save Nuclear Physics?
February 8, 1983	J. Carroll UCLA	Proton-Proton Correlations – Past, Present, and Future
February 15, 1983	Y. Karant LBL	A Consideration of Anomalon Signatures for the Design of Experiments

February 22, 1983	H. Crawford SSL	Atomic and Nuclear Physics with 1 GeV/n Uranium
March 8, 1982	M. Gyulassy LBL	Tevalac Physics at Brookhaven
March 15, 1983	H-A Gustafsson LBL	A Search for Short-Lived Anomalons in Projectile Fragmentation
March 17, 1983	B. Jacak MSU	Fragment Production in Intermediate Energy Heavy Ion Reactions
March 25, 1983	S. Nagamiya Univ. of Tokyo	A Question on the Mechanism of High Momentum Transfer
March 29, 1983	H. Stocker MSU	Nuclear Collisions from 50 MeV/n to 5 GeV/n
April 12, 1983	P. Danielewicz LBL	Jacobian Free Global Event Analysis
April 26, 1983	J. Ainsworth LBL	Bevalac Biomedical Program – Overview
May 3, 1983	D. Keane UC Riverside	Full Event Analysis Using the Streamer Chamber
May 17, 1983	H. Wieman GSI/LBL	Nuclear Stopping and Thermalization and Two Particle Correlations
May 31, 1983	Y. Kitazoe LBL	A Systematic Analysis of High Energy Heavy Ion Collisions Using Improved Cascade Calculations
June 14, 1983	J-P Dufour CEN/LBL	A System for the Electrostatic Collection of Nuclei and Application to Reactions of 86 MeV/nucleon 12C
June 20, 1983	J. Kapusta Univ of Minnesota	Deuteron and Entropy Production and the Nuclear Liquid-Gas Phase Transition
July 5, 1983	D. Strottman LASL	Global Analysis and Hydrodynamics from 200 MeV to 200 GeV
July 12, 1983	T. Matsui LBL	Meson Radiation from Quark-Gluon Plasma

Appendix III

Seminars

Theory Seminars

January 10, 1983	Pedro Federman Argentina	A Microscopic look at Nuclear Deformation
January 26, 1983	Joachen Wombach Julich, W. Germany	Correlations in Giant Resonances
March 2, 1983	Dr. Cseperley LLL	Monte Carlo Methods for Many Body Problems
April 5, 1983	J. Treiner ORSAY	Fission from Saddle to Exit: Influence of Curvature and Compression Energies
June 22, 1983	V. Ruuskanen Jyväskylä, Finland	Hydrodynamics Initialization
July 7, 1983	E. Remler Virginia	Relativistic Cascade Theory
July 8, 1983	A. L. Goodman New Orleans, Louisiana	Statistical Fluctuations in the Nuclear Liquid-Gas Phase Transition
July 11, 1983	B. Schurmann Munich, W. Germany	Kaons in Relativistic Collisions
July 13, 1983	K. Tanabe Saitama, Japan	Phase Transitions in Hot Rotating Nuclei with Pairing Conditions
July 26, 1983	D. Boal Burnaby, B.C., Canada	Thermal and Chemical Equilibrium in Proton Induced Reactions?
July 28, August 2 August 8, 1983	H. Sumiyoshi Tokyo, Japan	The Multichain Model for Hadron-Nucleus and Nucleus-Nucleus Collisions I-III
August 3, 1983	J. Kapusta Minnesota	Droplet Formation in Supersaturated Systems
August 9, 1983	D. Boal Burnaby, B.C., Canada	Kinetic Approach to Fragment Formation
August 22, 1983	A. Hosoya Osaka Univ.	Non-Equilibrium Field Theory: Computation of Transport Coefficients

September 13, 1983	P. Carruthers LANL	New Stochastic Dynamics Applied to Particle Physics
September 14, 1983	S. E. Koonin CalTech	Fusion Cross Sections and the Proximity Potential at Small Distances
September 19, 1983	C. C. Noack Bremen, W. Germany	Covariant Cascade Model

Author Index

Appendix IV

Abachi, S. 188
Abrams, P.C. 156
Agarwal, Y.K. 71
Albiston, C. 117,122,127
Albrecht, R. 279
Aleklett, K. 109,139,141,142,145,154
Andrews, H.R. 86
Armbruster, P. 71
Arthur, A.A. 293
Arvieux, J. 101

Baden, A. 262
Bai, X. 183,184
Baktash, C. 91
Banerjee, B. 236
Bangert, D. 172,191,192,283,284,285
Bantel, M. 117,122,127,275
Barasch, E. 188
Barnwell, J.M. 96
Barwick, S.W. 149
Baumgartner, M. 274
Beard, K. 186
Beckman, R. 154
Beiser, F. 253
Beleal, E. 292
Bendjaballah, N. 88
Benenson, W. 186
Bieser, F. 254,270,272
Birchall, J. 101,96
Bland, R.W. 156
Blann, M. 115
Blocki, J. 208
Bloomer, M.A. 155,251
Bowman, H. 169
Brady, P. 272
Brandt, R. 154
Brockmann, R. 172,191,192,283,284,285
Bronson, M. 287,292
Brown Jr., W.L. 293
Brown, J.D. 96
Browne, E. 295
Brüchle, W. 71
Brügger, M. 71
Buchwald, G. 227
Budzanowski, A. 115,117

Cable, M.D. 59,61,62
Canto, L.F. 214
Carroll, J. 180,188
Castenada, C. 272
Cerny, Joseph 59,61,62
Chan, Y.D. 104,107,115,117,122,127,275,277
Chang, C.C. 180
Christie, W. 272
Chung, K.C. 229
Clark, D.J. 256,258
Clarke, N.M. 96
Cline, D. 91
Conzett, H.E. 96,98,100,101,102
Countryman, P.J. 117,122,127,275,277
Crawford, H.J. 175,179,272,274,290
Csernai, L.P. 225
Czosnyka, T. 91

Døssing, T. 202,205
Dacal, A. 172,191,283
Danielewicz, P. 227,229
Daniels, W.R. 124
Deleplanque, M.A. 81,84,86,130
Dersch, G. 154
DiGregorio, D. 117
Diamond, R.M. 79,81,86,88,91,130
Dietrich, F.S. 102
Dines, E.L. 81,86,130
Donangelo, R. 214,229
Dornhöfer, H. 71
Draper, J.E. 81,130
Duarts, S.B. 229
Dufour, J.-P. 71

Eitner, P. 283,284
Ellis-Akovali, Y. 88
Eskola, K. 123
Eversheim, D. 96,102

Fa'i, G. 225
Firestone, R.B. 295
Fischer, P. 188
Flores, I. 272
Fowler, M.M. 71,123,124
Frankel, K.A. 227,247
Friedlander, E.M. 147,154,155,163,293
Frink, C. 71

Gäggeler, H. 71
Ganezer, K. 188
Garrett, J.D. 88
Ghiorso, A. 71,73,252
Gilot, J.-F. 186
Glendenning, N.K. 233,236
Gould, H. 175,179
Graebner, G. 227
Gregorich, K.E. 71,72,77,124,132
Greiner, D.E. 175,179,253,270,272

Greiner, W. 227
Greulich, N. 71
Griffiths, R.J. 96
Grotowski, K. 117
Gu, H.H. 108
Gu, J.H. 113,125
Guarino, G. 104,107,113,125,266
Gustafsson, H.-A. 153,160,189,190,260,279
Gutbrod, H.H. 153,160,189,190,260,262,279
Gyulassy, M. 227,230,231,236

Häusser, O. 86
Hagebø, E. 145
Hagstrom, R. 253
Hahn, A.A. 156
Halback, K. 252
Haldorsen, I.R. 145
Hallman, T. 180
Hamagaki, H. 183,184
Hanspal, J.S. 96
Harris, J.W. 172,186,191,192,283,284,285
Haruhn, J. 227
Harvey, B.G. 127,212
Hashimoto, O. 183,184
Hasselgren, L. 91
Heckman, H.H. 147,155,163,251,293
Herrmann, G. 71
Herskind, B. 88
Hessberger, F.P. 71
Hickmann, U. 71
Hicks, K.H. 169
Hildebrand, N. 71
Hodges, C.L. 156
Hoffman, D.C. 124,71
Hoffman, S. 71
Homeyer, H. 117,122,127,212
Honkanen, J. 59,61,62,65,69
Horn, D. 86
Hou, W. 283,284
Hulet, E.K. 91
Hunter, J.B. 267

Igo, G. 188
Ingersoll, J.G. 169

Johnson, R.T. 156
Jones, R.W. 293
Jongen, Y. 256
Joyce, D.C. 156
Juergens, P. 77

Kadota, S. 184
Kajantie, K. 231
Karant, Y.J. 147,155,163,251,293
Kazeminzhad, F. 188
Kidd, J. 175
Kimura, K. 183,184
Kirk, P.N. 180,186
Kluge, H. 91
Knoop, T.D. 156
Kobayashi, T. 183
Kodama, T. 229
Koike, M. 169
Kolb, B. 153,160,189,190,260,279,294
Koontz, R. 180
Kot, W. 72,109,132
Kratz, J.V. 71
Kraus, Jr., R.H. 142,145
Krebs, G. 180,186
Kudo, H. 134
Kurki-Suonio, H. 231

Lackner, K.S. 156
Lamontagne, C.R. 101
Lanza, E.G. 220
Lapointe, C. 96
Larimer, R.M. 96
Lee, D. 71,72,75,77,123,124,132
Leino, M. 71
Lemmertz, P.K. 65,69,71,280
Lindenberger, K.H. 88
Lindgren, M.A. 156
Lindstrom, P.J. 175,179,272,287,290
Liu, Y.-F. 75
Liu, Z.H. 108
Löhner, H. 160,189,190,260,262,279
Lone, M.A. 86
Lougheed, R.W. 91
Loveland, W. 109,139,141,142,145,154
Ludewigt, B. 153,160,189,190,260,279
Lund, T. 145,154
Lyneis, C.M. 256

Macchiavelli, A.O. 81,86,130
Madansky, L. 180
Maier, M. 172,191,192,283,284,285
Matsui, T. 200,230,233,236
McCulloch, R.A. 96
McDonald, R.J. 108,113,125,266,271
McFarland, R.M. 142
McGaughey, P.L. 139,142,145,154
McKee, J.S.C. 96
McLerran, L. 231
McParland, C. 254,272,287,289,292
Mendenhall, M. 264
Miake, Y. 183,184

Miller, J. 186
Möhring, K. 210
Möller, P. 198
Moody, K.J. 71,72,75,77,124,132,134,136,142
Moretto, L.G. 104,107,108,113, 125,217,220,223,224
Morita, Y. 75,145
Morrissey, D.J. 109,139
Münzenberg, G. 71
Mulera, T. 180,188
Murphy, D. 166
Murphy, M.J. 127,277
Musser, J.A. 149,269
Myers, W.D. 197,198,199

Nagamiya, S. 183,184
Nazareth, R.A.M.S. 229
Newton, J.O. 88
Nitschke, J.M. 65,69,280

Odyniec, G. 172,191,192,283,284,285
Oertel, C.P. 139
Ohm, H. 123
Oliveira, L.F. 214
Olson, D. 292
Omata, K. 184
Ortiz, M. 172,191,283

Pacheco, A.J. 104,107,113
Padgett, M.L. 104,107,108
Parry, R.F. 59,61
Perez-Mendez, V. 188
Peter, J. 169
Planeta, R. 117
Poppe, C.H. 102
Poppensieker, K. 71
Porile, N.T. 154
Poskanzer, A.M. 153,160,189,190,260,262,279
Price, P.B. 151,269
Pugh, H.G. 156,172,180,186,191, 192,283,284,285

Radi, H.M.A. 166,214,247
Randrup, J. 202,205,207,225,229
Rasmussen, J.O. 166,169,214,241,243,247
Rauch, W. 172,191,283,284,285
Reiff, J.E. 62
Reisdorf, W. 71
Renfordt, R.E. 172,191,192,283,284,285
Renner, T. 153,160,189,190,260,262,279
Ridout, J. 166
Riedesel, H. 153,160,189,190,260,262,279
Rioux, C. 101,102
Ritter, H.G. 153,160,189,190,260,262,279
Roche, G. 180,186
Roman, S. 96
Romero, J. 272
Roulet, C. 91
Rowley, D. 102
Roy, R. 101

Sandoval, A. 172,191,192,283,284,285
Sann, H. 272
Savage, M.H. 156
Schädel, M. 71
Schall, D. 172,191,192,284,285
Schimmerling, W. 175
Schloemer, E.C. 62
Schmidt, K.-H. 71,197
Schneider, J.H.R. 71
Schneider, W.F.W. 71
Scholz, M.H. 156
Schroeder, L. 180,186,192
Schuck, C. 88
Seaborg, G.T. 71,72,73,75,77,109,123,124, 132,134,136,139,141,142,145,154
Shapiro, G. 183
Shaw, G.L. 156
Sherill, B. 186
Shida, Y. 183,184
Shor, A. 188
Signarbieux, C. 108
Skensved, P. 86
Slansky, R. 156
Slobodrian, R.J. 101,101
Sobotka, L.G. 104,107,108,113,125,266,267,271
Song, H.C. 247
Stelzer, H. 279
Stephens, F.S. 81,86,88,93,130
Stevenson, J.D. 149,269
Stöcker, H. 227
Stock, R. 172,191,192,283,284,285
Stokstad, R.G. 104,107,115,117,122, 127,264,275,277
Stroebele, H. 172,191,192,283,284,285
Sümmerer, K. 71
Sugihara, T.T. 109,145
Sullivan, J.P. 169,247
Świątecki, W.J. 198,199,207,208,210
Symons, T.J.M. 175,179

Tanaka, S. 136
Tanihata, I. 183,184
Taras, P. 86
Tincknell, M.L. 151
Tittel, K. 192

Appendix IV Author Index

Tombrello, T. 264
Trautmann, N. 71
Treher, E.N. 123
Trentalange, S. 188
Tserruya, I. 104,107,115,127,277
Tull, C. 272
Turney, A.D. 293

Van Bibber, K. 122,127,277
van der Pflicht, H. 186
Vermeulen, D. 71
Vicente, J. 180,186
von Gunten, H.R. 71,75,124

Wada, Ryoichi 274
Wald, S. 104,107,115,117,122, 127,275,277,287
Wang, C.S. 199
Ward, T.E. 169
Warwick, A.I. 153,160,189,190,260,262,279
Weik, F. 160,189,260
Weiner, R.M. 154
Welch, R.B. 71,72,124,132
Wenxin, Li 141
Wieman, H. 153,160,189,190,260,262,279
Wilhelmy, J.B. 123
Wilmarth, P.A. 65,69,71,280
Wirth, G. 71
Wolf, K.L. 172,192
Wozniak, G.J. 104,106,107,108,113, 125,266,267,271
Wu, C.Y. 91

Yao, Z.Q. 108,125,266
Yashita, S. 71,252
Yoshikawa, N. 184
Young, B.A. 156

Zeitz, W.-D. 65,280
Zhou, S.H. 59,61,62,117
Zhou, Z.Y. 59,61,62,117
Zielińska-Pfabé, M. 210

This report was done with support from the Department of Energy. Any conclusions or opinions expressed in this report represent solely those of the author(s) and not necessarily those of The Regents of the University of California, the Lawrence Berkeley Laboratory or the Department of Energy.

Reference to a company or product name does not imply approval or recommendation of the product by the University of California or the U.S. Department of Energy to the exclusion of others that may be suitable.

Technical Information Department
Lawrence Berkeley Laboratory
University of California
Berkeley, California 94720